Tube-building annelids from hydrothermal vents and cold seeps:

Tube morphology, fossilisation, and evolutionary history

Magdalena Nikolaeva Georgieva

Submitted in accordance with the requirements for the degree of
Doctor of Philosophy

The University of Leeds
School of Earth and Environment

September 2016

Intellectual Property and Publication Statement

The candidate confirms that the work submitted is her own, except where work which has formed part of jointly-authored publications has been included. The contribution of the candidate and the other authors to this work has been explicitly indicated below. The candidate confirms that appropriate credit has been given within the thesis where reference has been made to the work of others.

The work in Chapter 2 of the thesis has appeared in publication as follows:

Georgieva, M. N., Wiklund, H., Bell, J. B., Eilertsen, M. H., Mills, R. A., Little, C. T. S. and Glover, A. G. (2015) A chemosynthetic weed: the tubeworm *Sclerolinum contortum* is a bipolar, cosmopolitan species. *BMC Evolutionary Biology* 15, 280. doi:10.1186/s12862-015-0559-y.

I was involved in the design and coordination of this study, performed all measurements, imaging, chemical, and the majority of genetic analyses (a subset of the DNA sequencing was performed by other authors). I also wrote the manuscript. Helena Wiklund helped to design the study and with all aspects of the molecular work - Helena taught me how to perform the genetic analyses used for this study, and provided guidance with the interpretation of the results. James B. Bell processed the samples from the JC55 cruise, and therefore picked out many of the worms that were used for this study. He also provided the SHRIMP imagery in Figure 2.5. Mari H. Eilertsen sequenced the DNA of the worms from Loki's Castle. Rachel A. Mills collected the sulphurous chunk with embedded *Sclerolinum* tubes that was analysed as part of this study, and provided guidance with the parts of the manuscript that deal with biogeochemistry. Crispin T. S. Little provided guidance with the parts of the manuscript dealing with fossilisation. Adrian G. Glover collected the Antarctic *S. contortum* material that formed the basis for this study, imaged specimens live at sea, conceived of the study, participated in its coordination, and provided guidance during the writing of the manuscript.

The work in Chapter 3 of the thesis has appeared in publication as follows:

Georgieva, M. N., Little, C. T. S., Ball, A. D. and Glover, A. G. (2015) Mineralization of *Alvinella* polychaete tubes at hydrothermal vents. *Geobiology* 13, 152-169. doi:152–169. 10.1111/gbi.12123.

I contributed to the design of this study, performed all analyses, and wrote the manuscript. Crispin T. S. Little collected the material that was used, conceived of the study, contributed to its design, and provided guidance during the writing of the manuscript. Alexander D. Ball also contributed to study design, and provided guidance with analytical techniques. Adrian G. Glover was involved in designing the study, and provided guidance during the writing of the manuscript.

The work in Chapter 4 of the thesis reproduces a manuscript in the final stages of preparation for submission to the *Journal of Systematic Palaeontology*:

Georgieva, M. N., Little, C. T. S., Watson, J. S., Sephton, M. S., Ball, A. D. and Glover, A. G. (in prep.) Worm tubes from ancient hydrothermal vents and cold seeps – towards improving identification.

I contributed to the design of this study, performed the majority of analyses, and wrote the manuscript. Crispin T.S. Little collected much of the material used, conceived of the study, and provided guidance during the study design and manuscript preparation. Jonathan S. Watson provided assistance with py-GC-MS and FTIR analytical techniques and interpretation of results, and Mark S. Sephton facilitated my use of Imperial College laboratory facilities. Alexander D. Ball provided assistance with imaging techniques, and Adrian G. Glover also assisted with the study design, and provided guidance during the writing of the manuscript.

The work in Chapter 5 of this thesis reproduces a manuscript in the final stages of preparation for submission to the journal *Geology*:

Georgieva, M. N., Little, C. T. S., Ball, A. D. and Glover, A. G. (in prep.) Microbial-tubeworm associations in a 440-million-year-old hydrothermal vent community.

I contributed to the design of this study, performed all analyses, and wrote the manuscript. Crispin T. S. Little assisted with the design of the study, and provided guidance during the writing of the manuscript. Alexander D. Ball provided guidance with analytical techniques.

Adrian G. Glover also assisted with the study design, and provided guidance during the writing of the manuscript.

Acknowledgements

This PhD was funded by a NERC CASE studentship (no. NE/K500847/1) which is gratefully acknowledged. It has taken me on an incredible journey in its pursuit of a better understanding of the deep sea, annelid tubes and their fossils and I am very thankful for the opportunity to work on this diverse and challenging subject. Firstly I would like to express my sincere gratitude to my supervisors Dr Crispin Little, Dr Adrian Glover and Dr Alex Ball for their continued support and guidance, for encouraging me to think more, for being inspiring mentors, and for being overall great people to work with. Many people have helped to make my PhD experience fun and enriching and I would also like to thank friends and colleagues at the University of Leeds and at the Natural History Museum for their companionship and support, and especially Dr Helena Wiklund for guidance with molecular work and all aspects of academic life. A special thanks also to Tony Wighton for his perseverance with making many tube thin sections!

One of the best aspects of this PhD has been getting to know the polychaete, palaeontology, and deep-sea research communities which have been truly inspiring, have provided many happy times and who it has been a great pleasure to get to know. My PhD project would not have been possible without the help of a global network of scientists who provided material for me to study, and a great number of support staff that made its collection possible. Thank you all! A special thanks to Eve Southward for providing tube samples, inspiring discussion, and a tour of the Marine Biological Association of the UK.

I am also indebted to Adrian for taking me on my first deep-sea research expedition, and to Dr Bob Vrijenhoek and Dr Charlie Paull for their invitations to join another deep-sea research cruise, and to work with them at MBARI for 6 weeks.

I would also like to thank my family, friends and James for their unwavering love and support throughout my PhD.

Abstract

Problems with the identification of tubular fossils from ancient hydrothermal vent and cold seep deposits have hindered understanding of the evolutionary history of vent and seep communities. This thesis aims to (1) improve knowledge of lesser-studied tubicolous annelids occupying vents and seeps, (2) study the diversity of tubes at vents and seeps, (3) investigate the fossilisation of tubes within modern vents and seeps, (4) better interpret the fossil record, and (5) provide insights into the palaeoecology these environments. Results presented here on investigations of *Sclerolinum contortum*, a species belonging to a little-studied genus of the major vent/seep dwelling annelid family Siboglinidae, demonstrate that it exhibits tube morphological plasticity, wide habitat preferences and a global distribution spanning the Arctic to the Southern Ocean. These results also suggest that this species has dispersed throughout this range using chemosynthetic habitats as stepping stones. A detailed investigation of the full mineralisation process of *Alvinella* (Alvinellidae) tubes at modern hydrothermal vents shows that these tubes are fossilised by pyrite and silica that template organic tube layers, and that microorganisms living on tube surfaces are also exceptionally well-preserved alongside the tubes. No known ancient vent tube fossils resemble mineralised *Alvinella* tubes. A major morphological and compositional comparison of both modern and fossil tubes from vents and seeps revealed that two fossil tube types from the Mesozoic were likely made by vestimentiferans (Siboglinidae), suggesting that this major vent and seep annelid lineage has a longer history within vents and seeps than proposed by molecular clock age estimates. This analysis also demonstrates the need for greater caution in assigning affinities to fossil vent and seep tubes. Finally, this thesis reports the remarkable preservation of filamentous microorganisms on the walls of Silurian vent tube fossils, giving the first insights into ecological associations between microbes and metazoans within the oldest known hydrothermal vent community.

Contents

List of Figures

List of Tables

Abbreviations

16S	Mitochondrial Large Subunit Ribosomal RNA
18S	Nuclear Small Subunit ribosomal RNA
AIC	Akaike Information Criterion
AMOVA	Analysis of Molecular Variance
ANME	Anaerobic Methanotrophic Archaea
AOM	Anaerobic Oxidation of Methane
BMNH	Natural History Museum, UK
BSE	Backscattered Electrons
CLSM	Confocal Laser Scanning Microscopy
COI	Cytochrome Oxidase Subunit I
EBSD	Electron Back-Scatter Diffraction
EDS	Energy Dispersive X-ray Spectroscopy
EPMA	Electron Probe Micro-Analysis
EPR	East Pacific Rise
EPS	Extracellular Polymeric Substances
FTIR	Fourier Transform Infrared Spectroscopy
Ga	Billion Years Before Present
GMRT	Global Multi-Resolution Topography
GoM	Gulf of Mexico
HMMV	Håkon Mosby Mud Volcano
ICL	Imperial College London, UK
JC55	RRS James Cook Expedition 055
JdFR	Juan de Fuca Ridge
K2P	Kimura 2 Parameter

LACMIP	Invertebrate Paleontology, Natural History Museum of Los Angeles, USA
Ma	Million Years Before Present
MAFFT	Multiple Alignment using Fast Fourier Transform
MBARI	Monterey Bay Aquarium Research Institute
μ-CT	Micro-Computed Tomography
MUSCLE	Multiple Sequence Comparison by Log-Expectation
NASA	National Aeronautics and Space Administration, USA
NCBI	National Center for Biotechnology Information, USA
NERC	Natural Environment Research Council, UK
NHM	Natural History Museum, UK
NHMUK	Natural History Museum, UK
NOAA	National Oceanic and Atmospheric Administration, USA
NSF	National Science Foundation, USA
PCO	Principal Coordinates Analysis
PCR	Polymerase Chain Reaction
py-GC-MS	Pyrolysis Gas Chromatography Mass Spectrometry
RL	Reflected Light Microscopy
ROV	Remotely-Operated Vehicle
SEM	Scanning Electron Microscopy
SHRIMP	Seafloor High Resolution Imaging Platform
SMS	Seafloor Massive Sulphide
UL	University of Leeds, UK
VMS	Volcanogenic Massive Sulphide
WDS	Wavelength Dispersive X-ray Spectroscopy
WHOI	Woods Hole Oceanographic Institution
XRD	X-Ray Diffraction

1 Introduction

Hydrothermal vents, characterised by the ejection of hot, reduced and mineral-rich fluids from the seafloor, have existed in the deep ocean since the Hadean, the earliest period of Earth's history 4.6-4.0 billion years ago (Ga; Russell and Hall, 1997; Martin *et al.*, 2008). Yet hydrothermal vents and related cold seep environments, from which cooler reducing fluids emanate, have only been known to scientists since late 1970s to early 1980s (Lonsdale, 1977; Corliss *et al.*, 1979; Paull *et al.*, 1984), when their initial exploration revealed that these systems support exceptional abundances of life in the otherwise largely resource-limited deep sea. Their discovery also profoundly changed understanding of life on Earth, as vent and seep ecosystems were found to be fuelled by the oxidation of reduced inorganic compounds entrained within vent and seep fluids rather than sunlight, a process termed chemosynthesis.

Hydrothermal vents and cold seeps have received much scientific attention in the years since their discovery (Van Dover, 2000), with even life itself proposed to have emerged within ancient vents (Reysenbach and Cady, 2001; Martin *et al.*, 2008; Weiss *et al.*, 2016). However, we know very little about a substantial part of the history of these ecosystems, exemplified by fundamental questions such as when and how animals adapted to survive within the sulphidic conditions presented by vents and seeps, and how these chemosynthetic ecosystems function over evolutionary timescales (Kiel, 2010). Windows into deep time that have enabled these questions to be addressed are provided by numerous examples of fossilised vents and seeps (Campbell, 2006). These have shown the occupation of these environments to be incredibly ancient, with the oldest known animal fossils in these habitats dating to the Silurian (443 - 419 Ma (million years ago)) (Little *et al.*, 1997; Barbieri *et al.*, 2004) and the oldest vent microbial fossils reaching 3.24 Ga (Rasmussen, 2000).

A prominent animal group inhabiting and structuring hydrothermal vents and cold seeps in the modern ocean, which have also become the icons of the former century's deep-sea discoveries, are tube-building annelid worms. Their prominence also within ancient vent and seep communities is attested by frequently encountered tubular fossils within these deposits spanning the Silurian to the Miocene, making them an essential component of, and potentially ideal subjects through which to study, the evolutionary history of vents and

seeps. But poor understanding of how tube morphology relates to established annelid taxonomy, in addition to a limited knowledge of the fossilisation of annelid tubes at vents and seeps, has limited the ability to interpret the fossil record. The above are major themes addressed in this thesis.

This chapter will firstly provide a brief overview of the abiotic characteristics of hydrothermal vents and cold seeps, essential to understanding the conditions within which life exists and under which it may be fossilised within these settings. Then background on vent and seep fauna, both in the modern ocean and in the ancient past will be provided, with a focus on the annelid worms, their tubes, and what is currently known about their fossilisation.

1.1 Hydrothermal vents and cold seeps: geology and chemistry

1.1.1 Hydrothermal vents

Hydrothermal vents occur predominantly along the axis of mid-ocean ridges, which form a ~64,000 km long global system that crosscuts the ocean floor (Hannington *et al.*, 2011). These submerged mountain chains result from the separation of oceanic tectonic plates, the divergence of which causes magma to rise between them and form new ocean crust (Van Dover, 2000). Within this setting, seawater that has percolated deep within the crust through fissures and fractures is heated by the upwelling magma, loaded with dissolved minerals and reduced gases such as hydrogen sulphide, and is subsequently convected upwards, erupting as hydrothermal vents on the seafloor. While the majority of hydrothermal vents currently known (57%; Beaulieu 2013) occur at mid-ocean ridges (Figure 1.1), hydrothermal circulation can also occur at forearc, island arc and back-arc settings of subduction zones, as well as at active submerged volcanoes or seamounts (Seyfried and Mottl, 1995).

When hydrothermal fluids eventually surface at the seabed, their interaction with surrounding cooler seawater causes minerals to precipitate. Commonly, modern vent deposits, also known as seafloor massive sulphides (SMS), take the form of towering chimneys termed black- or white-smokers depending on the temperature and composition of the vent fluid which they emit. Primary vent fluids are hot, reaching 350-407°C (Koschinsky *et al.*, 2008; Hannington *et al.*, 2011), and laden with metals such as iron, copper and zinc. The chimneys that precipitate from these fluids can form incredibly

quickly (up to 30 cm per day; Tivey 1995), and have a complex mineralogy that evolves as a chimney grows. They initiate with the precipitation of a porous anhydrite skeleton (Figure 1.2A) (Tivey, 1995), that isolates vent fluid from seawater and acts as a template for the deposition of sulphide minerals (Haymon, 1983). Chalcopyrite (copper-iron sulphide) is subsequently precipitated on inner chimney walls, while pore spaces within the anhydrite matrix are progressively infilled by iron and zinc sulphides, which are zoned according to the steep temperature and chemical gradients that develop within the growing vent chimney (Haymon, 1983; German and Von Damm, 2006). White-smoker chimneys typically vent fluids of intermediate temperatures (100-300°C; Van Dover 2000), and their pale plumes and deposit mineralogies reflect a vent fluid composition of silica, anhydrite and barite. At temperatures below 100°C, diffuse venting may emanate from the verges of active vent chimneys or directly from cracks in the seafloor. This typically does not result in significant mineral deposition due to the low temperatures of the fluid, however in some cases significant iron oxide deposits may form in association with low temperature venting (Little *et al.*, 2004a).

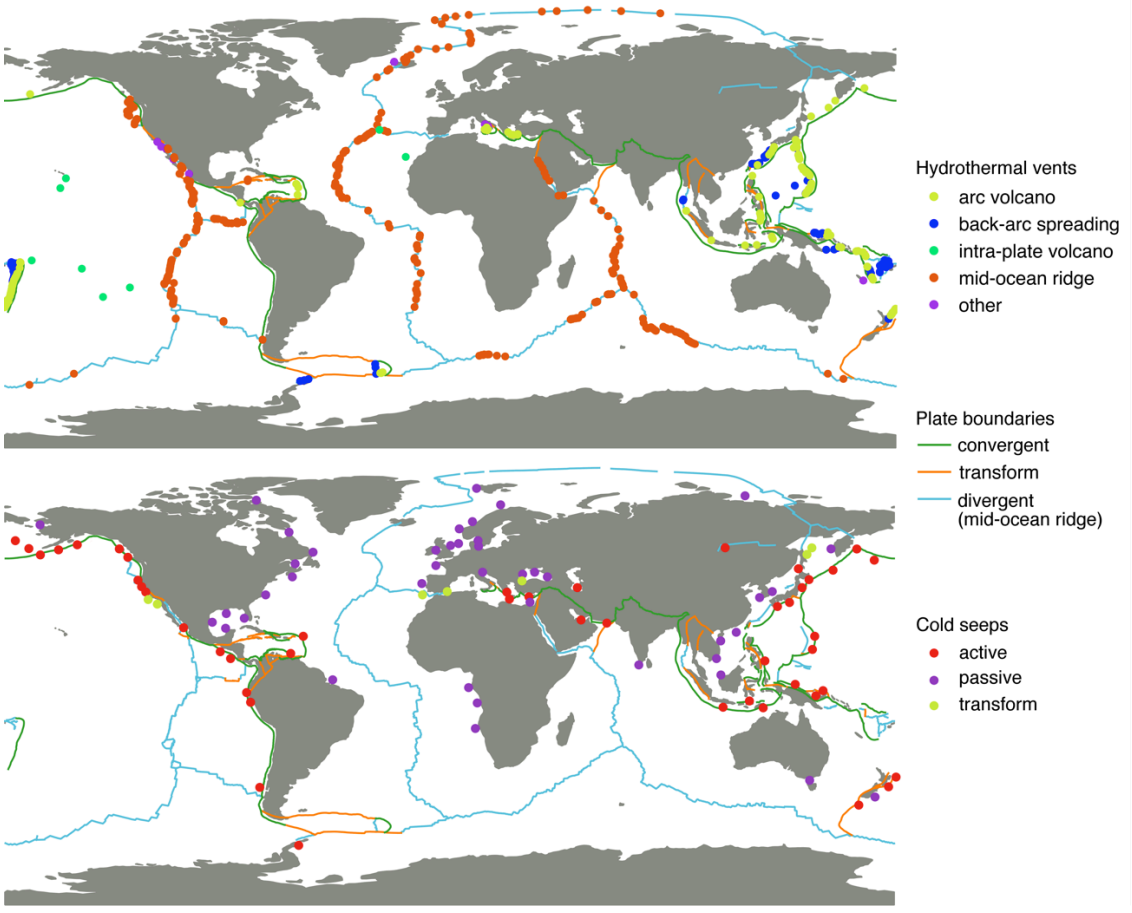

Figure 1.1 Currently known hydrothermal vent and cold seep sites. Locations are labelled by tectonic setting. Vent locations are based on the InterRidge Vents Database v. 3.3 (Beaulieu, 2013), and seep sites on Torres & Bohrmann (2014). Tectonic plate boundary shapefiles were obtained from the University of Texas PLATES Project (Coffin *et al.*, 1998).

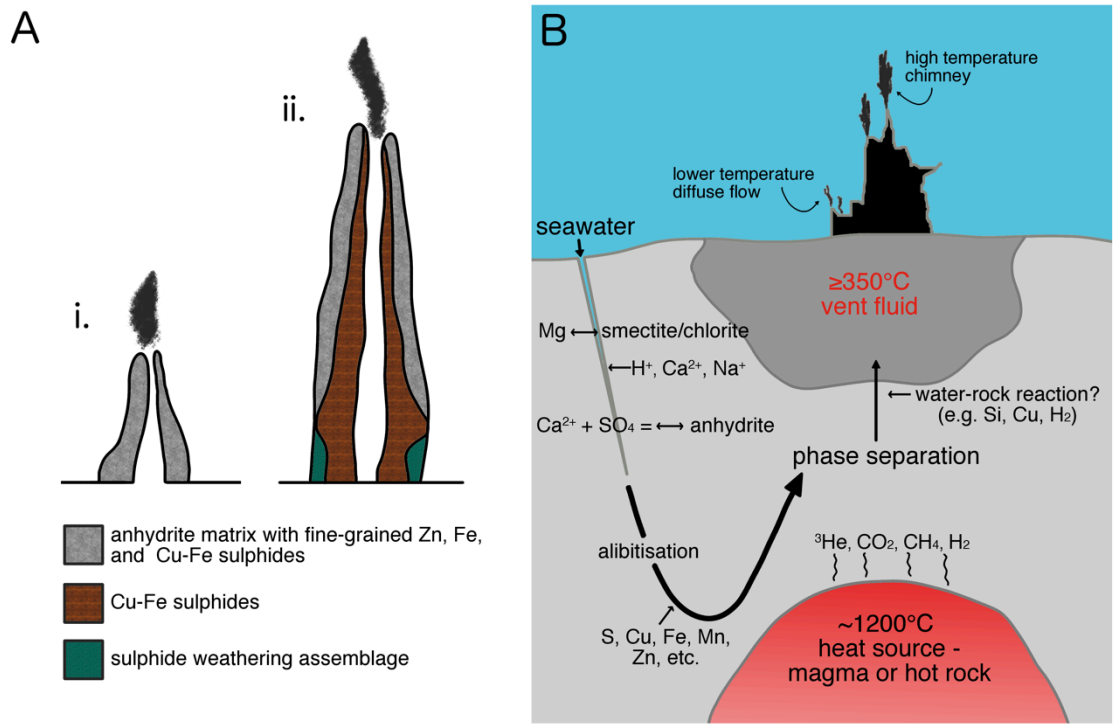

Figure 1.2 Vent chimney formation and processes affecting vent fluid composition within seafloor hydrothermal systems. **A,** schematic drawing of vertical cross-sections of black smoker vent chimneys, showing both early-stage (i) and late-stage (ii) chimney growth. Adapted from Tivey (1995). **B,** schematic drawing of a hydrothermal system within oceanic crust, showing the processes that affect the composition of vent fluids, adapted from Tivey (2007).

Although vent fluids are commonly acidic, reducing, sulphur and metal rich (Hannington *et al.*, 1995), large variations in their chemistry can result from subsurface reaction conditions and processes such as phase-separation (Von Damm, 1995) (Figure 1.2B), which can in turn affect the mineralogy of deposits at different sites (Hannington *et al.*, 1995). For example, highly unusual vent chimneys comprised largely of elemental sulphur occur within Kemp Caldera, a submerged volcano in the Southern Ocean, due to probable input of magmatic volatiles (Cole, 2013; Cole *et al.*, 2014). The morphology of sulphide deposits also varies in response to fluid flow dynamics, seafloor spreading rate and internal plumbing, discrepancies of which can manifest as 'beehive' and 'flange' structures on vent chimneys, subseafloor deposits and complex sulphide mounds. The occurrence of venting through sediment results in the mixing of vent fluids with seawater in the subseafloor, and can lead to further alteration of vent fluid (Van Dover, 2000) as well as mineral deposition at depth (Von Damm *et al.*, 1985).

In addition to showing high spatial heterogeneity, vents are also temporal variability as a result of mineral accretion and tectonic events such as volcanic eruptions (Tunnicliffe *et al.*,

2003). The stability, and much of the architecture of a vent site, also relates to the rate of seafloor spreading (Van Dover, 2000), which have resulted in the evolution of markedly different vent sites along the global mid-ocean ridge system. Volcanic eruptions occur more frequently on fast-spreading ridge segments such as the East Pacific Rise (EPR) than slow-spreading ridges (Fornari *et al.*, 2012). Slow spreading can favour the formation of unusual serpentinite-hosted hydrothermal vent systems, such as the 'Lost City' vent site which occurs ~15 km from the main spreading axis of the Mid-Atlantic Ridge. This site differs from known Mid-Atlantic Ridge along-axis vent sites due to the high pH (9-11) of vent fluids, and the precipitation of carbonate chimneys (Kelley *et al.*, 2001).

1.1.2 Cold seeps

Cold seeps (Figure 1.3) occur wherever sulphide and methane emanate from seafloor sediments but without the high temperatures characteristic of hydrothermal vents (Levin, 2005). Seeps are concentrated along both active and passive continental margins (Figure 1.1), but can also arise within inland lakes and seas such as within the world's largest body of freshwater (by volume), Lake Baikal (Van Rensbergen *et al.*, 2002). Processes such as high pore-fluid pressures resulting from tectonic movement, "salt tectonics", artesian flow, catastrophic erosion events and submarine slides can all result in fluid seepage (Tunnicliffe *et al.*, 2003). In addition to methane, the most common seepage component, seep fluid may contain other hydrocarbon gases, petroleum, asphalt, hypersaline brines and gas hydrate solutes (Tunnicliffe *et al.*, 2003; Levin, 2005).

Cold seeps are considered to have less fluctuating conditions in comparison to hydrothermal vents (Sibuet and Olu, 1998), but seepage can occur against a large range of flow rate, temporal stability, and geological contexts (Tunnicliffe *et al.*, 2003; Levin, 2005). Seeps in the modern ocean may manifest as gas bubbling out of the seafloor, microbial mats, gas hydrates, authigenic carbonates and bioherms, and may form topographic features such as pockmarks, mounds, mud volcanoes and diapirs (Levin, 2005).

Many cold seep sites are characterised by the presence of carbonate, which is precipitated at seeps through a microbial process known as the anaerobic oxidation of methane (AOM) (Figure 1.3). The methane that many seeps emanate commonly forms in marine sediments either thermogenically or via microbial processes (Tunnicliffe *et al.*, 2003), and major reservoirs of methane often develop in areas of high organic content such as beneath upwelling areas where productivity in the water column is high (Levin, 2005). Through

AOM, the majority of this methane (>90%) is converted to bicarbonate and hydrogen sulphide by microorganisms, using sulphate as the final electron acceptor (Knittel and Boetius, 2009; Blumenberg, 2010). AOM is carried out through direct coupling between anaerobic methanotrophic archaea (ANME) and sulphate-reducing bacteria (Nauhaus *et al.*, 2002; Knittel and Boetius, 2009), that likely achieve syntrophy through extracellular transfer of electrons (Wegener *et al.*, 2015; Scheller *et al.*, 2016). The production of carbonate through AOM results in an increase in alkalinity, which induces the precipitation of authigenic carbonate (Ritger *et al.*, 1987; Aloisi *et al.*, 2002). Seep carbonates can take the shape of mounds, platforms and crusts, and normally exhibit some depletion in ^{13}C that corresponds to their carbon source (Schrag *et al.*, 2013). However, in reality seep carbonates can show wide isotopic and mineralogical variation that likely reflects local controls on their formation (Naehr *et al.*, 2007).

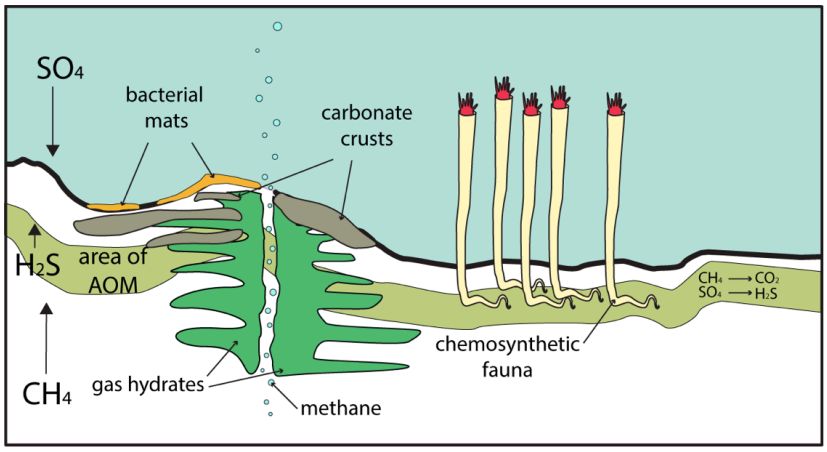

Figure 1.3 Schematic illustration of a cold seep. Methane emanating from marine sediments is commonly converted to hydrogen sulphide through AOM, which results in carbonate precipitation. Methane and hydrogen sulphide also support fauna such as mat-forming microorganisms and chemosynthetic animals. Illustration modified from Torres and Bohrmann (2014).

1.1.3 Hydrothermal vent and cold seeps in the geological record

Hydrothermal vent and cold seep deposits have been known long before their modern equivalents were found in the deep ocean (Stanton, 1895; Ivanov, 1959), but were not interpreted as such until the discoveries in the late 1970s and early 1980s. The fossil equivalent of SMS are volcanogenic massive sulphide deposits (VMS), which are defined as strata-bound sulphide mineral accumulations that have formed at or immediately below the seafloor in association with contemporaneous volcanism (Franklin *et al.*, 2005). They are a major source of zinc, copper, lead, silver and gold (Galley *et al.*, 2007) and thus have been mined on land for centuries (Laznicka, 2010).

Ancient vent and seep deposits occur in a wide range of sizes, lithologies, geotectonic settings and ages, and also have varied biotic compositions (Campbell, 2006). In the last compilation, there were 46 geographic groupings of fossiliferous seep deposits spanning the Silurian to the Pleistocene, and 13 vent fossiliferous deposits ranging from the Eocene to the Archean (Little *et al.*, 1998; Campbell, 2006). The ages of known fossil vent deposits are concentrated in the Silurian, Devonian and Cretaceous with large gaps existing in between, whereas most seep deposits are known from the Cenozoic of western USA, Japan and Italy (Little and Vrijenhoek, 2003).

Multiple lines of evidence are often evaluated to assess whether a particular deposit represents an ancient hydrothermal vent or seep, beginning with the settings of the deposits. The authigenic precipitates formed at vents and seeps often occur in geological settings comparable to modern vent and seep environments, such as rift zones, forearc and back-arc basins, or accretionary complexes (Campbell, 2006). VMS deposits occur within accreted volcanic arcs and ophiolites, the latter of which represents old oceanic crust obducted onto continental margins (Little and Vrijenhoek, 2003). The majority of ancient vent deposits are considered to have formed within arc and back-arc settings, which may be a result of preferential preservation of VMS deposits within these situations (Ross and Mercier-Langevin, 2014). Many of the known ancient seep deposits are subduction-related, however fossil seeps have also been located in settings representing passive margins and epicontinental seas (Majima *et al.*, 2005; Campbell, 2006; Kiel, 2010).

For ancient vent deposits, fossilised vent chimneys and fauna, mineralogical textures, isotopic data and palaeo-fluid temperatures similar to those of present-day vents are also central to their identification in the fossil record as well as helping to determine the palaeo-setting in which venting occurred (Herrington *et al.*, 1998). In addition, carbon and sulphur isotopes as well as biomarkers may provide evidence of microbial activity (Herrington *et al.*, 1998; Blumenberg, 2010). Cold seeps are broadly recognised by their occurrence as authigenic carbonate lenses hosted by deep-water sedimentary sequences, often containing fossilised fauna and exhibiting depletion in ^{13}C indicative of methane oxidation (Campbell, 2006). Furthermore, biomarkers specific to anaerobic methane-oxidising Archaea may be used to provide additional evidence of methane oxidation at ancient seeps (Peckmann *et al.*, 1999; Thiel *et al.*, 1999), and mineralogical and isotopic signatures can also provide insights into the composition of ancient seep fluids (Peckmann *et al.*, 2001).

1.2 Life at hydrothermal vents and cold seeps, in the modern ocean and throughout Earth history

Much of the deep sea is a food-limited environment, in which benthic organisms rely on the downward flux of minute fragments of organic material from the euphotic zone (Van Dover, 2000). Within this context, hydrothermal vents and cold seeps can be viewed as nutritional oases, as they fuel greatly increased production within the deep sea. The high concentrations of reduced chemicals (such as sulphide, methane, hydrogen, iron II) within fluids emitted at these environments are used by chemolithotrophic microorganisms to fix carbon (Le Bris *et al.*, 2015), which in turn support generally low diversity but high abundance assemblages of many unusual, endemic fauna. The sulphide chimney and carbonate pavement deposits generated at vents and seeps (respectively) additionally provide long-lasting hard substrate that is generally rare in the deep sea, which many organisms may utilise for attachment or shelter (Levin *et al.*, 2016).

The origin of the often highly specialised and unusual vent and seep fauna, and the occupation of vents and seeps by life over evolutionary time, is addressed through several lines of enquiry. Phylogeography, or spatio-genetic patterns of organisms, can help to assess the more recent histories of vent and seep organisms. Deeper in time, fossils, as well as molecular clock analyses that estimate faunal divergences based on mutation rates of DNA, are used.

1.2.1 Life at modern vents and seeps

Vents and seeps represent an assortment of habitats displaying a complexity of physico-chemical conditions (differing in temperature, salinity, pH, sulphide, oxygen, carbon dioxide, hydrocarbon and metal content, etc.) (Le Bris *et al.*, 2015), which vary over both space and time. This provides a wide diversity of niches, many of which can be exploited by microorganisms.

Microorganisms at vents and seeps occur as mats of filaments on rock surfaces and the seabed, within the sub-seafloor, vent and seep fluids, mineral deposits, and as ecto- and endosymbionts of animals (Takai *et al.*, 2006; Jørgensen and Boetius, 2007; Dubilier *et al.*, 2008). Bacteria belonging to the groups Epsilonproteobacteria and Aquificales, as well as Alpha- and Gammaproteobacteria, are abundant at hydrothermal vents, some of which have been identified as major chemolithoautotrophs within these environments (Sievert and Vetriani, 2012). Archaea show a greater abundance at vents compared to within ocean

sediments, and belong mainly to the groups Euryarchaea, Thermococcales and Methanococcales. At seeps, AOM is carried out by methanotrophic Archaea in the groups Euryarchaeota and Crenarchaeota, while sulphate-reduction is dominated by the Deltaproteobacteria (Jørgensen and Boetius, 2007).

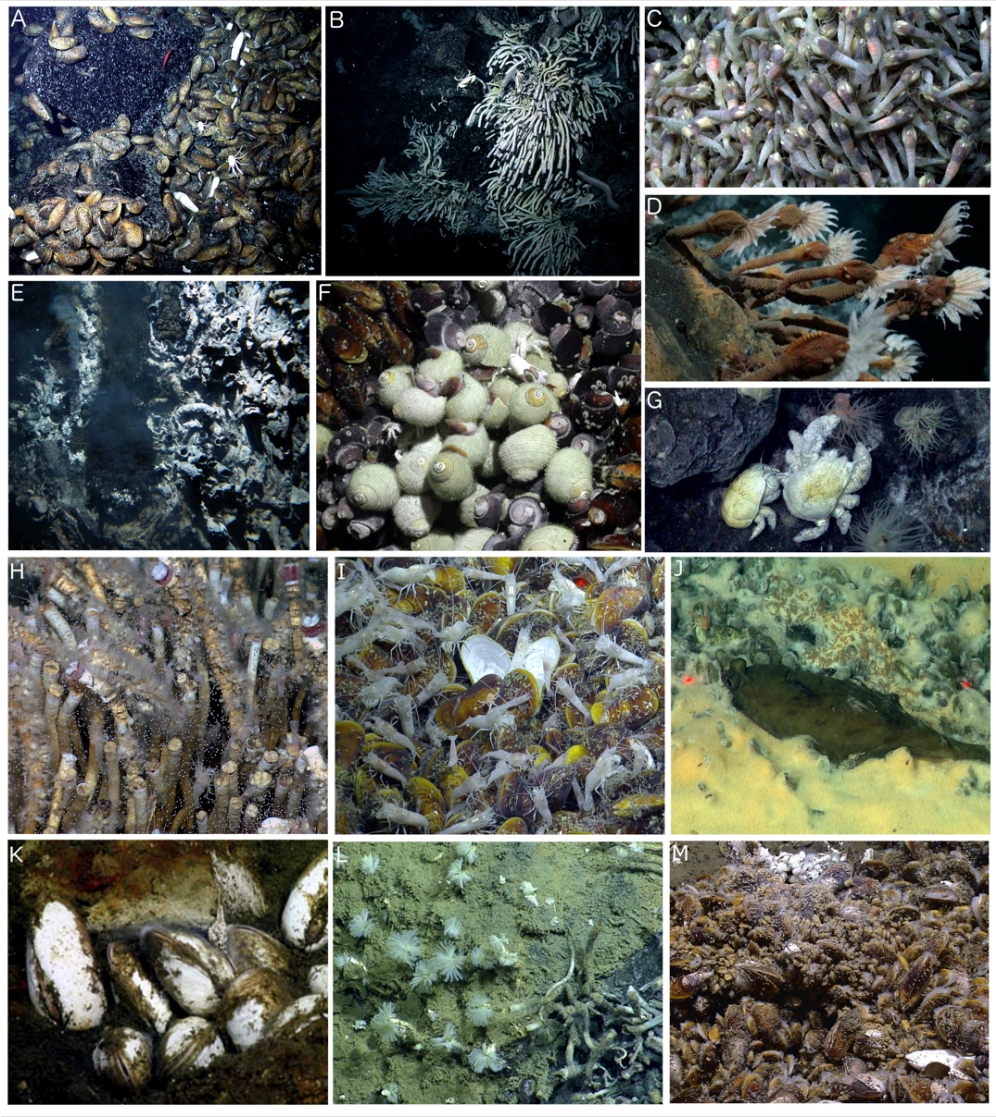

Figure 1.4 Modern vent (**A-G**) and seep (**H-M**) fauna. **A,** *Bathymodiolus* vent mussels, East Pacific Rise hydrothermal vents, image credit: WHOI. **B,** Siboglinid tubeworm bushes, East Pacific Rise hydrothermal vents, image credit: WHOI. **C,** vent shrimp *Rimicaris hybisae* from Caribbean hydrothermal vents, image credit: Chris German, WHOI/NSF, NASA/ROV Jason ©2012 WHOI. **D,** *Vulcanolepas* filter-feeding goose barnacles, Lau Back-Arc Basin. Image credit: Charles Fisher, Penn State. **E,** *Alvinella* spp. tubeworms, East Pacific Rise, image credit: WHOI. **F,** *Alviniconcha* spp. gastropods, Lau Basin vents. Image credit: Charles Fisher, WHOI. **G,** *Kiwa tyleri*, East Scotia Ridge hydrothermal vents. Image credit: NERC. **H,** *Lamellibrachia* sp., Gulf of Mexico cold seeps. Image credit: NOAA Okeanos Explorer. **I,** *Bathymodiolus* cf. *childressi* mussels and Alvinocaridae shrimp, El Pilar cold seeps (off Trinidad). Image credit: Ocean Exploration Trust. **J,** Microbial mat, grazing polychaete worms and a flatfish, cold seeps off southern California. Image credit: MBARI. **K,** vesicomyid clams, Sur Ridge cold seeps, off California. Image credit: NOAA/MBARI. **L,** serpulid and siboglinid tubeworms at cold seeps off Trinidad. Image credit: Ocean Exploration Trust. **M,** mussel bed with numerous small gastropods, Veatch Canyon cold seeps, U.S. continental margin. Image credit: NOAA Okeanos Explorer 2013.

Many of the dominant metazoans at hydrothermal vents and cold seeps are sustained through symbioses with chemoautotrophic microorganisms. Large microbial symbiont-bearing aggregations of annelid tubeworms (mainly Siboglinidae), mussels (mainly Bathymodiolinae), clams (mainly Vesicomyidae), gastropods (Provannidae), shrimp (Alvinocarididae) and crabs (Kiwa) can dominate at vents (Desbruyères *et al.*, 2006), while clams (Solemyidae, Lucinidae, Thyasiridae, Vesicomyidae), mussels (mainly Bathymodilinae) and tubeworms (mainly Siboglinidae) often populate seeps, and in both environments a diversity of heterotrophic animals live in association with the dominant fauna above (Bergquist *et al.*, 2005) (Figure 1.4). More than 700 species have been recorded from vents, and 600 from cold seeps (German *et al.*, 2011). Families, genera or species may be shared between vents and seeps, as well as with organic falls such as whale- or wood-falls and reducing sediments (Bernardino *et al.*, 2012), due to the similar sulphidic conditions encountered within all of these habitats. Seeps also commonly share fauna with surrounding non-seep sediments (Levin *et al.*, 2010), but it is increasingly recognised that vent and seep environments grade into the surrounding deep sea habitats, followed by similar transitions in biological assemblages (Levin *et al.*, 2016). Many of the dominant animals occupying vents and seeps may be considered as weedy taxa, as they are well adapted to the disturbed, and often ephemeral nature of many vent and some seep environments. Thus, they exhibit characteristics of effective dispersal, rapid growth and early reproduction (Baker, 1965; Vrijenhoek, 2010).

Complex symbioses with microorganisms have enabled vent and seep fauna to thrive within these habitats, such as the growth of filamentous microorganisms on body tissues. Annelids of the genus *Alvinella* (Alvinellidae) residing on vent chimneys have dorsal epidermal expansions densely colonised by filamentous microorganisms, which this worm has been shown to be partly sustained by (Gaudron *et al.*, 2012). Similarly, the seep-inhabiting crab *Kiwa puravida* feeds on filamentous bacteria colonising its claws (Thurber *et al.*, 2011). Chemolithotrophic microorganisms living inside the tissues of vent and seep animals (endosymbionts) can also provide their hosts with nutrition, which is observed in members of the prominent vent and seep tubicolous annelid family Siboglinidae. This family comprises the four monophyletic lineages 'vestimentifera', *Sclerolinum*, 'frenulata', and *Osedax*, the former two of which may generally be found in a range of reducing environments such as vents, seeps, whale- and wood-falls, while frenulates occur mainly within reducing sediments, and *Osedax* are specialist consumers of vertebrate-falls (Hilário *et al.*, 2011). Siboglinid worms lack a functioning gut, having instead developed a specialised organ, the trophosome, that houses endosymbiotic bacteria (Southward *et al.*, 2005). This is

the only annelid family for which such a mode of nutrition has been reported, whereas for bivalve molluscs, a chemosynthetic lifestyle has evolved independently at least five times (Taylor and Glover, 2010; Roeselers and Newton, 2012).

1.2.2 Fossil vent and seep communities

The fossil history of hydrothermal vents and cold seeps demonstrates that these environments have undergone dynamic faunal transitions over evolutionary time (Little and Vrijenhoek, 2003; Kiel and Little, 2006; Vrijenhoek, 2013), largely disproving a theory that vents and seeps are stable deep-sea refugia where relict faunas have survived undisturbed for hundreds of millions of years (McLean, 1981; Newman, 1985). This fossil history is biased towards organisms possessing hard outer structures such as shells and tubes (Figure 1.5), as soft body tissues are generally not found to preserve within vents and seeps.

Apart from two Precambrian occurrences of filamentous microorganisms at ancient vents (Rasmussen, 2000; Li and Kusky, 2007), much of the fossil history of vent and seep communities relates to occurrences since the Silurian (Campbell, 2006) (Figure 1.6). Palaeozoic vents were dominated by now extinct bivalve families (ambonychiids and modiomorphids), lingulate brachiopods that do not occur at modern vents, a monoplacophoran belonging to an extinct early Palaeozoic family, with the only animals ascribed to modern vent faunas being tubular fossils attributed to the annelids (Little *et al.*, 1999a; Little, 2002; Little and Vrijenhoek, 2003). A number of these Palaeozoic tubes have been suggested to be vestimentiferans, which comprise the larger members of Siboglinidae, however this has caused some controversy (see later). Similarly at Palaeozoic seeps, tubular fossils occur in many of the known deposits, some of which have also been ascribed to the vestimentiferans, as well as several types of bivalves such as solemyids (Campbell, 2006; Hryniewicz *et al.*, 2016). Additionally, many Palaeozoic and some Mesozoic seeps were dominated by giant rhynchonelloid brachiopods, which no longer occur within seeps (Sandy, 2010).

The Mesozoic generally marks a transition between Palaeozoic and Cenozoic vent and seep faunas (Little and Vrijenhoek, 2003; Vrijenhoek, 2013). Tube fossils also feature prominently in Mesozoic vents and seeps, some of which are again attributed to vestimentiferans. In addition to tubes, Mesozoic faunas comprised brachiopods and gastropods (possibly Provannidae) at vents (Little *et al.*, 1999b; c, 2004b), and more diverse assemblages of sponges, a variety of molluscs, brachiopods, echinoids, and crustaceans at

seeps (Campbell, 2006). Several extant mollusc taxa first appear at early Cretaceous seeps, such as lucinid bivalves and abyssochrysoid (the superfamily to which Provannidae belongs) gastropods (Kiel and Little, 2006; Kaim and Kelly, 2009).

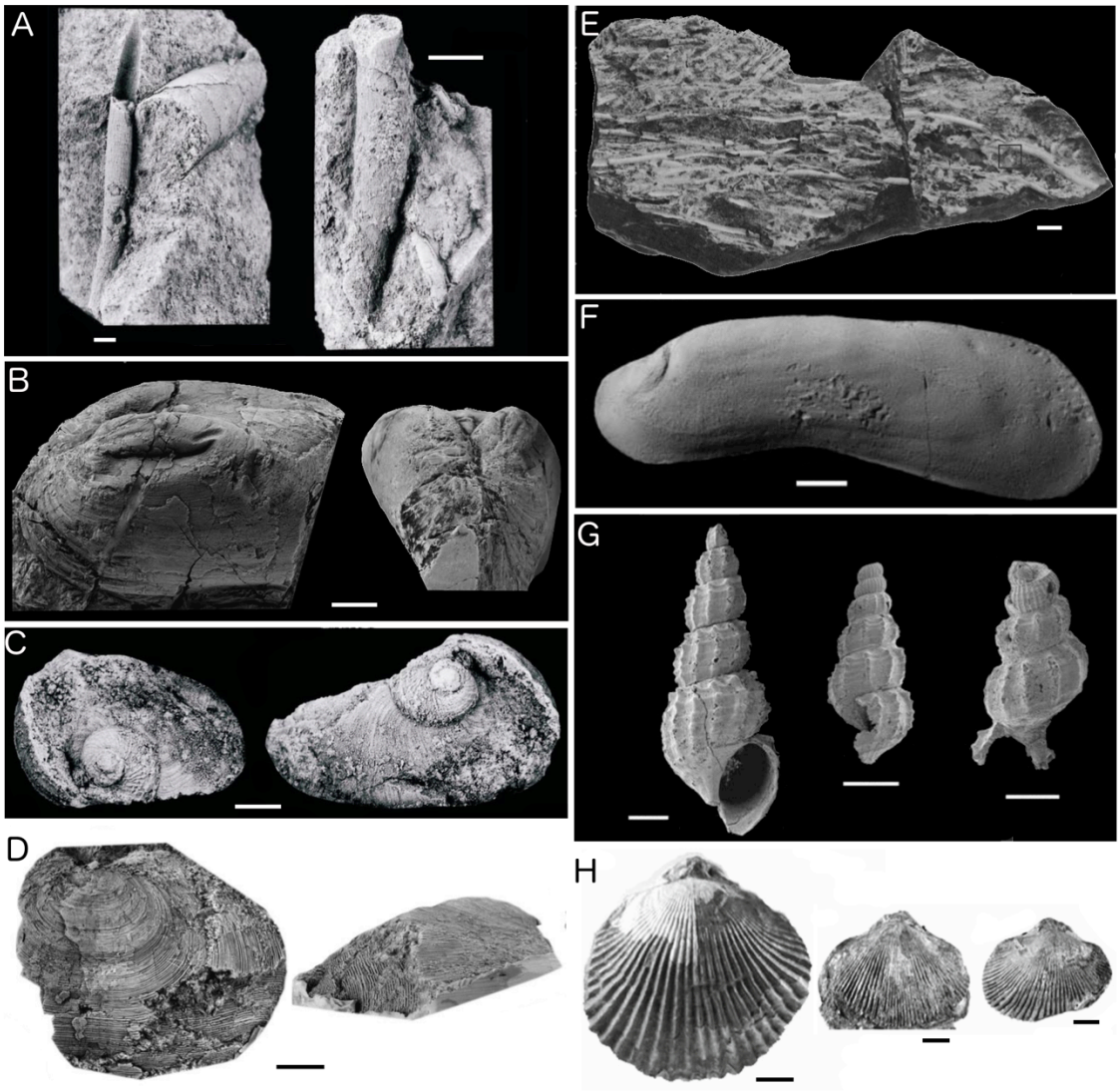

Figure 1.5 Fossil vent (**A-D**) and seep (**E-H**) fauna. **A,** tubeworm fossils, Figueroa deposit, early Jurassic. Scale of left image is 1.5 mm, and 5 mm in the right image. Image credit: Little *et al.* (2004b). **B,** *Sibaya ivanovi* modiomorphid bivalve, Sibay deposit, Devonian. Scale is 10 mm. Image credit: Little *et al.* (1999a). **C,** *Francisciconcha maslennikovi* vetigastropod, Figueroa deposit, early Jurassic. Scale is 2 mm. Image credit: Little *et al.* (2004b). **D,** *Pyrodiscus lorrainae* lingulate brachiopod, Yaman Kasy deposit, Silurian. Scale is 10 mm. Image credit: Little *et al.* (1999a). **E,** vestimentiferan tubeworms, Lincoln Creek Formation, Eocene. Scale is 20 mm. Image credit: Goedert *et al.* (2000). **F,** *Ataviaconcha wendti* modiomorphid bivalves from Hollard Mound, middle Devonian. Scale is 10 mm. Image credit: Hryniewicz *et al.* (2016). **G,** *Desbruyeresia kanajirisawensis* provannid gastropod, Hokkaido seep carbonates, Upper Cretaceous. Scales are 1 mm, 1 mm, and 0.5 mm from left to right. Image credit: Kaim *et al.* (2008). **H,** ancient seep brachiopods in the genus *Peregrinella*, all scales are 10 mm. Image credit: Sandy (2010).

Only one ancient hydrothermal vent site is known from the Cenozoic, from the Eocene Barlo Mine in the Philippines, which also contains worm tubes reported to be

vestimentiferan (Boirat and Fouquet, 1986). In contrast, the majority of known fossil seep sites are of Cenozoic age, which also share many taxa with modern seeps (Kiel and Tyler, 2010). Dominant bivalves at modern vents and seeps such as vesicomyid clams and bathmodiolin mussels first appear during the early Cenozoic (Kiel and Little, 2006; Vrijenhoek, 2013), as do decapods and several gastropod genera, with tubeworms again being abundant within many of these sites (Campbell, 2006).

While the fossil record can provide a definitive date for the first fossil occurrence of a taxon, the quality of preservation at vents and seeps can be variable, especially at vents where the original mineralogies of calcareous structures are lost (Little and Vrijenhoek, 2003). Identifications based on hard outer structures that provide much of the evidence of life at ancient vents and seeps are further made difficult as these structures can sometimes exhibit convergence, and the fact that many identifications of modern taxa are based largely on soft tissue morphology and molecular phylogenetic analyses.

Attempts to identify worm tubes throughout the fossil record of vent and seeps clearly exemplify the above issues. Many of these tubes have been reported to be those of vestimentiferans, based on characters shared with modern vestimentiferan tubes such as concentric tube wall lamination and outer wall collars and/or longitudinal ridges (Little *et al.*, 1999a; b, 2004b; Peckmann *et al.*, 2005). However, it has been pointed out that these tube characters are not unique to vestimentiferan tubes, as they also occur in the tubes of chaetopterids, an annelid family not closely related to siboglinids (Kiel and Dando, 2009), calling the fossil vestimentiferan identifications into question.

1.2.3 Evolutionary ages from molecular clocks

Molecular clock analyses provide an alternative means through which to evaluate the evolutionary histories of vent and seep fauna, and are the only means to assess this for taxa without a fossil record. However, molecular clocks can only be used to assess the potential ages of living taxa, and come with several further problems (Graur and Martin, 2004; Kumar, 2005). They are best applied when they can be calibrated with reliable fossil data, but for taxa where no fossil record is available, mutation rates over deep time are often inferred, and are calibrated against large-scale geological events. These analyses are also reliant on the use of appropriate genetic markers that evolve at slow rates, which may not be readily available. These assumptions can lead to inaccurate estimates of evolutionary age,

but patterns within these data, as well as consistencies with the fossil record, can improve the reliability of molecular clock age estimates (Vrijenhoek, 2013).

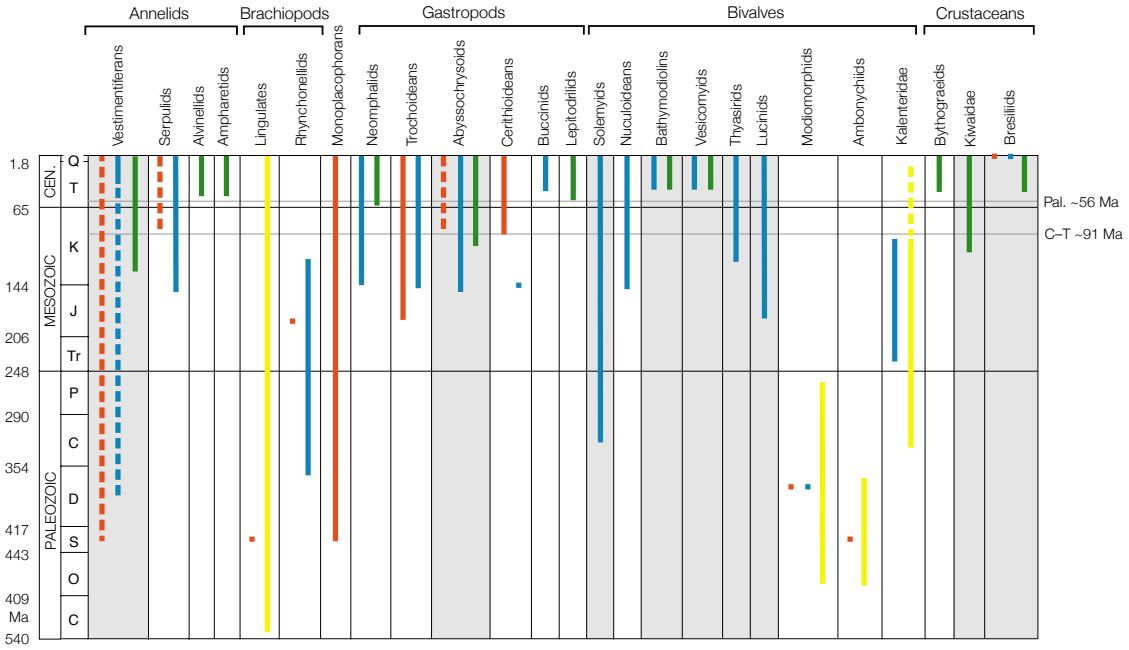

Figure 1.6 Stratigraphic ranges and molecular divergence estimates of hydrothermal vent and cold seep fauna. Red bars – stratigraphic ranges of fauna at hydrothermal vents, blue bars – stratigraphic ranges of fauna at cold seeps, yellow bars - stratigraphic ranges of fauna within other marine environments, green bars – molecular clock age estimates for vent and seep fauna. Interrupted bars indicate uncertain stratigraphic records. Squares indicate single fossil occurrences. Cen. Cenozoic. The Cenomanian–Turonian oceanic anoxic/dysoxic event (C–T) and end Palaeocene oceanic anoxic/dysoxic event (Pal.) are labelled. Majority of data is from Vrijenhoek (2013), Kiwaidae data from Roterman *et al.* (2013), and this figure is adapted from Little and Vrijenhoek (2003).

Evolutionary ages for the main vent and seep taxa including annelids, bivalves, gastropods and crustaceans also suggest Cenozoic radiations for these groups (Figure 1.6). The alvinellids, for which there is no definitive fossil record despite several suggested affinities (Haymon *et al.*, 1984; Little *et al.*, 1999a), a molecular clock age is estimated as 41-51 Ma, whereas the species *Paralvinella pandorae* that shows greater divergence is inferred to have split from other members of this family 98-121 Ma (Vrijenhoek, 2013). *Amphisamytha*, closely related annelids in the family Ampharetidae that are also common at vents and seeps, have a similar estimated evolutionary age of 44-55 Ma. For the siboglinids, and the vestimentiferans in particular, a range of age estimates have been suggested spanning 50-126 Ma (Black *et al.*, 1997; Hurtado, 2002; Vrijenhoek, 2013), but none back a Palaeozoic origin for this group. The majority of above estimates fall within the Cenozoic period, further calling into question fossil worm tubes identified as vestimentiferans from vents and seep deposits older than the Cenozoic. However, recent discoveries of fossil traces of the bone-eating siboglinid genus *Osedax* in Cretaceous plesiosaur and turtle bones (Danise

and Higgs, 2015) suggest the Cretaceous evolutionary age estimates for siboglinids may be more likely, and that the younger molecular clock estimates are likely erroneous.

For vesicomyids and bathymodiolins, ages of 50-63 Ma (Peek *et al.*, 1997; Vrijenhoek, 2013) and 58-61 Ma (Jones and Vrijenhoek, 2006; Vrijenhoek, 2013) are estimated respectively. Similar ages are also obtained for neomphaline and lepetodrilid limpets, and slightly younger ages for several groups of vent and seep crustaceans (Vrijenhoek, 2013). While some of the above estimates have large ranges, all generally fall within the Cenozoic, apart from Kiwaidae, which are estimated to have split from their sister clade Chirostylidae approximately 106 Ma (Roterman *et al.*, 2013).

1.2.4 Phylogeography

Phylogeography seeks to understand the historical processes that have led to contemporary geographical distribution patterns of genealogical lineages (Avise, 2000). These patterns are often explained in terms of dispersal and diversification histories of closely-related organisms in relation to physical factors (such as plate tectonics, chemistry, hydrography), historical factors (such as vicariance, range expansions) as well as biological factors (such as life histories, behaviours, demography and symbioses) (Vrijenhoek, 2010). This field is increasingly applied in the deep sea, especially in hydrothermal vents and manganese nodule fields that have been targeted for mining, because it can be applied to assess levels of relatedness and gene flow between populations. Through these studies, phylogeography can provide an indication of whether certain species may recover after mining activities (Breusing *et al.*, 2015). Phylogeography can also provide insights into the evolutionary context of the biodiversity that is to be conserved, and into the pathways of adaptation of vent and seep fauna to these sulphidic environments.

Traditionally, attempts have been made to classify vent sites into biogeographic provinces based on observed faunal distribution patterns to gain insight into evolutionary and ecological processes (Tunnicliffe *et al.*, 1998; Van Dover *et al.*, 2002; Bachraty *et al.*, 2009; Rogers *et al.*, 2012; Moalic *et al.*, 2012). However, such classifications have proved difficult as information on phylogenetic relationships across the range of deep-sea chemosynthetic environments has not been fully-integrated into the above classifications (Vrijenhoek, 2010), and as many vent sites are still unexplored. For example, recent exploration of the Pescadero Basin, Gulf of California, has revealed vent sites characterised by dense colonies

of the siboglinid *Oasisia alvinae*, which has not been observed to dominate in other Gulf of California or eastern Pacific vent sites (MBARI, 2015).

Vesicomyid clams, mytilid mussels and siboglinid worms are all suggested to have initially diversified in seeps or other chemosynthetic environments and to subsequently have populated vents several times (Vrijenhoek, 2010 and references therein). Whale-falls are also considered to have acted as ecological or evolutionary stepping stones, as well as sites of diversification, depending on the lineage in question (reviewed in Smith *et al.*, 2015). For siboglinid annelids, whale-falls likely acted as a diversification site due to the specialism of a whole lineage from this family (*Osedax*) to these environments (Smith *et al.*, 2015). However, better knowledge of phylogeography, systematics and ecology for lesser-studied members of the Siboglinidae is needed to understand the adaptation history of this family to chemosynthetic environments.

1.3 The annelids and their tubes

The previous section highlights that understanding the evolutionary history of some of the most prominent vent and seep occupants, the tube-building annelid worms, is hindered by problems identifying fossil tubes, and an incomplete knowledge of evolutionary biology for the main vent and seep-dwelling annelid family, the siboglinids. This section provides background on the annelid phylum, the tubes made by this group, the lineages that inhabit modern vents and seeps, and what is currently known about their fossilisation within vents and seeps.

1.3.1 The annelids

The annelid (or segmented) worms comprise a major metazoan phylum of over 21,000 species that occupy marine, freshwater and terrestrial environments, that includes the polychaetes (or bristle-worms), earthworms and leeches (Bleidorn *et al.*, 2015; Weigert *et al.*, 2016). Earthworms and leeches are now understood to be derived polychaete-like annelids (Weigert and Bleidorn, 2016), while the greater majority of polychaetes are marine. As such, the major radiation of annelids occurred within the oceans. Polychaetes are found to occupy almost every type of marine habitat ranging from the intertidal to the hadal zone (Rouse and Pleijel, 2001), and are often highly abundant and diverse within hydrothermal vents and cold seeps. Many mobile forms including predators, scavengers and grazers take

advantage of these organically-enriched habitats (Turnipseed *et al.*, 2004; Desbruyères *et al.*, 2006). However, tube-builders are often the most conspicuous vent and seep annelids, and particularly those within the family Siboglinidae. This is due to the extreme specialism of obtaining nutrition exclusively from endosymbiotic microorganisms observed for this family, and the large bush-like aggregations which this feeding mode enables them to establish within vents and seeps (Hilário *et al.*, 2011).

Annelids comprise a wealth of body forms, life modes, feeding and reproductive strategies and developmental styles (Rouse and Pleijel, 2001), and have traditionally been classified according to their morphology (Rouse and Fauchald, 1997; Westheide, 1997). However, their relationships received major revision with the application of molecular phylogenetic techniques, which has resulted in a more stable annelid phylogeny and has also revealed several surprising relations (Bleidorn *et al.*, 2015; Weigert *et al.*, 2016). According to recent analyses, annelids can be broadly subdivided into errant (which crawl, swim or burrow) and sedentary forms (which construct dwelling tubes, or are more sessile burrowers), with several additional groups forming a basal grade external to this main radiation (Figure 1.7) (Weigert and Bleidorn, 2016). Groups such as Sipuncula (peanut worms), Pogonophora (vent and seep tubeworms, now Siboglinidae), Echiura (spoon worms) and Myzostomida (small, parasites of crinoids) that were considered to be separate phyla are now included within the annelid radiation (Weigert *et al.*, 2014; Weigert and Bleidorn, 2016).

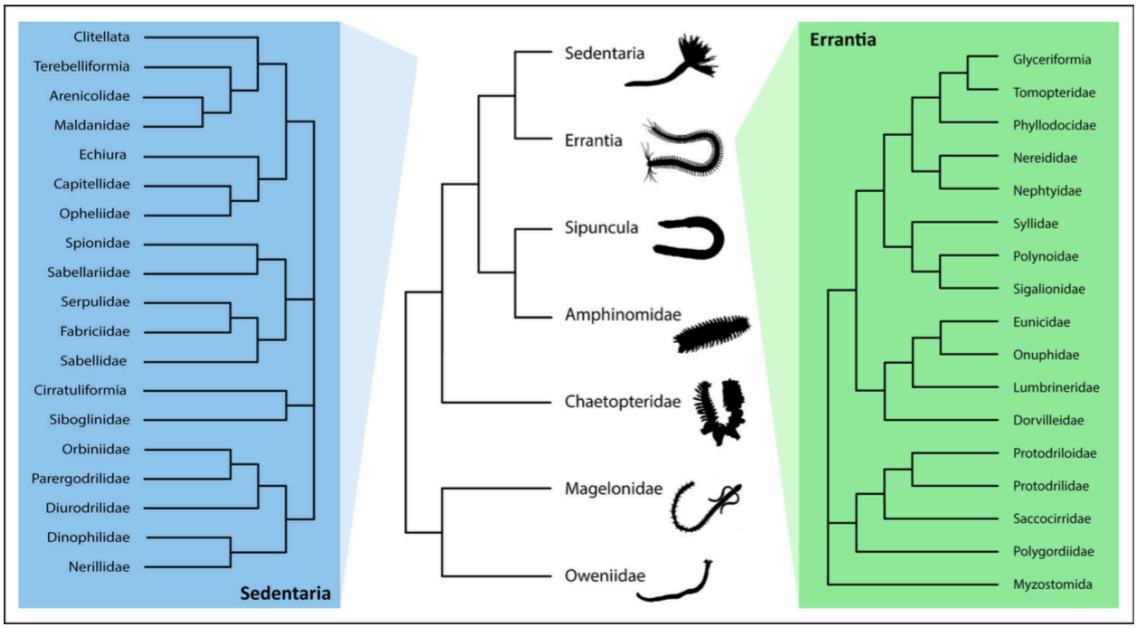

Figure 1.7 Current status of annelid phylogeny. Figure is derived from Weigert and Bleidorn (2016) and is based on phylogenomic data (Struck, 2011; Weigert *et al.*, 2014; Struck *et al.*, 2015).

The annelids are also an ancient lineage that dates to at least the early Cambrian, evidenced by exceptionally preserved body fossils from ~520 million year old lagerstätte deposits of the Sirius Passet, North Greenland (Conway Morris and Peel, 2008; Vinther *et al.*, 2011), Guanshan, China (Liu *et al.*, 2015), as well as the slightly younger Burgess Shale, Canada (Conway Morris, 1979; Eibye-Jacobsen, 2004). Aside from instances of exceptional preservation, annelids in general leave a very scant fossil record as they are soft-bodied, however, their borrows, or harder structures such as jaws and dwelling tubes, are occasionally preserved. Jaw pieces belonging to Eunicida and Phyllodocida are also known as scolecodonts, and have a fossil record dating from the latest Cambrian (Hints and Eriksson, 2007). Tube fossils can provide robust evidence for the origins of several annelid groups, especially for those that build calcareous tubes (Parry *et al.*, 2014). Tubes are also the only structures associated with annelids found to preserve within hydrothermal vents and cold seeps.

1.3.2 Annelid tubes

Many marine animals such as molluscs, crustaceans, anemones and phoronids may produce dwelling tubes primarily for protection from predators, currents, and thermal and chemical extremes, but tubes are most commonly observed, and are most morphologically and compositionally diverse, in the annelids (Merz, 2015) (Figure 1.8). As well as providing evidence of annelid occurrence throughout the fossil record, and being important providers of habitat structure that can shape ecosystems (e.g. Dubois *et al.*, 2002), annelid tubes are also of ongoing interest in materials science (Morin and Dufresne, 2002; Shah *et al.*, 2014). Supplementary Table A.1 provides information on polychaete lineages in which tubes are regularly observed.

Some annelids may produce only thin temporary mucus tubes (e.g. Nereididae), while a range of lineages also produce tubes of greater durability that have a greater likelihood of being preserved within the fossil record. These are generally formed of fibrous secretions produced by the worm that are laid down in successive layers that vary in orientation, which resembles the structure of plywood and gives the tube strength (Merz, 2015). More permanent annelid tubes may be divided into three broad categories based on their composition: 1) calcareous tubes, 2) agglutinated tubes, and 3) purely organic tubes.

Calcareous tubes are observed in the families Serpulidae, Sabellidae and Cirratulidae (Vinn and Mutvei, 2009). All serpulids build calcareous tubes, whereas this behaviour is restricted

only to a single genus in each of Cirratulidae and Sabellidae (Ippolitov *et al.*, 2014). Calcareous tubes may be formed either of calcite, aragonite or both (deposited within an organic mucopolysaccharide matrix), and may exhibit distinct ultrastructural crystal morphologies (Vinn *et al.*, 2008a).

Figure 1.8 Diversity of annelid tubes. **A,** chitin-protein tube of the siboglinid *Paraescarpia echinospica*, with attached goose barnacles. **B,** organic branched tube of the chaetopterid *Phyllochaetopterus socialis*. **C,** calcareous serpulid tubes encrusting a piece of wood. **D,** agglutinated tubes of oweniids, which attach sediment grains in an overlapping roof-tile pattern. **E,** detail of a serpulid tube. **F,** cluster of the agglutinated tubes of ampharetids. **G,** thick, agglutinated tube of a terebellid. **H,** agglutinated sabellid tube. **I,** agglutinated pectinariid tube, which are cone-shaped and formed of neatly arranged sand grains. **J,** agglutinated tube of the terebellid *Lanice* cf. *conchilega*, which has a crown-like branched anterior ending.

Agglutinated tubes are comprised of organic secretions such as mucus that are used to adhere sediment particles onto the tube wall. Sediment grains of varying sizes may be used for tube-building, from sand grains to mud particles, as well as other small marine debris such as sponge spicules and foraminiferal tests. Agglutinated tubes are commonly observed in the annelid families Sabellidae, Terebellidae, Pectinariidae, Sabellariidae, Oweniidae, Maldanidae, Ampharetidae, or in a subset of taxa within a family, e.g. *Diopatra* (Onuphidae) and *Mesochaetopterus* (Chaetopteridae).

Robust tubes produced solely of organic secretions (hereafter referred to as 'organic' tubes) appear in the families Siboglinidae, Chaetopteridae, Alvinellidae and Onuphidae, the varying compositions of which demonstrate that annelids can make use of a diversity of organic substances for tube-building. Several genera of the family Onuphidae produce quill-shaped organic tubes, which have been found to contain onuphic acid. This sugar phosphate polymer is rarely encountered in animals, aside from within the backbone of nucleic acids (Graham *et al.*, 1965; Defretin, 1971). The tubes of *Alvinella* (Alvinellidae) are predominantly formed of protein (Vovelle and Gaill, 1986), whereas analyses of the composition of various vestimentiferans and several frenulate tubes (Siboglinidae) have revealed these tubes to be constructed of a β-chitin and protein complex (Blackwell *et al.*, 1965; Foucart *et al.*, 1965; Gaill and Hunt, 1986; Gaill *et al.*, 1989; Shillito *et al.*, 1995). Chitin has also been detected in the tubes of oweniids and spionids (Guggolz *et al.*, 2015), and while also suggested to be present in chaetopterid tubes (Ippolitov *et al.*, 2014; Parry *et al.*, 2014), has not yet been detected. Instead, their fibrous component is suggested to be a highly ordered protein within a carbohydrate matrix (Gaill and Hunt, 1988), and to also contain furfural and a substance similar to onuphic acid (Berkeley, 1922; Zola, 1967).

Builders of calcareous, agglutinated and organic tubes all occur at modern hydrothermal vents and cold seeps (Figure 1.9). Serpulids are often abundant at the periphery of vents (Kupriyanova *et al.*, 2010), but can form large aggregations at seeps (Olu *et al.*, 1996a; b; Levin *et al.*, 2012). Agglutinated tubes from many families occur at vents and seeps. Maldanids (Kongsrud and Rapp, 2012), terebellids (Reuscher *et al.*, 2012) and ampharetids (Zottoli, 1983; Stiller *et al.*, 2013) are reported from hydrothermal vents, while maldanids, terebellids, ampharetids, sabellids and trochobranchiids can all occur at seeps (Levin *et al.*, 2003; Turnipseed *et al.*, 2004; Levin and Mendoza, 2007). Out of the organic tube-building annelids, the siboglinids are often the most prominent inhabitants of vents and seep environments (Hilário *et al.*, 2011). Chaetopterids can also occur both at vents (Nishi and Rouse, 2007; Morineaux *et al.*, 2010) and seeps (Olu *et al.*, 1997; Sibuet and Olu, 1998; Nishi

et al., 1999; Levin *et al.*, 2000; Van Dover *et al.*, 2003), while alvinellids occur at hydrothermal vents of the Eastern and Western Pacific, and the Central Indian Ridge (Desbruyères *et al.*, 2006; Nakamura *et al.*, 2012).

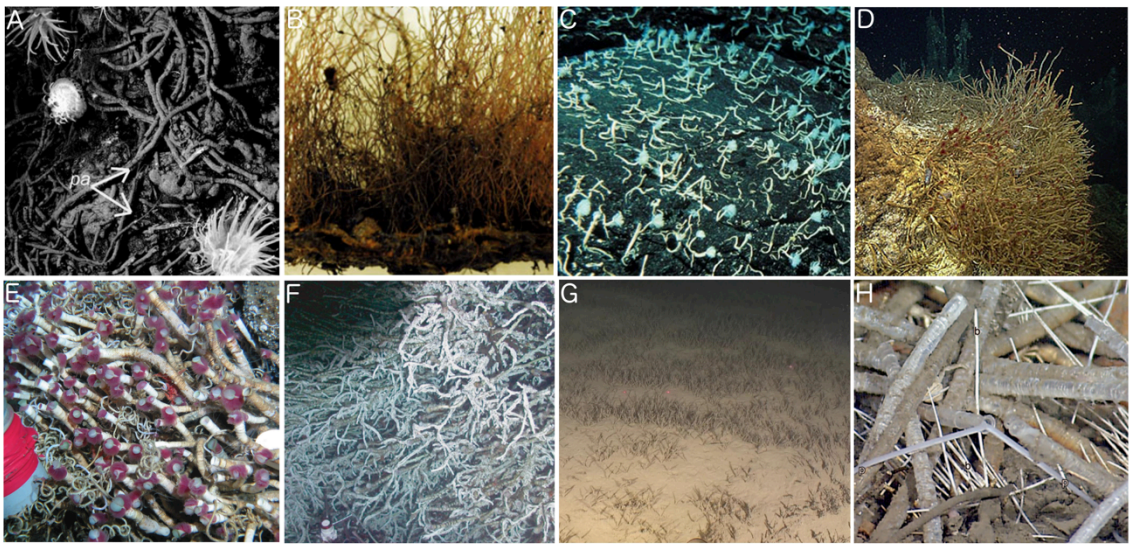

Figure 1.9 Tube-building annelids at modern hydrothermal vents (**A-D**) and cold seeps (**E-H**). **A,** *Phyllochaetopterus polus*, Ashadze -1, Mid-Atlantic Ridge, image credit: Ifremer, Morineaux *et al.* (2010). **B,** mat of the maldanid *Nichomache* (*Loxochona*) *lokii* and siboglinid *Sclerolinum contortum* from Loki's Castle, Mohn Ridge. Image credit: Kongsrud and Rapp (2012). **C,** serpulids, *Laminatubus alvini*, image credit: WHOI. **D,** colony of the siboglinid *Oasisia alvinae*, Pescadero Basin, Gulf of California. Image credit: MBARI. **E,** the siboglinids *Lamellibrachia sagami* and *Alaysia spiralis* from cold seeps off Hatsushima, Japan. Image credit: Kobayashi *et al.* (2015). **F,** serpulids encrusting the tubes of the vestimentiferan *Lamellibrachia barhami* at cold seeps off Costa Rica, image credit: Levin *et al.* (2012). **G,** *Oligobrachia* tubeworm fields at Arctic cold seeps, image credit: MBARI. **H,** *Phyllochaetopterus gigas* living on a whale-fall in Monterey Bay, image credit: Nishi and Rouse (2014).

1.3.3 Fossilisation of annelid tubes at vents and seeps

While it is often possible to determine the probable builder of a tube when dealing with modern material, this is increasingly difficult upon its conversion to fossil form, and means it is imperative to understand the taphonomy and fossilisation of tubes at vents and seeps. Despite the remoteness of deep-sea vent and seep environments, and their possession of chemical conditions difficult to recreate in a laboratory, such studies are possible through the collection and analysis of hard animal structures that exist in various stages of fossilisation.

Some of the hard structures created by metazoans can persist for some time after the death of the animal, for example the chitinous tubes of the siboglinid *Riftia pachyptila* may persist for approximately 2.5 years without maintenance by the worm (Ravaux *et al.*, 2003). Combined with the rapidity of mineral accretion at vents (Section 1.1), fossilisation within this setting may occur much more readily compared to within a typical soft sediment

fossilisation setting. Mineralised versions of the hard structures created by modern vent animals may therefore be found within contemporary vent sites, or experimentally generated (Little, 2009; Little *et al.*, in prep.). On the Juan de Fuca Ridge, fossilised tubes that likely belonged to the abundant siboglinid *Ridgeia piscesae* have been collected, and their mineralogical evolution documented (Cook and Stakes, 1995). Early-stage mineral precipitation in the unfossilised walls of *R. piscesae* tubes has also been observed, and is considered to be linked to microbial presence (Peng *et al.*, 2008, 2009). The full mineralisation of annelid tubes at vents however, has not yet been documented. Such studies are greatly needed to provide insights into exactly how a tube is modified by mineralisation, as well as into the variability, the level of detail, and the range of minerals and mineral textures associated with this process. The fossilisation of calcareous tubes at vents has also not been studied, but the fossilised shells of molluscs from ancient vents are always replaced by sulphides (e.g. Little *et al.*, 1999a, 2004b), indicating that tubes of similar original composition would be too.

At seeps, the crystalline nature of calcareous shelled/walled organisms is often retained, making it easier to recognise them in the fossil record. While mineral accretion at seeps is slower than at vents, mineralised versions of organic-walled seep tubeworms have also been collected, such as the tubes of the vestimentiferan *Escarpia southwardae* (Haas *et al.*, 2009). Following fossilisation, these tubes retain relict textures, such as the fine, concentric multi-layering of their tube walls.

1.3.4 Tube morphology and fossil identification

Calcareous tubes have the greatest potential for preservation in the fossil record, and because of this, the serpulids have the best fossil record of all annelids (Ippolitov *et al.*, 2014). Identifications of fossil serpulids are based on a range of morphological features, such as type of aggregation, coiling/curvature, substrate attachment, external ornamentation, degree of tapering, presence of internal tube structures, wall opacity, size, and opercular morphology (Ippolitov *et al.*, 2014). Ultrastructural details may also aid the identification of fossil forms (Vinn *et al.*, 2008a; b). The earliest occurrence of calcareous tube-building polychaetes are Late Carboniferous tubes ascribed to the sabellids (Ippolitov *et al.*, 2014). The first definitive serpulids date to the Mid-Triassic (Vinn and Mutvei, 2009; Ippolitov *et al.*, 2014), but there are also examples of Permian fossil tubes that are likely to be serpulid (Sanfilippo *et al.*, 2016). Tubes of an originally calcareous composition are so far

unknown from the fossil record of hydrothermal vents, whereas the presence of serpulids at seeps extends to the latest Jurassic (Vinn *et al.*, 2013, 2014).

Agglutinated tubes generally have a poor fossil record, and have not yet been reported from ancient vents and seeps. Within other marine environments, the earliest agglutinated tube fossil specimens with suggested annelid affinities date to the Carboniferous (Ettensohn, 1981; Zaton *et al.*, 2012), and like many modern agglutinated annelid tubes, are long, possess openings at both ends, and evidence of grain sorting when choosing sediment for tube construction. More definitive fossil agglutinated annelid tubes are reported from the Late Cretaceous, which demonstrate distinctly cone-shaped tubes (Figure 1.8I) typical of Pectinariidae (Vinn and Luque, 2013). Additional morphological features that may help to identify agglutinated annelid tubes in the fossil record include anterior ornament (e.g. *Lanice*, Figure 1.8J), arrangement of sediment grains (e.g. *Galathowenia*; Capa *et al.*, 2012), and rolling of anterior tube opening (e.g. *Sabellides*). However, many agglutinated annelid tubes lack such diagnostic features, making their identification difficult.

Organic annelid tubes have also proved difficult to identify in the fossil record, and much of the debate about problematic ancient vent and seep annelids outlined in Section 1.2 concerns tubes considered to originally have had organic compositions. It is often possible to identify whether a tube belongs to a siboglinid or chaetopterid worm when looking at modern material, as siboglinid tubes are characteristically long and may taper posteriorly, show differentiation along their length and ornamentation such as rings and collars (Webb, 1971; Hilário *et al.*, 2011). In addition, chaetopterid tubes may be branched, and are never as hard as some vestimentiferan and frenulate tubes. However, identifying fossils that are often fragmentary and exhibit morphological characteristics such as longitudinal ridges that are shared between the above two families can cause confusion (Kiel and Dando, 2009). The ranges of tube morphologies present across the Siboglinidae and Chaetopteridae families have not been fully investigated and compared to assess if there are characteristics that may tell them and other similar tubes apart, even in fossil material. Recently, siboglinid tubes have also been reported from the Ediacaran (Moczydłowska *et al.*, 2014), further contradicting molecular and fossil data on the evolutionary history of vent and seep groups, and making it even more imperative to gain a better understanding of the morphologies of siboglinid and other similar tubes, and determine what can and what cannot be deemed a fossil siboglinid.

1.4 Thesis aims and objectives

At present, knowledge of ancient hydrothermal vent and cold seep communities is limited by poor understanding of the evolutionary history of tube-building annelids within these environments, especially of taxa that build organic tubes. In particular, interpretations of the numerous tube fossils from ancient vents and seeps are impeded by insufficient understanding of the evolutionary biology, fossilisation, and tube morphologies of annelid lineages occupying present day vents and seeps.

In this thesis, I aim to enhance understanding of the evolutionary history of vent and seep communities through the study of tube-building annelid worms from these environments. In summary, the objectives of this thesis are to improve knowledge of:

1. the evolutionary biology of lesser-studied annelid tube-builders from vents and seeps
2. the morphological (and also compositional) diversity of annelid tubes occurring within modern hydrothermal vents and cold seeps
3. the fossilisation of annelid tubes within hydrothermal vents and cold seeps
4. the taxonomy of problematic worm tubes from ancient vents and seeps, and
5. the palaeoecology of ancient vent and seep environments

I address the above objectives through the use of a broad range of existing morphological and chemical characterisation techniques, as well as by applying modern phylogenetic methodologies to resolve taxonomical uncertainties.

In Chapter 2, I compare material belonging to the little-studied tubeworm genus *Sclerolinum* (Siboglinidae) from Antarctic hydrothermal vents to Arctic and Gulf of Mexico populations, to gain insight into the phylogeography, ecology (and thereby evolutionary longevity and dispersal), morphological plasticity, and potential fossilisation of this genus. This chapter supports the first, second and third thesis objectives.

In Chapter 3, I document the full mineralisation of the organic tubes constructed by the genus *Alvinella* at hydrothermal vents. A model is presented that demonstrates in detail how an organic annelid tube of this type may fossilise at vents, and the mineralised *Alvinella* tubes are compared to ancient tube fossils from vent deposits. This chapter supports mainly the third, but also the fourth thesis objectives.

In Chapter 4, I present a comprehensive morphological and compositional comparison of modern and fossil tubes from vents and seeps, that attempts to resolve problematic identifications of ancient worm tube fossils from these environments. This chapter supports the fourth and also the third thesis objectives.

In Chapter 5, I document the discovery of filamentous microorganisms fossilised alongside tubes from the oldest known hydrothermal vent community, preserved in the Silurian Yaman Kasy deposit. The locations, morphology and fossilisation of the microfossils are described, and the palaeoecological implications of their discovery are evaluated. This chapter supports the fifth thesis objective.

1.5 References

Aloisi, G., Bouloubassi, I., Heijs, S. K., Pancost, R. D., Pierre, C., Sinninghe Damsté, J. S., Gottschal, J. C., Forney, L. J. and Rouchy, J.-M. (2002) CH_4-consuming microorganisms and the formation of carbonate crusts at cold seeps. *Earth and Planetary Science Letters* **203**, 195–203. doi:10.1016/S0012-821X(02)00878-6.

Avise, J. C. (2000) *Phylogeography: The History and Formation of Species*. Harvard University Press, Cambridge, MA.

Bachraty, C., Legendre, P. and Desbruyères, D. (2009) Biogeographic relationships among deep-sea hydrothermal vent faunas at global scale. *Deep-Sea Research I* **56**, 1371–1378. doi:10.1016/j.dsr.2009.01.009.

Baker, H. (1965) Characteristics and modes of origin of weeds. In *Genetics of Colonizing Species* (ed. Baker, H. and Stebbins, G.), pp. 147–172. Academic Press, New York.

Barbieri, R., Ori, G. G. and Cavalazzi, B. (2004) A Silurian cold-seep ecosystem from the Middle Atlas, Morocco. *Palaios* **19**, 527–542.

Beaulieu, S. E. (2013) InterRidge Vents Database Ver. 3.3. *InterRidge Global Database of Active Submarine Hydrothermal Vent Fields*. http://irvents-new3.whoi.edu.

Bergquist, D. C., Fleckenstein, C., Knisel, J., Begley, B., MacDonald, I. R. and Fisher, C. R. (2005) Variations in seep mussel bed communities along physical and chemical environmental gradients. *Marine Ecology Progress Series* **293**, 99–108.

Berkeley, C. (1922) An organic constituent of the tube of *Mesochaetopterus taylori*, Potts. *Journal of Biological Chemistry* **50**, 113–120.

Bernardino, A. F., Levin, L. A., Thurber, A. R. and Smith, C. R. (2012) Comparative composition, diversity and trophic ecology of sediment macrofauna at vents, seeps and organic falls. *PLOS ONE* **7**, e33515. doi:10.1371/journal.pone.0033515.

Black, M. B., Halanych, K. M., Maas, P. A. Y., Hoeh, W. R., Hashimoto, J., Desbruyeres, D., Lutz, R. A. and Vrijenhoek, R. C. (1997) Molecular systematics of vestimentiferan tubeworms from hydrothermal vents and cold-water seeps. *Marine Biology* **130**, 141–149.

Blackwell, J., Parker, K. and Rudall, K. (1965) Chitin in pogonophore tubes. *Journal of Marine Biological Association of the UK* **45**, 51–54.

Bleidorn, C., Helm, C., Weigert, A. and Aguado, M. T. (2015) Annelida. In *Evolutionary Developmental Biology of Invertebrates 2*, pp. 193–230. Springer Vienna, Vienna doi:10.1007/978-3-7091-1871-9_9.

Blumenberg, M. (2010) Microbial chemofossils in specific marine hydrothermal and methane cold seep settings. In *The Vent and Seep Biota* (ed. Kiel, S.), pp. 73–106. Springer Netherlands, Dordrecht. doi: 10.1007/978-90-481-9572-5_4.

Boirat, J. M. and Fouquet, Y. (1986) Decouverte de tubes de vers hydrothermaux fossils dans un amas sulfure de l'Eocene superieur (Barlo, ophiolite de Zambales, Philippines). *Comptes Rendue, Serie II* **302**, 941–946.

Breusing, C., Johnson, S. B., Tunnicliffe, V. and Vrijenhoek, R. C. (2015) Population structure and connectivity in Indo-Pacific deep-sea mussels of the *Bathymodiolus septemdierum* complex. *Conservation Genetics* **16**, 1415-1430. doi:10.1007/s10592-015-0750-0.

Campbell, K. A. (2006) Hydrocarbon seep and hydrothermal vent paleoenvironments and paleontology: Past developments and future research directions. *Palaeogeography, Palaeoclimatology, Palaeoecology* **232**, 362–407. doi:10.1016/j.palaeo.2005.06.018.

Capa, M., Parapar, J. and Hutchings, P. (2012) Phylogeny of Oweniidae (Polychaeta) based on morphological data and taxonomic revision of Australian fauna. *Zoological Journal of the Linnean Society* **166**, 236–278. doi:10.1111/j.1096-3642.2012.00850.x.

Coffin, M. F., Gahagan, L. M. and Lawver, L. A. (1998) Present-day plate boundary digital data compilation. *University of Texas Institute for Geophysics Technical Report* **174**, 5.

Cole, C. S. (2013) Biogeochemistry of Hydrothermal Systems in the Scotia Sea. PhD Thesis, University of Southampton.

Cole, C. S., James, R. H., Connelly, D. P. and Hathorne, E. C. (2014) Rare earth elements as indicators of hydrothermal processes within the East Scotia subduction zone system. *Geochimica et Cosmochimica Acta* **140**, 20–38. doi:10.1016/j.gca.2014.05.018.

Conway Morris, S. (1979) Middle Cambrian polychaetes from the Burgess Shale of British Colombia. *Philosophical Transactions of the Royal Society of London B* **285**, 227–274.

Conway Morris, S. and Peel, J. S. (2008) The earliest annelids: lower Cambrian polychaetes from the Sirius Passet Lagerstätte, Peary Land, North Greenland. *Acta Palaeontologica Polonica* **53**, 137–148. doi:10.4202/app.2008.0110.

Cook, T. and Stakes, D. (1995) Biogeological mineralization in deep-sea hydrothermal deposits. *Science* **267**, 1975–1979.

Corliss, J., Dymond, J., Gordon, L., Edmond, J., von Herzen, R., Ballard, R., Green, K., Williams, D., Bainbridge, A., Crane, K. and van Andel, T. (1979) Submarine thermal springs on the Galapagos Rift. *Science* **203**, 1073–1083.

Danise, S. and Higgs, N. D. (2015) Bone-eating *Osedax* worms lived on Mesozoic marine reptile deadfalls. *Biology Letters* **11**, 20150072.

Defretin, R. (1971) The tubes of polychaete annelids. *Comprehensive Biochemistry* **26**, 713–747.

Desbruyères, D., Segonzac, M. and Bright, M. (2006) *Handbook of deep-sea hydrothermal vent fauna*. 2nd edition, p. 544. Biologiezentrum der Oberösterreichische Landesmuseen, Linz.

Dubilier, N., Bergin, C. and Lott, C. (2008) Symbiotic diversity in marine animals: the art of harnessing chemosynthesis. *Nature Reviews Microbiology* **6**, 725–740. doi:10.1038/nrmicro1992.

Dubois, S., Retière, C. and Olivier, F. (2002) Biodiversity associated with *Sabellaria alveolata* (Polychaeta: Sabellariidae) reefs: effects of human disturbances. *Journal of the Marine Biological Association of the UK* **82**, 817–826.

Eibye-Jacobsen, D. (2004) A reevaluation of *Wiwaxia* and the polychaetes of the Burgess Shale. *Lethaia* **37**, 317–335. doi:10.1080/00241160410002027.

Ettensohn, F. R. (1981) *Crininicaminus haneyensis*, a new agglutinated worm from the Chesterian of east-central Kentucky. *Journal of Paleontology* **55**, 479–482.

Fornari, D., Von Damm, K., Bryce, J., Cowen, J., Ferrini, V., Fundis, A., Lilley, M., Luther, G., Mullineaux, L., Perfit, M., Meana-Prado, M. F., Rubin, K., Seyfried, W., Shank, T.,

Soule, S. A., Tolstoy, M. and White, S. (2012) The East Pacific Rise between 9°N and 10°N: twenty-five years of integrated, multidisciplinary oceanic spreading center studies. *Oceanography* **25**, 18–43. doi:10.5670/oceanog.2012.02.

Foucart, M. F., Bricteux-Gregoire, S. and Jeuniaux, C. (1965) Composition chimique du tube d'un pogonophore (*Siboglinum* sp.) et des formations squelettiques de deux pterobranches. *Sarsia* **20**, 36–41.

Franklin, J. M., Gibson, H. L., Jonasson, I. R. and Galley, A. G. (2005) Volcanogenic massive sulfide deposits. In *Economic Geology One Hundredth Anniversary Volume* (ed. Hedenquist, J. W., Thompson, J. F. H., Goldfarb, R. J. and Richards, J. P.), pp. 523–560. Society of Economic Geologists.

Gaill, F. and Hunt, S. (1986) Tubes of deep sea hydrothermal vent worms *Riftia pachyptila* (Vestimentifera) and *Alvinella pompejana* (Annelida). *Marine Ecology Progress Series* **3**, 267–274.

Gaill, F. and Hunt, S. (1988) Tubes. In *The Ultrastructure of Polychaeta* (ed. Westheide, W. and Hermans, C. O.), pp. 61-70. Fischer, New York.

Gaill, F., Chanzy, H. and Vuong, R. (1989) Structural organisation and localisation of the β chitin secreted by deep sea hydrothermal vent worms. *Biologie Cellulaire* **66**, 8a.

Galley, A. G., Hannington, M. D. and Jonasson, I. R. (2007) Volcanogenic massive sulphide deposits. In *Mineral Deposits of Canada: A Synthesis of Major Deposit-Types, District Metallogeny, the Evolution of Geological Provinces, and Exploration Methods* (ed. Goodfellow, W. D.), pp. 141–161. Geological Association of Canada, Mineral Deposits Division, Special Publication No. 5.

Gaudron, S. M., Lefebvre, S., Nunes Jorge, A., Gaill, F. and Pradillon, F. (2012) Spatial and temporal variations in food web structure from newly-opened habitat at hydrothermal vents. *Marine Environmental Research* **77**, 129–40. doi:10.1016/j.marenvres.2012.03.005.

German, C. and Von Damm, K. (2006) Hydrothermal processes. In *The Oceans and Marine Geochemistry* (ed. Elderfield, H., Holland, H. and Turekian, K.), pp. 181–222. Elsevier, Oxford.

German, C. R., Ramirez-Llodra, E., Baker, M. C. and Tyler, P. A. (2011) Deep-water chemosynthetic ecosystem research during the Census of Marine Life decade and beyond: a proposed deep-ccean road map. *PLOS ONE* **6**, e23259. doi:10.1371/journal.pone.0023259.

Goedert, J., Peckmann, J. and Reitner, J. (2000) Worm tubes in an allochthonous cold-seep carbonate from lower Oligocene rocks of western Washington. *Journal of Paleontology* **74**, 992–999.

Graham, G. N., Kelly, P. G., Pautard, F. G. E. and Wilson, R. (1965) Onuphic acid - a sugar phosphate polymer from the tube of *Hyalinoecia tubicola*. *Nature* **206**, 1256–1257. doi:10.1038/2061256b0.

Graur, D. and Martin, W. (2004) Reading the entrails of chickens: molecular timescales of evolution and the illusion of precision. *Trends in Genetics* **20**, 80–86. doi:10.1016/j.tig.2003.12.003.

Guggolz, T., Henne, S., Politi, Y., Schütz, R., Mašić, A., Müller, C. H. G. and Meißner, K. (2015) Histochemical evidence of β-chitin in parapodial glandular organs and tubes of Spiophanes (Annelida, Sedentaria: Spionidae), and first studies on selected Annelida. *Journal of Morphology* **276**, 1433–1447. doi:10.1002/jmor.20432.

Haas, A., Little, C. T. S., Sahling, H., Bohrmann, G., Himmler, T. and Peckmann, J. (2009) Mineralization of vestimentiferan tubes at methane seeps on the Congo deep-sea fan. *Deep-Sea Research I* **56**, 283–293. doi:10.1016/j.dsr.2008.08.007.

Hannington, M. D., Jonasson, I. R., Herzig, P. M. and Petersen, S. (1995) Physical and chemical processes of seafloor mineralization at mid-ocean ridges. In *Seafloor Hydrothermal Systems: Physical, Chemical, Biological, and Geological Interactions* (ed. Humphris, S. E., Zierenberg, R. A., Mullineaux, L. S. and Thomson, R. E.), pp. 115–157. American Geophysical Union, Washington, D. C. doi:10.1029/GM091p0115.

Hannington, M., Jamieson, J., Monecke, T., Petersen, S. and Beaulieu, S. (2011) The abundance of seafloor massive sulfide deposits. *Geology* **39**, 1155–1158. doi:10.1130/G32468.1.

Haymon, R. (1983) Growth history of hydrothermal black smoker chimneys. *Nature* **301**, 695–698.

Haymon, R. M., Koski, R. A. and Sinclair, C. (1984) Fossils of hydrothermal vent worms from Cretaceous sulfide ores of the Samail Ophiolite, Oman. *Science* **223**, 1407–1409.

Herrington, R. J., Maslennikov, V. V., Spiro, B., Zaykov, V. V. and Little, C. T. S. (1998) Ancient vent chimney structures in the Silurian massive sulphides of the Urals. In *Modern Ocean Floor Processes and the Geological Record* (Mills, R. A. and Harrison, K.), pp. 241–258. Special Publication of the Geological Society, London.

Hilário, A., Capa, M., Dahlgren, T. G., Halanych, K. M., Little, C. T. S., Thornhill, D. J., Verna, C. and Glover, A. G. (2011) New perspectives on the ecology and evolution of siboglinid tubeworms. *PLOS ONE* **6**, e16309. doi:10.1371/journal.pone.0016309.

Hints, O. and Eriksson, M. E. (2007) Diversification and biogeography of scolecodont-bearing polychaetes in the Ordovician. *Palaeogeography, Palaeoclimatology, Palaeoecology* **245**, 95–114. doi:10.1016/j.palaeo.2006.02.029.

Hryniewicz, K., Jakubowicz, M., Belka, Z., Dopieralska, J. and Kaim, A. (2016) New bivalves from a Middle Devonian methane seep in Morocco: the oldest record of repetitive shell morphologies among some seep bivalve molluscs. *Journal of Systematic Palaeontology* 1–23. doi:10.1080/14772019.2015.1136900.

Hurtado, L. A. (2002) Evolution and biogeography of hydrothermal vent organisms in the Eastern Pacific Ocean. PhD Thesis, Rutgers University.

Ippolitov, A., Vinn, O., Kupriyanova, E. and Jäger, M. (2014) Written in stone: history of serpulid polychaetes through time. *Memoirs of Museum Victoria* **71**, 123–159.

Ivanov, S. N. (1959) Discussion of some modern question of the genesis of the Uralian massive sulphide deposits. *Publications of the Mining-Geology Institute* **43**, 7–78.

Jones, W. J. and Vrijenhoek, R. C. (2006) Evolutionary relationships within the '*Bathymodiolus*' *childressi* group. *Cahiers de Biologie Marine* **47**, 403–407.

Jørgensen, B. B. and Boetius, A. (2007) Feast and famine - microbial life in the deep-sea bed. *Nature Reviews Microbiology* **5**, 770–781. doi:10.1038/nrmicro1745.

Kaim, A. and Kelly, S. R. A. (2009) Mass occurrence of hokkaidoconchid gastropods in the Upper Jurassic methane seep carbonate from Alexander Island, Antarctica. *Antarctic Science* **21**, 279–284.

Kaim, A., Jenkins, R. G. and Waren, A. (2008) Provannid and provannid-like gastropods from the Late Cretaceous cold seeps of Hokkaido (Japan) and the fossil record of the Provannidae (Gastropoda: Abyssochrysoidea). *Zoological Journal of the Linnean Society* **154**, 421–436. doi:10.1111/j.1096-3642.2008.00431.x.

Kelley, D. S., Karson, J. A., Blackman, D. K., Früh-Green, G. L., Butterfield, D. A., Lilley, M. D., Olson, E. J., Schrenk, M. O., Roe, K. K., Lebon, G. T., Rivizzigno, P. and the AT3-60 Shipboard Party (2001) An off-axis hydrothermal vent field near the Mid-Atlantic Ridge at 30°N. *Nature* **412**, 145–149. doi:10.1038/35084000.

Kiel, S. (2010) *The Vent and Seep Biota*. (ed. Kiel, S.) Springer Netherlands, Dordrecht.

doi:10.1007/978-90-481-9572-5.

Kiel, S. and Dando, P. R. (2009) Chaetopterid tubes from vent and seep sites: implications for fossil record and evolutionary history of vent and seep annelids. *Acta Palaeontologica Polonica* **54**, 443–448. doi:10.4202/app.2009.0022.

Kiel, S. and Little, C. T. S. (2006) Cold-seep mollusks are older than the general marine mollusk fauna. *Science* **313**, 1429–1431. doi:10.1126/science.1126286.

Kiel, S. and Tyler, P. A. (2010) Chemosynthetically-driven ecosystems in the deep sea. In *The Vent and Seep Biota* (ed. Kiel, S.), pp. 1–14. Springer Netherlands, Dordrecht. doi:10.1007/978-90-481-9572-5_1.

Knittel, K. and Boetius, A. (2009) Anaerobic oxidation of methane: progress with an unknown process. *Annual Review of Microbiology* **63**, 311–334. doi:10.1146/annurev.micro.61.080706.093130.

Kobayashi, G., Miura, T. and Kojima, S. (2015) *Lamellibrachia sagami* sp. nov., a new vestimentiferan tubeworm (Annelida: Siboglinidae) from Sagami Bay and several sites in the northwestern Pacific Ocean. *Zootaxa* **4018**, 97. doi:10.11646/zootaxa.4018.1.5.

Kongsrud, J. A. and Rapp, H. T. (2012) *Nicomache* (*Loxochona*) *lokii* sp. nov. (Annelida: Polychaeta: Maldanidae) from the Loki's Castle vent field: An important structure builder in an Arctic vent system. *Polar Biology* **35**, 161–170. doi:10.1007/s00300-011-1048-4.

Koschinsky, A., Garbe-Schönberg, D., Sander, S., Schmidt, K., Gennerich, H.-H. and Strauss, H. (2008) Hydrothermal venting at pressure-temperature conditions above the critical point of seawater, 5°S on the Mid-Atlantic Ridge. *Geology* **36**, 615. doi:10.1130/G24726A.1.

Kumar, S. (2005) Molecular clocks: four decades of evolution. *Nature Reviews Genetics* **6**, 654–662. doi:10.1038/nrg1659.

Kupriyanova, E., Nishi, E., Kawato, M. and Fujiwara, Y. (2010) New records of Serpulidae (Annelida, Polychaeta) from hydrothermal vents of North Fiji, Pacific Ocean. *Zootaxa* **2389**, 57–68.

Laznicka, P. (2010) Oceans and young island arc systems. In *Giant Metallic Deposits*, pp. 81–108. Springer Berlin Heidelberg, Berlin, Heidelberg doi:10.1007/978-3-642-12405-1_5.

Le Bris, N., Arnaud-Haond, S., Beaulieu, S., Cordes, E., Hilario, A., Rogers, A., van de

Gaever, S. and Watanabe, H. (2015) Chapter 45. Hydrothermal vents and cold seeps. In *First Global Integrated Marine Assessment*, p. 18. United Nations.

Levin, L. A. (2005) Ecology of cold seep sediments: interactions of fauna with flow, chemistry and microbes. In *Oceanography and Marine Biology: An Annual Review* (ed. Gibson, R. N., Atkinson, R. J. A. and Gordon, J. D. M.), pp. 1–46. CRC Press, Boca Raton.

Levin, L. A. and Mendoza, G. F. (2007) Community structure and nutrition of deep methane-seep macrobenthos from the North Pacific (Aleutian) Margin and the Gulf of Mexico (Florida Escarpment). *Marine Ecology* **28**, 131–151. doi:10.1111/j.1439-0485.2006.00131.x.

Levin, L. A., James, D. W., Martin, C. M., Rathburn, A. E., Harris, L. H. and Michener, R. H. (2000) Do methane seeps support distinct macrofaunal assemblages? Observations on community structure and nutrition from the northern California slope and shelf. *Marine Ecology Progress Series* **208**, 21–39. doi:10.3354/meps208021.

Levin, L., Ziebis, W., Mendoza, G., Growney, V., Tryon, M., Brown, K., Mahn, C., Gieskes, J. and Rathburn, A. (2003) Spatial heterogeneity of macrofauna at northern California methane seeps: influence of sulfide concentration and fluid flow. *Marine Ecology Progress Series* **265**, 123–139. doi:10.3354/meps265123.

Levin, L. A., Mendoza, G. F., Gonzalez, J. P., Thurber, A. R. and Cordes, E. E. (2010) Diversity of bathyal macrofauna on the northeastern Pacific margin: the influence of methane seeps and oxygen minimum zones. *Marine Ecology* **31**, 94–110. doi:10.1111/j.1439-0485.2009.00335.x.

Levin, L. A., Orphan, V. J., Rouse, G. W., Rathburn, a. E., Ussler, W., Cook, G. S., Goffredi, S. K., Perez, E. M., Waren, A., Grupe, B. M., Chadwick, G. and Strickrott, B. (2012) A hydrothermal seep on the Costa Rica margin: middle ground in a continuum of reducing ecosystems. *Proceedings of the Royal Society B: Biological Sciences* **279**, 2580–2588. doi:10.1098/rspb.2012.0205.

Levin, L. A., Baco, A. R., Bowden, D. A., Colaco, A., Cordes, E. E., Cunha, M. R., Demopoulos, A. W. J., Gobin, J., Grupe, B. M., Le, J., Metaxas, A., Netburn, A. N., Rouse, G. W., Thurber, A. R., Tunnicliffe, V., Van Dover, C. L., Vanreusel, A. and Watling, L. (2016) Hydrothermal vents and methane seeps: rethinking the sphere of influence. *Frontiers in Marine Science* **3**, 72. doi:10.3389/fmars.2016.00072.

Li, J. and Kusky, T. M. (2007) World's largest known Precambrian fossil black smoker

chimneys and associated microbial vent communities, North China: implications for early life. *Gondwana Research* **12**, 84–100. doi:10.1016/j.gr.2006.10.024.

Little, C. T. S. (2002) The fossil record of hydrothermal vent communities. *Cahiers de Biologie Marine* **43**, 313–316.

Little, C. T. S. (2009) Hot stuff in the deep sea. NERC *Planet Earth Online*, http://planetearth.nerc.ac.uk/features/story.aspx? id=576.

Little, C. T. S. and Vrijenhoek, R. C. (2003) Are hydrothermal vent animals living fossils? *Trends in Ecology & Evolution* **18**, 582–588. doi:10.1016/j.tree.2003.08.009.

Little, C. T. S., Herrington, R. J., Maslennikov, V. V., Morris, N. J. and Zaykov, V. V. (1997) Silurian hydrothermal-vent community from the southern Urals, Russia. *Nature* **385**, 146–148. doi:10.1038/385146a0.

Little, C. T. S., Herrington, R. J., Maslennikov, V. V. and Zaykov, V. V. (1998) The fossil record of hydrothermal vent communities. *Geological Society, London, Special Publications* **148**, 259–270. doi:10.1144/GSL.SP.1998.148.01.14.

Little, C. T. S., Maslennikov, V. V, Morris, N. J. and Gubanov, A. P. (1999a) Two Palaeozoic hydrothermal vent communities from the southern Ural mountains, Russia. *Palaeontology* **42**, 1043–1078.

Little, C. T. S., Cann, J. R., Herrington, R. J. and Morisseau, M. (1999b) Late Cretaceous hydrothermal vent communities from the Troodos ophiolite, Cyprus. *Geology* **27**, 1027–1030.

Little, C. T. S., Herrington, R. J., Haymon, R. M. and Danelian, T. (1999c) Early Jurassic hydrothermal vent community from the Franciscan Complex, San Rafael Mountains, California. *Geology* **27**, 167–170.

Little, C. T. S., Glynn, S. E. J. and Mills, R. A. (2004a) Four-hundred-and-ninety-million-year record of bacteriogenic iron oxide precipitation at sea-floor hydrothermal vents. *Geomicrobiology Journal* **21**, 415–429. doi:10.1080/01490450490485845.

Little, C. T. S., Danelian, T., Herrington, R. and Haymon, R. (2004b) Early Jurassic hydrothermal vent community from the Franciscan Complex, California. *Journal of Paleontology* **78**, 542–559.

Liu, J., Ou, Q., Han, J., Li, J., Wu, Y., Jiao, G. and He, T. (2015) Lower Cambrian polychaete from China sheds light on early annelid evolution. *The Science of Nature* **102**, 34. doi:10.1007/s00114-015-1285-4.

Lonsdale, P. (1977) Clustering of suspension-feeding macrobenthos near abyssal hydrothermal vents at oceanic spreading centers. *Deep Sea Research* **24**, 857–863.

Majima, R., Nobuhara, T. and Kitazaki, T. (2005) Review of fossil chemosynthetic assemblages in Japan. *Palaeogeography, Palaeoclimatology, Palaeoecology* **227**, 86–123. doi:10.1016/j.palaeo.2005.04.028.

Martin, W., Baross, J., Kelley, D. and Russell, M. J. (2008) Hydrothermal vents and the origin of life. *Nature Reviews Microbiology* **6**, 805–814. doi:10.1038/nrmicro1991.

MBARI (2015) MBARI researchers discover deepest known high-temperature hydrothermal vents in Pacific Ocean. *Monterey Bay Aquarium Research Institute*. http://www.mbari.org/mbari-researchers-discover-deepest-known-high-temperature-hydrothermal-vents-in-pacific-ocean/.

McLean, J. H. (1981) The Galapagos Rift limpet *Neomphalus*: relevance to understanding the evolution of a major Paleozoic–Mesozoic radiation. *Malacologia* **11**, 291–336.

Merz, R. A. (2015) Textures and traction: how tube-dwelling polychaetes get a leg up. *Invertebrate Biology* **134**, 61–77. doi:10.1111/ivb.12079.

Moalic, Y., Desbruyeres, D., Duarte, C. M., Rozenfeld, A. F., Bachraty, C. and Arnaud-Haond, S. (2012) Biogeography revisited with network theory: retracing the history of hydrothermal vent communities. *Systematic Biology* **61**, 127–137. doi:10.1093/sysbio/syr088.

Moczydłowska, M., Westall, F. and Foucher, F. (2014) Microstructure and biogeochemistry of the organically preserved Ediacaran metazoan *Sabellidites*. *Journal of Paleontology* **88**, 224–239. doi:10.1666/13-003.

Morin, A. and Dufresne, A. (2002) Nanocomposites of chitin whiskers from *Riftia* tubes and poly(caprolactone). *Macromolecules* **35**, 2190–2199. doi:10.1021/ma011493a.

Morineaux, M., Nishi, E., Ormos, A. and Mouchel, O. (2010) A new species of *Phyllochaetopterus* (Annelida: Chaetopteridae) from deep-sea hydrothermal Ashadze-1 vent field, Mid-Atlantic Ridge: taxonomical description and partial COI DNA sequence. *Cahiers Biologie Marine* **51**, 239–248.

Naehr, T. H., Eichhubl, P., Orphan, V. J., Hovland, M., Paull, C. K., Ussler, W., Lorenson, T. D. and Greene, H. G. (2007) Authigenic carbonate formation at hydrocarbon seeps in continental margin sediments: a comparative study. *Deep-Sea Research II* **54**, 1268–1291. doi:10.1016/j.dsr2.2007.04.010.

Nakamura, K., Watanabe, H., Miyazaki, J., Takai, K., Kawagucci, S., Noguchi, T., Nemoto, S., Watsuji, T. o., Matsuzaki, T., Shibuya, T., Okamura, K., Mochizuki, M., Orihashi, Y., Ura, T., Asada, A., Marie, D., Koonjul, M., Singh, M., Beedessee, G., Bhikajee, M. and Tamaki, K. (2012) Discovery of new hydrothermal activity and chemosynthetic fauna on the Central Indian ridge at 18°-20°S. *PLOS ONE* **7**, e32965. doi:10.1371/journal.pone.0032965.

Nauhaus, K., Boetius, A., Kruger, M. and Widdel, F. (2002) In vitro demonstration of anaerobic oxidation of methane coupled to sulphate reduction in sediment from a marine gas hydrate area. *Environmental Microbiology* **4**, 296–305.

Newman, W. (1985) The abyssal hydrothermal vent invertebrate fauna: A glimpse of antiquity? *Bulletin of the Biological Society of Washington* **6**, 231–242.

Nishi, E. and Rouse, G. (2007) A new species of *Phyllochaetopterus* (Chaetopteridae: Annelida) from near hydrothermal vents in the Lau Basin, western Pacific Ocean. *Zootaxa* **1621**, 55–64.

Nishi, E. and Rouse, G. W. (2014) First whale fall chaetopterid; a gigantic new species of *Phyllochaetopterus* (Chaetopteridae: Annelida) from the deep sea off California. *Proceedings of the Biological Society of Washington* **126**, 287–298.

Nishi, E., Miura, T. and Bhaud, M. (1999) A new species of *Spiochaetopterus* (Chaetopteridae: Polychaeta) from a cold-seep site off Hatsushima in Sagami Bay, central Japan. *Proceedings of the Biological Society of Washington* **112**, 210–215.

Olu, K., Duperret, A., Sibuet, M., Foucher, J. and Fiala-Medoni, A. (1996a) Structure and distribution of cold seep communities along the Peruvian active margin: relationship to geological and fluid patterns. *Marine Ecology Progress Series* **132**, 109–125.

Olu, K., Sibuet, M., Harmegnies, F., Foucher, J. and Fiala-Medoni, A. (1996b) Spatial distribution of diverse cold seep communities living on various diapiric structures of the southern Barbados prism. *Progress in Oceanography* **38**, 347–376.

Olu, K., Lance, S., Sibuet, M., Henry, P., Fiala-Médioni, A. and Dinet, A. (1997) Cold seep communities as indicators of fluid expulsion patterns through mud volcanoes seaward of the Barbados accretionary prism. *Deep-Sea Research I* **44**, 811–841. doi:10.1016/S0967-0637(96)00123-9.

Parry, L., Tanner, A. and Vinther, J. (2014) The origin of annelids. *Palaeontology* **57**, 1091–1103. doi:10.1111/pala.12129.

Paull, C., Hecker, B., Commeau, R., Freeman-Lynde, R., Neumann, A., Corso, W., Golubic, S., Hook, J., Sikes, E. and Curray, J. (1984) Biological communities at Florida Escarpment resemble hydrothermal vent communities. *Science* **226**, 965–967.

Peckmann, J., Thiel, V., Michaelis, W., Clari, P., Gaillard, C., Martire, L. and Reitner, J. (1999) Cold seep deposits of Beauvoisin (Oxfordian, southeastern France) and Marmorito (Miocene, northern Italy): microbially induced authigenic carbonates. *International Journal of Earth Sciences* **88**, 60–75.

Peckmann, J., Gischler, E., Oschmann, W. and Reitner, J. (2001) An Early Carboniferous seep community and hydrocarbon-derived carbonates from the Harz Mountains, Germany. *Geology* **29**, 271–274. doi:10.1130/0091-7613(2001)029<0271:AECSCA>2.0.CO;2.

Peckmann, J., Little, C. T. S., Gill, F. and Reitner, J. (2005) Worm tube fossils from the Hollard Mound hydrocarbon-seep deposit, Middle Devonian, Morocco: Palaeozoic seep-related vestimentiferans? *Palaeogeography, Palaeoclimatology, Palaeoecology* **227**, 242–257. doi:10.1016/j.palaeo.2005.04.021.

Peek, A., Gustafson, R., Lutz, R. and Vrijenhoek, R. (1997) Evolutionary relationships of deep-sea hydrothermal vent and cold-water seep clams (Bivalvia: Vesicomyidae): results from the mitochondrial cytochrome oxidase subunit I. *Marine Biology* **130**, 151–161.

Peng, X., Zhou, H. H., Tang, S., Yao, H., Jiang, L. and Wu, Z. (2008) Early-stage mineralization of hydrothermal tubeworms: New insights into the role of microorganisms in the process of mineralization. *Chinese Science Bulletin* **53**, 251–261. doi:10.1007/s11434-007-0517-1.

Peng, X., Zhou, H., Yao, H., Li, J. and Wu, Z. (2009) Ultrastructural evidence for iron accumulation within the tube of Vestimentiferan *Ridgeia piscesae*. *Biometals* **22**, 723–732.

Rasmussen, B. (2000) Filamentous microfossils in a 3,235-million-year-old volcanogenic massive sulphide deposit. *Nature* **405**, 676–679.

Ravaux, J., Zbinden, M., Voss-Foucart, M. F., Compère, P., Goffinet, G. and Gaill, F. (2003) Comparative degradation rates of chitinous exoskeletons from deep-sea environments. *Marine Biology* **143**, 405–412.

Reuscher, M., Fiege, D. and Wehe, T. (2012) Terebellomorph polychaetes from hydrothermal vents and cold seeps with the description of two new species of

Terebellidae (Annelida: Polychaeta) representing the first records of the family from deep-sea vents. *Journal of the Marine Biological Association of the United Kingdom* **92**, 997–1012. doi:10.1017/S0025315411000658.

Reysenbach, A. L. and Cady, S. L. (2001) Microbiology of ancient and modern hydrothermal systems. *Trends in Microbiology* **9**, 79–86. doi:10.1016/S0966-842X(00)01921-1.

Ritger, S., Carson, B. and Suess, E. (1987) Methane-derived authigenic carbonates formed by subduction-induced pore-water expulsion along the Oregon/Washington margin. *Geological Society of America Bulletin* **98**, 147. doi:10.1130/0016-7606(1987)98<147:MACFBS>2.0.CO;2.

Roeselers, G. and Newton, I. L. G. (2012) On the evolutionary ecology of symbioses between chemosynthetic bacteria and bivalves. *Applied Microbiology and Biotechnology* **94**, 1–10. doi:10.1007/s00253-011-3819-9.

Rogers, A. D., Tyler, P. A., Connelly, D. P., Copley, J. T., James, R., Larter, R. D., Linse, K., Mills, R. A., Garabato, A. N., Pancost, R. D., Pearce, D. A., Polunin, N. V. C., German, C. R., Shank, T., Boersch-Supan, P. H., Alker, B. J., Aquilina, A., Bennett, S. A., Clarke, A., Dinley, R. J. J., Graham, A. G. C., Green, D. R. H., Hawkes, J. A., Hepburn, L., Hilario, A., Huvenne, V. A. I., Marsh, L., Ramirez-Llodra, E., Reid, W. D. K., Roterman, C. N., Sweeting, C. J., Thatje, S. and Zwirglmaier, K. (2012) The discovery of new deep-sea hydrothermal vent communities in the Southern Ocean and implications for biogeography. *PLOS Biology* **10**, e1001234. doi:10.1371/journal.pbio.1001234.

Ross, P.-S. and Mercier-Langevin, P. (2014) Igneous Rock Associations 14. The Volcanic Setting of VMS and SMS Deposits: A Review. *Geoscience Canada* **41**, 365. doi:10.12789/geocanj.2014.41.045.

Roterman, C. N., Copley, J. T., Linse, K. T., Tyler, P. A. and Rogers, A. D. (2013) The biogeography of the yeti crabs (Kiwaidae) with notes on the phylogeny of the Chirostyloidea (Decapoda: Anomura). *Proceedings of the Royal Society B* **280**, 20130718. http://dx.doi.org/10.1098/rspb.2013.0718.

Rouse, G. W. and Fauchald, K. (1997) Cladistics and polychaetes. *Zoologica Scripta* **26**, 139–204.

Rouse, G. W. and Pleijel, F. (2001) *Polychaetes*. Oxford University Press, Oxford.

Russell, M. J. and Hall, A. J. (1997) The emergence of life from iron monosulphide bubbles at a submarine hydrothermal redox and pH front. *Journal of the Geological Society* **154**, 377–402. doi:10.1144/gsjgs.154.3.0377.

Sandy, M. R. (2010) Brachiopods from ancient hydrocarbon seeps and hydrothermal vents. In *The Vent and Seep Biota* (ed. Kiel, S.), pp. 279–314. Springer Netherlands, Dordrecht. doi:10.1007/978-90-481-9572-5_9.

Sanfilippo, R., Rosso, A., Reitano, A. and Insacco, G. (2016) A new tubeworm of possible serpulid affinity from the Permian of Sicily. *Acta Palaeontologica Polonica* **61**, 621–626. doi:10.4202/app.00209.2015.

Scheller, S., Yu, H., Chadwick, G. L., McGlynn, S. E. and Orphan, V. J. (2016) Artificial electron acceptors decouple archaeal methane oxidation from sulfate reduction. *Science* **351**, 703–707. doi:10.1126/science.aad7154.

Schrag, D. P., Higgins, J. A., Macdonald, F. A. and Johnston, D. T. (2013) Authigenic carbonate and the history of the global carbon cycle. *Science* **339**, 540–543.

Seyfried, W. E. and Mottl, M. J. (1995) Geologic Setting and Chemistry of Deep-Sea Hydrothermal Vents. In *The Microbiology of Deep-Sea Hydrothermal Vents* (ed. Karl, D. M.), pp. 1–34. CRC Press, Boca Raton.

Shah, D. U., Vollrath, F., Porter, D., Stires, J. and Deheyn, D. D. (2014) Housing tubes from the marine worm *Chaetopterus* sp.: biomaterials with exceptionally broad thermomechanical properties. *Journal of The Royal Society Interface* **11**, 20140525. doi:10.1098/rsif.2014.0525.

Shillito, B., Lechaire, J.-P., Goffinet, G. and Gaill, F. (1995) Composition and morphogenesis of the tubes of vestimentiferan worms. *Geological Society, London, Special Publications* **87**, 295–302. doi:10.1144/GSL.SP.1995.087.01.22.

Sibuet, M. and Olu, K. (1998) Biogeography, biodiversity and fluid dependence of deep-sea cold-seep communities at active and passive margins. *Deep-Sea Research II* **45**, 517–567.

Sievert, S. and Vetriani, C. (2012) Chemoautotrophy at deep-sea vents: past, present, and future. *Oceanography* **25**, 218–233. doi:10.5670/oceanog.2012.21.

Smith, C. R., Glover, A. G., Treude, T., Higgs, N. D. and Amon, D. J. (2015) Whale-fall ecosystems: recent insights into ecology, paleoecology, and evolution. *Annual Review of Marine Science* **7**, 571–596. doi:10.1146/annurev-marine-010213-135144.

Southward, E., Schulze, A. and Gardiner, S. (2005) Pogonophora (Annelida): form and

function. *Hydrobiologia* **535**, 227–251.

Stanton, T. W. (1895) Contributions to the Cretaceous paleontology of the Pacific coast: the fauna of the Knoxville beds. *U.S. Geological Survey Bulletin* **133**, 1–132.

Stiller, J., Rousset, V., Pleijel, F., Chevaldonné, P., Vrijenhoek, R. C. and Rouse, G. W. (2013) Phylogeny, biogeography and systematics of hydrothermal vent and methane seep *Amphisamytha* (Ampharetidae, Annelida), with descriptions of three new species. *Systematics and Biodiversity* **11**, 35–65. doi:10.1080/14772000.2013.772925.

Struck, T. H. (2011) Direction of evolution within Annelida and the definition of Pleistoannelida. *Journal of Zoological Systematics and Evolutionary Research* **49**, 340–345. doi:10.1111/j.1439-0469.2011.00640.x.

Struck, T. H., Golombek, A., Weigert, A., Franke, F. A., Westheide, W., Purschke, G., Bleidorn, C. and Halanych, K. M. (2015) The evolution of annelids reveals two adaptive routes to the interstitial realm. *Current Biology* **25**, 1993–1999. doi:10.1016/j.cub.2015.06.007.

Takai, K., Nakagawa, S., Reysenbach, A.-L. and Hoek, J. (2006) Microbial ecology of mid-ocean ridges and back-arc basins. In *Geophysical Monograph Series*, pp. 185–213. doi:10.1029/166GM10.

Taylor, J. D. and Glover, E. A. (2010) Chemosymbiotic Bivalves. In *The Vent and Seep Biota* (ed. Kiel, S.), pp. 107–135. Springer Netherlands, Dordrecht. doi:10.1007/978-90-481-9572-5_5.

Thiel, V., Peckmann, J., Seifert, R., Wehrung, P., Reitner, J. and Michaelis, W. (1999) Highly isotopically depleted isoprenoids: molecular markers for ancient methane venting. *Geochimica et Cosmochimica Acta* **63**, 3959–3966. doi:10.1016/S0016-7037(99)00177-5.

Thurber, A. R., Jones, W. J. and Schnabel, K. (2011) Dancing for food in the deep sea: bacterial farming by a new species of yeti crab. *PLOS ONE* **6**, e26243. doi:10.1371/journal.pone.0026243.

Tivey, M. K. (1995) Modeling chimney growth and associated fluid flow at seafloor hydrothermal vent sites. In *Seafloor Hydrothermal Systems: Physical, Chemical, Biological, and Geological Interactions* (ed. Humphris, S. E., Zierenberg, R. A., Mullineaux, L. S. and Thomson, R. E.), pp. 158–177. American Geophysical Union, Washington, D. C. doi:10.1029/GM091p0158.

Tivey, M. (2007) Generation of seafloor hydrothermal vent fluids and associated mineral deposits. *Oceanography* **20**, 50–65. doi:10.5670/oceanog.2007.80.

Torres, M. E. and Bohrmann, G. (2014) Cold Seeps. In *Encyclopedia of Marine Geosciences* (ed. Harff, J., Meschede, M., Petersen, S. and Thiede, J.), pp. 1–8. Springer Netherlands, Dordrecht doi:10.1007/978-94-007-6644-0_153-1.

Tunnicliffe, V., McArthur, A. G. and McHugh, D. (1998) A biogeographical perspective of the deep-sea hydrothermal vent fauna. *Advances in Marine Biology* **34**, 353–442.

Tunnicliffe, V., Juniper, S. K. and Sibuet, M. (2003) Reducing environments of the deep-sea floor. In *Ecosystems of the Deep Oceans* (ed. Tyler, P. A.), pp. 81–110. Elsevier, Amsterdam.

Turnipseed, M., Jenkins, C. D. and Van Dover, C. L. (2004) Community structure in Florida Escarpment seep and Snake Pit (Mid-Atlantic Ridge) vent mussel beds. *Marine Biology* **145**, 121–132. doi:10.1007/s00227-004-1304-z.

Van Dover, C. (2000) *The ecology of deep-sea hydrothermal vents*. Princeton University Press.

Van Dover, C. L. L., German, C. R. R., Speer, K. G. G., Parson, L. M. M. and Vrijenhoek, R. C. C. (2002) Evolution and biogeography of deep-sea vent and seep invertebrates. *Science* **295**, 1253–1257. doi:10.1126/science.1067361.

Van Dover, C. L., Aharon, P., Bernhard, J. M., Caylor, E., Doerries, M. B., Flickinger, W., Gilhooly, W., Goffredi, S. K., Knick, K. E., Macko, S. A., Rapoport, S., Raulfs, E. C., Ruppel, C., Salerno, J. L., Seitz, R. D., Sen Gupta, B. K., Shank, T. M., Turnipseed, M. and Vrijenhoek, R. C. (2003) Blake Ridge methane seeps: characterization of a soft−sediment, chemosynthetically based ecosystem. *Deep-Sea Research I* **50**, 281–300.

Van Rensbergen, P., De Batist, M., Klerkx, J., Hus, R., Poort, J., Vanneste, M., Granin, N., Khlystov, O. and Krinitsky, P. (2002) Sublacustrine mud volcanoes and methane seeps caused by dissociation of gas hydrates in Lake Baikal. *Geology* **30**, 631. doi:10.1130/0091-7613(2002)030<0631:SMVAMS>2.0.CO;2.

Vinn, O. and Luque, J. (2013) First record of a pectinariid-like (Polychaeta, Annelida) agglutinated worm tube from the Late Cretaceous of Colombia. *Cretaceous Research* **41**, 107–110.

Vinn, O. and Mutvei, H. (2009) Calcareous tubeworms of the Phanerozoic. *Estonian Journal of Earth Sciences* **58**, 286–296. doi:10.3176/earth.2009.4.07.

Vinn, O., Ten-Hove, H., Mutvei, H. and Kirsimae, K. (2008a) Ultrastructure and mineral

composition of serpulid tubes (Polychaeta, Annelida). *Zoological Journal of the Linnean Society* **154**, 633–650.

Vinn, O., Jäger, M. and Kirsimäe, K. (2008b) Microscopic evidence of serpulid affinities of the problematic fossil tube Serpula etalensis from the Lower Jurassic of Germany. *Lethaia* **41**, 417–421.

Vinn, O., Kupriyanova, E. K. and Kiel, S. (2013) Serpulids (Annelida, Polychaeta) at Cretaceous to modern hydrocarbon seeps: Ecological and evolutionary patterns. *Palaeogeography, Palaeoclimatology, Palaeoecology* **390**, 35–41. doi:10.1016/j.palaeo.2012.08.003.

Vinn, O., Hryniewicz, K., Little, C. T. S. and Nakrem, H. A. (2014) A Boreal serpulid fauna from Volgian-Ryazanian (latest Jurassic-earliest Cretaceous) shelf sediments and hydrocarbon seeps from Svalbard. **36**, 527–540.

Vinther, J., Eibye-Jacobsen, D. and Harper, D. A. (2011) An Early Cambrian stem polychaete with pygidial cirri. *Biology Letters* **7**, 929–932.

Von Damm, K. L. (1995) Controls on the chemistry and temporal variability of seafloor hydrothermal fluids. In *Seafloor Hydrothermal Systems: Physical, Chemical, Biological, and Geological Interactions* (ed. Humphris, S. E., Zierenberg, R. A., Mullineaux, L. S. and Thomson, R. E.), pp. 222–247. American Geophysical Union, Washington, D. C. doi:10.1029/GM091p0222.

Von Damm, K. L., Edmond, J. M., Measures, C. I. and Grant, B. (1985) Chemistry of submarine hydrothermal solutions at Guaymas Basin, Gulf of California. *Geochimica et Cosmochimica Acta* **49**, 2221–2237. doi:10.1016/0016-7037(85)90223-6.

Vovelle, J. and Gaill, F. (1986) Donnees morphologiques, histochimiques et microanalytiques sur l'elaboration du tube organo-mineral d'*Alvinella pompejana*, polychete des sources hydrothermales, et leurs implications phylogenetiques. *Zoologica Scripta* **15**, 33–43.

Vrijenhoek, R. C. (2010) Genetic diversity and connectivity of deep-sea hydrothermal vent metapopulations. *Molecular Ecology* **19**, 4391–4411. doi:10.1111/j.1365-294X.2010.04789.x.

Vrijenhoek, R. C. (2013) On the instability and evolutionary age of deep-sea chemosynthetic communities. *Deep-Sea Research II* **92**, 189–200. doi:10.1016/j.dsr2.2012.12.004.

Webb, M. (1971) The morphology and formation of the pogonophoran tube and its value in systematics. *Journal of Zoological Systematics and Evolutionary Research* **9**, 169–181. doi:10.1111/j.1439-0469.1971.tb00895.x.

Wegener, G., Krukenberg, V., Riedel, D., Tegetmeyer, H. E. and Boetius, A. (2015) Intercellular wiring enables electron transfer between methanotrophic archaea and bacteria. *Nature* **526**, 587–590. doi:10.1038/nature15733.

Weigert, A. and Bleidorn, C. (2016) Current status of annelid phylogeny. *Organisms Diversity & Evolution* **16**, 345–362. doi:10.1007/s13127-016-0265-7.

Weigert, A., Helm, C., Meyer, M., Nickel, B., Arendt, D., Hausdorf, B., Santos, S. R., Halanych, K. M., Purschke, G., Bleidorn, C. and Struck, T. H. (2014) Illuminating the base of the annelid tree using transcriptomics. *Molecular Biology and Evolution* **31**, 1391–1401. doi:10.1093/molbev/msu080.

Weigert, A., Golombek, A., Gerth, M., Schwarz, F., Struck, T. H. and Bleidorn, C. (2016) Evolution of mitochondrial gene order in Annelida. *Molecular Phylogenetics and Evolution* **94**, 196–206. doi:10.1016/j.ympev.2015.08.008.

Weiss, M. C., Sousa, F. L., Mrnjavac, N., Neukirchen, S., Roettger, M., Nelson-Sathi, S. and Martin, W. F. (2016) The physiology and habitat of the last universal common ancestor. *Nature Microbiology* **1**, 16116. doi:10.1038/nmicrobiol.2016.116.

Westheide, W. (1997) The direction of evolution within the Polychaeta. *Journal of Natural History* **31**, 1–15.

Zaton, M., Kano, Y., Wilson, M. A. and Filipiak, P. (2012) Unusual tubular fossils associated with microbial crusts from the Middle Jurassic of Poland: agglutinated polychaete worm tubes? *Palaios* **27**, 550–559. doi:10.2110/palo.2012.p12-013r.

Zola, H. (1967) Sugar phosphate polymers in polychaete tubes and in mineralized animal tissues. *Comparative Biochemistry and Physiology* **21**, 179–183. doi:10.1016/0010-406X(67)90127-2.

Zottoli, R. A. (1983) *Amphisamytha galapagensis*, a new species of ampharetid polychaete from the vicinity of abyssal hydrothermal vents in the Galapagos Rift, and the role of this species in rift ecosystems. *Proceedings of the Biological Society of Washington* **96**, 379–391.

2 A chemosynthetic weed: the tubeworm *Sclerolinum contortum* is a bipolar, cosmopolitan species

Magdalena N. Georgieva[1,2], Helena Wiklund[2], James B. Bell[2,3], Mari H. Eilertsen[4,5], Rachel A. Mills[6], Crispin T. S. Little[1], Adrian G. Glover[2]

[1]*School of Earth and Environment, University of Leeds, Leeds, United Kingdom*

[2]*Life Sciences Department, Natural History Museum, London, United Kingdom*

[3]*School of Geography, University of Leeds, Leeds, United Kingdom*

[4]*Centre for Geobiology, University of Bergen, Bergen, Norway*

[5]*Department of Biology, University of Bergen, Bergen, Norway*

[6]*Ocean and Earth Science, National Oceanography Centre Southampton, University of Southampton, Southampton, United Kingdom*

2.1 Abstract

Sclerolinum (Annelida: Siboglinidae) is a genus of small, wiry deep-sea tubeworms that depend on an endosymbiosis with chemosynthetic bacteria for their nutrition, notable for their ability to colonise a multitude of reducing environments. Since the early 2000s, a *Sclerolinum* population has been known to inhabit sediment-hosted hydrothermal vents within the Bransfield Strait, Southern Ocean, and whilst remaining undescribed, it has been suggested to play an important ecological role in this ecosystem. Here, we show that the Southern Ocean *Sclerolinum* population is not a new species, but more remarkably in fact belongs to the species *S. contortum*, first described from an Arctic mud volcano located nearly 16,000 km away. Our new data coupled with existing genetic studies extend the range of this species across both polar oceans and the Gulf of Mexico. Our analyses show that the populations of this species are structured on a regional scale, with greater genetic differentiation occurring between rather than within populations. Further details of the external morphology and tube structure of *S. contortum* are revealed through confocal and SEM imaging, and the ecology of this worm is discussed. These results shed further insight

into the plasticity and adaptability of this siboglinid group to a range of reducing conditions, and into the levels of gene flow that occur between populations of the same species over a global extent.

2.2 Introduction

The vastness and inaccessibility of the deep sea has challenged scientists seeking to understand its diversity (Brandt *et al.*, 2007; McClain and Schlacher, 2015). A major area of this research concerns improving knowledge on the ranges of deep-sea species, which has become particularly pertinent in light of growing human impacts in this environment (Hilário *et al.*, 2015). Molecular tools have been applied to this field and have revealed that certain deep-sea species with widespread distributions can exhibit similar morphology but considerable genetic differentiation between regions, and may thereby represent several closely related but geographically restricted species – so called 'cryptic species' (Goffredi *et al.*, 2003; Zardus *et al.*, 2006; Raupach *et al.*, 2007; Brix *et al.*, 2011; Havermans *et al.*, 2013). Contrastingly, other studies have also revealed that some taxa can indeed be incredibly widespread, displaying distributions that can span both poles, i.e. bipolar. This pattern has been confirmed in bacteria and archaea (Brinkmeyer *et al.*, 2003; Bano *et al.*, 2004), in benthic foraminifera (Pawlowski *et al.*, 2007), deep-sea coral (Herrera *et al.*, 2012) and a lineage of the amphipod *Eurythenes gryllus* (Havermans *et al.*, 2013). While there are problems with the use of molecular data to delimit species, the examination of genetic variation at multiple (both mitochondrial and nuclear) loci within an evolutionary context has become an important addition to our definition of a species alongside morphological, biological and ecological observations (Vogler and Monaghan, 2007; Vrijenhoek, 2009; Nygren, 2014), as well as a critical tool in the investigation of species biogeography. Here we investigate the range and ecological adaptations of a deep-sea siboglinid tubeworm over the near 16,000 km spanning from the Arctic to the Antarctic.

The family Siboglinidae is a monophyletic lineage of annelid worms comprised of the vestimentiferans, or giant tubeworms, the bone-eating genus *Osedax*, and two groups of slender tubeworms – *Sclerolinum* and the frenulates (Hilário *et al.*, 2011). Siboglinidae is exceptional among the annelids due to this family's almost complete reliance on endosymbiotic bacteria for nutrition, and the unusual morphology which its members have adopted for this specialism (Southward *et al.*, 2005). The majority of siboglinids (except for *Osedax* and a number of frenulates capable of oxidising methane) harbour sulphur-oxidising

symbionts (Dubilier *et al.*, 2008) and are characteristically long, often acting like a 'bridge' between a sulphidic substrate where their posterior end is located, and oxygenated seawater into which they extend their anterior end (Dando *et al.*, 2008).

Although siboglinids are found within all of the world's major oceans, the distribution and genetic structure of certain lineages is poorly constrained. Hydrothermal vent vestimentiferans endemic to the East Pacific Rise (EPR) are perhaps the best studied, where species such as *Riftia pachyptila* and *Tevnia jerichonana* show extensive ranges along the length of this mid ocean ridge system, while the degree of genetic differentiation between populations increases with distance (Coykendall *et al.*, 2011; Zhang *et al.*, 2015). Vestimentiferans that can colonise seeps, whale and wood falls have the potential to be even more widely distributed. The genus *Escarpia* is found in a variety of reducing environments, and occupies several ocean basins with the three described species *Escarpia laminata*, *E. southwardae*, and *E. spicata* occurring in the Gulf of Mexico (GoM), West Africa, and in the eastern Pacific respectively. However, while there is high genetic similarity between the three species, geographical and hydrological barriers still appear to limit gene flow between them (Cowart *et al.*, 2013).

The genus *Sclerolinum*, which forms the sister clade to the vestimentiferans (Li *et al.*, 2015), also exhibits a widespread distribution. The seven formally described species are reported from the northeast Atlantic (Webb, 1964a; Smirnov, 2000), GoM and Caribbean (Southward, 1972; Eichinger *et al.*, 2013), and southeast Asia (Southward, 1961; Ivanov and Selivanova, 1992), however there are also a number of known but not currently described *Sclerolinum* populations from Antarctica, Hawaii (Sahling *et al.*, 2005), the Sea of Okhotsk (Sahling *et al.*, 2003) and off Kushiro, Japan (Kojima *et al.*, 1997, 2003), that extend the range of this genus even further. This little studied genus of small, wiry tubeworms have also been found to possesses peculiar organisation that has made it challenging to determine its position in relation to other siboglinids, have been shown to perform important ecological functions within deep-sea sediments, and is capable of colonising a multitude of reducing environments (Southward, 1972; Ivanov and Selivanova, 1992; Smirnov, 2000; Sahling *et al.*, 2005; Eichinger *et al.*, 2013; Aquilina *et al.*, 2014).

Remarkable substrate choice and geographical range is demonstrated by just one *Sclerolinum* species, *S. contortum*. Initially described from soft sediments at Håkon Mosby Mud Volcano (HMMV) (Smirnov, 2000), this species was later also found to be residing in the nearby cold seeps of the Storegga Slide, Norwegian Sea (Vanreusel *et al.*, 2009; Lazar *et al.*, 2010) as well as in diffuse flow areas of the Arctic vents of Loki's Castle (Pedersen *et al.*, 2010;

Kongsrud and Rapp, 2012). Colonisation experiments in the northeast Atlantic have shown that in addition to soft sediments, *S. contortum* can inhabit wood, other decaying plant debris, as well as mineral substrates (Gaudron *et al.*, 2010). A population of *Sclerolinum contortum* notably also occurs within the cold seeps of the GoM, a distance of over 7600 km from the nearest northeast Atlantic population (Eichinger *et al.*, 2013).

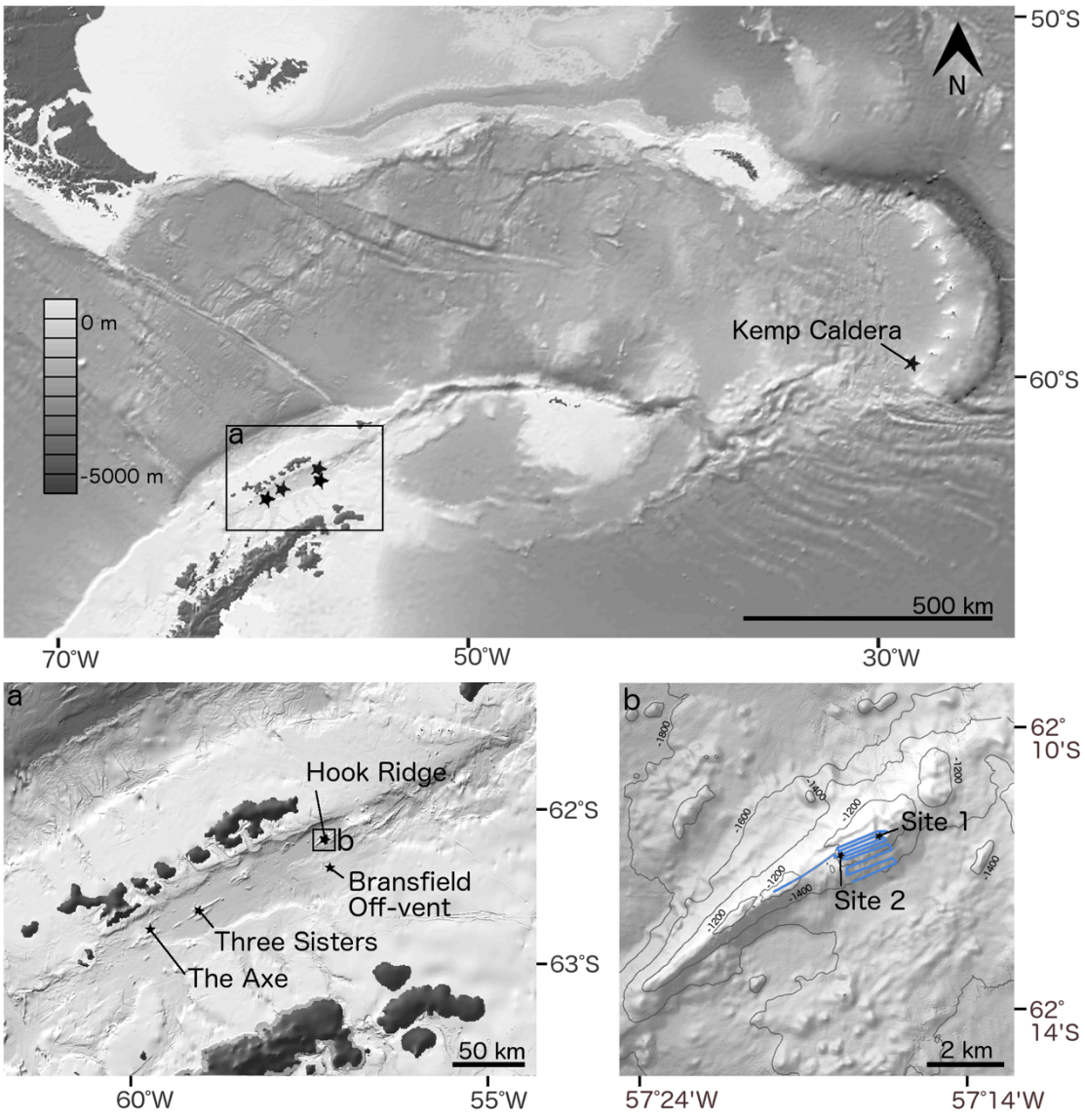

Figure 2.1 Southern Ocean sampling sites from which *Sclerolinum* sp. was collected. Box **A** shows the locations of JC55 Bransfield Strait sampling locations, and **B** shows detail of Hook Ridge sampling sites (Hook Ridge Site 1 and Hook Ridge Site 2), as well as the path traversed by the SHRIMP (in blue). Map created using GeoMapApp (http://www.geomapapp.org) using data from the Global Multi-Resolution Topography (GMRT) Synthesis (Ryan *et al.*, 2009).

Considerable sampling of the deep waters around Antarctica in recent years has revealed this region to be much more diverse, and not as isolated as traditionally thought (Chown *et al.*, 2015). These exploration efforts have also shown that the Southern Ocean possesses a

variety of deep-sea chemosynthetic habitats that include areas of high temperature and diffuse venting, cold seeps, and whale falls (Klinkhammer *et al.*, 2001; Domack *et al.*, 2005; Rogers *et al.*, 2012; Amon *et al.*, 2013). Hydrothermal activity is currently known to occur within the Bransfield Strait (Klinkhammer *et al.*, 2001; Aquilina *et al.*, 2013), along the East Scotia Ridge (German *et al.*, 2000), Pacific-Antarctic Ridge (Winkler *et al.*, 2010), Australian-Antarctic Ridge (Hahm *et al.*, 2015), and within Kemp Caldera (Tyler, 2011), and to support unique vent ecosystems distinct from those of the main mid-ocean ridge systems (Rogers *et al.*, 2012).

Since 2001, *Sclerolinum* has been known to inhabit the sedimented hydrothermal vents of Hook Ridge, Bransfield Strait (Figure 2.1) (Klinkhammer *et al.*, 2001). This population was recently suggested to play an important role in mediating the release of iron and manganese from sediments to the water column (Aquilina *et al.*, 2014). However while aspects of the habitat and function of this population have been investigated (Sahling *et al.*, 2005; Aquilina *et al.*, 2014), the morphology of these worms, their extent within the Southern Ocean, and how this population relates to other known *Sclerolinum* populations remain unknown. This study aims to provide a detailed description of the Antarctic *Sclerolinum* population, place it within a phylogenetic context and thereby establish its relationships to other *Sclerolinum* populations worldwide, and discern its extent and ecology within the Southern Ocean.

2.3 Results

2.3.1 Systematics

Phylum Annelida

Family Siboglinidae Caullery, 1914

Genus *Sclerolinum* Southward, 1961

***Sclerolinum contortum* Smirnov, 2000**

(Figures 2.2-2.4)

Material examined. Southern Ocean, *Hook Ridge Site 1*, 62.1969°S 57.2975°W, 1174 m depth: JC55_19 (RRS *James Cook* operation no.), 15 tube fragments. JC55_19, tubes attached to sampling gear (non-quantitative), 234 tube fragments [NHMUK 2015.1140-1146]. JC55_20, 5 tube fragments [NHMUK 2015.1153-1155]. JC55_21, 1 worm fragment

with forepart, 7 tube fragments [NHMUK 2015.1147-1152]. JC55_25, 29 worm fragments with forepart, 302 additional tube fragments [NHMUK 2015.1156-1157, 1188-1189 (subset of examined material]. *Hook Ridge Site 2*, 62.1924°S 57.2783°W, 1054 m depth: JC55_30, 8 tube fragments attached to sampling gear [NHMUK 2015.1158].

Description. Anterior extremity of tubes pale white in colour, thin walled (2 to 7 μm) and flattened. Posteriorly, wall thickness increases (to maximum of 28 μm) and tubes generally exhibit several smooth bends (Figure 2.2A). Majority of tube is pale brown/green in colour (Figure 2.2A-B), flexible and elastic, often possessing closely but irregularly spaced transverse wrinkles as well as faint longitudinal wrinkles on its outer surface (Figure 2.3A), occasional microbial filament and rust patches are also present on outer tube surfaces. Tube walls are multi-layered, comprised of superimposed fibrous sheets in which fibres show an overall disorganised arrangement, inner tube surface shows a similar texture (Figure 2.3C-D). Towards posterior extremity, tubes are increasingly thin walled and collapsed, outer tube wall generally smooth but with patches of attached sediment grains (Figure 2.3B). Tube diameter ranges from 0.22 to 0.30 mm, longest tube fragment measured 155 mm. Several tubes exhibit branch-like abnormalities (Figure 2.2E), a subset of Hook Ridge Site 1 tubes were very dark brown to black in colour (similar to tubes from Kemp Caldera, see later (Figure 2.6B)).

Longest animal measured 52 mm in length (from tip of the cephalic lobe) but all were incomplete with posterior extremity missing, therefore opisthosomal characters could not be elucidated. Animals are bright red when alive, this colouration being most pronounced in trunk tissues (Figure 2.3E-F). Two tentacles (Figure 2.2C) often slightly different in length in individuals, tentacle lengths overall varied greatly between measured worms, from 0.83 to 3.00 mm. Tentacles smooth or occasionally wrinkled on inner surfaces, longitudinal blood vessels visible within them (Figure 2.4A-B). Dense epidermal glands occur around the base of tentacles, which are more scattered distally (Figure 2.4A-B). Diameter of forepart ranges between 0.15 to 0.23 mm. Cephalic lobe had a small, rounded triangular tip 55 to 75 μm in length that protrudes from forepart (Figures 2.3H, 2.4B). Dorsal furrow deep and wide, extending from base of tentacles (Figures 2.3I, 2.4A). Frenulum positioned 0.13 to 0.37 μm from tip of cephalic lobe. Region surrounding frenulum shows dense covering of glands, present on both dorsal and ventral surfaces. Frenulum comprised of 9-19 oval to elongated plaques measuring 14 to 46 μm in diameter (Figure 2.3J), occurring as a slightly sparse or dense row. Frenular plaques occur dorsolaterally and ventrally with middle ventral plaque often missing, plaques in middle ventral and middle dorsal areas

often smaller (Figures 2.3H-I, 2.4A-B). Densely ciliated band present posterior to frenulum on ventral side of animal, that widens with increasing distance from frenulum (Figures 2.3H, K, 4B). Region posterior to frenulum and around the ciliated band contains scattered glands, visible as slits in SEM images (Figure 2.3I).

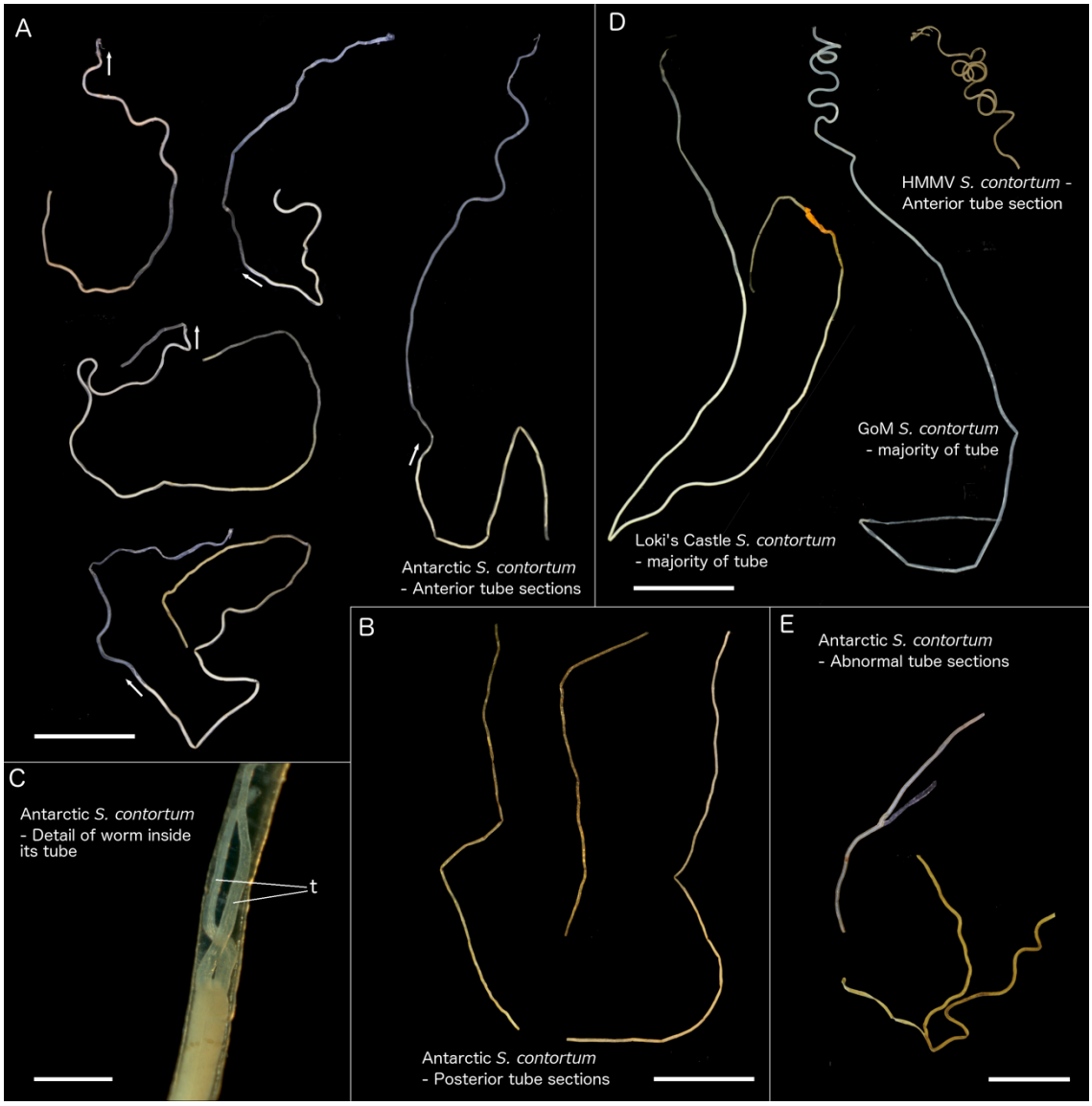

Figure 2.2 Broad morphology of *Sclerolinum contortum* tubes. **A,** Antarctic *S. contortum* anterior tube sections, arrows indicate position and orientation of the worms' heads. **B,** Posterior sections of Antarctic *S. contortum* tubes. **C,** detail of tube with worm inside it, t – tentacles. **D,** tubes of *S. contortum* from Loki's Castle, GoM and HMMV. **E,** Antarctic *S. contortum* tube sections showing abnormalities. Scale bars for **A-B** and **D** are 10 mm, 400 μm for **C** and 5 mm for **E**.

Transition between ending of dorsal furrow and beginning of a narrower, highly wrinkled and densely papillated trunk region clearly distinguished anterior and posterior zones of Antarctic *S. contortum* animals (Figure 2.3G), with this forepart region measuring 1.7 to 4.8 μm in length from the tip of the cephalic lobe to the beginning of the trunk. The trunk

(Figures 2.3L-N, 2.4C) comprised much of length of animals and was characterised by the presence of scattered oval plaques positioned on top of papillae (Figure 2.3L-N). Large papillae without plaques, possibly openings of pyriform glands, also present in trunk region (Figure 2.3N).

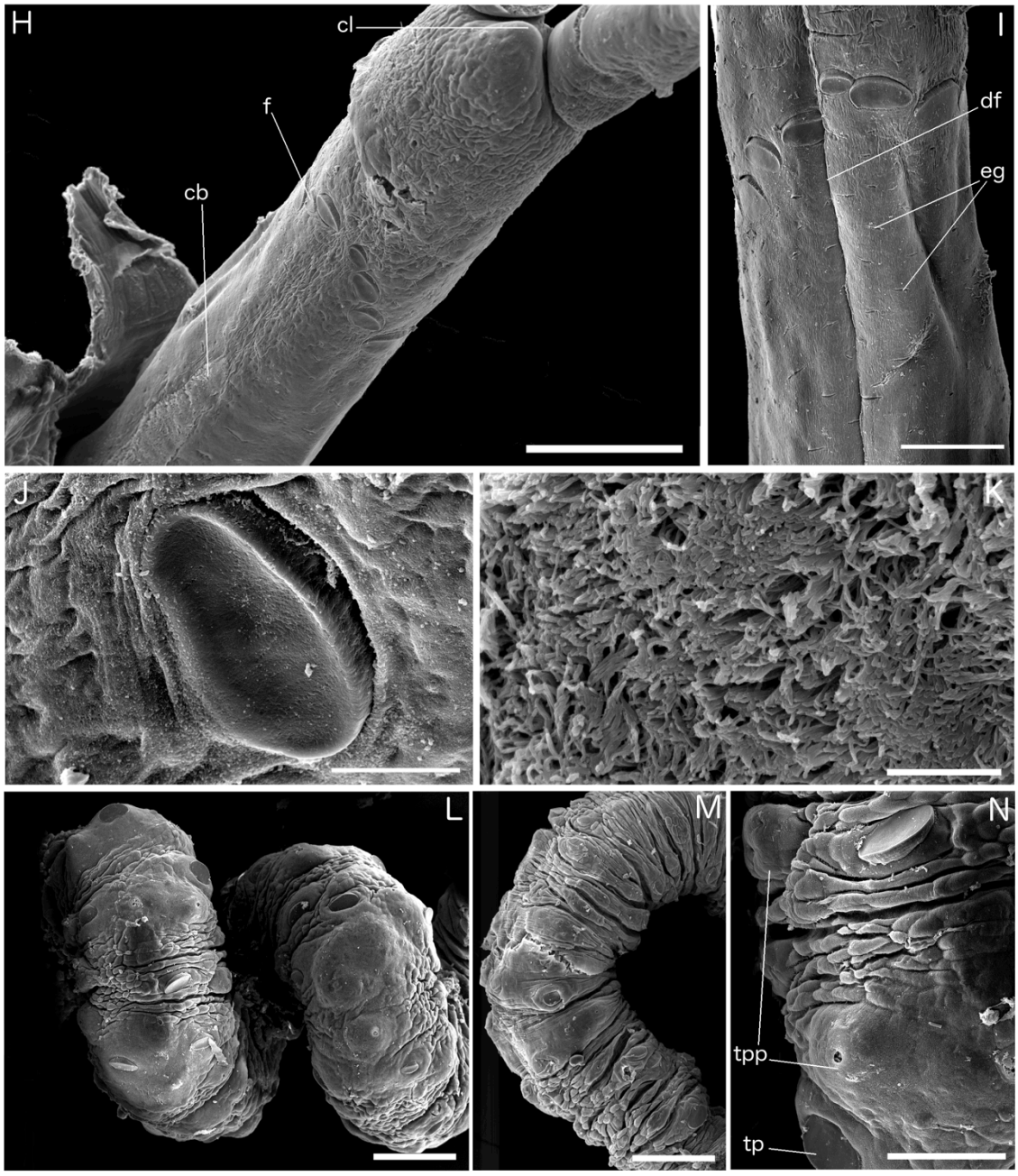

Figure 2.3 Details of tubes and tissues of Antarctic *Sclerolinum contortum*. **A,** anterior section of tube showing more pronounced transverse wrinkles and faint longitudinal wrinkles, scale bar is 200 μm. **B,** posterior section of tube showing a smooth tube wall with attached sediment, scale bar is 200 μm. **C,** detail of tube wall showing its multi-layered, fibrous structure, scale bar is 10 μm. **D,** detail of tube wall interior, scale bar is 5 μm. **E,** anterior portion of a live worm, scale bar is 300 μm. **F,** trunk tissue of a live worm, scale bar is 500 μm. **G,** anterior portion of a worm showing the transition between the forepart and trunk (arrow), scale bar is 500 μm. **H,** the anterior of a worm in ventral view, scale bar is 100 μm. **I,** detail of the frenulum and surrounding gland openings, dorsal view. Scale bar is 50 μm. **J,** detail of a frenular plaque, scale bar is 10 μm. **K,** detail of the ventral ciliary field, scale bar is 5 μm. **L-N,** trunk tissues of a worm, scale bars in **L-M** are 100 μm and 50 μm in **N**. cb – ciliated band; cl – cephalic lobe; df – dorsal furrow; eg – epidermal glands; f – frenulum; tp – trunk plaque; tpp – trunk papillae.

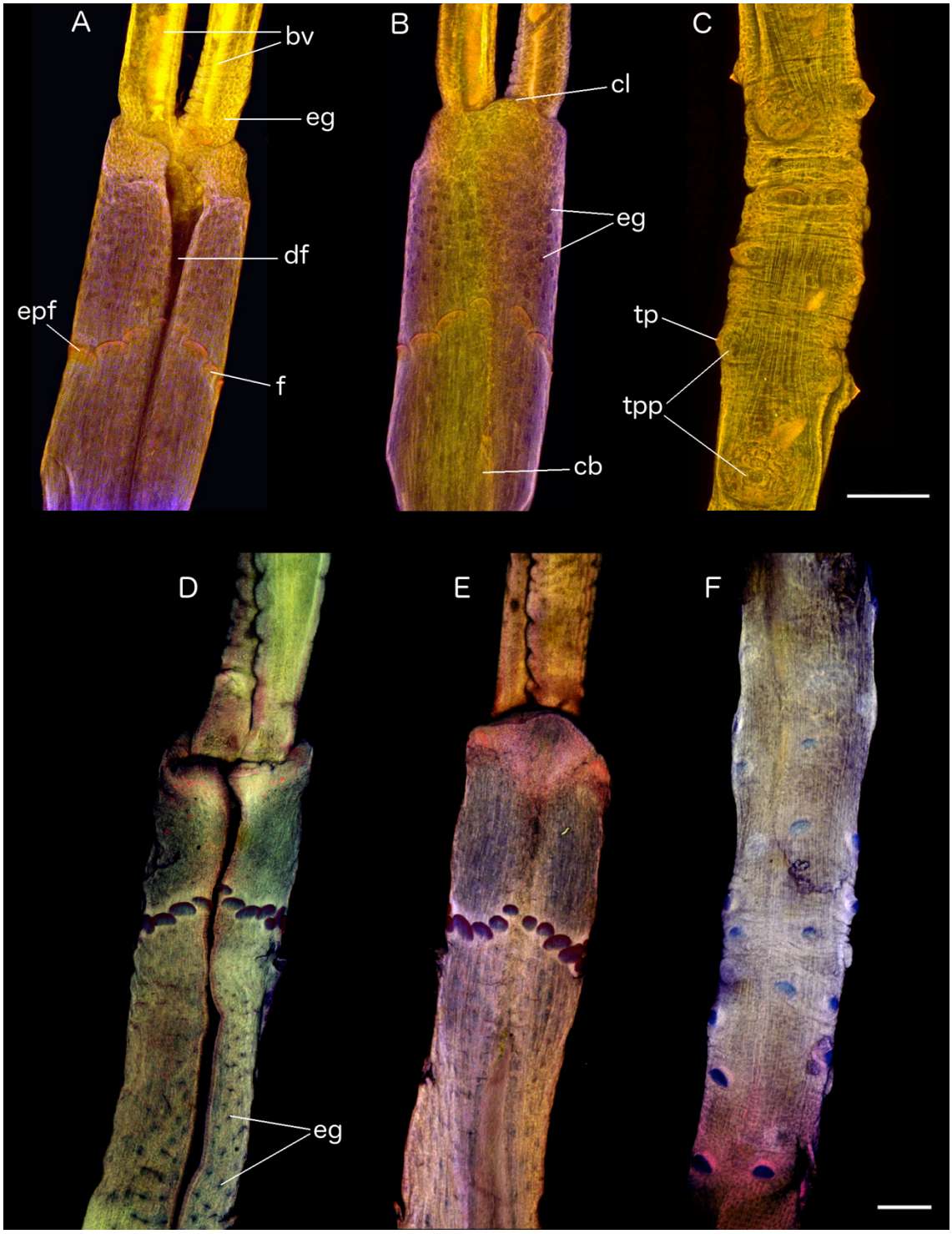

Figure 2.4 Confocal laser scanning microscopy images of *Sclerolinum contortum*. **A-C** show Antarctic *S. contortum*, and **D-F** show *S. contortum* from Loki's Castle. **A, D,** anterior section, dorsal view; **B, E,** anterior section, ventral view; **C, F,** – portion of trunk. All scale bars are 100 μm. bv – blood vessels; cb – ciliated band; cl – cephalic lobe; df – dorsal furrow; eg – epidermal glands; epf – elongated plaque of frenulum; f – frenulum; tp – trunk plaque; tpp – trunk papillae.

Remarks. The conspecificity of Antarctic *Sclerolinum* with HMMV, Loki's Castle and GoM *S. contortum* is strongly supported by genetic data (see later). *S. contortum* (from HMMV) was originally distinguished from all other species in this genus based on its long opisthosoma

with few segments, and a strongly twisted anterior tube region (Smirnov, 2000). The anterior regions of tubes from the Antarctic however lack the characteristic prominent, knot-like contortions that lend *S. contortum* its name, being instead only faintly wavy. These contortions are also absent in some of the Loki's Castle specimens (Figure 2.2). In addition, the GoM population shows that *S. contortum* opisthosoma can be longer than those of *S. magdalenae* (Southward, 1972) and possess a similar number of segments. Hence we do not believe the wavy nature of the tube and the length of the ophisthosome are useful characters to delineate species. *S. magdalenae* also has a similar frenulum to *S. contortum*, making these two species difficult to distinguish based on currently used characters. This raises the question of whether *S. magdalenae* may be the same species as *S. contortum* and thereby represent yet a further example of the wide range of this species; molecular analyses on *S. magdalenae* would be needed to clarify this.

Antarctic *S. contortum* most closely resembles the HMMV population in terms of size (diameter of tube and animal, forepart length, frenular plaque size and number; Supplementary Table B.1). Although animals from the various populations show broad similarity (Figure 2.4) (Smirnov, 2000; Eichinger *et al.*, 2013), this species is known to show pronounced morphological plasticity of its soft tissues (Eichinger *et al.*, 2013) and incorporating data from the Antarctic and Loki's Castle extends the ranges of taxonomic characters for this species even further (Supplementary Table B.1).

Ultrastructurally, tubes do not vary much between the Arctic, GoM and Antarctic populations and all exhibit both transverse and longitudinal wrinkles, while the tube abnormalities pictured in Figure 2.2E are similar to those recorded for *Sclerolinum brattstromi*, *Siboglinum ekmani* and *Siboglinum fiordicum* (Webb, 1964b).

Ecology. Living animals were most abundant at Hook Ridge Site 1, where *S. contortum* has been reported to live at high densities (up to 800 individuals m^{-2} (Sahling *et al.*, 2005)), and tube fragments with tissue were also abundant at Hook Ridge Site 2. However, the distribution of *S. contortum* at Hook Ridge appears to be patchy as one of the megacore samples contained only a single specimen with a head, while another contained 71 individuals (Bell *et al.*, 2015). Worm specimens were not visible within the megacore tubes until the samples were processed, suggesting that the majority of the tubes were buried within sediments. The posterior ends of the tubes were recorded as occurring at 15 cm depth by Sahling et al. (Sahling *et al.*, 2005), where temperatures are approximately 20°C and hydrogen sulphide concentrations reach 150 μm L^{-1}, increasing at greater depths (Aquilina *et al.*, 2014). No temperature anomalies were observed in any sediments during

sampling in 2011 (Aquilina *et al.*, 2014). A fully oxic water column, and oxygen penetration to depths of 2-5 cm into the sediment (Aquilina *et al.*, 2014) require little of the tubes to project above the sediment. *Sclerolinum* is not reported from parts of the Hook Ridge where temperatures reach 49°C and siliceous crusts form over the sediments (Dählmann *et al.*, 2001). SHRIMP (Seafloor High Resolution Imaging Platform) images (Figure 2.5) in the vicinity of Hook Ridge Site 1 give an indication of the habitat of this species. Diffuse hydrothermal flow in this area is evidenced through the presence of what are inferred to be patchy bacterial mats (white patches in Figure 2.5A). These mats also occurred around vent chimneys present at this site (Figure 2.5B) the activity of which is unknown but again no temperature anomaly was observed within the shimmering water emanating from the chimney structure (Aquilina *et al.*, 2013).

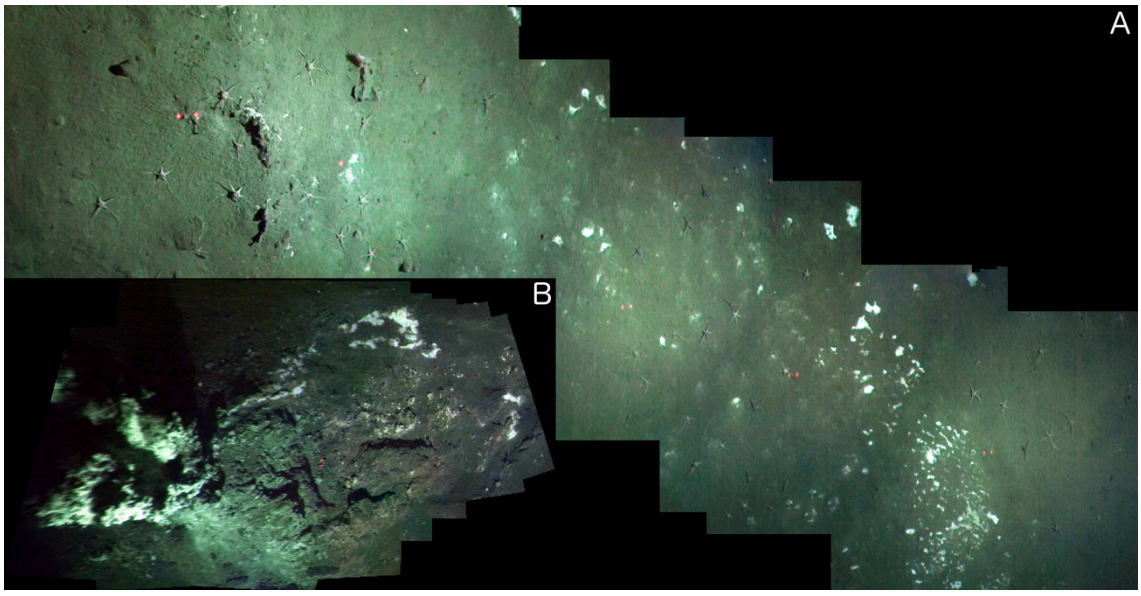

Figure 2.5 SHRIMP images of Hook Ridge, Southern Ocean. Images were taken near to where megacore samples containing the highest density of *Sclerolinum contortum* were collected (maximum of 20 m distance). **A,** soft sediment with bacterial mats; **B,** vent chimney of unknown activity with associated bacterial mats.

Sclerolinum sp. Southward, 1961

(Figure 2.6)

Material examined. *Kemp Caldera*, 59.6948°S 28.35°W, 1432 m depth: JC55_106, lump of sulphurous material attached to sampling gear with embedded tubes. 91 tube fragments

removed from lump, and 4 possible tissue fragments removed from tubes and preserved separately [NHMUK 2015.1159-1166].

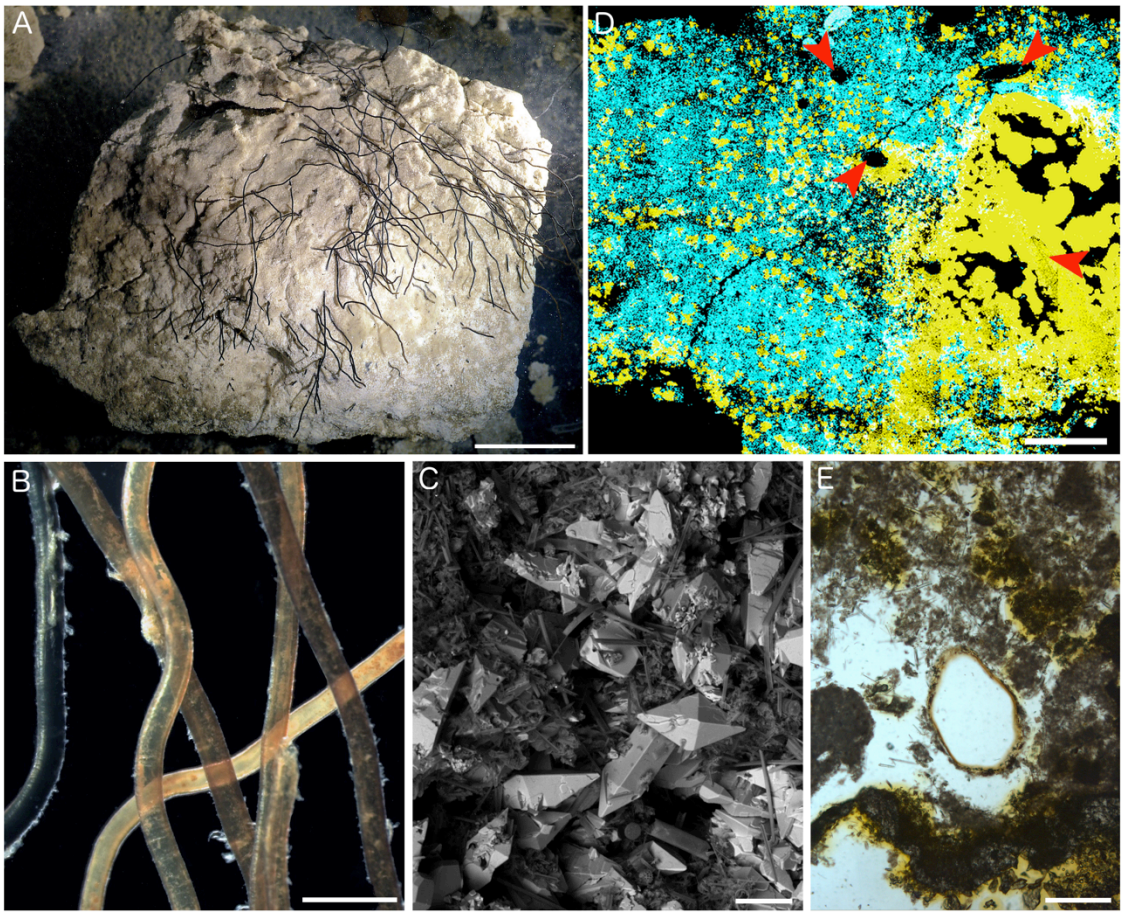

Figure 2.6 Sulphurous lump with embedded *Sclerolinum* tubes collected from Kemp Caldera. **A,** sulphurous lump with embedded *Sclerolinum* tubes collected from Kemp Caldera, scale bar is 30 mm. **B,** detail of the tubes embedded in the sulphurous lump pictured in **A**, scale bar is 1 mm. **C,** SEM image of the surface of subsample of the sulphurous lump, scale bar is 50 μm. The bright crystals in this image showed a large sulphur peak when examined using energy dispersive x-ray spectroscopy (EDS). **D,** EDS elemental map of sulphur lump subsample, yellow colours highlight the distribution of sulphur, blue of silicon. Red arrows show *Sclerolinum* tubes in section, scale bar is 2 mm. **E,** detail of *Sclerolinum* tube section that is embedded within the sulphurous lump, scale bar is 200 μm.

Description. Tubes clustered and tightly embedded into upper surface of sulphurous material (Figure 2.6A), 0.23-0.34 mm in diameter (n = 10) and with a tube wall thickness of approximately 30 μm. Wavy to near straight in appearance. Outer tube surfaces exhibit prominent, irregular transverse wrinkles and faint longitudinal wrinkles (Figure 2.6B). Tube walls are multi-layered and fibrous, and in some cases have a very rough appearance due to fragmentation of outer tube layers. SEM and EDS (energy dispersive x-ray spectroscopy) of the surface of the sulphurous lump shows large crystalline sulphur grains within a silica matrix (Figure 2.6C). When mapped in thin section, sulphur and silica show some zonation

but also many sulphur grains incorporated into areas of silica (Figure 2.6D). *Sclerolinum* tubes are rooted beneath the surface of the sulphur lump, Figure 2.6E shows detail of the sulphurous material with one of the embedded tubes.

Remarks. These tubes show very similar overall and detailed morphology to those made by *Sclerolinum contortum* from Hook Ridge, and it is very likely that they were therefore made by this species, however as no intact animals were found (unidentifiable tissue was present) it was not possible to confirm this. The significant lengths of the tubes (Figure 2.6A) suggest that the colony may have reached maturity, however the absence of good quality animal tissue, the inability to DNA sequence tube contents, and the rough appearance of some of the tube walls suggest that the colony had started degrading and that conditions may have become unfavourable for *Sclerolinum*. The sulphur chunk also demonstrates a pathway through which *Sclerolinum* tubes may fossilise, preserved as *Sclerolinum* tube-shaped voids within its matrix (Figure 2.6D).

Ecology. Areas of diffuse venting within Kemp Caldera would be favourable habitats for *Sclerolinum*, however the occurrence of these animals within such a highly acidic environment, within a substrate composed largely of sulphur has not previously been observed.

2.3.2 Phylogeny and genetic diversity of *S. contortum*

The three combined molecular analysis runs for the family Siboglinidae converged on the same tree topology and near identical posterior probability values (maximum variation of 4%). The 50% majority rule consensus tree (Figure 2.7) indicated overall strong branch support for the monophyly of the major clades of Vestimentifera, *Sclerolinum*, *Osedax* and Frenulata. Antarctic *Sclerolinum* falls within a clade comprised of *S. contortum* from GoM and the Arctic, where GoM worms form a sister group to *S. contortum* from the Arctic and Antarctic *Sclerolinum*, with strong branch support. However, support for the sister relationship between Antarctic *Sclerolinum* and Arctic *S. contortum* is weaker. 18S was identical between *S. brattstromi,* HMMV *S. contortum*, and Antarctic *Sclerolinum*, whereas for 16S, one change (a transversion) was detected between Antarctic *Sclerolinum*, and *S. contortum* from GoM, Loki's Castle and HMMV (*S. brattstromi* 16S was very different). COI K2P (Kimura 2 Parameter) and '*p*' distances within the *Sclerolinum* clade varied from 0% between *S. contortum* populations, to 1.4% between *S. contortum* and Antarctic *Sclerolinum*, and were almost an order of magnitude greater between these taxa and *S. brattstromi* where

the minimum distance detected was 8.8% (Supplementary Table B.2). Within the *S. contortum* clade, the lowest genetic distances occurred between Loki's Castle and HMMV populations, and the greatest between the Arctic and Antarctic populations (Supplementary Table B.2).

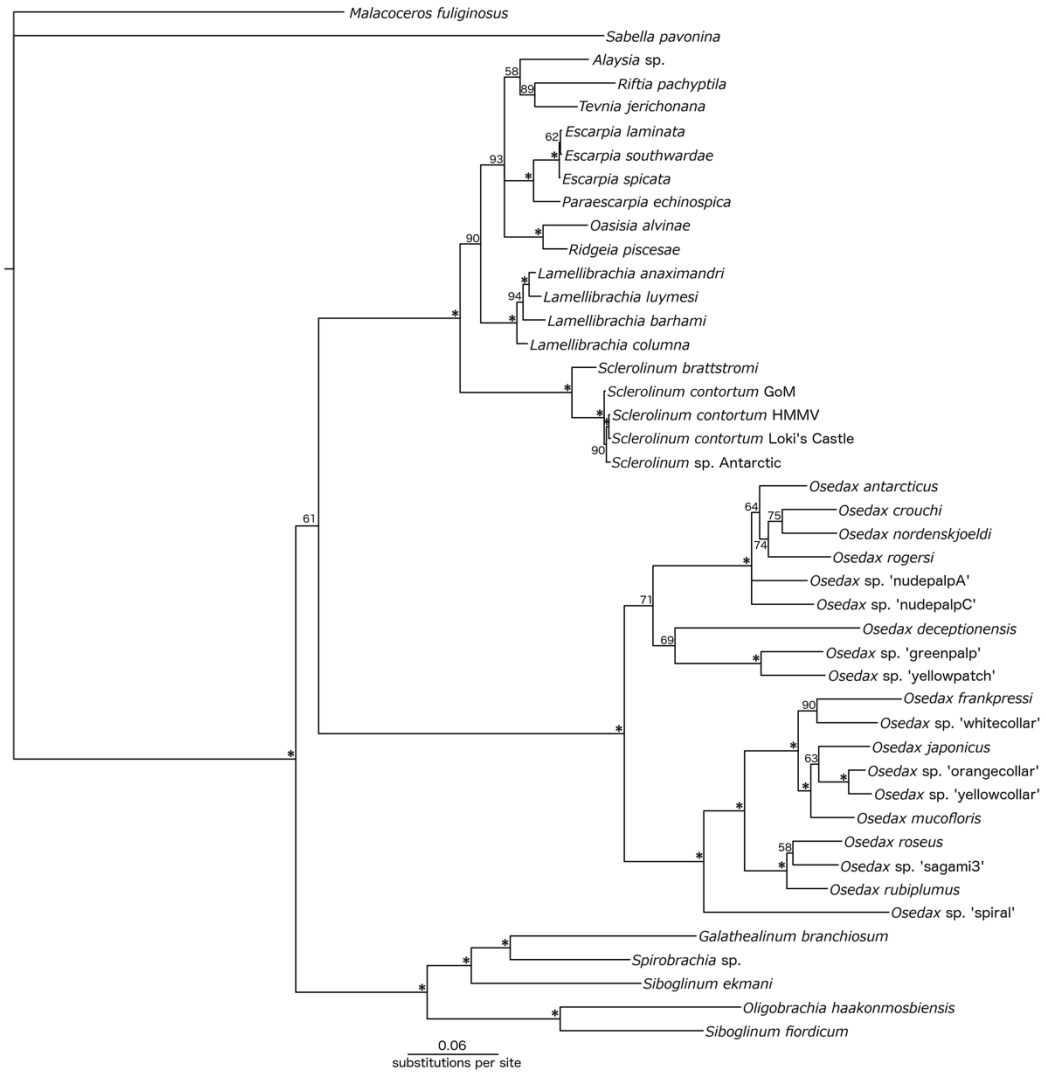

Figure 2.7 Phylogeny of the annelid family Siboglinidae. This analysis was performed by applying a Bayesian approach and using a combined dataset of the three genes COI, 16S and 18S. The phylogeny is a 50% consensus tree, in which numbers represent posterior probability values out of 100, and branches marked with an asterisk (*) indicate posterior probabilities equal to or greater than 95.

The phylogenetic and haplotype analyses based on 65 *S. contortum* COI sequences showed 14 distinct haplotypes (Figure 2.8; Table 2.1; maximum variation of 3% for posterior probability values within the phylogenetic analysis). The number of haplotypes within the Arctic and GoM populations were greater than within the Antarctic population, in which all 27 individuals form a single haplotype despite having the largest sample size. An HMMV individual fell within the same haplotype as Loki's Castle worms, and as genetic

distances were lowest between these two populations (Supplementary Table B.2), HMMV and Loki's Castle sequences were henceforth pooled into a single Arctic population. Nucleotide diversity (π) and mean K2P distances within populations were on the whole low, and a non-synonymous substitution was found within the Arctic population (Table 2.1). The results of the analysis of molecular variance (AMOVA) (Table 2.2) show that the largest percentage of variation occurs between the three regional populations, which also resulted in a large F_{ST} value, whereas within population variation is considerably lower. Pairwise F_{ST} values are high, significant, and increase with distance between populations, being greatest between the Antarctic and Arctic populations and lowest between the Arctic and GoM populations.

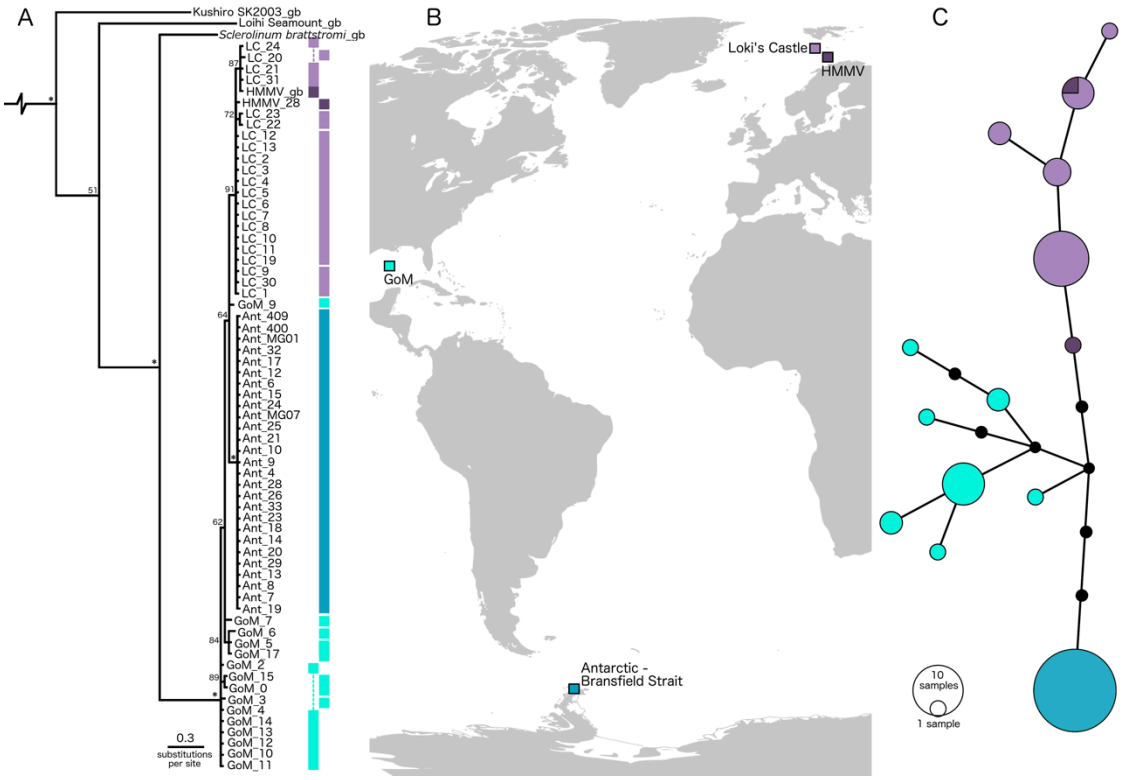

Figure 2.8 Results of phylogenetic and haplotype network analyses for *Sclerolinum contortum*. **A,** phylogeny of *S. contortum* individuals using the COI gene with vertical bars representing haplotype groups, coloured according to population location; HMMV -dark purple, Loki's Castle (prefix LC) – light purple, GoM – light blue, and the Antarctic (prefix Ant) – dark blue. The siboglinids *Riftia pachyptila* and *Siboglinum ekmani* were used as outgroups (not shown), and sequences obtained from NCBI GenBank have the suffix '_gb' (see Supplementary Table B.4 for accession numbers). **B,** map of the Atlantic and part of the Southern Ocean showing the locations of the four *S. contortum* populations used in this study, world map source: Wikipedia (https://en.wikipedia.org/wiki/Contemporary_history#/media/File:WorldMap.svg). **C,** haplotype network constructed using the gene COI, sequenced from animals from four different *S. contortum* populations. Gaps were treated as missing data, and the connection limit was set to 95%. Each line represents one change, and black dots represent missing haplotypes. Haplotype network was drawn using PopART (http://popart.otago.ac.nz).

Table 2.1 Measures of COI sequence variation within *S. contortum* populations**.**

Locality	*N*	No. of haplo-types	Haplotype diversity (h)	Nucleotide diversity (π)	No. of polymorphic sites (S)	No. of synonymous/non-synonymous substitutions	Mean K2P distance (%)
Arctic	23	6	0.700 ±0.088	0.002 ±0.0004	5	4/1	0.2
GoM	15	7	0.781 ±0.102	0.004 ±0.0008	10	10/0	0.4
Antarctic	27	1	0	0	0	0	0
Total	65	14					

N - *sample size, standard deviations are given for h and π.*

Table 2.2 Results of the AMOVA for the various *S. contortum* populations.

Source of variation	Degrees of freedom	Sum of Squares	Variance components	Percentage of variation
Among populations	2	102.573	2.41055 Va	84.5
Within populations	62	27.424	0.44232 Vb	15.5
Total	64	129.997	2.85287	
Fixation index (F_{ST})	0.84496			
Pairwise F_{ST} values				
	Arctic	GoM		
GoM	**0.7211**			
Antarctic	**0.9095**	**0.8621**		

F_{ST} *values in bold are significant ($p < 0.05$).*

2.4 Discussion

2.4.1 First record of a bipolar siboglinid: geographic and genetic patterns

Our data strongly supports the notion that *Sclerolinum contortum* is a bipolar species, with records that span almost 16,000 km from the Arctic to the Antarctic and making it the only siboglinid for which such a range has been observed. Our combined phylogenetic analysis using extended molecular data for the *Sclerolinum* genus demonstrates high levels of similarity of three barcoding genes COI, 16S and 18S between Antarctic *Sclerolinum* and *S. contortum* from the Arctic and GoM, and clearly distinguishes another *Sclerolinum* species (*S. brattstromi*) from this group (Figure 2.7). In addition, the mitochondrial marker COI also differentiates an additional two *Sclerolinum* species from the *S. contortum* clade (Kushiro SK2003 and Loihi Seamount; Figure 2.8). COI genetic distances are more than 6 times greater between *S. contortum* (including the Antarctic population) and *S. brattstromi* compared to within the former clade (Supplementary Table B.2), in which divergence is well below 3%, the generally accepted threshold for delimiting species (Hebert *et al.*, 2003; Carr *et al.*, 2011). The morphology of Antarctic *Sclerolinum* also generally fits within the variation observed for *S. contortum* from other areas, most closely resembling the soft tissue morphology of the most distant population, from HMMV (Supplementary Table B.1).

Classifying Antarctic *Sclerolinum* as *S. contortum* despite the great distances between populations highlights the important taxonomic observation that annelids with very similar morphology and DNA can be spread over vast geographical areas, with their distributions controlled by habitat availability and local ecology.

Bipolarity has so far been observed in only a handful of deep-sea organisms, but demonstrates that steep temperature gradients and limited water exchange between the Southern and surrounding oceans have not completely restricted the spread of deep-sea fauna across these barriers (Chown *et al.*, 2015). Southern Ocean vent sites such as the East Scotia Ridge differ from sites on Mid-Atlantic Ridge and East Pacific Rise in that fauna such as vestimentiferan and alvinellid polychaetes, vesicomyid clams, bathymodiolid mussels, and alvinocaridid shrimp are absent (Rogers *et al.*, 2012). However the ability of *S. contortum* to have migrated across Southern Ocean dispersal barriers suggests that the absence of vestimentiferans at Antarctic vent sites may not be the result of historical dispersal limitation (vicariance). The extensive, bipolar nature of this deep-sea chemosynthetic tubeworm also accentuates that being widespread in the deep-sea is a real and common pattern, with examples supported by molecular data emerging from a variety of additional taxa in recent years (Havermans *et al.*, 2013; O'Hara *et al.*, 2014; Walz *et al.*, 2014; Longmore *et al.*, 2014; Breusing *et al.*, 2015).

Although our data support *S. contortum* conspecificity across the Arctic, GoM and Antarctic, at a population level there is evidence that distance is a barrier to gene flow. While mixing appears to occur between the HMMV and Loki's Castle populations that are separated by approximately 270 km (Figure 2.8), this does not seem to be the case between the Arctic, GoM and Antarctic. Though these three regional populations show very high genetic similarity, the structure presented by the COI haplotype network (Figure 2.8), and the F_{ST} values obtained for population pairs (Table 2.2), suggest that geographic distance does present a barrier to gene flow for this species. This is largely consistent with research into the connectivity of hydrothermal vent vestimentiferans on the EPR, where for both *Riftia pachyptila* and *Tevnia jerichonana* there appears to be little gene flow between the most distant populations of these species (Coykendall *et al.*, 2011; Zhang *et al.*, 2015). Pairwise F_{ST} values between the most distant populations of these two species are similar to those reported for *S. contortum* in this study, however it is obvious that many populations of *S. contortum* are likely to exist between those sampled in this study, and sampling gaps have been found to inflate F_{ST} (Audzijonyte and Vrijenhoek, 2010).

High genetic correspondence with lack of gene flow over large distances is also characteristic of *Escarpia* spp., species of which show high levels of similarity in the mitochondrial genes 16S, COI and cytochrome *b*, but can be differentiated on their morphology, as well as by using a nuclear gene (haemoglobin subunit B2 intron) and microsatellite markers (Cowart *et al.*, 2013). Our interpretation of geographically distant *Sclerolinum* populations belonging to one species contrasts with the division of *Escarpia* into three separate species despite their genetic similarity, however we believe our classification to be justified based on the reasons outlined above, and recommend greater caution in describing genetically-similar but geographically distant populations of siboglinids as new species based on morphology.

Despite the evidence for low gene flow at regional scales, *Sclerolinum contortum* has managed to spread to both poles as well as subtropical latitudes, and the question remains as to how this was achieved. Nothing is presently known of the larvae of *Sclerolinum*, but when the larvae of the vestimentiferan *Riftia pachyptila* are considered, which can disperse 100 km along the EPR ridge axis (Marsh *et al.*, 2001), it is unlikely that *S. contortum* larvae travelled the ~10,000 km between the GoM and Hook Ridge in a single journey. As *S. contortum* appears to be capable of colonising a large range of substrates, dispersal over wide areas through the use of a variety of chemosynthetic habitats as 'stepping stones' (Feldman *et al.*, 1998; Glover *et al.*, 2005) might be the most plausible explanation for this species. Such a hypothesis may be supported by our results which show that there is greater genetic similarity between the spatially closer Arctic and GoM populations, and GoM and Antarctic populations, than there is between the two polar populations (Arctic and Antarctic; Table 2.2). However, the presently known number of *S. contortum* populations is too low to conduct a test for the above scenario, therefore whether this is the best model cannot be resolved at present. Stepping-stone dispersal would suggest that *S. contortum* is more widespread than currently supposed, which does appear to be the case in the Antarctic. The large mass of tubes recovered from Kemp Caldera suggests that *S. contortum* populations come and go, taking advantage of reducing conditions where they are encountered and dying out when these temporary oases dry up.

Such a lifestyle may also explain the low COI haplotype diversity observed within the Antarctic population in comparison to the Arctic and GoM worms used for this study. The Antarctic population may be demonstrating the effects either of a founder event or bottleneck (Fuerst and Maruyama, 1986), where a founder effect may arise as a result of a number of opportunistic *S. contortum* individuals finding suitable conditions and settling at

Hook Ridge, and persisting in the sustained diffuse hydrothermal flow at this site. However, the ephemeral nature of hydrothermal circulation within the Bransfield Strait (Aquilina *et al.*, 2013), and repeated glacial-interglacial events affecting the Southern Ocean mean that it may also be plausible for the Antarctic *S. contortum* population to have undergone a bottleneck (loss of genetic diversity following a population crash) (Riesgo *et al.*, 2015). Evidence of a genetic bottleneck linked to glacial cycles has been detected for a number of Antarctic species (see (Allcock and Strugnell, 2012) for a review), and ultimately more samples from a wider area of the Southern Ocean would be required to test this in *S. contortum*. *Sclerolinum* has also been shown to be capable of asexual reproduction via breaking and regenerating missing ends (Webb, 1964c; Southward, 1999), which may also account for the low genetic diversity of the Antarctic population.

There is currently no fossil record for *Sclerolinum*. As well as demonstrating a pathway through which *Sclerolinum* tubes may become preserved in the fossil record, this study shows that any future reports of *Sclerolinum* fossil discovery should be mindful of the following: fossils found in a range of ancient chemosynthetic environments, from very distant parts of the world, and exhibiting varying degrees of tube contortion may belong to the same species. Recent reports of Cretaceous *Osedax* fossils (Danise and Higgs, 2015) imply that Siboglinidae has more ancient origins than indicated by molecular clock estimates (Halanych *et al.*, 1998; Chevaldonné *et al.*, 2002; Hurtado, 2002), suggesting that the widespread distribution, morphological and habitat plasticity exhibited by *Sclerolinum* may have contributed to the survival of this genus over long evolutionary timescales too (Jablonski, 1991).

2.4.2 Natural history of *S. contortum* in the Southern Ocean

We have shown that *S. contortum* can exhibit even greater morphological plasticity than was previously noted for this species by Eichinger *et al.* (2013). Much of this plasticity is in the tubes constructed by this worm after which the species is named. Tube morphology may be a condition that is dictated by environmental factors, as has previously been shown for the highly plastic tubes built by the vent dwelling vestimentiferan *Ridgeia piscesae* (Southward *et al.*, 1995). Environmental factors can also influence the physiology of these worms, thereby affecting their genetic diversity (Tunnicliffe *et al.*, 2014). While environmental parameters were not measured by the present study, we speculate that contortion of the anterior of *S. contortum* tubes increases their surface area to volume ratio, thus improving

the efficiency of oxygen uptake and may therefore result from settlement in lower oxygen conditions.

The obvious morphological plasticity of *Sclerolinum contortum* is matched by its remarkable ecological and habitat plasticity. With our new data from the Antarctic we can now show that it is able to colonise a vast range of chemosynthetic habitats including high-temperature acidic white smoker vent fields, low-temperature sedimented diffuse vent fields, hydrocarbon cold seeps and mud volcanoes. Chemosynthetic invertebrates have been likened to terrestrial weeds (Baker, 1974) in virtue of their ability to colonise ephemeral/disturbed environments, as well as their effective dispersal, rapid growth rates, and early reproduction (Van Dover *et al.*, 2002; Vrijenhoek, 2010), and in this sense, we can also think of *S. contortum* as a 'chemosynthetic weed' due to its ability to quickly populate a wide range of sulphur-rich habitats and spread over great distances.

Weedy species can have a dramatic influence on the environments they colonise. Their impacts are well-documented particularly in reference to terrestrial non-native species, and have demonstrated the ability of weedy species to have pronounced ecosystem, community and population-level effects (Macdonald *et al.*, 1989; Gordon, 1998). Supporting the concept of the *Sclerolinum* weed is the observation that the species can have dramatic influence on the biogeochemistry of the sediment at the sediment-hosted Bransfield hydrothermal vents (Aquilina *et al.*, 2014). Along with the maldanid *Nicomache lokii*, *S. contortum* forms a complex three-dimensional habitat for free-living invertebrates at Loki's Castle (Kongsrud and Rapp, 2012), as well as in the Nyegga seep area of the Storegga Slide where filamentous bacteria cover *S. contortum* tube surfaces, thereby also providing substrate and food for associated organisms (Vanreusel *et al.*, 2009). *S. contortum* therefore represents an important keystone species within the range of reducing environments it inhabits.

2.5 Conclusions

Since their initial discovery alongside hydrothermal vent chimneys in the late 1970s, siboglinid worms have continued to surprise and amaze with their unusual adaptations to a mode of life in the deep sea dependant solely on endosymbionts. By investigating in detail the DNA, morphology and a novel inhabiting substrate of the very poorly studied *Sclerolinum* genus, the present study has found that they too conform to this pattern, by possessing extraordinary morphological and ecological plasticity that has allowed them to

occupy a remarkable range that spans across all of the world's oceans. However, fundamental knowledge of the biology of these worms is still lacking - there is presently no information on *Sclerolinum* reproduction, larvae and their dispersal, and symbionts from the range of chemosynthetic environments which this genus occupies. We therefore suggest these areas as potential directions for future research into this group.

2.6 Methods

2.6.1 Sample collection

Antarctic sample collection was conducted on board RRS *James Cook* expedition JC55 during January-February 2011 (Table 2.3), during which *Sclerolinum* was collected from two locations: Hook Ridge, Bransfield Strait, and Kemp Caldera. At Hook Ridge, venting occurs through sediment as low temperature discharge of phase-separated fluids that are highly diluted by seawater (Aquilina *et al.*, 2013). At Kemp Caldera, both hot and diffuse venting has been found that is characterised by unusual, highly acidic and sulphidic fluid composition. At a site named 'Winter Palace', crumbly chimneys release white smoker-type hydrothermal fluids up to 212°C, while at 'Great Wall' a seafloor fissure releases low temperature diffuse fluids from which sulphur-rich minerals precipitate (Cole *et al.*, 2014; Copley *et al.*, *unpublished data*).

Samples were obtained using a Bowers & Connelly megacorer fitted with multiple 10 cm-diameter polycarbonate core tubes. *Sclerolinum* sp. tubes containing animal tissues and empty *Sclerolinum* sp. tubes were collected from two Hook Ridge sites, Hook Ridge Site 1 and Hook Ridge Site 2 (Figure 2.1; Table 2.3). *Sclerolinum* sp. tubes from Kemp Caldera were acquired using a gravity corer, to which a sulphurous lump containing embedded tubes had become attached. Possible Siboglinidae tube fragments were collected from The Axe and Bransfield Off-vent, the latter comprising a non-active site located approximately 21 km south of the Hook Ridge sites. Samples were preserved in 80% ethanol or 6% formalin on board the ship. SHRIMP was used to visualise the seabed within a 20 m radius of Hook Ridge Site 1. *S. contortum* specimens from Loki's Castle and HMMV, Arctic Ocean, and the GoM (Appendix B: Methods Supplement) were used for morphological and genetic comparisons with Antarctic *Sclerolinum* sp. (Table 2.3).

Table 2.3 Collection details of Siboglinidae specimens examined within this study.

Locality	Taxon	Site	Latitude	Longitude	Depth (m)	No. of tube fragments*
Antarctic	*Sclerolinum* sp.	Hook Ridge Site 1	-62.1969	-57.2975	1174	686*
		Hook Ridge Site 2	-62.1924	-57.2783	1054	87*
		Kemp Caldera	-59.6948	-28.35	1432	95*
Arctic	*S. contortum*	Loki's Castle CG2009	73.5662	8.1585	2357	33*
		Loki's Castle CG2008	73.5662-73.5683	8.1585-8.1563	-	8*
		HMMV CG2010	71.9975-71.9999	14.7329-14.7316	1262	1*
		HMMV VICKING 2006	72.0013	14.7225	1270	50+
GoM	*S. contortum*	Walker Ridge WR269	26.6833	-91.65	1954	21*

Asterisk (*) denotes samples within which a subset of the tube fragments contained animal tissues.

2.6.2 Morphological and compositional analysis

Taxonomic characters were measured in 10 Antarctic and 10 Loki's Castle worms. Unfortunately no complete animals were found, therefore only characters of the anterior and trunk regions of the worms were recorded. Tubes were either cut around sections of the worms, or they were visualised through their tubes using a ZEISS Discovery V.20 stereomicroscope. Measurements were performed using ZEISS AxioVision digital processing software as well as ImageJ (version 1.46r). To visualise taxonomic characters more clearly, sections of Antarctic and Loki's Castle worms were cut out of their tubes, and imaged using laser-induced autofluorescence within a Nikon A1-Si Confocal microscope at the Natural History Museum, UK (NHM), operated in spectral imaging mode. In addition, the forepart and trunk regions of a *Sclerolinum* sp. worm fragment from the Antarctic were critical-point dried, coated in gold-paladium, and imaged using a secondary electron detector within a FEI Quanta 650 FEG-ESEM (NHM).

A subsection of the sulphurous lump with embedded *Sclerolinum* sp. tubes (recovered from Kemp Caldera, Southern Ocean) was viewed within a LEO 1455VP SEM (at the NHM), and point EDS spectra were obtained from its surface within the same SEM. The subsection was then prepared into a polished thin section and its elemental composition was mapped using EDS within a Carl Zeiss Ultra Plus Field Emission SEM, also at the NHM.

2.6.3 Phylogenetic sequencing and analyses

Total genomic DNA was extracted from 64 *Sclerolinum* worm fragments: 27 Antarctic *Sclerolinum* sp., 15 *S. contortum* from the GoM, 21 *S. contortum* from Loki's Castle, and one *S. contortum* individual from HMMV. Worm fragments with tentacles and forepart, and long worm fragments were selected for extractions to increase the likelihood of sampling from different individuals. DNA extractions of Antarctic and GoM specimens were performed using a Hamilton Microlab STAR Robotic Workstation combined with a DNeasy kit (Qiagen, Valencia, CA). Approximately 400 bp of the mitochondrial gene 16S, 600 bp of the mitochondrial gene COI, and 840-1370 bp of the nuclear 18S gene were amplified (all primers used for PCRs and sequencing are listed in Supplementary Table B.3). PCR mixtures for Antarctic and GoM specimens contained 1 µl of each primer (10µM), 2 µl of DNA template, and 21 µl of *Taq* PCR Master Mix (Qiagen). The PCR profile was as follows: 94ºC/300s, (94ºC/60s, 50ºC/60s, 72ºC/120s)*35cycles, 72ºC/300s. PCR products were visualised on 1.5% agarose gels following electrophoresis, and sequenced using an Applied Biosystems 3730XL DNA Analyser at the NHM. DNA extraction and PCR of Arctic specimens (Loki's Castle and HMMV) were carried out at the Biodiversity Laboratories, University of Bergen (BDL, DNA-lab section, Department of Biology) where an Applied Biosystems 3730XL DNA Analyser was used for sequencing. The PCR mixtures for amplification of 16S and COI contained 1 µl of each primer (10µM), 1 µl of DNA template, 2.5 µl Qiagen CoralLoad buffer (10x), 1µl Qiagen MgCl (25 µM), 2 µl dNTPs (TaKaRa; 2.5 µM of each dNTP), 0.15 µl TaKaRa HS taq, and 16.35 µl PCR water. The PCR profile for 16S was as follows: 95ºC/300s, (95ºC/30s, 50ºC/30s, 72ºC/90s)*35 cycles, 72ºC/600s, while the following profile was used for COI: 95ºC/300s, (95ºC/45s, 45ºC/45s, 72ºC/60s)*5 cycles, (95ºC/45s, 51ºC/45s, 72ºC/60s)*35 cycles, 72ºC/600s. In total, 16S was sequenced for 28 worm fragments, COI for 64, and 18S for two worm fragments.

Molecular phylogenetic analyses were performed using a combined dataset of 16S, COI and 18S sequences for members of the family Siboglinidae. A total of 44 terminal taxa were included in the analyses, of which five were *Sclerolinum*, and 39 were from other Siboglinidae genera. For the above analyses 111 sequences were obtained from NCBI Genbank, accession numbers for which are listed in Supplementary Table B.4. The sabellid *Sabella pavonina* and spionid *Malacoceros fuliginosus* were used as outgroup taxa, of which *M. fuliginosus* was used to root the tree. Outgroup choice was based on the analyses of Rousset et al. (2004) and Weigert et al. (2014). Overlapping sequence fragments were concatenated

into consensus sequences using Geneious (Kearse *et al.*, 2012), and aligned using the following programs (provided as plug-ins in Geneious): MUSCLE for COI (Edgar, 2004), and MAFFT for 18S and 16S (Katoh *et al.*, 2002). The evolutionary models used for each gene were selected using jModelTest (Posada, 2008). Based on the Akaike Information Criterion (AIC), the best fitting models of nucleotide substitution were TIM1+I+G for COI and 18S, and TIM2+G for 16S. As the model GTR+I+G is the closest approximation of the TIM models available in MrBayes, the GTR+I+G model was used for all three genes in the combined analysis. A Bayesian molecular phylogenetic analysis was conducted using MrBayes 3.1.2 (Ronquist and Huelsenbeck, 2003). Analyses of the combined dataset were run three times for 10,000,000 generations, with 2,500,000 generations discarded as burn-in. Genetic distances for the COI gene within the genus *Sclerolinum* were calculated using the K2P model, and *p*-distances were determined in MEGA 5.1 (Tamura *et al.*, 2011).

2.6.4 Genetic diversity

A close relationship between Antarctic *Sclerolinum* sp. and *S. contortum* was detected from the above investigations, therefore an additional alignment was used for a phylogenetic analysis using a total of 68 COI *Sclerolinum* sp. sequences (*S. brattstromi*, Kushiro-SK-2003 *Sclerolinum* sp., Loihi Seamount *Sclerolinum* sp., 27 Antarctic *Sclerolinum* sp., 15 GoM, 21 Loki's Castle, and 2 HMMV *S. contortum*) for which two additional siboglinid COI sequences (*Riftia pachyptila* and *Siboglinum ekmani*) were used as outgroups. The alignment was trimmed to standardise sequence lengths, and the analysis was performed in the same way as the combined analysis outlined above. In addition, a haplotype distribution was created using only Antarctic *Sclerolinum* sp. and *S. contortum* sequences in TCS 1.21 (Clement *et al.*, 2000) and drawn in PopART (http://popart.otago.ac.nz). Gaps were treated as missing data, and the connection limit was set to 95%. There appeared to be little genetic differentiation between HMMV and Loki's Castle *S. contortum* therefore sequences from these localities were subsequently pooled into one Arctic population, while GoM *S. contortum* and Antarctic *Sclerolinum* sp. were treated as two additional populations. Haplotype diversity, nucleotide diversity, and number of polymorphic sites were calculated within each population (Arctic, GoM and Antarctic) using DnaSP 5.10.1 (Librado and Rozas, 2009). Average genetic distances (K2P) within each population were calculated using MEGA 5.1 (Tamura *et al.*, 2011). Pairwise F_{ST} values and an AMOVA were computed using Arlequin 3.5.1.3

(Excoffier and Lischer, 2010). The AMOVA was performed using K2P distances and 1000 permutations.

2.6.5 Ethics statement

Ethics approval is not required for the collection and investigation of the morphology and DNA of annelid worms. Antarctic specimens were collected under the Foreign and Commonwealth Office Antarctic permit number S5-4/2010 issued to National Marine Facilities for the JC55 research expedition. Permits were not required by the collectors of Arctic and Gulf of Mexico material.

2.7 Availability of supporting data

Morphological data supporting the results of this article are included within Appendix B: Supplementary Table B.1. Occurrence data on specimens used in this study (in DarwinCore Archive format) and additional data sets (DNA sequence alignments) are available in the figshare repository (http://dx.doi.org/10.6084/m9.figshare.1613855). DNA sequences are available in GenBank (http://www.ncbi.nlm.nih.gov/genbank/), with NCBI accession numbers detailed in Supplementary Table B.4 (a sequence for each detected *Sclerolinum contortum* COI haplotype is available).

2.8 Acknowledgements

We would like to thank the masters and crews of the NERC 'Chemosynthetically-driven ecosystems in the Southern Ocean' (ChEsSo) research cruise on RRS *James Cook* JC055 (Professor Paul Tyler PI), the National Oceanography Centre technicians who operated the SHRIMP and ROV *Isis* platforms, the University of Bergen Centre for Geobiology expeditions on RV G. O. Sars during 2008-2010, the NOAA *Ronald H. Brown* expedition no. RB-07-04, and the 2006 VICKING cruise on board R/V *Pourquoi pas?* for their help in collecting specimens used in this study. We are also especially indebted to the following scientists for their generous donations of material for use in this study: Prof. Hans Tore Rapp and Dr. Jon Anders Kongsrud for material from Loki's Castle hydrothermal vent field, Prof. Monika Bright for material from the Gulf of Mexico, and Dr. Ann Andersen

for material from Håkon Mosby Mud Volcano. Thank you to Laura Hepburn for guidance regarding sulphur lump analyses, and to Dr. Gabrielle Kennaway, and Tony Wighton (NHM) for their help in the preparation of thin sections. Thank you also to Bob Vrijenhoek and Shannon Johnson for valuable comments on this work. MG is funded by NERC CASE PhD studentship no. NE/K500847/1. JB is funded by NERC CASE PhD studentship no. NE/L501542/1. The ChEsSo programme was funded by a NERC Consortium Grant (NE/DO1249X/1) which is gratefully acknowledged.

2.9 References

Allcock, A. L. and Strugnell, J. M. (2012) Southern Ocean diversity: New paradigms from molecular ecology. *Trends in Ecology and Evolution* **27**, 520–528. doi:10.1016/j.tree.2012.05.009.

Amon, D. J., Glover, A. G., Wiklund, H., Marsh, L., Linse, K., Rogers, A. D. and Copley, J. T. (2013) The discovery of a natural whale fall in the Antarctic deep sea. *Deep-Sea Research II* **92**, 87–96. doi:10.1016/j.dsr2.2013.01.028.

Aquilina, A., Connelly, D. P., Copley, J. T., Green, D. R. H., Hawkes, J. A., Hepburn, L. E., Huvenne, V. A. I., Marsh, L., Mills, R. A. and Tyler, P. A. (2013) Geochemical and visual indicators of hydrothermal fluid flow through a sediment-hosted volcanic ridge in the central Bransfield basin (Antarctica). *PLOS ONE* **8**, e54686. doi:10.1371/journal.pone.0054686.

Aquilina, A., Homoky, W. B., Hawkes, J. A., Lyons, T. W. and Mills, R. A. (2014) Hydrothermal sediments are a source of water column Fe and Mn in the Bransfield Strait, Antarctica. *Geochimica et Cosmochimica Acta* **137**, 64–80. doi:10.1016/j.gca.2014.04.003.

Audzijonyte, A. and Vrijenhoek, R. C. (2010) When gaps really are gaps: Statistical phylogeography of hydrothermal vent invertebrates. *Evolution* **64**, 2369–2384.

Baker, H. G. (1974) The evolution of weeds. *Annual Review of Ecology and Systematics* **5**, 1–24. doi:10.1146/annurev.es.05.110174.000245.

Bano, N., Ruffin, S., Ransom, B. and Hollibaugh, J. (2004) Phylogenetic composition of Arctic Ocean Archaeal assemblages and comparison with Antarctic assemblages. *Applied and Environmental Microbiology* **70**, 781–789.

Bell, J. B., Woulds, C., Brown, L. E., Little, C. T. S., Sweeting, C. J., Reid, W. D. and Glover, A. G. (2015) Macrofaunal ecology of sedimented hydrothermal vents in the Bransfield Strait, Antarctica. *Frontiers in Marine Science* **3**, 32. doi:10.3389/fmars.2016.00032.

Brandt, A., De Broyer, C., De Mesel, I., Ellingsen, K. E., Gooday, A. J., Hilbig, B., Linse, K., Thomson, M. R. A. and Tyler, P. A. (2007) The biodiversity of the deep Southern Ocean benthos. *Philosophical Transactions of the Royal Society B* **362**, 39–66. doi:10.1098/rstb.2006.1952.

Breusing, C., Johnson, S. B., Tunnicliffe, V. and Vrijenhoek, R. C. (2015) Population structure and connectivity in Indo-Pacific deep-sea mussels of the *Bathymodiolus septemdierum* complex. *Conservation Genetics* **16**, 1415-1430. doi:10.1007/s10592-015-0750-0.

Brinkmeyer, R., Knittel, K., Jürgens, J., Weyland, H., Amann, R. and Helmke, E. (2003) Diversity and structure of bacterial communities in Arctic versus Antarctic pack ice. *Applied and Environmental Microbiology* **69**, 6610–6619.

Brix, S., Riehl, T. and Leese, F. (2011) First genetic data for species of the genus *Haploniscus* Richardson, 1908 (Isopoda: Asellota: Haploniscidae) from neighbouring deep-sea basins in the South Atlantic. *Zootaxa* **2838**, 79–84.

Carr, C. M., Hardy, S. M., Brown, T. M., Macdonald, T. A. and Hebert, P. D. N. (2011) A tri-oceanic perspective: DNA barcoding reveals geographic structure and cryptic diversity in Canadian polychaetes. *PLOS ONE* **6**, e22232. doi:10.1371/journal.pone.0022232.

Chevaldonné, P., Jollivet, D., Desbruyeres, D., Lutz, R. and Vrijenhoek, R. C. (2002) Sister-species of eastern Pacific hydrothermal vent worms (Ampharetidae, Alvinellidae, Vestimentifera) provide new mitochondrial COI clock calibration. *Cahiers Biologie Marine* **43**, 367–370.

Chown, S. L., Clarke, A., Fraser, C. I., Cary, S. C., Moon, K. L. and McGeoch, M. A. (2015) The changing form of Antarctic biodiversity. *Nature* **522**, 431–438. doi:10.1038/nature14505.

Clement, M., Posada, D. and Crandall, K. (2000) TCS: a computer program to estimate gene genealogies. *Molecular Ecology* **9**, 1657–1660.

Cole, C. S., James, R. H., Connelly, D. P. and Hathorne, E. C. (2014) Rare earth elements as indicators of hydrothermal processes within the East Scotia subduction zone

system. *Geochimica et Cosmochimica Acta* **140**, 20–38. doi:10.1016/j.gca.2014.05.018.

Cowart, D. A., Huang, C., Arnaud-Haond, S., Carney, S. L., Fisher, C. R. and Schaeffer, S. W. (2013) Restriction to large-scale gene flow vs. regional panmixia among cold seep *Escarpia* spp. (Polychaeta, Siboglinidae). *Molecular Ecology* **22**, 4147–4162. doi:10.1111/mec.12379.

Coykendall, D. K., Johnson, S. B., Karl, S. A., Lutz, R. A. and Vrijenhoek, R. C. (2011) Genetic diversity and demographic instability in *Riftia pachyptila* tubeworms from eastern Pacific hydrothermal vents. *BMC Evolutionary Biology* **11**, 96. doi:10.1186/1471-2148-11-96.

Dählmann, A., Wallmann, K., Sahling, H., Sarthou, G., Bohrmann, G., Petersen, S., Chin, C. S. and Klinkhammer, G. P. (2001) Hot vents in an ice-cold ocean: Indications for phase separation at the southernmost area of hydrothermal activity, Bransfield Strait, Antarctica. *Earth and Planetary Science Letters* **193**, 381–394. doi:10.1016/S0012-821X(01)00535-0.

Dando, P. R., Southward, A. J., Southward, E. C., Lamont, P. and Harvey, R. (2008) Interactions between sediment chemistry and frenulate pogonophores (Annelida) in the north-east Atlantic. *Deep-Sea Research I* **55**, 966–996. doi:10.1016/j.dsr.2008.04.002.

Danise, S. and Higgs, N. D. (2015) Bone-eating *Osedax* worms lived on Mesozoic marine reptile deadfalls. *Biology Letters* **11**, 20150072.

Domack, E., Ishman, S., Leventer, A., Sylva, S., Willmott, V. and Huber, B. (2005) A chemotrophic ecosystem found beneath Antarctic Ice Shelf. *Eos, Transactions, American Geophysical Union* **86**, 269–276. doi:10.1029/2005EO290001.

Dubilier, N., Bergin, C. and Lott, C. (2008) Symbiotic diversity in marine animals: the art of harnessing chemosynthesis. *Nature Reviews Microbiology* **6**, 725–740. doi:10.1038/nrmicro1992.

Edgar, R. C. (2004) MUSCLE: multiple sequence alignment with high accuracy and high throughput. *Nucleic Acids Research* **32**, 1792–1797.

Eichinger, I., Hourdez, S. and Bright, M. (2013) Morphology, microanatomy and sequence data of *Sclerolinum contortum* (Siboglindae, Annelida) of the Gulf of Mexico. *Organisms Diversity and Evolution* **13**, 311–329. doi:10.1007/s13127-012-0121-3.

Excoffier, L. and Lischer, H. (2010) Arlequin suite version 3.5: a new series of programs to perform population genetics analyses under Linux and Windows. *Molecular Ecology*

Resources **10**, 564–567.

Feldman, R., Shank, T., Black, M., Baco, A., Smith, C. and Vrijenhoek, R. (1998) Vestimentiferan on a whale fall. *Biological Bulletin* **194**, 116–119.

Fuerst, P. A. and Maruyama, T. (1986) Considerations on the conservation of alleles and of genic heterozygosity in small managed populations. *Zoo Biology* **5**, 171–179.

Gaudron, S. M., Pradillon, F., Pailleret, M., Duperron, S., Le Bris, N. and Gaill, F. (2010) Colonization of organic substrates deployed in deep-sea reducing habitats by symbiotic species and associated fauna. *Marine Environmental Research* **70**, 1–12. doi:10.1016/j.marenvres.2010.02.002.

German, C. R., Livermore, R. A., Baker, E. T., Bruguier, N. I., Connelly, D. P., Cunningham, A. P., Morris, P., Rouse, I. P., Statham, P. J. and Tyler, P. A. (2000) Hydrothermal plumes above the East Scotia Ridge: an isolated high-latitude back-arc spreading centre. *Earth and Planetary Science Letters* **184**, 241–250.

Glover, A. G., Källström, B., Smith, C. R. and Dahlgren, T. G. (2005) World-wide whale worms? A new species of *Osedax* from the shallow north Atlantic. *Proceedings of the Royal Society B* **272**, 2587–2592. doi:10.1098/rspb.2005.3275.

Goffredi, S. K., Hurtado, L. A., Hallam, S. and Vrijenhoek, R. C. (2003) Evolutionary relationships of deep-sea vent and cold seep clams (Mollusca: Vesicomyidae) of the "*pacifica/lepta*" species complex. *Marine Biology* **142**, 311–320. doi:10.1007/s00227-002-0941-3.

Gordon, D. R. (1998) Effects of invasive, non-indigenous plant species on ecosystem processes: Lessons from Florida. *Ecological Applications* **8**, 975–989.

Hahm, D., Baker, E. T., Rhee, T. S., Won, Y.-J., Resing, J. A., Lupton, J. E., Lee, W.-K., Kim, M. and Park, S.-H. (2015) First hydrothermal discoveries on the Australian-Antarctic Ridge: Discharge sites, plume chemistry, and vent organisms. *Geochemistry, Geophysics, Geosystems* **16**,. doi:10.1002/2015GC005926.

Halanych, K., Lutz, R. and Vrijenhoek, R. (1998) Evolutionary origins and age of vestimentiferan tube-worms. *Cahiers Biologie Marine* **39**, 355–358.

Havermans, C., Sonet, G., d'Acoz, C. D., Nagy, Z. T., Martin, P., Brix, S., Riehl, T., Agrawal, S. and Held, C. (2013) Genetic and morphological divergences in the cosmopolitan deep-sea amphipod *Eurythenes gryllus* reveal a diverse abyss and a bipolar species. *PLOS ONE* **8**, e74218. doi:10.1371/journal.pone.0074218.

Hebert, P., Ratnasingham, S. and DeWaard, J. (2003) Barcoding animal life: cytochrome c oxidase subunit 1 divergences among closely related species. *Proceedings of the Royal Society B* **270**, S96–99.

Herrera, S., Shank, T. M. and Sánchez, J. A. (2012) Spatial and temporal patterns of genetic variation in the widespread antitropical deep-sea coral *Paragorgia arborea*. *Molecular Ecology* **21**, 6053–6067. doi:10.1111/mec.12074.

Hilário, A., Capa, M., Dahlgren, T. G., Halanych, K. M., Little, C. T. S., Thornhill, D. J., Verna, C. and Glover, A. G. (2011) New perspectives on the ecology and evolution of siboglinid tubeworms. *PLOS ONE* **6**, e16309. doi:10.1371/journal.pone.0016309.

Hilário, A., Metaxas, A., Gaudron, S. M., Howell, K. L., Mercier, A., Mestre, N. C., Ross, R. E., Thurnherr, A. M. and Young, C. (2015) Estimating dispersal distance in the deep sea: challenges and applications to marine reserves. *Frontiers in Marine Science* **2**, 1–14. doi:10.3389/fmars.2015.00006.

Hurtado, L. A. (2002) Evolution and biogeography of hydrothermal vent organisms in the Eastern Pacific Ocean. PhD Thesis, Rutgers University.

Ivanov, A. and Selivanova, R. (1992) *Sclerolinum javanicum* sp.n., a new pogonophoran living on rotten wood. A contribution to the classification of Pogonophora. *Biologiya Morya (Vladivostok)* **1-2**, 27–33.

Jablonski, D. (1991) Extinctions: a paleontological perspective. *Science* **253**, 754–757. doi:10.1126/science.253.5021.754.

Katoh, K., Misawa, K., Kuma, K. and Miyata, T. (2002) MAFFT: a novel method for rapid multiple sequence alignment based on fast Fourier transform. *Nucleic Acids Research* **30**, 3059–3066.

Kearse, M., Moir, R., Wilson, A., Stones-Havas, S., Cheung, M., Sturrock, S., Buxton, S., Cooper, A., Markowitz, S., Duran, C., Thierer, T. and Ashton, B., Meintjes, P. Drummond, A. (2012) Geneious Basic: An integrated and extendable desktop software platform for the organization and analysis of sequence data. *Bioinformatics* **28**, 1647–1649.

Klinkhammer, G. P., Chin, C. S., Keller, R. A., Dählmann, A., Sahling, H., Sarthou, G., Petersen, S., Smith, F. and Wilson, C. (2001) Discovery of new hydrothermal vent sites in Bransfield Strait, Antarctica. *Earth and Planetary Science Letters* **193**, 395–407. doi:10.1016/S0012-821X(01)00536-2.

Kojima, S., Segawa, R., Hashimoto, J. and Ohta, S. (1997) Molecular phylogeny of vestimentiferans collected around Japan, revealed by the nucleotide sequences of mitochondrial DNA. *Marine Biology* **127**, 507–513. doi:10.1007/s002270050039.

Kojima, S., Ohta, S., Yamamoto, T., Yamaguchi, T., Miura, T., Fujiwara, Y., Fujikura, K. and Hashimoto, J. (2003) Molecular taxonomy of vestimentiferans of the western Pacific, and their phylogenetic relationship to species of the eastern Pacific III. *Alaysia*-like vestimentiferans and relationships among families. *Marine Biology* **142**, 625–635. doi:10.1007/s00227-002-0954-y.

Kongsrud, J. A. and Rapp, H. T. (2012) *Nicomache* (*Loxochona*) *lokii* sp. nov. (Annelida: Polychaeta: Maldanidae) from the Loki's Castle vent field: An important structure builder in an Arctic vent system. *Polar Biology* **35**, 161–170. doi:10.1007/s00300-011-1048-4.

Lazar, C. S., Dinasquet, J., Pignet, P., Prieur, D. and Toffin, L. (2010) Active archaeal communities at cold seep sediments populated by Siboglinidae tubeworms from the Storegga Slide. *Microbial Ecology* **60**, 516–527. doi:10.1007/s00248-010-9654-1.

Li, Y., Kocot, K. M., Schander, C., Santos, S. R., Thornhill, D. J. and Halanych, K. M. (2015) Mitogenomics reveals phylogeny and repeated motifs in control regions of the deep-sea family Siboglinidae (Annelida). *Molecular Phylogenetics and Evolution* **85**, 221–229. doi:10.1016/j.ympev.2015.02.008.

Librado, P. and Rozas, J. (2009) DnaSP v5: A software for comprehensive analysis of DNA polymorphism data. *Bioinformatics* **25**, 1451–1452.

Longmore, C., Trueman, C. N., Neat, F., Jorde, P. E., Knutsen, H., Stefanni, S., Catarino, D., Milton, J. A., Mariani, S. and Gillanders, B. (2014) Ocean-scale connectivity and life cycle reconstruction in a deep-sea fish. *Canadian Journal of Fisheries and Aquatic Sciences* **71**, 1312–1323. doi:10.1139/cjfas-2013-0343.

Macdonald, I., Loope, L., Usher, M. and Hamann, O. (1989) Wildlife conservation and the invasion of nature reserves by introduced species: a global perspective. In *Biological Invasions: A Global Perspective* (eds. Drake, J. A. *et al.*), pp. 215–255. Wiley, New York.

Marsh, A. G., Mullineaux, L. S., Young, C. M. and Manahan, D. T. (2001) Larval dispersal potential of the tubeworm *Riftia pachyptila* at deep-sea hydrothermal vents. *Nature* **411**, 77–80. doi:10.1038/35075063.

McClain, C. R. and Schlacher, T. A. (2015) On some hypotheses of diversity of animal life at great depths on the sea floor. *Marine Ecology* **36**, 849-872. doi:10.1111/maec.12288.

Nygren, A. (2014) Cryptic polychaete diversity: A review. *Zoologica Scripta* **43**, 172–183. doi:10.1111/zsc.12044.

O'Hara, T. D., England, P. R., Gunasekera, R. M. and Naughton, K. M. (2014) Limited phylogeographic structure for five bathyal ophiuroids at continental scales. *Deep-Sea Research I* **84**, 18–28. doi:10.1016/j.dsr.2013.09.009.

Pawlowski, J., Fahrni, J., Lecroq, B., Longet, D., Cornelius, N., Excoffier, L., Cedhagen, T. and Gooday, A. J. (2007) Bipolar gene flow in deep-sea benthic foraminifera. *Molecular Ecology* **16**, 4089–4096. doi:10.1111/j.1365-294X.2007.03465.x.

Pedersen, R. B., Rapp, H. T., Thorseth, I. H., Lilley, M. D., Barriga, F. J. A. S., Baumberger, T., Flesland, K., Fonseca, R., Früh-Green, G. L. and Jorgensen, S. L. (2010) Discovery of a black smoker vent field and vent fauna at the Arctic Mid-Ocean Ridge. *Nature Communications* **1**, 126. doi:10.1038/ncomms1124.

Posada, D. (2008) jModelTest: Phylogenetic Model Averaging. *Molecular Biology and Evolution* **25**, 1253– 1256.

Raupach, M. J., Malyutina, M., Brandt, A. and Wägele, J. W. (2007) Molecular data reveal a highly diverse species flock within the munnopsoid deep-sea isopod *Betamorpha fusiformis* (Barnard, 1920) (Crustacea: Isopoda: Asellota) in the Southern Ocean. *Deep-Sea Research II* **54**, 1820–1830. doi:10.1016/j.dsr2.2007.07.009.

Riesgo, A., Taboada, S. and Avila, C. (2015) Evolutionary patterns in Antarctic marine invertebrates: An update on molecular studies. *Marine Genomics* **23**, 1–13. doi:10.1016/j.margen.2015.07.005.

Rogers, A. D., Tyler, P. A., Connelly, D. P., Copley, J. T., James, R., Larter, R. D., Linse, K., Mills, R. A., Garabato, A. N., Pancost, R. D., Pearce, D. A., Polunin, N. V. C., German, C. R., Shank, T., Boersch-Supan, P. H., Alker, B. J., Aquilina, A., Bennett, S. A., Clarke, A., Dinley, R. J. J., Graham, A. G. C., Green, D. R. H., Hawkes, J. A., Hepburn, L., Hilario, A., Huvenne, V. A. I., Marsh, L., Ramirez-Llodra, E., Reid, W. D. K., Roterman, C. N., Sweeting, C. J., Thatje, S. and Zwirglmaier, K. (2012) The discovery of new deep-sea hydrothermal vent communities in the Southern Ocean and implications for biogeography. *PLOS Biology* **10**, e1001234. doi:10.1371/journal.pbio.1001234.

Ronquist, F. and Huelsenbeck, J. P. (2003) Mrbayes 3: Bayesian phylogenetic inference under mixed models. *Bioinformatics* **19**, 1572–1574.

Rousset, V., Rouse, G. W., Siddall, M. E., Tillier, A. and Pleijel, F. (2004) The phylogenetic

position of Siboglinidae (Annelida) inferred from 18S rRNA, 28S rRNA and morphological data. *Cladistics* **20**, 518–533.

Ryan, W. B. F., Carbotte, S. M., Coplan, J. O., O'Hara, S., Melkonian, A., Arko, R., Weissel, R. A., Ferrini, V., Goodwillie, A., Nitsche, F., Bonczkowski, J. and Zemsky, R. (2009) Global multi-resolution topography synthesis. *Geochemistry, Geophysics, Geosystems* **10**, Q03014. doi:10.1029/2008GC002332.

Sahling, H., Galkin, S., Salyuk, A., Greinert, J., Foerstel, H., Piepenburg, D. and Suess, E. (2003) Depth-related structure and ecological significance of cold-seep communities - a case study from the Sea of Okhotsk. *Deep-Sea Research I* **50**, 1391–1409. doi:10.1016/j.dsr.2003.08.004.

Sahling, H., Wallmann, K., Dählmann, A., Schmaljohann, R. and Petersen, S. (2005) The physicochemical habitat of *Sclerolinum* sp. at Hook Ridge hydrothermal vent, Bransfield Strait, Antarctica. *Limnology and Oceanography* **50**, 598–606. doi:10.4319/lo.2005.50.2.0598.

Smirnov, R. V. (2000) Two new species of Pogonophora from the arctic mud volcano off northwestern Norway. *Sarsia* **85**, 141–150. doi:10.1080/00364827.2000.10414563.

Southward, E. C. (1961) Pogonophora. In *Siboga - Expeditie* (ed. Weber, M.), pp. 1–22. E. J. Brill, Leiden.

Southward, E. C. (1972) On some Pogonophora from the Carribbean and the Gulf of Mexico. *Bulletin of Marine Science* **22**, 739–776.

Southward, E. C. (1999) Development of Perviata and Vestimentifera (Pogonophora). In *Reproductive Strategies and Developmental Patterns in Annelids* (ed. Dorresteijn, A. W. C. and Westheide, W.), pp. 185–202. Springer Netherlands.

Southward, E. C., Tunnicliffe, V. and Black, M. (1995) Revision of the species of *Ridgeia* from northeast Pacific hydrothermal vents, with a redescription of *Ridgeia piscesae* Jones (Pogonophora: Obturata = Vestimentifera). *Canadian Journal of Zoology* **73**, 282–295. doi:10.1139/z95-033.

Southward, E., Schulze, A. and Gardiner, S. (2005) Pogonophora (Annelida): Form and function. *Hydrobiologia* **535**, 227–251.

Tamura, K., Peterson, D., Peterson, N., Stecher, G., Nei, M. and Kumar, S. (2011) MEGA5: Molecular evolutionary genetics analysis using maximum likelihood, evolutionary distance, and maximum parsimony methods. *Molecular Biology and*

Evolution **28**, 2731–2739.

Tunnicliffe, V., St. Germain, C. and Hilário, A. (2014) Phenotypic variation and fitness in a metapopulation of tubeworms (*Ridgeia piscesae* Jones) at hydrothermal vents. *PLOS ONE* **9**, e110578. doi:10.1371/journal.pone.0110578.

Tyler, P. A. (2011) Cruise Report No. 05 RRS James Cook Cruise JC55 13 JAN-22 FEB 2011 Bransfield Strait, the East Scotia Ridge and the Kemp Seamount Calderas. Cruise 3 of the NERC Consortium Grant *"Chemosynthetically-driven ecosystems in the Southern Ocean."* British Oceanographic Data Centre.

Van Dover, C. L. L., German, C. R. R., Speer, K. G. G., Parson, L. M. M. and Vrijenhoek, R. C. C. (2002) Evolution and biogeography of deep-sea vent and seep invertebrates. *Science* **295**, 1253–1257. doi:10.1126/science.1067361.

Vanreusel, A., Andersen, A. C., Boetius, A., Connelly, D., Cunha, M. R., Decker, C., Heeschen, K., Hilario, A., Kormas, K. A., Maignien, L., Olu, K., Pachiadaki, M., Ritt, B., Rodrigues, C., Sarrazin, J., Tyler, P. A., Van Gaever, S. and Vanneste, H. (2009) Biodiversity of cold seep ecosystems along the European margins. *Oceanography* **22**, 118–435.

Vogler, A. P. and Monaghan, M. T. (2007) Recent advances in DNA taxonomy. *Journal of Zoological Systematics and Evolutionary Research* **45**, 1–10. doi:10.1111/j.1439-0469.2006.00384.x.

Vrijenhoek, R. C. (2009) Cryptic species, phenotypic plasticity, and complex life histories: Assessing deep-sea faunal diversity with molecular markers. *Deep-Sea Research II* **56**, 1713–1723. doi:10.1016/j.dsr2.2009.05.016.

Vrijenhoek, R. C. (2010) Genetic diversity and connectivity of deep-sea hydrothermal vent metapopulations. *Molecular Ecology* **19**, 4391–4411. doi:10.1111/j.1365-294X.2010.04789.x.

Walz, K. R., Clague, D. A., Barry, J. P. and Vrijenhoek, R. C. (2014) First records and range extensions for two *Acesta* clam species (Bivalvia: Limidae) in the Gulf of California, Mexico. *Marine Biodiversity Records* **7**, e60. doi:10.1017/S1755267214000165.

Webb, M. (1964a) A new bitentaculate pogonophoran from Hardangerfjorden, Norway. *Sarsia* **15**, 49–55.

Webb, M. (1964b) Tube abnormality in *Siboglinum ekmani*, *S. fiordicum* and *Sclerolinum brattstromi* (Pogonophora). *Sarsia* **15**, 69–70.

Webb, M. (1964c) Additional notes on *Sclerolinum brattstromi* (Pogonophora) and the establishment of a new family, Sclerolinidae. *Sarsia* **16**, 47–58.

Weigert, A., Helm, C., Meyer, M., Nickel, B., Arendt, D., Hausdorf, B., Santos, S. R., Halanych, K. M., Purschke, G., Bleidorn, C. and Struck, T. H. (2014) Illuminating the base of the annelid tree using transcriptomics. *Molecular Biology and Evolution* **31**, 1391–1401. doi:10.1093/molbev/msu080.

Winkler, G., Newton, R., Schlosser, P. and Crone, T. (2010) Mantle helium reveals Southern Ocean hydrothermal venting. *Geophysical Research Letters* **37**, L05601.

Zardus, J. D., Etter, R. J., Chase, M. R., Rex, M. A. and Boyle, E. E. (2006) Bathymetric and geographic population structure in the pan-Atlantic deep-sea bivalve *Deminucula atacellana* (Schenck, 1939). *Molecular Ecology* **15**, 639–651. doi:10.1111/j.1365-294X.2005.02832.x.

Zhang, H., Johnson, S. B., Flores, V. R. and Vrijenhoek, R. C. (2015) Intergradation between discrete lineages of *Tevnia jerichonana*, a deep-sea hydrothermal vent tubeworm. *Deep-Sea Research II* **121**, 53-61. doi:10.1016/j.dsr2.2015.04.028.

3 Mineralisation of *Alvinella* polychaete tubes at hydrothermal vents

Magdalena N. Georgieva[1,2], Crispin T. S. Little[1], Alexander D. Ball[3], Adrian G. Glover[2]

[1]*School of Earth and Environment, University of Leeds, Leeds, United Kingdom*

[2]*Life Sciences Department, Natural History Museum, London, United Kingdom*

[3]*Imaging and Analysis Centre, Natural History Museum, London, United Kingdom*

3.1 Abstract

Alvinellid polychaete worms form multi-layered organic tubes in the hottest and most rapidly-growing areas of deep-sea hydrothermal vent chimneys. Over short periods of time, these tubes can become entirely mineralised within this environment. Documenting the nature of this process in terms of the stages of mineralisation, as well as the mineral textures and end-products that result, is essential for our understanding of the fossilisation of polychaetes at hydrothermal vents. Here we report in detail the full mineralisation of *Alvinella* spp. tubes collected from the East Pacific Rise, determined through the use of a wide range of imaging and analytical techniques. We propose a new model for tube mineralisation, whereby mineralisation begins as templating of tube layer and sub-layer surfaces, and results in fully mineralised tubes comprised of multiple concentric, colloform, pyrite bands. Silica appeared to preserve organic tube layers in some samples. Fine-scale features such as protein fibres, extracellular polymeric substances and two types of filamentous microbial colonies were also found to be well preserved within a subset of the tubes. The fully mineralised *Alvinella* spp. tubes do not closely resemble known ancient hydrothermal vent tube fossils, corroborating molecular evidence suggesting that the alvinellids are a relatively recent polychaete lineage. We also compare pyrite and silica preservation of organic tissues within hydrothermal vents to soft tissue preservation in sediments and hot springs.

3.2 Introduction

The annelid worms are an ancient lineage of animals dating to at least the earliest Cambrian period, ~540 Ma (Conway Morris and Peel, 2008; Vinther *et al.*, 2011). Over evolutionary time, they have radiated into almost all marine habitats including deep-sea hydrothermal vents. Many vent sites in the Pacific are characterised by spectacular colonies of tube-dwelling polychaetes in the families Siboglinidae and Alvinellidae (Van Dover, 2000). Our understanding of the evolutionary history of these polychaetes and the vent ecosystems more generally is limited by a poor fossil record of soft-bodied organisms. Typically, preservation of soft tissues occurs through early authigenic mineralisation (the impregnation and/or replication of an organic structure by minerals), and usually involves the minerals phosphate, carbonate, pyrite or silica (Briggs *et al.*, 1991; Akahane *et al.*, 2004). Much research has focused on organic tissue mineralisation within soft sediments and terrestrial hot springs (e.g. Raff *et al.*, 2008; Farrell *et al.*, 2013), but mineralisation of organic animal and prokaryotic remains within hydrothermal vent environments, which also involves pyrite and silica (Cook and Stakes, 1995; Maginn *et al.*, 2002; Boyce *et al.*, 2003), is poorly understood. Documenting this process at modern hydrothermal vents is key to understanding taphonomy within this chemically distinct setting, and to improving the interpretation of ancient vent fossils.

Worm-tube fossils with diverse morphologies are known from vent sites in the geological record back to the early Silurian period, ~430 million years ago (Little *et al.*, 1998, 1999, 2004, 2007; Hilário *et al.*, 2011), but little is known about the animals that formed them. Although some have been assigned to extant vent polychaete groups, morphological identifications are not generally consistent with estimates of molecular divergence (Little and Vrijenhoek, 2003; Vrijenhoek, 2013) and there is potential confusion with morphologically-similar polychaete tubes (Kiel and Dando, 2009).

An endemic tube-forming polychaete genus within extant hydrothermal vents on the East Pacific Rise (EPR) is *Alvinella* Desbruyères & Laubier, 1986, comprising two species: *Alvinella pompejana* and *A. caudata*. Both are renowned for their occupation of high-temperature vent chimneys and role as biogeoengineers within this habitat (Desbruyères *et al.*, 1998; Le Bris and Gaill, 2007). After colonisation, *Alvinella* spp. can alter local vent fluid flow and composition, creating a range of micro-environments that allow the establishment of other hydrothermal vent biota less tolerant to high temperatures, and also promoting additional mineral precipitation and thus modifying chimney morphology (Juniper and Martineu, 1995; Pradillon *et al.*, 2005). In part, this biological habitat modification arises

from *Alvinella* spp. irrigating the interior of their tubes with cool seawater from above the alvinellid colony. This results in an inner tube environment with a lower temperature and a more neutral pH (temp. of ~29-81°C, pH ~7) compared to conditions on the surface of the vent chimney substrate (temp. of ~120°C, pH ~4) (Di Meo-Savoie *et al.*, 2004; Le Bris *et al.*, 2005), and creates buffered micro-niches which are colonised by micro-organisms (Le Bris *et al.*, 2005).

Colonisation of fresh vent chimneys by *Alvinella* spp. is considered to be strongly dependent on the properties of their unique tubes, which are attached directly onto vent chimney walls. These tubes possess high thermal and chemical stability (Gaill and Hunt, 1986), and can be secreted incredibly quickly, at a maximum rate of 1 cm day^{-1} in length (Pradillon *et al.*, 2009). The tubes of *Alvinella pompejana* and *A. caudata* are identical in appearance, and are formed from granules primarily composed of protein (Vovelle and Gaill, 1986). The resulting tubes are fibrous and concentrically multi-layered, with each tube layer comprised of superimposed sub-layers of parallel fibrils that vary in direction between adjacent sub-layers (Gaill and Hunt, 1986; Desbruyères *et al.*, 1998). Both the inner and outer surfaces of *Alvinella* spp. tubes are covered by a patchy, but dense microbial community that includes filamentous, rod-shaped, and coccoid forms (Desbruyeres *et al.*, 1985), belonging primarily to the epsilon subdivision of the proteobacteria (Haddad *et al.*, 1995; Campbell and Cary, 2001; Campbell *et al.*, 2003). Micro-organisms on the insides of the tubes can become trapped between the tube layers as more organic material is deposited during tube growth, to form distinctive microbial layers within the tube wall (Gaill and Hunt, 1986; Zbinden *et al.*, 2001; Maginn *et al.*, 2002).

Within the extreme environment of the EPR hydrothermal vents (see Fornari *et al.* (2012) and references therein for an overview of the EPR spreading centre), minerals can precipitate onto occupied *Alvinella* tubes remarkably quickly, such that an 11-day-old alvinellid colony can have 88% mineral content (Pradillon *et al.*, 2009). During the early stages of this mineralisation, minerals progressively coat the inner and outer tube surfaces (Gaill and Hunt, 1991) and accumulate within the tube walls, where they occur as nanocrystalline iron or zinc sulphides that assemble along sub-layer surfaces (Zbinden *et al.*, 2001, 2003; Maginn *et al.*, 2002; Le Bris *et al.*, 2008). Mineral precipitation has been observed particularly in tube layers containing trapped micro-organisms, and pyrite may occasionally replace organic tube layers (Maginn *et al.*, 2002). Over time, *Alvinella* spp. tubes can become entirely mineral in composition (fully mineralised) (Haymon *et al.*, 1984; Haymon and Koski, 1985). Full mineralisation of originally organic polychaete tubes has

also been observed by Cook and Stakes, (1995) for siboglinid worm tubes at vent sites on the Juan de Fuca Ridge (JdFR), but the details of how *Alvinella* spp. tubes are fully mineralised, including the gross and fine-scale mineral textures and distributions, have not been documented.

Here we provide a detailed account of the complete mineralisation process of *Alvinella* spp. tubes to show how polychaete tubes can be fossilised at vent sites such as the EPR. A large number of *Alvinella* spp. tube specimens exhibiting varying degrees of mineralisation have been analysed to better understand a) the identity of the main minerals replacing the tubes, b) the nature and distribution of the mineral textures, and c) the stages and timing of mineralisation of the tubes. The identification of problematic tubular fossils from ancient vent sites is discussed, and mineralisation of *Alvinella* spp. tubes is compared to preservation of organic tissues by silica and sulphide minerals within other environments.

3.3 Methods

3.3.1 Sample collection and storage

The studied samples comprised vent chimney material containing *Alvinella* spp. tubes exhibiting varying degrees of mineralisation. These were collected from the tops of nine active vent chimneys and one inactive chimney (Alvinellid Pillar) located along the EPR axial summit trough at depths of ~2500 m (Figure 3.1). The material was collected on 10 dives of the submersible *Alvin*, during three Woods Hole Oceanographic Institution cruises of the RV Atlantis (AT15-13, AT15-27 and AT15-38, Table 3.1). Some of the vent sites were sampled on more than one of the cruises (Table 3.1), but different vent chimneys within these sites were sampled on each cruise. A small number of the studied samples were obtained through experimental fossilisation cages, deployed at vent sites for approximately 1 year, during the same RV Atlantis cruises (outlined in Little (2009); see Methods Supplement). After recovery from the sea-floor, the *Alvinella* spp. tubes that were largely non-mineralised were removed from the vent chimneys and preserved in 95% ethanol (hereafter referred to as partially mineralised *Alvinella* spp. tubes). Samples of vent chimney sulphides with fully mineralised *Alvinella* spp. tubes were dried and stored at room temperature post-collection (Figure 3.2A). During post-collection storage, some of the sulphide chimney samples started to oxidise, forming secondary sulphate minerals; these were washed off prior to analyses. This oxidation may have resulted in the formation of

iron oxides in addition to those formed in-situ (in-situ iron oxides were evidenced by a red colour on recovery; Figure 3.2A), and we hence excluded iron oxide analysis from the study.

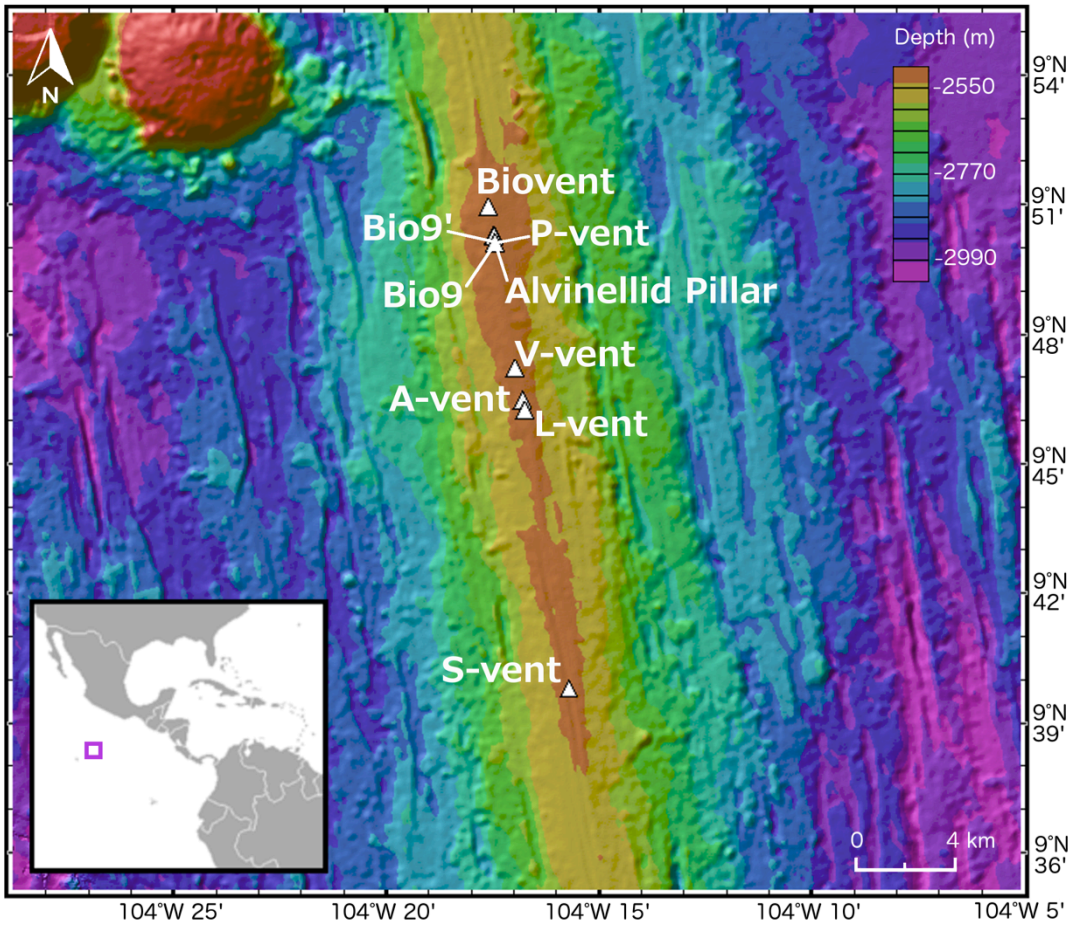

Figure 3.1 Location of the East Pacific Rise vent sites between 9° 41' and 9° 51' North from which the *Alvinella* spp. tube material was collected. *Insert*, Location of the study area in relation to Central America. The map was created using GeoMapApp© and vent locations were plotted using data from the Marine Geoscience Data System (http://www.marine-geo.org/).

3.3.2 Micro-CT analyses

Five partially mineralised *Alvinella* spp. tubes (Specimens 44, 46, 47, 48, 49; Table 3.1) were initially scanned using a Metris X-Tek HMX ST 225 micro-computed tomography (μ-CT) system at the Natural History Museum, London, UK (NHM), to visualise the distribution of minerals on and within the tubes. Data volumes were constructed using CT Pro ver. 2.1 (Metris X-Tek, UK), and analysed using Drishti ver. 2.0 (Limaye, 2006). All five tube scans had a resolution of 71 μm or better. Mineral and organic tube components were separated based on grayscale values that represent x-ray attenuation, which closely corresponds to material density. To verify that the two were being accurately distinguished, one of the

scanned specimens (Specimen 44) was embedded in resin, cross-sectioned and polished for reflected light microscopy to cross-reference the presence/absence of minerals with the μ-CT scan reconstruction.

Table 3.1 Information on the *Alvinella* spp. tube material used for this study. Specimen numbers were assigned during this study. Vent location, depth, temperature and pH data were obtained from the Marine Geoscience Data System (Bryce *et al.*, 2007, 2008) (http://www.marine-geo.org/).

Vent	Alvin Dive	Collection Date	Latitude of vent site	Longitude of vent site	Depth of vent site (m)	Temp. (°C)	pH	Specimens	Fossilisation cage sample?
Bio9'	4274	24-Nov-06	N9° 50.311	W104° 17.480	2509	382	4.4	45, 66, 69	No
Bio9	4274	24-Nov-06	N9° 50.312	W104° 17.484	2509	388	3.6	55, 67, 71	No
	4375	11-Dec-07	N9° 50.312	W104° 17.484	2509	358	3.9	47, 56, 61, 70, 72	Yes - 370 days
L-vent	4276	26-Nov-06	N9° 46.256	W104° 16.749	2519	341	4.4	46, 54	No
	4377	13-Dec-07	N9° 46.256	W104° 16.749	2519	279	3.6	62, 65	No
	4467	01-Nov-08	N9° 46.256	W104° 16.749	2519	-	-	57, 60	Yes - 319 days
P-vent	4278	28-Nov-06	N9° 50.280	W104° 17.473	2509	392	4.5	44	No
Alvinellid Pillar	4281	01-Dec-06	N9° 50.125	W104° 17.456	2504	-	-	68	No
Biovent	4374	10-Dec-07	N9° 50.963	W104° 17.617	2501	349	4.1	49	No
A-vent	4377	13-Dec-07	N9° 46.500	W104° 16.810	2541	136	5.4	74	No
V-vent	4378	14-Dec-07	N9° 47.231	W104° 16.989	2517	363	3.6	48, 58	No
S-vent	4379	15-Dec-07	N9° 39.816	W104° 15.714	2510	326	4.3	59	No

3.3.3 Microscopic and chemical analyses

The ethanol-preserved tubes were critically point dried, and, along with the fully mineralised tubes, were cut, impregnated in resin, and made into polished blocks of both transverse and longitudinal tube sections. Polished blocks of mineralised *Alvinella* spp. tubes contained both tubes and a section of the surrounding vent chimney matrix. The polished blocks were coated with an approximately 17 nm carbon layer, and imaged using the following scanning electron microscopes (SEM) with backscattered electron detectors: a LEO 1455VP SEM, a Carl Zeiss Ultra Plus Field Emission SEM, and an FEI Quanta 650 FEG-ESEM both at the NHM and at the University of Leeds, UK (Leeds). Two fully mineralised *Alvinella* spp. tubes (Table 3.1) were also imaged uncoated in the environmental chamber of a Philips XL 30 FEG-SEM at Leeds.

The elemental composition of mineral phases, and elemental distribution, were determined using both energy-dispersive X-ray spectroscopy (EDS) within the SEMs above, and wavelength-dispersive spectrometry (WDS) using a Cameca SX-100 electron microprobe (EPMA) at the NHM. An accelerating voltage of 20 kV was used for EDS point-analyses and maps, whereas in the EPMA these were carried out using an accelerating voltage of 15

kV and a probe current of 40 nA for mapping and 20 nA for point analyses. Reflected light microscopy was used to identify the mineral phases within approximately half of the specimens (Supplementary Table C.1). X-ray diffraction (XRD) was performed on a Bruker D8 instrument (Cu Kα radiation source, 40kV voltage and 40mA of current) in Leeds on bulk material from a single vent chimney section and attached fully mineralised *Alvinella* spp. tube (Specimen 57) to identify the crystalline form of the zinc sulphide phase. In addition, confocal laser scanning microscopy (CLSM) using a Nikon A1-Si Confocal microscope at the NHM and operated in spectral imaging mode, was used to visualise the structure of the organic tube layers, and microbial filaments on the inner surface of an *Alvinella* spp. tube (Specimen 44) by laser-induced autofluorescence.

3.3.4 Measurements of mineral textures

The dimensions of mineral textures preserved within *Alvinella* spp. tubes were measured from SEM images using the program ImageJ (version 1.46r; National Institutes of Health, USA; http://rsb.info.nih.gov/ij). Pores and filaments were prevalent mineral textures within the samples, which are likely to be fossilised microbial filaments (see later). When measuring the dimensions of these textures, only pores with a distinctly circular or elliptical transverse section i.e. those likely to be biogenic in origin, were measured. For statistical tests, diameter measurements from pore and filament textures were grouped into two types. Shapiro-Wilk normality tests were used to determine if diameter measurements were normally distributed, and *F*-tests to compare variances between data pairs. Two-sample Kolmogorov-Smirnov tests were subsequently used to compare the cumulative distributions between pairs of diameter measurements. All three types of statistical test were performed in R (R Core Team, 2013).

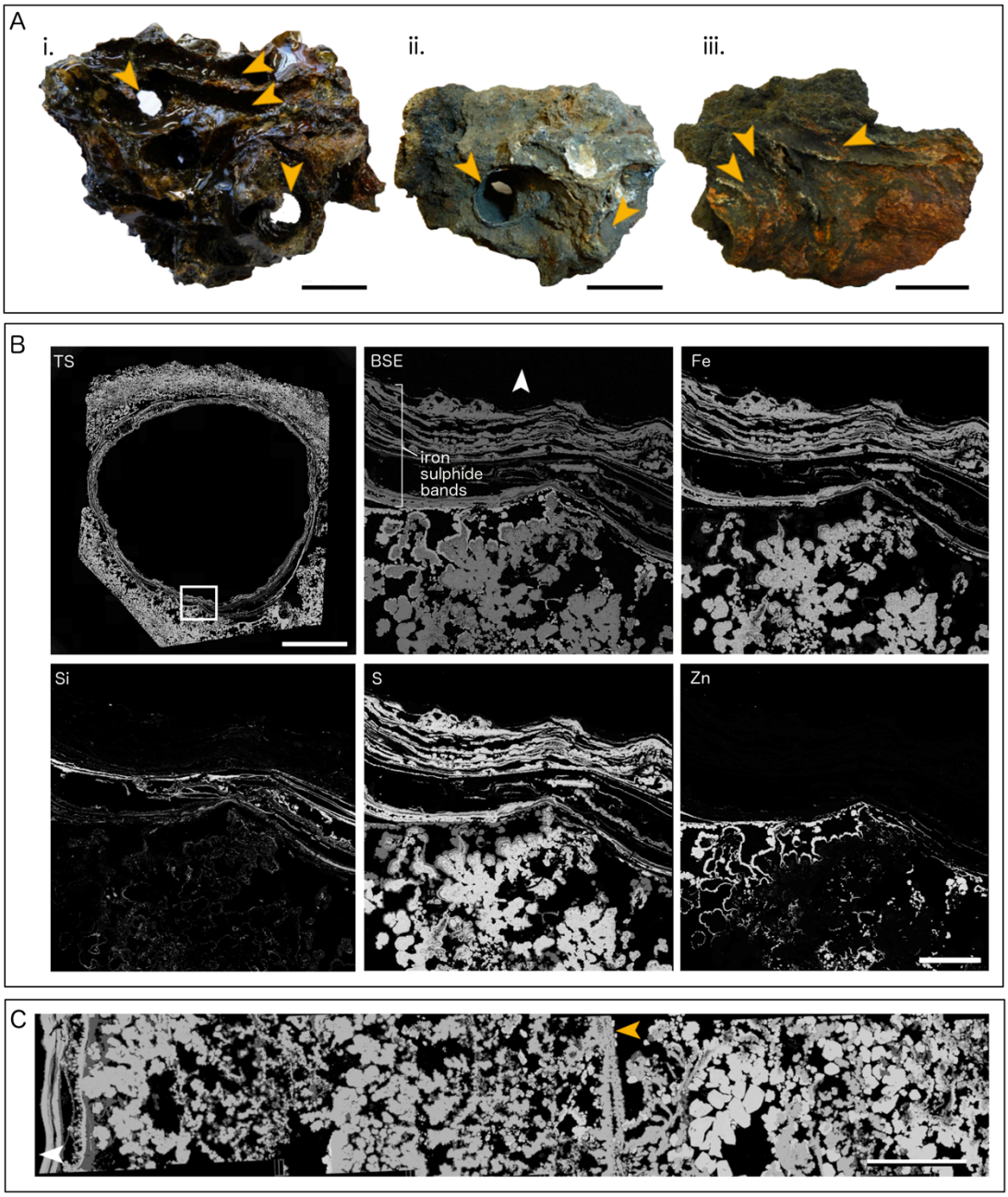

Figure 3.2 Fully mineralised *Alvinella* spp. tubes and associated vent chimney fragments. **A,** blocks of sulphide from vent chimneys containing fully mineralised *Alvinella* spp. tubes (orange arrows). **i-ii,** chimney blocks containing complex intertwined *Alvinella* spp. tubes, some of which have been mineralised completely as cylindrical structures; **iii,** sulphide block with *Alvinella* spp. tubes mineralised on the surfaces that were attached to the vent chimney wall. **i**, Specimen 74 (coated in epoxy resin); **ii**, Specimen 57; **iii**, Specimen 61. All scales in *A* are 30 mm. **B,** WDS elemental mapping of a fully mineralised *Alvinella* spp. tube in transverse section (Polished Block 57.1) and associated vent chimney minerals. TS, Transverse section with the area analysed highlighted with white box; scale = 5 mm. BSE, Backscatter electron image of the analysed area, white arrow points towards tube centre; scale = 500 µm. Fe to Zn show the distribution of four elements within the area analysed (Fe – iron, Si – silicon, S – sulphur, Zn – zinc). **C,** Backscatter SEM composite of Polished Block 60.2 showing variation in mineral texture and composition from a fully mineralised *Alvinella* spp. tube (extreme left) to several millimetres into the vent chimney. Brightest minerals = zinc sulphides, medium grey = iron sulphides, and dullest grey = silica. The linear texture towards the middle of the image (orange arrow) likely represents an overgrown, older fully mineralised *Alvinella* spp. tube; scale = 1 mm. White arrows point towards tube centres.

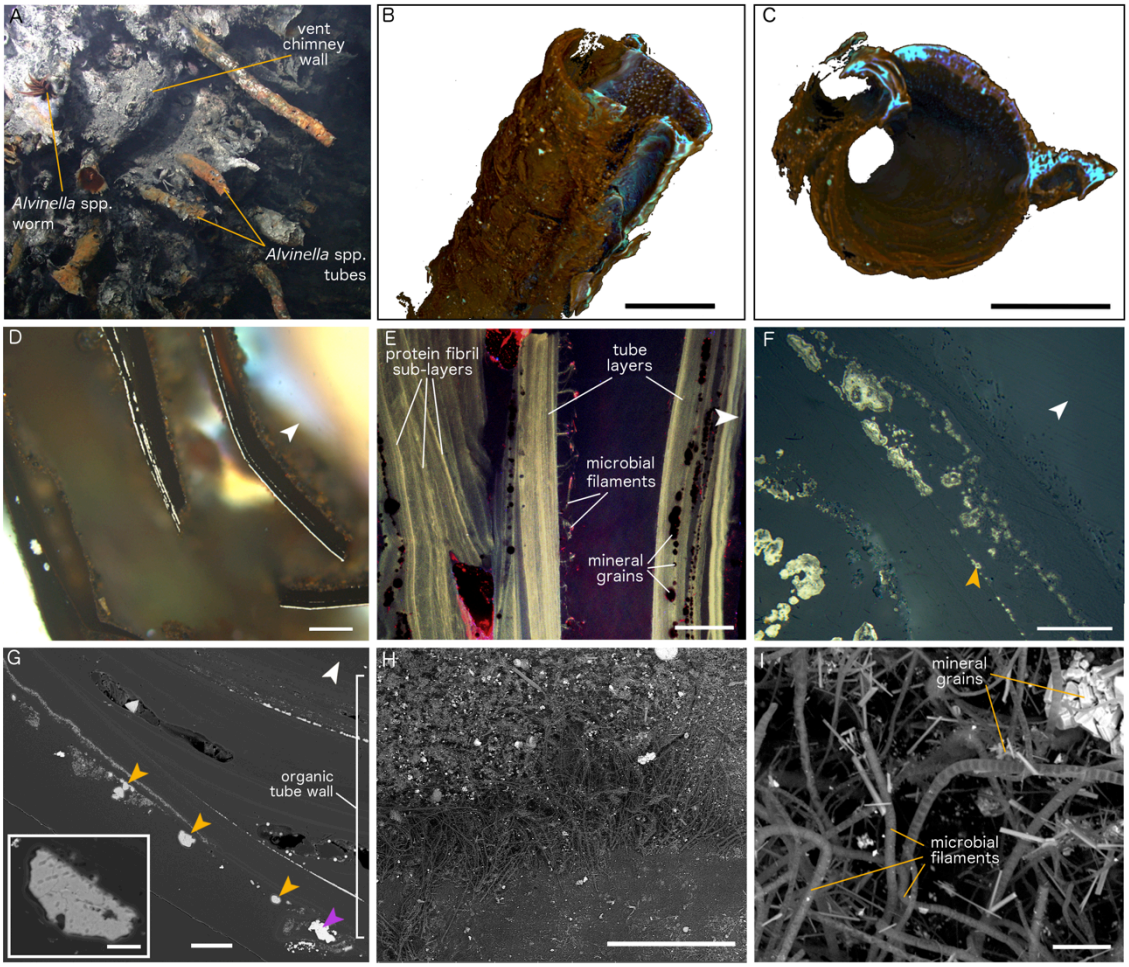

Figure 3.3 Partially mineralised *Alvinella* spp. tubes. **A,** *Alvinella* spp. tubes on a hydrothermal vent chimney (L-vent, AT15-27, Alvin dive 4382), with an *Alvinella* spp. worm at its tube opening. Image credit: Woods Hole Oceanographic Institution. **B-C,** reconstructions of a single *Alvinella* spp. tube (Specimen 46) using micro-computed tomography (μ-CT). Blues and purples highlight dense areas where minerals have precipitated, while browns constitute the organic tube wall; scales = 10 mm. **B**, tube in oblique side view; **C**, tube in transverse section. **D,** bands of mineral growth within and on surfaces of organic *Alvinella* spp. tube layers, scale = 300 μm (Polished Block 46.1). **E,** confocal image of a transverse section though an *Alvinella* spp. tube (Polished Block 44.1), showing organic tube layers, microbial filaments trapped between layers, and the texture of protein fibrils within the organic tube. Scale = 100μm. **F,** detail of an organic tube layer where mineralisation begins as small iron sulphide cores, which join up upon further mineral precipitation to form distinct colloform pyrite bands. Cores and bands often occur along distinct surfaces within the organic layers (orange arrow) (Polished Block 44.1); scale = 50 μm. **G,** transverse section of an *Alvinella* spp. tube (Polished Block 44.1) with mineral grain (purple arrow) and elemental sulphur grains (orange arrows); scale = 100 μm. *Insert*, detail of elemental sulphur grain showing pitted texture; scale = 20 μm. **H,** SEM image of the interior surface of an *Alvinella* spp. tube (Specimen 44) showing patchily distributed microbial filaments and mineral grains, scale = 500 μm. **I,** detail of **H**, scale = 10 μm. White arrows point towards tube centres.

3.4 Results

3.4.1 Vent chimney minerals around *Alvinella* spp. tubes

The fragments of vent chimneys onto which *Alvinella* spp. tubes were attached (Figure 3.2A) were formed largely of iron (pyrite, marcasite), zinc and copper (chalcopyrite, minor isocubanite) sulphides, silica, anhydrite and galena (Figure 3.2B-C). An XRD trace for a vent chimney sample with an attached tube (Specimen 57) showed the zinc sulphide to be sphalerite, but it is likely that both sphalerite and wurtzite were common in the samples (these polymorphs are difficult to discriminate when intergrown). The distribution of mineral phases within these vent chimney fragments was variable, but generally fine-grained marcasite occurred directly adjacent to *Alvinella* spp. tube walls on the outside of vent chimneys, which was sometimes overgrown by zinc sulphides (Figure 3.2B). This was succeeded by zinc sulphides and amorphous silica further into the vent chimney, which in turn was succeeded by larger-grained marcasite or zinc sulphides, then chalcopyrite or anhydrite (Figure 3.2C). The vent chimney minerals exhibited crystalline morphologies and porosity associated with fine-grained marcasite growth, while colloform (finely concentric and radiating) textures were rare and did not delineate consistent shapes. An exception were continuous thin bands of colloform iron sulphide (Figure 3.2C), found on the interiors of three chimney sections (Polished Blocks 57.3, 60.2, and 62.1). These were similar to the mineral layers comprising fully mineralised *Alvinella* spp. tubes (see later).

3.4.2 Partially mineralised *Alvinella* spp. tubes

Examples of in-situ partially mineralised *Alvinella* spp. tubes are shown in Figure 3.3A. Three-dimensional μ-CT reconstructions of partially mineralised *Alvinella* spp. tubes showed that minerals were often concentrated along one longitudinal surface of the tubes (Figure 3.3B) (in Specimens 44, 46, 48, 49), which in one tube (Specimen 44) was known to have been the side that was directly attached to the vent chimney. Minerals occurred as grains and crusts coating inner and outer tube wall surfaces, and were also abundant between the concentric organic layers that comprise the *Alvinella* spp. tube walls (Figure 3.3C). Detailed microscopy revealed that minerals were templating (here defined as the growth of minerals on a surface) certain organic tube layer and sub-layer surfaces (Figure 3.3D-G), where mineral growth appears to begin as small cores, often less than 1 μm in diameter. These cores appeared to fuse with adjacent cores following further mineral precipitation, to form multiple bands of mineralisation parallel to the natural layering of the

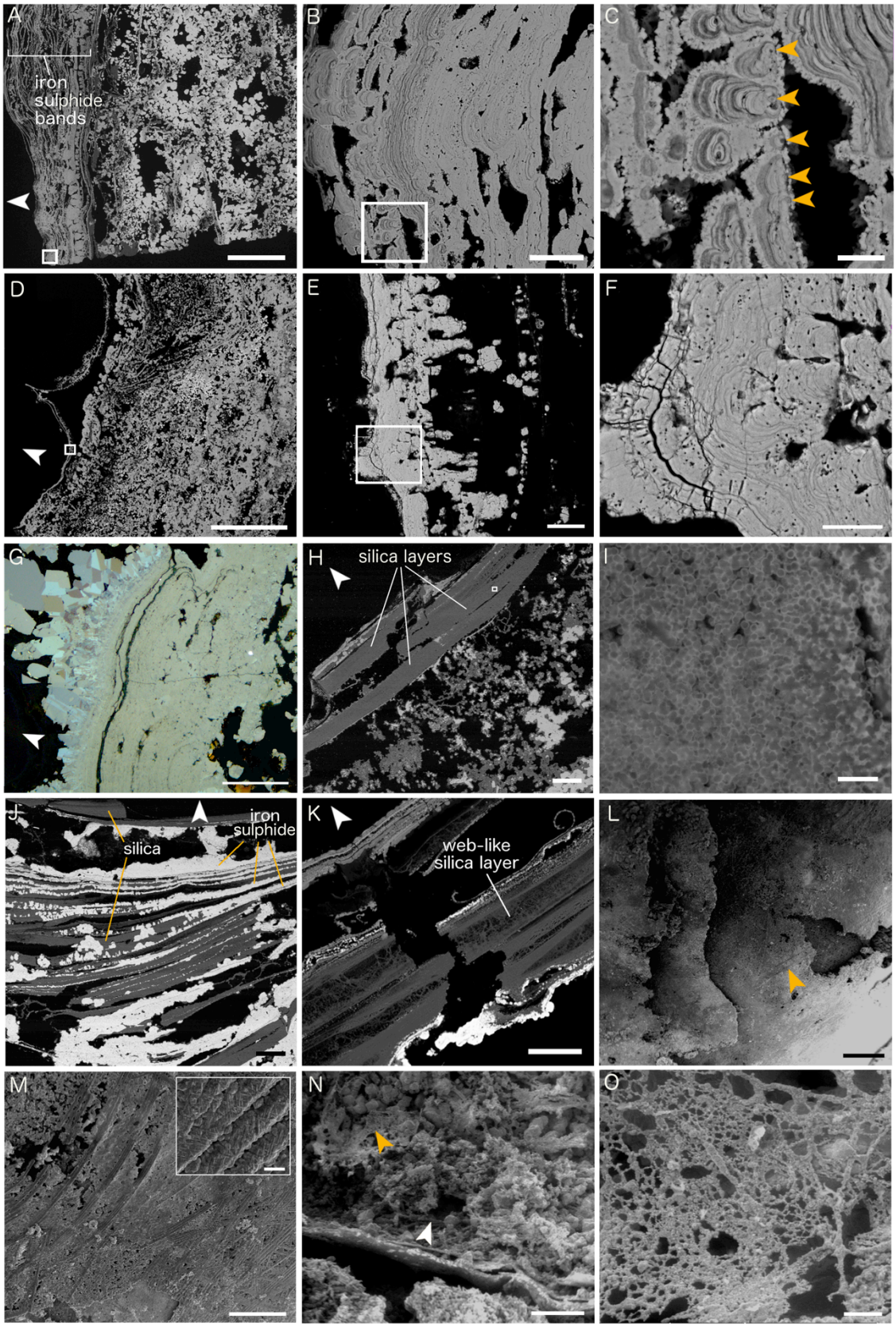
A
iron sulphide bands
B
C
D
E
F
G
H
silica layers
I
J
silica
iron sulphide
K
web-like silica layer
L
M
N
O

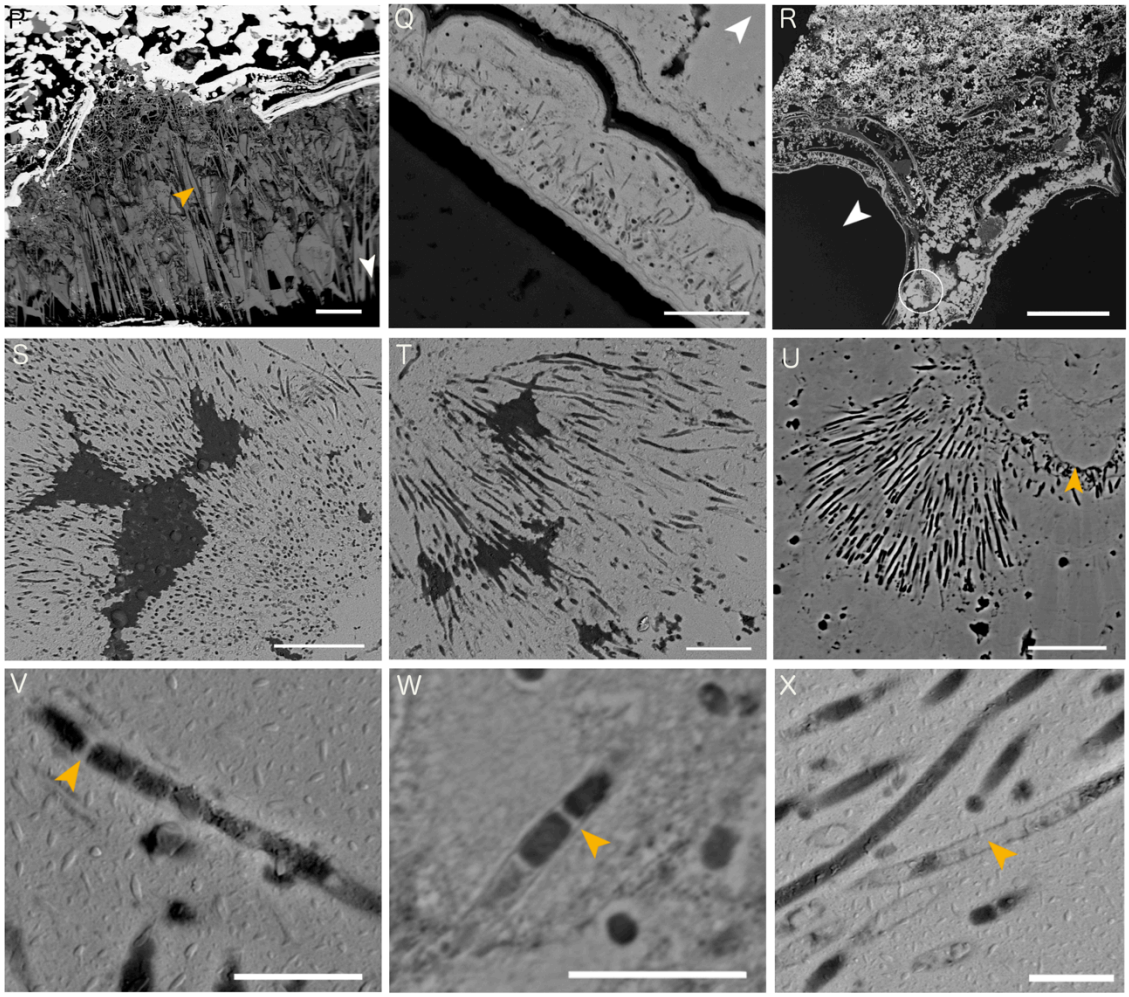

Figure 3.4 Fully mineralised *Alvinella* spp. tubes. **A,** longitudinal section of a tube (Polished Block 60.3) with a large number of iron sulphide (pyrite) bands replacing the tube wall; scale = 1 mm. White box shows location of **B**. **B,** detail of boxed area in **A** showing bands of colloform pyrite; scale = 50 µm. White box shows location of **C**. **C,** detail of boxed area in **B** showing colloform micro-stromatolitic structures with orange arrows pointing towards the cores from which they originate; scale = 10 µm. **D,** transverse section through two adjacent *Alvinella* spp. tubes; white box shows location of *E*, scale = 4mm. **E,** bands of pyrite comprising the mineralised tube, white box shows location of *F*; scale = 50 µm. **F,** pore and filament textures within colloform pyrite (association 1); scale = 20 µm. **G,** bands of colloform pyrite overgrown by marcasite; scale = 100 µm (Polished Block 70.1). **H,** amorphous silica appears to be replacing organic tube layers (Polished Block 58.1). Scale = 200 µm; white box shows location of **I**. **I,** detail of tube in *H* showing small silica spheres that comprise some of the amorphous silica layers; scale = 4 µm. **J,** interlaminated silica and pyrite, where silica appears to have preserved parts of disintegrating organic tube layers, and surrounds iron sulphide cores (Polished Block 57.2). Scale = 200 µm. **K,** silica layer within a mineralised *Alvinella* spp. tube (Polished Block 62.1) exhibiting a web-like texture; scale = 200 µm. **L,** view of the external wall of a fully mineralised *Alvinella* spp. tube (Specimen 54A) showing four mineralised layers; orange arrow points to texture in **M**. Scale = 500 µm. **M,** detail of iron sulphide 'fibres' that are cross-cutting and/or bundled; scale = 250 µm. *Insert*, detail of adjacent fibres showing surface covering of small cross-hatched striations; scale = 10 µm. **N,** interior of a mineralised *Alvinella* spp. tube (Specimen 55A) which has been partially filled by minerals. The mineralised tube wall runs horizontally along bottom third of image; orange arrow points towards location of EPS-like mineral texture. Scale = 1 mm. **O,** detail of EPS-like mineral

texture from the tube in **N**; scale = 50 μm. **P,** anhydrite growing on the inside of an *Alvinella* spp. tube (orange arrow); scale = 500 μm. **Q,** pore and filament texture (association 1) occurring within one of the outer pyrite bands of a fully mineralised *Alvinella* spp. tube (Polished Block 57.1); scale = 20 μm. **R,** transverse section of *Alvinella* spp. tubes (Polished Block 60.1); white circle shows the location of clumped pores and filaments (association 2) in **S** and **T**; scale = 500 μm. **S,** pore and filament clump showing a change in orientation from the clump base (bottom right) to the edge (left and top); scale = 20 μm. **T,** clumped radiating filaments; scale = 10 μm. **U,** clumped pore and filament association (Specimen 63979) that appears to be rooted onto a distinct iron sulphide layer (orange arrow), scale = 20 μm. **V-W,** filaments from various samples with preserved septae (orange arrows). **V**, polished Block 60.1; **W**, polished Block 62.1. **X,** detail of filaments infilled by pyrite (orange arrow) (Polished Block 60.1). Scales in **V-X** are 3 μm. White arrows point towards tube centres.

tubes (Figure 3.3D-G). The composition of the minerals found within partially mineralised *Alvinella* spp. tubes generally reflected the mineralogy of vent chimney sections, with the mineral cores found to be predominantly comprised of iron sulphide, but occasionally also contained zinc and copper (Supplementary Table C.1). The cores tended to be larger and more abundant in the outer layers of tube walls, and likely acted as loci for subsequent colloform iron sulphide growth. Large mineral grains, as well as large grains of elemental sulphur (Figure 3.3G), also occurred between organic tube layers and on both inner and outer tube surfaces. The elemental sulphur grains were usually 10s of micrometers in size, but some were up to 468 μm across. They had a pitted texture (Figure 3.3G, *insert*), and were rarely observed in the fully mineralised tubes.

3.4.3 Fully mineralised *Alvinella* spp. tubes

The fully mineralised *Alvinella* spp. tubes occurred in two forms: as tubes fully enclosed within vent chimney sulphides, in which the entire circumference of the tube wall had been preserved and tube interiors were mostly hollow (Figure 3.2Ai-ii), or as partial tube walls attached to the surfaces of vent chimney fragments (Figure 3.2Aiii). The fully mineralised *Alvinella* spp. tubes that were obtained from the fossilisation experiment lasting approximately 1 year (319 days and 370 days; Table 3.1; Methods Supplement), demonstrate that full tube mineralisation can occur within this time period.

The composition of fully mineralised *Alvinella* spp. tubes also reflected the mineralogy of adjacent vent chimney fragments. Mineral *Alvinella* spp. tube walls were mainly iron sulphide (pyrite and marcasite) and amorphous silica (Figure 3.2B; Supplementary Table C.1) in composition, with small quantities of zinc sulphides (sphalerite and/or wurtzite), and minor quantities of copper containing sulphides (chalcopyrite, isocubanite), galena, and anhydrite. The majority of fully mineralised *Alvinella* spp. tubes were comprised of multi-

layered iron sulphide (pyrite) sheets that broadly mirrored the layering of organic tube walls, which appeared as concentric pyrite bands or horizons in transverse and longitudinal section (Figures 3.2B-C, 3.4A-F). The pyrite bands occasionally showed weak anisotropy, and contained overgrowths of crystalline marcasite that increased in crystal size away from the tube wall (Figure 3.4G).

The number of pyrite bands comprising fully mineralised *Alvinella* spp. tubes varied greatly between different tube samples (Supplementary Table C.1; Figures 3.2B, 3.4A, D). Pyrite band number, thickness, and the degree to which they joined with adjacent bands also varied between different parts of the same tube. The pyrite bands were characterised by colloform textures, the development of which could in some instances be traced to small iron sulphide cores very similar to those recorded within partially mineralised *Alvinella* spp. tubes (Figures 3.4C, F; 3.3D-F). Sustained mineral precipitation onto the iron sulphide cores appears to have resulted in the formation of colloform micro-stromatolitic structures, up to 218 μm in length, comprised of fine-scale pyrite layers less than 1 μm thick (Figure 3.4B-C, E-F). Colloform layering tended to become increasingly sheet-like with distance away from the cores and as adjacent micro-stromatolitic structures fused (Figure 3.4B, E, G). Most micro-stromatolitic iron sulphide structures were oriented towards the inside of the tubes. Electron microprobe transects through the colloform textures (Supplementary Tables C.2-C.5; Supplementary Figures C.2-C.5) showed silicon or zinc to be present within some of the fine mineral layers, however, the small size of individual layers made it difficult to determine their elemental composition independently of the surrounding layers.

Amorphous silica was often present filling voids between pyrite bands in the fully mineralised *Alvinella* spp. tubes (Figure 3.2B). However, in four of the polished blocks (numbers 57.2, 57.3, 58, 62.1), the mineral tube wall was mainly comprised of layers of silica that resembled organic tube layers in thickness and shape (Figure 3.4H, I). These silica layers also contained rows of iron sulphide cores, much like those observed to have grown within the organic walls of partially mineralised *Alvinella* spp. tubes (Figure 3.4J). The silica layers were made up of small (less than 1 μm diameter) silica spheres, and in some places the thick silica layers exhibited web-like or stringy textures (Figure 3.4I, K).

Additional mineral textures found within fully mineralised *Alvinella* spp. tubes comprised mainly of pyrite include a texture of cross-cutting and/or bundled 'fibres' (Figure 3.4L-M), which occurred on the external surface of a tube. Under higher magnification, these bundled 'fibres' showed a surface covering of smaller cross-hatched striations less than 1 μm in width (Figure 3.4M, *insert*). Another tube also contained mineral infilling of pyrite

crystals, and a fine mesh-like structure also formed of pyrite (Figure 3.4N-O), while anhydrite was observed to have overgrown the inside of a different fully mineralised *Alvinella* spp. tube (Figure 3.4P).

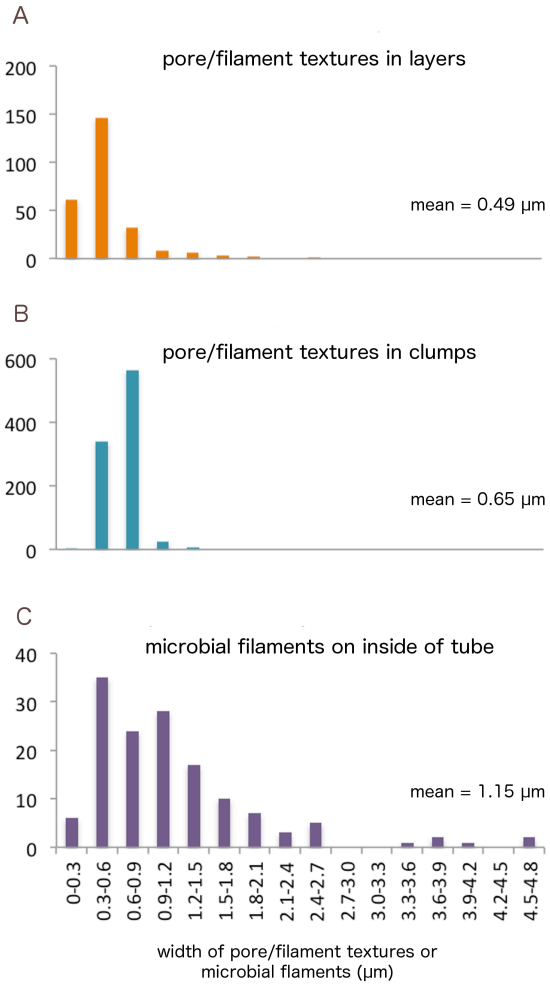

Figure 3.5 Frequency distribution plots showing diameter measurements for **A,** pores and filaments occurring within mineralised bands of *Alvinella* spp. tubes (association 1); **B,** those occurring as clumps (association 2); and **C,** confirmed microbial filaments from the inside of an *Alvinella* spp. tube (Specimen 44).

3.4.4 Pore and filament textures

Another texture prevalent in the fully mineralised tube samples was porosity. The pyrite minerals of several tubes contained circular pores 0.1 µm to several micrometers in diameter, in association with sinuous, unbranched filaments of a uniform diameter (Figure 3.4F, Q, S-U) (hereafter referred to as pore and filament associations). A few of these filaments contained cross-walls resembling septae (Figure 3.4V-W). Pore and filament textures were found to crosscut colloform structures, and in some samples, the filaments appeared 'rooted' to individual pyrite layers (Figure 3.4Q, U). Two types of pore and filament associations were identified, based on their mode of occurrence. The first (association 1) occurred within the pyrite layers comprising fully mineralised *Alvinella* spp.

tubes (Figure 3.4F, Q), and had pores and filaments ranging from 0.13 μm to 2.62 μm in diameter (mean = 0.49 μm; Figure 3.5) that were in some instances very densely packed (Supplementary Table C.6). Association 1 filaments were hollow. The second type of pore and filament association (association 2) occurred as clumps of pores and filaments preserved within pyrite minerals adjacent to the outer layers of fully mineralised *Alvinella* spp. tubes (Figure 3.4R-U). Association 2 pores and filaments had diameters of a smaller size range (0.26 μm to 1.36 μm; mean = 0.65 μm) (Figure 3.5), and were often more densely packed than pores and filaments in association 1 (Supplementary Table C.6). Association 2 filaments at times also exhibited changes in orientation within the clumps, appearing in transverse section towards the centre of the clumps, and in longitudinal section towards the clump perimeters (Figure 3.4S, U). The filaments were mostly hollow but some were infilled by pyrite (Figure 3.4X).

Table 3.2 Results of statistical tests performed on pore and filament mineral textures preserved in mineral layers and as clumps, and microbial filaments from the inner surface of an *Alvinella* spp. tube (Specimen 44).

		P/F in layers	P/F in clumps	Microbial filaments
Shapiro-Wilk test	n	259	939	142
	W	0.7337	0.9550	0.8181
	p	< 2.2E-16	2.34E-16	5.47E-12
		P/F in clumps vs.	P/F in layers vs.	P/F in clumps vs.
F-test	*F*	0.1861	0.1392	0.0259
	p	0.000	0.000	0.000
Kolmogorov-Smirnov test	*D*	0.5678	0.5584	0.5103
	p	< 2.2E-16*	< 2.2E-16*	< 2.2E-16*

*Due to the presence of ties, *p*-values are approximate. P/F = pores/filaments.

Confirmed microbial filaments occurring on the inner tube surface of a partially mineralised *Alvinella* spp. tube (Figure 3.3H-I) were measured for comparison with the two pore and filament associations, and had a mean filament diameter of 1.15 μm (Figure 3.5). The three diameter measurement data sets (pores and filaments in layers; pores and filaments in clumps; and microbial filaments from an inner tube surface) were not normally distributed, and *F*-tests revealed the variances to be significantly different between all three data types (Table 3.2). Subsequent two-sample Kolmogorov-Smirnov tests between the data type pairs were all significant (Table 3.2). However, the *p*-values are approximate due to the presence of ties in the data.

3.5 Interpretations and discussion

3.5.1 *Alvinella* spp. tube mineralisation process

Model of mineralisation. Micro-CT reconstructions (Figure 3.3B-C) of the partially mineralised *Alvinella* spp. tubes show that tube mineralisation begins preferentially along the longitudinal surfaces of the tubes which are attached to, or nearest to the vent chimney walls (Figure 3.6A). From these surfaces, mineralisation likely spreads through the remainder of the tubes. This directional mineralisation appears to result from a greater supply of mineral ions from the vent chimney. The greater amount of sulphide minerals in the outer tube layers of partially mineralised tubes suggests that, at least initially, mineralisation begins along the exterior surfaces of tubes. Mineralisation appears to then progress within the organic walls of *Alvinella* spp. tubes, where fine iron sulphide (plus or minus a zinc and/or copper content) cores template tube layer and sub-layer surfaces (Figures 3.3D-F, 3.6C-D). Space to accommodate the growth of these cores may be provided by breaks between adjacent protein sub-layers, possibly created by a poorer organisation of their protein fibrils (Zbinden *et al.*, 2001). The sulphide cores may also form within these particular layers because of an accumulation of metal ions (e.g. iron (Le Bris *et al.*, 2008)), and/or by seeding on mineral grains (including elemental sulphur) trapped between tube layers (Maginn *et al.*, 2002) (Figures 3.3F, 3.6B-C). In addition, sulphide mineralisation within *Alvinella* spp. tube walls may also be aided by the creation of oxygen poor microenvironments between tube layers. Newly-secreted *Alvinella* spp. tubes are permeable to hydrogen sulphide (Le Bris *et al.*, 2008). If hydrogen sulphide is trapped within such crevices as it diffuses into the tube, a greater influence of anoxic vent fluid over seawater may favour the precipitation of sulphide minerals in tube wall interspaces.

The small sulphide mineral cores formed along the *Alvinella* spp. organic tube layer and sub-layer surfaces continue to grow in a directed manner, amalgamating to produce bands of iron sulphides (pyrite). These run in parallel to the organic tube layering (Figures 3.3C-F, 3.4A-F, 3.6D), and are often more numerous than the original organic tube layers. These pyrite bands show an increasingly colloform texture as they thicken, and can preserve fine-scale details of the original fibrous structure of the organic tubes (Figure 3.4L-M), possibly even individual protein fibres (Figure 3.4M, *insert*). The growing sulphide bands may also incorporate and fossilise the microbial community present between the organic tube layers, leading to the formation of layers of pyrite with pore and filament textures (as proposed by Maginn *et al.* (2002)). Delamination of adjacent protein sub-layers, probably resulting from iron sulphide growth and/or decay of the organic material, may expose additional surfaces

for further templating by pyrite. This process could account for the very large number of pyrite bands observed in some of the fully mineralised tubes (Figure 3.4A-B). In other samples where the fully mineralised tubes comprise of only up to 3-5 mineral bands (Figures 3.4C-E, 3.6G-H), the original organic tubes may not have been very thick, perhaps the result of a tube which was built and vacated fairly quickly by the worm (Zbinden *et al.* (2003) found 3-6 layers in 70 day old *Alvinella* spp. tubes), or a tube that was being rapidly elongated to keep pace with rapid chimney growth as suggested by previous authors (Gaill and Hunt, 1991; Chevaldonne and Jollivet, 1993).

As the organic tube walls eventually decompose, sulphide mineral precipitation continues through the accretion of thin colloform pyrite layers onto existing mineral bands (Figures 3.4B-C, E-F, 3.6E). At this stage, mineral precipitation appears to be greater on the inside of the tubes, which is shown by the orientation of micro-stromatolitic iron sulphide structures towards the tube interiors. The colloform pyrite bands that at this stage comprise the *Alvinella* spp. tube wall are subsequently overgrown by more crystalline marcasite (Figures 3.4G, 3.6E-F, H). The mineral precipitation orientation change, and the growth of later marcasite minerals, can be explained by the absence of the worms at this stage of tube mineralisation. During the life of *Alvinella* spp. the fluids in the tube are both cooler than end-member vent fluids and less acidic (pH ~7 inside the tube compared to pH 4-5 outside (Le Bris *et al.*, 2005)), because of active mixing with seawater by the worms. However, once an *Alvinella* spp. worm has left its tube, the increasingly mineralised tubes can act as conduits for fluids that are closer in composition to end-member vent fluids, including being more acidic. Marcasite is precipitated preferentially to pyrite under conditions of lower pH (Murowchick and Barnes, 1986; Schoonen and Barnes, 1991a; b; Benning *et al.*, 2000). Therefore while a tube is occupied, the higher pH within the tube would result in preferential pyrite precipitation within the tube layers, which reflects mineralogical observations (Supplementary Table C.1). Some marcasite may, however, also be precipitated while the worm is still occupying the tube. For example, in the case of the alvinellid *Paralvinella sulphincola*, marcasite is thought to be precipitated in local acidic conditions regulated by the production of tube mucus that is rich in elemental sulphur (Juniper and Sarrazin, 1995).

At this stage, silica may form layers between the pyrite bands (Figure 3.6E-F). This likely occurs due to convective cooling, which induces silica saturation and promotes its precipitation after the tube has already been mineralised by iron sulphides (Hannington and Scott, 1988; Juniper and Fouquet, 1988; Halbach *et al.*, 2002). However, the silica layers that

resemble organic tube layers and contain bands of iron sulphide cores (Figure 3.4H-K) suggest that the iron sulphide cores initially templated organic tube layers, which were later directly preserved by silica. These observations therefore suggest that silica can be intimately involved in the tube fossilisation process, rather than occurring just as a late-stage mineral phase. These silica layers are unlikely to have formed through replacement (i.e. substitution of a mineral phase by another phase, or of organic matter by a mineral) of iron sulphides, as there is no evidence in our samples of the oxidised products (i.e. no iron oxides) that one might expect from this process.

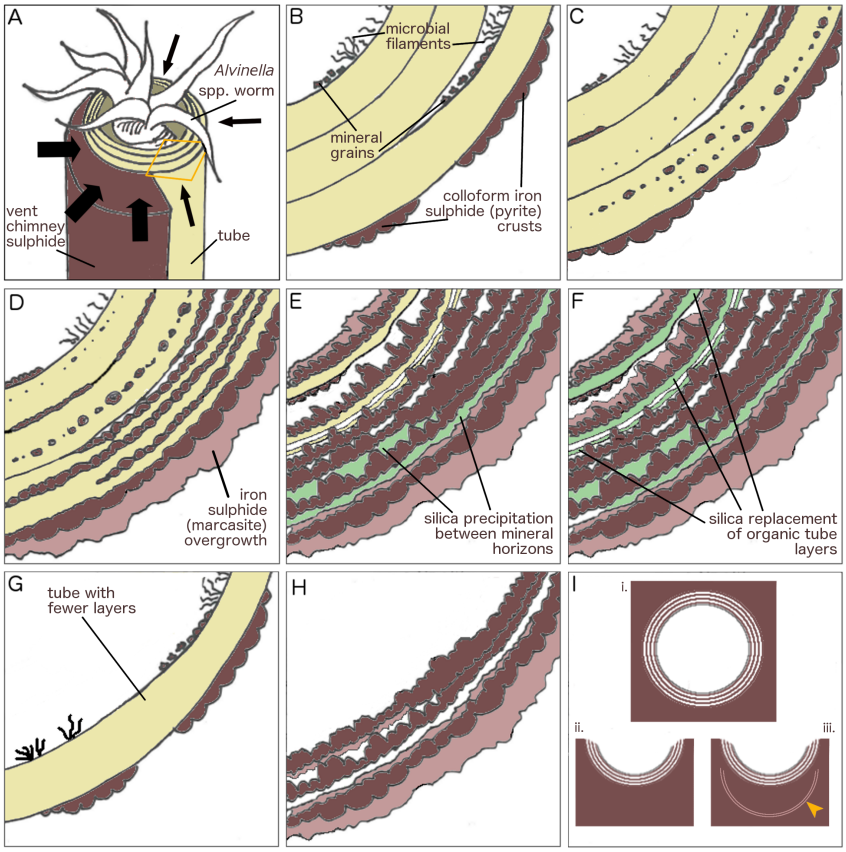

Figure 3.6 Stages of *Alvinella* spp. tube mineralisation. **A,** *Alvinella* spp. worm inside multi-layered organic tube attached to vent chimney sulphide. Mineralisation (black arrows) progresses from the outside of the tube towards the inside, and is more prevalent from the vent chimney side. Orange area shows transverse section in **B-F**. **B,** transverse section of tube in **A**. Mineralisation begins as colloform iron sulphide (pyrite) crusts forming on outer layers, and mineral grains becoming trapped in microbial filaments acting as nuclei for further mineral precipitation. **C,** minerals precipitate onto distinct surfaces within organic layers and sub-layers, as small predominantly iron sulphide cores. **D,** further mineral precipitation results in the formation of concentric colloform pyrite bands. More crystalline iron sulphide (marcasite) overgrows initial iron sulphides deposited on the outside of the tube. **E,** organic matter degrades and silica occasionally fills gaps where it previously occurred. The supply of dissolved minerals changes to being from inside the tube, and growing colloform iron sulphides orient towards the tube interior. **F,** in some instances, silica may directly preserve the degrading organic matter. Further overgrowth of more crystalline iron sulphide occurs. **G-H**, mineralisation of a tube with fewer layers and without silica, **G,** early stage; **H,** late stage. **I,** end-products of *Alvinella* spp. tube mineralisation recorded in this study. In transverse section: **i,** full tube cylinder preserved, **ii,** partial tube preservation, **iii,** partial tube preservation with preservation of a previous tube beneath it (orange arrow).

The fully mineralised *Alvinella* spp. tubes may be preserved within the vent chimneys in several different forms (Figure 3.6I). Rapid mineral precipitation may surround entire tubes to create the porous structures in Figure 3.2Ai-ii, which are analogous to those observed by previous studies of EPR chimney sulphides (Hekinian *et al.*, 1980; Haymon and Kastner, 1981; Haymon and Koski, 1985). Alternatively, only the sides of the tubes that are attached to the vent chimney may be mineralised, resulting in the partial tubes observed on the mineral blocks used in this study (Figure 3.2Aiii). The concentric continuous layers of colloform pyrite that comprise fully mineralised *Alvinella* spp. tubes clearly distinguish them from vent chimney minerals, and such layers inside some of the vent chimney samples likely represent the mineralisation of earlier tubes, which have been subsequently overgrown by vent chimney sulphides and other *Alvinella* spp. tubes (Figure 3.2C). Tubes may eventually be infilled by the precipitation of later-stage sulphides, including higher grade minerals (e.g. copper-rich sulphides), as noted by Cook and Stakes (1995) for mineralised siboglinid tubes from the JdFR.

The fully mineralised *Alvinella* spp. tubes collected from the fossilisation experiment provide a maximum-time estimate for annelid tubes to be completely mineralised at hydrothermal vents (~1 year). However, one should be cautious about deriving an actual rate of mineralisation from the above, as it is not known at what point during the deployment period *Alvinella* spp. colonised the fossilisation cages. Mineralisation rates are also likely to be highly variable on small spatial scales due to the heterogeneous nature of vent environments (Van Dover, 2000). It is therefore very likely that *Alvinella* spp. tubes can become fully mineralised much more rapidly than within one year, as suggested by the very high mineral content observed within an 11 day-old alvinellid colony (Pradillon *et al.*, 2009).

Microbial preservation. We interpret the pore and filament textures in pyrite found within and around the mineralised *Alvinella* spp. tubes to be the fossils of microbial filaments. This is because they demonstrate all of the suggested characteristics of *bona fide* microbial fossils (Westall, 1999; Schopf *et al.*, 2010), are morphologically closely analogous to the microbial community associated with partially mineralised *Alvinella* spp. tubes (Gaill *et al.*, 1987; Desbruyères *et al.*, 1998; Zbinden *et al.*, 2001; Maginn *et al.*, 2002), and occur in a range of orientations throughout the matrix of the iron sulphides in which they are present (cf. pyrite leaching/oxidation by microbes (Verati *et al.*, 1999; Edwards *et al.*, 2003)). The microbial fossils appear to be mostly external filament molds, but exhibit some evidence of replacement of septae and external sheaths by iron sulphide (Figure 3.4W-X)

demonstrating that extremely fine-scale preservation can occur at hydrothermal vent sites. The difference in diameter distributions (Figure 3.5; Table 3.2) between the fossil and the non-fossil microbial filaments may occur due to mineral replacement of microbial sheaths in the former. The significantly different diameter distributions between the fossil filaments occurring in iron sulphide bands (association 1) of the *Alvinella* spp. mineralised tube wall, and those occurring as clumps around the tube (association 2) (Figure 3.5; Table 3.2) are likely due to the fossilisation of two distinct microbial communities. Micro-organisms sampled from whole *Alvinella pompejana* tubes have been shown to differ to those sampled from tube interiors through molecular studies (Campbell *et al.*, 2003), which likely reflects the variation in microhabitats between the tube interior and exterior. Microbial mats are commonly encountered on hydrothermal vent chimneys in areas colonised by *Alvinella* spp. (Taylor *et al.*, 1999), and the position of the clumped filament fossils relative to the *Alvinella* spp. tubes in our samples indicates that the microbial filaments inhabited crevices next to the tubes, which may have provided some protection from thermal and chemical extremes. The marked differences in temperature and pH along an *Alvinella* spp. tube (temp. of ~20°C, pH ~8 at tube openings; temp. of ~120°C, pH ~4 adjacent to vent chimney substrate) (Le Bris *et al.*, 2005) may explain the patchy distribution of the clumped filaments in our samples, and why they were only found within a few of the examined specimens. The observation that the filaments in clumps are sometimes 'rooted' onto specific iron sulphide layers (Figure 3.4U) indicates a complex intergrowth of microbial mats and sulphide mineral precipitation.

The mesh-like pyritised structure associated with sulphide minerals precipitated in the internal space of the fully mineralised *Alvinella* spp. tube shown in Figure 3.4N-O likely represents mineralised EPS, due to the irregular sizes of the fibres comprising the mesh. In addition, the mesh in Figure 3.4O bears a strong resemblance to mineralised microbial EPS textures observed in hot spring deposits (Handley *et al.*, 2008; Tobler *et al.*, 2008; Peng and Jones, 2012). Many hydrothermal vent micro-organisms are known to secrete EPS (Raguenes *et al.*, 1996, 1997a), including those associated with the integument of *Alvinella pompejana* (Vincent *et al.*, 1994; Raguenes *et al.*, 1997b; Cambon-Bonavita *et al.*, 2002). However as the mesh observed in this study is positioned on top of minerals infilling an *Alvinella* spp. tube, we hypothesise that the mesh was created in the absence of an *Alvinella* spp. polychaete.

3.5.2 Comparison with previous accounts of vent tube mineralisation

Our observations of early-stage mineral precipitation in *Alvinella* spp. tubes are similar to that reported by Maginn *et al.* (2002), as we also observed early-stage iron sulphide mineralisation along sub-layers in *Alvinella* spp. tubes. However, we did not find pyrite to be directly replacing the organic walls of *Alvinella* spp. tubes in our samples, finding instead more evidence for the growth of sulphides on the organic layer surfaces (i.e. templating). The small iron sulphide cores we observed along tube sub-layer surfaces appear analogous to the nanocrystalline zinc-iron sulphides reported by Zbinden *et al.* (2001, 2003). However, the general absence of zinc sulphides in our tube samples may be explained by different chemical and/or thermal characteristics of the vent fluids in the 9°N EPR area at the time that our samples were collected, compared to when the *Alvinella* spp. tubes studied by Zbinden *et al.* (2001, 2003) were obtained, as it is well established that EPR 9°N vent fluid temperature and chemistry varies temporally (Von Damm, 2000, 2004; Von Damm and Lilley, 2004). Previous studies on early-stage mineralisation have also proposed that the presence of trapped micro-organisms within the organic tube walls of *Alvinella* spp. (Maginn *et al.*, 2002) and siboglinid tubes (Peng *et al.*, 2008, 2009) may have a direct control on their mineralisation. However, mineral growth along the organic sub-layers within our *Alvinella* spp. tubes often did not originate where trapped microbial filaments occurred, suggesting that mineralisation may also take place in the absence of micro-organisms, in spaces between the protein fibril layering of *Alvinella* spp. tubes. This may also account for the absence of fossilised microbial filaments in many of the pyrite bands.

The fully mineralised *Alvinella* spp. tubes described here differ from the recently mineralised siboglinid worm tubes described by Cook and Stakes (1995) because at all stages of mineralisation of the latter, the tubes are represented by a single layer of minerals, and do not show the concentric multi-layered banding of the *Alvinella* spp. tubes. This likely reflects the structural differences of siboglinid tubes compared to *Alvinella* spp. tubes (Gaill and Hunt, 1986; Shillito *et al.*, 1995), and suggests that it may be possible to distinguish tubes from these two polychaete families in the fossil record, if their mineralised products are not substantially altered through diagenesis.

3.5.3 Comparison with ancient hydrothermal vent tubeworm fossils

Our mineralised *Alvinella* spp. tubes differ in several respects from all fossil vent tubes described to date (Little *et al.*, 1998). The Silurian vent tube species *Eoalvinellodes annulatus*

(Little *et al.*, 1999) occupied a similar ecological habitat as *Alvinella* spp., being found on the exterior of vent chimney walls, but the mineralised tubes of *E. annulatus* are formed of a single layer (0.04–0.60 mm thick) of framboidal and/or colloform pyrite, that is externally smooth but with internal ornament of concentric and sub-concentric annulations. Further, *E. annulatus* tubes are generally smaller than *Alvinella* spp. tubes. The tubes of the Silurian vent species *Yamankasia rifeia* (Little *et al.*, 1997, 1999) are equivalent in size to *Alvinella* spp. tubes, and have tube walls formed of several thin layers (0.01-0.08 mm thick) of arsenian pyrite, however they show an external ornament of concentric growth lines, fine longitudinal ridges that are absent in *Alvinella* spp. tubes. However, some *Y. rifeia* tube wall have a thick coating (up to 2.7 mm) of micro-laminated colloform pyrite with ~1 μm diameter holes (Little *et al.*, 1997), which are very much like the microbial fossils in *Alvinella* spp. tubes.

Haymon *et al.* (1984) and Haymon and Koski (1985) compared fully mineralised *Alvinella* spp. tubes from 21°N EPR with Upper Cretaceous (Bayda, Oman) tubular fossils formed of 2-3 concentric pyrite layers, with interlaminations silica or void space. While these fossil tubes are morphologically similar to our *Alvinella* spp. tubes in terms of size and the presence of multi-layering in the tube wall, they do not show all the characteristics outlined above for *Alvinella* spp. tubes, such as some tube walls being comprised of many more than three pyrite layers. In addition, the Bayda tubes exhibit annulations and longitudinal ornamentation which are more closely associated with siboglinid or chaetopterid tubes (Kiel and Dando, 2009; Hilário *et al.*, 2011), and are generally absent from *Alvinella* spp. tubes. Because of this, we suggest that no known ancient vent fossil tubes are equivalent to present day *Alvinella* spp. tubes. This interpretation is currently supported by molecular evidence suggesting that modern alvinellids diverged from 41 to 51 Ma (Eocene) (Vrijenhoek, 2013), whereas the majority of well-preserved tubular vent fossils are Mesozoic or Palaeozoic in age (Little *et al.*, 1997, 1998, 1999).

3.5.4 Soft tissue preservation by silica and pyrite

Our study shows that the proteinaceous organic tube walls of *Alvinella* spp. and associated microbial cells can be rapidly preserved by both sulphide minerals and silica at vent sites. Soft tissue preservation by pyrite is on the whole rare and only seen at sites of exceptional preservation, e.g. Beecher's Trilobite Bed, Upper Ordovician, New York State USA, or the Hunsrückschiefer, Devonian, western Germany (Briggs *et al.*, 1991; Briggs and Bartels, 2001; Raiswell *et al.*, 2008; Farrell *et al.*, 2013). In these cases, soft tissues are preserved by

an infilling or templating of pyrite occurring as framboids, pyritohedra and euhedral crystals generally less than 20 μm in size (Briggs *et al.*, 1991, 1996). Sulphide mineralisation within this setting is biogenically-mediated as it results from the decay of the soft tissues and leads to the localisation of sulphide mineral precipitation on and around these tissues. Within hydrothermal vent environments, mineral precipitation generally occurs abiogenically as a result of the mixing of hot, mineral-rich vent fluid with cooler seawater. However, the role of decay products on mineralisation within vents is largely unknown. Elevated dissolved sulphide, low oxygen and low pH conditions that may be especially concentrated around decomposing *Alvinella* spp. tube surfaces could act to induce local supersaturation of iron and sulphide at these sites, and thereby promote more intense iron sulphide precipitation. The micro-stromatolitic, fine-scale nature of pyrite that preserves *Alvinella* spp. tubes could be indicative of this process, as small pyrite grain sizes suggest abundant nucleation, which is considered a product of high degrees of supersaturation and the formation of colloform pyrite (Barrie *et al.*, 2009). Decay-induced local supersaturation may thereby account for the widespread association and organisation of colloform iron sulphide textures with *Alvinella* spp. tubes, compared to their relative rarity within vent chimney minerals. The role of decay products in hydrothermal vent mineralisation therefore could have parallels with (albeit different products to) pyritisation within soft sediments, but warrants further investigation.

Within terrestrial hydrothermal systems, i.e. hot springs, detailed preservation of organic matter by early-stage silica microspheres has been widely documented for micro-organisms (Westall *et al.*, 1995; Jones *et al.*, 1997, 1998; Konhauser *et al.*, 2001) as well as for wood (Akahane *et al.*, 2004). The mechanisms of preservation can be diverse, and both micro-organisms and plant tissues may be replaced or templated by silica (Jones and Renaut, 2003), or silica can infill the lumina of plant cells (Akahane *et al.*, 2004). Analogous mechanisms might be proposed for silica mineralisation within the similar setting of deep-sea hydrothermal vent environments. In the *Alvinella* spp. tubes, the mechanism through which silica appears to have preserved organic tube walls does not seem to be void-filling, as silica mimics the appearance of tube layers rather than gaps between or within them. Instead, silica seems to have either replaced organic matter directly, or to have universally templated protein fibres within the tube walls. These modes of mineralisation can account for the stringy, web-like appearance of silica in some of the fully mineralised tubes (Figure 3.4K). As in terrestrial hot springs, several modes of organic matter preservation by silica may be occurring simultaneously within hydrothermal vents, but if silica templating is a

pathway through which *Alvinella* spp. tubes are mineralising, it seems to be occurring in an altogether different manner to pyrite templating.

3.6 Conclusions

Documenting in detail the mineralisation of modern polychaete tubes is critical to ensuring the validity of fossil-modern comparisons, and to advancing current understanding of the taphonomy and palaeontology of polychaete worms. We have shown how *Alvinella* tubes can be fully mineralised within a modern hydrothermal vent setting as multiple concentric pyrite bands, that include fine-scale features such as protein fibres and associated micro-organisms. Our ability to interpret ancient fossils will always be limited by paucity of material and diagenetic alteration, and it is important to be mindful of these factors when comparing ancient to recently mineralised material. Fortunately, many ancient hydrothermal vent tube fossils appear well preserved, with some of the oldest specimens exhibiting fine colloform layering which suggests that they have not been significantly altered. These tubes will make ideal targets for investigating the preservation and nature of interactions between micro-organisms and tubeworms, a largely unknown aspect of the ecology of ancient vent communities.

3.7 Acknowledgements

MNG is funded by a NERC CASE PhD studentship (NE/K500847/1). For sample collection cruises to the East Pacific Rise, the authors would like to thank Karen Von Damm (deceased), Stefan Sievert and Timothy Shank specifically, and the Woods Hole Oceanographic Institution in general. Funding for these cruises was from the NSF Ridge2000 project (AT15-13 and AT15-27 - OCE03-27126; AT15-38 - MCB07-02677). NERC Small Grant NE/C000714/1 funded the fossilisation experiments of CTSL associated with these cruises. Thank you to Chris Stanley (NHM) for help with mineralogical observations, and to Claire Stevenson for observations of anhydrite and rooted filaments in the *Alvinella* spp. tubes. Thanks also to Harri Wyn Williams, Richard Walshaw, Lesley Neve, Geoff Lloyd, David Wallis, Liane Benning (Leeds); Tomasz Goral, Farah Ahmed, Daniel Sykes, and John Spratt (NHM) for guidance and assistance with analytical techniques.

3.8 References

Akahane, H., Furuno, T., Miyajima, H., Yoshikawa, T. and Yamamoto, S. (2004) Rapid wood silicification in hot spring water: an explanation of silicification of wood during the Earth's history. *Sedimentary Geology* **169**, 219–228.

Barrie, C. D., Boyce, A. J., Boyle, A. P., Williams, P. J., Blake, K., Ogawara, T., Akai, J. and Prior, D. J. (2009) Growth controls in colloform pyrite. *American Mineralogist* **94**, 415–429. doi:10.2138/am.2009.3053.

Benning, L., Wilkin, R. and Barnes, H. (2000) Reaction pathways in the Fe–S system below 100°C. *Chemical Geology* **167**, 25–51.

Boyce, A. J., Little, C. T. S. and Russel, M. J. (2003) A new fossil vent biota in the Ballynoe barite deposit, Silvermines, Ireland: evidence for intracratpnic sea-floor hydrothermal activity about 352 Ma. *Ecolomic Geology* **98**, 649–656.

Briggs, D. E. G. and Bartels, C. (2001) New arthropods from the Lower Devonian Hunsrück Slate (Lower Emsian, Rhenish Massif, Western Germany). *Palaeontology* **44**, 275–303.

Briggs, D. E. G., Bottrell, S. H. and Raiswell, R. (1991) Pyritization of soft-bodied fossils: Beecher's Trilobite Bed, Upper Ordovician, New York State. *Geology* **19**, 1221–1224. doi:10.1130/0091-7613(1991)019<1221.

Briggs, D. E. G., Raiswell, R., Bottrell, S. H., Hatfield, D. T. and Bartels, C. (1996) Controls on the pyritization of exceptionally preserved fossils; an analysis of the Lower Devonian Hunsrueck Slate of Germany. *American Journal of Science* **296**, 633–663.

Bryce, J., Prado, F. and Von Damm, K. (2007) Vent Fluid Chemistry Data, including Metals Fractions and Dissolved Majors, from fluid samples acquired with HOV Alvin during Atlantis expedition AT15-13 (2006) at the East Pacific Rise 9N site. Integrated Earth Data Applications (IEDA). doi: http://dx.doi.org/10.1594/IEDA/317364.

Bryce, J., Prado, F. and Von Damm, K. (2008) Vent Fluid Chemistry Data, including Metals Fractions and Dissolved Majors, from fluid samples acquired with HOV Alvin during Atlantis expedition AT15-27 (2007) at the East Pacific Rise 9N site. Integrated Earth Data Applications (IEDA). doi: http://dx.doi.org/10.1594/IEDA/317603.

Cambon-Bonavita, M.-A., Raguenes, G., Jean, J., Vincent, P. and Guezennec, J. (2002) A novel polymer produced by a bacterium isolated from a deep-sea hydrothermal vent polychaete annelid. *Journal of Applied Microbiology* **93**, 310–315. doi:10.1046/j.1365-

2672.2002.01689.x.

Campbell, B. J. and Cary, S. C. (2001) Characterization of a novel Spirochete associated with the hydrothermal vent polychaete annelid, *Alvinella pompejana*. *Applied and Environmental Microbiology* **67**, 110–117. doi:10.1128/AEM.67.1.110.

Campbell, B., Stein, J. and Cary, S. (2003) Evidence of chemolithoautotrophy in the baterial community associated with *Alvinella pompejana*, a hydrothermal vent polychaete. *Applied and Environmental Microbiology* **69**, 5070– 5078.

Chevaldonne, P. and Jollivet, D. (1993) Videoscopic study of deep-sea hydrothermal vent alvinellid polychaete populations: biomass estimation and behaviour. *Marine Ecology Progress Series* **95**, 251–262.

Conway Morris, S. and Peel, J. S. (2008) The earliest annelids: lower Cambrian polychaetes from the Sirius Passet Lagerstätte, Peary Land, North Greenland. *Acta Palaeontologica Polonica* **53**, 137–148. doi:10.4202/app.2008.0110.

Cook, T. and Stakes, D. (1995) Biogeological mineralisation in deep-sea hydrothermal deposits. *Science* **267**, 1975–1979.

Desbruyeres, D., Gaill, F., Laubier, L. and Fouquet, Y. (1985) Polychaetous annelids from hydrothermal vent ecosystems: an ecological overview. *Bulletin of the Biological Society of Washington* **6**, 103–116.

Desbruyères, D., Chevaldonné, P., Alayse, A.-M., Jollivet, D., Lallier, F. H., Jouin-Toulmond, C., Zal, F., Sarradin, P.-M., Cosson, R., Caprais, J.-C., Arndt, C., O'Brien, J., Guezennec, J., Hourdez, S., Riso, R., Gaill, F., Laubier, L. and Toulmond, A. (1998) Biology and ecology of the "Pompeii worm" (*Alvinella pompejana* Desbruyères and Laubier), a normal dweller of an extreme deep-sea environment: A synthesis of current knowledge and recent developments. *Deep-Sea Research II* **45**, 383–422.

Di Meo-Savoie, C. A., Luther, G. W. and Cary, S. C. (2004) Physicochemical characterization of the microhabitat of the epibionts associated with *Alvinella pompejana*, a hydrothermal vent annelid. *Geochimica et Cosmochimica Acta* **68**, 2055–2066. doi:10.1016/j.gca.2003.10.039.

Edwards, K. J., McCollom, T., Konishi, H. and Buseck, P. (2003) Seafloor bioalteration of sulfide minerals: results from in situ incubation studies. *Geochimica et Cosmochimica Acta* **67**, 2843–2856. doi:10.1016/S0016-7037(00)00089-9.

Farrell, U. C., Briggs, D. E. G., Hammarlund, E. U., Sperling, E. A. and Gaines, R. R.

(2013) Paleoredox and pyritization of soft-bodied fossils in the Ordovician Frankfort Shale of New York. *American Journal of Science* **313**, 452–489. doi:10.2475/05.2013.02.

Fornari, D., Von Damm, K., Bryce, J., Cowen, J., Ferrini, V., Fundis, A., Lilley, M., Luther, G., Mullineaux, L., Perfit, M., Meana-Prado, M. F., Rubin, K., Seyfried, W., Shank, T., Soule, S. A., Tolstoy, M. and White, S. (2012) The East Pacific Rise between 9°N and 10°N: twenty-five years of integrated, multidisciplinary oceanic spreading center studies. *Oceanography* **25**, 18–43. doi:10.5670/oceanog.2012.02.

Gaill, F. and Hunt, S. (1986) Tubes of deep sea hydrothermal vent worms *Riftia pachyptila* (Vestimentifera) and *Alvinella pompejana* (Annelida). *Marine Ecology Progress Series* **3**, 267–274.

Gaill, F. and Hunt, S. (1991) The biology of annelid worms from high temperature hydrothermal vent regions. *Reviews in Aquatic Sciences* **4**, 107–137.

Gaill, F., Desbruyères, D. and Prieur, D. (1987) Bacterial communities associated with "Pompei Worms" from the East Pacific Rise hydrothermal vents: SEM, TEM observations. *Microbial Ecology* **13**, 129–139.

Haddad, A., Camacho, F., Durand, P. and Cary, S. C. (1995) Phylogenetic characterization of the epibiotic bacteria associated with the hydrothermal vent polychaete *Alvinella pompejana*. *Applied and Environmental Microbiology* **61**, 1679–1687.

Halbach, M., Halbach, P. and Luders, V. (2002) Sulfide-impregnated and pure silica precipitates of hydrothermal origin from the Central Indian Ocean. *Chemical Geology* **182**, 357–375.

Handley, K. M., Turner, S. J., Campbell, K. A. and Mountain, B. W. (2008) Silicifying biofilm exopolymers on a hot-spring microstromatolite: templating nanometer-thick laminae. *Astrobiology* **8**, 747–70. doi:10.1089/ast.2007.0172.

Hannington, M. D. and Scott, S. D. (1988) Mineralogy and geochemistry of a hydrothermal silica-sulfide-sulfate in the caldera of Axial Seamount, Juan de Fuca ridge. *Canadian Mineralogist* **26**, 603–625.

Haymon, R. M. and Kastner, M. (1981) Hot spring deposits on the East Pacific Rise at 21°N: preliminary description of mineralogy and genesis. *Earth and Planetary Science Letters* **53**, 363–381.

Haymon, R. and Koski, R. (1985) Evidence of an ancient hydrothermal vent community: fossil worm tubes in Cretaceous sulfide deposits of the Samail Ophiolite, Oman.

Bulletin of the Biological Society of Washington **6**, 57–65.

Haymon, R. M., Koski, R. A. and Sinclair, C. (1984) Fossils of hydrothermal vent worms from Cretaceous sulfide ores of the Samail Ophiolite, Oman. *Science* **223**, 1407–1409.

Hekinian, R., Fevrier, M., Bischoff, J. L., Picot, P. and Shanks, W. (1980) Sulfide deposits from the East Pacific Rise near 21°N. *Science* **207**, 1433–1444.

Hilário, A., Capa, M., Dahlgren, T. G., Halanych, K. M., Little, C. T. S., Thornhill, D. J., Verna, C. and Glover, A. G. (2011) New perspectives on the ecology and evolution of siboglinid tubeworms. *PLOS ONE* **6**, e16309. doi:10.1371/journal.pone.0016309.

Jones, B. and Renaut, R. W. (2003) Hot spring and geyser sinters: the integrated product of precipitation, replacement, and deposition. *Canadian Journal of Earth Sciences* **40**, 1549–1569. doi:10.1139/e03-078.

Jones, B., Renaut, R. W. and Rosen, M. R. (1997) Biogenicity of silica precipitation around geysers and hot-spring vents, North Island, New Zealand. *Journal of Sedimentary Research* **67**, 88–104.

Jones, B., Renaut, R. W. and Rosen, M. R. (1998) Microbial biofacies in hot-spring sinters: a model based on Ohaaki Pool, North Island, New Zealand. *Journal of Sedimentary Research* **68**, 413–434.

Juniper, S. K. and Fouquet, Y. (1988) Filamentous iron-silica deposits from modern and ancient hydrothermal sites. *Canadian Mineralogist* **26**, 859–869.

Juniper, S. and Martineu, P. (1995) Alvinellids and sulfides at hydrothermal vents of the eastern Pacific: a review. *American Zoologist* **35**, 174–185.

Juniper, S. K. and Sarrazin, J. (1995) Interaction of vent biota and hydrothermal deposits: Present evidence and future experimentation. In *Seafloor Hydrothermal Systems: Physical, Chemical, Biological, and Geological Interactions* (ed. Humphris, S. E., Zierenberg, R. A., Mullineaux, L. S. and Thomson, R. E.), pp. 178–193. American Geophysical Union, Washington, D. C.

Kiel, S. and Dando, P. R. (2009) Chaetopterid tubes from vent and seep sites: implications for fossil record and evolutionary history of vent and seep annelids. *Acta Palaeontologica Polonica* **54**, 443–448. doi:10.4202/app.2009.0022.

Konhauser, K. O., Phoenix, R. R., Bottrell, S. H., Adams, D. G. and Head, I. M. (2001) Microbial–silica interactions in Icelandic hot spring sinter: possible analogues for some Precambrian siliceous stromatolites. *Sedimentology* **48**, 415–433.

Le Bris, N. and Gaill, F. (2007) How does the annelid *Alvinella pompejana* deal with an extreme hydrothermal environment? *Reviews in Environmental Science and Biotechnology* **6**, 197–221. doi:10.1007/s11157-006-9112-1.

Le Bris, N., Zbinden, M. and Gaill, F. (2005) Processes controlling the physico-chemical micro-environments associated with Pompeii worms. *Deep-Sea Research I* **52**, 1071–1083.

Le Bris, N., Anderson, L., Chever, F. and Gaill, F. (2008) Sulfide diffusion and chemoautotrophy requirements in an extremophilic worm tube. In *Biological Oceanography Research Trends* (ed. Mertens, L. P.), pp. 157–175. Nova Science Publishers Inc, New York.

Limaye, A. (2006) Drishti: Volume Exploration and Presentation Tool. Australian National University, Canberra.

Little, C. T. S. (2009) Hot stuff in the deep sea. NERC *Planet Earth Online*, http://planetearth.nerc.ac.uk/features/story.aspx? id=576.

Little, C. T. S. and Vrijenhoek, R. C. (2003) Are hydrothermal vent animals living fossils? *Trends in Ecology & Evolution* **18**, 582–588. doi:10.1016/j.tree.2003.08.009.

Little, C. T. S., Herrington, R. J., Maslennikov, V. V., Morris, N. J. and Zaykov, V. V. (1997) Silurian hydrothermal-vent community from the southern Urals, Russia. *Nature* **385**, 146–148. doi:10.1038/385146a0.

Little, C. T. S., Herrington, R. J., Maslennikov, V. V. and Zaykov, V. V. (1998) The fossil record of hydrothermal vent communities. *Geological Society, London, Special Publications* **148**, 259–270. doi:10.1144/GSL.SP.1998.148.01.14.

Little, C. T. S., Maslennikov, V. V, Morris, N. J. and Gubanov, A. P. (1999) Two Palaeozoic hydrothermal vent communities from the southern Ural mountains, Russia. *Palaeontology* **42**, 1043–1078.

Little, C. T. S., Danelian, T., Herrington, R. and Haymon, R. (2004) Early Jurassic hydrothermal vent community from the Franciscan Complex, California. *Journal of Paleontology* **78**, 542–559.

Little, C. T. S., Magalashvili, A. and Banks, D. (2007) Neotethyan Late Cretaceous volcanic arc hydrothermal vent fauna. *Geology* **35**, 835–838.

Maginn, E., Little, C. T. S., Herrington, R. and Mills, R. (2002) Sulphide mineralisation in the deep sea hydrothermal vent polychaete, *Alvinella pompejana*: implications for fossil

preservation. *Marine Geology* **181**, 337–356.

Murowchick, J. and Barnes, H. (1986) Marcasite precipitation from hydrothermal solutions. *Geochimica et Cosmochimica Acta* **50**, 2615–2629.

Peng, X. and Jones, B. (2012) Rapid precipitation of silica (opal-A) disguises evidence of biogenicity in high-temperature geothermal deposits: Case study from Dagunguo hot spring, China. *Sedimentary Geology* **257-260**, 45–62. doi:10.1016/j.sedgeo.2012.01.013.

Peng, X., Zhou, H. H., Tang, S., Yao, H., Jiang, L. and Wu, Z. (2008) Early-stage mineralisation of hydrothermal tubeworms: New insights into the role of microorganisms in the process of mineralisation. *Chinese Science Bulletin* **53**, 251–261. doi:10.1007/s11434-007-0517-1.

Peng, X., Zhou, H., Yao, H., Li, J. and Wu, Z. (2009) Ultrastructural evidence for iron accumulation within the tube of Vestimentiferan *Ridgeia piscesae*. *Biometals* **22**, 723–732.

Pradillon, F., Zbinden, M., Mullineaux, L. and Gaill, F. (2005) Colonisation of newly-opened habitat by a pioneer species, *Alvinella pompejana* (Polychaeta: Alvinellidae), at East Pacific Rise vent sites. *Marine Ecology Progress Series* **302**, 147–157. doi:10.3354/meps302147.

Pradillon, F., Zbinden, M., Le Bris, N., Hourdez, S., Barnay, A. S. and Gaill, F. (2009) Development of assemblages associated with alvinellid colonies on the walls of high-temperature vents at the East Pacific Rise. *Deep-Sea Research II* **56**, 1622–1631. doi:10.1016/j.dsr2.2009.05.009.

R Core Team (2013) *R: A Language and Environment for Statistical Computing*. 3.0.2. R Foundation for Statistical Computing, Vienna, Austria.

Raff, E. C., Schollaert, K. L., Nelson, D. E., Donoghue, P. C. J., Thomas, C.-W., Turner, F. R., Stein, B. D., Dong, X., Bengtson, S., Huldtgren, T., Stampanoni, M., Chongyu, Y. and Raff, R. A. (2008) Embryo fossilisation is a biological process mediated by microbial biofilms. *Proceedings of the National Academy of Sciences* **105**, 19360–19365. doi:10.1073/pnas.0810106105.

Raguenes, G., Pignet, P., Gauthier, G., Peres, A., Christen, R., Rougeaux, H., Barbier, G. and Guezennec, J. (1996) Description of a new polymer-secreting bacterium from a deep-sea hydrothermal vent, *Alteromonas macleodii* subsp. *fijiensis*, and preliminary characterization of the polymer. *Applied and Environmental Microbiology* **62**, 67–73.

Raguenes, G., Peres, A., Ruimy, R., Pignet, P., Christen, R., Loaec, M., Rougeaux, H.,

Barbier, G. and Guezennec., J. G. (1997a) *Alteromonas infernus* sp. nov., a new polysaccharide-producing bacterium isolated from a deep-sea hydrothermal vent. *Journal of Applied Microbiology* **82**, 422–430.

Raguenes, G., Christen, R., Guezennec, J. G., Pignet, P. and Barbier, G. (1997b) *Vibrio diabolicus* sp. nov., a new polysaccharide-secreting organism isolated from a deep-sea hydrothermal vent polychaete annelid, *Alvinella pompejana*. *International Journal of Systematic Bacteriology* **47**, 989–995.

Raiswell, R., Newton, R., Bottrell, S. H., Coburn, P. M., Briggs, D. E. G., Bond, D. P. G. and Poulton, S. W. (2008) Turbidite depositional influences on the diagenesis of Beecher's Trilobite Bed and the Hunsruck Slate; sites of soft tissue pyritization. *American Journal of Science* **308**, 105–129. doi:10.2475/02.2008.01.

Schoonen, M. and Barnes, H. (1991a) Reactions forming pyrite and marcasite from solution: I. Nucleation of FeS_2 below 100°C. *Geochimica et Cosmochimica Acta* **55**, 1495–1504.

Schoonen, M. and Barnes, H. (1991b) Reactions forming pyrite and marcasite from solution: II. Via FeS precursors below 100°C. *Geochimica et Cosmochimica Acta* **55**, 1505–1514.

Schopf, J. W., Kudryavtsev, A. B., Sugitani, K. and Walter, M. R. (2010) Precambrian microbe-like pseudofossils: A promising solution to the problem. *Precambrian Research* **179**, 191–205. doi:10.1016/j.precamres.2010.03.003.

Shillito, B., Lechaire, J.-P., Goffinet, G. and Gaill, F. (1995) Composition and morphogenesis of the tubes of vestimentiferan worms. *Geological Society, London, Special Publications* **87**, 295–302. doi:10.1144/GSL.SP.1995.087.01.22.

Taylor, C. D., Wirsen, C. O. and Gaill, F. (1999) Rapid microbial production of filamentous sulfur mats at hydrothermal vents. *Applied and Environmental Microbiology* **65**, 2253–2255.

Tobler, D. J., Stefánsson, A. and Benning, L. G. (2008) In-situ grown silica sinters in Icelandic geothermal areas. *Geobiology* **6**, 481–502. doi:10.1111/j.1472-4669.2008.00179.x.

Van Dover, C. (2000) *The ecology of deep-sea hydrothermal vents*. Princeton University Press, New Jersey.

Verati, C., Donato, P. De, Prieur, D. and Lancelot, J. (1999) Evidence of bacterial activity

from micrometer-scale layer analyses of black-smoker sulfide structures (Pito Seamount Site, Easter microplate). *Chemical Geology* **158**, 257–269.

Vincent, P., Pignet, P., Talmont, F., Bozzi, L., Fournet, B., Guezennec, J., Jeanthon, C. and Prieur, D. (1994) Production and characterization of an exopolysaccharide excreted by a deep-sea hydrothermal vent bacterium isolated from the polychaete annelid *Alvinella pompejana*. *Applied and Environmental Microbiology* **60**, 4134–4141.

Vinther, J., Eibye-Jacobsen, D. and Harper, D. A. (2011) An Early Cambrian stem polychaete with pygidial cirri. *Biology Letters* **7**, 929–932.

Von Damm, K. L. (2000) Chemistry of hydrothermal vent fluids from 9°-10°N, East Pacific Rise: " Time zero," the immediate posteruptive period. *Journal of Geophysical Research* **105**, 11,203–11,222.

Von Damm, K. L. (2004) Evolution of the hydrothermal system at East Pacific Rise 9°50′ N: Geochemical evidence for changes in the upper oceanic crust. *Geophysical Monograph Series* **148**, 285–304.

Von Damm, K. L. and Lilley, M. D. (2004) Diffuse flow hydrothermal fluids from 9°50′ N East Pacific Rise: Origin, evolution and biogeochemical controls. *Geophysical Monograph Series* **144**, 245–268.

Vovelle, J. and Gaill, F. (1986) Donnees morphologiques, histochimiques et microanalytiques sur l'elaboration du tube organo-mineral d'*Alvinella pompejana*, polychete des sources hydrothermales, et leurs implications phylogenetiques. *Zoologica Scripta* **15**, 33–43.

Vrijenhoek, R. C. (2013) On the instability and evolutionary age of deep-sea chemosynthetic communities. *Deep-Sea Research II* **92**, 189–200. doi:10.1016/j.dsr2.2012.12.004.

Westall, F. (1999) The nature of fossil bacteria: A guide to the search for extraterrestrial life. *Journal of Geophysical Research* **104**, 16437–16451. doi:10.1029/1998JE900051.

Westall, F., Boni, L. and Guerzoni, E. (1995) The experimental silicification of microorganisms. *Palaeontology* **38**, 495–528.

Zbinden, M., Martinez, I., Guyot, F., Cambon-Bonavita, M.-A. and Gaill, F. (2001) Zinc-iron sulphide mineralisation in tubes of hydrothermal vent worms. *European Journal of Mineralogy* **13**, 653–658. doi:10.1127/0935-1221/2001/0013-0653.

Zbinden, M., Le Bris, N., Compère, P., Martinez, I., Guyot, F. and Gaill, F. (2003)

Mineralogical gradients associated with alvinellids at deep-sea hydrothermal vents. *Deep-Sea Research I* **50**, 269–280. doi:10.1016/S0967-0637(02)00161-9.

4 Worm tubes from ancient hydrothermal vents and cold seeps – towards improving identification

Magdalena N. Georgieva[1,2], Crispin T. S. Little[1], Jonathan S. Watson[3], Mark A. Sephton[3], Alexander D. Ball[4], Adrian G. Glover[2]

[1]*School of Earth and Environment, University of Leeds, Leeds, United Kingdom*

[2]*Life Sciences Department, Natural History Museum, London, United Kingdom*

[3]*Department of Earth Science and Engineering, Imperial College London, London, United Kingdom*

[4]*Core Research Laboratories, Natural History Museum, London, United Kingdom*

4.1 Abstract

One of the main limitations to understanding the evolutionary history of hydrothermal vents and cold seeps is the identification of tube fossils from ancient deposits representing these environments. Tube-dwelling annelids are some of the most conspicuous inhabitants of modern vent and seep ecosystems, and ancient vent and seep tubular fossils are typically considered to have been made by annelids. However, the actual taxonomic affinities of many tube fossils from vents and seeps are contentious, or have remained largely undetermined due to difficulties in identification. In this study, we employ a detailed chemical and morphological assessment of both modern annelid and fossil tubes from hydrothermal vent and cold seep environments. This allows better constraint on the identity of fossil tubes, and thus enhances knowledge of the evolutionary history of vent and seep communities. For the first time, we have investigated the systematics of ancient vent and seep tubes within a cladistic framework. Results of these investigations suggest that two types of tubes from ancient vent localities were made by the annelid family Siboglinidae, which often dominates modern vents and seeps, but also highlight that many vent and seep tube fossils formerly thought to be annelids cannot be assigned annelid affiliation with any certainty. The above findings overall improve the level of quality control with regard to interpretations of fossil tubes, and most importantly, suggest that

siboglinids likely occupied Mesozoic vents and seeps, greatly increasing the minimum age of the clade relative to earlier molecular estimates.

4.2 Introduction

Annelids are some of the most conspicuous dwellers of hydrothermal vent and cold seep ecosystems, occurring as large habitat-forming tubeworm bushes, on the walls of vent chimneys, and showing remarkable adaptations that enable them to thrive in these environments. Not long after the discovery of abundant life fuelled by chemosynthesis at modern vent and seep ecosystems in the late 1970s and early 1980s (Lonsdale, 1977; Corliss *et al.*, 1979; Paull *et al.*, 1984), multiple fossil analogues of these communities were also described. These showed the occupation of vents and seeps by animal life to be ancient, dating back to the Silurian period approximately 443-419 Ma (Little *et al.*, 1997; Barbieri *et al.*, 2004). Ancient vents and seeps often contain tubular fossils considered to have been made by annelids, as well as brachiopods, gastropods, and bivalves. While the taxonomy of non-tube fossil groups is generally uncontroversial, that of the tube fossils has remained elusive. Many tubular fossils are referred to simply as 'worm tubes', rather than being assigned to specific modern or fossil lineages, or have received controversial assignments (Campbell, 2006; Vrijenhoek, 2013). This has hindered our ability to understand the evolutionary history of chemosynthetic communities.

The majority of annelids are soft-bodied and in general this group has a very poor fossil record. However, the dwelling tubes that many annelids create are often more robust structures that have a greater likelihood of becoming preserved as fossils (Ippolitov *et al.*, 2014; Georgieva *et al.*, 2015a), and are usually the only remnants of annelid occupation at ancient vents and seeps. Some annelids can produce only thin, temporary mucus tubes, but many construct dwelling tubes with greater durability (Gaill and Hunt, 1988). These are generally comprised primarily of a fibrous secretion produced by the worm that is laid down in successive layers, with varying fibre orientations between adjacent sheets. This results in tube walls with a plywood-like organisation that imparts them strength (Merz, 2015).

Robust annelid tubes can be divided into three broad categories: calcium carbonate tubes, agglutinated tubes comprised of inner organic layers and outer exogenous material (e.g. sediment grains), and tubes comprised purely of an organic secretion. Calcareous tubes are

almost exclusively confined to the family Serpulidae, but a single genus of extant sabellids and cirratulids also produce calcareous tubes (Ippolitov *et al.*, 2014). Calcareous tubes can be formed of either calcite, aragonite, or both, and may also exhibit distinct crystal microstructures (Vinn *et al.*, 2008). Agglutinated tubes occur in families such as Sabellidae and Terebellidae, or only in a subset of members of a family, e.g. the genus *Mesochaetopterus* (Chaetopteridae). Purely organic tubes (referred to as 'organic' tubes hereafter) often have a high protein content which co-occurs with a carbohydrate (Merz, 2015). For example, chaetopterid tubes are considered to be formed of a highly ordered fibrous protein embedded within a carbohydrate matrix (Gaill and Hunt, 1988), and also to contain furfural (Berkeley, 1922). The tubes of *Alvinella* spp. (Alvinellidae) are primarily comprised of protein (Vovelle and Gaill, 1986). Other organic tubes may be formed of a β-chitin and protein complex. The latter composition most notably occurs in the tubes of siboglinids (Brunet and Carlisle, 1958; Shillito *et al.*, 1995), which constitute the most prominent tubicolous annelid family occupying modern vents and seeps. Chitin content can vary throughout the length of siboglinid tubes (Julian *et al.*, 1999), and has also recently been detected in the tubes of spionids and oweniids (Guggolz *et al.*, 2015).

Annelid builders of calcareous, agglutinated and organic tubes all occur at modern hydrothermal vents and cold seeps (Olu *et al.*, 1996; Desbruyères *et al.*, 2006; Levin and Mendoza, 2007; Kupriyanova *et al.*, 2010). Many of the tubular fossils at ancient vent and seep sites are considered to have originally been organic in composition (e.g. Little *et al.*, 1999a; b; Goedert *et al.*, 2000; Himmler *et al.*, 2008), but identifications based on their morphologies has proved difficult. This is because (i) many fossil tubes lack diagnostic characters; (ii) often only short fossil tube fragments are found, making it difficult to assess the morphology of the whole tube; (iii) the same type of tube can exhibit a range of preservations; (iv) and tube surfaces with diagnostic characters may be obscured by mineralisation. Existing taxonomic designations of fossil tubes to the annelids are made based on their resemblance at various morphological scales to tubicolous annelid lineages as well as on environmental considerations in some instances. Potential annelid affinities of originally calcareous fossil tubes may also be evaluated on their ultrastructure if this is well preserved (e.g. Taylor and Vinn, 2006), and Palaeozoic fossil tubes are also assessed for their resemblance to non-annelid tube builders from this period such as cornulitids, microconchids, and tentaculitids (e.g. Vinn *et al.*, 2015).

Based on the above considerations, such as tube morphology and occurrence within an ancient vent environment, many ancient vent and seep tubes have been assigned to the

vestimentiferans (a subgroup of siboglinids comprising its larger members) (Little *et al.*, 1999a, 2004; Shpanskaya *et al.*, 1999). However, these identifications have been challenged as the morphological characters used to make these diagnoses are not unique to the vestimentiferans, being also present in other annelid families as well as non-annelid fossil taxa (Kiel and Dando, 2009). Such characters include longitudinal wavy ridges, tube collars (or flanges), multi-layered tube walls, as well as the size and mass occurrence of tubes. However, no comprehensive comparison of annelid tubes has yet been attempted to determine whether there are clear morphological features that can distinguish tubicolous annelid lineages in the fossil record.

Interpretations of Palaeozoic and Mesozoic vent and seep tubes as vestimentiferans are also at odds with the age of the siboglinids as determined through molecular clock methods. The oldest putative vent siboglinid, *Yamankasia rifeia*, is ~440 million years old, which vastly exceeds the range of molecular age estimates for the Siboglinidae family of 50-126 million years (Little and Vrijenhoek, 2003; Vrijenhoek, 2013). Recently discovered borings of the bone-eating siboglinid worm *Osedax* in Late Cretaceous (~100 million year old) plesiosaur and turtle bones (Danise and Higgs, 2015) however suggest that the older molecular age estimates for this family may be more accurate. The above study also highlights that better morphological assessment of fossils is needed to clarify the evolutionary ages of vent and seep fauna.

Identification of fossil vent and seep tubes is further complicated by poor understanding of the taphonomy and fossilisation of different tube types within these settings. The few existing studies show that vestimentiferan and alvinellid tubes at hydrothermal vents are preserved primarily by iron sulphides (Cook and Stakes, 1995; Georgieva *et al.*, 2015a). At seeps, aragonite can preserve the original finely multi-layered structure of the tube walls of the vestimentiferan *Escarpia southwardae* (Haas *et al.*, 2009). While it is known that organic compounds (biomarkers) specific to methane and sulphur cycling micro-organisms may be preserved at vents and seeps (Peckmann *et al.*, 2004; Blumenberg *et al.*, 2012), the preservation of annelid tube biomarkers during fossilisation within these environments has not been investigated. If preserved, biomarkers can potentially provide additional information to morphology to aid in the identification of problematic vent and seep tube fossils due to the different compositions of organic annelid tubes (Gaill and Hunt, 1988).

To enhance the understanding of the evolutionary history of deep-sea hydrothermal vents and cold seep communities, this study aims to improve the taxonomy of the abundant but problematic fossil annelid tubes from ancient vents and seeps. Firstly, we aim to define a

range of morphological criteria to improve identification of fossil tubes from vents and seeps. Secondly, we aim to clarify whether modern organic annelid tubes exhibit significantly different chemical compositions, and whether these can be detected in ancient vent and seep worm tubes to aid in their identification.

4.3 Materials and methods

4.3.1 Modern and fossil tube selection

Fossil tubes for identification were selected based on the availability of material, and are therefore a representative subsample of all the reported tubes from fossil vent and seep localities (Supplementary Table D.1). An effort made to include tubes from a range of geological time periods and exhibiting a range of morphologies (summarised in Supplementary Table D.2).

Tubes from modern annelid families for in-depth study and comparison with fossil material (Supplementary Table D.3) were chosen on the basis of two main criteria: (i) annelid families that occur within modern vents and seep environments, and (ii) families for which difficulties in discrimination in the fossil record of vents and seeps have been noted. As potential confusion between siboglinid and chaetopterid tubes in the fossil record has been highlighted (Kiel and Dando, 2009), analyses of modern material were focused on tubes from these two families, with an effort made to cover the range of tube morphologies exhibited by each family (Supplementary Table D.3).

In addition to vestimentiferans, the Siboglinidae family includes another two monophyletic lineages that construct durable organic tubes; the frenulates and the genus *Sclerolinum*. Both of these build long, small-diameter tubes, however frenulate tubes often exhibit greater morphological diversity. The tubes of vestimentiferans, *Sclerolinum* and frenulates were all included in tube comparisons. Siboglinid tubes are known to exhibit variation from their anterior to posterior sections (Southward *et al.*, 2005). Vestimentiferan tubes can produce extensive posterior tube regions to access sulphide that lack ornamentation and are sometimes termed 'roots' (Dattagupta *et al.*, 2006). For such tubes, the morphology of the anterior, middle, and posterior regions were noted. Chaetopterid tubes can also show morphological variation along their length (although this is more rarely observed than in siboglinid tubes).

Serpulid tubes that may resemble siboglinid tubes were also included in tube comparisons, as were the tubes of the genera *Alvinella* and *Glyphanostomum* because they construct organic tubes and occur at vents (also seeps for the latter genus) (Reuscher *et al.*, 2009, 2012). Agglutinated tubes from several families (Sabellidae, Chaetopteridae, Oweniidae) were included for comparison with non-agglutinated tubes. Palaeozoic fossil tubes were also compared to the tubes of Palaeozoic non-annelids, using existing literature describing the latter.

4.3.2 Morphological analysis

Fossil tubes were photographed and measured in hand specimen, and a selection of these were also viewed uncoated using a scanning electron microscope (SEM; FEI Quanta 650 FEG-ESEM) at the Natural History Museum, UK. Fossil tubes from each locality were also prepared into polished thin sections, and visualised using light microscopy. Selected modern tubes were initially photographed, after which lengths of approximately 10 mm were cut from a subset of these for further analyses. For tubes that showed differentiation along their length, 10 mm sections were cut from each differing region (e.g. the anterior, middle, and posterior portions of frenulate tubes). For tubes preserved in ethanol, sections were initially critical-point dried, and all tube sections were subsequently visualised using SEM. Following this, tube sections were embedded in resin, prepared into polished thin sections and visualised using light microscopy.

Aspects of the broad morphology, ultrastructure and composition (see later) exhibited by modern tubes were used to identify characters that can be used to distinguish annelid tubes, with an attempt made to include all of the features that a tube may exhibit. This was important as tubes, especially when fossilised, generally possess relatively few characters compared to annelid soft tissues. The 48 characters (see Results) are all binary to maximise the amount of information obtainable from relatively few tube features.

4.3.3 Principal co-ordinate and phylogenetic analyses

Selected tube characters were used to create a character matrix (Supplementary Table D.4), in which morphological and compositional aspects of modern and fossil tubes were scored using both findings from this study as well as from existing literature. During creation of the character matrix, the differing anterior and posterior sections of four vestimentiferan tubes were scored individually to assess any effects of this. Fossil tubes from two localities

(Bear River, Wilbur Springs) were also removed from the character matrix prior to any subsequent analyses. These tubes were only available in thin section, therefore broader tube morphology could not be assessed.

The resulting character matrix was firstly used to conduct a principal co-ordinate analysis (PCO), to assess the similarity of tubes based on the 48 identified characters within a low-dimensional space. PCO was performed using PAST (Hammer *et al.*, 2001), and was used due to its ability to handle an incomplete matrix. Similarity was computed with the Gower Similarity index.

The tube character matrix was also used to conduct phylogenetic analyses to determine whether compositional and morphological criteria can reconstruct currently accepted relationships of modern annelid lineages as inferred from soft tissues and DNA (Rouse and Fauchald, 1997; Weigert and Bleidorn, 2016), and where fossils fit in relation to these. These were performed using the parsimony program TNT v.1.1 (Tree analysis using New Technology) (Goloboff *et al.*, 2008), using the following two datasets: 1. modern taxa, tube data only (43 taxa, 48 characters); 2. modern and fossil taxa, tube data only (64 taxa, 48 characters). To explore congruence between DNA-based phylogenies and tube morphology, an additional three datasets were created that include molecular data for modern annelids (Supplementary Table D.5). These datasets were analysed using the Bayesian program MrBayes v.3.2.6 (Ronquist and Huelsenbeck, 2003) (see Appendix D, Methods Supplement 1). Outgroup choice for all analyses was based on the findings of Weigert *et al.* (2014).

For analyses performed using TNT, all characters were treated as non-additive (unordered) and were weighted using implied character weighting which is deemed more appropriate for datasets in which homoplasy is likely to occur (Goloboff, 1993; Legg *et al.*, 2013). The degree to which homoplastic characters are downweighted during the analysis is determined by the concavity constant k, which is set to 3 by default in TNT. Greater values of k down-weigh homoplastic characters to a lesser extent, and our datasets were analysed with both k=3 and k=4 due to suggested high potential for homoplasy when dealing with tubicolous annelids (Merz and Woodin, 2006; Kiel and Dando, 2009). Tree searching was conducted using the new technology search option, as this is regarded the most suitable search tool for finding the shortest trees when handling datasets that contain 50 or more taxa (Goloboff, 1999). Tree search parameters were as follows: 200 random stepwise addition sequences, 3000 iterations each of drifting and ratcheting, and 100 rounds of tree

fusing. Symmetric resampling of 1,000 replicates was used to measure nodal support as this technique is unaffected by character weighting (Goloboff *et al.*, 2003; Legg *et al.*, 2013).

4.3.4 Tube compositional analysis

Several modern organic tubes covering a range of annelid families were initially analysed using Fourier Transform Infra-red Spectroscopy (FTIR). This technique is used to identify the types of bonds or functional groups present within an organic sample (Williams and Fleming, 1980), and was employed to provide an overview of similarity in organic composition between tubes from various taxonomic lineages. FTIR analyses were performed using a Nicolet Nexus FTIR bench unit (Thermo Scientific, Waltham, MA, USA) at Imperial College London, UK (ICL) in attenuated total reflectance mode. Spectra were collected at a resolution of four data points per reciprocal centimetre, and converted to absorbance using Nicolet OMNIC software (Thermo Scientific).

A subset of the modern organic tubes that showed different FTIR spectra were then analysed in more detail using pyrolysis gas-chromatography mass-spectrometry (py-GC-MS; also performed at ICL), to identify the structural components of the tubes. Py-GC-MS is widely employed for analysis of organics preserved in fossils, as it allows rapid detection of complex polymers and requires very little material (Gupta and Cody, 2011). For this analysis, small pieces of modern dry annelid tube were placed inside quartz pyrolysis tubes plugged with quartz wool at each end. Further details of the py-GC-MS methods used can be found in Appendix D, Methods Supplement 2.

To determine whether fossil tubes contained any preserved organic matter (and would hence make good targets for py-GC-MS), fossil tube thin sections were initially viewed using confocal laser scanning microscopy (CLSM) using a Nikon A1-Si confocal microscope at the NHM, operated in auto-fluorescence mode. Fossil tubes which showed pronounced fluorescence relative to surrounding minerals with CLSM (and were therefore suspected to contain preserved organic matter), were selected for py-GC-MS. For py-GC-MS, the walls of fossil tubes were carefully separated from the host rock. These were subsequently ground to a fine powder, placed inside pyrolysis tubes, and were analysed using the same instrument parameters as modern tubes. Fossil tubes from two localities (Humptulips, Waipiro) were assessed only for organics content (with py-GC-MS; Supplementary Table D.2) and were therefore not included in the character matrix.

4.3.5 Organisation of results

The results section follows a systematic review of ancient vent and seep tube fossils organised by geological age (youngest to oldest), followed by descriptions of the identified tube characters. Results of principal coordinates, phylogenetic and tube compositional analyses are subsequently presented.

Sample identification codes for fossil tube material in the systematics section (e.g. RK-5) are locality codes and/or codes assigned by collectors/donors of material. Commonly used abbreviations: **UL**, University of Leeds, Leeds, UK; **LACMIP**, Natural History Museum of Los Angeles County, Invertebrate Paleontology section, USA; **BMNH**, Natural History Museum, London, UK; **don**., donated; **coll.**, collected; **loc.**, locality.

4.4 Systematic palaeontology

Kingdom **Animalia**

Phylum **Annelida**

Tubes, 'rocky knob' *incertae sedis*

(Figure 4.1)

Material. RK-5: block of many large-diameter tubes, mostly in the same orientation. RK-15B-6: block of small-diameter tubes mostly in the same orientation. RNT1: many similarly sized tubes, mostly in the same orientation. RNT2: dense aggregation of small-diameter tubes in a range of orientations. C.T.S. Little collection, UL, don. K.A. Campbell and coll. C.T.S. Little.

Occurrence. Rocky Knob, northern Hawke's Bay area, east coast of North Island, New Zealand (~38°19'S, 177°56'E). Seep carbonates occurring as isolated lenses in mudstone, Bexhaven Limestone Formation, Tolaga Group, Middle Miocene (Campbell *et al.*, 2008; Saether, 2011).

Description. Tubes are mostly straight and exhibiting a wide range of diameters, from 1.0-7.9 mm, and are preserved in clusters mostly of similarly sized tubes (Figure 4.1A-B). In some clusters, tubes are preserved in the same orientation (Figure 4.1B). The tubes are non-branching, large-diameter fragments are somewhat tapering (Figure 4.1A), and some tube walls appear to be touching others (Figure 4.1B, F). Tube walls are mostly smooth (Figure 4.1C), however one tube exhibits round concretions on its surface (Figure 4.1D),

while another small-diameter tube bears fine, long, continuous longitudinal wrinkles (Figure 4.1B). Tube walls are fibrous, in places torn fibres are preserved (Figure 4.1E), and show high organic content (Figure 4.1F; Supplementary Table D.9). The tubes also appear to originally have been flexible as well as multi-layered (Figure 4.1E-G), with delamination occurring between some layers (Figure 4.1G). Some tube sections show well-consolidated lamination that is many layers thick (Figure 4.1F-G).

Remarks. Tubes from Rocky Knob have previously tentatively been ascribed to the siboglinids (Saether, 2011), however cluster and cladistic analyses (Figures 4.22, 4.24) failed to place these tubes among the siboglinids or any of the other annelid families included in the analyses. We therefore presently assign these tubes to the annelids only, as more information would be required to assign these tubes to the siboglinids or otherwise. However, their similarity to vestimentiferan tubes is noted, and for this reason these tubes have been assigned to the annelids. The high abundance of these tubes at this ancient seep, large diameter range, the generally smooth organic tube walls, and the thick, neatly multi-layered tube wall appearance in some of the specimens do suggest a vestimentiferan affinity, but specimens with better preserved morphology or additional analyses of tube organics would be required to prove this affinity. The round concretions (Figure 4.1D) present on the surface of a large-diameter tube may constitute epiphytic foraminifera that were fossilised alongside the tube.

Kingdom **Animalia**

Tubes, 'upper waiau river' *incertae sedis*

(Figure 4.2)

Material. UWT3-4: clumps of tubes preserved mostly in the same orientation, one large-diameter tube has a very grainy tube wall. C.T.S. Little collection, UL, don. K.A. Campbell.

Occurrence. Upper Waiau River, northern Hawke's Bay area, east coast of North Island, New Zealand (~38°13'S, 178°5'E). Seep carbonates occurring as isolated lenses in mudstone, Bexhaven Limestone Formation, Tolaga Group, ?late Early Miocene-Middle Miocene (Campbell *et al.*, 2008; Saether, 2011).

Description. Relatively straight tubes, 2.3-6.6 mm in diameter (Figure 4.2A). Tube walls smooth (Figure 4.2A) or with a grainy appearance (Figure 4.2B-C) created by what seems to be aragonite growth around many small round concretions. In section, tube walls appear to have a high organic content (Figure 4.22; Supplementary Table D.9), and are comprised

of multiple brown layers of varying thickness. Preserved tears (Figure 4.2D) also suggest that the original tube wall had an organic component. The brown layers sometimes have with a thick calcareous band occurring along their outer edge (Figure 4.2D-E). The small concretions that likely give the tube its grainy appearance are located on the outside of the thick calcareous layer (Figure 4.2D).

Remarks. These tubes were resolved among siboglinids only within the cladistic analysis allowing more homoplasy (Figure 4.24), however the amount of missing data for these tubes (Supplementary Table D.4) makes this result uncertain. In addition, the small concretions present on the surface of these tubes make them difficult to place. These spheres are not located on top of the organic fibrous layers as would be expected in an agglutinated tube. Instead, the spheres are located on top of another layer of mineralisation, suggesting that they became part of the tubes after the tube was mineralised. Similarly preserved tubes have been observed in the Devonian Hollard Mound deposit (Peckmann *et al.*, 2005). The tube assemblage at Upper Waiau River warrants further investigation and therefore these tubes are not presently assigned to a modern annelid lineage or otherwise.

Kingdom **Animalia**

Phylum **Annelida**

Family **Serpulidae** Rafinesque, 1815

Serpulidae sp. 'bexhaven'

(Figure 4.3)

Material. BXG: many small-diameter tubes occurring clustered together (Figure 4.3A). C.T.S. Little collection, UL, coll. C.T.S. Little.

Occurrence. Bexhaven locality, northern Hawke's Bay area, east coast of North Island, New Zealand (~38°3'S, 178°5'E). Seep carbonates occurring as isolated lenses in mudstone, Bexhaven Limestone Formation, Tolaga Group, Middle Miocene (Campbell *et al.*, 2008; Saether, 2011).

Description. Tubes 0.5-1.9 mm in diameter, non-branching, somewhat sinuous (wavy), and appear to have originally been rigid (Figure 4.3A). Tubes do not taper in the fragments observed. Tube wall surfaces exhibit numerous fine, parallel transverse wrinkles (Figure 4.3B). Tubes are clearly attached to each other (Figure 4.3C-D), and show chevron-like multi-layered tube wall structure (Figure 4.3E), while in some cases the tube walls have

been replaced (Figure 4.3D). Tube walls do not appear to contain preserved organic matter (Figure 4.22).

Remarks. The attachment exhibited by these tubes, and the chevron-like structure of the tube walls clearly point to them having been made by serpulids, and they are identified as such by both cluster and cladistic analyses (Figures 4.22, 4.24). The tube wall ornamentation of fine closely-spaced transverse wrinkles is also seen in many members of this family (e.g. *Serpula* spp.). Serpulids are commonly encountered within fossil seep deposits (Vinn *et al.*, 2013, 2014), and have tentatively been suggested to occur at the Haunui and Ugly Hill localities (Saether, 2011).

Kingdom **Animalia**

Phylum **Annelida**

Family ?**Siboglinidae** Caullery, 1914

?Siboglinidae sp. 'west fork satsop river'

(Figure 4.4)

Material. JLG459C 1&2, 3B: several wavy tubes. C.T.S. Little collection, UL, don. J.L. Goedert.

Occurrence. West Fork Satsop River, Grays Harbor County, Washington State, USA (~47°16'N, 123°33'W). Float seep limestone blocks. Lincoln Creek Formation, Oligocene (Campbell and Bottjer, 1993; Kiel and Amano, 2013).

Description. Tubes up to 2.4 mm in diameter, somewhat sinuous, non-branching, and do not appear to have been agglutinated or to taper in the observed fragments (Figure 4.4A-B). Tubes appear inflexible, unattached, and the tube walls are free of ornamentation. In thin section, the tube walls are brown, of variable thickness but finely multi-layered (Figure 4.4C-D). Tears in the tube wall can be observed showing fibre endings (Figure 4.4D), and an originally organic composition of the tube walls is supported by confocal microscopy (Figure 4.22).

Remarks. These tubes were resolved only within the cladistic analysis allowing for more homoplasy (Figure 4.24B), in which they fall among siboglinids. The fibrous organic composition and concentrically multi-layered walls are however also consistent with the tubes of chaetopterids, although the smooth walls and sinuosity of these tubes suggest that

they are possibly more likely to have been made by siboglinids. We therefore tentatively suggest a siboglinid affinity for these tubes.

Kingdom **Animalia**

Phylum **Annelida**

Family ?**Siboglinidae** Caullery, 1914

?Siboglinidae sp. 'murdock creek'

(Figure 4.5)

Material. LACMIP loc. 6295: One spiralling tube (Figure 4.5A), another tube with a ~90° bend, and a smaller tube observed in thin section only. C.T.S. Little collection, UL, don. J.L. Goedert.

Occurrence. Murdock Creek, Clallam County, Washington State, USA (~48°9'N, 123°52'W). Loose seep carbonate blocks. Pysht Formation, late Early Oligocene (Goedert and Squires, 1993; Vinn *et al.*, 2013; Kiel and Amano, 2013).

Description. Tubes 0.7-3.0 mm in diameter, appearing non-branched, non-agglutinated and non-tapering in the tube fragments observed. The spiralling tube (Figure 4.5A) appears to have coarse longitudinal wrinkles on its tube wall surface, but whether these are original is uncertain. In thin section, tube walls are thick and concentrically multi-layered (Figure 4.5 B-D), and occasionally delaminated (Figure 4.5B). Some of the tubes appear to have originally been flexible (Figure 4.5C) and have had been fibrous walls due to visible tears in thin section (Figure 4.5D).

Remarks. These tubes appear to have been organic originally due to preserved tube wall tears that reveal a fibrous nature. The size of the tubes, their thick, multi-layered walls and the spiralling that they exhibit suggests that the tubes may have been made by vestimentiferans as the combination of these features are not commonly encountered in other organic tube-building annelids that occur at vents and seeps. Due to a limited amount of material available for study, and as these tubes were only resolved among those of siboglinids when homoplastic characters are downweighted less within cladistic analyses (Figure 4.24B), these tubes are only tentatively assigned to the siboglinids.

Kingdom **Animalia**

Phylum **Annelida**

Family ?**Siboglinidae** Caullery, 1914

?Siboglinidae sp. 'canyon river'

(?vestimentifera)

(Figure 4.6)

Material. LACMIP 16957: several large straight tubes preserved in the same orientation. JLG 473: tubes embedded in carbonate matrix, thin sections of tubes only. C.T.S. Little collection, UL, don. J.L. Goedert.

Occurrence. Canyon River, south-west Washington State, USA (47°18.18'N, 123°30.52'W). Carbonate within siltstone, Lincoln Creek Formation, lower Oligocene (Goedert *et al.*, 2000; Peckmann *et al.*, 2002).

Description. Tubes from this locality were originally described by Goedert *et al.* (2000). They measure 1.1-7.0 mm in diameter, and are non-branching, non-agglutinated, and not attached to other tubes (Figure 4.6A-C). Tubes taper slightly, and the walls of the majority of tubes are smooth and lack ornamentation (Figure 4.6A-B), while longitudinal wrinkles are present in one small-diameter tube (Figure 4.6C). Tube walls are thick and multi-layered, at times delaminated, and in one of the tubes examined a tear of the tube wall indicative of an originally fibrous composition can be seen (Figure 4.6D). The tubes appear to have originally been rigid as walls are generally not compressed, both in hand specimen (Figure 4.6A-C) and thin section (Figure 4.6E), and fluorescence during CLSM analysis of the tube walls further suggests that the tubes were originally organic (Figure 4.6F).

Remarks. These tubes were deemed to have been made by vestimentiferans by Goedert *et al.* (2000), resembling tubes made by the genus *Escarpia*. Despite these tubes being largely unresolved within the cladistic and cluster analyses (Figures 4.22, 4.24), these tubes closely resemble those of vestimentiferans due to their smooth walls and columnar morphology. The diameter range of these tubes, as well as the hard, organic, mostly thick and multi-layered nature of the tube walls which are typical of most vestimentiferans. We therefore suggest that vestimentiferans are the most likely builders of these tubes, but this assignment is tentative due to the poor resolution of these tubes through cladistics.

Kingdom **Animalia**

Tubes, 'bear river' *incertae sedis*

(Figure 4.7)

Material. LACMIP 5802 BRB-1: Several small tubes preserved in close proximity and embedded within the carbonate matrix. C.T.S. Little collection, UL, don. J.L. Goedert.

Occurrence. Bear River, Pacific County, Washington State, USA (46°19.94'N, 123°55.96'W). Large seep deposit, siltstone of Cliff Point, late Eocene (Vinn *et al.*, 2013).

Description. Tubes are 0.4-2.3 mm in diameter, appear non-agglutinated, and not attached to other tubes (Figure 4.7A). As the tubes are fairly round in thin section, it is inferred that they were originally rigid (Figure 4.7A). Whether the tubes taper and details of wall ornamentation could not be assessed. In thin section, the tube walls are thick (Figure 4.7B-C) and in places remnants of tube wall appear multi-layered (Figure 4.7C). The brown, filmy nature of the tube walls (Figure 4.7B-C) suggests that they were likely originally organic in composition.

Remarks. The thick, multi-layered organic tube walls suggest that these tubes could potentially have been made by annelids, perhaps siboglinids. However due to the inability to assess outer tube wall characters and availability of only a limited number of sections, these tubes have not presently been assigned to a modern annelid lineage or otherwise.

Kingdom **Animalia**

Phylum **Annelida**

Family **?Siboglinidae** Caullery, 1914

?Siboglinidae sp. 'omagari'

(?vestimentifera)

(Figure 4.8)

Material. Many small, similar-diameter tubes preserved together. OMG03-4a: pinkish calcite with many worm tubes with brown walls (Figure 4.8A-B). OMG03-1: many tubes in muddy, crumbly matrix (Figure 4.8C-D). OMG03-2, OMG03-3a, OMG03-3b: many tubes with light-coloured walls preserved in hard cement. C.T.S. Little collection, UL, don. Y. Hikida.

Occurrence. Omagari, Nakagawa-cho region, north-western Hokkaido, northern Japan (44°39.58'N, 142°2.22'E). Aprroximately 10 m wide seep carbonate deposit, Omagari

Formation, Yezo Supergroup, Campanian, Cretaceous (Hikida *et al.*, 2003; Majima *et al.*, 2005; Kiel *et al.*, 2008).

Description. Non-agglutinated tubes that do not appear to be branching (Figure 4.8A-D), and with walls that, where visible, appear smooth (Figure 4.8B, D). Tube diameters range between 0.8-2.7 mm, and tubes do not appear to distinctly taper along their length. Tube walls are uncompressed suggesting that they may have originally been rigid, and are multi-layered (Figure 4.8E-F). Tube walls are generally not very thick, apart from in a subset tubes in which walls are thick and exhibit many layers (Figure 4.8F). Preserved tears of the tube wall reveal an originally fibrous nature (Figure 4.8G).

Remarks. These tubes have been interpreted as those of vestimentiferans by earlier work (Hikida *et al.*, 2003), but are difficult to identify due to their lack of ornamentation. They fall among siboglinids when more homoplasy is permitted in the cladistic analysis (Figure 4.24B). The tubes are clearly organic, due to preserved wall tears that reveal a fibrous nature. Transverse ornamentation typical of some frenulates or chaetopterids is absent, and the size, clumped nature of the tubes, combined with walls that are sometimes thick and neatly multi-layered suggests that the Omagari tubes are most likely the roots/posterior portions of vestimentiferan tubes. The morphology of Omagari tube clumps very closely resembles a clump of the roots of the seep vestimentiferan *Lamellibrachia luymesi* (Figure 4.8H-I). We therefore tentatively suggest that the Omagari tubes may be vestimentiferan tube roots.

Kingdom **Animalia**

Phylum **Annelida**

Tubes, 'okukinenbetsu yellow' *incertae sedis*

(Figure 4.9A-D)

Material. OKb4-5: similarly sized tubes with yellowish walls preserved in a range of orientations. C.T.S. Little collection, UL, don. F. Gill.

Occurrence. Okukinenbetsu River (Kanajirisawa Creek), Obira-machi, north-western Hokkaido, northern Japan. Mudstone of Middle Ezo Group, Cenomanian, Cretaceous (Majima *et al.*, 2005; Kiel *et al.*, 2008).

Description. Small tubes, 1.1-2.4 mm in diameter, fairly straight, non-branching and non-agglutinated (Figure 4.9A). Tubes are not attached to each other, do not appear to taper

much, and the tube walls appear to have originally been somewhat flexible (Figure 4.9A). The only ornamentation visible on the tubes is fine, continuous longitudinal wrinkles which occasionally bifurcate (Figure 4.9A-B). In thin section, the tube walls are preserved as brown-yellow rims showing evidence of multi-layering and mineral growth between tube layers (delamination) (Figure 4.9C-D). Some of the tube sections also show signs of compression and/or shrinkage.

Remarks. Fine longitudinal wrinkles such as those found on these tubes are most often associated with vestimentiferan tubes, and they very closely resemble the small-diameter tubes with longitudinal wrinkles from Canyon River. However, these tubes could not be resolved by cladistics (Figure 4.24) likely due to the poor state of preservation of their wall structure, and are therefore presently only ascribed to the annelids.

Kingdom **Animalia**

Phylum **Annelida**

Family ?**Siboglinidae** Caullery, 1914

?Siboglinidae sp. 'okukinenbetsu brown'

(Figure 4.9E-I)

Material. OKb4-3: larger tubes with brown walls largely obscured by rock matrix. C.T.S. Little collection, UL, don. F. Gill.

Occurrence. Okukinenbetsu River (Kanajirisawa Creek), Obira-machi, north-western Hokkaido, northern Japan. Mudstone of Middle Ezo Group, Cenomanian, Cretaceous (Majima *et al.*, 2005; Kiel *et al.*, 2008).

Description. Larger brown tubes 3.7-4.3 mm in diameter, uncompressed in section (Figure 4.9E) and with clear multi-layering (Figure 4.9F-I) that is very thick and well consolidated in some of the tubes (Figure 4.9I). Highly frayed edges can be seen, suggesting that tubes were originally organic and fibrous (Figure 4.9F).

Remarks. The clear round transverse sections of the larger brown tubes suggests that the tubes were originally rigid. Their size may indicate that the inhabitants were not frenulates, while the structure of the tube wall indicates that they are more likely to have been made by siboglinids than chaetopterids due to the thick, well-consolidated multi-layering. These

tubes fall among siboglinids when more homoplasy is permitted in cladistic analyses (Figure 4.24B), therefore this affinity is only tentatively suggested.

Kingdom **Animalia**

Phylum **Annelida**

Family ?**Siboglinidae** Caullery, 1914

?Siboglinidae sp. 'troodos collared'

(?vestimentifera)

(Figure 4.10A-C)

Material. Kambia 401b, 4061, 4062; Kapedhes 2031, 2051, 2081; Memi 212b2, 2021; Sha 3011: Small worm tubes with collars, generally occurring with other similar tubes. C.T.S. Little collection, UL, coll. C.T.S. Little.

Occurrence. Troodos Ophiolite, Cyprus. Turonian, Late Cretaceous (Little *et al.*, 1999c).

Description. Worm tubes 0.6-1.9 mm in diameter, appear to have been hard, sinuous, non-branching and not attached to other tubes (Figure 4.10A-B). It is not discernable whether tubes are tapering. The tubes possess short collars which are sometimes slightly flaring and at times are positioned in an oblique angle in relation to the tube (Figure 4.10C). The tube surface between adjacent collars appears smooth and unornamented (Figure 4.10B).

Remarks. The similarity of these tubes to those made by vestimentiferans was highlighted by Little *et al.* (1999b), in particular to the spiralling tubes of *Alaysia spiralis*. Siboglinid, chaetopterid and serpulid tubes may all possess collars and occur at vents, and siboglinid and serpulid tubes may both be highly spiralling. While the cladistic analysis groups these tubes with siboglinids when more homoplasy is allowed (Figure 4.24B), they cluster near serpulids within the PCO plot (Figure 4.22). Although small, the collars of these tubes are at times flaring and attached in an oblique angle with respect to the tube, which are features more readily observable on siboglinid tubes. These tubes are therefore tentatively suggested to have been made by vestimentiferans rather than serpulids.

Kingdom **Animalia**

Phylum **Annelida**

Family **Siboglinidae** Caullery, 1914

Siboglinidae sp. 'troodos wrinkled'

(vestimentifera)

(Figure 4.10D-E)

Material. Kambia 4051, 4061, 6061, t3; Kapedhes 204b, 2101: Worm tubes with walls ornamented by transverse and longitudinal wrinkles. C.T.S. Little collection, UL, coll. C.T.S. Little.

Occurrence. Troodos Ophiolite, Cyprus. Turonian, Late Cretaceous (Little *et al.*, 1999c).

Description. Generally straight or slightly curving tubes 1.2-4.5 mm in diameter, which do not show signs of being flexible and are not attached to other tubes (Figure 4.10D-E). Whether tubes taper cannot be assessed with certainty due to the short length of preserved fragments. Tubes do not have collars, and instead possess fine transverse and longitudinal wrinkles on their surfaces, with the transverse wrinkles often being more pronounced and fairly regular (Figure 4.10D). Longitudinal wrinkles are fine and occasionally bifurcating (Figure 4.10E). One tube specimen has a smaller tube preserved within it.

Remarks. These tubes are resolved among siboglinids by both cladistic and cluster analyses (Figures 4.22-4.24), as a result of the fine, bifurcating longitudinal wrinkles as well as the fine transverse wrinkles which they possess. The features above are not observed on serpulid tubes, which sometimes possess coarse longitudinal wrinkles. The longitudinal wrinkles of chaetopterid tubes are often coarser (Kiel and Dando, 2009), and have not been observed to be crosscut by fine transverse wrinkles. We therefore suggest that the most likely builders of these tubes are vestimentiferans, which do exhibit such an ornamentation pattern (cf. *Ridgeia piscesae* tubes, Figure 4.15G).

Kingdom **Animalia**

Phylum **Annelida**

Tubes, 'troodos attached' *incertae sedis*

(Figure 4.10F-G)

Material. Kinousa 2023; Memi 2021: Sinuous worm tubes that appear attached to a surface, several tubes often occurring together. C.T.S. Little collection, UL, coll. C.T.S. Little.

Occurrence. Troodos Ophiolite, Cyprus. Turonian, Late Cretaceous (Little *et al.*, 1999c).

Description. Tubes 0.2-0.5 mm in diameter, very sinuous (Figure 4.10F-G). The tubes have the appearance of being attached to a surface as they are mostly sinuous in two dimensions. Some of the tubes have smooth walls (Figure 4.10G) whereas others possess regular fine transverse wrinkles (Figure 4.10F). The wrinkled tubes are also somewhat tapering, whereas the smooth tubes do not appear to taper in the fragments observed.

Remarks. These tubes are resolved near siboglinids in cladistic analyses when more homoplasy is permitted (Figure 4.24B), and cluster near to serpulids within the PCO plot (Figure 4.22). The attachment exhibited by these tubes suggests an annelid affinity to a lineage such as Serpulidae, Alvinellidae or vestimentifera (posterior tube sections), in which this characteristic is often observed. For the tubes that exhibit closely spaced transverse wrinkles and taper, Serpulidae are the most likely tube builders as these characters are not observed in the tubes of Alvinellidae or in the posterior sections of vestimentiferan tubes. However this is less clear for the smooth tubes, and it is difficult to tell if the smooth and transversely wrinkled tubes were made by the same or different taxa. Therefore these tubes are presently only assigned to the annelids.

Kingdom **Animalia**

Phylum **Annelida**

Family **?Siboglinidae** Caullery, 1914

?Siboglinidae sp. 'ellef ringnes'

(?vestimentifera)

(Figure 4.11A-B, D-E)

Material. C-581891 QQA 10-22 Ellef Ringnes Island: clustered broken fragments of large tubes, mostly in various orientations however some tubes are aligned parallel to each other. C.T.S. Little collection, UL, don. S.E. Grasby.

Occurrence. Ellef Ringnes Island, Arctic, Canada. Christopher Formation, Lower Albian, Cretaceous.

Description. Large tubes: Tubes are non-branching, do not appear attached to other tubes, and are not agglutinated (Figure 4.11A-B). They are 2.0-10.0 mm in diameter, more or less straight, and have smooth walls. In thin section, the tubes show very thick,

concentrically multi-layered walls (Figure 4.11D-E) that are very likely organic due to the presence of breaks in the tube wall that reveal possible torn fibres (Figure 4.11D-E). Larger breaks in the tube wall look cleaner (Figure 4.11E), and combined with the round cross sections this suggests that the tubes are likely to originally have been rigid and inflexible.

Remarks. These tubes have previously been considered to have been made by serpulids (Beauchamp and Savard, 1992; Williscroft, 2013). However, evidence of an originally calcareous tube wall such as chevron-like layering is absent, while torn fibres point to the tubes having originally been organic in composition. The thick tube walls and neat, well-consolidated multi-layering are very characteristic of vestimentiferan tubes, and the size of these tubes and their hardness support this interpretation. However these tubes only group among modern siboglinid tubes when more homoplasy is permitted within the cladistic analysis (Figure 4.24B). For the above reasons, we tentatively suggest that the large tubes from Ellef Ringnes Island are likely the anterior sections of vestimentiferan tubes.

Kingdom **Animalia**

Phylum **Annelida**

Family **?Siboglinidae** Caullery, 1914

?Siboglinidae sp. 'prince patrick'

(?vestimentifera)

(Figure 4.11C, F-G)

Material. C-453952 1-4 Prince Patrick Island: many small tubes cemented together in a large bundle. C.T.S. Little collection, UL, don. S.E. Grasby.

Occurrence. Prince Patrick Island, Arctic, Canada. Christopher Formation, Lower Albian, Cretaceous.

Description. Tubes mostly 1.0 mm in diameter but tubes of up to 5 mm are also cemented in these clumps (Figure 4.11C). Tubes are unattached, non-branching and non-agglutinated. Ornamentation of the tube walls is largely obscured due to surface mineralisation. In thin section, the tube walls are very similar to those of the large tubes from the same deposit – they are mostly thick and comprised of many superimposed layers (Figure 4.11F) but some are also thin-walled (Figure 4.11G). Tube cross-sections are distinctly round (Figure 4.11F) suggesting that tubes were originally hard. Some of the smaller tubes contain round pellets within their interior (Figure 4.11G).

Remarks. Tubes from Prince Patrick Island have also been interpreted as having been made by serpulids (Beauchamp and Savard, 1992). However, these tubes are unlikely to have originally been calcareous in composition due to the absence of chevron-like layering, their neatly laminated tube walls and the separation of wall layers in places, which is unlikely to occur in cemented mineral tubes. Although outer tube wall ornamentation could not be assessed, the at times thick walls that these tubes possess, in combination with the morphology of the tube cluster, suggest that these tubes may represent the fossilised root portions of vestimentiferan tubes (cf. Figure 4.8I). These tubes are resolved near siboglinid tubes in the PCO plot (Figure 4.22) and near vestimentiferans in the less conservative cladistic analysis (4.24B), and are therefore also tentatively assigned to the vestimentiferans.

Kingdom **Animalia**

Phylum **Annelida**

Tubes, 'cold fork cottonwood creek' *incertae sedis*

(Figure 4.12)

Material. CFCC-2A, 2B, CC-F8: Yellowish tubes, many occurring together in a range of orientations. C.T.S. Little collection, UL, don. K.A. Campbell.

Occurrence. Cold Fork Cottonwood Creek, northern California, USA. Carbonate lenses and nodules with complex cement sequence, Great Valley Group, Aptian-Albian, Cretaceous (Campbell, 1995; Campbell *et al.*, 2002).

Description. Tubes are 0.2-5.4 mm in diameter, non-branching, wavy, non-agglutinated and not appearing to taper along their length (Figure 4.12A). Tube walls are smooth in several samples (Figure 4.12B) but are generally obscured by the host rock. Tube walls appear poorly preserved (Figure 4.12C) but seem to have originally been organic due to the presence of folds in the tube layers visible in thin section (Figure 4.12D). In places the tubes also appear multi-layered (Figure 4.12E). Internal septae have been observed in some of the tubes (Campbell *et al.*, 2002), but not during the present study.

Remarks. These tubes have been likened to those of vestimentiferans due to their diameter range (Campbell *et al.*, 2002) but apart from within the tubes of *Riftia pachyptila* (Gaill *et al.*, 1997), internal septae are not reported in the tubes of vestimentiferans. Septae are more commonly observed in chaetopterid tubes, and for this reason these tubes group among chaetopterids in the cladistic analyses. However, these tubes are on the whole

difficult to interpret due to the inability to assess tube ornamentation and the poor state of preservation of the tube walls, therefore they have not been assigned to a modern annelid lineage.

Kingdom **Animalia**

Tubes, 'wilbur springs' *incertae sedis*

(Figure 4.13)

Material. WS45A: Single tapering tube with a smooth wall, more tubes revealed in thin section. C.T.S. Little collection, UL, don. K.A. Campbell.

Occurrence. Wilbur Springs, northern California, USA. Carbonate lenses in serpentenites and siltstone turbidites, Great Valley Group, Hauterivian, Cretaceous (Campbell, 1995; Campbell *et al.*, 2002).

Description. The single tapering tube section (27 mm long) measures 2.4-3.6 mm in diameter. Tube wall is smooth and shiny (Figure 4.13A). In thin section, carbonates from Wilbur Springs reveal two types of tubes – thick walled tubes ~2.3 mm in diameter which appear to have been replaced by large calcite crystals (Figure 4.13B), and similarly-sized tubes that exhibit tube walls with a hazy brown rim (Figure 4.13C-E). However, due to the poor state of preservation, very few characters can be discerned from either type of tube.

Remarks. These tubes are not preserved well enough to be assigned to a particular animal group, and were not included in cladistic and cluster analyses as so few characters could be coded. However it is worth noting that the degree of tapering and smooth wall of the single tube in hand specimen resemble the shells made by scaphopods.

Kingdom **Animalia**

Phylum **Annelida**

Tubes, 'svalbard' *incertae sedis*

(Figure 4.14)

Material. Svalbard 2007-03: long tube with yellowish wall. Svalbard 2009-01: single tube with dark black wall. 2009-03: single tube with longitudinal wrinkles. Selection of thin sections of different tubes. C.T.S. Little collection, UL, don. K. Hryniewicz.

Occurrence. Sassenfjorden area, Svalbard. Seep carbonates in shale and shale and siltstone, Slottsmøya Member, upper Agardhfjellet Formation, Volgian-Ryazanian (latest Jurassic-earliest Cretaceous) (Hammer *et al.*, 2011; Hryniewicz *et al.*, 2012, 2015; Vinn *et al.*, 2014).

Description. The tube sections measure 2.9-5.7 mm in diameter and are all fairly straight, and not attached to other tubes. The long tube appears unornamented (Figure 4.14A), the tube with a black wall is smooth and shows no ornamentation apart from a possible small collar (Figure 4.14B), while the remaining tube fragment bears what may be faint longitudinal wrinkles (Figure 4.14C). In thin section, some of the tubes exhibit thick, neatly multi-layered walls (Figure 4.14D-E). Curving delaminated layers can also be observed in some of the tube sections (Figure 4.14F), suggesting that they were originally organic in composition. A subset of tubes exhibit hazy (poorly preserved?) tube walls (Figure 4.14G).

Remarks. Non-serpulid, originally organic-walled tubes from the Sassenfjorden area are suggested to have been made by siboglinids (Hammer *et al.*, 2011; Hryniewicz *et al.*, 2015). However the tubes examined do not clearly group with the tubes of modern annelid families included in cladistic and cluster analyses (Figures 4.22, 4.24). The tube sections with thick, neatly multi-layered walls that were observed within this study were possibly made by vestimentiferans for which this tube structure is widely observed. However, the broad morphology of this tube is presently unknown, and tubes from this deposit in general warrant further investigation as several different tube types are present. Hence these tubes are broadly ascribed to the annelids.

Kingdom **Animalia**

Phylum **Annelida**

Family **Siboglinidae** Caullery, 1914

Siboglinidae sp. 'figueroa'

(vestimentifera)

(Figure 4.15)

Material. FF-10, FFC-00, FFC-12, FFC-18, FFC-19, FFC-37: Blocks of vent chimney sulphides containing fossilised tube fragments, tubes often occurring singly. C.T.S. Little collection, UL, coll. C.T.S. Little.

Occurrence. Figueroa, San Rafael Mountains, southern California, USA. VMS deposit of Franciscan Complex, Pliensbachian, Lower Jurassic (Little *et al.*, 1999b, 2004).

Description. Tubes are 0.3-6.9 mm in diameter, appear to have originally been rigid as they do not exhibit fossilised folds depressions in their walls, and are fairly straight (Figure 4.15A). One long tube fragment appears to taper along its length (Figure 4.15A). Tubes possess collars (Figure 4.15B-D) which are large and flaring in some cases (Figure 4.15B, D), some tubes show several collars in short succession (Figure 4.15B) and collars are also sometimes oriented obliquely (Figure 4.15C). The tube walls are ornamented with fine, bifurcating longitudinal and irregular transverse wrinkles (Figure 4.15A-C, E-F). In section, tube walls are preserved by colloform and framboidal pyrite, and it is unclear if tubes were originally multi-layered (Figure 4.15H-I).

Remarks. These tubes group with siboglinids in both PCO and cladistic analyses (Figures 4.22, 4.24). The presence of large, flaring collars suggests these tubes are unlikely to have been made by chaetopterids. Serpulids and vestimentiferans both produce collars which are large and flaring, however the pattern of fine longitudinal and irregular transverse wrinkles on tube surfaces suggests that the tubes are more likely to have been made by vestimentiferans, as fine longitudinal wrinkles are not commonly observed in serpulid tubes. The ornamentation of the Figueroa tubes also greatly resembles that of *Ridgeia piscesae* tubes (Figure 15G). Therefore, we infer that the most likely tube-builders of the Figueroa tubes are vestimentiferans.

Kingdom **Animalia**

Phylum **Annelida**

Tevidestus serriformis, incertae sedis Shpanskaya, Maslennikov and Little, 1999

(Figure 4.16)

Material. BMNH VF 71: Single tube fragment. Coll. C.T.S. Little.

Occurrence. Sibay, southern Ural Mountains, Russia (52° 41.66'N, 58° 38.15'E). VMS deposit, Middle-Lower Devonian (Little *et al.*, 1999a; Shpanskaya *et al.*, 1999).

Description. Tubes 10-20 mm in diameter possessing closely-spaced spaced collars that can have curved edges (Figure 4.16A) (Shpanskaya *et al.*, 1999). Collars may be short (Figure 4.16B) or slightly flaring. The outer tube wall exhibits a fine mesh of what appear to

be pyritised fibres (Figure 4.16B-C), which cross each other at near right angles and suggest that these tubes were originally organic in composition.

Remarks. When compared with modern annelid tubes, the fibrous and collared appearance of *T. serriformis* tubes suggests they are most likely to have been made by an annelid such as a siboglinid or chaetopterid. These tubes group near chaetopterids and ampharetids in the PCO (Figure 4.22), group with chaetopterids in the more conservative cladistic analysis (Figure 4.24A), but are unresolved when more homoplasy is permitted (Figure 4.24B). The chaetopterid genera *Phyllochaetopterus* and *Spiochaetopterus* were found to produce tubes with a distinct fibre alignment whereby the sheets of parallel fibres overlap with adjacent sheets at near right angles (Figure 4.16D) (Bhaud, 1998). However, the fibres that comprise chaetopterid tubes are much finer than those observed on the tube of *T. serriformis*. The presence of both small and large flaring collars on *T. serriformis* tubes would be more indicative of vestimentiferan tubes, however, as such large fibres are not observed on vestimentiferan tube walls either, it was not possible to assign *T. serriformis* tubes to a particular modern annelid group. *T. serriformis* tubes also do not resemble Palaeozoic non vent/seep tubes. *T. serriformis* tubes are not rapidly-tapering like cornulitids (Vinn and Mutvei, 2005) and *Hyolithellus* (Skovsted, 2006). *Gaojishania cyclus* tubes bear small annulations resembling collars (Cai *et al.*, 2013), however these tubes are more irregular along their length, while *Conotubus* fossils do not possess the mesh-fibre pattern preserved on *T. serriformis* tubes. *T. serriformis* tubes are therefore presently assigned to the annelids, as these originally organic tubes resemble those of annelids more closely.

Kingdom **Animalia**

Phylum **?Annelida**

Tubes, 'sibay' *incertae sedis*

(Figure 4.17)

Material. Indeterminate ?annelid, BMNH VF 71: cluster of tubes. Coll. C.T.S. Little.

Occurrence. Sibay, southern Ural Mountains, Russia (52° 41.66'N, 58° 38.15'E). VMS deposit, Middle-Lower Devonian (Little *et al.*, 1999a; Shpanskaya *et al.*, 1999).

Description. These tubes are 0.3-7.0 mm in diameter, non-tapering, sometimes gently curved and with smooth walls (Figure 4.17A-B) (Little *et al.*, 1999a). The tube walls were originally described to be formed of fine-grained pyrite which is occasionally colloform

(Little *et al.*, 1999a). In thin sections examined by the present study, the tube walls appear thick, may be multi-layered (Figure 4.17C), and some also appear to be comprised of framboidal pyrite (Figure 4.17D).

Remarks. These tubes exhibit few distinguishing characteristics, which lead to their previous diagnosis indeterminate ?annelid tubes (Little *et al.*, 1999a). As we were unable to find further characters, these tubes were largely unresolved within cluster and cladistic analyses (Figures 4.22, 4.24). The indeterminate status of these tubes is therefore maintained. They are tentatively suggested to be annelid tubes due to their smooth, thick and possibly multi-layered walls, and as they do not closely resemble the tubes of other Palaeozoic tubicolous animals.

Kingdom **Animalia**

Eoalvinellodes annulatus, incertae sedis Little et al., 1999

(Figure 4.18)

Material. BMNH VF 50-55, 57, 60-61, 102: Tubes occurring either singly or in small clumps. Coll. C.T.S. Little.

Occurrence. Yaman Kasy, southern Ural Mountains, Russia (51° 24.43'N, 57° 41.63'E). VMS deposit, late Ordovician or earliest Silurian (Little *et al.*, 1999a; Shpanskaya *et al.*, 1999; Buschmann and Maslennikov, 2006).

Description. Small tubes 0.1-3.5 mm in diameter, non-branching and slightly tapering (Figure 4.18A-B) (Little *et al.*, 1999a; Buschmann and Maslennikov, 2006). Tubes are straight to wavy, and do not show evidence having been flexible before fossilisation (Figure 4.18A-C). The tubes show ornamentation of pronounced transverse wrinkles, which occasionally bifurcate, on what is considered to be their inner surface, and are smooth externally (Little *et al.*, 1999a). In section, tube walls are comprised of a single thick layer of framboidal pyrite (Little *et al.*, 1999a), or can be preserved with thick walls comprised of finely layered colloform pyrite (Figure 4.18D-F).

Remarks. When formerly described, these tubes were suggested to have been made by an alvinellid-like polychaete due to the proximity of *Eoalvinellodes annulatus* tubes to hydrothermal vent chimneys (Little *et al.*, 1999a). However, alvinellid tubes do not exhibit the neat, bifurcating transverse wrinkles that *E. annulatus* tubes possess - alvinellid tubes often being much more disorganised. Similar transverse folded fabric-like texture occurs on

the tubes of chaetopterids, some frenulates, and the Palaeozoic fossils *Sabellidites cambriensis* (Moczydłowska *et al.*, 2014) and *Sinotubulites* (Cai *et al.*, 2015). This texture is however much finer on frenulate and *S. cambriensis* tubes than *E. annulatus* tubes. *E. annulatus* tubes group with those of chaetopterids when more homoplasy is permitted within the cladistic analysis (Figure 4.24B) due to the coarse transverse wrinkles which they both exhibit. The wrinkles on *E. annulatus* tubes have a somewhat neater appearance, and also resemble *Glyphanostomum* tubes (Figure 4.20N). As several types of annelid and non-annelid tubes are found to possess this type of tube wall ornamentation, it has not been possible to clearly discern what these tubes may have been made by.

Kingdom **Animalia**

Yamankasia rifeia, incertae sedis Little et al., 1999

(Figure 4.19)

Material. BMNH VF 78, 80, 84, 89, 97: Very large tubes mostly preserved singly. Coll. C.T.S. Little.

Occurrence. Yaman Kasy Deposit Silurian Ural Mountains, Russia (51° 24.43'N, 57° 41.63'E). VMS deposit, late Ordovician or earliest Silurian (Little *et al.*, 1999a; Shpanskaya *et al.*, 1999; Buschmann and Maslennikov, 2006).

Description. These are the largest of the fossil vent and seep tubes, being 3.0-39.0 mm in diameter (Figure 4.19A). They are not branching and are thought to taper at their base (Little *et al.*, 1999a; Buschmann and Maslennikov, 2006). The tubes appear to have originally been flexible as they often show folding and creases (Figure 4.19B), suggesting an originally fibrous and organic nature, and one tube also exhibits possible fossilised fibres on its surface (Figure 4.19C). The tubes are fairly straight, and some well-preserved tubes show very fine parallel and closely spaced longitudinal wrinkles on their outer tube surfaces (Figure 4.19D). The tubes may also be transversely wrinkled (Buschmann and Maslennikov, 2006). In thin section, the tubes are comprised of several concentric layers of framboidal pyrite (Figure 4.19E-F), while in some specimens colloform pyrite in the shape of tube wall is interpreted as having grown onto the outside of the tubes (Figure 4.19G) (Little *et al.*, 1999a).

Remarks. These tubes are unique amongst hydrothermal vent and cold seep fossils because of their size, and also the distinctly fine and parallel longitudinal wrinkles which

they possess. Very large tubes at modern hydrothermal vents are constructed by the species *Riftia pachyptila*, however these do not show the same ornamentation. The root tubes of some vestimentiferans show similar ornamentation of parallel closely-spaced longitudinal wrinkles, but it is unlikely that the tubes of *Y. rifeia* are root portions because of their size. Their size also means that they are unlikely to be frenulate tubes, despite grouping with frenulates in the cladistic and PCO analyses (Figures 4.22, 4.24). The above characteristics are also not consistent with the tubes of other Palaeozoic tubicolous animals, therefore *Y. rifeia* tubes are not likened to a particular modern annelid group or otherwise.

Table 4.1 Summary of systematic designations of tubes from ancient hydrothermal vent and cold seep environments. Fossil tubes from ancient hydrothermal vent localities are highlighted.

Fossil vent/seep tubes	Previous designation	Present designation	Notes
Rocky Knob	?Siboglinidae (Saether, 2011)	Annelida *incertae sedis*	Not resolved by PCO or cladistics, broadly resemble vestimentiferan tubes.
Upper Waiau River	-	Animalia *incertae sedis*	Not resolved more conservative cladistic analysis (Figure 4.24A), missing data and surface concretions make them difficult to place.
Bexhaven	-	Serpulidae	Well preserved calcareous walls, resolved near serpulids by all analyses.
West Fork Satsop River	-	?Siboglinidae	Less conservative cladistic analysis (Figure 4.24B), suggests possible siboglinid affinity.
Murdock Creek	-	?Siboglinidae	Less conservative cladistic analysis (Figure 4.24B), suggests possible siboglinid affinity.
Canyon River	Siboglinidae vestimentifera (Goedert *et al.*, 2000)	?Siboglinidae ?vestimentifera	Not resolved by cladistic analyses, however closely resemble vestimentiferan tubes.
Bear River	-	Animalia *incertae sedis*	Outer morphology of these tubes could not be assessed.
Omagari	Siboglinidae vestimentifera (Hikida *et al.*, 2003)	?Siboglinidae ?vestimentifera	Less conservative cladistic analysis (Figure 4.24B), suggests possible siboglinid affinity, resemble vestimentiferan roots.
Okukinenbetsu - yellow tubes	-	Annelida *incertae sedis*	Not resolved by cladistic analyses, outer morphology suggests likely annelid affinity.
Okukinenbetsu - brown tubes	-	?Siboglinidae	Less conservative cladistic analysis (Figure 4.24B), suggests possible siboglinid affinity.
Troodos - collared tubes	Siboglinidae vestimentifera (Little *et al.*, 1999c)	?Siboglinidae ?vestimentifera	Less conservative cladistic analysis (Figure 4.24B), suggests possible siboglinid affinity. Also resemble serpulid tubes, but siboglinid tubes more closely.
Troodos - wrinkled tubes	Siboglinidae vestimentifera (Little *et al.*, 1999c)	Siboglinidae vestimentifera	Resolved near vestimentiferans by all analyses.
Troodos - attached tubes	Siboglinidae vestimentifera (Little *et al.*, 1999c)	Annelida *incertae sedis*	Less conservative cladistic analysis (Figure 4.24B), suggests possible siboglinid affinity, but cluster near serpulids in PCO plot. Characters consistent with both annelid families.
Christopher Fm. - Ellef Ringnes Island	Serpulidae (Beauchamp and Savard, 1992)	?Siboglinidae ?vestimentifera	Less conservative cladistic analysis (Figure 4.24B), suggests possible vestimentiferan affinity.
Christopher Fm. - Prince Patrick Island	Serpulidae (Beauchamp and Savard, 1992)	?Siboglinidae ?vestimentifera	Less conservative cladistic analysis (Figure 4.24B), suggests possible vestimentiferan affinity.
Cold Fork Cottonwood Creek	?Siboglinidae ?vestimentifera (Campbell *et al.*, 2002)	Annelida *incertae sedis*	Cladistic analyses suggest possible chaetopterid affinity but outer tube morphology could not be assessed.
Wilbur Springs	-	Animalia *incertae sedis*	Poorly preserved walls, single tube for which outer morphology could be assessed resembles scaphopod.
Svalbard	?Siboglinidae ?vestimentifera (Hammer *et al.*, 2011; Hryniewicz *et al.*, 2015)	Annelida *incertae sedis*	Do not clearly group within a modern annelid family in cladistic analyses, although one tube resembles those of siboglinids in section.
Figueroa	Siboglinidae vestimentifera (Little *et al.*, 2004)	Siboglinidae vestimentifera	Resolved among vestimentiferans by all analyses.
Tevidestus serriformis	Siboglinidae vestimentifera (Little *et al.*, 1999a; Shpanskaya *et al.*, 1999)	Annelida *incertae sedis*	Group near chaetopterid tubes in more conservative cladistic analysis (Figure 4.24A), unresolved by less conservative cladistic analysis. Also resemble siboglinid tubes in some respects.
Indeterminate annelid Sibay	?Annelida *incertae sedis* (Little *et al.*, 1999a)	?Annelida *incertae sedis*	Unresolved by cladistic analyses, tubes possibly resemble those of annelids more than those of other tubicolous animals.
Eoalvinellodes annulatus	Annelida *incertae sedis* (Little *et al.*, 1999a)	Animalia *incertae sedis*	Less conservative cladistic analysis (Figure 4.24B), suggests possible chaetopterid affinity, but morphology consistent with several annelid and potentially non-annelid lineages.
Yamankasia rifeia	Siboglinidae vestimentifera (Little *et al.*, 1999a; Shpanskaya *et al.*, 1999)	Animalia *incertae sedis*	Group with frenulates in cladistic analyses, but the combination of large size and fine parallel wrinkles does not closely resemble any of the modern annelid tubes investigated.

Figure 4.1 Rocky Knob tubes, Middle Miocene, New Zealand. **A,** larger tube fragments in hard specimen, scale bar is 20 mm. **B,** smaller, parallel-aligned tubes, with one tube exhibiting fine longitudinal wrinkles on its surface (blue arrow), scale bar is 5 mm. **C,** detail of smooth tube wall, scale bar is 2mm. **D,** tube exhibiting round concretions on its surface, scale bar is 1 mm. **E,** tube in transverse section showing preserved torn fibres, scale bar is 100 μm. **F,** detail of join between three tubes with thick, multi-layered walls in transverse section, imaged using confocal laser scanning microscopy. Scale bar is 200 μm. **G,** detail of tube transverse section showing delamination of its thick, multi-layered tube wall, scale bar is 200 μm.

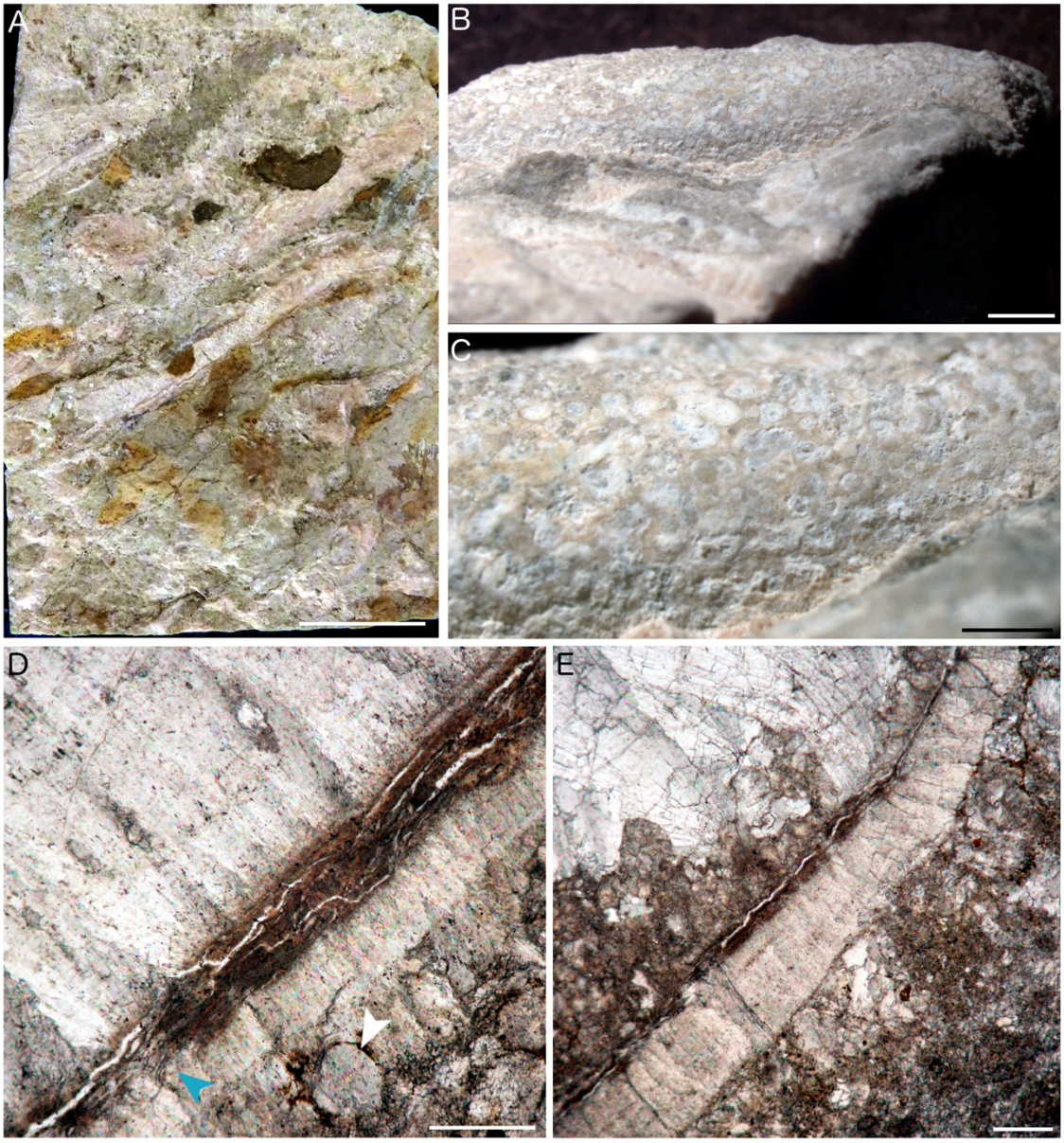

Figure 4.2 Upper Waiau River tubes, ?late Early Miocene-Middle Miocene, New Zealand. **A,** tubes in hand specimen, sale bar is 20 mm. **B,** tube with grainy wall in hand specimen, scale bar is 2 mm. **C,** detail of tube wall in **B**, scale bar is 1 mm. **D,** detail of tube wall in near transverse section showing brown bands that make up the multi-layered tube wall, where a tear in the wall is also preserved (blue arrow). A small sphere is preserved towards the outside of the tube (white arrow). Scale bar is 200 μm. **E,** detail of tube wall in transverse section showing a thick calcareous band occurring on the outside of the brown tube wall layers, scale bar is 200 μm.

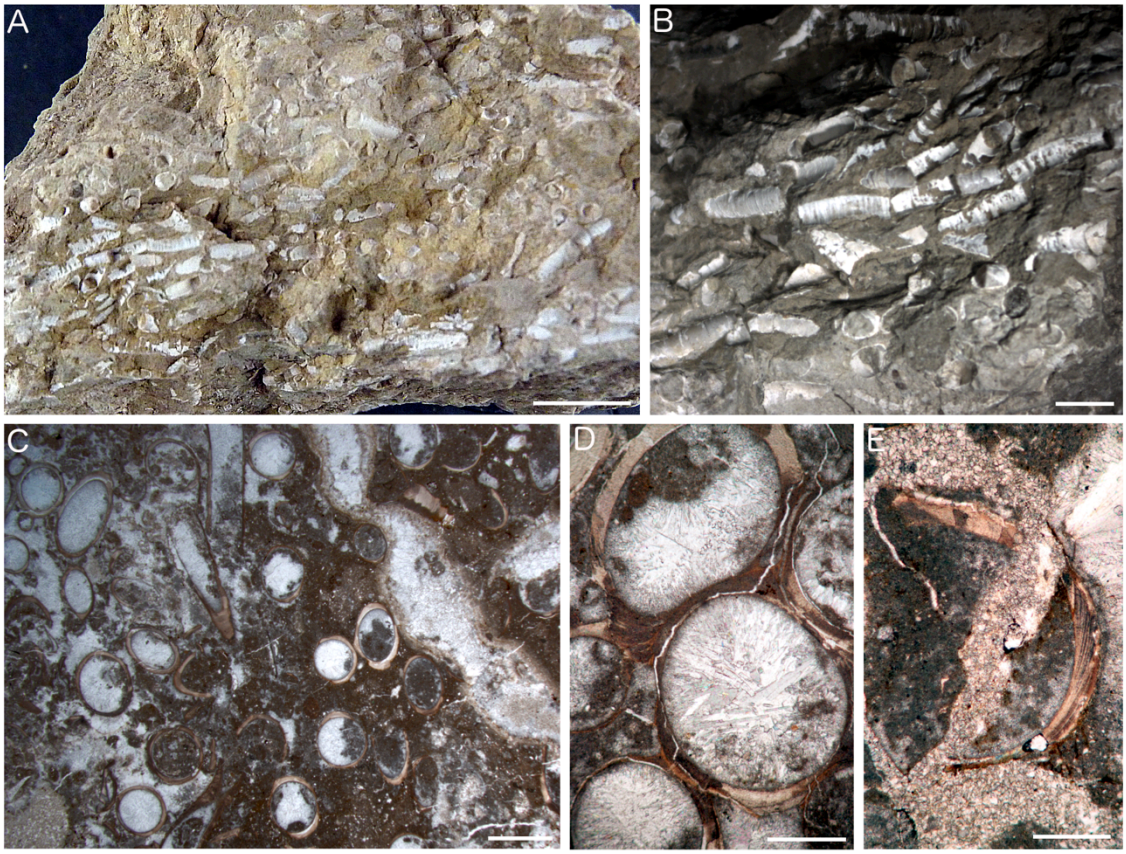

Figure 4.3 Bexhaven tubes, Middle Miocene, New Zealand. **A,** tubes in hand specimen, scale bar is 20 mm. **B,** detail of tubes in hand specimen showing fine parallel transverse wrinkles on tube surfaces, scale bar is 3 mm. **C,** tubes in section, scale bar is 2 mm. **D,** cluster of five attached tubes in transverse section, scale bar is 500 μm. **E,** detail of partial transverse section of tube wall showing its chevron-like appearance, scale bar is 500 μm.

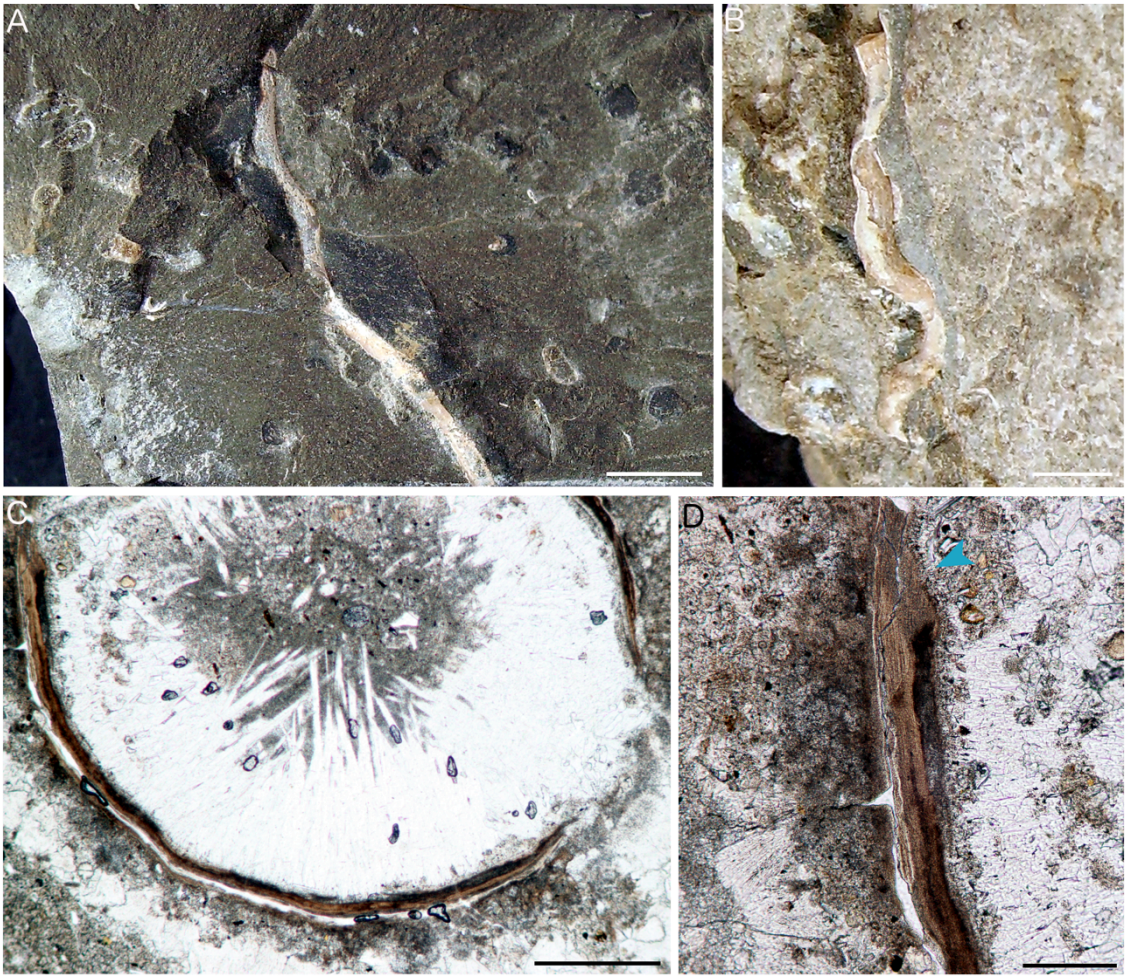

Figure 4.4 West Fork Satsop River tubes, Oligocene, WA, USA. **A-B,** tubes in had specimen wavy nature and smooth tube walls, scale bar in **A** is 10 mm, and 5 mm in **B**. **C,** transverse section of tube showing multi-layered brown walls of varying thickness, scale bar is 300 μm. **D,** detail of tube wall where a tear occurs, revealing fibre endings (blue arrow), scale bar is 100 μm.

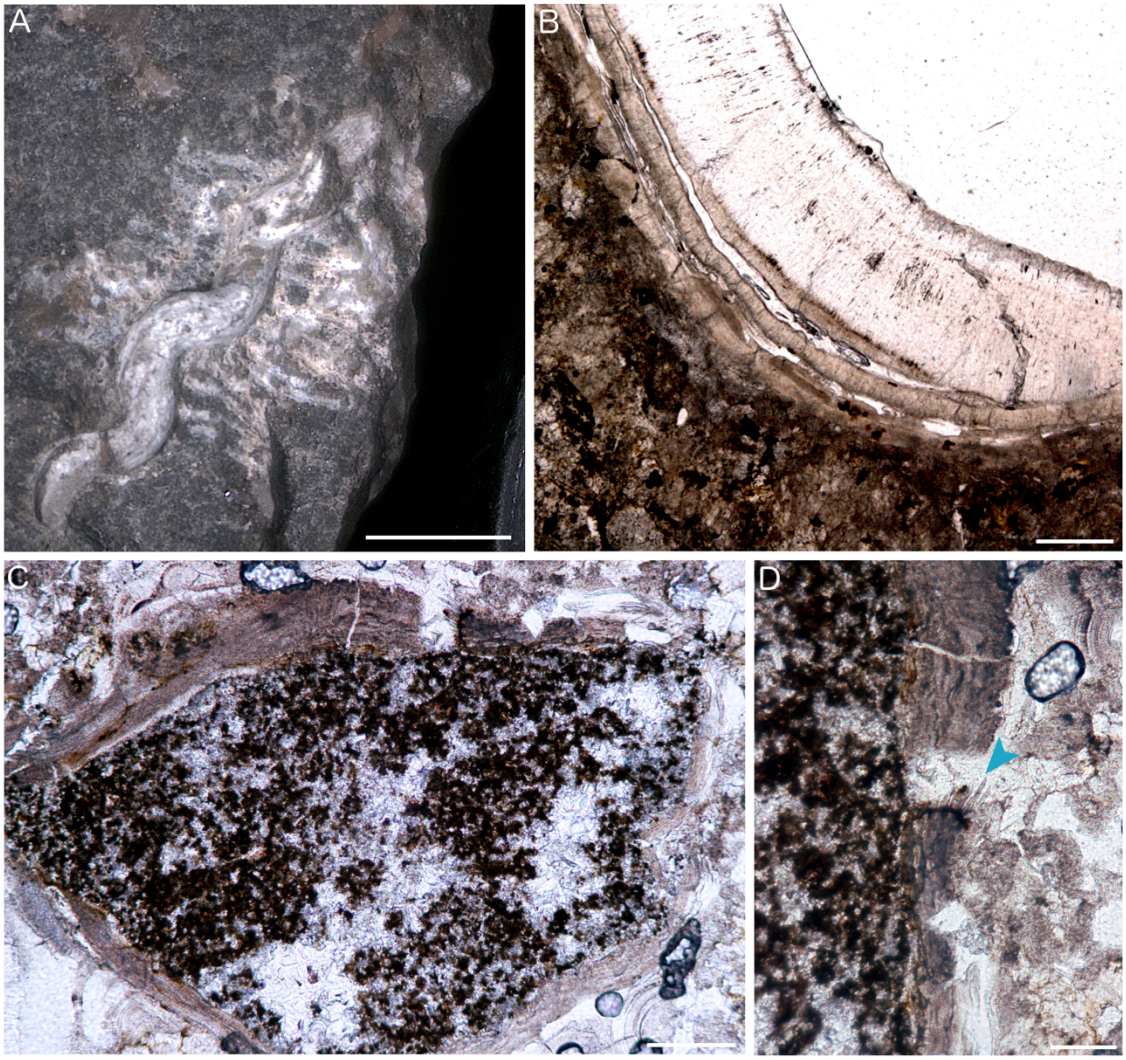

Figure 4.5 Murdock Creek tubes, Early Oligocene, WA, USA. **A,** a single tube in hand specimen possibly bearing longitudinal wrinkles, scale bar is 5 mm. **B,** detail of tube wall in transverse section with thick, multi-layered and delaminated tube wall, scale bar is 150 μm. **C,** transverse section of tube which appears to have originally been flexible, scale bar is 100 μm. **D,** detail of tube wall where a tear occurs, revealing fibre endings (blue arrow), scale bar is 50 μm.

Figure 4.6 Canyon River tubes, Oligocene, WA, USA. **A,** large-diameter tubes in hand specimen, scale bar is 20 mm. **B,** smooth small-diameter tubes, scale bar is 5 mm. **C,** small-diameter tube with longitudinal wrinkles, scale bar is 3 mm. **D,** delaminated tube wall with a fragment of preserved multi-layered and fibrous tube wall (blue arrow), scale bar is 150 μm. **E,** uncompressed transverse section of a small diameter tube, scale bar is 300 μm. **F,** detail of tube wall showing fluorescent bands that likely indicate the presence of preserved organic matter from the tube wall, imaged using confocal laser scanning microscopy. Scale bar is 30 μm.

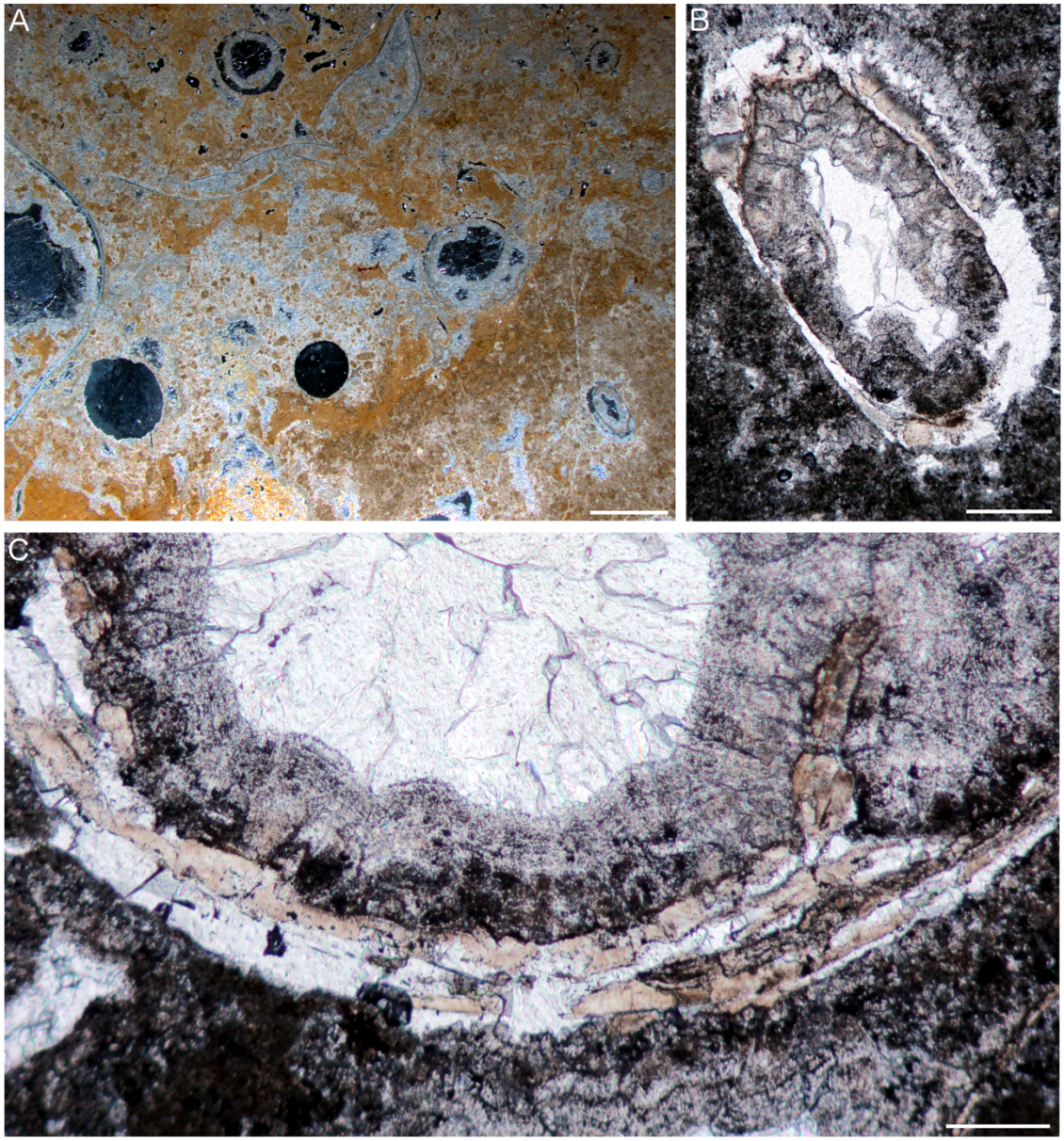

Figure 4.7 Bear River tubes, late Eocene, WA, USA. **A,** multiple tubes in transverse section with neat round profiles, scale bar is 2 mm. **B,** small-diameter tube with thick wall, scale bar is 300 μm. **C,** large-diameter tube with thick wall and showing evidence of multi-layering, scale bar is 200 μm.

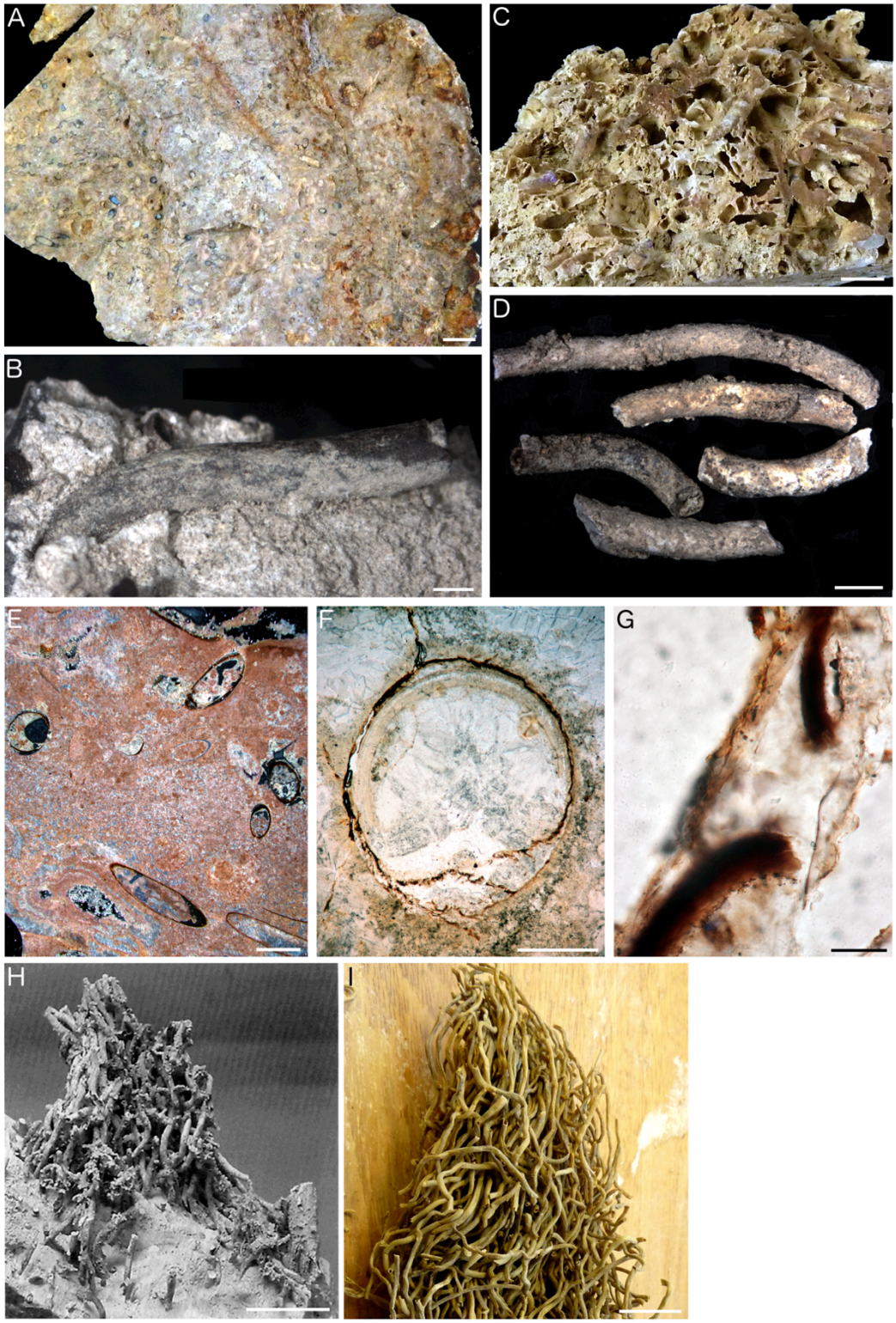

Figure 4.8 Omagari tubes, Campanian, Hokkaido, Japan. **A,** hand specimen with many, similar-diameter tubes with brown walls encased in carbonate, scale bar is 10 mm. **B,** detail of tube with brown wall, outer wall appears smooth, scale bar is 1 mm. **C,** cluster of tubes with mineralised walls but not encased in carbonate, scale bar is 5 mm. **D,** detail of individual tubes from specimen in **C**, scale bar is 2 mm. **E,** tubes with brown walls in section, scale bar is 2 mm. **F,** large-diameter tube in transverse section with wall comprised of many layers, scale bar is 500 μm. **G,** preserved tear in the wall of a tube suggesting an originally fibrous nature, scale bar is 50 μm. **H,** clump of Omagari tubes, reproduced from Hikida *et al.* (2003), scale bar is 20 mm. **I,** clump of the roots of the seep vestimentiferan *Lamellibrachia luymesi*, scale bar is 20 mm.

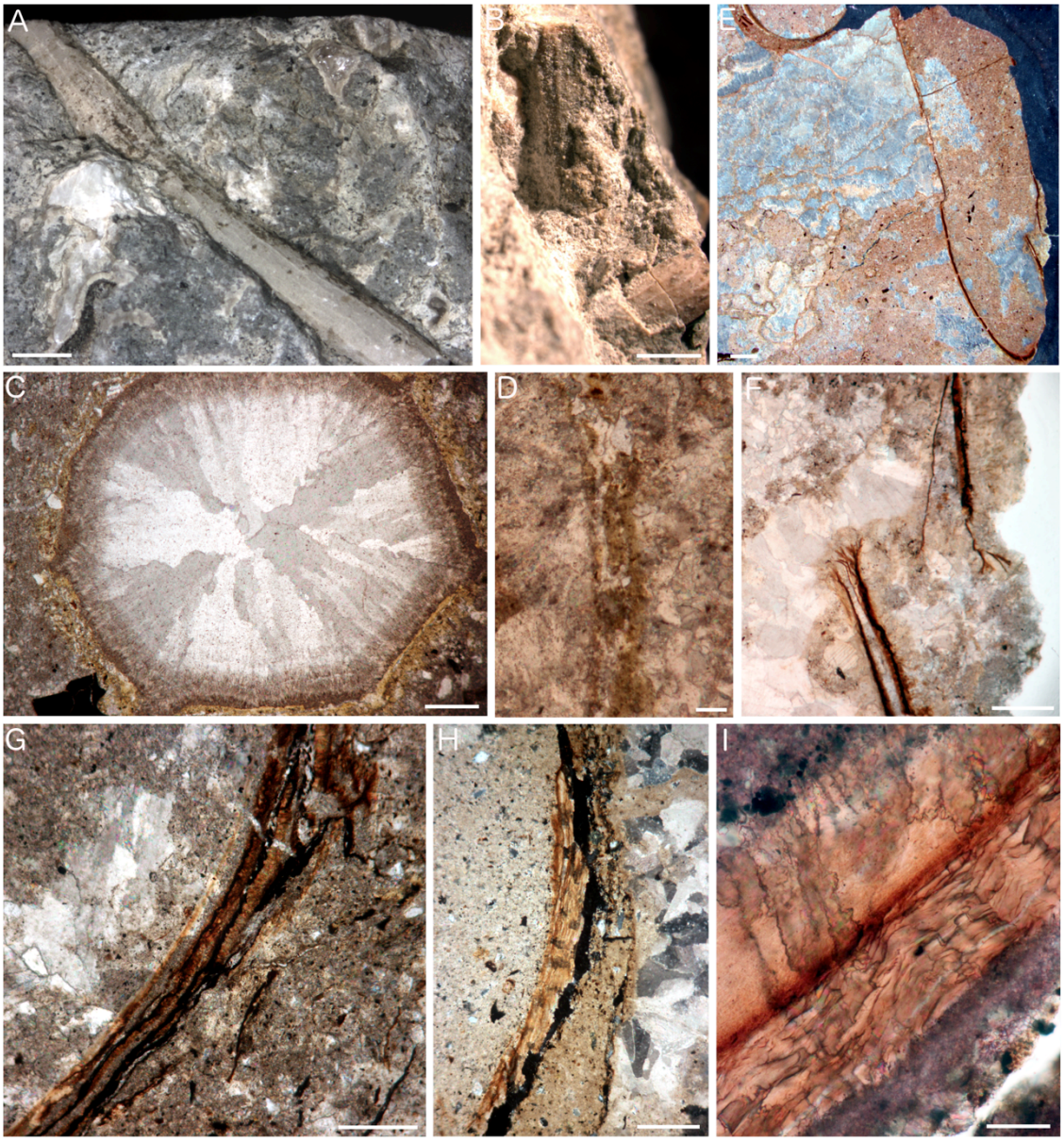

Figure 4.9 Okukinenbetsu River tubes, Cenomanian, Japan. **A-D**, yellow-walled tubes, **E-I**, brown-walled tubes. **A,** long fragment of a tube exhibiting fine longitudinal wrinkles, scale bar is 2 mm. **B,** short tube fragments also exhibiting fine longitudinal wrinkles, scale bar is 2 mm. **C,** transverse section of tube with yellowish walls, scale bar is 300 μm. **D,** detail of a yellow tube wall, showing some evidence of multi-layering, scale bar is 50 μm. **E,** partial longitudinal and transverse sections of a tube with brown walls, scale bar is 1 mm. **F,** detail of brown-walled tube revealing a multi-layered, fibrous nature, scale bar is 300 μm. **G-I,** detail of thick, multi-layered brown-walled tubes. Scale bars are 150 μm in **G**, 200 μm in **H**, and 50 μm in **I**.

Figure 4.10 Troodos Ophiolite tubes, Turonian, Cyprus. **A-B,** sinuous worm tubes with collars, scale bars are 1 mm. **C,** worm tube with collar attached at an oblique angle, scale bar is 1mm. **D-E,** worm tubes bearing longitudinal and transverse wrinkles, scale bars are 1 mm in D and 0.5 mm in E. **F-G,** sinuous tubes that appear attached to a surface, tubes in **F** bear fine parallel transverse wrinkles. Scale bars are 1 mm.

Figure 4.11 Christopher Formation tubes, Albian, Canada. **A-B**, **D-E**, larger tubes from Ellef Ringnes Island. **C**, **F-G**, smaller tubes from Prince Patrick Island. **A,** Ellef Ringnes Island tubes in hand specimen, scale bar is 10 mm. **B,** sections of Ellef Ringnes Island tubes, scale bar is 10 mm. **C,** Prince Patrick Island tubes in hand specimen, scale bar is 10 mm. **D,** detail of a transverse section of a Ellef Ringnes Island tube showing thick, multi-layered tube walls, with some possible torn fibres (blue arrow), scale bar is 1 mm. **E,** detail of a transverse section of an Ellef Ringnes Island tube showing a break in the tube wall where it appears fibrous but brittle, scale bar is 500 um. **F,** transverse section of a Prince Patrick Island tube exhibiting thick, multi-layered tube walls, scale bar is 1 mm. **G,** longitudinal section of a Prince Patrick Island tube with thinner walls containing round pellets, scale bar is 1 mm.

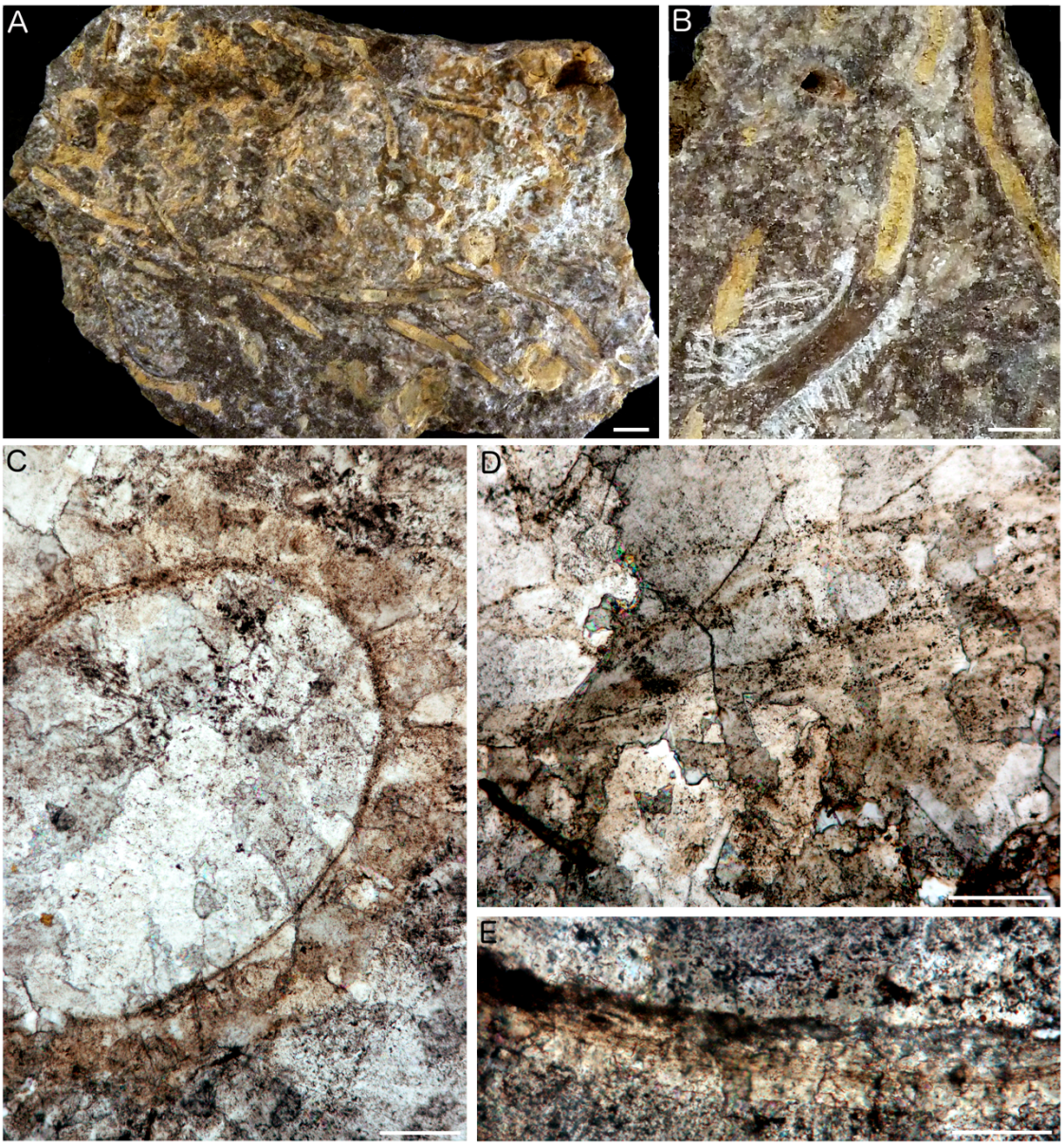

Figure 4.12 Cold Fork Cottonwood Creek tubes, Hauterivian, CA, USA. **A,** tubes in hand specimen, walls largely obscured by rock matrix, scale bar is 10 mm. **B,** tube with some visible wall which appears smooth, scale bar is 5 mm. **C,** transverse section of a tube showing the hazy nature of the walls, scale bar is 100 μm. **D,** detail of tube wall in transverse section showing delaminated, curving tube layers, scale bar is 100 μm. **E,** detail of tube wall in transverse section showing multi-layered nature, scale bar is 50 μm.

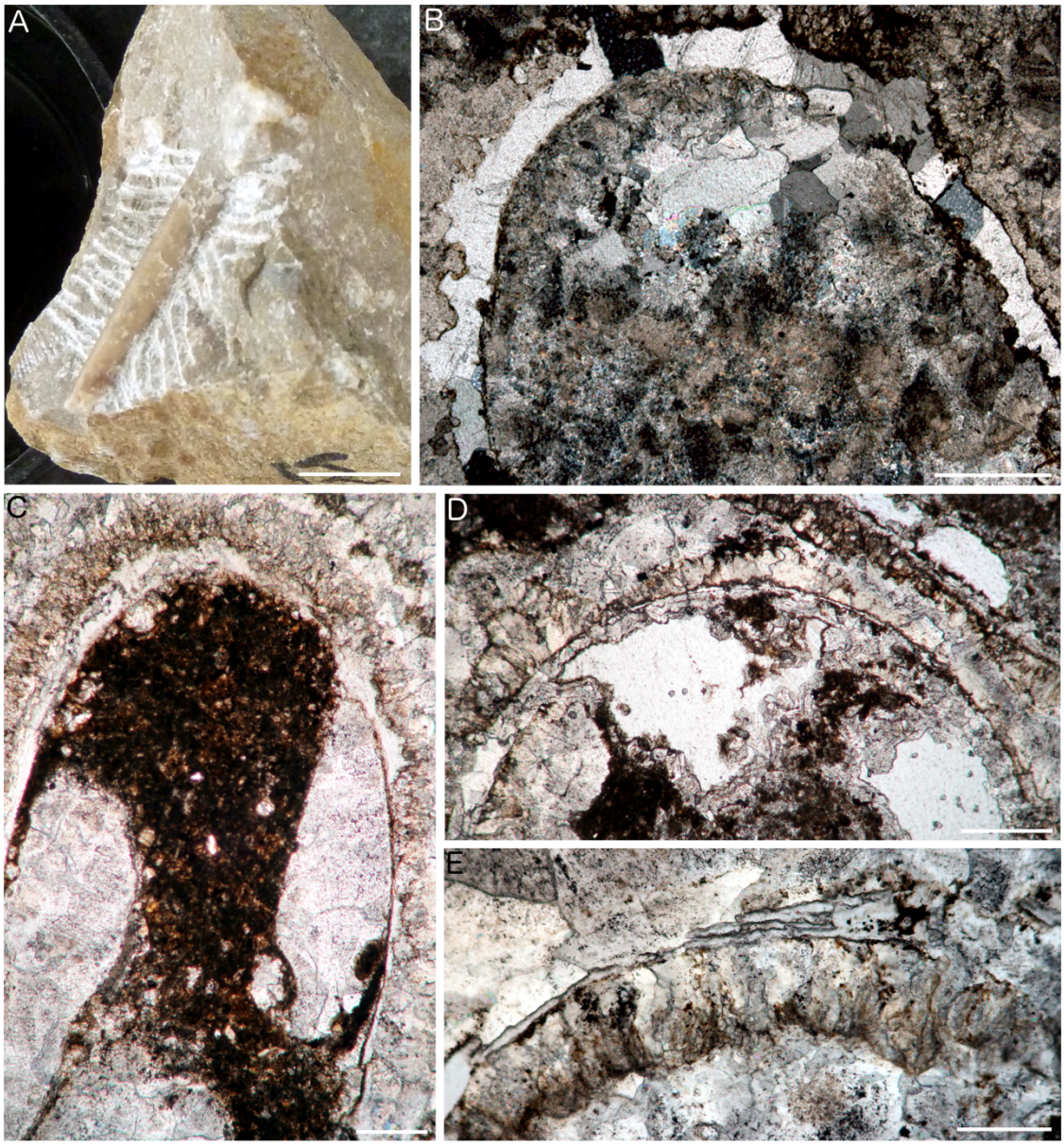

Figure 4.13 Wilbur Springs tubes, Hauterivian, CA, USA. **A,** smooth-walled, tapering tube in hand specimen, scale bar is 10 mm. **B,** transverse section of tube with replaced wall that may have originally been calcareous in composition, scale bar is 500 μm. **C-E,** tube walls in near-transverse section with poorly preserved walls that may have originally been organic in composition. Scale bars are 200 μm in **C**, 400 μm in **D** and 200 μm in **E**.

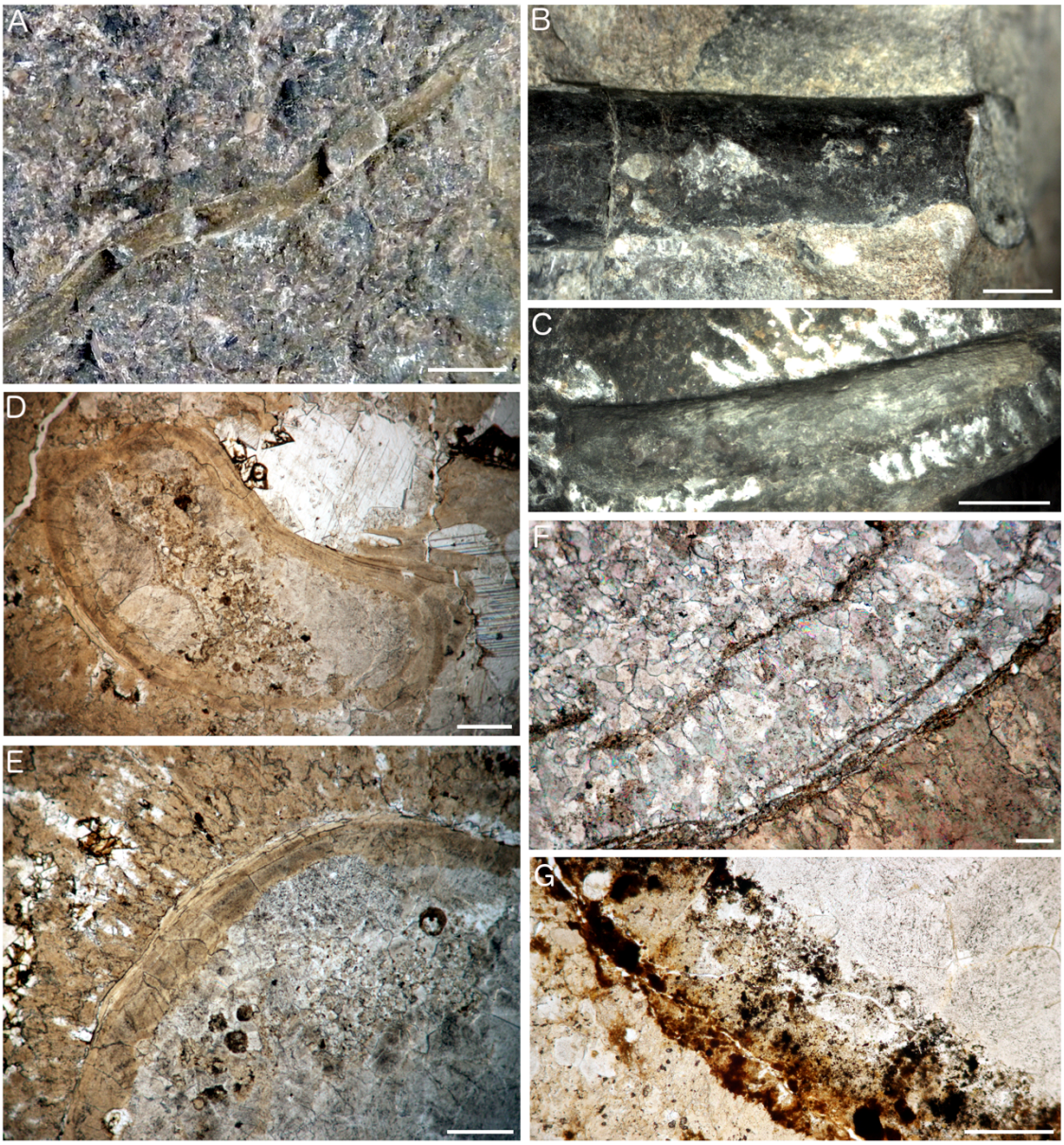

Figure 4.14 Sassenfjorden area tubes, Volgian-Ryazanian, Svalbard. **A-C,** hand specimens of Sassenfjorden tubes, **A,** long tube with poorly preserved walls, scale bar is 10 mm. **B,** smooth-walled tube possibly with a small collar, scale bar is 2 mm. **C,** tube with possible longitudinal wrinkles, scale bar is 5 mm. **D-E,** near-transverse sections of tubes with thick, neatly-multi-layered walls, scale bars are 300 μm. **F,** detail from transverse section of a tube where the tube exhibits curving layers that have separated, scale bar is 100 μm. **G,** tube with poorly preserved walls, scale bar is 200 μm.

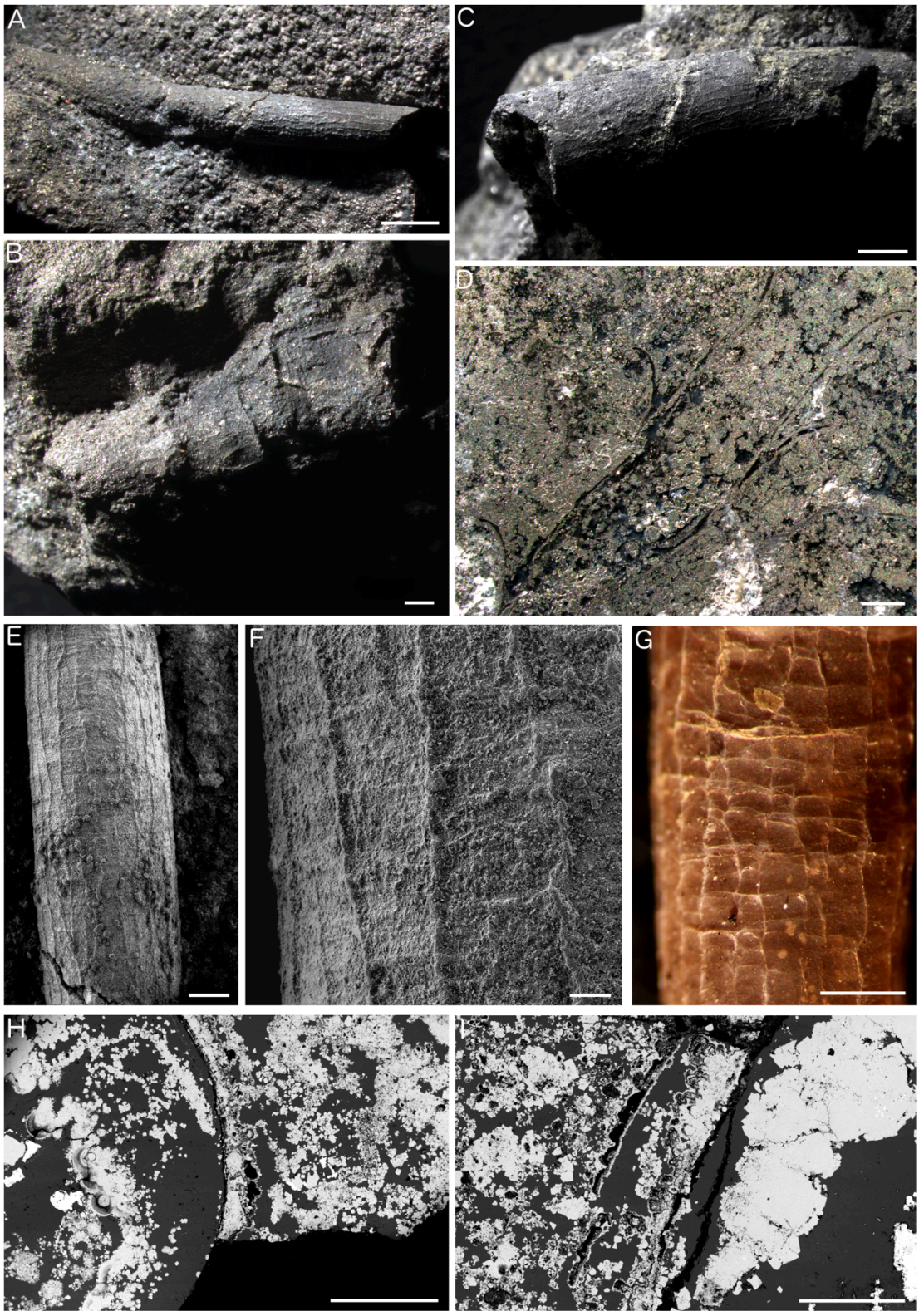

Figure 4.15 Figueroa tubes, Pleinsbachian, CA, USA. **A-C,** tubes in hand specimen. **A,** straight, tapering tube with fine longitudinal wrinkles, scale bar is 2mm. **B,** tube fragment bearing ongitudinal wrinkles and collars, scale bar is 1 mm. **C,** tube with longitudinal wrinkles and a fine, obliquely-positioned collar, scale bar is 2mm. **D,** longitudinal section of tube exhibiting long, flaring collars, scale bar is 1 mm. **E,** SEM image showing details of tube wall ornamentation, scale is 500 μm. **F,** greater detail of tube in E, scale is 100 μm. **G,** detail of the ornamentation of a *Ridgeia piscesae* (Siboglnidae) tube, scale is 1mm. **H,** detail of tube transverse section showing preservation of tube walls, scale bar is 1 mm. **I,** detail of tube wall in transverse section, scale bar is 300 μm.

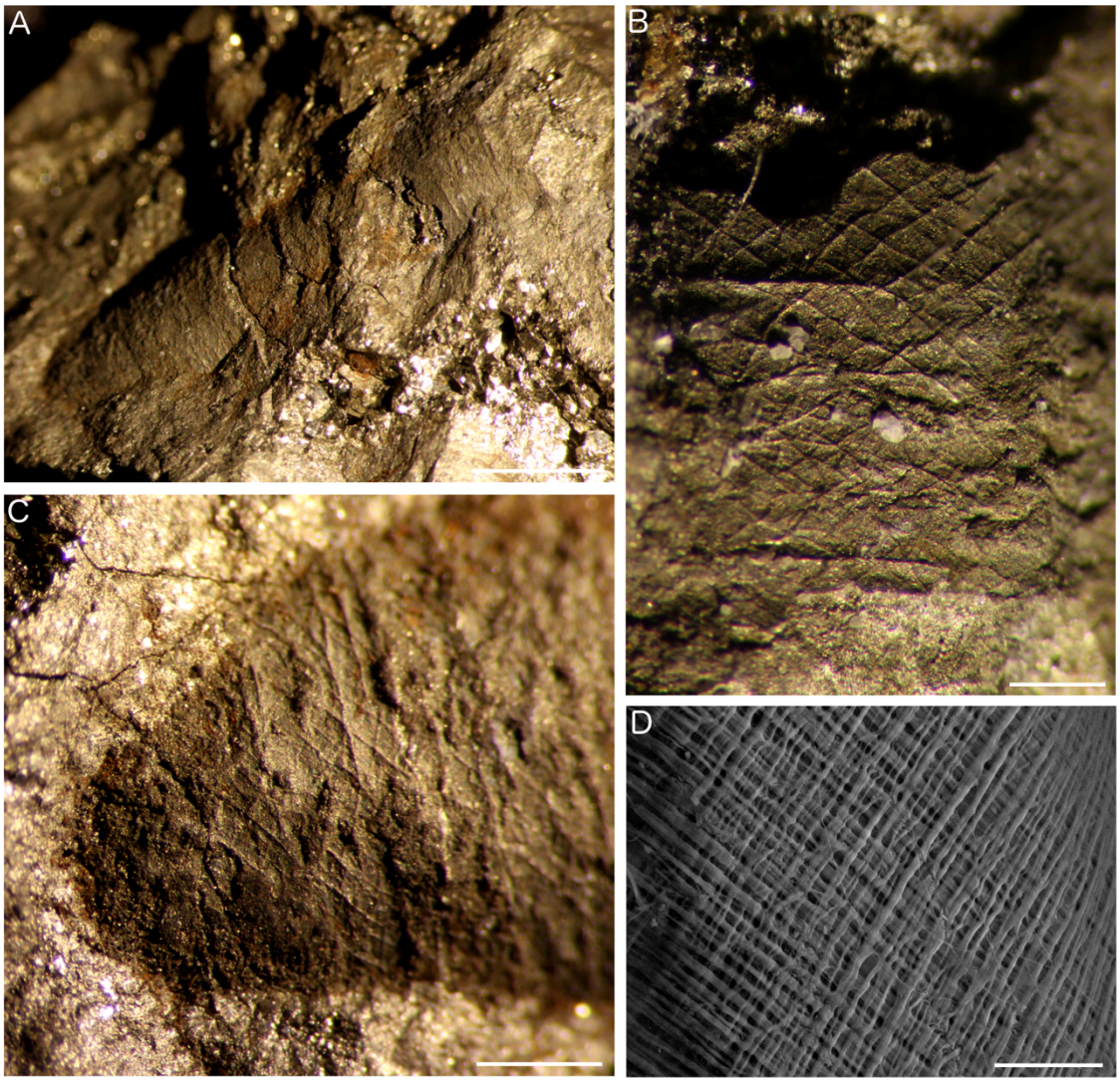

Figure 4.16 *Tevidestus serriformis* tubes, Devonian, Sibay, Russia. **A,** tube fragment exhibiting numerous short collars, scale bar is 4 mm. **B-C,** detail of tube wall showing small collars and meshwork of fibres, scale bars are 1 mm. **D,** detail of the outer tube wall of *Phyllochaetopterus prolifica* for comparison, scale bar is 10 μm.

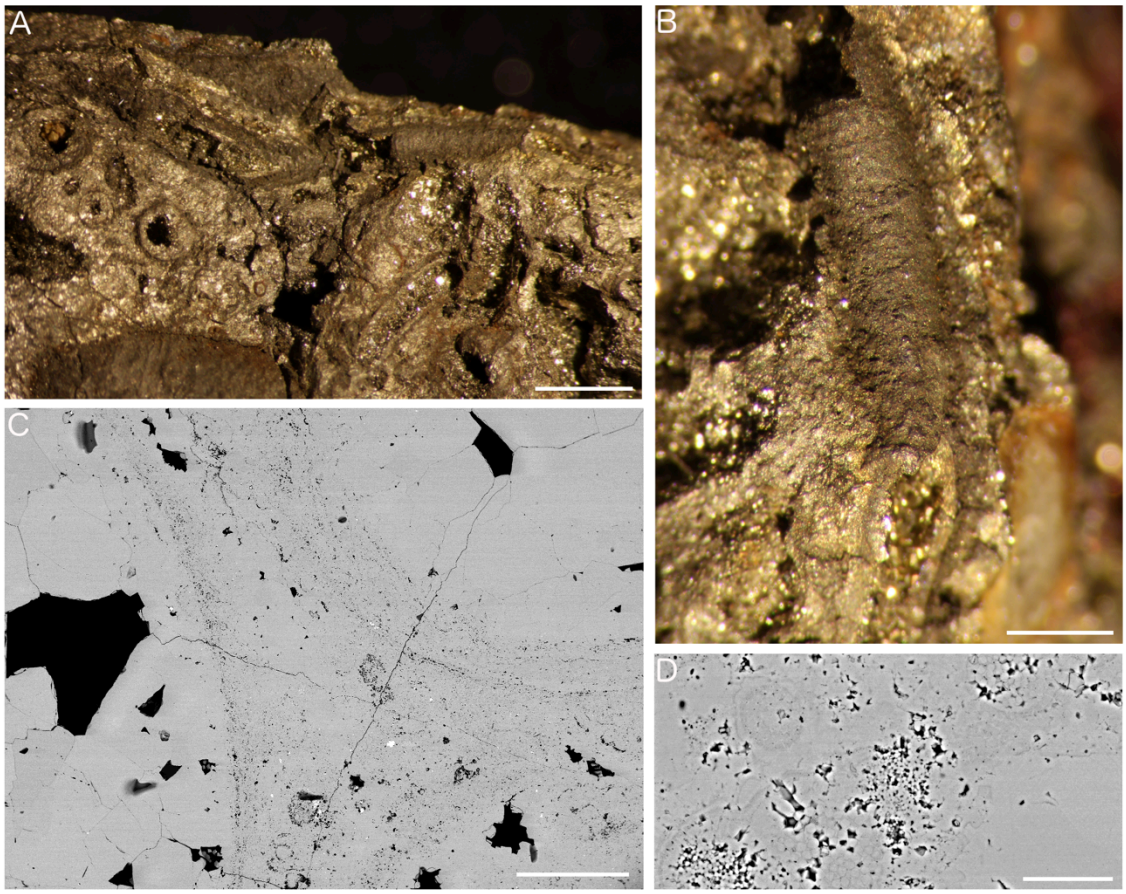

Figure 4.17 Indeterminate annelid tubes, Devonian, Sibay, Russia. **A,** hand specimen showing cluster of tubes in various orientations, scale bar is 3 mm. **B,** detail of tube wall showing smooth appearance, scale bar is 1 mm. **C,** detail of the walls of three adjacent tubes in transverse section, walls appear thick and multi-layered. Scale bar is 500 μm. **D,** detail of framboidal pyrite preserving tube walls, scale bar is 10 μm.

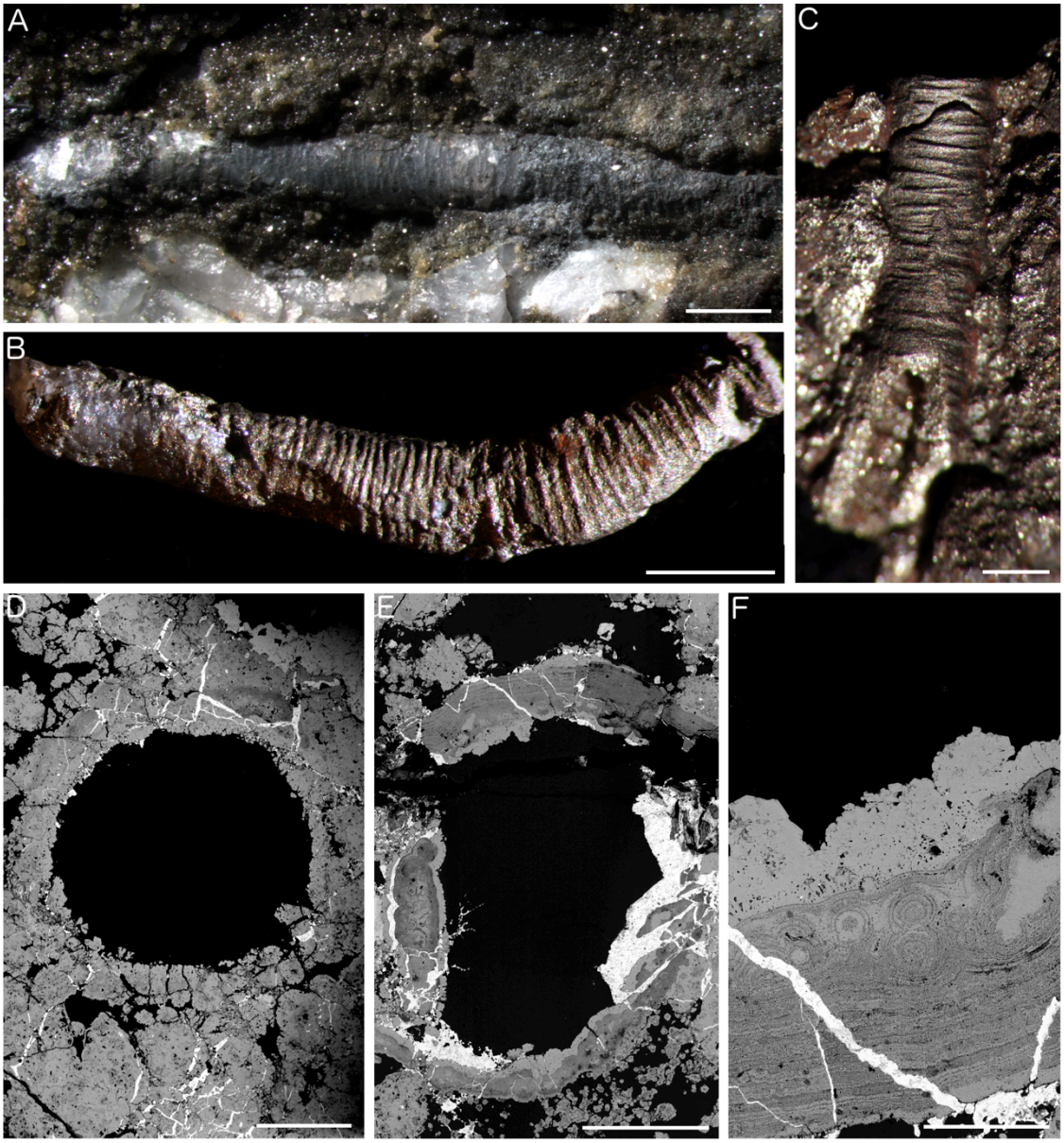

Figure 4.18 *Eoalvinellodes annulatus* tubes, Silurian, Yaman Kasy, Russia. **A-C,** hand specimens of gently curving tubes with folded fabric-like tube wall texture, scale bar in **A** is 2mm, in **B** is 2mm, and in **C** is 1mm. **D-E,** transverse sections of tubes showing thick walls with thick, possibly multi-layered walls, scale bars in **D** and **E** are 500 μm. **F,** detail of tube wall in transverse section showing preservation by colloform pyrite many layers thick, scale bar is 100 μm.

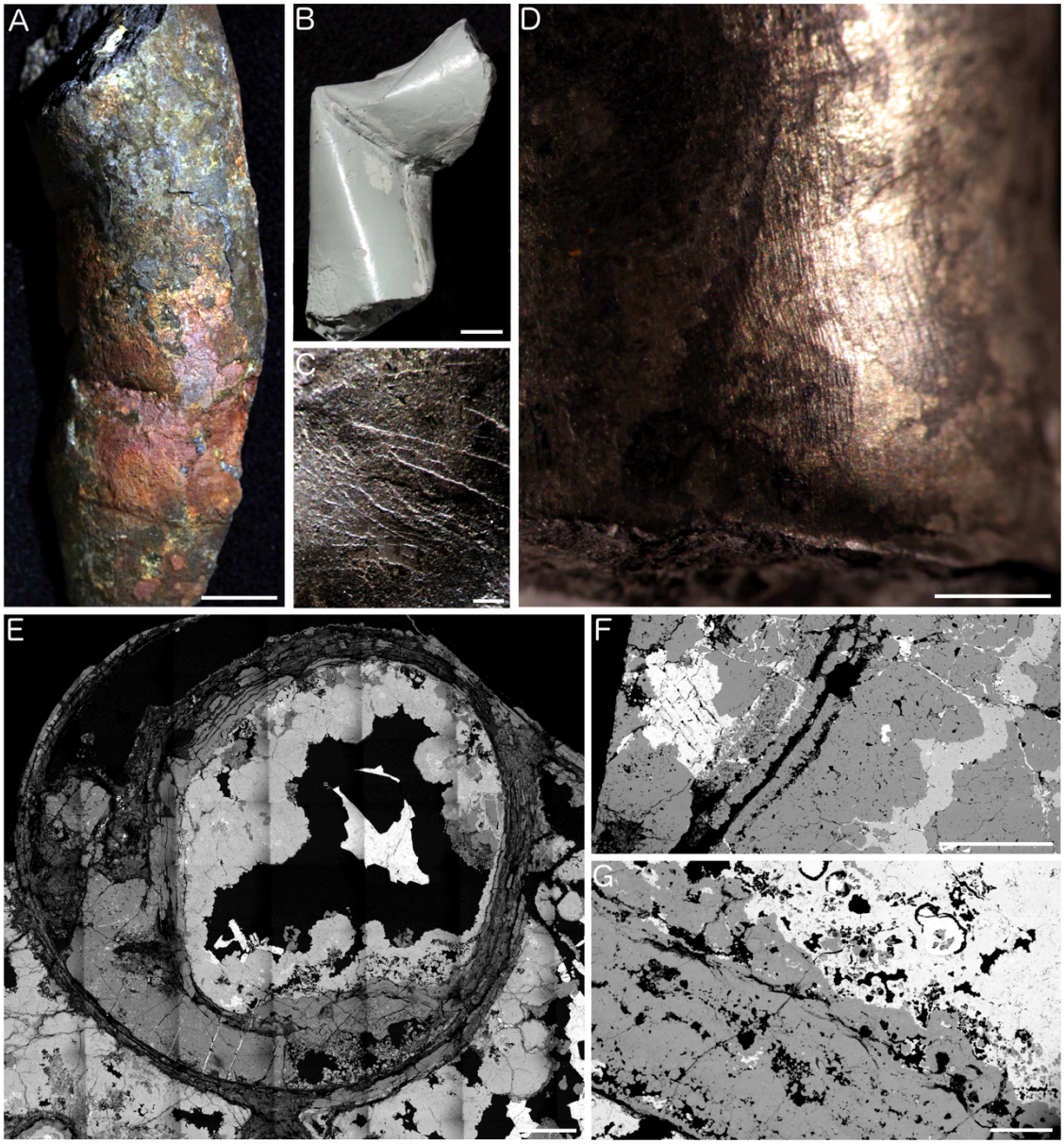

Figure 4.19 *Yamankasia rifeia* tubes, Silurian, Yaman Kasy, Russia. **A,** large tube in hand specimen, scale bar is 10 mm. **B,** cast of tube exhibiting fold, scale bar is 5 mm. **C,** pyritised fibres or filamentous micro-organisms preserved on the outside of a tube, scale bar is 500 μm. **D,** fine longitudinal wrinkles preserved on outer tube surface, scale bar is 3 mm. **E,** tube in transverse section with thick, multi-layered wall, scale bar is 1.5 mm. **F,** tube wall in transverse section preserved as several layers, scale bar is 500 μm. **G,** detail of tube transverse section showing colloform pyrite interpreted as having grown on the outside of the tube, scale bar is 500 μm.


A
B
C
D
E
F
G
H
I
J
K
L
M
N
O
P
Q
S
U
W
Y
Z
R
T
V
X
A'

Figure 4.20 Morphology of tubes made by annelid lineages occurring at modern hydrothermal vents and cold seeps. **A,** disorganised tubes of *Alvinella* spp. (Alvinellidae), scale bar is 10 mm. **B,** agglutinated tube of *Mesochaetopterus taylori* (Chaetopteridae), scale bar is 10 mm. **C,** agglutinated Sabellidae tube, scale bar is 5 mm. **D,** branched tube of *Phyllochaetopterus claparedii* (Chaetopteridae), scale bar is 10 mm. **E,** segmented tubes of *Spiochaetopterus costarum* (Chaetopteridae), scale bar is 10 mm. **F,** *Phyllochaetopterus polus* (Chaetopteridae) tubes bearing short collars and wrinkled-fabric ornamentation, scale bar is 10 mm. **G,** collared Serpulidae tubes (likey *Serpula narconensis*). **H,** collared tubes of *Serpula vermicularis* (Serpulidae), scale bar is 10 mm. **I,** large tube of the vestimentiferan *Riftia pachyptila* (Siboglinidae), scale bar is 10 mm. **J,** collared, ornamented tube of the vestimentiferan *Ridgeia piscesae* (Siboglinidae), scale bar is 10 mm. **K,** smooth tube of the vestimentiferan *Escarpia southwardae* (Siboglinidae), scale bar is 20 mm. **L,** collared tubes of the frenulate *Polybrachia canadensis* (Siboglinidae), scale bar is 5 mm. **M,** Hard tubes of the frenulate Siphonobrachia lauensis (Siboglinidae), scale bar is 10 mm. **N,** *Glyphanostomum* tube, scale bar is 1 mm. **O,** detail of the wall of an *Alvinella* spp. tube in transverse section, scale bar is 200 μm. **P,** detail of the wall of an *M. taylori* tube in transverse section. **Q,** detail of the wall of a *Megalomma vesiculosum* (Sabellidae) tube in transverse section. **R,** detail of the wall of a Serpulidae tube in transverse section, scale bar is 50 μm. **S,** detail of the wall of a *Spiochaetopterus typicus* (Chaetopteridae) tube in transverse section, **T,** is detail of the wall of the same tube in longitudinal section. **U,** detail of the wall of a *P. polus* tube in transverse section, **V,** is detail of the wall of the same tube in longitudinal section. **W,** detail of the anterior tube wall of an *E. southwardae* tube in transverse section, **X,** shows a transverse section of the posterior tube wall of the same species, scale bar is 125 μm. **Y,** transverse section of the very anterior portion of the tube of the frenulate *Unibrachium colombianum* (Siboglinidae), **Z,** shows a longitudinal section of the ringed middle region of the same tube, and **A',** shows a transverse section of the middle tube region.

4.5 Tube characters

Comparisons of modern tubes from a range of annelid families that mostly occur at vents and seeps (Figure 4.20), as well as fossil tubes from these environments, allowed the formulation of 48 potentially useful characters for the identification of fossil tubes (illustrated in Figure 4.21). The selected characters below are numbered with their character states outlined, and are preceded by an explanation of each character.

Tube diameter. The size of tubes is difficult to code as a character due to the large range of diameters that a single annelid tube may exhibit, for example the tubes of the vestimentiferan *Paraescarpia echinospica* range from 25 mm at their anterior end to 1 mm at their posterior end (Southward *et al.*, 2002). Therefore diameter measurements strongly depend on where a tube is measured. For fossil tubes, which are mainly fragments, this information is largely unknown. However despite these difficulties, tube diameter does contain taxonomically useful information as only certain annelids build tubes that reach very large diameters (e.g. *Riftia pachyptila*; Figure 4.20I), or tubes with diameters that are never above a certain size. Therefore, tube diameter has been divided into two characters to account for this information - tubes that reach a maximum diameter of over 20 mm, and tubes that have a maximum diameter of less than 1 mm.

1. Maximum diameter greater than 20 mm: (0) below 20 mm (1) above 20 mm

2. Maximum diameter less than 1 mm: (0) above 1 mm (1) below 1 mm

Clustering. As highlighted by Kiel and Dando (2009), whether tubes occur singly or are clustered is a difficult criterion to base tube identification upon, as the same type of tube under different conditions can occur either singly or as part of a clump e.g. *Tevnia jerichonana* (Rybakova and Galkin, 2015). Nevertheless, siboglinid tubes are often clustered at hydrothermal vents and cold seeps creating large habitat-forming bushes, which are characteristic of these habitats. The roots of these tubes, which have greater potential for become fossilised, are also distinct as the clusters are often very dense and tubes are highly intertwined within them. In order to include this information within the data matrix, clustering is divided into three to characters, the first of which distinguishes between tubes that often occur alongside conspecific tubes and those that mostly do not. The further

characters allow for tubes that are found to cluster either as a dense mass, and/or as a minimum of two tubes together.

3. Clustering: (0) absent (1) present

4. Several tubes occurring together: (0) absent (1) present

5. Dense cluster of intertwined tubes: (0) absent (1) present

Attachment. This character can be used to distinguish the tubes of serpulids from those built by other annelid families, as serpulid tubes are often attached to a hard substrate such as rock or other serpulid tubes (Ippolitov *et al.*, 2014). While siboglinids and chaetopterids often occur in clumps of many individuals, their tubes are generally not attached to surfaces or to other tubes. However, exceptions do occur for the siboglinids. Examples include the tubes of *Tevnia jerichonana*, which attach to hard surfaces at vents using a chitinous plate located at their posterior extremity, and small tubes can sometimes be found winding around larger vestimentiferan tubes. To ensure that this character can distinguish between serpulid and siboglinid tubes, attachment is only determined to be present for fossil tubes when it can be seen to occur between three or more tubes along most of their lengths, and if the tube appears attached to a surface, it is also attached along most of its length.

6. Attachment to a surface or other tubes: (0) absent (1) present

Outer wall organisation. Tubes that do not have a regular pattern of ornamentation and possess very uneven, roughly textured walls are classed as disorganised. Examples include the outer walls of *Alvinella* tubes (Figure 4.20A), which are often comprised of a scaly arrangement of organic layers. This character is useful for distinguishing the organic tubes of alvinellids from those of siboglinids and the majority of chaetopterids.

7. Organisation: (0) present (1) absent

Agglutination. Evidence of outer wall sediment attachment is classed as agglutination. This character is useful for distinguishing between annelid lineages that always build agglutinated tubes, such as sabellids, terebellids and maldanids, and those that do not, e.g. siboglinids and many chaetopterids. Character 8 distinguishes between tubes that are not fully agglutinated, but often have sediment grains incorporated into them, and tubes that are completely agglutinated, where sediment homogeneously covers most of the tube.

Coating sediments can vary in size between different types of tube, but are most often sand (e.g. the tubes of *Mesochaetopterus taylori*; Figure 4.20B, P) or mud particles (e.g. sabellids tubes; Figure 4.20C, Q). Characters 9 and 10 distinguish between these two types of construction materials, but both are included to account for instances where a tube may exhibit both. A further character (11) distinguishes completely agglutinated tubes on which sand grains are oriented into a distinct pattern, this can often be seen in the tubes of oweniids which can arrange sediment grains on their tubes into an overlapping roof-tile pattern (Capa *et al.*, 2012).

8. Agglutination:	(0) absent	(1) present
9. Some sediment or complete:	(0) some sediment	(1) complete
10. Coating sediments is coarse/sandy:	(0) no	(1) yes
11. Coating sediment is fine-grained:	(0) no	(1) yes
12. Sediment grains are oriented:	(0) no	(1) yes

Organic composition. Based on the results of organics analyses (see later), two compositional characters are included to differentiate between organic tubes that contain chitin, which is largely associated with the siboglinids, and those that contain furfural such as chaetopterid tubes. For siboglinid tubes in which chitin content was not directly determined by the present or previous studies, chitin has been inferred to occur. Similarly, furfural has been assumed to occur in all chaetopterid tubes. The recently detected occurrence of chitin in oweniid tubes has also been coded into the data matrix (Guggolz *et al.*, 2015).

13. Chitin:	(0) absent	(1) present
14. Furfural:	(0) absent	(1) present

Branching. The division of single a tube into several distinct branches was most frequently observed in the chaetopterid genera *Spiochaetopterus* and *Phyllochaetopterus* (Figure 4.20D). While certain frenulate and *Sclerolinum* tubes can exhibit deformities that resemble branching (Webb, 1964; Georgieva *et al.*, 2015b), true tube branching was not found within siboglinid tubes. This character, if observed, may therefore suggest a chaetopterid affinity for the tube in question.

15. Branching: (0) absent (1) present

Sinuosity. Sinuosity is also difficult to code into a taxonomically useful character as tubes may exhibit both straight and highly sinuous sections, and it is the combination of these characters that may be useful for identification (e.g. the straight anterior sections and highly coiled root sections of *Escarpia* tubes; Figure 4.20K). To accommodate this variation, three sinuosity characters are included which score whether a tube possesses very straight sections along a length of approximately 10x the tube diameter, whether the tube has sections with s-bends, or sections in which the tube is highly contorted or twisted into a tight spiral. These characters allow for plasticity in tube sinuosity, as observed in some siboglinid tubes (Georgieva *et al.*, 2015b), and allow for the highly sinuous tubes of certain serpulids (Ippolitov *et al.*, 2014) and siboglinids (e.g. *Sclerolinum contortum*, *Alaysia spiralis*) to be distinguished from others.

16. Straight sections: (0) absent (1) present

17. Sections with s-bends: (0) absent (1) present

18. Highly contorted/spiralling sections: (0) absent (1) present

Flexibility. For modern taxa, tubes are hereby defined as rigid if when pressed between two fingers, they do not give way or break. For fossils, tubes are coded as 'flexible' if they show any signs of compression or folding of the tube wall (before it was fossilised), both in hand specimen and thin section, whereas tubes are coded as 'rigid' if they have clear circular cross sections and hand specimens have no preserved compressional features. The tubes of serpulids are always hard, as were those of certain vestimentiferan species. This character can therefore be useful in distinguishing the tubes of serpulids and some vestimentiferans from the flexible tubes built by other organic tube dwellers.

19. Flexibility: (0) rigid (1) flexible

Tapering. Any tube that shows a distinct change in diameter throughout its length is coded as tapering. Very gradual tapering can be difficult to classify as this may look like an untapered tube if only a fragment is available – in cases where fossil tube fragments are very short, tubes are coded with a '?' for this character. Siboglinid and serpulid tubes were often tapered in one direction, albeit for some exceptions such as the frenulate

Zenkevitchiana longissima. Chaetopterid tubes on the other hand were rarely observed to be tapering, but exceptions also exist in this family e.g. the tubes of *Chaetopterus variopedatus* are sometimes tapering at both ends.

20. Tapering: (0) absent (1) present

Collars. Collars are distinct structures, formed when layers of the outermost tube wall partially overlap tube layers beneath them. They can occur in siboglinid, chaetopterid, and serpulid tubes. Collars are defined as small if they are only several millimetres in length and do not overlap other tube layers very much. Short collars were the only type observed in chaetopterid tubes (e.g. Figure 4.20F). Alternatively, collars can be longer, and flare away from the tube wall. Vestimentiferans often produce this latter type of collar, as do some serpulids. Collars can also curve under - this characteristic was mostly associated with the tubes of vestimentiferans such as the collars on *Tevnia jerichonana* tubes. The angle at which collars are oriented with respect to the tube was also observed to vary between different tube-building annelid lineages. Chaetopterids and serpulids appeared to mostly build collars that were formed straight around the tube circumference, while a subset of siboglinids had collars that were oriented obliquely with respect to the tube wall. Thick-edged collars were uncommon in siboglinid and chaetopterid tubes but the collars of several of the examined serpulids were of this type (Figure 4.20G-H), discriminating them from other tube-builders. Spacing between collars also varied between different tubes. Closely-spaced collars are defined as those occurring at intervals equal to or less that the tube diameter, while distantly-spaced collars are defined as generally occurring at intervals greater than the diameter of the tube. Closely-spaced collars were observed on the tubes of several frenulates, vestimentiferans and chaetopterids, while distantly spaced collars occurred mostly on vestimentiferan and serpulid tubes (Figure 4.20G-H, J). Whether collars show regularity over a distance of tube length ~10 times the tube diameter was also considered, which distinguished the anterior regions of frenulate tubes (e.g. Figure 4.20L) from other tube types. The shapes of collar interspaces was also found to vary among the tubes examined. Several vestimentiferans and serpulids possessed cone-shaped collar interspaces, whereas the interspaces between chaetopterid and frenulate collars were mostly straight.

21. Collars present/absent: (0) absent (1) present

22. Collar spacing: (0) closely-spaced (1) distant spacing

23. Collar regularity: (0) irregular (1) regular

24. Collar angle: (0) only straight (1) some oblique

25. Collar interspace shape: (0) straight (1) cone-shaped

26. Collar length: (0) small (1) large, flaring

27. Collar curled: (0) absent (1) present

28. Collar thickness: (0) thin (1) thick

Segments. Segments are defined as tube wall lengths delineated by grouped wrinkles encircling the entire tube circumference, that occur at regular intervals along the outer tube wall. Examples include the segments on the tubes of *Zenkevitchiana longissima* and *Spiochaetopterus costarum* (Figure 4.20E). Segments are also observable in longitudinal section as regular wrinkles along the tube wall.

29. Segments: (0) absent (1) present

Rings. Rings are defined as regular stripes of the outer tube wall that also encircle the entire tube circumference, which are also followed by a distinct change in outer tube wall thickness that corresponds to the rings (Figure 4.20Z). Rings are typical of frenulate tubes especially in the genus *Siboglinum*, and certain frenulate tubes can have both rings and segments, e.g. *Siboglinum ekmani*. Rings can also be observed in longitudinal sections of tubes, within which differences in tube wall thickness between the rings and interspaces can be clearly seen.

30. Rings: (0) absent (1) present

Undulations. Undulations describe tubes with an outer wall that bears smooth waves. This texture was only observed in three *Phyllochaetopterus* tubes therefore it is possible that this ornamentation may be unique to the chaetopterids.

31. Undulations: (0) absent (1) present

Annulations. Annulations are here defined as a fine, outwardly-projecting wrinkle-like undulations of the outer tube wall that encircle the entire tube circumference. These are particularly apparent on the tubes of the ampharetid *Glyphanostomum* sp., where they are

very closely spaced and regularly occurring (Figure 4.20N). Annulations were also found to occur on the tubes of chaetopterids, however they were much more irregular in appearance, being distantly and unevenly spaced.

32. Annulations: (0) absent (1) present

33. Annulations regular/irregular: (0) irregular (1) regular

Transverse indentations. These differ from segments as indentations are often finer, occur individually, and where observed, show no regular pattern along the tube. Some transverse indentations were found to encircle the whole tube, but they could also occur as short sections only, and not encircle the tube circumference. While irregular indentations were also sometimes present on other tubes, they were most commonly associated with *Sclerolinum* tubes and the anterior regions of vestimentiferan tubes.

34. Encircling transverse indentations: (0) absent (1) present

35. Short transverse indentations: (0) absent (1) present

Transversely crumpled fabric texture. Folded-fabric-like texture is defined as smooth, closely-spaced wrinkles that sometimes bifurcate and resemble crumpled fabric, and was observed mostly in chaetopterid tubes (Figure 4.20F) where wrinkles tended to be coarser. However, the same texture was also visible in the anterior portions of frenulate tubes, albeit with wrinkles being finer.

36. Transversely crumpled fabric texture: (0) absent (1) present

37. Transversely crumpled fabric texture size: (0) fine (1) coarse

Parallel transverse wrinkles. Fine, parallel and closely spaced transverse wrinkles were very common on the outsides of serpulid tubes where they tended to have distinct round edges.

38. Parallel closely-spaced transverse wrinkles: (0) absent (1) present

Longitudinal ornamentation. Four types of longitudinal wrinkles were found – fine closely spaced parallel longitudinal wrinkles, which occurred on the walls of the fossil vent

tube *Yamankasia rifeia*, around the collars of the vestimentiferan *Lamellibrachia anaximandri*, and several vestimentiferan tube roots. Coarser, parallel and more distantly spaced longitudinal wrinkles can occur on serpulid tubes (Ippolitov *et al.*, 2014). Longer fine, bufircating longitudinal wrinkles, as well as short fine longitudinal wrinkles, were found on the anteriors of many vestimentiferan tubes. While chaetopterid tubes from vents and seeps have been reported to often possess longitudinal wrinkles (Kiel and Dando, 2009), the majority of those examined during the present study did not, and if present, they were not clearly fine and bifurcating, cross-cut by irregular transverse indentations or a consistent feature of the tube as on vestimentiferan tubes. The potential issue that longitudinal wrinkles are confined to the anterior portions of vestimentiferan tubes highlighted by Kiel and Dando (2009) is only a problem if only posterior tube sections have been fossilised. In that case, different criteria are required to identify them. Fine, bifurcating longitudinal wrinkles were absent on frenulate and *Sclerolinum* tubes, therefore they are not diagnostic of Siboglinidae in general. The fossils examined also show that very fine longitudinal wrinkles on tubes can be fossilised, especially at hydrothermal vents (Figures 4.10D, 4.15A), which further suggests that they are a useful feature to aid in the identification of fossils.

39. Longitudinal ornamentation:	(0) absent	(1) present
40. Parallel, fine, closely-spaced:	(0) absent	(1) present
41. Parallel, coarse, widely-spaced:	(0) absent	(1) present
42. Long, fine and bifurcating:	(0) absent	(1) present
43. Short, fine:	(0) absent	(1) present

Internal septae. This type of structure occurs in some serpulid tubes, in which they are referred to as tabulae (Ippolitov *et al.*, 2014), and they can also be common in the tubes of chaetopterids such as *Spiochaetopterus* (Bhaud, 1998; Nishi *et al.*, 2004). Internal tube septae have also been reported from several fossil seep tubes (Campbell *et al.*, 2002; Nobuhara *et al.*, 2008).

44. Internal septae:	(0) absent	(1) present

Tube wall structure. Particularly at seeps, the original wall structure of an annelid tube may be preserved, allowing the determination of whether the tube was originally calcareous

or organic. In thin section, calcareous tubes exhibited multi-layering that forms unique, chevron-like structures, while tubes of an originally organic composition possess only concentric multi-layering, and sometimes show fibrous tears, or layers that have come away from others, i.e. delamination. At vents, it is not presently known whether the different wall structures of calcareous and organic tubes can be distinguished when viewed in section, however sometimes even very fine organic fibres may be replicated by iron sulphides. Differences in the arrangement of the fibres that comprise the tube structure were also observed between chaetopterids and other organic tube builders. All of the examined *Phyllochaetopterus* and *Spiochaetopterus* tubes were comprised of fibres that crossed at near right angles (Figure 4.16D), whereas the fibre arrangement of other organic tube builders tended to be largely disorganised.

When observed in thin section, the organic walls of vestimentiferan, *Sclerolinum* and frenulate tubes can be very thick in places, with the tube diameter being 4-10 times the wall thickness (Figure 4.20W). The walls of chaetopterids are rarely as thick, measuring approximately 1/14th of the diameter of the tube. The walls of chaetopterid (Figure 4.20S-T, U-V) and alvinellid (Figure 4.20O) tubes are also tended to be poorly consolidated in comparison to siboglinid tubes, and showed greater spaces in between adjacent tube layers, while siboglinid tubes were neatly multi-layered with good adhesion between adjacent tube layers (Figure 4.20W-X, A').

45. Wall structure: (0) fibrous (1) calcareous

46. Fibre arrangement: (0) disorganised (1) crossed

47. Organic wall thickness: (0) thin (1) very thick in places

48. Organic wall consolidation: (0) poorly consolidated (1) well-consolidated

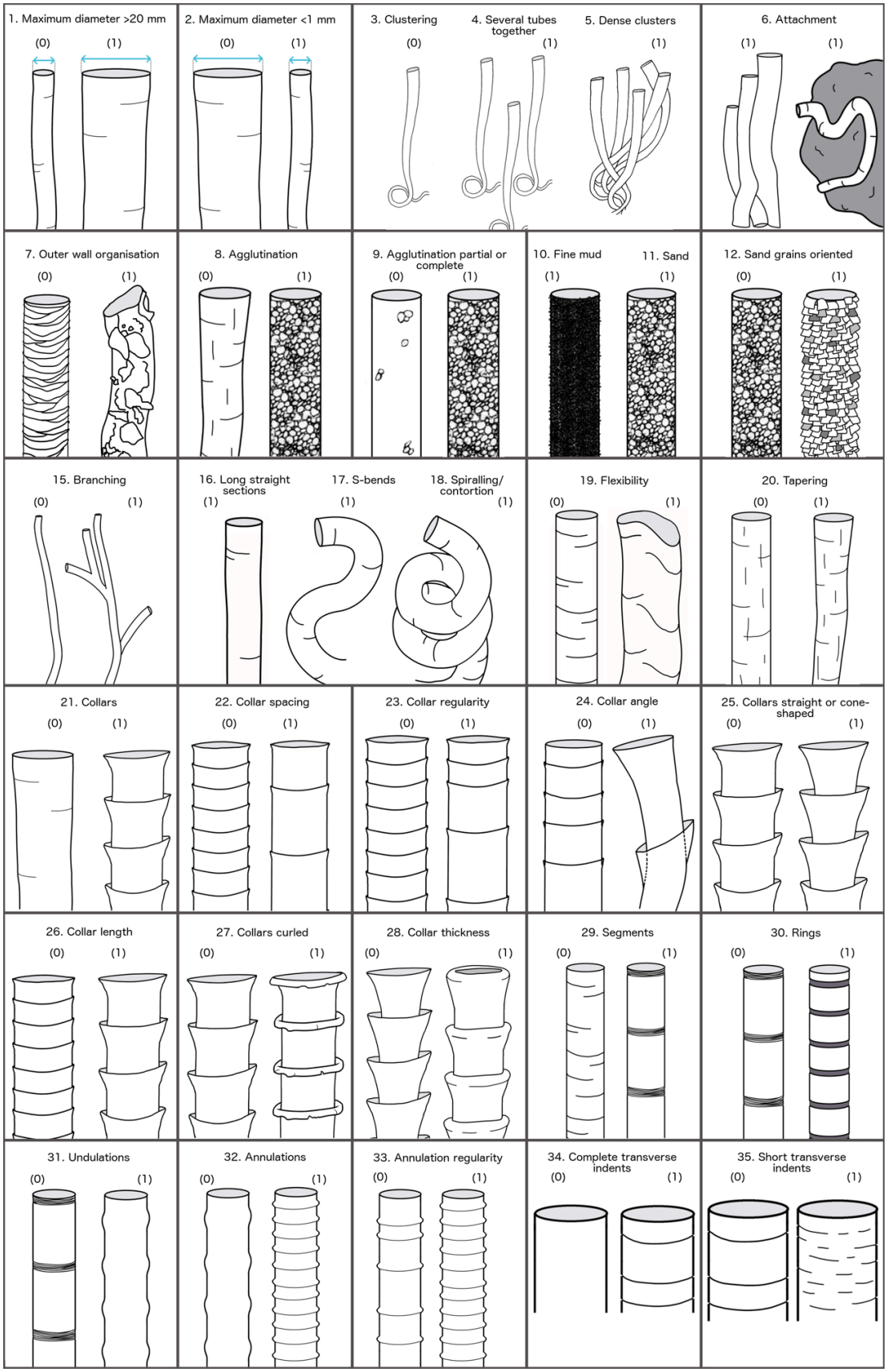
1. Maximum diameter >20 mm
(0) (1)
2. Maximum diameter <1 mm
(0) (1)
3. Clustering
4. Several tubes together
5. Dense clusters
(0) (1) (1)
6. Attachment
(1) (1)
7. Outer wall organisation
(0) (1)
8. Agglutination
(0) (1)
9. Agglutination partial or complete
(0) (1)
10. Fine mud
11. Sand
(1) (1)
12. Sand grains oriented
(0) (1)
15. Branching
(0) (1)
16. Long straight sections
17. S-bends
18. Spiralling/ contortion
(1) (1) (1)
19. Flexibility
(0) (1)
20. Tapering
(0) (1)
21. Collars
(0) (1)
22. Collar spacing
(0) (1)
23. Collar regularity
(0) (1)
24. Collar angle
(0) (1)
25. Collars straight or cone-shaped
(0) (1)
26. Collar length
(0) (1)
27. Collars curled
(0) (1)
28. Collar thickness
(0) (1)
29. Segments
(0) (1)
30. Rings
(0) (1)
31. Undulations
(0) (1)
32. Annulations
(0) (1)
33. Annulation regularity
(0) (1)
34. Complete transverse indents
(0) (1)
35. Short transverse indents
(0) (1)

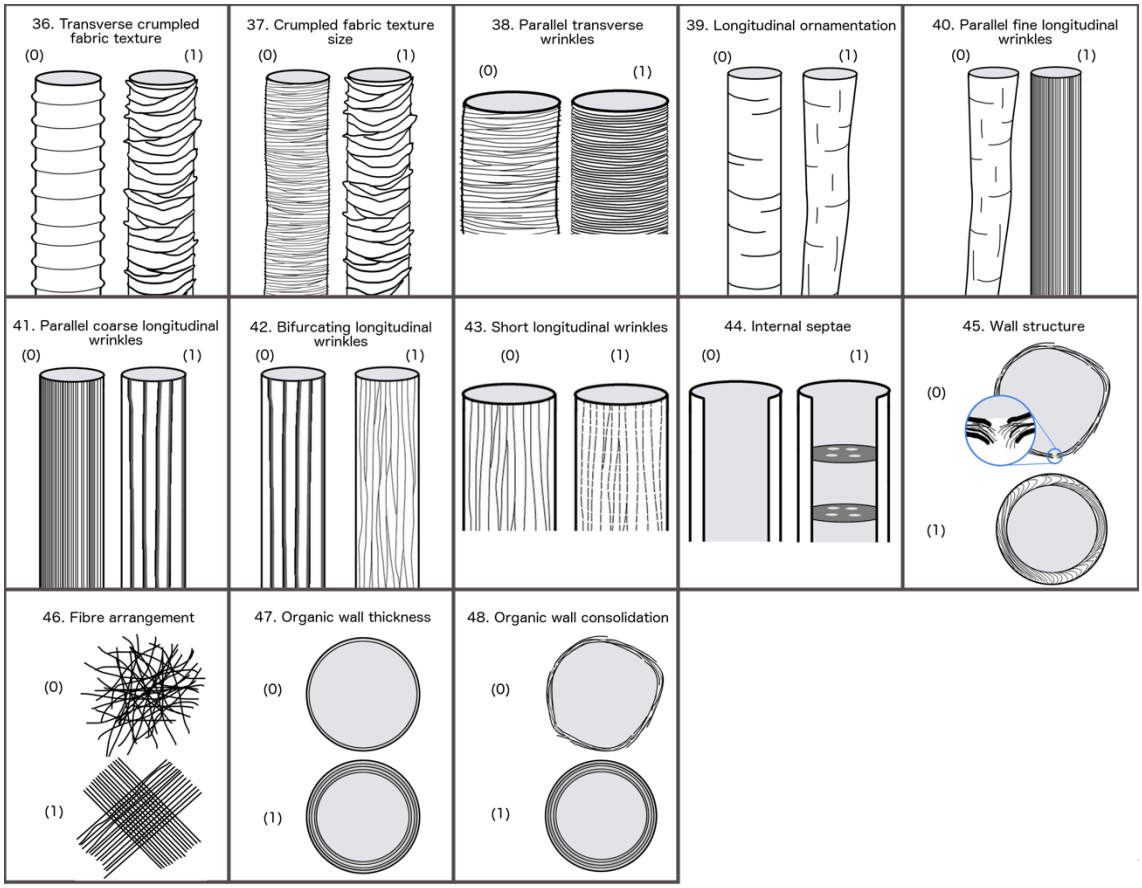

Figure 4.21 Illustrations of the 48 tube characters selected to aid in the identification of fossil annelid tubes. The compositional characters 13 and 14 are not included.

4.6 Tube similarity and phylogenetic relationships

The results of analyses described within this section were used to inform the systematic assessment of fossil tubes above.

The PCO analysis, which was used to explore similarity of tubes based on their character coding, showed distinct clustering of modern annelid tubes according to family (Figure 4.22). Fossil tubes were largely positioned between modern tube groupings, although a number of fossil taxa plotted in greater proximity to siboglinid tubes. Scores for the first two coordinate axes account for approximately 30% of the variation in the data (Supplementary Table D.6).

The cladistic analysis of modern tubes only (Figure 4.23) was able to group the majority of taxa according to established annelid taxonomic lineages based on the 48 defined tube morphological characters above. The majority of chaetopterids grouped with other chaetopterid species, and all serpulids grouped together, despite also grouping with chaetopterids. Siboglinid and sabellid tubes also mostly grouped with members of the same family. However the defined characters did not resolve relationships between annelid families according to established annelid phylogenies (e.g. Weigert *et al.*, 2014).

When fossils are included in the analyses, many taxa, including the majority of fossils, are left unresolved when homoplastic characters are down-weighted to a greater extent ($k = 3$; Figure 4.24A). Under a scenario in which homoplastic characters are down-weighted less ($k = 4$; Figure 4.24B), a greater proportion of fossil taxa are resolved, however with both of these analyses modern siboglinid and chaetopterid tubes are divided. Consistency and retention indices for the cladistic analysis reflect a high degree of homoplasy, and that characters mostly retain potential synapomorphies in the modern taxa only (Figure 4.23) and the $k = 4$ fossils-included analyses (Figure 4.24B), but not within the $k = 3$ analysis including fossils (Figure 4.24A). The inclusion of molecular data for the modern tubicolous annelids improved the resolution of evolutionary relationships between annelid families (Supplementary Figures D.1-D.2). However, this did not improve the resolution of trees containing fossil taxa (Supplementary Figure D.3).

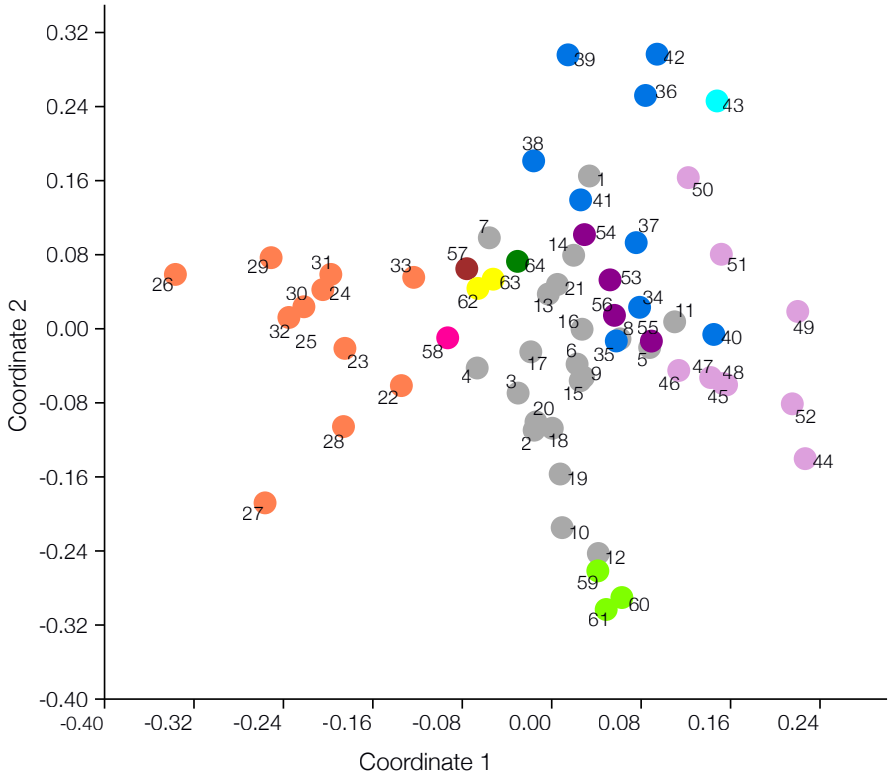

Figure 4.22 Principal coordinate analysis (PCO) plot of modern and fossil annelid tubes, based on the 48 characters for which they were scored during this study. Fossils (grey dots): 1. *Yamankasia rifeia*; 2, *Eoalvinellodes annulatus*; 3, Indeterminate annelid Sibay; 4, *Tevidestus serriformis*; 5, Figueroa; 6, Svalbard; 7, Cold Fork Cottonwood Creek; 8, Christopher Fm. Prince Patrick Island tubes; 9, Christopher Fm. Ellef Ringnes Island tubes; 10, Troodos attached tubes; 11, Troodos wrinkled tubes; 12, Troodos collared tubes; 13, Okukinenbetsu yellow tubes; 14, Okukinenbetsu brown tubes; 15, Omagari; 16, Canyon River; 17, Murdock Creek; 18, West Fork Satsop River; 19, Bexhaven; 20, Upper Waiau River; 21, Rocky Knob. Modern tubes - Chaetopteridae (orange dots): 22, *Chaetopterus* cf. *variopedatus*; 23, Chaetopteridae id83; 24, *Phyllochaetopterus polus*; 25, *P. gigas*; 26, *P. claparedii*; 27, *P. prolifica*; 28, *P. socialis*; 29, *Spiochetopterus izuensis*; 30, *S. sagamiensis*; 31, *S. costarum*; 32, S. *typicus*; 33, *Mesochaetopterus taylori*. Siboglinidae, frenulata (dark blue dots): 34, *Galathealinum arcticum*; 35, *Lamellisabella denticulata*; 36, *Oligobrachia gracilis*; 37, *Polybrachia canadensis*; 38, *Siboglinum ekmani*; 39, *S. lacteum*; 40, *Siphonobrachia lauensis*; 41, *Unibrachium colombianum*; 42, *Zenkevitchiana longissima*; 43. Siboglinidae, *Sclerolinum* (light blue dot): *S. contortum*. Siboglinidae, vestimentifera (light purple dots): 44, *Alaysia spiralis*; 45, *Arcovestia ivanovi*; 46, *Escarpia southwardae*; 47, *Lamellibrachia anaximandri*; 48, *Paraescarpia echinospica*; 49, *Ridgeia piscesae*; 50, *Riftia pachyptila*; 51, *Tevnia jerichonana*; 52, *Seepiophila jonesi*. Siboglinidae, vestimentifera roots (dark purple dots): 53, *E. southwardae* root; 54, *L. anaximandri* root; 55, *S. jonesi* root; 56, *P. echinospica* root. Alvinellidae (maroon dot): 57, *Alvinella* sp. Ampharetidae (fuchsia dot): 58, *Glyphanostomum* sp. Serpulidae (lime dots): 59, Serpulidae sp. JCR; 60, *Serpula vermicularis*; 61, *Vermiliopsis infundibulum*. Sabellidae (yellow dots): 62, *Sabella pavonina*; 63, *Megalomma vesiculosum*. Oweniidae (dark green dot): 64. *Owenia fusiformis*.

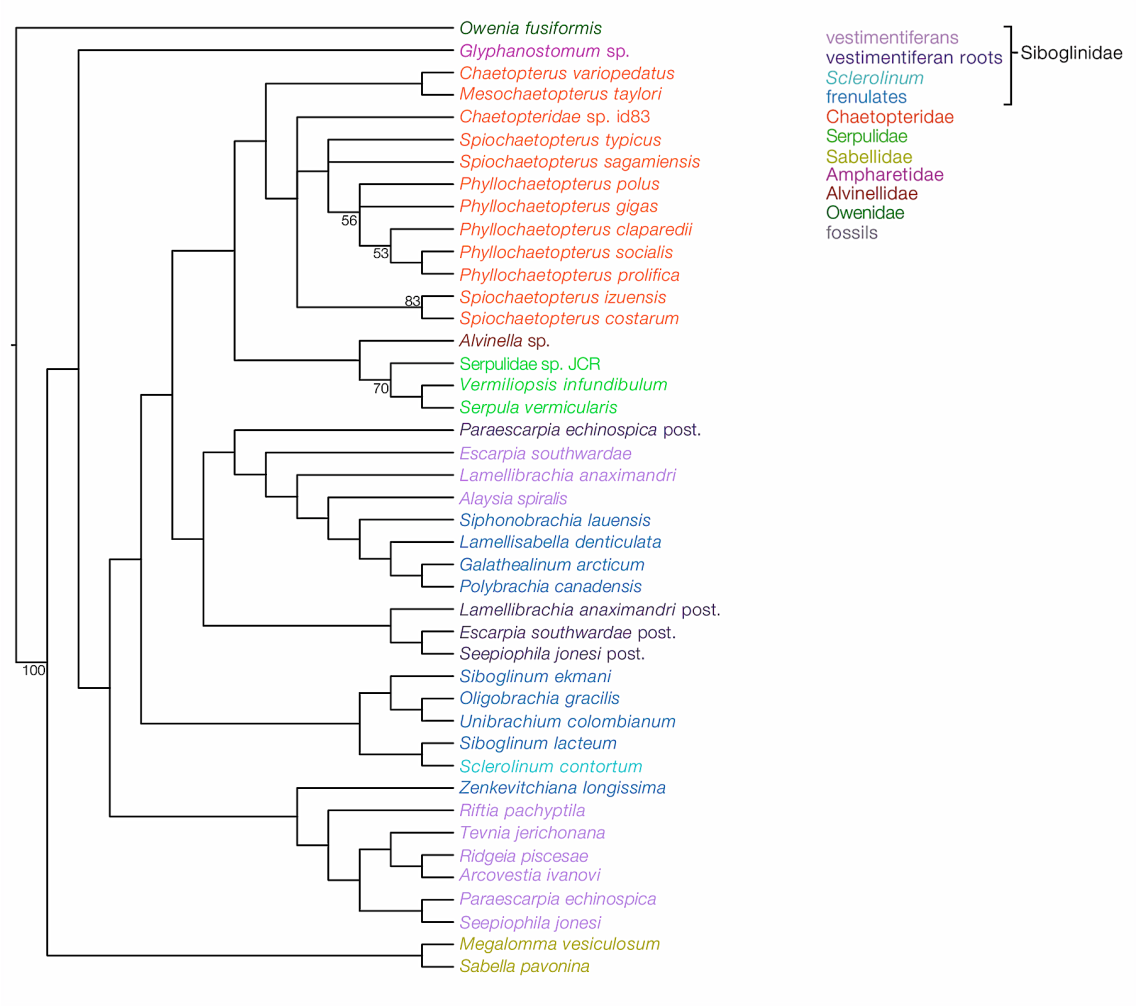

Figure 4.23 Strict consensus cladogram of 3 most parsimonious trees of tubes built by a total of 43 modern annelid taxa (best score = 14.344, consistency index = 0.308, retention index = 0.629). The analysis was based on the 48 mostly morphological tube characters and was performed using implied character weighting (k = 3). Numbers on nodes represent groups present/contradicted support values. Taxa are coloured according to taxonomic groups.

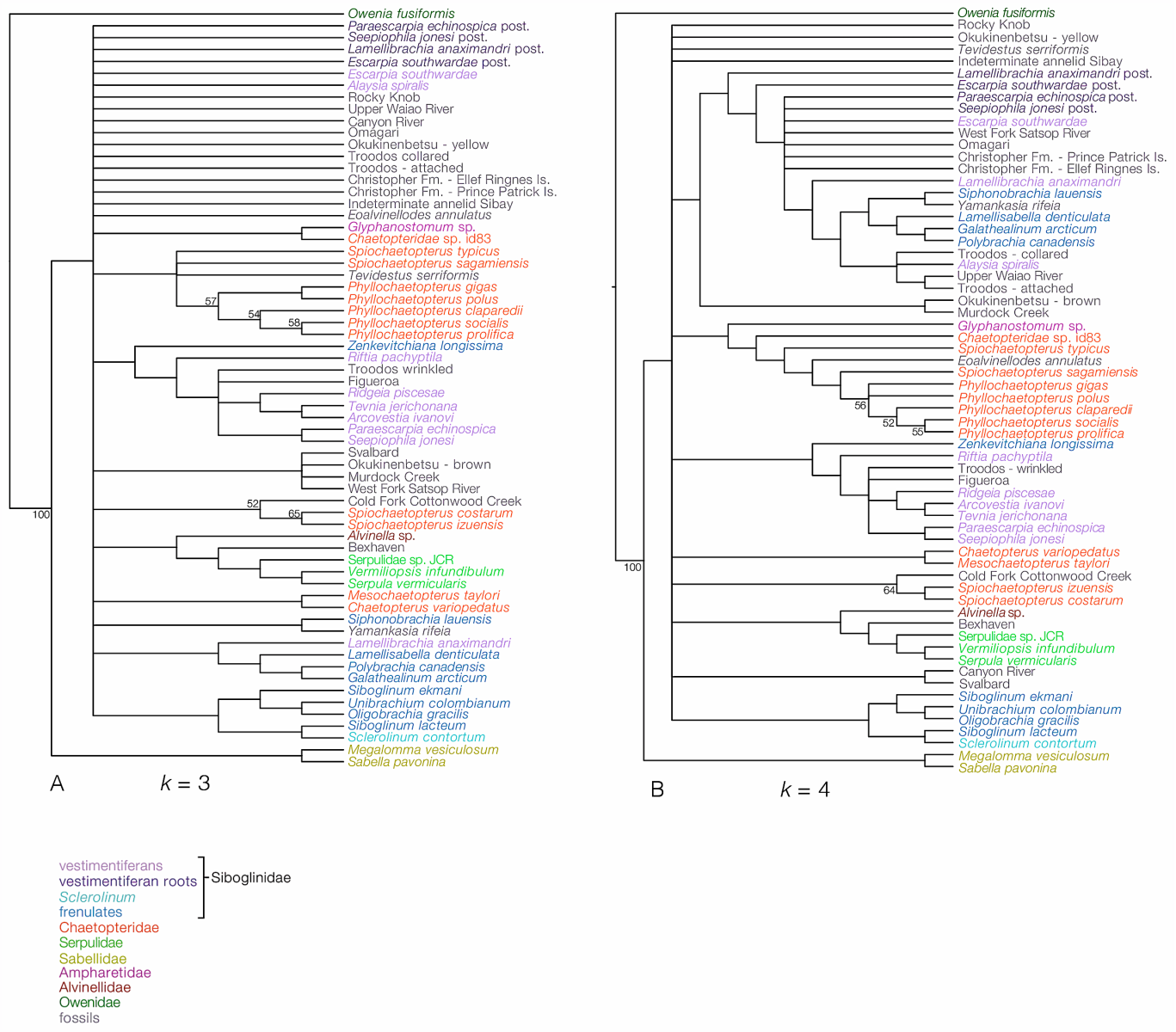

Figure 4.24 Strict consensus cladograms constructed using a total of 64 modern and fossil annelid taxa and 48 mostly morphological tube characters. Analyses were performed using implied character weighting, with the concavity constant set as default (*k* = 3; A), and also set to downweigh homoplastic characters less (*k* = 4; B). Numbers on nodes represent groups present/contradicted support values. Modern taxa are coloured according to taxonomic groups, fossil taxa are in grey. A, consensus of 271 most parsimonious trees (best score = 15.387, consistency index = 0.195, retention index = 0.264). B, consensus of 60 most parsimonious trees (best score = 13.568, consistency index = 0.232, retention index = 0.569). Taxa are coloured according to taxonomic groups.

4.7 Organic constituents of modern tubes and their preservation

Screening of organic tubes for potential differences in composition using FTIR showed that tubes from the annelid families Siboglinidae and Alvinellidae had distinctly different FTIR spectra to Chaetopteridae tubes (Figure 4.25). Chaetopterid tube spectra lacked -NH peaks and showed only weak -CH peaks. The *Alvinella* tube spectrum generally resembled those of several siboglinids such as *Sclerolinum contortum*, which only showed one -NH peak, whereas vestimentiferan and frenulate tubes exhibited two -NH peaks.

More in-depth analyses of the compositions of these modern tubes using py-GC-MS (Supplementary Table D.7) revealed divergent compositions between siboglinid, chaetopterid and alvinellid tubes, with siboglinid tubes (both anterior and posterior tube regions) being rich in the compounds 3-acetamido-5-methylfuran and acetamido-pyrones, and often also acetamide and 3-acetamidofuran. A single alvinellid and five chaetopterid tubes largely lacked these compounds which are considered amongst the most important pyrolysis products indicative of chitin (Gupta and Cody, 2011). Tubes from all three families were however rich in compounds considered to be pyrolysis products of proteins, and several of the analysed chaetopterid tubes also contained furfural.

Assessment of fossil tubes for preserved organic matter was performed using confocal microscopy. The walls of recently mineralised vestimentiferan tubes from cold seeps emitted a distinct fluorescence signal compared to surrounding minerals (Figure 4.26A), suggesting that tube wall organics had been preserved during the mineralisation process. A similar fluorescence pattern was also obtained for a number of ancient tubes from seep deposits (Figure 4.26B-C). Fossil serpulid tube walls from ancient seeps showed no fluorescence (Figure 4.26D), suggesting that the observed fluorescence is unique to tubes considered to have originally been organic. When organic components preserved in recently mineralised and ancient fossil tubes from seeps were analysed in more detail through py-GC-MS, mineralised roots of *Escarpia southwardae* and *Lamellibrachia luymesi* tubes did not the contain characteristic chitin pyrolysis products recorded in unmineralised tubes. Sixteen ancient fossil tube samples from seeps also showed that although organics were present in the tube walls, these were mostly protein constituents and none could be associated with a particular modern annelid group (Supplementary Table D.9).

For recently mineralised *Alvinella* and *Ridgeia piscesae* tubes from hydrothermal vents (Supplementary Table D.8), py-GC-MS analyses detected sulphurous compounds, but none of the characteristic pyrolysis products of chitin and proteins recorded in unmineralised tube specimens.

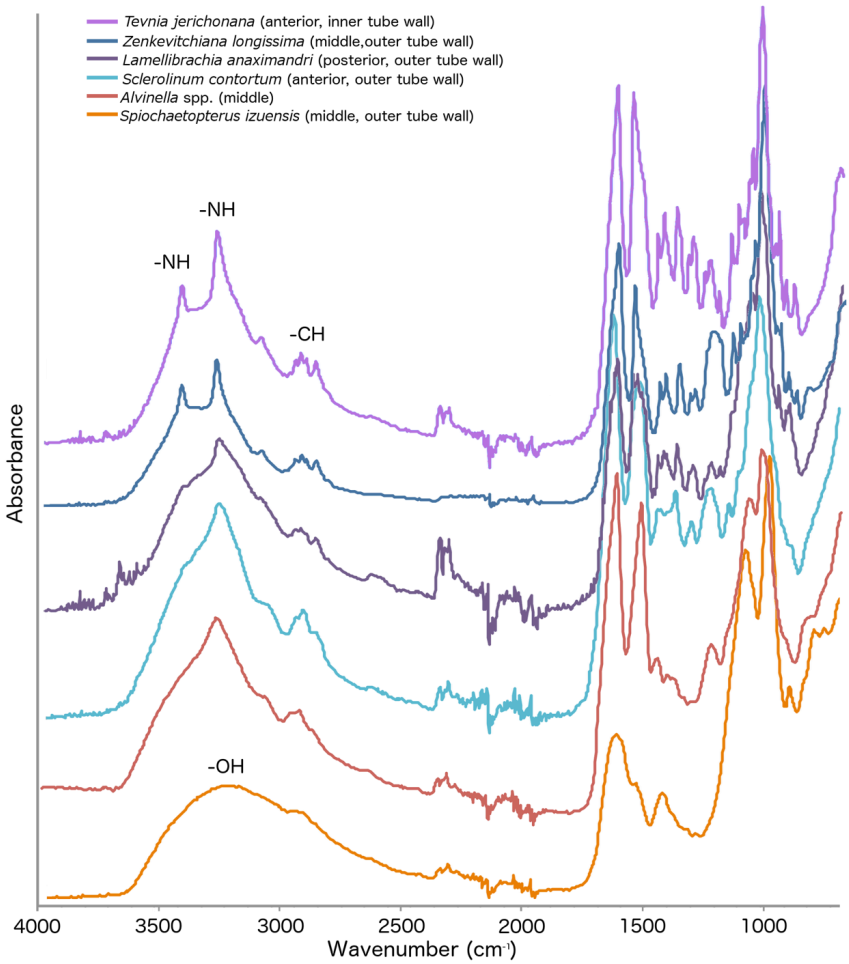

Figure 4.25 Fourier transform infrared (FTIR) spectroscopy spectra of the organic tubes of vent and seep dwelling annelids. Spectra are offset on the absorbance axis, and key spectral absorbance peaks are labelled with the types of chemical bonds they represent: -NH, nitrogen-hydrogen; -CH, carbon-hydrogen; -OH, oxygen-hydrogen. The region of the tube (anterior, mid, posterior; inner or outer tube wall) from which the spectra were collected is also indicated.

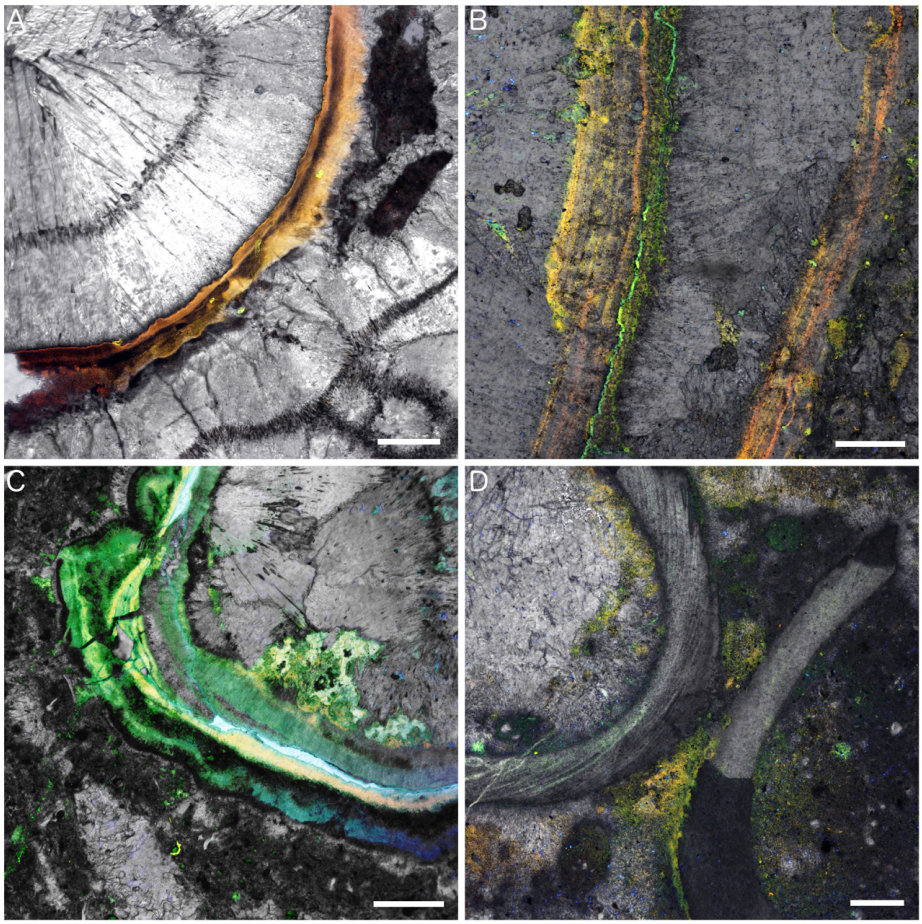

Figure 4.26 Results of confocal laser-scanning microscopy (CLSM) of recently mineralised and ancient fossil annelid tubes. Tubes are imaged in auto-fluorescence mode, where areas of fluorescence likely reflect the presence of organic matter. **A,** detail of mineralised *Escarpia southwardae* (Siboglinidae) tube transverse section, scale bar is 100 μm. **B,** fossil tube from Upper Waiau River, New Zealand, detail of transverse section, scale bar is 200 μm. **C,** fossil tube from West Fork Satsop River, WA, USA, detail of transverse section, scale bar is 200 μm. **D,** fossil tubes from Bexhaven, New Zealand, detail of two near-transverse sections, scale bar is 200 μm.

4.8 Discussion

4.8.1 Can tube organics help to identify fossil vent and seep tubes?

This study constitutes the first major comparative evaluation of the organic compositions of modern annelid tubes, which were initially screened using FTIR and then analysed in greater detail through py-GC-MS. Assessment of the organic constituents of alvinellid, chaetopterid and siboglinid tubes firstly confirms the different compositions of the tubes built by these families, thereby suggesting that tube organics can be taxonomically informative. While there has been some confusion as to whether chaetopterid tubes contain chitin (Barnes, 1964; Ippolitov *et al.*, 2014; Parry *et al.*, 2014), our FTIR (Figure 4.25) and py-GC-MS (Supplementary Table D.7) results from all four chaetopterid genera

suggest that they do not, as three major chitin marker pyrolysis products that were commonly observed in siboglinid tubes were absent from the tubes of chaetopterids. Py-GC-MS showed that the majority of chaetopterid tubes analysed contained furfural, as has previously been reported (Berkeley, 1922). The absence of key chitin markers, as well as furfural, distinguished *Alvinella* tubes from those of the siboglinids and chaetopterids, respectively. The above analyses also confirmed the presence of chitin in *Sclerolinum*, as well as the root portions of two vestimentiferan tubes (Supplementary Table D.7), and the inclusion of tube organic constituents within the tube character matrix also helped to resolve modern annelid families within cladistic analyses (Figure 4.23).

The utility of organic composition for tube identification does however appear to diminish upon fossilisation at vents and seeps. While confocal microscopy (Figure 4.26) and py-GC-MS revealed that organic matter had been preserved in the walls of recently mineralised vestimentiferan tubes from seeps, only one sample showed the presence of chitin markers upon pyrolysis (Supplementary Table D.8). This suggests that chitin does not generally fossilise within seep environments. A selection of ancient tube fossils from seeps also showed preserved organics but no traces of chitin or furfural derivatives (Supplementary Table D.9). We were therefore unable to determine whether ancient seep tubes could potentially have been built by siboglinids or chaetopterids based on the above analyses. At vents, recently mineralised tubes of *Alvinella* spp. and *Ridgeia piscesae* showed very little organic constituents at all (Supplementary Table D.8). While chitin has been detected in fossils through py-GC-MS (e.g. Stankiewicz *et al.*, 1997), it is generally considered to have a low preservation potential within sedimented fossilisation settings (Sephton *et al.*, 2009), and it appears that this is also the case within hydrothermal vent and cold seep environments. Although our analyses of organics in fossil tubes proved inconclusive, tube wall organics may still aid in the identifications of fossil seep material through the development of additional biomarkers for organic annelid tubes that are less affected by fossilisation, or in cases where tube walls are exceptionally well preserved.

4.8.2 Tube morphology

As annelid dwelling tubes are not joined to the annelid body and adaptive evolution of tubes is considered independent to that of soft tissues (Ippolitov *et al.*, 2014), tubes have generally been considered to have limited utility in taxonomy. However, there are recognised characters of fossil tubes, such as tube wall structure in fossil serpulid tubes from seeps, that can enable taxonomic designation. In this study, tube characters that are

important for taxonomic determination have been expanded, as well as clarified. While aspects of tube morphology such as longitudinal ridges, tube wall structure, tube size, mode of occurrence, and collars have been highlighted as being problematic in fossil tube identification as they are shared by several modern lineages (Kiel and Dando, 2009), with many of these features we were able to show that they can still be taxonomically useful. This is due to additional details observed within this study, such as the orientation of collars with respect to the tube, collar size, the type of longitudinal wrinkles and how they combine with other tube morphological characters (Section 4.5). Features such as rings of frenulate tubes (Figure 4.20Z) appeared unique to this group, and are therefore a key identifying character for this lineage, whereas segments or wrinkled fabric-type textures that were observed in frenulate tubes can also occur in the tubes made by other families. Fossil tubes exhibiting the latter features would therefore be difficult to place, and for these reasons, we suggest that the fossil *Sabellidites cambriensis* may not have been made by a siboglinid as suggested by Moczydłowska *et al.* (2014).

It is also important to note that for tube morphology, absence of evidence is no evidence and not evidence of absence, and therefore the identification of a fossil tube is only possible if some diagnostic features of the tube have been retained following fossilisation. The tube-builders of poorly preserved tubes such as the Cold Fork Cottonwood Creek specimens are therefore unlikely to be uncovered using morphology. With such fossils it is difficult to determine whether there was an original absence of characters or whether these were not preserved (Sansom, 2015), which may be more of a problem for tubes fossilised at seeps as vent tubes occasionally retain very fine ornamental details (Little *et al.*, 1998).

4.8.3 Cladistic analyses

Through the application of a cladistic methodology, the taxonomic identification of fossil tube material from ancient vents and seeps has been placed within a modern comparative context, whereby affinities of vent and seep tubes could be assessed more objectively. In summary, this analysis revealed that out of eight fossil tube types that were previously interpreted as having been made by vestimentiferans, siboglinid affinities could be upheld for only two of these, three were changed to possibly siboglinid, two were ascribed to the annelids only, and one tube type to Animalia only (Table 4.1). Out of tube types that were not previously ascribed to siboglinids, an additional five are here suggested to have possibly been made by siboglinids. Notably, this includes mid-Cretaceous tubes from the

Christopher Formation in the Canadian Arctic, which were previously considered to have been made by serpulids (Beauchamp and Savard, 1992).

The ability of the cladistic analysis of modern tubes only (Figure 4.23) to resolve taxa among their family members, firstly confirms that tubes do possess enough information for taxonomic assignment. The above analysis also demonstrates that coding tube characters and analysing them within a cladistic framework does function to determine the probable identity of a tube, and can thus do so for a fossil tube, if it is sufficiently well preserved. The lack of correspondence of deeper annelid branches within our analyses to existing annelid molecular phylogenies however (e.g. Weigert *et al.*, 2014), even when molecular data were included (Supplementary Figures D.1-D.2), likely reflects the more limited sampling of annelid taxa within our analyses.

The on the whole poorer resolution of cladograms which included fossil tubes (Figure 4.24) further highlights that alteration during fossilisation is often significant, and the few characters that can subsequently be gleaned from fossil tubes make their identification difficult, even at broad taxonomic levels. This is also demonstrated by the PCO plot (Figure 4.22), in which the majority of fossil vent and seep tubes cluster with each other rather than with the tubes of modern annelid lineages, and is reflected in the overall increased uncertainly of fossil tube taxonomic interpretations (Table 4.1). The inclusion of molecular data worsened fossil taxon resolution (Supplementary Figure D.3), likely as a result of conflicts arising from homoplasies in the morphological data. The fossils-included cladistic analyses (Figure 4.24) especially appeared to encounter problems in placing smooth-walled tube fossils, which are how many of the fossil seep and several vent tubes are preserved. Even tubes from Canyon River, which are generally accepted as having been made by vestimentiferans, are not well resolved with cladistics. Tubes with more detailed outer wall ornamentation, for which there was greater information to base these identifications upon, resolved more definitively among modern annelid groups. These tubes comprised Cretaceous tubes from the Troodos Ophiolite, and Jurassic tubes from the Figueroa deposit, which were both resolved among modern vestimentiferan tubes (Figure 4.24).

While helping to resolve the identities of only a small proportion of the fossil tubes investigated, this study has nevertheless improved the level of quality control within palaeontological interpretations of fossil vent and seep tubes, which has been greatly needed (Kiel and Dando, 2009; Vrijenhoek, 2013). Gaining an understanding of evolutionary history also requires authors to be cautious, as over-identifications of fossils

where they are assigned to a lower-level taxon than can be demonstrated by data, can lead to false conclusions of taxon evolutionary ages (Bell *et al.*, 2010; Parham *et al.*, 2012). Cladistic comparative methods are widely used for fossil identifications because they increase transparency in the fossil identification process and clearly demonstrate which characters are attributed to each fossil, thereby adding objectivity to fossil identifications that may be inherently difficult (Crepet *et al.*, 2004). Overall, the use of cladistics has greatly improved knowledge of the types of characters that can be gleaned from both fossil and modern tubes, which of these are homoplastic, and also which characters can result in more definitive identifications.

The above methods however need to be applied with greater caution for very ancient tube fossils (such as those from the Palaeozoic), as the identity of these fossils will largely be evaluated with respect to modern tubes from which they are very distant in time. The Palaeozoic fossils are also the most likely to belong to now extinct taxa that do not have modern morphological analogues.

4.8.4 Implications for vent and seep evolutionary history

The evolutionary history of the annelid family Siboglinidae is controversial, owing to conflicting theories of its origins from fossil and molecular age estimates (Vrijenhoek, 2013). Our study suggests that late Cretaceous tubes from the Troodos Ophiolite and early Jurassic tubes from the Figueroa deposit were made by vestimentiferans, which greatly extends the age of this lineage beyond that suggested by molecular clock analyses. This finding comprises a further piece of independent evidence, after the discovery of mid Cretaceous-age *Osedax* fossils (Danise and Higgs, 2015), that the more derived siboglinid lineages have a Mesozoic origin. However, we were unable to find definitive evidence that Devonian and Silurian vent fossils were made by siboglinids, thereby reinforcing doubts that this lineage could extend back into the Palaeozoic (Vrijenhoek, 2013) and perhaps even into the Neo-Proterozoic (Moczydłowska *et al.*, 2014). Four types of tubes that are tentatively assigned to the vestimentiferans by this study are from Cretaceous deposits (Table 4.1), and while their designation remains uncertain, if vestimentifera originated during the Jurassic or earlier, its members are likely to have been abundant within Cretaceous vents and seeps.

The faunal compositions of hydrothermal vents and cold seeps have undergone dynamic shifts over evolutionary time. Although it has been difficult to attribute many of these

transitions to large-scale environmental upheaval events (Kiel and Little, 2006), much of the modern vent and seep fauna is considered to have originated during the Cenozoic (Vrijenhoek, 2013). The occurrence of Mesozoic siboglinid fossils however, constitutes a major diversion from this pattern. Perhaps these worms were able to withstand deep-sea anoxic/dysoxic events through the possession of weedy characteristics such as wide habitat preferences and distant dispersal abilities (Georgieva *et al.*, 2015b), as well as the ability of vestimentiferans, frenulates and *Sclerolinum* to build durable, non-calcified tubes that are less vulnerable to ocean acidification than the shells of molluscs. The surprising fossil discoveries of Danise and Higgs (2015) and the reinterpretations presented here emphasise that the evolutionary history of this remarkable family warrants further investigation, and we therefore urge that an earlier origin for the main tube-building vent and seep annelid lineage, the vestimentiferans, be considered, and incorporated into a much-needed new molecular age estimation for Siboglinidae.

4.9 Acknowledgements

We would like to thank all of the scientists who donated material for this study. Thank you also to Greg Edgecombe for advice regarding cladistic analyses, Tony Wighton and Enrica Bonato for the preparation of tube thin sections, Tomasz Goral for help with confocal microscopy, Richard Herrington, Jon Todd and Helena Toman for providing access to fossil vent material at the NHM and Emma Sherlock for help with accessing modern annelid tube material at the NHM. MNG is funded by NERC CASE PhD studentship no. NE/K500847/1.

4.10 References

Barbieri, R., Ori, G. G. and Cavalazzi, B. (2004) A Silurian cold-seep ecosystem from the Middle Atlas, Morocco. *Palaios* **19**, 527–542.

Barnes, R. (1964) Tube-building and feeding in the chaetopterid polychaete, *Spiochaetopterus oculatus*. *The Biological Bulletin* **127**, 397–412.

Beauchamp, B. and Savard, M. (1992) Cretaceous chemosynthetic carbonate mounds in the Canadian Arctic. *Palaios* **7**, 434–450.

Bell, C. J., Gauthier, J. A. and Bever, G. S. (2010) Covert biases, circularity, and

apomorphies: A critical look at the North American Quaternary Herpetofaunal Stability Hypothesis. *Quaternary International* **217**, 30–36. doi:10.1016/j.quaint.2009.08.009.

Berkeley, C. (1922) An organic constituent of the tube of *Mesochaetopterus taylori*, Potts. *Journal of Biological Chemistry* **50**, 113–120.

Bhaud, M. R. (1998) Species of *Spiochaetopterus* (Polychaeta, Chaetopteridae) in the Atlantic-Mediterranean biogeographic area. *Sarsia* **83**, 243–263. doi:10.1080/00364827.1998.10413685.

Blumenberg, M., Seifert, R., Buschmann, B., Kiel, S. and Thiel, V. (2012) Biomarkers reveal diverse microbial communities in black smoker sulfides from turtle pits (Mid-Atlantic Ridge, Recent) and Yaman Kasy (Russia, Silurian). *Geomicrobiology Journal* **29**, 66–75.

Brunet, P. C. J. and Carlisle, D. B. (1958) Chitin in Pogonophora. *Nature* **182**, 1689–1689. doi:10.1038/1821689a0.

Buschmann, B. and Maslennikov, V. V. (2006) The late Ordovician or earliest Silurian hydrothermal vent fauna from Yaman Kasy VMS deposit (South Uralides, Russia). *Freiberger Forschungshefte* **14**, 139–172.

Cai, Y., Hua, H. and Zhang, X. (2013) Tube construction and life mode of the late Ediacaran tubular fossil *Gaojiashania cyclus* from the Gaojiashan Lagerstätte. *Precambrian Research* **224**, 255–267.

Cai, Y., Xiao, S., Hua, H. and Yuan, X. (2015) New material of the biomineralizing tubular fossil *Sinotubulites* from the late Ediacaran Dengying Formation, South China. *Precambrian Research* **261**, 12–24. doi:10.1016/j.precamres.2015.02.002.

Campbell, K. A. (1995) Dynamic development of Jurassic-Pliocene cold-seeps, convergent margin of western North America. PhD Thesis, University of Southern California.

Campbell, K. A. (2006) Hydrocarbon seep and hydrothermal vent paleoenvironments and paleontology: Past developments and future research directions. *Palaeogeography, Palaeoclimatology, Palaeoecology* **232**, 362–407. doi:10.1016/j.palaeo.2005.06.018.

Campbell, K. A. and Bottjer, D. J. (1993) Fossil cold seeps. *National Geographic Research and Exploration* **9**, 326–343.

Campbell, K. A., Farmer, J. D. and Des Marais, D. (2002) Ancient hydrocarbon seeps from the Mesozoic convergent margin of California: carbonate geochemistry, fluids and palaeoenvironments. *Geofluids* **2**, 63–94. doi:10.1046/j.1468-8123.2002.00022.x.

Campbell, K. A., Francis, D. A., Collins, M., Gregory, M. R., Nelson, C. S., Greinert, J. and Aharon, P. (2008) Hydrocarbon seep-carbonates of a Miocene forearc (East Coast Basin), North Island, New Zealand. *Sedimentary Geology* **204**, 83–105. doi:10.1016/j.sedgeo.2008.01.002.

Capa, M., Parapar, J. and Hutchings, P. (2012) Phylogeny of Oweniidae (Polychaeta) based on morphological data and taxonomic revision of Australian fauna. *Zoological Journal of the Linnean Society* **166**, 236–278. doi:10.1111/j.1096-3642.2012.00850.x.

Cook, T. and Stakes, D. (1995) Biogeological mineralization in deep-sea hydrothermal deposits. *Science* **267**, 1975–1979.

Corliss, J., Dymond, J., Gordon, L., Edmond, J., von Herzen, R., Ballard, R., Green, K., Williams, D., Bainbridge, A., Crane, K. and van Andel, T. (1979) Submarine thermal springs on the Galapagos Rift. *Science* **203**, 1073–1083.

Crepet, W. L., Nixon, K. C. and Gandolfo, M. A. (2004) Fossil evidence and phylogeny: the age of major angiosperm clades based on mesofossil and macrofossil evidence from Cretaceous deposits. *American Journal of Botany* **91**, 1666–1682. doi:10.3732/ajb.91.10.1666.

Danise, S. and Higgs, N. D. (2015) Bone-eating *Osedax* worms lived on Mesozoic marine reptile deadfalls. *Biology Letters* **11**, 20150072.

Dattagupta, S., Miles, L. L., Barnabei, M. S. and Fisher, C. R. (2006) The hydrocarbon seep tubeworm *Lamellibrachia luymesi* primarily eliminates sulfate and hydrogen ions across its roots to conserve energy and ensure sulfide supply. *The Journal of Experimental Biology* **209**, 3795–3805. doi:10.1242/jeb.02413.

Desbruyères, D., Segonzac, M. and Bright, M. (2006) *Handbook of deep-sea hydrothermal vent fauna*. 2nd edition, p. 544. Biologiezentrum der Oberösterreichische Landesmuseen, Linz.

Gaill, F. and Hunt, S. (1988) Tubes. In *The Ultrastructure of Polychaeta* (ed. Westheide, W. and Hermans, C. O.), pp. 61-70. Fischer, New York.

Gaill, F., Shillito, B., Ménard, F., Goffinet, G. and Childress, J. J. (1997) Rate and process of tube production by the deep-sea hydrothermal vent tubeworm *Riftia pachyptila*. *Marine Ecology Progress Series* **148**, 135–143.

Georgieva, M. N., Little, C. T. S., Ball, A. D. and Glover, A. G. (2015a) Mineralization of *Alvinella* polychaete tubes at hydrothermal vents. *Geobiology* **13**, 152–169.

doi:10.1111/gbi.12123.

Georgieva, M. N., Wiklund, H., Bell, J. B., Eilertsen, M. H., Mills, R. A., Little, C. T. S. and Glover, A. G. (2015b) A chemosynthetic weed: the tubeworm *Sclerolinum contortum* is a bipolar, cosmopolitan species. *BMC Evolutionary Biology* **15**, 280. doi:10.1186/s12862-015-0559-y.

Goedert, J. L. and Squires, R. L. (1993) First Oligocene records of *Calyptogena* (Bivalvia: Vesicomyidae). *Veliger* **36**, 72–77.

Goedert, J., Peckmann, J. and Reitner, J. (2000) Worm tubes in an allochthonous cold-seep carbonate from lower Oligocene rocks of western Washington. *Journal of Paleontology* **74**, 992–999.

Goloboff, P. A. (1993) Estimating character weights during tree search. *Cladistics* **9**, 83–91.

Goloboff, P. A. (1999) Analyzing large datasets in reasonable times: solutions for composite optima. *Cladistics* **15**, 415–428.

Goloboff, P. A., Farris, J. S., Källersjö, M., Oxelman, B. and Szumik, C. A. (2003) Improvements to resampling measures of group support. *Cladistics* **19**, 324–332.

Goloboff, P., Farris, J. S. and Nixon, K. (2008) TNT, a free program for phylogenetic analysis. *Cladistics* **24**, 774–786.

Guggolz, T., Henne, S., Politi, Y., Schütz, R., Mašić, A., Müller, C. H. G. and Meißner, K. (2015) Histochemical evidence of β-chitin in parapodial glandular organs and tubes of *Spiophanes* (Annelida, Sedentaria: Spionidae), and first studies on selected Annelida. *Journal of Morphology* **276**, 1433–1447. doi:10.1002/jmor.20432.

Gupta, N. S. and Cody, G. D. (2011) Indentification and characterization of chitin in organisms. In *Chitin: Formation and Diagenesis* (ed. Gupta, N. S.), pp. 117–132. Springer Netherlands, Dordrecht doi:10.1007/978-90-481-9684-5.

Haas, A., Little, C. T. S., Sahling, H., Bohrmann, G., Himmler, T. and Peckmann, J. (2009) Mineralization of vestimentiferan tubes at methane seeps on the Congo deep-sea fan. *Deep-Sea Research I* **56**, 283–293. doi:10.1016/j.dsr.2008.08.007.

Hammer, Ø., Harper, D. and Ryan, P. (2001) Past: palaeontological statistics software package for education and data analysis. *Palaeontolia Electronica* **4**, 9.

Hammer, Ø., Nakrem, H. A., Little, C. T. S., Hryniewicz, K., Sandy, M. R., Hurum, J. H., Druckenmiller, P., Knutsen, E. M. and Høyberget, M. (2011) Hydrocarbon seeps from close to the Jurassic–Cretaceous boundary, Svalbard. *Palaeogeography,*

Palaeoclimatology, Palaeoecology **306**, 15–26. doi:10.1016/j.palaeo.2011.03.019.

Hikida, Y., Suzuki, S., Togo, Y. and Ijiri, A. (2003) An exceptionally well-preserved fossil seep community from the Cretaceous Yezo Group in the Nakagawa area, Hokkaido, northern Japan. *Paleontological Research* **7**, 329–342.

Himmler, T., Freiwald, A., Stollhofen, H. and Peckmann, J. (2008) Late Carboniferous hydrocarbon-seep carbonates from the glaciomarine Dwyka Group, southern Namibia. *Palaeogeography, Palaeoclimatology, Palaeoecology* **257**, 185–197. doi:10.1016/j.palaeo.2007.09.018.

Hryniewicz, K., Hammer, Ø., Nakrem, H. a. and Little, C. T. S. (2012) Microfacies of the Volgian-Ryazanian (Jurassic-Cretaceous) hydrocarbon seep carbonates from Sassenfjorden, central Spitsbergen, Svalbard. *Norsk Geologisk Tidsskrift* **92**, 113–131.

Hryniewicz, K., Nakrem, H. A., Hammer, Ø., Little, C. T. S., Kaim, A., Sandy, M. R. and Hurum, J. H. (2015) The palaeoecology of the latest Jurassic-earliest Cretaceous hydrocarbon seep carbonates from Spitsbergen, Svalbard. *Lethaia* **48**, 353–374. doi:10.1111/let.12112.

Ippolitov, A., Vinn, O., Kupriyanova, E. and Jäger, M. (2014) Written in stone: history of serpulid polychaetes through time. *Memoirs of Museum Victoria* **71**, 123–159.

Julian, D., Gaill, F., Wood, E., Arp, A. J. and Fisher, C. R. (1999) Roots as a site of hydrogen sulfide uptake in the hydrocarbon vestimentiferan *Lamellibrachia* sp. *The Journal of Experimental Biology* **202**, 2245–2257.

Kiel, S. and Little, C. T. S. (2006) Cold-seep mollusks are older than the general marine mollusk fauna. *Science* **313**, 1429–1431.

Kiel, S. and Dando, P. R. (2009) Chaetopterid tubes from vent and seep sites: implications for fossil record and evolutionary history of vent and seep annelids. *Acta Palaeontologica Polonica* **54**, 443–448. doi:10.4202/app.2009.0022.

Kiel, S. and Amano, K. (2013) The earliest bathymodiolin mussels: an evaluation of Eocene and Oligocene taxa from deep-sea methane seep deposits in western Washington State, USA. *Journal of Paleontology* **87**, 589–602. doi:10.1666/12-135.

Kiel, S., Amano, K. and Jenkins, R. G. (2008) Bivalves from cretaceous cold-seep deposits on Hokkaido, Japan. *Acta Palaeontologica Polonica* **53**, 525–537. doi:10.4202/app.2008.0310.

Kupriyanova, E., Nishi, E., Kawato, M. and Fujiwara, Y. (2010) New records of Serpulidae

(Annelida, Polychaeta) from hydrothermal vents of North Fiji, Pacific Ocean. *Zootaxa* **2389**, 57–68.

Legg, D. A., Sutton, M. D. and Edgecombe, G. D. (2013) Arthropod fossil data increase congruence of morphological and molecular phylogenies. *Nature Communications* **4**, 1–7. doi:10.1038/ncomms3485.

Levin, L. A. and Mendoza, G. F. (2007) Community structure and nutrition of deep methane-seep macrobenthos from the North Pacific (Aleutian) Margin and the Gulf of Mexico (Florida Escarpment). *Marine Ecology* **28**, 131–151. doi:10.1111/j.1439-0485.2006.00131.x.

Little, C. T. S. and Vrijenhoek, R. C. (2003) Are hydrothermal vent animals living fossils? *Trends in Ecology & Evolution* **18**, 582–588. doi:10.1016/j.tree.2003.08.009.

Little, C. T. S., Herrington, R. J., Maslennikov, V. V., Morris, N. J. and Zaykov, V. V. (1997) Silurian hydrothermal-vent community from the southern Urals, Russia. *Nature* **385**, 146–148. doi:10.1038/385146a0.

Little, C. T. S., Herrington, R. J., Maslennikov, V. V. and Zaykov, V. V. (1998) The fossil record of hydrothermal vent communities. *Geological Society, London, Special Publications* **148**, 259–270. doi:10.1144/GSL.SP.1998.148.01.14.

Little, C. T. S., Maslennikov, V. V, Morris, N. J. and Gubanov, A. P. (1999a) Two Palaeozoic hydrothermal vent communities from the southern Ural mountains, Russia. *Palaeontology* **42**, 1043–1078.

Little, C. T. S., Herrington, R. J., Haymon, R. M. and Danelian, T. (1999b) Early Jurassic hydrothermal vent community from the Franciscan Complex, San Rafael Mountains, California. *Geology* **27**, 167–170.

Little, C. T. S., Cann, J. R., Herrington, R. J. and Morisseau, M. (1999c) Late Cretaceous hydrothermal vent communities from the Troodos ophiolite, Cyprus. *Geology* **27**, 1027–1030.

Little, C. T. S., Danelian, T., Herrington, R. and Haymon, R. (2004) Early Jurassic hydrothermal vent community from the Franciscan Complex, California. *Journal of Paleontology* **78**, 542–559.

Lonsdale, P. (1977) Clustering of suspension-feeding macrobenthos near abyssal hydrothermal vents at oceanic spreading centers. *Deep Sea Research* **24**, 857–863.

Majima, R., Nobuhara, T. and Kitazaki, T. (2005) Review of fossil chemosynthetic

assemblages in Japan. *Palaeogeography, Palaeoclimatology, Palaeoecology* **227**, 86–123. doi:10.1016/j.palaeo.2005.04.028.

Merz, R. A. (2015) Textures and traction: how tube-dwelling polychaetes get a leg up. *Invertebrate Biology* **134**, 61–77. doi:10.1111/ivb.12079.

Merz, R. A. and Woodin, S. A. (2006) Polychaete chaetae: function, fossils, and phylogeny. *Integrative and Comparative Biology* **46**, 481–496.

Moczydłowska, M., Westall, F. and Foucher, F. (2014) Microstructure and biogeochemistry of the organically preserved Ediacaran metazoan *Sabellidites*. *Journal of Paleontology* **88**, 224–239. doi:10.1666/13-003.

Nishi, E., Bhaud, M. R. and Koh, B. S. (2004) Two new species of *Spiochaetopterus* (Annelida: Polychaeta) from Sagami Bay and Tokyo Bay, central Japan with a comparative table of species from Japanese and adjacent waters. *Zoological Science* **21**, 457–464.

Nobuhara, T., Onda, D., Kikuchi, N., Kondo, Y., Matsubara, K., Amano, K., Jenkins, R. G., Hikida, Y. and Majima, R. (2008) Lithofacies and fossil assemblages of the Upper Cretaceous Sada limestone, Shimanto City, Kochi Prefecture, Shikoku, Japan. *Fossils* **84**, 47–60.

Olu, K., Duperret, A., Sibuet, M., Foucher, J. and Fiala-Medoni, A. (1996) Structure and distribution of cold seep communities along the Peruvian active margin: relationship to geological and fluid patterns. *Marine Ecology Progress Series* **132**, 109–125.

Parham, J. F., Donoghue, P. C. J., Bell, C. J., Calway, T. D., Head, J. J., Holroyd, P. A., Inoue, J. G., Irmis, R. B., Joyce, W. G., Ksepka, D. T., Patane, J. S. L., Smith, N. D., Tarver, J. E., van Tuinen, M., Yang, Z., Angielczyk, K. D., Greenwood, J. M., Hipsley, C. A., Jacobs, L., Makovicky, P. J., Muller, J., Smith, K. T., Theodor, J. M., Warnock, R. C. M. and Benton, M. J. (2012) Best practices for justifying fossil calibrations. *Systematic Biology* **61**, 346–359. doi:10.1093/sysbio/syr107.

Parry, L., Tanner, A. and Vinther, J. (2014) The origin of annelids. *Palaeontology* **57**, 1091–1103. doi:10.1111/pala.12129.

Paull, C., Hecker, B., Commeau, R., Freeman-Lynde, R., Neumann, A., Corso, W., Golubic, S., Hook, J., Sikes, E. and Curray, J. (1984) Biological communities at Florida Escarpment resemble hydrothermal vent communities. *Science* **226**, 965–967.

Peckmann, J., Edert, J. L. G. O., Thielà, V., Michaelisà, W. and Reitner, J. (2002) A

comprehensive approach to the study of methane-seep deposits from the Lincoln Creek Formation, western Washington State, USA. *Sedimentology* **49**, 855–873.

Peckmann, J., Thiel, V., Reitner, J., Taviani, M., Aharon, P. and Michaelis, W. (2004) A microbial mat of a large sulfur bacterium preserved in a Miocene methane-seep limestone. *Geomicrobiology Journal* **21**, 247–255. doi:10.1080/01490450490438757.

Peckmann, J., Little, C. T. S., Gill, F. and Reitner, J. (2005) Worm tube fossils from the Hollard Mound hydrocarbon-seep deposit, Middle Devonian, Morocco: Palaeozoic seep-related vestimentiferans? *Palaeogeography, Palaeoclimatology, Palaeoecology* **227**, 242–257. doi:10.1016/j.palaeo.2005.04.021.

Reuscher, M., Fiege, D. and Wehe, T. (2009) Four new species of Ampharetidae (Annelida: Polychaeta) from Pacific hot vents and cold seeps, with a key and synoptic table of characters for all genera. *Zootaxa* **2191**, 1–40.

Reuscher, M., Fiege, D. and Wehe, T. (2012) Terebellomorph polychaetes from hydrothermal vents and cold seeps with the description of two new species of Terebellidae (Annelida: Polychaeta) representing the first records of the family from deep-sea vents. *Journal of the Marine Biological Association of the United Kingdom* **92**, 997–1012. doi:10.1017/S0025315411000658.

Ronquist, F. and Huelsenbeck, J. P. (2003) MrBayes 3: Bayesian phylogenetic inference under mixed models. *Bioinformatics* **19**, 1572–1574.

Rouse, G. W. and Fauchald, K. (1997) Cladistics and polychaetes. *Zoologica Scripta* **26**, 139–204.

Rybakova, E. and Galkin, S. (2015) Hydrothermal assemblages associated with different foundation species on the East Pacific Rise and Mid-Atlantic Ridge, with a special focus on mytilids. *Marine Ecology* **36**, 45–61. doi:10.1111/maec.12262.

Saether, K. P. (2011) A taxonomic and palaeobiogeographic study of the fossil fauna of Miocene hydrocarbon seep deposits, North Island, New Zealand. PhD Thesis, University of Auckland.

Sansom, R. S. (2015) Bias and sensitivity in the placement of fossil taxa resulting from interpretations of missing data. *Systematic Biology* **64**, 256–266. doi:10.1093/sysbio/syu093.

Sephton, M. A., Visscher, H., Looy, C. V., Verchovsky, A. B. and Watson, J. S. (2009) Chemical constitution of a Permian-Triassic disaster species. *Geology* **37**, 875-878. doi:

10.1130/G30096A.1.

Shillito, B., Lechaire, J.-P., Goffinet, G. and Gaill, F. (1995) Composition and morphogenesis of the tubes of vestimentiferan worms. *Geological Society, London, Special Publications* **87**, 295–302. doi:10.1144/GSL.SP.1995.087.01.22.

Shpanskaya, A. Y., Maslennikov, V. V. and Little, C. T. S. (1999) Vestimnetiferan tubes from the Early Silurian and Middle Devonian hydrothermal biota of the Uralian palaeobasin. *Paleontologicheskii Zhurnal* **33**, 222–228.

Skovsted, C. B. (2006) Small shelly fauna from the Upper Lower Cambrian Bastion and Ella Island Formations, north-east Greenland. *Journal of Paleontology* **80**, 1087–1112. doi:10.1666/0022-3360(2006)80[1087:SSFFTU]2.0.CO;2.

Southward, E. C., Schulze, A. and Tunnicliffe., V. (2002) Vestimentiferans (Pogonophora) in the Pacific and Indian Oceans: A new genus from Lihir Island (Papua New Guinea) and the Java Trench, with the first report of *Arcovestia ivanovi* from the North Fiji Basin. *Journal of Natural History* **36**, 1179–1197.

Southward, E., Schulze, A. and Gardiner, S. (2005) Pogonophora (Annelida): form and function. *Hydrobiologia* **535**, 227–251.

Stankiewicz, B. A., Briggs, D. E. G., Evershed, R. P., Flannery, M. B. and Wuttke, M. (1997) Preservation of chitin in 25-million-year-old fossils. *Science* **276**, 1541–1543. doi: 10.1126/science.276.5318.1541.

Taylor, P. D. and Vinn, O. (2006) Convergent morphology in small spiral worm tubes ('*Spirorbis*') and its palaeoenvironmental implications. *Journal of the Geological Society* **163**, 225–228. doi:10.1144/0016-764905-145.

Vinn, O. and Mutvei, H. (2005) Observations on the morphology and affinites of cornulitids from the Ordovician of Anticosti Island and the Silurian of Gotland. *Journal of Paleontology* **79**, 726–737.

Vinn, O., Ten-Hove, H., Mutvei, H. and Kirsimae, K. (2008) Ultrastructure and mineral composition of serpulid tubes (Polychaeta, Annelida). *Zoological Journal of the Linnean Society* **154**, 633–650.

Vinn, O., Kupriyanova, E. K. and Kiel, S. (2013) Serpulids (Annelida, Polychaeta) at Cretaceous to modern hydrocarbon seeps: ecological and evolutionary patterns. *Palaeogeography, Palaeoclimatology, Palaeoecology* **390**, 35–41. doi:10.1016/j.palaeo.2012.08.003.

Vinn, O., Hryniewicz, K., Little, C. T. S. and Nakrem, H. A. (2014) A Boreal serpulid fauna from Volgian-Ryazanian (latest Jurassic-earliest Cretaceous) shelf sediments and hydrocarbon seeps from Svalbard. **36**, 527–540.

Vinn, O., Zabini, C., Sene-Silva, G., Kirsimae, K. and Susan-Marcos, L. (2015) Possible polychaete tube worms from the Late Emsian (Early Devonian) of the Parana Basin, Brazil. *Acta Palaeontologica Polonica*. doi:10.4202/app.00206.2015.

Vovelle, J. and Gaill, F. (1986) Donnees morphologiques, histochimiques et microanalytiques sur l'elaboration du tube organo-mineral d'*Alvinella pompejana*, polychete des sources hydrothermales, et leurs implications phylogenetiques. *Zoologica Scripta* **15**, 33–43.

Vrijenhoek, R. C. (2013) On the instability and evolutionary age of deep-sea chemosynthetic communities. *Deep-Sea Research II* **92**, 189–200. doi:10.1016/j.dsr2.2012.12.004.

Webb, M. (1964) Tube abnormality in *Siboglinum ekmani*, *S. fiordicum* and *Sclerolinum brattstromi* (Pogonophora). *Sarsia* **15**, 69–70.

Weigert, A. and Bleidorn, C. (2016) Current status of annelid phylogeny. *Organisms Diversity & Evolution* **16**, 345–362. doi:10.1007/s13127-016-0265-7

Weigert, A., Helm, C., Meyer, M., Nickel, B., Arendt, D., Hausdorf, B., Santos, S. R., Halanych, K. M., Purschke, G., Bleidorn, C. and Struck, T. H. (2014) Illuminating the base of the annelid tree using transcriptomics. *Molecular Biology and Evolution* **31**, 1391–1401. doi:10.1093/molbev/msu080.

Williams, D. H. and Fleming, I. (1980) *Spectroscopic methods in organic chemistry*. McGraw-Hill, London.

Williscroft, K. (2013) Early Cretaceous methane seepage system and associated carbonates, biota and geochemistry, Sverdrup Basin, Ellef Ringnes Island, Nunavut. MSc Thesis, University of Calgary.

5 Microbial-tubeworm associations in a 440-million-year-old hydrothermal vent community

Magdalena N. Georgieva[1,2], Crispin T. S. Little[1], Alexander D. Ball[3], Adrian G. Glover[2]

[1] *School of Earth and Environment, University of Leeds, Leeds, United Kingdom*

[2] *Life Sciences Department, Natural History Museum, London, United Kingdom*

[3] *Imaging and Analysis Centre, Natural History Museum, London, United Kingdom*

5.1 Abstract

Microorganisms are the chief primary producers within present-day deep-sea hydrothermal vent ecosystems, and play a fundamental role in shaping the ecology of these unique environments. However, very little is known about the microbes that occurred within, and structured ancient vent communities. Their evolutionary history, diversity, and the nature of their interactions with hydrothermal vent animals are largely undetermined. The oldest known hydrothermal vent community that includes metazoans is preserved within the Yaman Kasy massive sulphide deposit of the Ural Mountains, Russia, which dates back to the late Ordovician-early Silurian, approximately 440 million years ago. This deposit contains two types of dwelling-tube fossils attributed to annelid worms – the large tubes of the fossil species *Yamankasia rifeia*, and the smaller tubes of *Eoalvinellodes annulatus*. A re-examination of the tube fossils preserved within the Yaman Kasy deposit using scanning electron microscopy reveals the preservation of filamentous microorganisms intimately associated with these tubes. The microfossils bear a strong resemblance to modern hydrothermal vent microbial filaments, including those preserved within the mineralised tubes of the vent polychaete genus *Alvinella*. The Yaman Kasy fossil filaments represent the oldest animal-microbial associations preserved within an ancient hydrothermal vent environment. They allude to a diverse microbial community, and also demonstrate that fine-scale microbial preservation can also be observed in ancient vent deposits, suggesting the possible existence of similarly-preserved microfossils in even older vent environments.

5.2 Introduction

Microorganisms are an intrinsic component of modern hydrothermal vent communities, being the chief primary producers within these ecosystems and sustaining remarkable biomass in the otherwise largely resource-limited deep sea (Sievert and Vetriani, 2012). They occupy a variety of niches at vents, including biological and mineral surfaces, hydrothermal plumes, and extend into the sub-seafloor. Microorganisms also constitute an important food source for grazing animals, and form unique and important associations with metazoan vent fauna such as large tubeworms, including ectosymbiosis, endosymbiosis and commensalism. In addition, vent microorganisms are highly diverse taxonomically, and are comprised of many novel lineages of archaea and bacteria, especially ε-Proteobacteria (Reysenbach *et al.*, 2000; Takai *et al.*, 2006; Huber *et al.*, 2007).

Hydrothermal vents have been suggested as the potential environments within which life may have originated (Martin *et al.*, 2008; Deamer and Georgiou, 2015; Weiss *et al.*, 2016), yet microbial fossils from ancient vent deposits are extremely rare. Microbial fossils, in addition to stromatolites considered to be fossil microbial mats, constitute the earliest morphological evidence for life on Earth (Allwood *et al.*, 2006; Knoll, 2012; Bontognali *et al.*, 2012), some of which occur within hydrothermally-influenced settings (Westall *et al.*, 2001; Hofmann, 2011). The oldest known microbial high-temperature vent fossils however, are poorly-preserved filamentous 'structures', reported from 3.24 Ga (Rasmussen, 2000) and 1.4 Ga (Li and Kusky, 2007).

Key to the interpretation of ancient microbial fossils are data from studies of fossilisation within modern hydrothermal vents. These have shown that filamentous microorganisms can be preserved in micron-scale detail by pyrite, and can retain very fine cellular morphological structures such as septae within filaments (Georgieva *et al.*, 2015). These microorganisms are fossilised within, and adjacent to, sulphide-replaced dwelling tubes of the vent annelid *Alvinella*, thereby demonstrating that microbial-animal interactions can potentially be observed in the fossil record given similar preservational processes.

The earliest metazoan fossils from hydrothermal vents occur in the late Ordovician-early Silurian Yaman Kasy volcanogenic massive sulphide (VMS) deposit, from which tubeworms have been described. Associated with these tubes, potential microbial structures have been observed, including 1 μm diameter holes (Little *et al.*, 1997; Buschmann and Maslennikov, 2006). But the nature of these structures has not yet been fully described, and their relationship to modern microbial fossilisation processes has not been elucidated.

Here we describe in detail for the first time, the preservational and morphological characteristics of filamentous microorganisms, associated with macrofossils from the Yaman Kasy VMS deposit. This study reveals an essential component of the oldest known hydrothermal vent community, the nature of microbial associations with ancient vent animals, as well as the potential for similar preservation of microorganisms within even older vent deposits.

5.3 Geological background

The Yaman Kasy VMS deposit is located in the southern Ural Mountains, Russia (51.4068°N, 57.6930°E; Supplementary Figure E.1). The age of this deposit is poorly constrained due to a lack of biostratigraphically useful fossils at the locality, but is considered be late Ordovician to early Silurian (Little *et al.*, 1999; Buschmann and Maslennikov, 2006), approximately 440 Ma. The deposit comprises a lens of Cu-Zn-rich massive sulphides up to 37 m thick and 90-100 m in diameter within calc-alkaline volcanic rocks (Little *et al.*, 1999; Buschmann and Maslennikov, 2006), interpreted to have formed within a back-arc basin (Zaykov *et al.*, 1995). Based on fluid inclusion analyses, the temperatures of the fluids from which sulphide minerals precipitated ranged from 103-371°C and did not boil, suggesting that the deposit was formed at approximately 1600 m depth (Herrington *et al.*, 1998). Sulphur isotopic ($\partial^{34}S$) analyses on fossil, chimney and mound sulphides indicate an igneous source for positive values, and a probable bacteriogenic source for the lightest $\partial^{34}S$ values (Herrington *et al.*, 1998). $\partial^{13}C$ carbon isotope analyses of organic material preserved in the Yaman Kasy deposit also yields values indicative of microbial fractionation, as well as biomarkers of potential microbial origin (Blumenberg *et al.*, 2012).

The Yaman Kasy fossils were found within the upper clastic sulphide sections of this deposit, and occur among colloform pyrite and black smoker vent chimney fragments (Herrington *et al.*, 1998). The fossil assemblage comprises a monoplacophoran mollusc (*Thermoconus shadlunae*), a ligulate brachiopod (*Pyrodiscus lorrainae*), an ambonychiid bivalve (*Mytilarca* sp.), an indeterminate vetiagastropod, as well as two morphotypes of tubes (Little *et al.*, 1999). The smaller tubes (*Eoalvinellodes annulatus*) are 0.2-3 mm in diameter, while the larger tubes (*Yamankasia rifeia*) range from 3-39 mm in diameter. The original walls of the tubes are not preserved, but were likely organic in composition due to the fossil tubes exhibiting folds or wrinkled textures (Shpanskaya *et al.*, 1999). The fossilised tube walls are

formed either of framboidal or colloform pyrite, and also retain fine details of the external tube wall ornamentation. *E. annulatus* tubes often have thick walls comprised of colloform pyrite that is many layers thick, and show external ornament of transverse, bifurcating wrinkles (Little et al., 1999; Buschmann and Maslennikov, 2006). Small holes in *E. annulatus* tube walls have been interpreted as molds of microorganisms by Buschmann and Maslennikov (2006). *Y. rifeia* tubes are either preserved as several (2-3) layers of pyrite, or by a single layer of colloform pyrite that is interpreted as having grown onto the outside of the tube (Little *et al.*, 1999). These tubes show external ornament of fine parallel longitudinal striations (Little *et al.*, 1999; Buschmann and Maslennikov, 2006). *Y. rifeia* tubes also possess small holes suggested to be microbial fossils, which occur in the colloform pyrite tube coatings (Little *et al.*, 1997; Buschmann and Maslennikov, 2006).

5.4 Methods

Fragments of fossil *Yamankasia rifeia* and *Eoalvinellodes annulatus* tubes from Yaman Kasy material housed in the collections of the Natural History Museum, UK (NHMUK) were embedded in resin blocks and then polished (finishing with 1 μm diamond). They were subsequently examined with optical microscopy (in reflected light), then given a ~10 nm thick carbon coating for backscattered electron imaging using a FEI Quanta 650 FEG-ESEM at NHMUK. Elemental composition of mineral phases at various scales was determined through energy dispersive x-ray spectroscopy (EDS) using a Bruker Flat Quad 5060F detector fitted within the above SEM. Tube-scale maps were collected at 12-20 kV. For putative microfossil-scale maps (hereafter putative microfossils are referred to as 'microfossils'), an accelerating voltage of 10 kV was used, and x-rays collected for 31-85 minutes with counts averaging 144,000-160,000 counts per second for each map. Interaction volumes for all detailed maps were estimated as 0.4 μm in diameter and 0.4 μm deep by the Bruker Esprit software used to analyse the data. Electron probe micro-analysis was also performed to assess the composition of pyrite directly around microfossils, and in nearby non-fossiliferous pyrite (see Appendix E, Methods Supplement for details). Phosphorus content, which has been posited as a proxy for fossilised organic matter at vents (Maginn *et al.*, 2002), was also evaluated using this technique.

Measurements of microfossils were made from SEM images using the software ImageJ v. 1.46r (Schneider *et al.*, 2012). Only microstructures with a distinctly circular or elliptical cross section i.e. those likely to have a biogenic in origin, were measured. For statistical

tests, diameter measurements from microfossils were divided into four data groups based on their location of occurrence. Shapiro-Wilk normality tests were used to determine if microfossil diameters were normally distributed, and *F*-tests to compare variances between data pairs. Two-sample Kolmogorov-Smirnov tests were subsequently used to compare the cumulative distributions of diameter measurements between data pairs. All three types of statistical test were performed in R (R Core Team, 2013).

Modern unmineralised and recently mineralised microbial filaments occurring on the tubes of the hydrothermal vent polychaetes *Alvinella* sp. were imaged using SEM for comparison with the Yaman Kasy microfossils. Unmineralised microorganisms were coated with 20 nm gold-palladium, while mineralised microbes were embedded in resin blocks, polished, and coated with carbon as for the Yaman Kasy material.

5.5 Results

5.5.1 Occurrence of microfossils

Microfossils were found in three sections of tubes from Yaman Kasy. They occurred in pyrite with colloform (or finely layered) growth, and fine-grained non-colloform pyrite. Tubes preserved by framboidal pyrite showed no evidence of the occurrence of microfossils.

Microfossils were found in a transverse and a longitudinal section of two separate *Yamankasia rifeia* tubes (Figure 5.1A-C, D-F) and a transverse section of an *Eoalvinellodes annulatus* tube (Figure 5.1G-I). In the *Y. rifeia* transverse section (Yr_61633; Figure 5.1A-C), microfossils occurred in a ~2 mm thick layer of colloform pyrite that is considered to have grown on the exterior tube wall surface (Little *et al.*, 1999). Within this layer, small microfossils occurred along the inner rim closest to where the original outer tube wall would have been, and slightly larger microfossils occurred towards the outer rim of the pyrite layer (Figure 5.1A, C). Microfossils (Figure 5.1F) in the *Y. rifeia* longitudinal section (Yr_OR6468; Figure 5.1D) were found within a ~3 mm thick layer of fine-grained pyrite in which spaces were infilled by silica (Figure 5.1E). This pyrite layer is also positioned on the outside of the fossil tube wall (Figure 5.1F). In the *E. annulatus* tube transverse section (Eo_YKB1; Figure 5.1G), microfossils occurred within a section of the fossil tube wall preserved as finely interlayered colloform pyrite and silica (Figure 5.1H-I). Many of these microfossils were observed to crosscut the pyrite-silica banding.

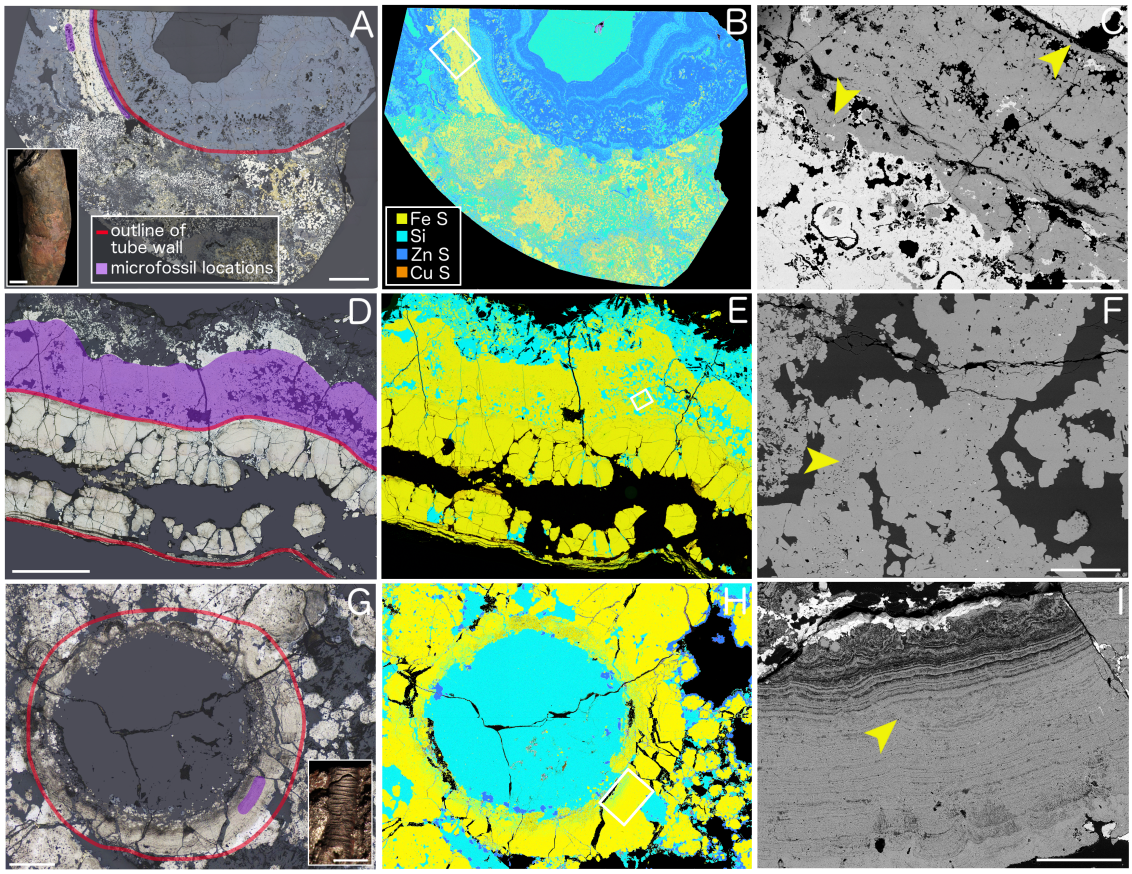

Figure 5.1 Sections of fossilised tubes from the Yaman Kasy deposit associated with microfossils. **A, D, G** - reflected light images (tube rims and areas containing microfossils are highlighted), **B, E, H** - elemental maps, **C, F, I** - detail of areas where microfossils occur. **A,** transverse section of a *Yamankasia rifeia* tube (Yr_61633) in which only a section of colloform pyrite that formed on the outer tube surface has been preserved, scale is 3 mm. *Inset - left*, an example of a *Y. rifeia* tube in hand specimen, scale bar is 10 mm. *Insert - right*, key to colours in **A**, **D** and **G**. **B,** elemental map of **A**; *insert*, key to elemental maps **B**, **E** and **H**. **C,** SEM image of boxed area in **B** showing the colloform pyrite band in greater detail, and where microfossils occur within it. Small filaments occur along the inner surface of the band, and larger filaments are found along its outer edge (yellow arrows). Scale bar is 500 µm. **D,** longitudinal section of an additional *Y. rifeia* tube (Yr_OR6468), in which microfossils occur in a ~2 mm thick band of pyrite located on the outside of the fossilised tube, scale bar is 3 mm. **E,** elemental map of section in **D**. **F,** detail of boxed area in **E** showing abundant microbial clumps in this region (yellow arrow), scale bar is 100 µm. **G,** transverse section of an *Eoalvinellodes annulatus* tube (Eo_YKB1), in which microfossils occur in a small area of colloform pyrite forming the tube wall, scale bar is 400 µm. *Insert*, example of an *E. annulatus* tube in hand specimen, scale bar is 1 mm. **H,** elemental map of section in **G**. **I,** detail of boxed area in **H** showing tube wall containing microfossils (yellow arrow), scale bar is 100 µm.

5.5.2 Morphology and preservation of microfossils

The Yaman Kasy microfossils occur in a variety of orientations, with occasional longitudinal sections revealing filamentous morphologies (Figure 5.2). They generally form clusters of microfossils with a similar diameter, but the density of filaments within these clusters varied between the four locations where microfossils were found (the four locations being: Yr_61633 inner rim of colloform pyrite (Figure 5.2A-C); Yr_61633 outer

rim of colloform pyrite (Figure 5.2D-F); Yr_OR6468 (Figure 5-2G-I); Eo_YKB1 (Figure 5.2J-L)) (Supplementary Figure E.6). The distributions of microfossil diameter measurements also varied between the four above locations (Supplementary Figure E.6), and were significantly different for all location data pairs (Supplementary Tables E.3 to E.5). Occasionally, filaments with visibly different diameters were preserved alongside each other, such as the orange-arrowed filament in Figure 5.2B, and the adjacent smaller, vertically-oriented filaments.

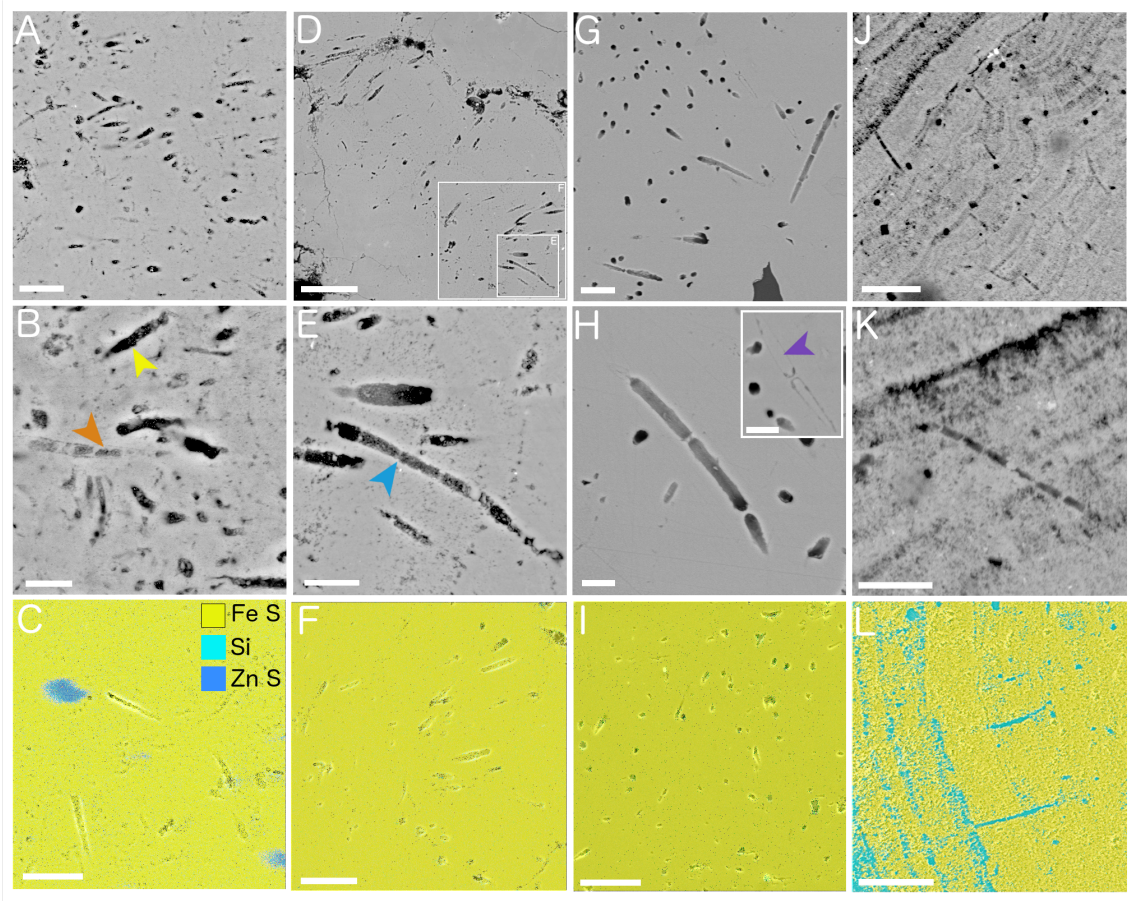

Figure 5.2 Morphology and elemental composition of microfossils associated with Yaman Kasy worm tube fossils. **A-C**, microfossils found along the inner rim of the colloform pyrite band within Yr_61633. **A,** cluster of filamentous microfossils, scale bar is 5 µm. **B,** Detail of filamentous microfossils in **A**, showing preservation of many hollow filaments (yellow arrow) as well as one which appears to retain a sheath (orange arrow), scale bar is 2 µm. **C,** elemental map of Yr_61633 inner pyrite rim microfossils, scale bar is 5 µm. (*Note*, **A-C** are all of different areas). **D-F**, microfossils found along the outer rim of the colloform pyrite band within Yr_61633. **D,** cluster of filamentous microfossils, scale bar is 20 µm (locations of **E** and **F** are shown). **E,** detail of a microfossil with septae (blue arrow), scale bar is 4 µm. **F,** elemental map of Yr_61633 outer pyrite rim microfossils, scale bar is 10 µm. **G-I,** microfossils preserved in *Y. rifeia* longitudinal section (Yr_OR6468). **G,** cluster of filamentous microfossils resembling chains of rods, scale bar is 5 µm. **H,** detail of microfossils of the type pictured in **G**, scale bar is 2 µm. *Insert*, microfossil infilled by pyrite (purple arrow), scale bar is 2 µm. **I,** elemental map of Yr_OR6468 microfossils, scale bar is 10 µm. **J-L,** microfossils preserved in *E. annulatus* transverse section (Eo_YKB1) (*Note*, **G-I** are all of different areas). **J,** cluster of septate filamentous microfossils, scale bar is 10 µm. **K,** detail of a septate microfossil from Eo_YKB1, scale bar is 5 µm. **L,** elemental map of Eo_YKB1 microfossils, scale bar is 10 µm (*Note*, **J-L** are all of different areas).

The filamentous microfossils were often curved (Figure 5.2A-E, H-J), and a subset were cross-cut by transverse septae that occurred at regular intervals (Figure 5.2B, E, H, K). Distances between septae (in relation to filament diameter) were visibly greater for microfossils in Yr_OR6468 than in Yr_61633 and Eo_YKB1. In addition, individual Yr_OR6468 'cells' (Figure 5.2G-H) had a rod-like appearance, whereas the endings of 'cells' of septate microfossil filaments from Yr_61633 and Eo_YKB1 showed a large area of attachment to one another. A microfossil in Figure 5.2B (arrowed) has the appearance of a sheathed microbial filament, due to the encasement of cell-like bodies within a tubular structure.

Detailed EDS maps of the Yaman Kasy microfossils show that they are mainly preserved by iron sulphides (Figure 5.2C, F, I, L; confirmed to be pyrite using RL) as hollow moulds delineated by pyrite, with silica infilling cells within one of the specimens (Figure 5.2L). Occasionally the microfossils were also infilled by pyrite (Figure 5.2B, H *insert*), and septae were also formed of pyrite. There appeared to be no clear variation in pyrite composition of sample areas containing microfossils, and those that did not. Phosphorus was not detected around microfossils in either Yr_61633 or Yr_OR6468 by EPMA (Appendix E; Supplementary Figures E.2 to E.5; Supplementary Tables E.1 to E.2).

5.6 Interpretations and discussion

The microfossils found in association with fossil tubes from Yaman Kasy meet many of the suggested criteria for genuine biogenic microbial fossils (Brasier and Wacey, 2012). Importantly, they occur within an appropriate context, as a diverse range of microorganisms are often found growing on the surfaces of annelid tubes and vent chimney sulphides in modern vent environments (Campbell *et al.*, 2003; López-García *et al.*, 2003; Duperron *et al.*, 2009). All of the Yaman Kasy microstructures occur as a population of filaments of a similar size and morphology, which are often clustered together (Figure 5.2A, D, G) and thus resemble clumps of modern vent microbial filaments (Georgieva *et al.*, 2015). The small filaments within sample Yr_61633 especially have a mat-like appearance, as they are distributed within a very narrow zone of pyrite that is thought to have grown directly onto the outer tube wall (Little *et al.*, 1999). The microstructures themselves have tubular morphologies with mostly constant diameters, a curved appearance of filaments suggesting that they were originally flexible, mostly hollow interiors apart from where infilled by silica or pyrite, and the septate divisions within many

of the filaments delineate spaces indicative of cells. The observed microfossil textures are not the result of microbial leaching of pyrite (Verati *et al.*, 1999; Edwards *et al.*, 2003) as they occur throughout the pyrite matrix in which they are preserved, and are present in a range of orientations.

The interpretation of the Yaman Kasy filaments as fossilised microorganisms is further supported by both their very close resemblance to modern day hydrothermal vent filamentous microorganisms, and studies which have shown that microorganisms as small as 1 μm in diameter can be fossilised by pyrite at vents with high fidelity (Georgieva *et al.*, 2015). Like the Yaman Kasy microfossils, modern vent microbial filaments can be tapering as well as septate (Jannasch and Wirsen, 1981; Jannasch and Mottl, 1985; López-García *et al.*, 2003). For example, septate, non-septate, chain-of rods (Figure 5.3A) and tapering (Figure 5.3B) microbial morphologies can all be observed on the surfaces of *Alvinella* tubes. Following mineralisation, the original cluster (Figure 5.3C) and mat-like (Figure 5.3D) growth habits of these microorganisms are maintained. At modern vents, pyrite and silica also preserve fine details such as septae, microbial sheaths, and cell contents (Figure 5.3E-F), and occasionally infill microfossils preserved as moulds (Figure 5.5E-F, Supplementary Figure E.7). While phosphorus was not detected around the Yaman Kasy microfossils (Supplementary Figures E.2 to E.5; Supplementary Tables E.1 to E.2), the retention of this element upon the mineralisation of organic matter at modern vents (Maginn *et al.*, 2002) may be specific to *Alvinella* tubes and their particular microbial community.

Based on the observed Yaman Kasy microfossil morphologies, there are a number of preservational pathways and original microbial growth-types from which the fossils could have resulted (Figure 5.4). Bacteria are known to concentrate minerals along their surfaces (Schultze-Lam *et al.*, 1996; Li *et al.*, 2013) and may also induce mineralisation at vents (Peng *et al.*, 2007, 2009). Thus, the range of preservations observed in ancient and recently mineralised microorganisms may also be linked to preferential mineral accumulations within various parts of the microbial filaments/cells. Empty filamentous microfossil pyrite moulds (e.g. Figure 5.2B) may have either formed from filaments that contained no cells, or if cells were present, mineralisation may have been concentrated along the outer sheath walls, thus preventing mineralisation of inner cells (Figure 5.4A). For microfossils that exhibit septate divisions but no sheath (Figure 5.2E, H, K), there may, or may not, have originally been a sheath that was completely replaced by pyrite, while mineralisation appears to have been concentrated along the cell walls (Figure 5.4B). Infilling of cells was likely contemporaneous with cell wall mineralisation (Peng *et al.*, 2007), while the empty

nature of some cells could have resulted from their cell walls mineralising before vent fluids were able to penetrate into the cell interior. Microfossils that demonstrate preservation of both cells and sheaths (Figure 5.2B) indicate that the sheath and cell walls had similar resistance and were likely mineralised at the same time (Figure 5.4C). Microbial sheaths were only well preserved in a subset of recently mineralised vent microorganisms (Figure 5.3D-F), suggesting that this type of preservation may be on the whole rarer. While the preservation of microfossils also appears to not affect pyrite composition at a broader scale that can be detected by EPMA (Supplementary Figures E.2 to E.5; Supplementary Tables E.1 to E.2), finer scale analyses that target pyrite directly delineating microfossils could shed insights into any effects of microbial presence on mineral precipitation.

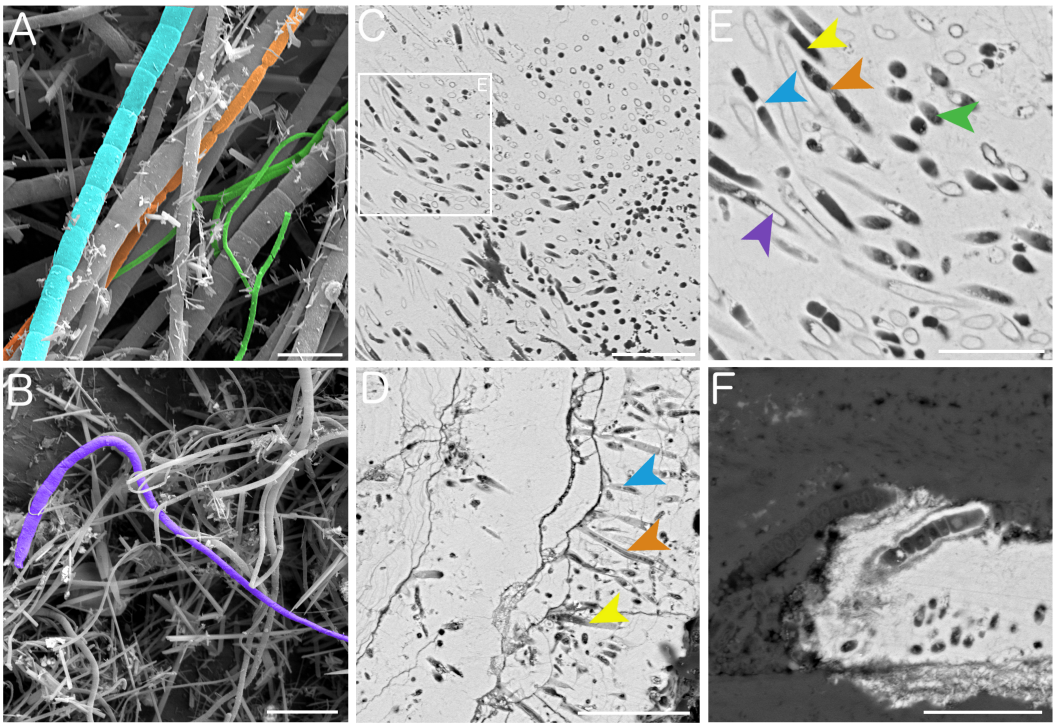

Figure 5.3 Microorganisms associated with the tubes of the hydrothermal vent annelid *Alvinella* sp. **A-B,** unmineralised filamentous microorganisms from the inside surface of an *Alvinella* sp. tube exhibiting a variety of morphologies, including non-septate filaments (green), septate filaments (blue), 'chain-of-rods'-type filament and a tapering filament (purple). Scale bars are 5 µm in **A** and 10 µm in B. **C-F,** microorganisms mineralised alongside *Alvinella* sp. tubes. **C,** clump of filaments in a variety of orientations, scale bar is 10 µm. **D,** filaments arranged longitudinally within a band of pyrite thereby demonstrating mat-like growth, scale bar is 10 µm. Some of the filaments appear hollow (yellow arrow), whereas others exhibit septae (blue arrow) as well as replacement of a microbial sheath by pyrite (orange arrow). **E,** detail of area in **C** showing hollow filaments (yellow arrow), filaments with septae formed of pyrite (blue arrow), septae and sheath formed of silica (orange arrow), as well as filaments infilled by pyrite (purple arrow) and others infilled by silica (green arrow). Scale bar is 5 µm. **F,** filamentous microorganisms preserved in exceptional detail by both pyrite and silica (silica - dark grey, pyrite - light grey), that reveals sub-cellular aspects, scale bar is 5 µm.

It is difficult to infer the taxonomic identity of the Yaman Kasy microfossils, as microorganisms from modern vent environments are largely described using molecular methods (e.g. Schrenk et al., 2003; Anderson et al., 2015). Microorganisms can also exhibit convergent morphologies, and microbial morphologies may vary in relation to environmental conditions (Reysenbach and Cady, 2001). Archaea, ε-Proteobacteria and *Aquificales* have all been identified as prominent members of modern vent microbial communities (Takai *et al.*, 2006; Sievert and Vetriani, 2012), and while bacteria are more likely to occur as filaments, Archaea can occasionally also take this form (Muller *et al.*, 2010). Nevertheless, the Yaman Kasy microfossils are perhaps more likely those of bacteria, as bacteria are more abundant in modern vents and often form mats of filaments in this environment. Despite their unknown identity, the occurrence of both 'chain of rods' microfossils (Figure 5.2H) with curved endings resembling a *Streptobaccillus*-type morphology, and microfossils resembling microbial trichomes (Pelczar *et al.*, 2010) (Figure 5.2B, E, K), as well as mixing of different sizes of filaments (Figure 5.2B), alludes to a diversity of different microorganisms occurring around the Yaman Kasy tube fossils. The original microbial diversity of the Yaman Kasy palaeocommunity was undoubtedly greater than the microfossils described here suggest, as microbial morphologies such as coccoids that are observed to occur within modern vent environments (Harmsen *et al.*, 1997; Reysenbach *et al.*, 2000) were likely not fossilised. By how much that original diversity is underestimated is currently unknown.

In addition to their morphologies, the different diameter distributions of Yaman Kasy microfossils from the four near-tube locations, as well as variations in microfossil density, show that these ancient microbial assemblages were heterogeneous. This reflects the characteristics of microbial mats within modern day hydrothermal vent environments, which are often diverse and exhibit spatial variation in the degree to which micro-organisms of a particular type are mixed in with other sizes and morphotypes of microorganisms (Takai *et al.*, 2006) (Figure 5.3A-B). This results from the wide range of niches available at vents, and this study demonstrates the first evidence that microorganisms, in association with macrofaunal-sized metazoan animals, were taking advantage of the assortment of niches available at vents ~440 million years ago.

The locations of a subset of the Yaman Kasy microfossils (Figure 5.1A, E) suggest that microorganisms were living on and around metazoan tube surfaces and were fossilised alongside the tubes, very similar to the preservation of annelid tubes and their epiphytic microorganisms recently observed within modern vent environments (Georgieva *et al.*,

2015). This preservation demonstrates that associations between microorganisms and animals that have been observed within modern vents, such as commensalism and episymbioses (Desbruyeres *et al.*, 1983; Duperron *et al.*, 2009; Thurber *et al.*, 2011), may also be detected within the fossil record of ancient vent communities. For some of the resulting microfossils, such as those for which pyrite may preserve cellular details, it may also be possible to gain a good understanding of what the original microorganisms looked like (Figure 5.4). These results also show that microbial colonisation of metazoan tubes is an association that has a very long fossil history, stretching back to the earliest known hydrothermal vent community, and demonstrates the potential for detailed microbial preservation within even older hydrothermal vent deposits.

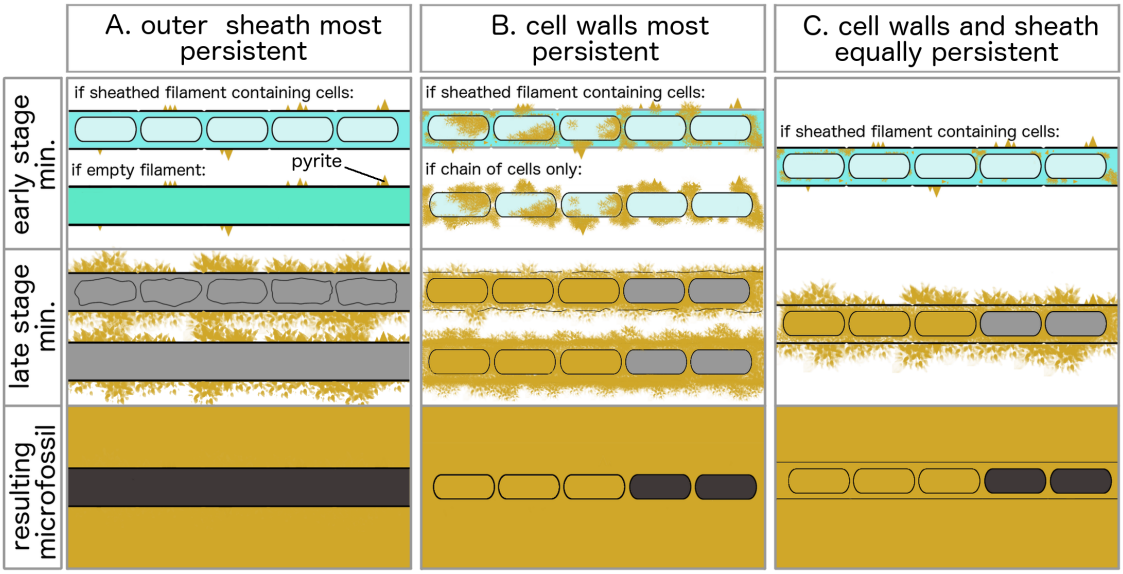

Figure 5.4 Fossilisation models for hydrothermal vent microorganisms. In scenario **A,** the resulting microfossil is an empty filament moulded of pyrite. There could be two starting microorganism types for this - a filament containing cells in which the cells are not preserved, and a filament that does not contain cells. With both of these starting filaments, mineralisation would need to be confined to mainly the outer wall, while any contents degrade within the pyrite tomb. Under scenario **B,** the resulting microfossil looks like a chain of cells. Either these cells never had a sheath, or such a sheath was not preserved. Mineralisation likely propagated along the cell walls, with the cell volume also being infilled in some cases. The microfossil that results in scenario **C** shows preservation of both microbial cells and an outer sheath, therefore the starting filament must have contained both of these features. Both the cell walls and sheath walls likely had equal persistence, and cell volumes may also be infilled as these filaments are mineralising.

5.7 Acknowledgements

The authors would like to thank Richard Herrington, Helena Toman and Jon Todd (NHMUK) for access to Yaman Kasy material, Tomasz Goral for assistance with EDS

analyses, and John Spratt for assistance with EPMA. MNG is funded by a NERC CASE studentship (NE/ K500847/1).

5.8 References

Allwood, A., Walter, M., Kamber, B., Marshall, C. and Burch, I. (2006) Stromatolite reef from the early Archaean era of Australia. *Nature* **441**, 714–718.

Anderson, R. E., Sogin, M. L. and Baross, J. A. (2015) Biogeography and ecology of the rare and abundant microbial lineages in deep-sea hydrothermal vents. *FEMS Microbiology Ecology* **91**, 1–11. doi:10.1093/femsec/fiu016.

Blumenberg, M., Seifert, R., Buschmann, B., Kiel, S. and Thiel, V. (2012) Biomarkers reveal diverse microbial communities in black smoker sulfides from turtle pits (Mid-Atlantic Ridge, Recent) and Yaman Kasy (Russia, Silurian). *Geomicrobiology Journal* **29**, 66–75.

Bontognali, T. R. R., Sessions, A. L., Allwood, A. C., Fischer, W. W., Grotzinger, J. P., Summons, R. E. and Eiler, J. M. (2012) Sulfur isotopes of organic matter preserved in 3.45-billion-year-old stromatolites reveal microbial metabolism. *Proceedings of the National Academy of Sciences* **109**, 15146–15151. doi:10.1073/pnas.1207491109.

Brasier, M. D. and Wacey, D. (2012) Fossils and astrobiology: new protocols for cell evolution in deep time. *International Journal of Astrobiology* **11**, 217–228. doi:10.1017/S1473550412000298.

Buschmann, B. and Maslennikov, V. V. (2006) The late Ordovican or earliest Silurian hydrothermal vent fauna from Yaman Kasy VMS deposit (South Uralides, Russia). *Freiberger Forschungshefte* **14**, 139–172.

Campbell, B., Stein, J. and Cary, S. (2003) Evidence of chemolithoautotrophy in the baterial community associated with *Alvinella pompejana*, a hydrothermal vent polychaete. *Applied and Environmental Microbiology* **69**, 5070– 5078.

Deamer, D. W. and Georgiou, C. D. (2015) Hydrothermal conditions and the origin of cellular life. *Astrobiology* **15**, 1091–1095. doi:10.1089/ast.2015.1338.

Desbruyeres, D., Gaill, F., Laubier, L., Prieur, D. and Rau, G. H. (1983) Unusual nutrition of the "Pompeii worm" *Alvinella pompejana* (polychaetous annelid) from a hydrothermal vent environment: SEM, TEM, 13C and 15N evidence. *Marine Biology* **75**, 201–205.

Duperron, S., De Beer, D., Zbinden, M., Boetius, A., Schipani, V., Kahil, N. and Gaill, F. (2009) Molecular characterization of bacteria associated with the trophosome and the tube of *Lamellibrachia* sp., a siboglinid annelid from cold seeps in the eastern Mediterranean. *FEMS Microbiology Ecology* **69**, 395–409. doi:10.1111/j.1574-6941.2009.00724.x.

Edwards, K. J., McCollom, T., Konishi, H. and Buseck, P. (2003) Seafloor bioalteration of sulfide minerals: Results from in situ incubation studies. *Geochimica et Cosmochimica Acta* **67**, 2843–2856. doi:10.1016/S0016-7037(00)00089-9.

Georgieva, M. N., Little, C. T. S., Ball, A. D. and Glover, A. G. (2015) Mineralization of *Alvinella* polychaete tubes at hydrothermal vents. *Geobiology* **13**, 152–169. doi:10.1111/gbi.12123.

Harmsen, H., Prieur, D. and Jeanthon, C. (1997) Distribution of microorganisms in deep-sea hydrothermal vent chimneys investigated by whole-cell hybridization and enrichment culture of thermophilic subpopulations. *Applied and Environmental Microbiology* **63**, 2876–2883.

Herrington, R. J., Maslennikov, V. V., Spiro, B., Zaykov, V. V. and Little, C. T. S. (1998) Ancient vent chimney structures in the Silurian massive sulphides of the Urals. In *Modern Ocean Floor Processes and the Geological Record* (ed. Mills, R. A. and Harrison, K.), pp. 241–258. Special Publication of the Geological Society, London.

Hofmann, A. (2011) Archaean hydrothermal systems in the Barberton Greenstone Belt and their significance as a habitat for early life. In *Earliest Life on Earth: Habitats, Environments and Methods of Detection* (ed. Golding, S. D. and Glikson, M.), pp. 51–78. Springer Netherlands, Dordrecht doi:10.1007/978-90-481-8794-2_3.

Huber, J. A., Welch, D. B. M., Morrison, H. G., Huse, S. M., Neal, P. R., Butterfield, D. A. and Sogin, M. L. (2007) Microbial population structures in the deep marine biosphere. *Science* **318**, 97–100. doi:10.1126/science.1146689.

Jannasch, H. W. and Mottl, M. J. (1985) Geomicrobiology of deep-sea hydrothermal vents. *Science* **229**, 717–725. doi:10.1126/science.229.4715.717.

Jannasch, H. W. and Wirsen, C. O. (1981) Morphological survey of microbial mats near deep-sea thermal vents. *Applied and Environmental Microbiology* **41**, 528–538.

Knoll, A. H. (2012) The fossil record of microbial life. In *Fundamentals of Geobiology* (ed. Knoll, A. H., Canfield, D. E. and Konhouser, K. O), pp. 297–314. John Wiley & Sons, Chichester. doi:10.1002/9781118280874.ch16.

Li, J. and Kusky, T. M. (2007) World's largest known Precambrian fossil black smoker chimneys and associated microbial vent communities, North China: implications for early life. *Gondwana Research* **12**, 84–100. doi:10.1016/j.gr.2006.10.024.

Li, J., Benzerara, K., Bernard, S. and Beyssac, O. (2013) The link between biomineralization and fossilization of bacteria: Insights from field and experimental studies. *Chemical Geology* **359**, 49–69. doi:10.1016/j.chemgeo.2013.09.013.

Little, C. T. S., Herrington, R. J., Maslennikov, V. V., Morris, N. J. and Zaykov, V. V. (1997) Silurian hydrothermal-vent community from the southern Urals, Russia. *Nature* **385**, 146–148. doi:10.1038/385146a0.

Little, C. T. S., Maslennikov, V. V, Morris, N. J. and Gubanov, A. P. (1999) Two Palaeozoic hydrothermal vent communities from the southern Ural mountains, Russia. *Palaeontology* **42**, 1043–1078.

López-García, P., Duperron, S., Philippot, P., Foriel, J., Susini, J. and Moreira, D. (2003) Bacterial diversity in hydrothermal sediment and epsilonproteobacterial dominance in experimental microcolonizers at the Mid-Atlantic Ridge. *Environmental Microbiology* **5**, 961–976. doi:10.1046/j.1462-2920.2003.00495.x.

Maginn, E., Little, C. T. S., Herrington, R. and Mills, R. (2002) Sulphide mineralisation in the deep sea hydrothermal vent polychaete, *Alvinella pompejana*: implications for fossil preservation. *Marine Geology* **181**, 337–356.

Martin, W., Baross, J., Kelley, D. and Russell, M. J. (2008) Hydrothermal vents and the origin of life. *Nature Reviews Microbiology* **6**, 805–814. doi:10.1038/nrmicro1991.

Muller, F., Brissac, T., Le Bris, N., Felbeck, H. and Gros, O. (2010) First description of giant Archaea (Thaumarchaeota) associated with putative bacterial ectosymbionts in a sulfidic marine habitat. *Environmental Microbiology* **12**, 2371–2383. doi:10.1111/j.1462-2920.2010.02309.x.

Pelczar, M. J., Chan, E. and Krieg, N. R. (2010) *Microbiology: Application Based Approach*. Tata McGraw-Hill Education, New Delhi.

Peng, X., Zhou, H., Yao, H., Li, J., Tang, S., Jiang, L. and Wu, Z. (2007) Microbe-related precipitation of iron and silica in the Edmond deep-sea hydrothermal vent field on the Central Indian Ridge. *Chinese Science Bulletin* **52**, 3233–3238. doi:10.1007/s11434-007-0523-3.

Peng, X., Zhou, H., Yao, H., Li, J. and Wu, Z. (2009) Ultrastructural evidence for iron

accumulation within the tube of Vestimentiferan *Ridgeia piscesae*. *Biometals* **22**, 723–732.

R Core Team (2013) *R: A Language and Environment for Statistical Computing*. 3.0.2. R Foundation for Statistical Computing, Vienna, Austria.

Rasmussen, B. (2000) Filamentous microfossils in a 3,235-million-year-old volcanogenic massive sulphide deposit. *Nature* **405**, 676–679.

Reysenbach, A. L. and Cady, S. L. (2001) Microbiology of ancient and modern hydrothermal systems. *Trends in Microbiology* **9**, 79–86. doi:10.1016/S0966-842X(00)01921-1.

Reysenbach, A.-L., Longnecker, K. and Kirshtein, J. (2000) Novel bacterial and archaeal lineages from an in situ growth chamber deployed at a Mid-Atlantic Ridge hydrothermal vent. *Applied and Environmental Microbiology* **66**, 3798–3806. doi:10.1128/AEM.66.9.3798-3806.2000.

Schneider, C. A., Rasband, W. S. and Eliceiri, K. W. (2012) NIH Image to ImageJ: 25 years of image analysis. *Nature Methods* **9**, 671–675.

Schrenk, M. O., Kelley, D. S., Delaney, J. R. and Baross, J. A. (2003) Incidence and diversity of microorganisms within the walls of an active deep-sea sulfide chimney. *Applied and Environmental Microbiology* **69**, 3580–3592. doi:10.1128/AEM.69.6.3580-3592.2003.

Schultze-Lam, S., Fortin, D., Davis, B. S. and Beveridge, T. J. (1996) Mineralization of bacterial surfaces. *Chemical Geology* **132**, 171–181. doi:10.1016/S0009-2541(96)00053-8.

Shpanskaya, A. Y., Maslennikov, V. V. and Little, C. T. S. (1999) Vestimnetiferan tubes from the Early Silurian and Middle Devonian hydrothermal biota of the Uralian palaeobasin. *Paleontologicheskii Zhurnal* **33**, 222–228.

Sievert, S. and Vetriani, C. (2012) Chemoautotrophy at deep-sea vents: past, present, and future. *Oceanography* **25**, 218–233. doi:10.5670/oceanog.2012.21.

Takai, K., Nakagawa, S., Reysenbach, A.-L. and Hoek, J. (2006) Microbial ecology of mid-ocean ridges and back-arc basins. In *Geophysical Monograph Series*, pp. 185–213. doi:10.1029/166GM10.

Thurber, A. R., Jones, W. J. and Schnabel, K. (2011) Dancing for food in the deep sea: bacterial farming by a new species of yeti crab. *PLOS ONE* **6**, e26243. doi:10.1371/journal.pone.0026243.

Verati, C., Donato, P. De, Prieur, D. and Lancelot, J. (1999) Evidence of bacterial activity

from micrometer-scale layer analyses of black-smoker sulfide structures (Pito Seamount Site, Easter microplate). *Chemical Geology* **158**, 257–269.

Weiss, M. C., Sousa, F. L., Mrnjavac, N., Neukirchen, S., Roettger, M., Nelson-Sathi, S. and Martin, W. F. (2016) The physiology and habitat of the last universal common ancestor. *Nature Microbiology* **1**, 16116. doi:10.1038/nmicrobiol.2016.116.

Westall, F., de Wit, M. J., Dann, J., van der Gaast, S., de Ronde, C. E. and Gerneke, D. (2001) Early Archean fossil bacteria and biofilms in hydrothermally-influenced sediments from the Barberton greenstone belt, South Africa. *Precambrian Research* **106**, 93–116. doi:10.1016/S0301-9268(00)00127-3.

Zaykov, V. V., Shadlun, T. N., Maslennikov, V. V. and Bortnikov, N. C. (1995) Yaman-Kasy sulphide deposit – ancient black smoker in the floor of the Uralian Palaeoocean. *Geologia Rudnih Mestorogdeniy* **37**, 511–529.

6 Discussion: unravelling the evolutionary history of vent and seep communities through the study of annelid tubes

Deep-sea hydrothermal vents and cold seeps constitute some of the most astonishing environments in our oceans within which life has flourished, forming ecosystems reliant on novel carbon-fixation strategies in the absence of sunlight. When and how hydrothermal vents and cold seeps were colonised by life, and what ancient vents and seeps were like, remain some of the most stimulating questions regarding these environments to date. There are also ever-increasing opportunities to answer the above questions, provided by emerging fossil discoveries from ancient vent and seep deposits, such as the on-going excavations from the hundreds of Cretaceous fossil seeps dotting the U.S. Western Interior (Metz, 2010; Landman *et al.*, 2012), Boreal seeps in Svalbard (Hammer *et al.*, 2011; Vinn *et al.*, 2014), and from VMS deposits in the Ural Mountains (Ayupova *et al.*, 2016a; b), and through the application of new methods through which to study this material. For example, compound-specific isotope analysis of nitrogen within amino acids is now being developed to attempt to detect chemosynthesis within the fossil record (Hagehashi *et al.*, 2016).

This thesis set out to enhance understanding of the evolutionary history of hydrothermal vent and cold seep communities, by improving our knowledge of tube-building annelid worms from these environments. A substantial part of this work included the examination of tube fossils from ancient vents and seeps, which are frequently encountered within such deposits but are generally poorly identified. These fossils can only be properly interpreted with sufficient knowledge of modern tube-dwelling annelids, which are the primary tube-builders within, and often dominate, modern vents and seeps. The initial objectives of this thesis were therefore to: (1) improve understanding of the evolutionary biology of lesser-studied vent and seep tubeworms, (2) examine the range of morphologies and morphological plasticity exhibited by the main tube-dwelling vent and seep annelid lineages, and (3) to explore fossilisation of annelid tubes within vent and seep environments. This thesis also intended to use the above information to (4) better interpret the fossil record of tubes from ancient vents and seeps, and (5) provide insights into the palaeoecology of these environments.

Using cross-cutting themes distilled from the thesis objectives as structure, here I will synthesise the major findings of this thesis while also discussing how they have advanced understanding and can lead to future research directions.

6.1 Diversity of annelid tubes from hydrothermal vents and cold seeps

The discovery of vents and seeps spurred renewed scientific interest in the tubes made by annelids, due to the prominence of annelid tube-builders within these environments and the desire to understand how tubes help their inhabitants to deal with the conditions presented by vents and seeps (Gaill and Hunt, 1986). Annelids build tubes that can exhibit diverse morphologies at a range of scales, from tube cluster to ultrastructure, between and within species, and can also have diverse compositions. The above diversity is demonstrated by the annelid occupants of hydrothermal vents and cold seeps, and has significant implications for identifying tubular fossils from ancient vent and seep environments. In this thesis I have made several important discoveries regarding the morphological and compositional diversity of annelid tubes from vents and seeps:

1. A comprehensive analysis of organic constituents of alvinellid, chaetopterid and siboglinid tubes confirms that chaetopterid tubes do not contain chitin. Different lineages of vent and seep dwelling annelids can use different organic compounds in their tubes, hence the tube constituents can potentially be taxonomically informative. However, while remnants of organic material from the original tube walls are retained after fossilisation particularly at cold seeps, diagnostic compounds such as chitin likely degrade during the early stages of tube fossilisation (Chapter 4).
2. I show for the first time that cladistics can be applied to infer the broad taxonomic identity of extant vent and seep annelids, when tube morphological and compositional features are coded as characters. This suggests that the same technique can be used to improve identifications of fossil material, if sufficient details are retained by a tube during its fossilisation (Chapter 4).
3. Through a detailed (morphological and genetic) investigation of an Antarctic population belonging to the poorly-studied siboglinid lineage *Sclerolinum*, I have found that the species *S. contortum* exhibits morphological plasticity with respect to the sinuosity of the anterior portion of its tube. This species also has a remarkable

bipolar distribution spanning the Arctic to the Antarctic, but exhibits limited gene flow between more distant populations (Chapter 2).

Investigations into the compositions of annelid tubes are key to understanding their properties, the suitability of these biomaterials for a range of applications, and can shed insights into annelid evolution. The tubes of frenulates were the first among the siboglinids to have their composition assessed, revealing them to contain β-chitin (Brunet and Carlisle, 1958; Blackwell *et al.*, 1965; Foucart *et al.*, 1965), followed by those of the vestimentiferans (Gaill and Hunt, 1986; Shillito *et al.*, 1995). This thesis has confirmed chitin in the tubes of *Sclerolinum*, and this polysaccharide has also recently been detected spionid and oweniid tubes (Guggolz *et al.*, 2015). Chitin is an abundant polymer in nature used in a variety of structures by at least 19 animal phyla (Willmer, 1990), and in annelids is also used for the construction of jaws and chaetae (Daly, 1973). The annelid family Oweniidae is resolved at the base of the annelid tree by the latest phylogenetic assessments (Weigert *et al.*, 2014), suggesting that many annelids may have the potential to use chitin for tube-building. However, the finding of this study that chaetopterids and the genus *Alvinella* do not incorporate this polymer into their tubes highlights the diversity of organic compounds that may be employed by annelids to build durable tubes that can persist and protect their inhabitant even within the extreme conditions presented by vent and seep environments (Gaill and Hunt, 1986). The tubes of *Chaetopterus* have recently been shown to possess high thermal and chemical stability (Shah *et al.*, 2014), and to have considerable strength as a result of the orientation of organic nano-filaments. This genus has not yet been found to occupy vents and seeps, however these characteristics suggest that tube features that enable survival within other marine environments may also facilitate annelids with robust tube types to occupy vents and seeps.

Although compounds such as chitin do not appear to fossilise well at vents and seeps (Chapter 4), having an understanding of how annelid tube composition varies among and within different lineages can still be useful for fossil identification in cases where tube organics are exceptionally well preserved. As some remnant organic matter is still retained within fossil vent and seep tubes, it may still be possible to identify fossil tubes using their compositions through the use of additional techniques that target other aspects of the preserved organics. Research into the composition and structure of the diverse tubes produced by annelids also has utility for materials engineering such as in the construction of pipes (Shah *et al.*, 2014, 2015) and waste-management solutions (Morin and Dufresne,

2002), and will likely be revealed to have further applications within a context of increasing demand for sustainable, high-performance natural materials.

Figure 6.1 Differentiation of siboglinid tubes along their length. **A**, anterior region of a *Galathealinum arcticum* (frenulate) tube, scale bar is 1 mm. **B,** middle tube regions of the tube pictured in **A**, scale bar is 1 mm. **C,** anterior region of a *Seepiophila jonesi* (vestimentiferan) tube, scale bar is 5 mm. **D,** middle and posterior tube regions of the tube pictured in **C**, scale bar is 5 mm.

Annelid tubes can demonstrate high morphological diversity that can vary between species, within a species, and also along the length of a tube (Figure 6.1), making it particularly difficult to characterise, and compare to fossil tubes that have often undergone significant alteration during fossilisation, and for which only fragments are normally available. This is further compounded by convergent tube morphologies between distantly related annelid families (Kiel and Dando, 2009). These difficulties highlight the need for a broad-scale review of annelid tube characteristics, to determine if the builders of ancient vent and seep tubes can ever be identified with any certainty.

In this thesis I present the first attempt to compare annelid tube morphology in detail across a range of families, focusing on organic-walled tubes at vents and seeps and employing a more objective, cladistic approach, with fossil identification in mind. My cladistic analysis of modern tubes only (Chapter 4; Figure 4.23) demonstrates that tube variability can be distilled within a character-coding framework, and that the defined characters are effective in determining the broad identity of the tube. This suggests that it would be possible to identify well-preserved fossil tubes from these environments with a degree of certainty, and that tubes are useful for assessing the evolutionary history of tubicolous annelid lineages within vents and seeps. This approach was also key in providing

a better understanding of which tube characters are homoplastic, and of which fossil tubes cannot be identified with certainty based on currently available specimens and the morphological features they exhibit. The tube morphological analysis presented here forms a foundation for a larger comparison of tubes across many marine environments, and one which also incorporates other types of data as well as the tubes of non-annelids. It also paves the way towards a more careful and objective way of analysing tubes and their morphology. It is therefore important that authors of modern tubicolous animal descriptions provide a detailed description of tubes, in addition to the animal soft tissues. Only then can a complete picture of the degree of tube similarity between annelid lineages emerge, and also in relation to the tubes of non-annelids.

That the tubes made by a particular species of annelid can exhibit diversity in certain aspects of their morphology has previously been noted for the tubes of the siboglinid *Ridgeia piscesae*, in which case it had important taxonomic implications (Southward *et al.*, 1995), and can also be observed in *Lamellibrachia anaximandri* tubes (Southward *et al.*, 2011). A similar discovery for the tubes of *Sclerolinum contortum* within this thesis suggests that the potential for plasticity in aspects of tube morphology is widespread within the Siboglinidae family, and that the range of morphologies a tube made by a particular annelid may exhibit also needs to be considered for fossil identifications and to be incorporated into tube character coding systems. Studies of *S. contortum*, a species which was named after its contorted tube morphology, also highlight the value of genetic tools in assessing how taxonomically informative aspects of tube morphology are.

In addition to understanding the diversity of morphology an annelid tube may exhibit, genetic tools also enable us to understand other important aspects of vent and seep-dwelling animals such as their dispersal pathways and abilities, as well as range of habitat preferences. This information enables better interpretations of the fossil record, and allows further details such as ecological information to be gleaned from it. It can allow the prediction of what other types of palaeo-habitats may contain the fossils of vent and seep fauna, and also has significant collateral applications such as in the assessment of species vulnerability to human impacts in important deep-sea habitats such as hydrothermal vents and cold seeps (Hilário *et al.*, 2015; Baco *et al.*, 2016).

6.1.1 Recommendations for future research

Variation in tube composition across the annelid phylum is still not well understood, and it often appears that tube composition does not correspond with current phylogenies for the annelid phylum. For example, calcareous tubes are observed within serpulids, sabellids, and cirratulids (Vinn *et al.*, 2008), however cirratulids seem to not be closely related to the former two families but instead to siboglinids, which build chitinous tubes (Weigert *et al.*, 2014). Determining the compositions of tubes made by the breadth of annelid lineages would give a wider understanding of tube diversity within this phylum, providing a dataset that could be tested in terms of both functional and evolutionary significance. This may also shed insights into the occupation of extreme environments such as hydrothermal vents and cold seeps by diverse tube-building annelid lineages.

Additional techniques targeting tube biomarkers, such as compound-specific nitrogen isotopes (Hagehashi *et al.*, 2016), could also be employed to help identify problematic fossil tubes. This technique may provide the exciting possibility to identify metabolic signals (e.g. thiotrophy for vestimentiferans) preserved within fossil tube organic constituents from vents and seeps.

The tube character matrix provided here could be integrated with additional datasets such as DNA and soft tissue morphological characters. By scoring tube characters for members of annelid families across the sedentary and errant lineages, and by mapping the better-identified tube fossils to nodes within phylogenetic trees, deeper branches of the resulting trees may be better resolved (L.A. Parry, *personal communication*). In addition, a character scoring system whereby different regions (Figure 6.1) as well as morphotypes of a tube are scored separately could also be trialled to determine if fossil resolution in cladistic analyses is improved.

6.2 Fossilisation of annelid tubes within hydrothermal vents and cold seeps

In addition to providing conditions in which life can thrive, vents and seeps also present conditions under which inhabitants may be readily fossilised - from microbes to members of the animal community. Taphonomic and fossilisation studies are essential to understanding how tubes and other biogenic structures are altered during their conversion to mineral form. Several types of fossils from vents and seeps, such as microbial cell walls and annelid tubes, are structures that were originally purely organic in composition, and

remarkably, vents and seeps provide the otherwise rare conditions (Briggs, 2003) under which such non-mineralised structures may also be preserved. I present several key findings relating to the fossilisation of tubes within hydrothermal vents and cold seeps:

1. Annelid tubes at hydrothermal vents can be fossilised with hitherto unknown details, such as microbial communities that occupied tube wall surfaces. These microorganisms can be exceptionally-well preserved, demonstrating even sub-cellular details (Chapter 3). I also observed similarly-fossilised microorganisms along the walls of tube fossils from the oldest known hydrothermal vent community (Chapter 5).
2. Detailed preservation of tube morphology that can enable more conclusive identifications of fossils is more likely at hydrothermal vents. However, particularly at seep sites, tubes may be altered beyond definitive recognition through fossilisation (Chapter 4).
3. A detailed analysis of the full mineralisation process of *Alvinella* tubes at hydrothermal vents revealed that these organic structures are rapidly preserved by both iron sulphides and silica, most commonly resulting in a fossil tube comprised of many concentric layers of colloform pyrite. Silica was also found to play an important role in preserving the fibrous structure of organic tube layers (Chapter 3).
4. Unusual vent systems may also provide opportunities for fossilisation of vent fauna, albeit of a different nature to fossilisation within black smoker-type vent settings. The small tubes of *Sclerolinum* may be preserved inside a sulphurous-silica matrix within the hydrothermal vents of Kemp Caldera. Their fossilisation within this setting will likely retain the broad morphology of tube clumps but not ornamental details of tube walls (Chapter 2).

Fossil microbial filaments have been reported from seeps (Peckmann *et al.*, 2004) and have also been suggested to fossilise within vents (Maginn *et al.*, 2002; Peng *et al.*, 2009). In this thesis, I clearly demonstrate the fossilisation of microorganisms at vents, and that fossilised microorganisms can also be detected within ancient vent environments. Such fine-scale preservation by both pyrite and silica, even of structures within filaments less than 1 μm in diameter, has not previously been observed within high-temperature vent environments, and greatly changes our understanding of the scales at which fossilisation can occur within this setting. In combination with iron oxide deposits of hydrothermal vent origin (Little *et*

al., 2004), iron sulphides also appear to be key deposits for which to search for ancient life at hydrothermal vents.

Because of their proposed links to the origin of life on Earth (Martin *et al.*, 2008; Deamer and Georgiou, 2015; Weiss *et al.*, 2016), hydrothermal systems also constitute major environments within which to search for life on other planets (Pirajno, 2009; Shapiro and Schulze-Makuch, 2009). Several planetary bodies within our solar system including Jupiter's satellites Europa and Ganymede, and Saturn's moon Enceladus, possess liquid water and are geologically active (Pirajno, 2009). Mars is also considered to have possessed these features in the past (Schulze-Makuch *et al.*, 2007). These characteristics suggest that the above planetary bodies may harbour (or have harboured) hydrothermal systems within which extraterrestrial life may exist. Thus, the data presented here will also be informative for future astrobiological studies, based on sample return or data from meteorites.

In this thesis I also show that in many instances, fossilisation at vents and seeps alters annelid tubes significantly by removing signatures of characteristic organic tube compounds and by obscuring aspects of morphology. This has crucial implications for tube identification and thereby evolutionary history, and demonstrates that with many fossil vent tubes, the information that can presently be gleaned from them is not enough to confidently identify them. Such problems are also highlighted for the harder structures remaining upon the fossilisation of other taxa: their morphology may be insufficient to obtain an accurate identification of the fossil, and can distort phylogenies (Sansom and Wills, 2013; Sansom, 2015). It is important to highlight when observed fossil characters are inadequate for confident identification, and also to understand how the robust structures made by organisms that may be fossilised are altered by this process. Experimental fossilisation can be very useful within this respect (Briggs and McMahon, 2016), and results presented in Chapter 3 demonstrate that such experiments can even be performed within the extreme setting of hydrothermal vents.

Vents and seeps are very heterogeneous environments and as highlighted through studies of *Alvinella* tube mineralisation, fossilisation of just one type of tube can be highly variable (Figure 6.2). This variability also needs to be considered when attempting identifications of ancient vent and seep tubes. Despite variations in the appearance of many mineralised *Alvinella* tubes, aspects such as the widespread occurrence of collomorphic pyrite texture (Figure 6.3) associated with mineralised walls, and the involvement of silica in mineralisation (Figure 6.2) were consistently observed for these tubes. Authigenic pyrite and silica are known for their importance in preserving soft tissues within soft sediment

and terrestrial hot spring environments (Briggs and McMahon, 2016), and this thesis demonstrates the significance of these minerals for replicating organic structures within hydrothermal vents. The association between colloform pyrite and mineralised *Alvinella* tube walls (Figure 6.3) also suggests that colloform pyrite formation may potentially result from the interaction of organic tube decay products and minerals, and therefore could act as a proxy for organic matter in the fossil record of vents.

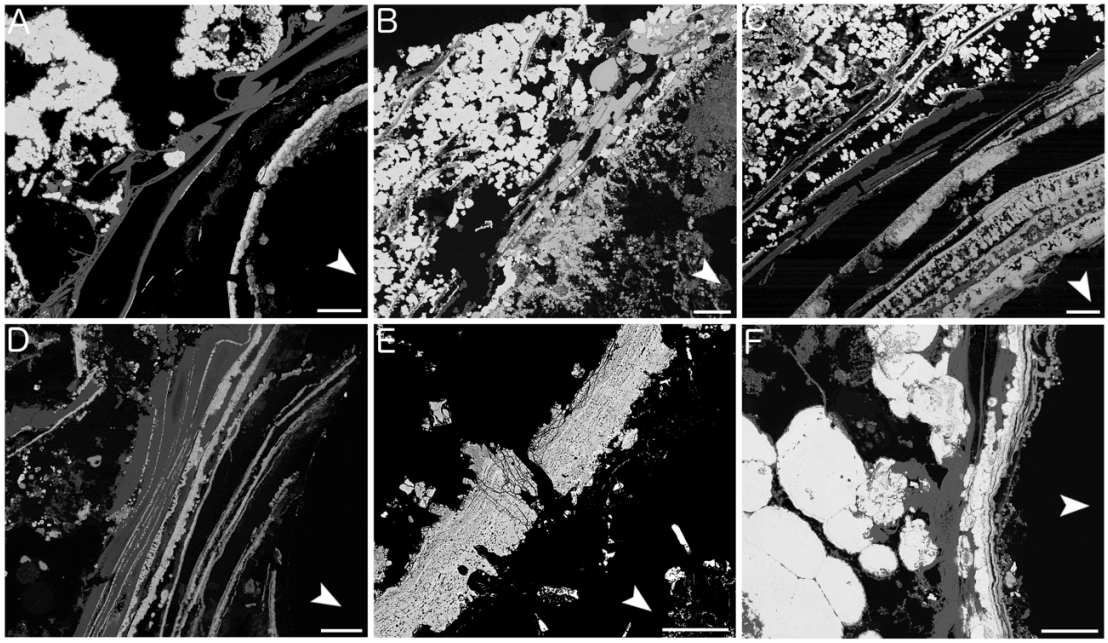

Figure 6.2 Different preservational styles of *Alvinella* tube walls. All images represent transverse sections of mineralised *Alvinella* spp. tubes. **A,** tube preserved as a thin inner pyrite band and several thin outer silica bands, scale bar is 200 μm. **B,** tube preserved as several thin pyrite bands encased in other minerals, scale bar is 200 μm. **C,** tube preserved by many pyrite bands that exhibit finger-like colloform pyrite growth. Some silica layers are also present towards the outer tube wall, scale bar is 200 μm. **D,** a tube in which thin pyrite bands are present within a thick outer layer of silica, scale bar is 200 μm. **E,** tube preserved as one thick layer of colloform pyrite, scale bar is 100 μm. **F,** tube wall preserved by pyrite with an ovoid texture, scale bar is 200 μm. White arrows point towards tube interior.

Fossilisation within vents has also been shown to be incredibly rapid, occurring in less than one year but likely on a faster timescale of days to several weeks (Pradillon *et al.*, 2009). Such rapid pyrite mineralisation has been observed in laboratory experiments on plant remains (Grimes *et al.*, 2001; Rickard *et al.*, 2007), and the data presented here adds to understanding of the environments within which such pyritisation can occur, and how ancient evidence of life may be interpreted. It also likely accounts for the level of detail of hydrothermal vent fossils reported in this thesis - of fibres from tube walls, sub-micron details of microbial filaments, and tube wall ornamentation. While pyrite and silica are important for preservation in mid-ocean ridge and arc-type hydrothermal vent settings,

conditions may be altogether different at vents associated with submerged volcanoes. Observations made within Chapter 2 suggest that within the sulphurous vents of Kemp Caldera, only moulds of *Sclerolinum* tubes would likely remain over geological time scales, but environmental conditions, tube clump morphology and tube size would likely be the remaining characters upon which tube identifications could be based.

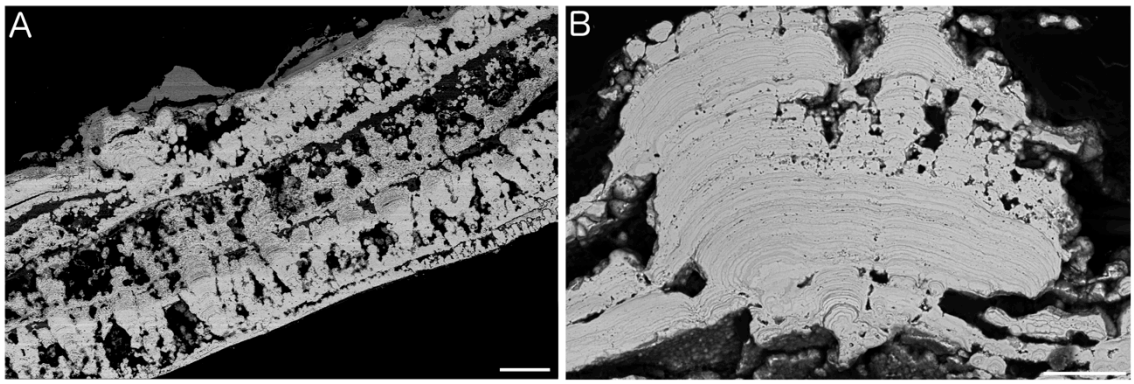

Figure 6.3 Colloform pyrite preserving *Alvinella* spp. tube walls. **A,** mineralised *Alvinella* tube wall characterised by preservation through the growth of finger-like colloform pyrite, scale bar is 100 μm. **B,** detail of many-layered colloform pyrite from the mineralised wall of an *Alvinella* tube, scale bar is 50 μm.

6.2.1 Recommendations for future research

The importance of research into decay and fossilisation within a range of settings is increasingly recognised (Raff *et al.*, 2008, 2013; Farrell *et al.*, 2013), and is also greatly needed within vents and seeps environments to further inform interpretations of their fossil record. The fossilisation experiments at vents from which a number of *Alvinella* tubes were collected (Supplementary Figure C.1) also show that tube morphological aspects may be altered if significant time is permitted for decomposition before mineralisation; the collars of *Tevnia jerichonana* tubes were lost when these tubes were emplaced within a diffuse flow vent setting during a fossilisation experiment (C.T.S. Little, *personal communication*). These effects warrant further study, as do comparisons between various types of annelid tube and robust structures produced by a range of animal phyla and microorganisms. Such studies should also try to perform experiments across a range of physico-chemical conditions that may be presented by different, as well as within particular, vent and seep sites.

At present, our understanding of fossilisation biases regarding vent and seep communities is also limited. Fossilisation studies have the potential to demonstrate which types of organisms and structures may be preferentially preserved at vents and seeps, and which

aspects of the community are unlikely to be found as fossils. This can enable better estimation of the original diversity of ancient vent and seep communities, and will also improve understanding of what types of fossils might be expected to occur on other planets.

6.3 Evolutionary history of hydrothermal vent and cold seep communities

Problems with the identification of tube fossils from ancient vents and seeps have presented a major challenge to our understanding of the evolutionary history of deep-sea chemosynthetic communities. Much remains to be learned about the builders of tube fossils from ancient vents and seeps, however despite the difficulties that these tube fossils can pose for palaeontologists, the work presented in this thesis demonstrates that their study is very much worthwhile. Investigations into the diversity of tubes from both modern fossil hydrothermal vent and cold seep environments, the characteristics of their builders, and into how these tubes fossilise within vents and seeps, have improved understanding of the evolutionary history of vent and seep communities through the following findings:

1. Detailed comparative analyses of modern and fossil tubes from vent and seep environments suggest that two fossil tube types of from ancient vent deposits were likely made by the vestimentiferan lineage of Siboglinidae. After discoveries of Cretaceous-age *Osedax* fossils (Danise and Higgs, 2015), this provides a second piece of independent evidence which suggests that siboglinids originated earlier than implied by molecular clock age estimates, within the Mesozoic. Furthermore, there appears to be no compelling evidence that vent tubes from the Palaeozoic were made by siboglinids (Chapter 4).

2. No ancient vent fossil tubes closely resemble the mineralised tubes of *Alvinella*, which at present corresponds with suggestions based on molecular clock age estimates that this is a relatively recent lineage (Chapter 3).

3. Remarkable habitat plasticity may be exhibited by just one species within the siboglinid genus *Sclerolinum*, *S. contortum*. This likely enabled its colonisation of distant chemosynthetic sites, and may have facilitated the persistence of this lineage over evolutionary timescales (Chapter 2).

4. Microorganisms fossilised alongside ancient tube fossils from the earliest known hydrothermal vent community suggest that ecological associations, whereby

microorganisms colonise the surfaces of tube-dwelling metazoans, have a very long fossil history that stretches into the Silurian (Chapter 5).

As new tube fossil interpretations emerge suggesting that siboglinids may even have occupied marine environments during the Proterozoic (Moczydłowska *et al.*, 2014), an analysis that constrains the unique aspects of tube morphologies made by this prominent vent and seep tubicolous family, such as that presented in Chapter 4 of this thesis, becomes ever more necessary. This analysis showed that even well-preserved Palaeozoic vent fossils such as *Yamankasia rifeia* and *Tevidestus serriformis* do not demonstrate sufficient tube characters to have definitively been made by siboglinids, thereby confirming doubts that the this family has ancient origins within the Silurian or earlier (Vrijenhoek, 2013). The finding presented in this thesis, that the best fossil evidence for fossil vent and seep vestimentiferans is from the Mesozoic, also does not reflect current molecular clock age estimates. However, this is consistent with the finding of Mesozoic-age *Osedax* fossils (Danise and Higgs, 2015) and provides another piece of independent evidence which indicates that more derived siboglinid lineages were already present by the mid-Cretaceous, and that a recalibration of molecular clocks for the Siboglinidae family is greatly needed. While the lack of an ancient fossil record for the genus *Alvinella* is consistent with recent molecular age estimates for this lineage, it may also reflect its restricted distribution within the East Pacific Rise. The fossil record of hydrothermal vents is inherently biased towards communities which occupied back-arc basin vents (Galley *et al.*, 2007), which would poorly represent lineages restricted to mid ocean ridges.

For siboglinids at hydrothermal vents and cold seeps, adaptation to a range of reducing conditions combined with an ability for distant dispersal, as observed within the vestimentiferan and *Sclerolinum* lineages (Figure 6.4), may be indicative of evolutionary longevity. The same could also be true for the siboglinid genus *Osedax*, which it is now recognised can live on a vast diversity of bone types such as the bones of fish (Rouse *et al.*, 2011) as well as those of plesiosaurs during the Cretaceous (Danise and Higgs, 2015). While it appears unlikely that vent and seep environments acted as stable refugia where relict faunas survived unperturbed for hundreds of millions of years (Little and Vrijenhoek, 2003; Kiel and Little, 2006; Vrijenhoek, 2013), perhaps once certain animal lineages had adapted to utilise the range of conditions presented by reducing environments, and developed dispersal abilities to be able to locate distant reducing conditions, they were able to persist over longer evolutionary timescales despite disturbance events.

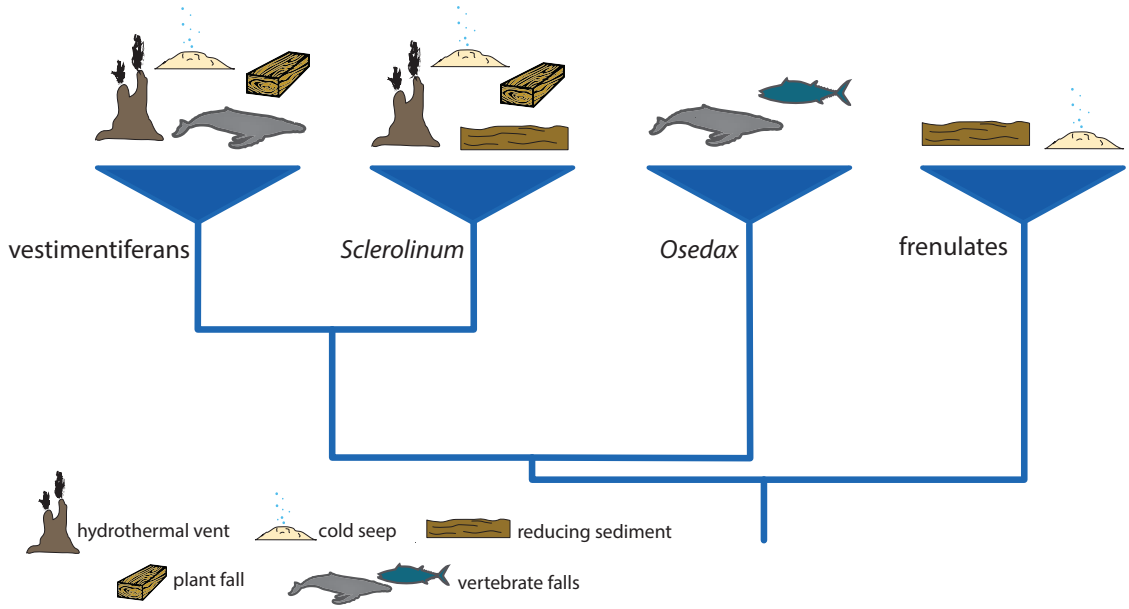

Figure 6.4 Adaptations of Siboglinidae to a range of reducing conditions mapped onto a phylogeny for this family (Chapter 2). The most ancestral lineage, the frenulates, are currently known to inhabit only reducing sediments and seeps. The genus *Osedax* is highly specialised to feeding on bones, but can survive on a range of bone types. The genus *Sclerolinum* and the vestimentiferans have broader habitat preferences, being able to also survive on plant-based organic falls and also at hydrothermal vents and cold seeps.

Although the majority of modern vent and seep fauna appear to have originated during the Cenozoic (Kiel, 2010; Vrijenhoek, 2013), animal lineages such as abyssochrysoid gastropods had already occupied vent and/or seep environments by the Jurassic (Kiel *et al.*, 2008; Kaim and Kelly, 2009). This suggests that rather than there being a common origination time period for modern vent and seep fauna, a more complex scenario may be more probable whereby the histories of occupation of these environments were likely individual to particular lineages, and now appear to be spread within the Cenozoic and Mesozoic. A similar situation is also exemplified by bivalve molluscs, for which the evolutionary pathways of specialisation to reducing conditions also appear to vary between different lineages. For example, solemyids are an ancient taxon dating to the early Ordovician that has likely been chemosymbiotic throughout its history (Taylor and Glover, 2010), whereas bathymodiolin mussels are a recent radiation of the Mytilidae family that seem to have colonised vents and seeps several times from organic falls (Duperron, 2010), and have a fossil record dating to the Eocene (Kiel and Little, 2006). Within the annelids, the history of *Alvinella* within vents currently also appears to have been different to that of the siboglinids. Varying histories within vents and seep environments even within closely related lineages may also reflect the longevities of different vent and seep settings - some back-arc basins only have a lifespan of 10 million years (Woodcock, 2004), and if also

poorly connected to other vents and seeps, may drive the rapid evolution of the existing deep-sea background fauna to utilise the high productivity within this setting. Such effects may form part of the explanation for surprising patterns of modern hydrothermal vent biogeography, such as the distinctive fauna of the East Scotia Ridge (Rogers *et al.*, 2012).

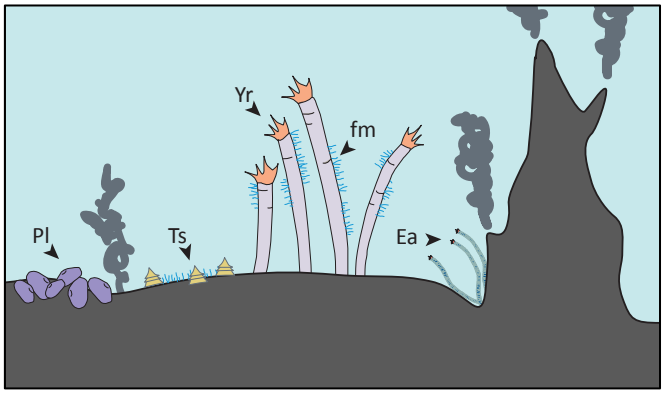

Figure 6.5 Reconstruction of the Yaman Kasy hydrothermal vent palaeo-community. Pl, *Pyrodiscus lorraine*; Ts, *Thermoconus shadlunae*; Yr, *Yamankasia rifeia*; fm, filamentous microorganisms; Ea, *Eoalvinellodes annulatus*.

By demonstrating the preservation of microorganisms even within a Silurian vent deposit, this thesis was also able to gain insights into the palaeoecology of the oldest known hydrothermal vent community. While it is still unknown whether members of the Yaman Kasy vent community contained microbial endosymbionts, the occurrence of microbial mats on animal surfaces within modern vent environments is known to be an important adaptation and feeding mechanism for a range of fauna. The results presented here allow us to gain a better understanding of very early vent communities and how they may have functioned (Figure 6.5), even when they are very remote in time.

6.3.1 Recommendations for future research

Firstly, an new molecular clock analysis that incorporates recent *Osedax* fossil discoveries (Danise and Higgs, 2015) and the vent and seep tube fossil identifications presented here, is needed to provide an updated estimate for the age of Siboglinidae. Phylogeographic studies of lesser studied siboglinids, such as the frenulates, could also be performed to gain a more complete understanding of the evolutionary history of siboglinids within reducing environments (Figure 6.4). Many frenulates occur in reducing sediments but some types transition into seeps, such as within the Gulf of Cadiz (Hilário *et al.*, 2010), and at HMMV

(Smirnov, 2000). Improving genetic sampling for this diverse group, and integrating it with habitat and distributional information, may yield interesting insights into the evolutionary pathways of specialism to a range of reducing environments for the Siboglinidae family.

Did animals occupy vents and seeps during the Silurian, or earlier? Although there are suggestions that animals had occupied vent environments earlier than the Silurian from Cambrian barite deposits in China (Yang *et al.*, 2008), more robust evidence of this is needed. There are however additional VMS deposits that pose as good candidates to search for animal fossils, such as the Ordovician Løkken and Cambrian Rosebery deposits. Assessing the presence of animal fossils within such deposits would enable determination of whether animals were able to move into chemosynthetic environments soon after their major radiation during the Cambrian. Unmetamorphosed parts of these deposits could also be examined for microbial fossils, and interactions they may have had with animals if they are also present.

Although the microbial metabolisms that drove chemosynthesis within ancient hydrothermal vent ecosystems may be expected to be similar to those observed within vents today, they are as yet unknown. Recent studies on ancient microfossils from other environments have demonstrated that their sulphur cycling metabolisms can be detected through the examination of stable isotopes of sulphur, even on very small spatial scales (Wacey *et al.*, 2010; Schopf *et al.*, 2015). Similar analyses could be attempted for the Yaman Kasy microfossils, to determine if they were chemosynthetic or were involved in other sulphur cycling pathways, thus providing information on their roles within the ancient vent community. Physiological studies on non-vent endemic fauna that have moved into vent and seep environments could also be attempted, to assess how they deal with the conditions presented by vents and seeps. These could offer insights into how, and over what timescales, more intricate adaptations to vent and seep environments arose.

6.4 Concluding remarks

Since their discovery, chemosynthetic environments have revolutionised our understanding of biology, and are even suggested to be where life on our planet may have begun. Animals are considered to have colonised vents and seeps perhaps 100 million years after undergoing major radiations within other marine environments, by which time they were capable of coping with sulphidic conditions to harness the energy within these settings.

Investigating the evolutionary history of these fascinating deep-sea communities can provide vital insights into the evolution of life on Earth, but presents major challenges due to the fragmentary nature of fossil evidence, and the difficulties in accessing modern vents and seeps for comparisons. Thus, this field requires the use of a diverse range of tools and approaches. To understand the history of tube-building annelids at vents and seeps, this thesis integrated genetic and morphological taxonomy, cladistics, population genetics, fossilisation experiments, mineralogy, and both organic and mineralogical chemical analysis. These studies have provided a clearer understanding of which annelid groups occupied vents and seeps over geological time, but also have far-reaching implications for a range of other fields such as palaeoecology, deep-sea biology, organic preservation and astrobiology. They also illuminate future research directions that can provide further exciting opportunities to understand long-term evolutionary change within, as well as the historic context of the modern deep oceans.

6.5 References

Ayupova, N. R., Maslennikov, V. V., Sadykov, S. A., Maslennikova, S. P. and Danyushevsky, L. V. (2016a) Evidence of Biogenic Activity in Quartz-Hematite Rocks of the Urals VMS Deposits. In *Biogenic—Abiogenic Interactions in Natural and Anthropogenic Systems* (ed. Frank-Kamenetskaya, O. V., Panova, E. G. and Vlasov, D. Y.), pp. 109–122. Springer International Publishing doi:10.1007/978-3-319-24987-2_10.

Ayupova, N. R., Maslennikov, V. V., Tessalina, S. G., Shilovsky, O. P., Sadykov, S. A., Hollis, S. P., Danyushevsky, L. V., Safina, N. P. and Statsenko, E. O. (2016b) Tube fossils from gossanites of the Urals VHMS deposits, Russia: Authigenic mineral assemblages and trace element distributions. *Ore Geology Reviews*. doi:10.1016/j.oregeorev.2016.08.003.

Baco, A. R., Etter, R. J., Ribeiro, P. A., von der Heyden, S., Beerli, P. and Kinlan, B. P. (2016) A synthesis of genetic connectivity in deep-sea fauna and implications for marine reserve design. *Molecular Ecology* **25**, 3276–3298. doi:10.1111/mec.13689.

Blackwell, J., Parker, K. and Rudall, K. (1965) Chitin in pogonophore tubes. *Journal of Marine Biological Association of the UK* **45**, 51–54.

Briggs, D. E. G. (2003) The role of decay and mineralization in the preservation of soft-

bodied fossils. *Annual Review of Earth and Planetary Sciences* **31**, 275–301. doi:10.1146/annurev.earth.31.100901.144746.

Briggs, D. E. G. and McMahon, S. (2016) The role of experiments in investigating the taphonomy of exceptional preservation. *Palaeontology* **59**, 1–11. doi:10.1111/pala.12219.

Brunet, P. C. J. and Carlisle, D. B. (1958) Chitin in Pogonophora. *Nature* **182**, 1689–1689. doi:10.1038/1821689a0.

Daly, J. M. (1973) Behavioural and secretory activity during tube construction by *Platynereis dumerilii* Aud & M. Edw. [Polychaeta: Nereidae]. *Journal of the Marine Biological Association of the United Kingdom* **53**, 521. doi:10.1017/S0025315400058732.

Danise, S. and Higgs, N. D. (2015) Bone-eating *Osedax* worms lived on Mesozoic marine reptile deadfalls. *Biology Letters* **11**, 20150072.

Deamer, D. W. and Georgiou, C. D. (2015) Hydrothermal conditions and the origin of cellular life. *Astrobiology* **15**, 1091–1095. doi:10.1089/ast.2015.1338.

Duperron, S. (2010) The diversity of deep-sea mussels and their bacterial symbioses. In *The Vent and Seep Biota* (ed. Kiel, S.), pp. 137–167. Springer Netherlands, Dordrecht. doi:10.1007/978-90-481-9572-5_6.

Farrell, U. C., Briggs, D. E. G., Hammarlund, E. U., Sperling, E. A. and Gaines, R. R. (2013) Paleoredox and pyritization of soft-bodied fossils in the Ordovician Frankfort Shale of New York. *American Journal of Science* **313**, 452–489. doi:10.2475/05.2013.02.

Foucart, M. F., Bricteux-Gregoire, S. and Jeuniaux, C. (1965) Composition chimique du tube d'un pogonophore (*Siboglinum* sp.) et des formations squelettiques de deux pterobranches. *Sarsia* **20**, 36–41.

Gaill, F. and Hunt, S. (1986) Tubes of deep sea hydrothermal vent worms *Riftia pachyptila* (Vestimentifera) and *Alvinella pompejana* (Annelida). *Marine Ecology Progress Series* **3**, 267–274.

Galley, A. G., Hannington, M. D. and Jonasson, I. R. (2007) Volcanogenic massive sulphide deposits. In *Mineral Deposits of Canada: A Synthesis of Major Deposit-Types, District Metallogeny, the Evolution of Geological Provinces, and Exploration Methods* (ed. Goodfellow, W. D.), pp. 141–161. Geological Association of Canada, Mineral Deposits Division, Special Publication No. 5.

Grimes, S. T., Brock, F., Rickard, D., Davies, K. L., Edwards, D., Briggs, D. E. G. and

Parkes, R. J. (2001) Understanding fossilization: Experimental pyritization of plants. *Geology* **29**, 123–126. doi:10.1130/0091-7613(2001)029<0123:UFEPOP>2.0.CO;2.

Guggolz, T., Henne, S., Politi, Y., Schütz, R., Mašić, A., Müller, C. H. G. and Meißner, K. (2015) Histochemical evidence of β-chitin in parapodial glandular organs and tubes of Spiophanes (Annelida, Sedentaria: Spionidae), and first studies on selected Annelida. *Journal of Morphology* **276**, 1433–1447. doi:10.1002/jmor.20432.

Hagehashi, D., Jenkins, R. G., Goto, A. S., Chikaraishi, Y. and Hasegawa, T. (2016) Evaluation of early diagenetic influence on nitrogen isotopes within fossil amino acids: towards an estimation of ancient food webs. In *1st International Workshop on Ancient Hydrocarbon Seep and Cognate Communities*, p. 11. 13-17 June 2016, Warsaw, Poland.

Hammer, Ø., Nakrem, H. a., Little, C. T. S., Hryniewicz, K., Sandy, M. R., Hurum, J. H., Druckenmiller, P., Knutsen, E. M. and Høyberget, M. (2011) Hydrocarbon seeps from close to the Jurassic–Cretaceous boundary, Svalbard. *Palaeogeography, Palaeoclimatology, Palaeoecology* **306**, 15–26. doi:10.1016/j.palaeo.2011.03.019.

Hilário, A., Johnson, S. B., Cunha, M. R. and Vrijenhoek, R. C. (2010) High diversity of frenulates (Polychaeta: Siboglinidae) in the Gulf of Cadiz mud volcanoes: A DNA taxonomy analysis. *Deep-Sea Research I* **57**, 143–150. doi:10.1016/j.dsr.2009.10.004.

Hilário, A., Metaxas, A., Gaudron, S. M., Howell, K. L., Mercier, A., Mestre, N. C., Ross, R. E., Thurnherr, A. M. and Young, C. (2015) Estimating dispersal distance in the deep sea: challenges and applications to marine reserves. *Frontiers in Marine Science* **2**, 1–14. doi:10.3389/fmars.2015.00006.

Kaim, A. and Kelly, S. R. A. (2009) Mass occurrence of hokkaidoconchid gastropods in the Upper Jurassic methane seep carbonate from Alexander Island, Antarctica. *Antarctic Science* **21**, 279–284.

Kiel, S. (2010) The fossil record of vent and seep mollusks. In *The Vent and Seep Biota* (ed. Kiel, S.), pp. 255–277. Springer Netherlands, Dordrecht. doi:10.1007/978-90-481-9572-5_8.

Kiel, S. and Dando, P. R. (2009) Chaetopterid tubes from vent and seep sites: implications for fossil record and evolutionary history of vent and seep annelids. *Acta Palaeontologica Polonica* **54**, 443–448. doi:10.4202/app.2009.0022.

Kiel, S. and Little, C. T. S. (2006) Cold-seep mollusks are older than the general marine mollusk fauna. *Science* **313**, 1429–1431. doi:10.1126/science.1126286.

Kiel, S., Campbell, K. A., Elder, W. P. and Little, C. T. S. (2008) Jurassic and Cretaceous gastropods from hydrocarbon seeps in forearc basin and accretionary prism settings, California. *Acta Palaeontologica Polonica* **53**, 679–703. doi:10.4202/app.2008.0412.

Landman, N. H., Cochran, J. K., Larson, N. L., Brezina, J., Garb, M. P. and Harries, P. J. (2012) Methane seeps as ammonite habitats in the U.S. Western Interior Seaway revealed by isotopic analyses of well-preserved shell material. *Geology* **40**, 507–510. doi:10.1130/G32782.1.

Little, C. T. S. and Vrijenhoek, R. C. (2003) Are hydrothermal vent animals living fossils? *Trends in Ecology & Evolution* **18**, 582–588. doi:10.1016/j.tree.2003.08.009.

Little, C. T. S., Glynn, S. E. J. and Mills, R. A. (2004) Four-hundred-and-ninety-million-year record of bacteriogenic iron oxide precipitation at sea-floor hydrothermal vents. *Geomicrobiology Journal* **21**, 415–429. doi:10.1080/01490450490485845.

Maginn, E., Little, C. T. S., Herrington, R. and Mills, R. (2002) Sulphide mineralisation in the deep sea hydrothermal vent polychaete, *Alvinella pompejana*: implications for fossil preservation. *Marine Geology* **181**, 337–356.

Martin, W., Baross, J., Kelley, D. and Russell, M. J. (2008) Hydrothermal vents and the origin of life. *Nature Reviews Microbiology* **6**, 805–814. doi:10.1038/nrmicro1991.

Metz, C. L. (2010) Tectonic controls on the genesis and distribution of late Cretaceous, Western Interior Basin hydrocarbon seep mounds (Tepee Buttes) of North America. *The Journal of Geology* **118**, 201–213. doi:10.1086/650181.

Moczydłowska, M., Westall, F. and Foucher, F. (2014) Microstructure and biogeochemistry of the organically preserved Ediacaran metazoan *Sabellidites*. *Journal of Paleontology* **88**, 224–239. doi:10.1666/13-003.

Morin, A. and Dufresne, A. (2002) Nanocomposites of chitin whiskers from *Riftia* tubes and poly(caprolactone). *Macromolecules* **35**, 2190–2199. doi:10.1021/ma011493a.

Peckmann, J., Thiel, V., Reitner, J., Taviani, M., Aharon, P. and Michaelis, W. (2004) A microbial mat of a large sulfur bacterium preserved in a Miocene methane-seep limestone. *Geomicrobiology Journal* **21**, 247–255. doi:10.1080/01490450490438757.

Peng, X., Zhou, H., Yao, H., Li, J. and Wu, Z. (2009) Ultrastructural evidence for iron accumulation within the tube of Vestimentiferan *Ridgeia piscesae*. *Biometals* **22**, 723–732.

Pirajno, F. (2009) Hydrothermal processes and systems on other planets and satellites: clues for the search of extraterrestrial life. In *Hydrothermal Processes and Mineral Systems*, pp.

1131–1211. Springer Netherlands, Dordrecht. doi:10.1007/978-1-4020-8613-7_12.

Pradillon, F., Zbinden, M., Le Bris, N., Hourdez, S., Barnay, A.-S. and Gaill, F. (2009) Development of assemblages associated with alvinellid colonies on the walls of high-temperature vents at the East Pacific Rise. *Deep-Sea Research II* **56**, 1622–1631. doi:10.1016/j.dsr2.2009.05.009.

Raff, E. C., Schollaert, K. L., Nelson, D. E., Donoghue, P. C. J., Thomas, C.-W., Turner, F. R., Stein, B. D., Dong, X., Bengtson, S., Huldtgren, T., Stampanoni, M., Chongyu, Y. and Raff, R. A. (2008) Embryo fossilization is a biological process mediated by microbial biofilms. *Proceedings of the National Academy of Sciences* **105**, 19360–19365. doi:10.1073/pnas.0810106105.

Raff, E. C., Andrews, M. E., Turner, F. R., Toh, E., Nelson, D. E. and Raff, R. A. (2013) Contingent interactions among biofilm-forming bacteria determine preservation or decay in the first steps toward fossilization of marine embryos. *Evolution & Development* **15**, 243–256. doi:10.1111/ede.12028.

Rickard, D., Grimes, S., Butler, I., Oldroyd, A. and Davies, K. L. (2007) Botanical constraints on pyrite formation. *Chemical Geology* **236**, 228–246. doi:10.1016/j.chemgeo.2006.09.011.

Rogers, A. D., Tyler, P. A., Connelly, D. P., Copley, J. T., James, R., Larter, R. D., Linse, K., Mills, R. A., Garabato, A. N., Pancost, R. D., Pearce, D. A., Polunin, N. V. C., German, C. R., Shank, T., Boersch-Supan, P. H., Alker, B. J., Aquilina, A., Bennett, S. A., Clarke, A., Dinley, R. J. J., Graham, A. G. C., Green, D. R. H., Hawkes, J. A., Hepburn, L., Hilario, A., Huvenne, V. A. I., Marsh, L., Ramirez-Llodra, E., Reid, W. D. K., Roterman, C. N., Sweeting, C. J., Thatje, S. and Zwirglmaier, K. (2012) The discovery of new deep-sea hydrothermal vent communities in the Southern Ocean and implications for biogeography. *PLOS Biology* **10**, e1001234. doi:10.1371/journal.pbio.1001234.

Rouse, G. W., Goffredi, S. K., Johnson, S. B. and Vrijenhoek, R. C. (2011) Not whale-fall specialists, *Osedax* worms also consume fishbones. *Biology Letters* **7**, 736–739. doi:10.1098/rsbl.2011.0202.

Sansom, R. S. (2015) Bias and sensitivity in the placement of fossil taxa resulting from interpretations of missing data. *Systematic Biology* **64**, 256–266. doi:10.1093/sysbio/syu093.

Sansom, R. S. and Wills, M. A. (2013) Fossilization causes organisms to appear erroneously

primitive by distorting evolutionary trees. *Scientific Reports* **3**, 2545. doi:10.1038/srep02545.

Schopf, J. W., Kudryavtsev, A. B., Walter, M. R., Van Kranendonk, M. J., Williford, K. H., Kozdon, R., Valley, J. W., Gallardo, V. A., Espinoza, C. and Flannery, D. T. (2015) Sulfur-cycling fossil bacteria from the 1.8-Ga Duck Creek Formation provide promising evidence of evolution's null hypothesis. *Proceedings of the National Academy of Sciences* **112**, 2087–2092. doi:10.1073/pnas.1419241112.

Schulze-Makuch, D., Dohm, J., Fan, C., Fairen, A., Rodriguez, J., Baker, V. and Fink, W. (2007) Exploration of hydrothermal targets on Mars. *Icarus* **189**, 308–324. doi:10.1016/j.icarus.2007.02.007.

Shah, D. U., Vollrath, F., Porter, D., Stires, J. and Deheyn, D. D. (2014) Housing tubes from the marine worm *Chaetopterus* sp.: biomaterials with exceptionally broad thermomechanical properties. *Journal of The Royal Society Interface* **11**, 20140525. doi:10.1098/rsif.2014.0525.

Shah, D. U., Vollrath, F., Stires, J. and Deheyn, D. D. (2015) The biocomposite tube of a chaetopterid marine worm constructed with highly-controlled orientation of nanofilaments. *Materials Science and Engineering: C* **48**, 408–415. doi:10.1016/j.msec.2014.12.015.

Shapiro, R. and Schulze-Makuch, D. (2009) The search for alien life in our Solar System: strategies and priorities. *Astrobiology* **9**, 335–343. doi:10.1089/ast.2008.0281.

Shillito, B., Lechaire, J.-P., Goffinet, G. and Gaill, F. (1995) Composition and morphogenesis of the tubes of vestimentiferan worms. *Geological Society, London, Special Publications* **87**, 295–302. doi:10.1144/GSL.SP.1995.087.01.22.

Smirnov, R. V. (2000) Two new species of Pogonophora from the arctic mud volcano off northwestern Norway. *Sarsia* **85**, 141–150. doi:10.1080/00364827.2000.10414563.

Southward, E. C., Tunnicliffe, V. and Black, M. (1995) Revision of the species of *Ridgeia* from northeast Pacific hydrothermal vents, with a redescription of *Ridgeia piscesae* Jones (Pogonophora: Obturata = Vestimentifera). *Canadian Journal of Zoology* **73**, 282–295. doi:10.1139/z95-033.

Southward, E. C., Andersen, A. C. and Hourdez, S. (2011) *Lamellibrachia anaximandri* n. sp., a new vestimentiferan tubeworm (Annelida) from the Mediterranean, with notes on frenulate tubeworms from the same habitat. *Zoosystema* **33**, 245–279.

Taylor, J. D. and Glover, E. A. (2010) Chemosymbiotic Bivalves. In *The Vent and Seep Biota* (ed. Kiel, S.), pp. 107–135. Springer Netherlands, Dordrecht. doi:10.1007/978-90-481-9572-5_5.

Vinn, O., Ten-Hove, H. and Mutvei, H. (2008) On the tube ultrastructure and origin of calcification in sabellids (Annelida, Polychaeta). *Palaeontology* **51**, 295–301.

Vinn, O., Hryniewicz, K., Little, C. T. S. and Nakrem, H. A. (2014) A Boreal serpulid fauna from Volgian-Ryazanian (latest Jurassic-earliest Cretaceous) shelf sediments and hydrocarbon seeps from Svalbard. *Geodiversitas* **36**, 527–540.

Vrijenhoek, R. C. (2013) On the instability and evolutionary age of deep-sea chemosynthetic communities. *Deep-Sea Research II* **92**, 189–200. doi:10.1016/j.dsr2.2012.12.004.

Wacey, D., McLoughlin, N., Whitehouse, M. J. and Kilburn, M. R. (2010) Two coexisting sulfur metabolisms in a ca. 3400 Ma sandstone. *Geology* **38**, 1115–1118. doi:10.1130/G31329.1.

Weigert, A., Helm, C., Meyer, M., Nickel, B., Arendt, D., Hausdorf, B., Santos, S. R., Halanych, K. M., Purschke, G., Bleidorn, C. and Struck, T. H. (2014) Illuminating the base of the annelid tree using transcriptomics. *Molecular Biology and Evolution* **31**, 1391–1401. doi:10.1093/molbev/msu080.

Weiss, M. C., Sousa, F. L., Mrnjavac, N., Neukirchen, S., Roettger, M., Nelson-Sathi, S. and Martin, W. F. (2016) The physiology and habitat of the last universal common ancestor. *Nature Microbiology* **1**, 16116. doi:10.1038/nmicrobiol.2016.116.

Willmer, P. (1990) *Invertebrate Relationships*. Cambridge University Press, Cambridge doi:10.1017/CBO9780511623547.

Woodcock, N. H. (2004) Life span and fate of basins. *Geology* **32**, 685–688. doi:10.1130/G20598.1.

Yang, R., Wei, H., Bao, M., Wang, W., Wang, Q., Zhang, X. and Liu, L. (2008) Discovery of hydrothermal venting community at the base of Cambrian barite in Guizhou Province, Western China: Implication for the Cambrian biological explosion. *Progress in Natural Science* **18**, 65–70. doi:10.1016/j.pnsc.2007.07.006.

Appendix A: Supplementary material to Chapter 1

Table A.1 Summary of tube building families, general information, and information on tubes. The majority of data is summarised from Rouse and Pleijel, (2001).

Family	All have tubes?	Tube material	Tube growth characters (e.g. clump)	Tube description	Size range	Substratum type	Depth range	Distribution
Eunicidae	No	Papery or parchment-like.	Tubes can be branching.	Tube may be attached to stones or within crevices of rocks or corals. Some species form complex tubes but most tubicolous species form less-complicated structures.	Worm: 5mm to >1m.	On various kinds of substratum from soft bottoms to rocky, on all bottoms but particularly on sub-tidal hard substrata.	Intertidal to abyssal depths.	Worldwide but more common in tropical and subtropical seas.
Onuphidae	Majority	Tough, parchment-like or softer, fragile mucous substance.	Solitary and largely unbranching.	Thin and ephemeral tube (e.g. Australonuphis) to tough and highly characteristic tube such as in *Hyalinoecia* which construct cylindrical, translucent and quill-like tube, or *Nothria conchylega*, which is distinctly flattened. Tubes usually have an inner lining of parchment, and large pieces of foreign particles on outside. Generally longer than inhabitant.	Worm: a few mm to several metres, sizes of a few cm are common.	Occur on all kinds of substrata.	From intertidal down to bathyal and abyssal depths.	Worldwide.
Acoetidae	Yes	Mud and chaetal fibres.	Solitary.	Unusual among scale worms as they construct big tubes of mud which are lined with cross-hatched chaetal fibres produced by the spinning glands. The tubes may exceed 1m in length and 3-4cm in width, are buried in sandy or muddy sediment with one end reaching or protruding from the sediment. The tubes harbour a number of commensals.	Tube: up to 1m long, 3-4 cm wide.	Muddy or sandy sediments.	Intertidal to 1500m depth.	Occur in most seas, although majority of records are from warm water temperate and tropical seas. Antarctic records lacking.
Fabriciidae	Yes	Mucus, parchment or sediment.		Mucus, parchment, or sediment tubes. Tubes often several times the length of the body and are attached to hard substrates, but tubes can also be immersed in soft sediments.	Worm: 0.85mm+.	Can be associated with hard surfaces or soft sediments.	From intertidal to abyssal depths.	Live in all seas.
Oweniidae	Yes	Sediment, shells.		Distinctive tightly fitting sedimentary tubes.	Worm: 10 - 300 mm.		Intertidal sediments down	Worldwide.

							to around 200m depth, although some have been described from abyssal regions.	
Sabellariidae	Yes	Sand, coarse sediment particles.	Reef-forming.	Distinctive hard tubes from sand or other coarse particles, and often seen forming colonies on rocky surfaces in intertidal marine environments.	Worm: 20-50mm.	Need hard substrate on which to build tube.	Often form reefs in intertidal to slightly sub-tidal areas, although many have been described from deep waters as well. Prefer areas of high wave action or current.	Worldwide.
Sabellidae	Yes	Mucus, parchment or sediment. One species constructs calcareous tubes.	Gregarious or solitary.	Mucus, parchment, or sediment tubes. Tubes often several times the length of the body and are attached to hard substrates, but tubes can also be immersed in soft sediments. *Glomerula piloseta* constructs calcareous tubes.	Worm: from minute to up to 45cm in length.	Can be associated with hard surfaces or soft sediments.	From intertidal to abyssal depths.	Live in all seas.
Serpulidae	Yes	Calcium carbonate interspersed with a mucopolysccharide matrix.	Reef-forming or solitary.	Tube is calcareous, sometimes embedded in coral.	Worm: <2mm - >100mm.	Nearly always associated with hard substrates, usually rocks. Can also be found epizoically. Serpulinae such as *Ditrupa* have free tubes that are not attached.	*Ditrupa* can be common in sediments on the continental shelf. Serpulidae occur from the intertidal, and are now known from some very deep waters.	Worldwide distribution in marine waters.
Siboglinidae	Majority	Chitin-protein complex.	Usually in clumps.	Tubes commonly vertical, with posterior end buried in sediment. Some attach their tubes to surfaces such as wood or other plant matter, e.g. *Sclerolinum*, or to rocks e.g. vestimentiferans.	Worm: 50mm - 1.5m.	Can be associated with hard surfaces or soft sediments.	20-10,000m depth, generally found in deep waters but exceptionally in some shallower settings.	Found in all seas. The need for reduced sulphur compounds or methane restricts the distribution of these worms. Can be present in high densities.

Maldanidae	Yes	Membranous lining with mud, shell or sand.	Can reach very high densities.	Tube has membranous lining and is covered with mud, shell or sand, although some 'tubes' are simple consolidated burrows.	Worm: 3mm - >200mm.	Shelf sediments, mudflats, in algae or seagrass.	Common in continental shelf sediments, also occur in shallow seagrass beds and mudflats, as well as intertidally in algal mats.	
Chaetopteridae	Yes	~	Can reach high population densities.	Brown fragile parchment to thick and leathery.	Worm: <10mm - 700mm.	Those that bury tubes are found in sands or muds, while others attach their tubes to hard substrates.	Intertidal sediments to abyssal regions.	Worldwide. Chaetopteridae can be extremely abundant and occur in very high densities.
Poecilochaetidae	Yes	Sand.	Solitary.	Long U-shaped or branching tubes made of loosely packed sand.	Worm: up to 90mm.		Recorded in sediments ranging in depth from the intertidal zone to over 10,000m, although the majority have been found in shallow waters.	Widely distributed taxa.
Spionidae	Majority	Sediment and mucus.	Can reach high population densities.	Sediment and mucus.	Worm: several mm to several cm.	Dominant polychaete component in sand and mud habitats.	From intertidal to abyssal depths, although most are described from shallow marine waters.	Recorded from all around the world.
Trochochaetidae	Yes	Sediment.		Fragile tubes made of sediment that are more like continuously created galleries than tube. Thulin (1921) gave account of *Trochochaeta multisetosa* living in complex U-shaped or branching mud-tube galleries that were around 3 times as long as the inhabitants.	Worm: >90 mm.		In sediments at depths ranging from 2m to more than 1000m.	Recorded mainly in northern hemisphere.
Uncispionidae	~	~		May live in tubes, and are thought to be tubicolous. But these have yet to be described	Worm: up to 5mm.		USA at 200-3000m, South America at	Found of western coast of USA in

				fully.			1500m (Green 1982).	sediments at 200-3000m, also off South America at 1500m (Green 1982).
Cirratulidae	No	Calcium carbonate.		Tubes can form colonies.	Worm: 7mm - >250mm.	Found in many different habitats.	From intertidal to abyssal depths.	Diverse group found all over the world. Some can form large colonies.
Fauveliopsidae	No	Cemented sand grains.		Generally not tubicolous, although some live in tubes of cemented sand grains.	Worm: 1.3mm - 20 mm.		Most members of this family occur in deep water sediments down to more than 6000m, although some have been described from depths of <100m, and up to 5m.	
Alvinellidae	Yes	Protein.	Can form colonies.	Tube can be parchment-like to more robust if more heavily mineralised	Worm: 15mm - 100mm.	Vent chimney sulphide.	Deep-sea hydrothermal vent environments - around 2000m and over.	Known only from sites associated with hydrothermal vents in the Pacific Ocean.
Ampharetidae	Yes	Sediment.			Worm: 10-60 mm.	Soft sediments.	Uncommon in shallow waters, mainly described from deeper soft sediments, including hydrothermal vents.	Worldwide.
Pectinariidae	Yes	Sand, shell, other small particles.	Solitary.	Elegant cone-shaped tubes, constructed from sand, small shells or other small particles.	Worm: 10-250mm.	All are burrowers and dig into the surface layers of sediment with their paleae, until completely buried, or with the posterior end of the tube projecting slightly. In soft	Mainly occur in shallow marine sediments.	Worldwide.

						muds, fine to coarse sand or coral sediment.		
Terebellidae	No	Mucus with sand and/or shells.	Can reach high population densities.		Worm: 10-300mm.		One of the most diverse groups of polychaetes. They are found in deep waters but tube-building ones require a hard surface onto which to attach their tubes, therefore a greater variety live in shallower waters.	Described from marine waters worldwide.
Trichobranchidae	Yes	Mud.		Some species live in muddy tubes. Reports suggest that they do not form well-consolidated tubes (Dales 1955) however Australian species do make well-constructed tubes of fine mud.		Soft sediments.	From shallow water to depths of 2700m. Possibly more common in cold waters, therefore in deep water habitats.	Worldwide.
Psammodrilidae	No	Mucus and sand-grain tube.	Solitary.	Some live in tubes or 'houses' constructed of sand grains.	Worm: up to 8mm.	Sand.	From shallow water marine sands, a beach in NZ, shallow waters, depths 15-50m	Recorded from only a few localities, mainly in Europe.

References

Rouse, G. W. and Pleijel, F. (2001) *Polychaetes*. Oxford University Press, Oxford.

Appendix B: Supplementary material to Chapter 2

Table B.1 Comparison of morphological characters between Antarctic *Sclerolinum* and three populations of *S. contortum*.

	S. contortum HMMV* n=18	*S. contortum* Loki's Castle n=10	*S. contortum* GoM** n=5	*Sclerolinum* sp. Antarctic n=10
Tube, general character	a - contorted, p - straight	a- wavy to contorted, p - straight	a - contorted, p - straight	a- wavy, p - straight
Tube diameter (mm)	0.20-0.39	0.33-0.42	0.35-0.61	0.22-0.30
Thickness of tube wall (µm)	56	43 (mean)	-	9 (mean)
Anterior zone breadth (mm)	0.13-0.24	0.22-0.29	-	0.15-0.23
Distance from apex of cephalic lobe to frenulum (mm)	0.27–0.30	0.25-0.52	0.32–0.59	0.13-0.37
Arrangement of frenular plaques	Dense row	Dense row but plaques occasionally missing	Dense row/ scattered	Dense row but plaques occasionally missing
Frenulum, position	d-l-(v)	d-l-(v)	d-l-v	d-l-(v)
Number of frenular plaques	10–14	18-23	12–20	9-19
Frenular plaques, shape	Oval	Roundish to elongated	Roundish to oval	Roundish to elongated
Frenular plaques, diameter (µm)	22–41	18-72	21–85	14-46
Dorsal furrow	Deep, narrow	Deep, wide or narrow	Deep, narrow	Deep, wide
Plaques of trunk, diameter (µm)	29-41	20-61	30-50	12-43
Transition between forepart and trunk	Abrupt	Abrupt	Abrupt	Abrupt
Forepart length (mm)	2.3-4.8	5.2-9.0	3.5-6.4	1.7-4.8
Trunk length (mm)	30-50	> 60.1	47.9-80.6	> 47.2
Opisthosoma length (mm)	0.45-0.6	-	1.4-1.8	-
Opisthosoma number of segments	3-5	-	13-16	-
Uncini of opisthosoma, diameter (µm)	5.5-6.3	-	4.5-6.5	-
Habitat	Mud sediments, mud volcano	Sediments close to hydrothermal vents	Mud sediments, cold seeps	Sediments weakly exposed to hydrothermal flow

*(v) - middle ventral plaque often missing, a - anterior, p - posterior. *Data from Smirnov (2000). **Data from Eichinger et al. (2013).*

Table B.2 P-distance (above diagonal) and K2P (below diagonal) genetic distances (in %) among the genus, as well as putative, *Sclerolinum*.

	Kushiro SK2003	Loihi Sea-mount	*S. bratt-stromi*	*S. conto-rtum* HMMV	*S. conto-rtum* Loki's Castle	*S. contor-tum* GoM	*Sclerolinum* sp. Antarctic
Kushiro SK2003		18.5	15.2	14.9	14.9	15.4	15.7
Loihi Seamount	21.6		15.7	15.2	15.2	15.2	14.9
S. brattstromi	17.1	17.8		9.4	9.4	8.8	9.4
S. contortum HMMV	16.7	17.0	10.2		0.0	0.8	1.4
S. contortum Loki's Castle	16.7	17.0	10.2	0.0		0.8	1.4
S. contortum GoM	17.5	17.0	9.5	0.8	0.8		0.8
Sclerolinum sp. Antarctic	17.8	16.7	10.2	1.4	1.4	0.8	

Methods Supplement: Details on the collection of additional *Sclerolinum contortum* specimens for comparison with Antarctic material.

Loki's Castle specimens (donated by Hans Tore Rapp) were collected during R/V G. O. Sars cruises during 2008-9 (samples S1-S13 were collected on ROV dive 8 [07/07/2009], 73°33.97'N 08°09.51'E, depth 2357 m; samples S17-24, and 30-31 were collected on ROV dive 11 [14/07/2008], 73°33.97'N-73°34.10'N 8°09.51'E-8°09.38'E, depth unknown). A single Håkon Mosby Mud Volcano (HMMV) specimen was used for DNA studies (S28) and was collected during 2010 on the R/V G. O. Sars (ROV dive 2 [10/07/2010], 71°59.852'N-71°59.993'N 14°43.975'E-14°43.897'E, depth 1262). Additional dried empty *S. contortum* tubes from HMMV (donated by Ann Andersen) were also used for comparisons with *Sclerolinum* tubes from other locations. These were collected during the June 2006 VICKING cruise on board R/V *Pourquoi pas?* (sample no. VI-103B, KGS 5, 72° 00.0785N, 14°43.3477E, 1270 m depth). Gulf of Mexico specimens (donated by Monika Bright) consisting of tubes with and without tissue and preserved in ethanol, were collected during NOAA *Ronald H. Brown* expedition no. RB-07-04 during June 2007 (Jason Dive 275, WR269, 26°41N, 91°39W, 1954 m depth).

Table B.3 Primers used for PCR and sequencing.

Primer	Sequence 5'-3'	References
16 AnnF	GCGGTATCCTGACCGTRCWAAGGTA	(Sjölin *et al.*, 2005)
16 AnnR	TCCTAAGCCAACATCGAGGTGCCAA	(Sjölin *et al.*, 2005)
16Sar	CGCCTGTTTATCAAAAACAT	(Palumbi, 1996)
16Sbr	CTCCGGTTTGAACTCAGATC	(Palumbi, 1996)
PolyLCO	GAYTATWTTCAACAAATCATAAAGATATTGG	(Carr *et al.*, 2011)
PolyHCO	TAMACTTCWGGGTGACCAAARAATCA	(Carr *et al.*, 2011)
LCO1490	GGTCAACAAATCATAAAGATATTGG	(Folmer *et al.*, 1994)
HCO2198	TAAACTTCAGGGTGACCAAAAAATCA	(Folmer *et al.*, 1994)
18SA	AYCTGGTTGATCCTGCCAGT	(Medlin *et al.*, 1988)
18SB	ACCTTGTTACGACTTTTACTTCCTC	(Nygren and Sundberg, 2003)
620F	TAAAGYTGYTGCAGTTAAA	(Nygren and Sundberg, 2003)
1324R	CGGCCATGCACCACC	(Cohen *et al.*, 1998)

Table B.4 Taxa used in Bayesian molecular analyses and GenBank accession numbers.

Terminal taxa	COI	18S	16S
Malacoceros fuliginosus	EF432015	EF446961	EF431961
Sabella pavonina	KF369181	U67144	AY340482
Alaysia sp.	FJ667536	FM995545	---
Escarpia laminata	KC357324	---	HE974467
Escarpia southwardae	KC870958	---	KC870952
Escarpia spicata	KC870961	AF168741	KC870943
Galathealinum brachiosum	U74066	AF168738	AF315040
Kushiro-SK-2003 pogonophoran	D50598		
Lamellibrachia anaximandri	KC832757	---	KF199248
Lamellibrachia barhami	AY129145	---	AF315047
Lamellibrachia columna	DQ996645	FJ347679	FJ347646
Lamellibrachia luymesi	GU059233	---	GU068251
'Loihi Seamount' pogonophoran	PSU74068		
Oasisia alvinae	AY646020	AF168743	AF315052
Oligobrachia haakonmosbiensis	FM178482	AM883186	---
Osedax antarcticus	KF444427	KF444420	KF444418
Osedax crouchi	KJ598038	KJ598035	KJ598032
Osedax deceptionensis	KF444428	KF444421	KF444419
Osedax frankpressi	FJ347607	AY577885	AY577876
Osedax japonicus	FM998111	FM995535	---
Osedax mucofloris	HM045513	AY941263	---
Osedax nordenskjoeldi	KJ598039	KJ598036	KJ598033
Osedax rogersi	KJ598040	KJ598037	KJ598034
Osedax roseus	JF509949	FJ347683	FJ347657
Osedax rubiplumus	EU852488	AY577894	AY577878
Osedax sp.'greenpalp'	FJ347641	FJ347694	FJ347655
Osedax sp. 'nudepalpA'	FJ347623	FJ347687	FJ347653
Osedax sp. 'nudepalpC'	EU267676	FJ347688	FJ347650
Osedax sp. 'orangecollar'	FJ431203	FJ347690	FJ347661
Osedax sp. 'sagami3'	FM998080	FM995537	---
Osedax sp. 'spiral'	FJ347637	FJ347693	FJ347647
Osedax sp. 'whitecollar'	FJ347613	FJ347684	FJ347659
Osedax sp. 'yellowcollar'	EU223338	FJ347689	FJ347660
Osedax sp. 'yellowpatch'	FJ347618	FJ347685	FJ347654
Paraescarpia echinospica	D50594	FM995546	---
Ridgeia piscesae	EU190708	AF168744	AF315054
Riftia pachyptila	FJ667529	AF168745	AF315050
Sclerolinum brattstromi	FJ347644	FJ347680	FJ347645
Sclerolinum contortum GoM	*KU214839	---	JX013982
Sclerolinum contortum HMMV	FM178480	AM883187	JX013984
Sclerolinum contortum Loki's Castle	*KU214833	---	*KU214831
Sclerolinum contortum Antarctica	*KU214832	*KU214829	*KU214830
Siboglinum ekmani	KF444429	AF315062	AF315038
Siboglinum fiordicum	---	AF315060	AF315039
Spirobrachia sp.	FJ480372	AF168740	AF315036
Tevnia jerichonana	FJ667531	AF168746	---

--- no sequence available, asterisk (*) denotes sequences provided as part of this study, grey highlight denotes sequences used for Sclerolinum *COI only Bayesian analysis (Figure 2.8).*

COI sequences submitted to GenBank (for each *Sclerolinum contortum* haplotype) and accession numbers:

Sclerolinum contortum G44 Antarctica-haplotype 1	(in table above)
Sclerolinum contortum S1 Loki's Castle-haplotype 1	(in table above)
Sclerolinum contortum S12 Loki's Castle-haplotype 2	KU214834
Sclerolinum contortum S20 Loki's Castle-haplotype 3	KU214835
Sclerolinum contortum S23 Loki's Castle-haplotype 4	KU214836
Sclerolinum contortum S24 Loki's Castle-haplotype 5	KU214837
Sclerolinum contortum S28 HMMV-haplotype 1	KU214838
Sclerolinum contortum G69 GoM-haplotype 1	KU214840
Sclerolinum contortum G72 GoM-haplotype 2	KU214841
Sclerolinum contortum G73 GoM-haplotype 3	KU214842
Sclerolinum contortum G74 GoM-haplotype 4	KU214843
Sclerolinum contortum G76 GoM-haplotype 5	KU214844
Sclerolinum contortum G78 GoM-haplotype 6	KU214845
Sclerolinum contortum G68 GoM-haplotype 7	(in table above)

References

Carr, C. M., Hardy, S. M., Brown, T. M., Macdonald, T. A. and Hebert, P. D. N. (2011) A tri-oceanic perspective: DNA barcoding reveals geographic structure and cryptic diversity in Canadian polychaetes. *PLOS ONE* **6**, e22232. doi:10.1371/journal.pone.0022232.

Cohen, B. L., Gawthrop, A. and Cavalier-Smith, T. (1998) Molecular phylogeny of brachiopods and phoronids based on nuclear-encoded small subunit ribosomal RNA gene sequences. *Philosophical Transactions of the Royal Society B: Biological Sciences* **353**, 2039–2061. doi:10.1098/rstb.1998.0351.

Eichinger, I., Hourdez, S. and Bright, M. (2013) Morphology, microanatomy and sequence data of *Sclerolinum contortum* (Siboglindae, Annelida) of the Gulf of Mexico. *Organisms Diversity and Evolution* **13**, 311–329. doi:10.1007/s13127-012-0121-3.

Folmer, O., Black, M., Hoeh, W., Lutz, R. and Vrijenhoek, R. (1994) DNA primers for amplification of mitochondrial cytochrome c oxidase subunit I from diverse metazoan invertebrates. *Molecular Marine Biology and Biotechnology* **3**, 294–299.

Medlin, L., Elwood, H. J., Stickel, S. and Sogin, M. L. (1988) The characterization of

enzymatically amplified eukaryotic 16S-like rRNA-coding regions. *Gene* **71**, 491–499. doi:10.1016/0378-1119(88)90066-2.

Nygren, A. and Sundberg, P. (2003) Phylogeny and evolution of reproductive modes in Autolytinae (Syllidae, Annelida). *Molecular Phylogenetics and Evolution* **29**, 235–249. doi:10.1016/S1055-7903(03)00095-2.

Palumbi, S. R. (1996) Nucleic acid II: the polymerase chain reaction. In *Molecular Systematics* (ed. Hillis, D. M., Moritz, C. and Mable, B. K.), pp. 205–247. Sinauer Associates, Sunderland, MA.

Sjölin, E., Erséus, C. and Källersjö, M. (2005) Phylogeny of Tubificidae (Annelida, Clitellata) based on mitochondrial and nuclear sequence data. *Molecular Phylogenetics and Evolution* **35**, 431–41. doi:10.1016/j.ympev.2004.12.018.

Smirnov, R. V. (2000) Two new species of Pogonophora from the arctic mud volcano off northwestern Norway. *Sarsia* **85**, 141–150. doi:10.1080/00364827.2000.10414563.

Appendix C: Supplementary material to Chapter 3

Methods Supplement: Fossilisation cage experiment

This experiment involved the deployment of replicate titanium mesh cages approximately 120 mm (length) x 120 mm (width) x 60 mm (height) in size, containing, per cage, invertebrate material (two *Bathymodiolus thermophilus* shell pieces, two gastropod shells, two *Ridgeia piscesae* tube pieces, one shrimp half carapace, one *Calyptogena magnifica* shell piece, and one *Tevnia jerichonana* tube), and a range of abiogenic control materials (Figure C.1A). These cages were placed at two different vent sites (Bio9 during AT15-13; L-vent during AT15-27) in conditions of high-temperature fluid flow, i.e. on top of vent chimneys (two cage stack) (Figure C.1B), and in adjacent areas of diffuse flow (two cage stack). In addition, a single control cage was placed away from hydrothermal fluid activity. The cages were deployed for approximately one year (Table 3.1), and during this time, sulphides (and other vent minerals) had grown on both the inside and outside of the cages deployed on the tops of chimneys (Figure C.1C). Fully mineralised *Alvinella* spp. tubes were apparent on the exterior surfaces of the sulphides that had grown onto the experimental cages (Figure C.1C). Inside one of the cages deployed in diffuse flow there were many non-mineralised and partially mineralised *Alvinella* spp. tubes (Figure C.1D).

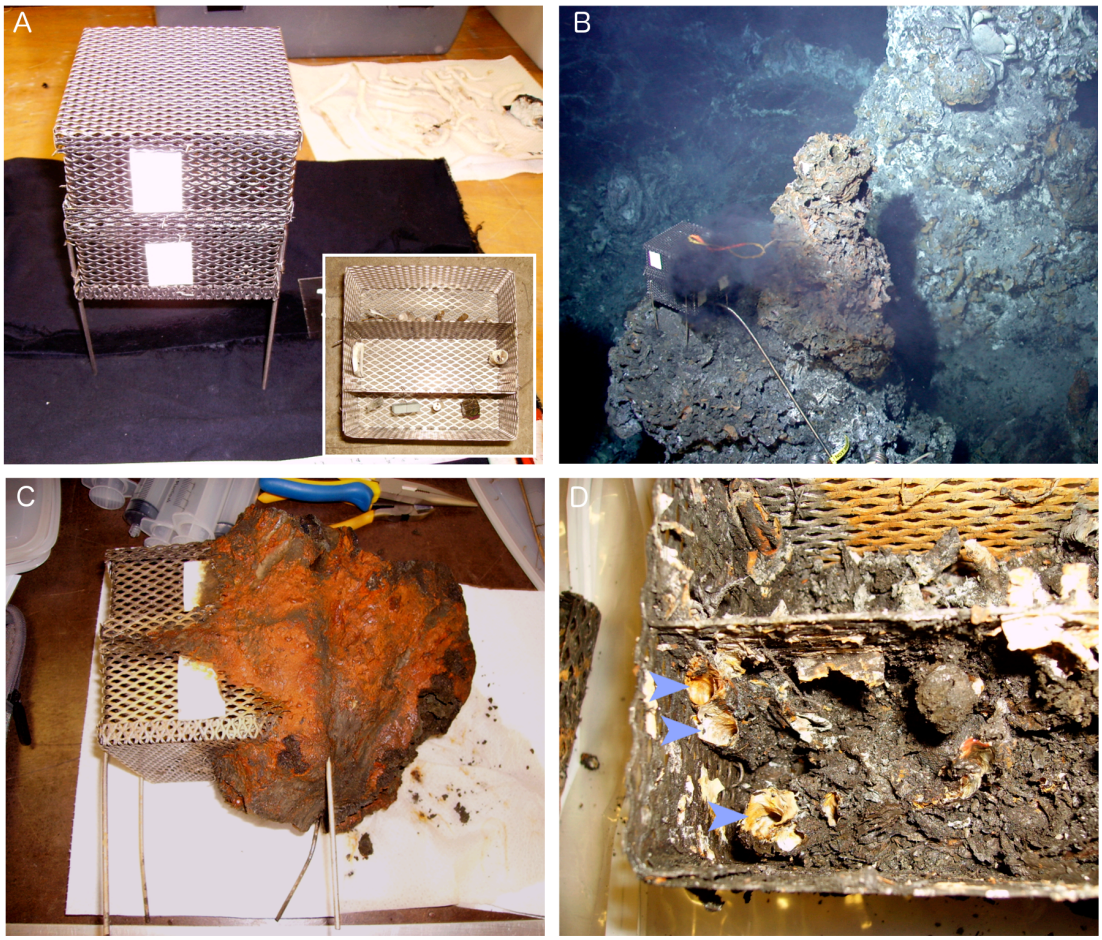

Figure C.1 The vent fossilisation experiment from which some of the samples used in this study were obtained. **A,** titanium cage pair before deployment. *Insert*, Contents of one cage (top compartment, from left to right: two *Bathymodiolus thermophilus* shell pieces, two gastropod shells, two *Ridgeia piscesae* tube pieces, one shrimp half carapace; middle compartment: one *Calyptogena magnifica* shell piece (left), one *Tevnia jerichonana* tube piece (right); bottom compartment: one calcite crystal, one glass square, one ceramic tube and one pyrite cube. **B,** high-temperature fluid flow cage pair *in situ* at L-vent; **C,** high-temperature fluid flow cage pair after recovery from Bio9 with sulphide growth inside and outside cages; **D,** *Alvinella* spp. tubes (blue arrows) inside the lower cage from L-vent diffuse flow site.

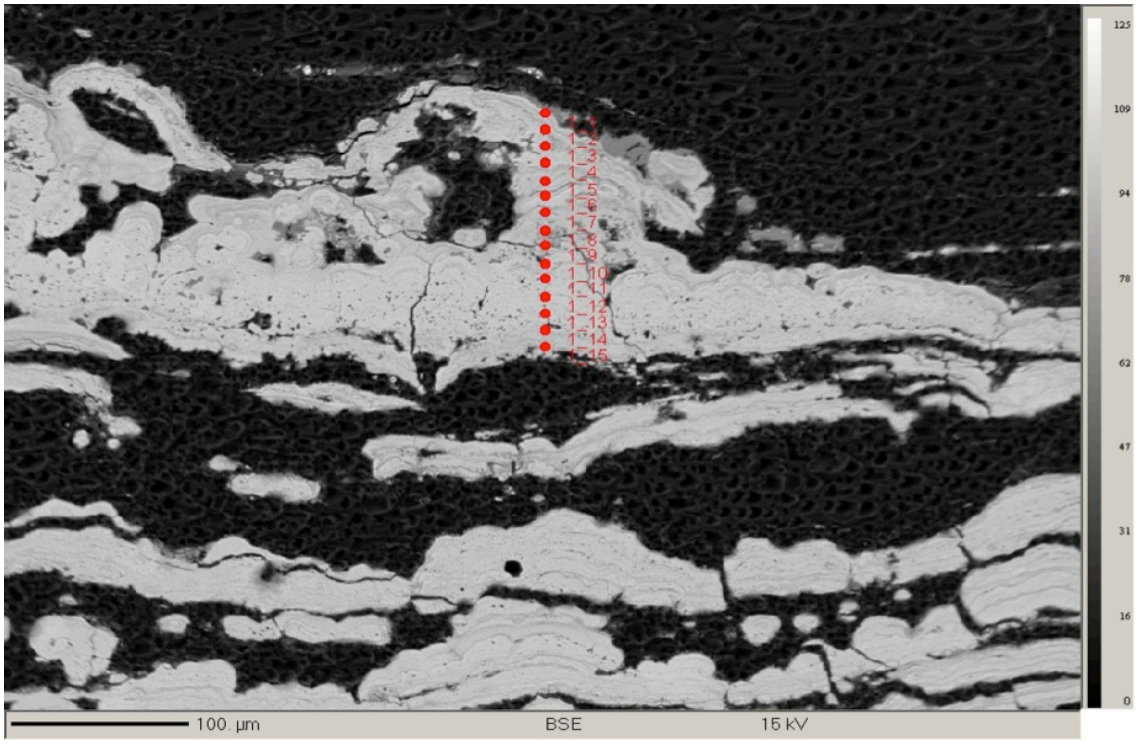

Figure C.2 Locations of EPMA point analyses for colloform mineral textures (polished Block 57.1). Elemental compositions of point are given in Table C.2.

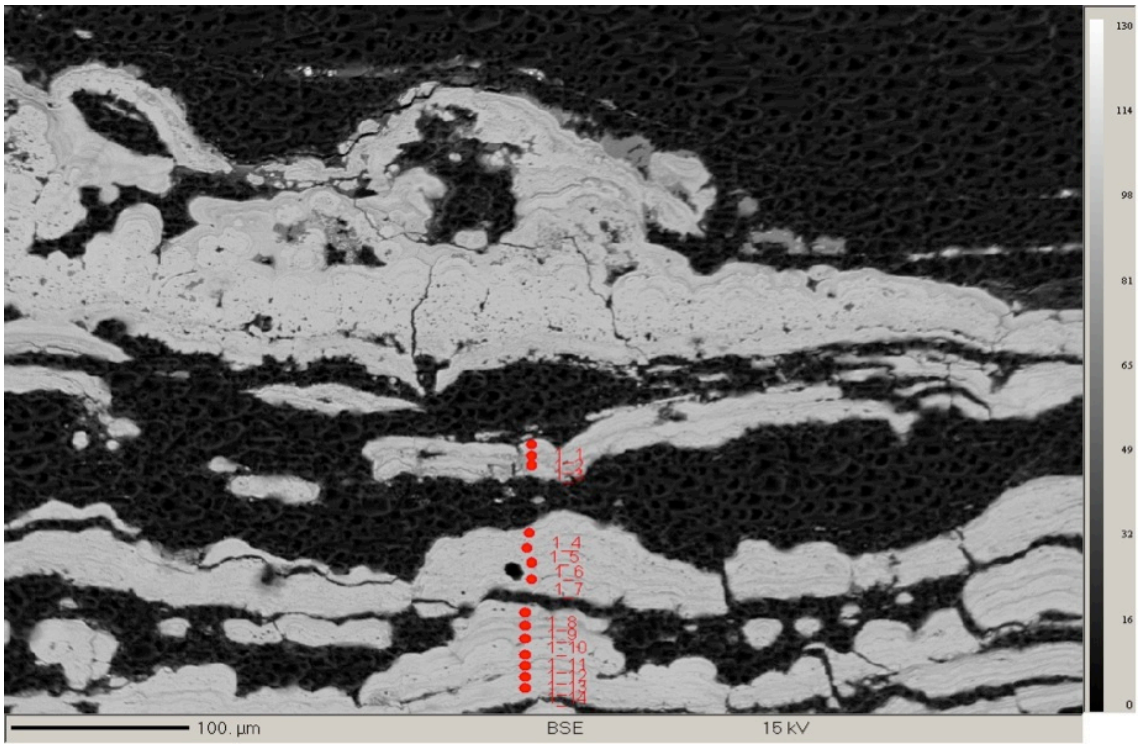

Figure C.3 Locations of EPMA point analyses for colloform mineral textures (polished Block 57.1). Elemental compositions of point are given in Table C.3.

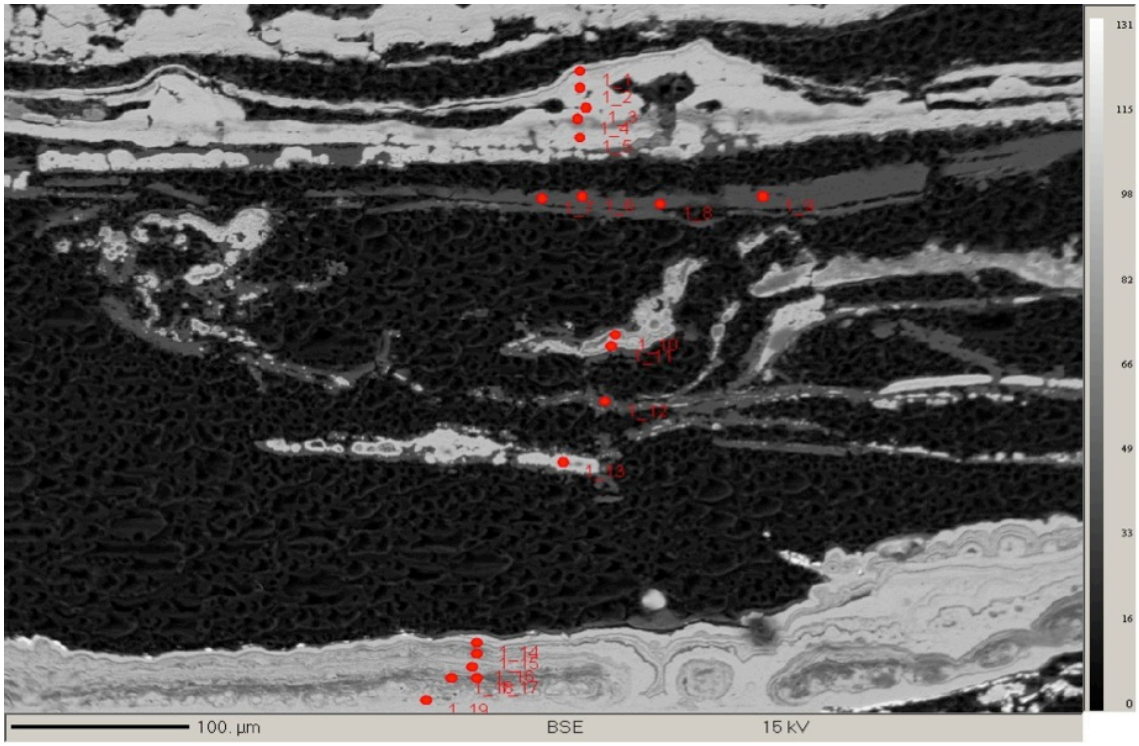

Figure C.4 Locations of EPMA point analyses for colloform mineral textures (polished Block 57.1). Elemental compositions of point are given in Table C.4.

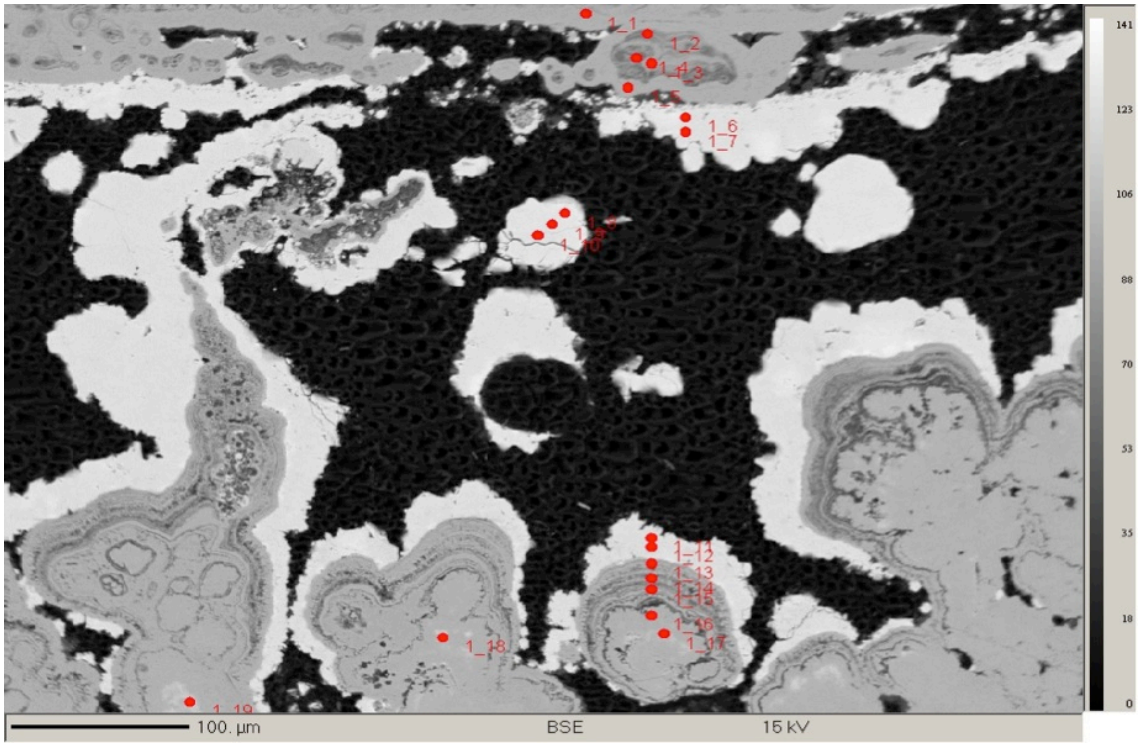

Figure C.5 Locations of EPMA point analyses for colloform mineral textures (polished Block 57.1). Elemental compositions of point are given in Table C.5.

Table C.1 Mineralogical observations for each of the polished blocks used in this study.

Specimen no.	Polished block no.	Type of tube section	From fossilisation cages?	Mineralisation state	Analysis techniques	No. of organic tube layers	No. of mineral horizons	Description of tube mineralogy	Description of mineralogy directly behind tube	Description of mineralogy of remainder of section (vent chimney sulphides)	Bacterial textures	Elemental sulfur grains
44	44.1	T, L	N	P	SEM, EDS, RL	3	2 - 8	colloform FeS, CuFeS, and mineral fragments on internal and outer organic layer surfaces	-	-	filaments on surface	I, O, B
44	44.2	T	N	P	RL	1	2 - 6	small colloform pyrite nodules, fine grained marcasite overgrowth	spongy pyrite-marcasite	-	filaments on surface	-
44	44.3	T	N	P	RL	2 - 3	1 - 3	small colloform pyrite nodules, fine grained marcasite overgrowth	spongy pyrite-marcasite	-	filaments on surface	-
45	45.1	T, L	N	P	SEM, EDS, RL	3 - 5	4 - 8	mainly organic, colloform deposition of FeS and CuFeS between layers, mineral fragments	-	-	filaments on surface	-
46	46.1	T, L	N	P	SEM, EDS, RL	4	5 - 11	mainly organic, FeOS layers some with Zn, grains CuZnFeS, ZnFeS, FeS	-	-	-	I, B
47	47.1	T, L	Y	P	SEM, EDS, RL	2	1 - 3	colloform FeS and CuFeS between tube layers, some with O, FeOCl deposition on outside of tube, CuFeSO and FeS on inside, with acicular FeS and CuFeS	-	-	-	-
47	47.2	T, L	Y	P	SEM, EDS	2	1 - 3	FeS FeCuS FeCuZnSO grains, FeOCl patches, acicular FeS all in between layers	-	-	-	-
48	48.1	T, L	N	P	SEM, EDS, RL	4	1 - 7	colloform FeS, and FeSCaO between layers with pores, CaSO grains on inside of tube, ZnFeS, FeS and CuZnFeS growth and CaSO between tube layers	-	-	pores in colloform FeS layers	B
49	49.1	T, L	N	P	SEM, EDS, RL	3	1 - 3	CaSO on outside, fine ZnFeS growth on inside, colloform FeS between layers with pores	-	-	pores in colloform FeS layers	I, B
54	63983	T	N	P	RL	4	2 - 17	FeS horizons stemming from	-	-	-	-

55	63979	T	N	F	SEM	_	2-6	thin layer, FeO in organic tube layers colloform bands of FeS, overgrown on inside of tube by CaSO	Mostly FeS with some ZnS	_	pores and filaments in colloform FeS	-
56	56.1	T	Y	P	SEM, EDS, RL	5	7	tube layers FeSO with some Ca, colloform FeS between layers	-	-	-	-
57	57.1	T	Y	F	SEM, EDS, XRD, EPMA	-	13 - 21	interlayered colloform FeS and SiO	ZnS overgrowth overgrown by PbS, little FeS	fine intergrained FeS SiO and ZnS, giving way to large crystaline ZnFeS	pores in colloform FeS, pores and filaments in distinct layer, clump	-
57	57.2	T, L	Y	F	SEM, EDS	-	3 - 18	interlayered colloform FeS and SiO, FeO on innermost tube layer	SiO and pyrite-marcasite crust	small to larger grained crystalline CuFeS	pores in colloform FeS layers	
57	57.3	T	Y	F	SEM, EDS	-	6 - 16	interlayered colloform FeS and SiO	large grained CaSO or ZnS overgrowing FeS and SiO, FeS stands in between other minerals	large grained CaSO or small grained mixture of ZnS, FeS and SiO	pores in colloform FeS, pores and filaments in distinct layers	
58	58.1	T	N	F	SEM, EDS	-	1 - 6	organic tube layers replaced mainly by small spheres of SiO with FeZnS present, some FeSO also	acicular ZnFeS and grains, abundant SiO, some PbS overgrowth	larger grained FeS and ZnFeS overgrown by SiO	-	-
59	59.1	T, L	N	F	SEM, EDS, RL	-	2 - 4	thin pyrite layers, FeSO on innermost tube	spongy pyrite-marcasite	-	-	-
59	59.2	T	N	F	SEM, EDS	-	2 - 4	thin FeS layers with some SiO, FeSO around FeS	spongy pyrite-marcasite, thin SiO	-	-	O

60	60.1	T	Y	F	SEM, EDS, RL	-	4 - 27	interlayered colloform pyrite and SiO, some ZnFeS between tube layers	strands large round-shaped pyrite with SiO in between gaps	FeS overgrown by ZnFeS leading into more ZnFeS	pores and filaments in colloform pyrite layers, clumps around tubes	-
60	60.2	L	Y	F	SEM, EDS	-	5	interlayered colloform FeS and SiO	SiO and spongy pyrite-marcasite, possible tube overgrown by minerals	FeS overgrown by ZnFeS, leading into intergrown FeS with SiO spheres and ZnFeS overgrowth	pores in colloform FeS layers	-
60	60.3	L	Y	F	SEM, EDS	-	15-57	highly colloform FeS layers	sheet SiO and FeS strands with ZnFeS overgrowth	large grained ZnFeS overgrowing smaller FeS, fine SiO also present	pores in colloform FeS layers	O
61	61.1	T	Y	F	SEM, EDS	-	3 - 4	thin FeS layers	spongy FeS, some ZnFeS overgrowth	spongy FeS, some ZnFeS overgrowth	pores in colloform FeS layers	-
61	61.2	T, L	Y	F	SEM, EDS	-	3 - 6	colloform bands of FeS	spongy pyrite-marcasite	acicular and granular FeS, small ZnS grains	pores in colloform FeS inner tube layers, clump colony	-
62	62.1	T, L	N	F	SEM, EDS, RL	-	9	thick FeSO layers interlayered with SiO, SiO web-like	spongy pyrite-marcasite, FeS strands and growth next to SiO, strands and spheres of SiO	spongy pyrite-marcasite, some FeS growth onto SiO, strands and spheres of SiO	filaments in round pyrite grains	-
62	62.2	T, L	N	F	SEM,	-	1 - 3	inner FeS layers only, inner	-	-	pore in	-

					EDS			bands overgrown by more crystalline FeS			distinct inner tube layers	
62	62.4	T, L	N	F	SEM, EDS	-	5 - 7	FeS stemming from some very thin bands, interlayering with SiO in some places	SiO and round pyrite-marcasite mixture	-	pores not very distinct	-
66	63976	T	N	F	RL	-	1 - 4	pyrite tube layers	pyrite overgrown by marcasite	pyrite overgrown by marcasite and ZnS, grains of chalcopyrite	-	-
67	63978	T	N	F	SEM	-	6-8	colloform bands of FeS, overgrown on inside of tube by CaSO	FeS then FeS overgrown by ZnS, CaSO fills some gaps	FeS then mainly ZnS with some CuFeS inclusions	pores in colloform FeS layers	-
68	63984	T	N	F	RL	-	2 - 3	fine-grained marcasite bands	mainly marcasite, spongy, with size of crystals increasing away from cores	intermixed fine and large grained ZnS, pyrite and chalocpyrite	-	-
69	63977	T	N	F	RL	-	2 - 4	thin pyrite bands overgrown by marcasite	intermixed small and large grained marcasite, some acicular	intermixed pyrite, ZnS and marcasite but less marcasite	-	-
70	70.1	T	Y	F	SEM, EDS, RL, EPMA	-	4 - 6	highly colloform pyrite or thin FeS bands, inside of tube overgrown by crystalline marcasite and ZnS	ZnS sometimes directly behind tube, some empty space, very porous FeS	mainly porous FeS with some ZnS	pores in colloform FeS layers	-
71	71.1	T	N	F	SEM, EDS	-	3 - 5	colloform bands of FeS make up thin tube rim	spongy pyrite-marcasite	fine grained FeS and ZnS with SiO, larger grained ZnS overgrowing	pores in colloform FeS inner tube layers	

	71	71.2	L	N	F	SEM, EDS, RL	-	4 - 7	colloform bands of FeS	spongy pyrite-marcasite, some overgrowth by thin band of ZnS with PbS	FeS FeS overgrown by ZnS	pores in colloform FeS inner tube layers	B
	71	71.3	T	N	F	SEM, EDS	-	7 - 9	bands with colloform FeS and more crystalline FeS overgrowth	spongy FeS	FeS and CuFeS in CaSO, then CuFeS	pores in colloform FeS inner tube layers	-
	72	72.1	T	Y	F	SEM, EDS	-	1 - 3	colloform bands of FeS	spongy FeS, overgrown by ZnS and FeO	FeS, needle-shaped FeO	pores and filaments in colloform FeS layers	-
	72	72.2	T	Y	F	SEM, EDS	-	4 - 6	colloform bands of FeS, mineral growth from distinct surfaces	spongy FeS, overgrown by ZnS and FeO	larger FeS, extensively overgrown by acicular FeO and smaller-grained ZnS	pores in colloform FeS, pores and filaments in distinct layers	-
	74	74.1	T	N	F	SEM, EDS	-	4 - 8	interlayered colloform FeS and SiO, FeS cores overgrown by more crystalline FeS	large round-shaped FeS and SiO in between	-	SiO clumps in large round FeS	B
	74	74.2	T	N	F	SEM, EDS	-	7 - 13	interlayered colloform FeS and SiO, FeS cores overgrown by more crystalline FeS	large round-shaped FeS and SiO in between	FeS growth from cores,overgrowth by ZnS, larger patches of FeS	pores and filaments in colloform FeS	-
	74	74.3	L	N	F	SEM, EDS	-	4	interlayered FeS and SiO, inner colloform FeS bands overgrown by more crystalline FeS	large round-shaped FeS and SiO in between	-	filaments in round FeS grains	-
	75	75.1	T	N	F	SEM, EDS	-	9 - 18	interlayered colloform FeS and SiO, thick SiO bands in some places with thin FeS horizons within them	patchy, stringy silica overgrown by ZnS	small grained FeS and SiO oergrown by larger ZnS, tube remnants	pores in colloform FeS	VCS
	75	75.2	T, L	N	F	SEM,	-	9 - 17	interlayered colloform FeS and	fine grained	patches of fine	pores in	-

					EDS			SiO	FeS and patchy, stringy SiO, or FeS overgrown by ZnS behind tube	grained FeS and SiO overgrown by large crystalline ZnS	colloform FeS	
75	75.3	T	N	F	SEM, EDS	-	4 - 7	thin colloform FeS bands, SiO behind	very fine and patchy FeS and SiO	colloform FeS, large grained ZnS behind, SiO present in layers	pores in colloform FeS	VCS

For type of tube section, T = transverse, L = longitudinal (T, L indicates that both section types are present within the polished block). For mineralisation state, P = partially mineralised, F = fully mineralised. For presence of elemental sulphur grains, I = occurring on inner tube surface, O = occurring on outer tube, B = between tube layers, and VCS = within vent chimney sulphide. Element combinations, e.g. FeS, indicate the main elemental constituents of minerals (these are not chemical formulae). ETOH = ethanol.

Table C.2 EPMA point analyses for colloform mineral textures (polished Block 57.1). Point locations are pictured in Figure C.2.

Point	Weight %								
	Mg	Si	P	S	Mn	Fe	Cu	Zn	As
1 / 1 .	0.000	0.029	-0.002	2.079	-0.003	1.986	0.022	0.024	-0.006
1 / 2 .	0.011	0.193	0.011	47.653	0.120	41.399	0.070	0.080	0.086
1 / 3 .	0.015	0.234	0.042	44.363	0.116	43.203	0.017	0.100	0.018
1 / 4 .	0.021	0.067	0.029	42.932	0.083	38.391	-0.041	0.025	0.112
1 / 5 .	0.018	0.064	-0.001	49.558	0.207	42.433	0.004	0.018	0.019
1 / 6 .	0.010	0.091	0.006	50.263	0.054	42.135	0.017	0.024	0.019
1 / 7 .	0.011	0.037	0.002	51.547	0.089	41.579	-0.014	0.040	0.013
1 / 8 .	0.009	0.049	0.010	44.511	0.150	38.627	0.009	0.012	0.129
1 / 9 .	0.015	0.280	0.034	35.967	0.127	37.664	0.012	0.156	0.217
1 / 10 .	0.018	0.058	0.008	47.821	0.350	40.289	0.000	0.084	0.050
1 / 11 .	0.016	0.125	0.008	48.564	0.085	41.870	-0.018	0.027	0.004
1 / 12 .	0.014	0.027	0.004	52.516	0.081	41.786	0.011	0.023	0.011
1 / 13 .	0.012	0.326	0.036	44.808	0.066	37.967	0.003	0.066	0.016
1 / 14 .	0.024	0.073	0.004	51.455	0.231	40.522	-0.002	0.017	-0.009
1 / 15 .	0.015	0.105	0.009	47.695	0.382	40.155	0.009	0.062	0.010
	Detection limit %								
1 / 1 .	0.008	0.009	0.011	0.020	0.024	0.034	0.037	0.045	0.018
1 / 2 .	0.013	0.013	0.015	0.048	0.042	0.059	0.076	0.090	0.025
1 / 3 .	0.012	0.013	0.016	0.046	0.041	0.060	0.072	0.091	0.024
1 / 4 .	0.013	0.013	0.014	0.045	0.042	0.055	0.074	0.088	0.026
1 / 5 .	0.012	0.012	0.017	0.047	0.043	0.058	0.073	0.093	0.024
1 / 6 .	0.012	0.013	0.016	0.046	0.044	0.060	0.075	0.091	0.024
1 / 7 .	0.012	0.013	0.017	0.049	0.042	0.060	0.073	0.088	0.025
1 / 8 .	0.012	0.013	0.016	0.047	0.042	0.059	0.072	0.089	0.025
1 / 9 .	0.013	0.013	0.014	0.043	0.040	0.057	0.070	0.087	0.025
1 / 10 .	0.013	0.013	0.015	0.047	0.043	0.059	0.072	0.088	0.026
1 / 11 .	0.012	0.013	0.015	0.048	0.042	0.059	0.077	0.092	0.025
1 / 12 .	0.013	0.013	0.015	0.049	0.045	0.056	0.073	0.091	0.025
1 / 13 .	0.012	0.012	0.015	0.045	0.043	0.060	0.072	0.087	0.024
1 / 14 .	0.012	0.013	0.016	0.048	0.042	0.060	0.072	0.091	0.025
1 / 15 .	0.012	0.013	0.015	0.048	0.041	0.059	0.072	0.090	0.025

Table C.3 EPMA point analyses for colloform mineral textures (polished Block 57.1). Point locations are pictured in Figure C.3.

Point	Weight %								
	Mg	Si	P	S	Mn	Fe	Cu	Zn	As
1 / 1 .	0.029	0.032	0.003	51.051	0.319	41.101	-0.006	0.033	0.026
1 / 2 .	0.016	0.217	0.029	42.511	0.365	39.611	0.008	0.094	0.145
1 / 3 .	0.008	0.168	0.016	34.354	0.234	36.780	0.020	0.135	0.432
1 / 4 .	0.023	0.064	0.005	51.192	0.372	41.203	0.002	0.045	0.025
1 / 5 .	0.014	0.237	0.009	51.405	0.351	40.717	-0.018	0.097	0.006
1 / 6 .	0.002	0.281	0.035	3.670	0.044	7.067	0.008	0.084	0.004
1 / 7 .	0.020	0.099	0.011	51.518	0.344	40.981	-0.050	0.042	0.013
1 / 8 .	0.013	0.167	0.006	50.146	0.320	41.635	0.035	0.094	0.015
1 / 9 .	0.012	0.048	0.005	51.874	0.346	40.169	0.004	0.089	0.011
1 / 10 .	0.011	0.059	0.004	50.707	0.449	40.988	-0.009	0.136	0.019
1 / 11 .	0.017	0.032	0.002	53.186	0.444	41.383	-0.002	-0.014	-0.010
1 / 12 .	0.017	0.061	0.000	51.389	0.328	40.755	-0.017	0.017	0.008
1 / 13 .	0.011	0.081	0.005	52.136	0.327	40.830	0.001	0.016	0.070
1 / 14 .	0.016	0.457	0.007	50.772	0.362	39.280	-0.019	0.047	0.080
	Detection limit %								
1 / 1 .	0.012	0.012	0.016	0.048	0.044	0.060	0.077	0.093	0.025
1 / 2 .	0.012	0.013	0.014	0.046	0.043	0.056	0.073	0.089	0.025
1 / 3 .	0.013	0.012	0.016	0.044	0.042	0.056	0.070	0.085	0.023
1 / 4 .	0.012	0.013	0.015	0.048	0.044	0.057	0.074	0.091	0.026
1 / 5 .	0.012	0.013	0.015	0.047	0.043	0.058	0.076	0.088	0.025
1 / 6 .	0.005	0.005	0.010	0.019	0.029	0.039	0.047	0.057	0.010
1 / 7 .	0.012	0.013	0.014	0.047	0.045	0.062	0.076	0.093	0.025
1 / 8 .	0.013	0.013	0.015	0.047	0.043	0.061	0.074	0.090	0.025
1 / 9 .	0.012	0.013	0.015	0.048	0.041	0.061	0.076	0.091	0.025
1 / 10 .	0.013	0.013	0.016	0.044	0.043	0.064	0.074	0.087	0.024

1 / 11 .	0.012	0.013	0.016	0.048	0.045	0.063	0.075	0.094	0.025
1 / 12 .	0.012	0.013	0.015	0.049	0.044	0.059	0.077	0.092	0.025
1 / 13 .	0.012	0.013	0.016	0.048	0.040	0.059	0.075	0.093	0.025
1 / 14 .	0.013	0.013	0.016	0.047	0.043	0.061	0.075	0.090	0.025

Table C.4 EPMA point analyses for colloform mineral textures (polished Block 57.1). Point locations are pictured in Figure C.4.

Point	Weight %								
	Mg	Si	P	S	Mn	Fe	Cu	Zn	As
1 / 1 .	-0.002	0.380	-0.002	2.177	0.008	1.007	-0.027	0.000	0.028
1 / 2 .	0.008	1.399	0.001	48.325	0.282	39.618	-0.030	0.052	0.022
1 / 3 .	0.004	0.998	0.007	48.592	0.042	42.504	0.007	0.022	0.032
1 / 4 .	0.001	0.365	0.004	52.166	0.124	43.029	0.011	0.008	0.007
1 / 5 .	0.018	2.119	0.002	46.179	0.106	38.310	-0.005	0.080	0.086
1 / 6 .	-0.002	1.014	-0.003	0.797	0.008	0.117	0.000	-0.017	0.005
1 / 7 .	-0.001	4.530	0.010	0.685	-0.006	0.157	-0.003	-0.003	0.026
1 / 8 .	-0.001	42.249	0.005	0.092	-0.012	0.207	-0.003	-0.001	0.004
1 / 9 .	0.004	46.634	0.003	0.068	0.003	0.229	-0.016	-0.027	0.008
1 / 10 .	-0.005	19.162	0.004	29.734	0.059	18.176	0.056	-0.008	0.373
1 / 11 .	0.000	5.239	0.005	45.927	0.024	34.594	0.036	0.028	0.119
1 / 12 .	-0.005	39.390	0.000	2.854	-0.003	1.775	-0.001	0.048	0.162
1 / 13 .	0.010	1.171	0.007	51.140	0.103	40.538	0.018	0.102	0.164
1 / 14 .	0.008	9.973	0.005	39.117	0.050	32.143	0.011	0.127	0.044
1 / 15 .	0.009	6.979	0.007	44.944	0.065	34.847	0.006	0.108	0.007
1 / 16 .	0.001	18.109	0.009	31.709	0.114	23.409	-0.028	0.090	0.045
1 / 17 .	0.019	8.185	0.005	39.423	0.279	32.313	-0.014	0.152	0.081
1 / 18 .	0.016	4.056	0.002	46.871	0.253	37.946	-0.006	0.171	0.059
1 / 19 .	0.003	0.040	0.004	53.749	0.100	43.360	0.021	0.226	0.010
	Detection limit %								
1 / 1 .	0.008	0.008	0.009	0.020	0.021	0.030	0.040	0.046	0.015
1 / 2 .	0.012	0.013	0.016	0.045	0.042	0.058	0.078	0.090	0.025
1 / 3 .	0.012	0.012	0.017	0.048	0.044	0.060	0.078	0.093	0.024
1 / 4 .	0.012	0.013	0.016	0.048	0.042	0.061	0.075	0.093	0.025
1 / 5 .	0.012	0.013	0.015	0.046	0.043	0.060	0.074	0.091	0.025
1 / 6 .	0.006	0.007	0.013	0.020	0.022	0.029	0.039	0.048	0.011
1 / 7 .	0.006	0.008	0.013	0.027	0.026	0.029	0.042	0.047	0.011
1 / 8 .	0.006	0.016	0.018	0.031	0.034	0.041	0.056	0.068	0.013
1 / 9 .	0.006	0.017	0.018	0.031	0.033	0.043	0.056	0.068	0.013
1 / 10 .	0.010	0.013	0.015	0.040	0.038	0.051	0.065	0.081	0.020
1 / 11 .	0.012	0.013	0.016	0.046	0.044	0.061	0.070	0.090	0.023
1 / 12 .	0.007	0.014	0.016	0.033	0.036	0.041	0.059	0.068	0.013
1 / 13 .	0.013	0.013	0.015	0.049	0.044	0.060	0.076	0.091	0.025
1 / 14 .	0.011	0.013	0.016	0.044	0.041	0.057	0.069	0.088	0.023
1 / 15 .	0.011	0.013	0.016	0.046	0.042	0.059	0.072	0.090	0.023
1 / 16 .	0.010	0.013	0.016	0.043	0.038	0.054	0.069	0.083	0.020
1 / 17 .	0.012	0.013	0.016	0.044	0.042	0.056	0.070	0.087	0.023
1 / 18 .	0.012	0.013	0.016	0.047	0.045	0.058	0.072	0.087	0.024
1 / 19 .	0.013	0.013	0.016	0.049	0.045	0.060	0.074	0.095	0.025

Table C.5 EPMA point analyses for colloform mineral textures (polished Block 57.1). Point locations are pictured in Figure C.5.

Point	Weight %								
	Mg	Si	P	S	Mn	Fe	Cu	Zn	As
1 / 1 .	0.018	2.241	0.014	47.715	0.243	40.174	-0.039	0.137	0.077
1 / 2 .	-0.001	0.034	0.003	52.768	0.063	44.600	0.034	0.094	0.011
1 / 3 .	0.007	6.362	0.010	44.719	0.123	37.389	-0.003	0.148	0.033
1 / 4 .	0.010	3.234	-0.002	49.817	0.150	40.659	0.040	0.134	0.020
1 / 5 .	0.006	14.065	0.001	37.239	0.116	29.145	0.039	0.248	0.019
1 / 6 .	-0.009	7.397	-0.006	30.593	0.041	8.986	-0.012	42.305	0.284
1 / 7 .	-0.024	0.004	-0.007	32.428	0.001	3.407	0.011	57.248	0.251
1 / 8 .	-0.020	0.054	0.006	31.626	0.003	2.305	0.057	54.982	0.315

1 / 9 .	-0.009	0.003	-0.009	32.125	0.014	3.233	0.060	54.631	0.188
1 / 10 .	-0.010	0.006	-0.008	32.070	0.015	2.952	0.032	55.486	0.186
1 / 11 .	-0.012	0.014	0.000	32.705	0.014	5.540	0.038	55.437	0.055
1 / 12 .	-0.004	0.009	0.004	32.998	0.017	7.630	-0.002	53.015	0.041
1 / 13 .	0.012	0.120	0.012	49.151	0.055	43.113	-0.010	0.797	0.021
1 / 14 .	0.029	5.948	0.013	42.590	0.051	37.970	0.021	0.589	0.012
1 / 15 .	0.008	5.642	0.014	45.683	0.065	38.943	-0.018	0.404	-0.004
1 / 16 .	0.005	0.007	0.006	53.999	0.038	43.159	-0.023	1.985	0.038
1 / 17 .	0.008	0.003	-0.003	54.027	0.023	43.045	0.003	1.939	0.021
1 / 18 .	-0.003	0.003	0.001	54.781	0.022	44.284	0.009	0.244	0.040
1 / 19 .	0.007	0.004	-0.006	54.517	0.077	44.312	0.013	0.274	0.013
	Detection limit %								
1 / 1 .	0.012	0.013	0.016	0.047	0.042	0.059	0.078	0.093	0.024
1 / 2 .	0.013	0.013	0.016	0.048	0.044	0.058	0.076	0.093	0.026
1 / 3 .	0.012	0.013	0.014	0.047	0.041	0.058	0.074	0.092	0.023
1 / 4 .	0.013	0.013	0.016	0.048	0.043	0.059	0.074	0.095	0.025
1 / 5 .	0.011	0.013	0.016	0.045	0.040	0.057	0.069	0.089	0.022
1 / 6 .	0.016	0.015	0.019	0.045	0.040	0.048	0.075	0.110	0.029
1 / 7 .	0.018	0.016	0.020	0.045	0.046	0.054	0.080	0.119	0.032
1 / 8 .	0.018	0.015	0.020	0.046	0.046	0.055	0.079	0.120	0.033
1 / 9 .	0.017	0.016	0.020	0.045	0.047	0.053	0.079	0.118	0.033
1 / 10 .	0.017	0.016	0.020	0.048	0.044	0.054	0.080	0.121	0.032
1 / 11 .	0.017	0.016	0.018	0.046	0.045	0.056	0.079	0.118	0.033
1 / 12 .	0.017	0.016	0.018	0.044	0.045	0.055	0.080	0.117	0.032
1 / 13 .	0.013	0.013	0.015	0.047	0.043	0.058	0.076	0.095	0.026
1 / 14 .	0.012	0.013	0.016	0.046	0.043	0.060	0.072	0.090	0.025
1 / 15 .	0.012	0.013	0.016	0.047	0.043	0.060	0.077	0.092	0.025
1 / 16 .	0.013	0.013	0.016	0.050	0.044	0.063	0.079	0.094	0.025
1 / 17 .	0.012	0.013	0.017	0.050	0.045	0.061	0.078	0.099	0.026
1 / 18 .	0.013	0.013	0.016	0.049	0.044	0.061	0.076	0.092	0.025
1 / 19 .	0.013	0.013	0.016	0.048	0.045	0.064	0.077	0.091	0.025

Table C.6 Information on the diameter measurements of pore and filament associations found within fully mineralised *Alvinella* spp. tubes, and of microbial filaments from the inner surface of an *Alvinella* spp. tube (Specimen 44). All measurements were taken from SEM images. P/F = pores/filaments.

Specimen no.	Object measured	Area measured (μm^2)	No. of pore/ filament diameters measured	Pore/ filament density (no. per 100 μm^2)	Maximum diameter (µm)	Minimum diameter (µm)	Average diameter (µm)	Standard deviation (µm)
48	P/F in layers	766	26	3.39	0.88	0.23	0.45	0.18
49	P/F in layers	3047	23	0.75	1.16	0.25	0.55	0.20
57	P/F in layers	506	59	11.67	0.64	0.13	0.32	0.11
57	P/F in layers	33201	66	0.20	1.24	0.21	0.49	0.21
59	P/F in layers	5230	51	0.98	1.40	0.19	0.40	0.21
71	P/F in layers	3311	34	1.03	2.62	0.25	0.91	0.55
60	P/F in clumps	5905	251	4.25	0.91	0.26	0.56	0.10
60	P/F in clumps	4239	104	2.45	0.96	0.36	0.61	0.11
74	P/F in clumps	2932	140	4.78	0.93	0.34	0.65	0.09
74	P/F in clumps	3495	297	8.50	1.00	0.37	0.66	0.11
61	P/F in clumps	8721	147	1.69	1.36	0.47	0.79	0.16
44	Microbial filaments	-	33	-	4.78	0.35	1.49	1.29
44	Microbial filaments	-	62	-	3.15	0.18	1.12	0.60
44	Microbial filaments	-	47	-	3.65	0.24	0.96	0.67

Appendix D: Supplementary material to Chapter 4

Methods Supplement 1: Additional phylogenetic datasets

Datasets including molecular data analysed using MrBayes (in addition to the two morphological datasets analysed using TNT):

3. Modern taxa, DNA data only (28 taxa, 7445 characters, analysis: MrBayes)

4. Modern taxa, tube and DNA data (43 taxa, 7493 characters, analysis: MrBayes)

5. Modern and fossil taxa, tube and DNA data (64 taxa, 7493 characters, analysis: MrBayes).

Bayesian phylogenetic analyses were conducted using DNA sequences from four genes (COI, 28S, 18S, 16S) obtained from NCBI Genbank (accession numbers are given in Table D.5). Morphological data was assessed according to the evolutionary model for standard discrete data provided in MrBayes. Model choice for molecular data was determined using jModelTest (Posada, 2008) and the Akaike Information Criterion (AIC). The GTR + I + G model was used for COI and 18S, and the GTR + G model for 28S and 16S. Analyses of the combined dataset were run for 10,000,000 generations with 2,500,000 discarded as burnin. Outgroup choice for all analyses was based on the findings of Weigert *et al.* (2014). For taxa for which tube morphology was assessed but DNA data was not available, sequences from close relatives were used (see Table D.5).

Methods Supplement 2: Pyrolysis gas-chromatography mass-spectrometry

Samples were initially purged with helium for 60 seconds inside the pyrolysis chamber (300°C) to remove any volatile contamination. Samples were subsequently pyrolysed for 15 seconds at 650°C using a CDS Pyroprobe 2000 and 1500 valve interface (both CDS Analytical, Oxford, Pennsylvania). Pyrolysis products were separated and identified using an Agilent Technologies 6890 gas chromatograph coupled to a 5973 mass spectrometer. Organic compounds were separated using a J&W DB5-MSui column (30 m length, 0.25 mm internal diameter, 0.25 μm film thickness), with helium at a column flow rate of 1.1 mL min^{-1} used as the carrier gas. The injection was at 10: 1 split, and the temperature of the injector was 270°C. The gas chromatographer oven temperature was held for 2 minutes at 40°C and then programmed at 5°C min^{-1} to 310°C. The final temperature was held for

10 minutes. The mass spectrometer was operated in electron impact mode (70 eV) with a scan range of 45-500 amu. Determination of organic constituents was based on previously published information on the pyrolysis products of expected compounds such as chitin (Stankiewicz *et al.*, 1996, 1998; Zeitsch, 2000; Flannery *et al.*, 2001).

Table D.1 Worm tubes in regional groupings of ancient hydrothermal vent (highlighted) and cold seep deposits. Adapted from Campbell (2006).

Location	Geotectonic/stratigraphic context	Age	Deposit type	Tubes	Inferred paleo-depth/setting	References (main refs referring to worm tubes in particular deposit)
Miura Peninsula, Kanagawa Prefecture, central Japan	Convergent/ Honshu Arc– Izu–Ogasawara Arc collision	Upper Pliocene Ikego, Urago & Nojima Fms.; & Miocene Misaki, Ochiai & Jike Fms.	Deep-sea fan tuffaceous sandstone & siltstone; faults, slump blocks, breccia & conglomerate	Worm tubes	Lower-upper bathyal	(Campbell, 2006)
Tertiary Piedmont Basin, northwest Italy	Margin of Tertiary Piedmont Basin	Late Miocene, Valle Versa Chaotic Complex	Lucina and brecciated limestones, carbonate beds with veins, conduits	Vestimentiferan worm tubes	Outer shelf to slope	(Natalicchio *et al.*, 2013)
Rocky Knob, Upper Waiau River (Puketawa, Totaranui), Waipiro, Bexhaven Limestone, Karikarihuata, Tauwharaepare, Turihaua, Moonlight North, Ugly Hill, Northern East Coast Basin, North Island, New Zealand	Convergent/ Hikurangi forearc	Lower to Upper Miocene, "Moonlight Limestone"	Micrite and fibrous aragonite lenses, pipes and nodules in siltstone	Siboglinidae? worm tubes, vestimentiferan worm tubes, worm tubes, serpulid worm tubes	?Bathyal	(Campbell, 2006; Campbell *et al.*, 2008a; Saether, 2011)
Kanagawa Prefecture, central Japan	Forearc	Lower to Middle Miocene (17.2-14.4 Ma), Hayama Group	Fault-induced brecciated zone, parauchthonous, carbonate concretions	Worm tubes	1200-1600 m	(Majima *et al.*, 2005)
Monferrato, Marmorito, northwest Italy	Transpressional	Miocene	Micrite cements, veins, fibrous aragonite	Worm tubes	-	(Peckmann *et al.*, 1999; Campbell, 2006))
Shipwreck Pt., Strait of Juan de Fuca, Washington State, USA	Convergent	Lower Oligocene, Makah Fm.	Allochthonous carbonate blocks of micrite, fibrous cement & spar, in siltstone	Vestimentiferan? worm tubes	?slope olistostrome	(Goedert and Campbell, 1995; Campbell, 2006)
Scotland district, northeast Barbados	Convergent	Eocene-Miocene, diapiric melange and Sub-Oceanic Fault Zone	Micritic carbonate blocks	Vestimentiferan worm tubes	Deep offshore	(Gill *et al.*, 2005; Campbell, 2006)
Barlo, Luzon, Philippines	Supra-subduction zone	Upper Eocene, Zambales Ophiolite	VMS deposit	Vestimentiferan? worm tubes	Deep offshore	(Boirat and Fouquet, 1986; Little *et al.*, 1998; Campbell, 2006)
Whiskey Creek, Strait of Juan de Fuca, Washington State, USA	Convergent	Upper Eocene, Pysht Fm.	Micrite, fibrous cement in boulders - bioturbated, brecciated; pyrite	Serpulid? worm tubes	Deep offshore	(Goedert *et al.*, 2003; Campbell, 2006)
Wagonwheel Mountain, central California, USA	Convergent	Upper Eocene, Wagonwheel Fm.	Calcareous sandstone lenses in silty mudstone	Serpulid worm tubes	Deep offshore	(Squires and Gring, 1996; Campbell, 2006)
Canyon River, Humptulips, West Fork Satsop River, Murdock Creek, Bear River, Washington State, USA	Convergent	Oligocene - Upper Eocene, Humptulips Fm., Lincoln Creek Fm.,	Lenses of micrite, fibrous cement and spar, in siltstone. Some allochthonous	Serpulid worm tubes, worm tubes, vestimentiferan? worm tubes	Bathyal, deep offshore	(Goedert and Squires, 1990b, 1993; Goedert *et al.*, 2000; Peckmann *et al.*, 2002; Campbell, 2006; Kiel, 2010; Vinn *et al.*, 2013)

Panoche Hills, central California, USA	Convergent/forearc	Cliff Pt. siltstone Paleocene, Moreno Fm.	Carbonate pavements, pipes; associated sandstone intrusions	Worm tubes	Shelf edge, 100-200 m	(Schwartz *et al.*, 2003; Campbell, 2006; Minisini and Schwartz, 2007)
Azema, New Caledonia	Oceanic spreading centre	Paleocene or Upper Cretaceous; ophiolite	VMS deposit	Worm tubes	Deep offshore	(Oudin *et al.*, 1985; Little *et al.*, 1998; Campbell, 2006)
Sada, Shikoku, Japan	-	Upper Cretaceous, Campanian-Maastrichtian), Sada Limestone	Large limestone boulders	Serpulid worm tubes	-	(Nobuhara *et al.*, 2008; Vinn *et al.*, 2013)
Lahanos, Killik, Cayeli beds, eastern Black Sea, Turkey	-	Upper Cretaceous	VMS deposits	Worm tubes	-	(Revan *et al.*, 2010)
Tepee Buttes, Colorado, South Dakota, Montana Wyoming, USA	Epeiric seaway/ basement faults, early Laramide orogeny	Upper Cretaceous, Late Campanian	Micrites in pipe-like core; irregular nodules	Worm tubes	Deep offshore	(Kauffman *et al.*, 1996; Shapiro and Fricke, 2002; Campbell, 2006)
Nakagawa-cho region, NW Hokkaido, north Japan	Convergent/ Yezo forearc	Upper Cretaceous, Cenomanian-Santonian, Omagari Fm., Yezo Supergroup	Upper worm tube boundstone & lower carbonate breccia, in muddy turbidite	Vestimentiferan worm tubes	Slope	(Hikida *et al.*, 2003; Majima *et al.*, 2005; Campbell, 2006)
Okukinenbetsu River, Obira-machi, NW Hokkaido, north Japan	Forearc	Upper Cretaceous, Lower Cenomanian (97 Ma), Middle Ezo Group	Mudstone	No worm tubes identified	Slope	(Majima *et al.*, 2005)
Kapedhes, Kinousa, Kambia, Memi, Sha, Peristerka sites, Cyprus	Supra-sbuduction zone	Upper Cretaceous, Turonian, Troodos ophiolite	VMS deposits	Vestimentiferan worm tubes, serpulid? worm tubes	Deep offshore	(Oudin and Constantinou, 1984; Little *et al.*, 1998, 1999a)
Bayda, Oman	Oceanic spreading center/ ?marginal basin	Upper Cretaceous, Cenomanian, Samail Ophiolite	VMS deposit	Vestimentiferan? worm tubes	Deep offshore	(Haymon *et al.*, 1984; Haymon and Koski, 1985; Little *et al.*, 1998; Campbell, 2006)
Ellef Rignes and Prince Patrick Islands, northern Canada	Sverdrup Basin/ faults associated with salt diapir or half-graben	Lower Cretaceous, Albian, Christopher Fm.	Carbonate lenses and nodules with complex cement sequence	Serpulid worm tubes	~ 400 m	(Beauchamp *et al.*, 1989; Beauchamp and Savard, 1992; Campbell, 2006; Williscroft, 2013)
Rocky Creek, Bear Creek, Cold Fork Cottonwood Creek, Wilbur Springs, Rice Valley, Paskenta, NW Berryessa, Little Indian Valley, California, USA	Convergent/forearc and accretionary prism	Lower Cretaceous - Upper Jurassic, Great Valley Group and Fransciscan Complex	Carbonate lenses and nodules in siltstone turbidites and serpentenites, some with complex cement sequence	Serpulid worm tubes, worm tubes, worm tubes?	Upper slope	(Campbell, 1995, 2006; Campbell *et al.*, 2002; Kiel and Campbell, 2005; Kiel *et al.*, 2008a)
Sassenfjorden area, Spitsbergen, Svalbard		Volgian-Ryazanian (latest Jurassic-earliest Cretaceous),	Seep and diagenetic carbonates in mudstones	Vestimentiferan? worm tubes	Middle to outer shelf	(Hammer *et al.*, 2011; Hryniewicz *et al.*, 2012, 2015; Vinn *et al.*, 2014)

Neuquen, Argentina	Fault-controlled rift depo-centers, early post-rift subsidence	Agardhfjellet Fm. Lower Jurassic, Lower Toarcian, Los Molles Fm.	Carbonate bioherm in shales & turbidite sandstones	Worm tubes	Offshore, 50-100 m	(Gomez-Perez, 2003; Campbell, 2006)
Figueroa, San Rafael Mountains, southern California	Mid-ocean ridge or seamount	Lower Jurassic, Pleinsbachian, Franciscan Complex	VMS deposit	Vestimentiferan worm tubes	Deep offshore	(Little *et al.*, 1999b, 2004; Campbell, 2006)
Gangobis, southern Namibia	Sediments accumulated within an intracontinental rift basin	Late Carboniferous, Dwyka Group, Gangobis Shale Member	Cementstone (banded/botryoidal cement, yellow calcite, microspar, spheroidal calcite), framboidal pyrite	Vestimentiferan? worm tubes	~600 m	(Himmler *et al.*, 2008)
Tynagh lead-zinc deposit, Ireland	Intracontinental basin adjacent to active fault/exhalative	Lower Carboniferous, Upper Tournaisian-Lower Viscean	Sediment-hosted Pb-Zn-barite deposit; pyrite chimneys	Pyritised worm tubes	<100 m	(Banks, 1985; Little *et al.*, 1998)
Ballynoe barite deposit, Silvermines, Ireland	Intracontinental basin adjacent to active fault/exhalative	Lower Carboniferous, late Tournaisian	Massive barite deposit	Worm tube	?	(Boyce *et al.*, 2003)
Red Dog Zn-Pb- Ag deposit, western Brooks Range, Alaska, USA	Active horst & graben/ long-lived starved sedimentary basin	Carboniferous, Kuna Formation	Barites and sulfides hosted in siliceous black shale and chert; seep-related	Worm tubes	Offshore	(Moore *et al.*, 1986; Campbell, 2006)
Sonora, Mexico & Roberts Mountain Allochthon, Nevada, USA	Extensional basins	Upper Devonian, Famennian	Stratiform barite deposits, associated with methane seeps on continental margin	Worm tubes	Deep offshore	(Dube, 1988; Torres *et al.*, 2003; Campbell, 2006)
Hollard Mound, Hamar Laghdad, Antiatlas, Morocco	Epeiric/ submarine rise and associated neptunian dikes	Middle Devonian, Eifelian- Givetian	Carbonate lenses with complex cement sequence	Vestimentiferan worm tubes	Offshore	(Peckmann *et al.*, 2005; Campbell, 2006)
Sibay, southern Ural Mountains, Russia	Inter-arc basin	Middle-Lower Devonian	VMS deposit	Annelid? worm tubes, Tevidestus serriformis (vestimentiferan? worm tube)	Deep offshore	(Little *et al.*, 1997, 1999c; Campbell, 2006)
Yaman Kasay, southern Ural Mountains, Russia	Back-arc basin	Silurian	VMS deposit	Eoalvinellodes annulatus (polychaete? worm tube), Yamankasia riftia (vestimentiferan? offshore worm tube)	1600+ m	(Little *et al.*, 1997, 1999c; Buschmann and Maslennikov, 2006; Campbell, 2006)

Table D.2 Fossil tubes examined.

Locality	No. examined	Specimen information	Site/tube description(s) consulted	Notes
Rocky Knob, Northern East Coast Basin, North Island, New Zealand	many	RK-5: block of many large-diameter tubes, mostly in the same orientation. RK-15B-6: block of small-diameter tubes mostly in the same orientation. RNT1: many similarly sized tubes, mostly in the same orientation. RNT2: dense aggregation of small-diameter tubes in a range of orientations.	(Campbell *et al.*, 2008b; Saether, 2011)	Collected by C.T.S. Little and donated by K.A. Campbell
Upper Waiau River, Northern East Coast Basin, North Island, New Zealand	8+	UWT3-4: clusters of tubes preserved mostly in the same orientation, one large-diameter tube has a very grainy tube wall.	(Campbell *et al.*, 2008b; Saether, 2011)	Donated by K.A. Campbell
Waipiro, Northern East Coast Basin, North Island, New Zealand	2	WAIP-1: several tubes preserved by large calcium carbonate crystals.		Collected by C.T.S. Little and used for py-GC-MS only
Bexhaven Limestone, Northern East Coast Basin, North Island, New Zealand	many	BXG: many small-diameter tubes occurring clustered together.	(Campbell *et al.*, 2008b; Saether, 2011)	Collected by C.T.S. Little
West Fork Satsop River, Grays Harbor County, Washington State, USA	2	JLG459C 1&2, 3B: several wavy tubes preserved near each other.	(Peckmann *et al.*, 2002; Vinn *et al.*, 2013)	Donated by J.L. Goedert
Murdock Creek, Clallam County, Washington State, USA	3	LACMIP 6295: One spiralling tube, another tube with a ~90° bend, and a smaller tube observed in thin section only.	(Goedert and Squires, 1993; Vinn *et al.*, 2013)	Donated by J.L. Goedert
Canyon River, SW Washington State, USA	18+	LCAMIP 16957: several large straight tubes preserved in the same orientation. JLG 473: tubes embedded in carbonate matrix, thin sections of tubes only.	(Goedert and Squires, 1990a; Goedert *et al.*, 2000; Peckmann *et al.*, 2002)	Donated by J.L. Goedert
Humptulips, Grays Harbor County, Washington State, USA	2	LACMIP 12385: several tubes with dark walls, one curving.	(Goedert and Squires, 1990a; Vinn *et al.*, 2013)	Donated by J. L. Goedert and E. Southward, used for py-GC-MS only
Bear River, Pacific County, Washington State, USA	5	LACMIP 5802 BRB-1: Several small tubes preserved in close proximity and embedded within the carbonate matrix.	(Vinn *et al.*, 2013)	Donated by J.L. Goedert
Omagari, Nakagawa-cho region, NW Hokkaido, north Japan	many	Many small, similar-diameter tubes preserved together. OMG03-1: many tubes in muddy, crumbly matrix. OMG03-2, OMG03-3a, OMG03-3b: many tubes preserved in hard cement with light-coloured tube walls. OMG03-4a: pinkish calcite with many worm tubes with brown walls.	(Hikida *et al.*, 2003; Majima *et al.*, 2005; Kiel *et al.*, 2008b)	Donated by Y. Hikida
Okukinenbetsu River, Obira-machi, NW Hokkaido, north Japan	many	OKb4-5: Similarly sized tubes preserved in a range of orientations. OKb4-3: larger tubes with brown walls largely obscured by rock matrix.	(Majima *et al.*, 2005; Kiel *et al.*, 2008b)	Donated by F.L. Gill
Kapedhes, Kinousa, Kambia, Memi, Sha sites, Cyprus	many	Kambia 401b, 4061, 4062; Kapedhes 2031, 2051, 2081; Memi 212b2, 2021; Sha 3011: Small worm tubes with collars, generally occurring with other similar tubes. Kambia 4051, 4061, 6061, t3; Kapedhes 204b, 2101: Worm tubes with walls ornamented by transverse and longitudinal wrinkles. Kinousa 2023; Memi 2021: Sinuous worm tubes, several tubes	(Oudin and Constantinou, 1984; Little *et al.*, 1999a)	Collected by C.T.S. Little

		often occurring together.		
Christopher Fm. Ellef Rignes and Prince Patrick Islands, northern Canada	many	C-581891 QQA 10-22 Ellef Ringnes Island: clustered broken fragments of large tubes, mostly in various orientations however some tubes are aligned parallel to each other. C-453952 1-4 Prince Patrick Island: many small tubes cemented together in a large bundle.	(Beauchamp *et al.*, 1989; Beauchamp and Savard, 1992; Williscroft, 2013)	Donated by S.E. Grasby
Cold Fork of Cottonwood Creek, northern California, USA	many	CFCC-2A, 2B, CC-F8: Yellowish tubes, many occurring together in a range of orientations.	(Campbell, 1995; Campbell *et al.*, 2002)	Donated by K.A. Campbell
Wilbur Springs, northern California, USA		WS45A: Single tapering tube with a smooth wall, more tubes revealed in thin section.	(Campbell, 1995; Campbell *et al.*, 2002)	Donated by K.A. Campbell
Sassenfjorden area, Spitsbergen, Svalbard	3	Svalbard 2007-03: long tube with yellowish wall. Svalbard 2009-01: single tube with dark black wall. 2009-03: single tube with longitudinal wrinkles.	(Hammer *et al.*, 2011; Hryniewicz *et al.*, 2012, 2015; Vinn *et al.*, 2014)	Donated by K. Hryniewicz
Figueroa, San Rafael Mountains, southern California	many	FF-10, FFC-00, FFC-12, FFC-18, FFC-19, FFC-37: Blocks of vent chimney sulphides containing fossilised tube fragments, tubes often occurring singly.	(Little *et al.*, 1999b, 2004)	Collected by C.T.S. Little
Sibay, southern Ural Mountains, Russia	6	*Tevidestus serriformis*: BMNH VF 71: Single tube fragment. Indeterminate ?annelid: BMNH VF 71: cluster of tubes.	(Little *et al.*, 1999c)	Collected by C.T.S. Little
Yaman Kasay, southern Ural Mountains, Russia	7	*Eoalvinellodes annulatus*: BMNH VF 50-55, 57, 60-61, 102: Tubes occurring either singly or in small clumps. *Yamankasia rifeia*: BMNH VF 78, 80, 84, 89, 97: Very large tubes mostly preserved singly.	(Little *et al.*, 1997, 1999c)	Collected by C.T.S. Little

Table D.3 Modern tubes examined.

Taxa	No. examined	Specimen information	Description(s) consulted	Notes
Galathealinum arcticum	1	NHMUK 1962.1.9.1; Thetis Bay, Herschel Island, Canada; 69.5333/-138.9500; 36 m.	(Southward, 1962)	
Lamellisabella denticulata	4	NHMUK 1978.3.21.2-5; Bay of Biscay, NE Atlantic; 45.583/-3.866; 4250 m.	(Southward, 1978a)	
Oligobrachia gracilis	4	NHMUK 1978.1.13.17-27; Bay of Biscay, NE Atlantic; 48.383/-9.85; 720-2215 m.	(Southward, 1978b)	
Polybrachia canadensis	4	NHMUK 1969.3.3.4-5; Off Vancouver Island Canada; 50.533/-129.033; 1900 m.	(Southward, 1969)	
Siboglinum ekmani	3	Skagerrak; 58.448-58.445/10.228-10.420; 434-471 m.		Donated by H. Wiklund
Siboglinum lacteum	1	NHMUK 1962.1.9.1; NE Atlantic; 48.50/-10.00; 1100-1250 m.	(Southward, 1963)	
Siphonobrachia lauensis	3	NHMUK 1991.1-3; Lau Basin, S Pacific; -22.533/-176.717; 1914 m.	(Southward, 1991)	
Unibrachium colombianum	1	NHMUK 1978.1.13.1; Off N Colombia; 11.300/-74.733; 605 m.	(Southward, 1972)	
Zenkevitchiana longissima	2	NHMUK 1960.10.1.1; Kurile-Kamschatka Trench N Pacific; Vitjas Stn 2217; 9220-8820 m .	(Ivanov, 1963)	
Sclerolinum contortum	many	Nyegga HMMV NE Atlantic, Walker Ridge Gulf of Mexico, Loki's Castle N Atlantic.	(Smirnov, 2000; Eichinger *et al.*, 2013)	Donated by A. Andersen, M. Bright, H.T. Rapp
Alaysia spiralis	-	Tube information included from original description.	(Southward, 1991)	
Arcovestia ivanovi	3	Manus Basin SW Pacific.	(Southward and Galkin, 1997)	Small fragments donated by E.C. Southward
Escarpia southwardae	9	Gabon Margin E Atlantic.	(Andersen *et al.*, 2004)	Donated by A. Andersen
Lamellibrachia anaximandri	9	Anaximander and Olimpi mud fields, wreck of S.S. Persia; 1945-2800 m.	(Southward *et al.*, 2011)	Donated by A. Andersen and D. Hughes
Paraescarpia echinospica	1	NHMUK 2001.6633; Edison Seamount Papua New Guinea; -3.232/152.592; 1600 m.	(Southward *et al.*, 2002)	
Ridgeia piscesae	many	Juan de Fuca Ridge NE Pacific.	(Southward *et al.*, 1995)	Donated by J. Copley
Riftia pachyptila	4	NHMUK 1981.1; Galapagos Rift E Pacific; 0.804/-86.225; 2450 m. NHMUK 2011.28; Guaymas Basin. 9°N E Pacific Rise; 2500 m.	(Jones, 1985)	EPR tubes collected by C.T.S. Little
Seepiophila jonesi	9	Green Canyon Lease Block Gulf of Mexico; 550 m	(Gardiner *et al.*, 2001)	Donated by C. Fisher
Tevnia jerichonana	6	9°N E Pacific Rise; ~2500 m.	(Jones, 1985)	Collected by C.T.S. Little
Chaetopteridae sp.	8	Wagner Basin Gulf of California; 31.062/-144.087; 103 m.	-	Small tube fragments, donated by P. Dando
Chaetopterus cf. *variopedatus*	6	Eddystone Plymouth Sound; 50.180/-4.267; 18 m.	(Enders, 1909)	Collected by A. Glover
Mesochaetopterus taylori	1	NHMUK 1935.12.19.36; Departure Bay Vancouver.	(Sendall *et al.*, 1995)	
Phyllochaetopterus claparedii	14	NHMUK 1885.12.1.268, NHMUK 1921.5.1.2807-12; Kobe Japan Challenger Stn 233; 15-91 m.		
Phyllochaetopterus gigas	1	'Ruby' whalefall Monterey Bay CA; 36.614/-122.435; 2893 m.	(Nishi and Rouse, 2014)	Collected by C.T.S. Little
Phyllochaetopterus polus	32	Ashadze Mid-Atlantic Ridge; 12.973/-44.863; 4080 m.	(Morineaux *et al.*, 2010)	Donated by M. Morineaux

Phyllochaetopterus prolifica	3	NHMUK 1915.5.1.4-6; NW Pacific.		
Phyllochaetopterus socialis	many	NHMUK 1930.10.8.2133-44; Elephant Bay Angola.		
Spiochaetopterus costarum	6	NHMUK 1928.4.26.585-8; Naples. NHMUK 1970.629; Komimbo Bay Solomon Islands.	(Barnes, 1964)	
Spiochaetopterus izuensis	5	Off Futo Izu Peninsula Japan; 12 m.	(Nishi *et al.*, 2004)	Donated by E. Nishi
Spiochaetopterus sagamiensis	1	Off Hatsushima Sagami Bay Japan; 35.017/139.200; 800-1100 m.	(Nishi *et al.*, 1999)	Donated by E. Nishi
Spiochaetopterus typicus	1	NHMUK 1900.5.1.354-5; Denmark.		
Serpulidae sp. JCR (*Serpula* cf. *narconensis*)	9	Southern Ocean; JR275 1565, 1615.		
Serpula vermicularis	many	NHMUK 1941.3.3.1469; BANZAR Expedition station 47; 150 m.		
Vermiliopsis infundibulum	3	NHMUK 1930.10.8.2677-79; Discovery station 283 Gulf of Guinea; 18-30 m.	(Radwanska, 1994)	Small fragments
Megalomma vesiculosum	1	Nord Ilot St Anne Pemoull Roscoff; intertidal.	-	Donated by A. Andersen
Sabella pavonina	1	Nord Ilot St Anne Pemoull Roscoff; intertidal.	-	Donated by A. Andersen
Alvinella spp.	9	9°N E Pacific Rise; 2500 m.	(Gaill and Hunt, 1986)	Collected by C.T.S. Little
Glyphanostomum sp.	2	Falkland Islands.	(Reuscher *et al.*, 2009, 2015)	Donated by Lenka Neal and Gordon Paterson
Lamellibrachia luymesi	many	Gulf of Mexico.	(Gardiner and Hourdez, 2003)	Donated by C. Fisher, used for py-GC-MS only
Spirobrachia triperia	1	Porto Mud Volcano Gulf of Cadiz.	(Hilário and Cunha, 2008)	Donated by A. Hilário, used for py-GC-MS only

Table D.4 Data matrix used in phylogenetic analyses. Fossil taxa are highlighted.

	1-5	6-10	11-15	16-20	21-25	26-30	31-35	36-40	41-45	46-48
Yamankasia rifeia	10110	000--	--??0	1?01?	0----	---00	00-11	?0011	00000	???
Eoalvinellodes annulatus	00110	000--	--??0	1100?	0----	---00	00-00	1100-	---0?	?1?
Indeterminate annelid - Sibay	00110	000--	--??0	??0??	0----	---00	00-00	0-00-	---0?	???
Tevidestus serriformis	000--	000--	--??0	1????	10100	1?000	00-00	0-00-	---00	1??
Figueroa	00110	000--	--??0	1?00?	11010	10000	00-?1	0-010	01100	???
Svalbard	000--	000--	--??0	1?00?	?10?0	??000	00-00	0-0?0	0?000	?11
Wilbur Srings	00110	0?0--	--???	?????	?????	?????	?????	?????	???00	???
Cold Fork Cottonwood Creek	00101	000--	--??0	0?010	0----	---00	00-??	0-???	???10	???
Christopher Fm. - Prince Patrick Is.	00101	000--	--??0	?1000	0----	---00	00-??	0-???	???00	?11
Christopher Fm. - Ellef Ringnes Is.	0011?	000--	--??0	1??0?	0----	---00	00-00	0-00-	---00	?11
Troodos - attached tubes	00110	100--	--??0	011??	0----	---00	00-?0	???0-	---0?	???
Troodos - wrinkled tubes	00110	000--	--??0	1??0?	0----	---00	00-11	0-010	0110?	???
Troodos - collared tubes	00110	000--	--??0	0110?	11010	00000	00-00	0-00-	---0?	???
Okukinenbetsu - yellow tubes	00110	000--	--??0	1??1?	0----	---00	00-00	0-010	0100?	???
Okukinenbetsu - brown tubes	000--	000--	--??0	1??1?	0----	---00	00-??	0-0??	???00	?11
Omagari	00101	000--	--??0	01000	0----	---00	00-??	0-?0-	---00	??1
Bear River	00110	000--	--???	???0?	?????	?????	?????	?????	???00	?1?
Canyon River	00111	000--	--??0	1??0?	0----	---00	00-00	0-010	??000	???
Murdock Creek	000--	000--	--??0	?1?1?	0----	---00	00-00	0-0?0	?0000	?11
West Fork Satsop River	000--	000--	--??0	?1?0?	0----	---00	00-00	0-00-	---00	??1
Bexhaven	00101	100--	--??0	1??0?	0----	---00	00-00	0-10-	---01	?--
Upper Waiau River	00110	00??0	?0??0	???0?	0----	---00	00-00	0-00-	---00	???
Rocky Knob	00110	000--	--??0	1??1?	0----	---00	00-00	0-010	01000	?1?
Chaetopterus cf. *variopedatus*	100--	0110-	--010	00011	0----	---00	00-00	0-00-	---00	010
Chaetopteridae - id83	00???	000--	--010	10000	0----	---00	01000	10010	10000	100
Phyllochaetopterus polus	00101	000--	--011	10010	10000	01000	00-00	1100-	---00	100
Phyllochaetopterus gigas	00110	000--	--011	10010	0----	---00	00-00	1100-	---00	100
Phyllochaetopterus claparedii	000--	000--	--011	10010	0----	---00	10-00	1100-	---10	100
Phyllochaetopterus prolifica	00010	000--	--011	01010	10000	00000	11000	1100-	---00	100
Phyllochaetopterus socialis	00101	000--	--011	00000	0----	---00	11000	0-00-	---00	101
Spiochaetopterus izuensis	00101	000--	--010	00010	0----	---10	00-00	1000-	---10	100
Spiochaetopterus sagamiensis	000--	000--	--010	10010	0----	---00	00-00	1100-	---00	100
Spiochaetopterus costarum	00110	000--	--010	10010	0----	---10	00-00	1000-	---10	110
Spiochaetopterus typicus	000--	000--	--010	10010	0----	---00	01000	1100-	---00	110
Mesochaetopterus taylori	000--	00110	10010	10010	0----	---00	00-00	0-00-	---00	001
Galathealinum arcticum	00110	000--	--100	1?011	10100	00001	00-00	0-00-	---00	011
Lamellisabella denticulata	00110	000--	--100	10001	10100	00000	00-00	1000-	---00	011
Oligobrachia gracilis	01101	000--	--100	10011	0----	---01	00-00	10010	01000	011
Polybrachia canadensis	00110	000--	--100	10011	11100	00001	00-00	10011	00000	011
Siboglinum ekmani	01101	000--	--100	00010	0----	---11	00-00	0-00-	---00	0??
Siboglinum lacteum	010--	000--	--100	10010	0----	---00	00-01	10010	01000	001
Siphonobrachia lauensis	00110	000--	--100	10-01	11010	00000	00-11	10001	00000	011
Unibrachium colombianum	01110	000--	--100	10011	0----	---01	00-00	1000-	---00	001
Zenkevitchiana longissima	00111	000--	--100	10010	0----	---10	00-11	10010	01000	011
Sclerolinum contortum	01101	000--	--100	11110	0----	---00	00-11	0-010	01000	001
Alaysia spiralis	00110	000--	--100	01101	11000	00000	00-??	0-0??	???00	011
Arcovestia ivanovi	00111	000--	--100	11001	11010	11000	00-00	0-010	11100	011
Escarpia southwardae	00111	000--	--100	11001	0----	---00	00-00	0-00-	---00	011
Lamellibrachia anaximandri	00111	000--	--100	11001	10000	00000	00-00	0-011	00000	011
Paraescarpia echinospica	10110	000--	--100	10001	11011	10000	00-10	0-00-	---00	011
Ridgeia piscesae	00111	000--	--100	11001	11010	11000	00-11	0-010	01100	001
Riftia pachyptila	10111	000--	--100	10010	11000	00000	00-11	0-010	01100	001
Tevnia jerichonana	00111	000--	--100	10001	10100	11000	00-01	0-010	01100	011
Seepiophila jonesi	00111	000--	--100	01001	11001	10000	00-10	0-010	01100	011
Escarpia southwardae - posterior	00101	000--	--100	01010	0----	---00	00-00	0-011	00000	011
Lamellibrachia anaximandri - posterior	00101	000--	--100	11010	0----	---00	00-00	0-011	00000	001
Paraescarpia echinospica - posterior	00101	000--	--100	01000	0----	---00	00-00	0-011	00000	011
Ridgeia piscesae - posterior	00101	000--	--100	11000	0----	---00	00-00	0-00-	---00	0?1
Alvinella spp.	10101	110--	--000	10010	0----	---00	00-00	0-00-	---00	010
Glyphanostomum sp.	00110	000--	--??0	00010	0----	---00	01100	0-00-	---00	???
Serpulidae JCR	00110	100--	--000	10001	11000	10?00	00-00	0-10-	---01	---
Serpula vermicularis	00111	000--	--000	01001	11001	10100	00-00	0-10-	---01	---
Vermiliopsis infundibulum	000--	100--	--000	0?001	11011	00?00	00-00	0-?10	10001	---
Sabella pavonina	00110	00111	0-??0	10010	0----	---00	01000	0-00-	---00	?11
Megalomma vesiculosum	000--	00111	0-??0	1001?	0----	---00	00-00	0-00-	---00	?11
Owenia fusiformis	00110	00110	11100	10010	0----	---00	00-00	0-00-	---00	???

Table D.5 NCBI Genbank accession numbers. Information in parentheses after a species name indicates the taxon for which tube morphology was assessed.

Taxon	COI	28S	18S	16S
Chaetopterus variopedatus (morph: cf. *variopedatus*)	AM503096	AY145399	U67324	
Chaetopteridae sp 83				
Phyllochaetopterus polus	GQ891958			
Phyllochaetopterus gigas	DQ209248	DQ209228	DQ209213	
Phyllochaetopterus prolifica	HM473564	HM473256		
Phyllochaetopterus socialis	DQ209247	DQ209227	DQ209212	
Mesochaetopterus taylori	DQ209251	DQ209232	DQ209217	
Galathealinum branchiosum (morph: *arcticum*)	U74066		AF168738	AF315040
Lamellisabella denticulata	FJ480376			
Oligobrachia haakonmosbiensis (morph: *gracilis*)	FM178481		AM883186	
Siboglinum ekmani	KF444429		AF315062	AF315038
Siphonobrachia ilyophora (morph: *lauensis*)				JX013985
Sclerolinum contortum	KU214832		KU214829	KU214830
Alaysia sp. (morph: *Alaysia spiralis*)	AB088670		FM995545	
Arcovestia ivanovi	AB073491			
Escarpia southwardae	KC357336	KJ603316		KC357356
Lamellibrachia anaximandri	KC832758			HE974474
Paraescarpia cf. *echinospica* (morph: *echinospica*)	D50593		FM995546	
Ridgeia piscesae	U87975	AY344665	AF168744	AF315048
Riftia pachyptila	KP119562	KP119582	KP119591	KP119573
Tevnia jerichonana	KM271059	Z21529	AF168746	AF315042
Seepiophila jonesi	KT429473			KT429520
Alvinella pompejana (morph: sp.)	GQ473219	X80646	AM159573	
Glyphanostomum sp.	DQ209260	DQ209240	DQ209225	
Serpula vermicularis	HM375142	DQ317148	DQ317128	
Vermiliopsis infundibulum			DQ140411	
Sabella pavonina	KR916924	AY612632	U67144	AY340482
Megalomma vesiculosum			KJ182980	
Owenia fusiformis	KR916900	KP119583	KP119590	KP119572

Table D.6 Summary statistics for first 10 PCO axes, computed in PAST .

Axis	Eigenvalue	Variance (%)
1	1.045	18.75
2	0.59713	10.714
3	0.48555	8.7117
4	0.3198	5.7378
5	0.24459	4.3885
6	0.19339	3.4698
7	0.18761	3.3661
8	0.16342	2.9321
9	0.14621	2.6233
10	0.12953	2.324

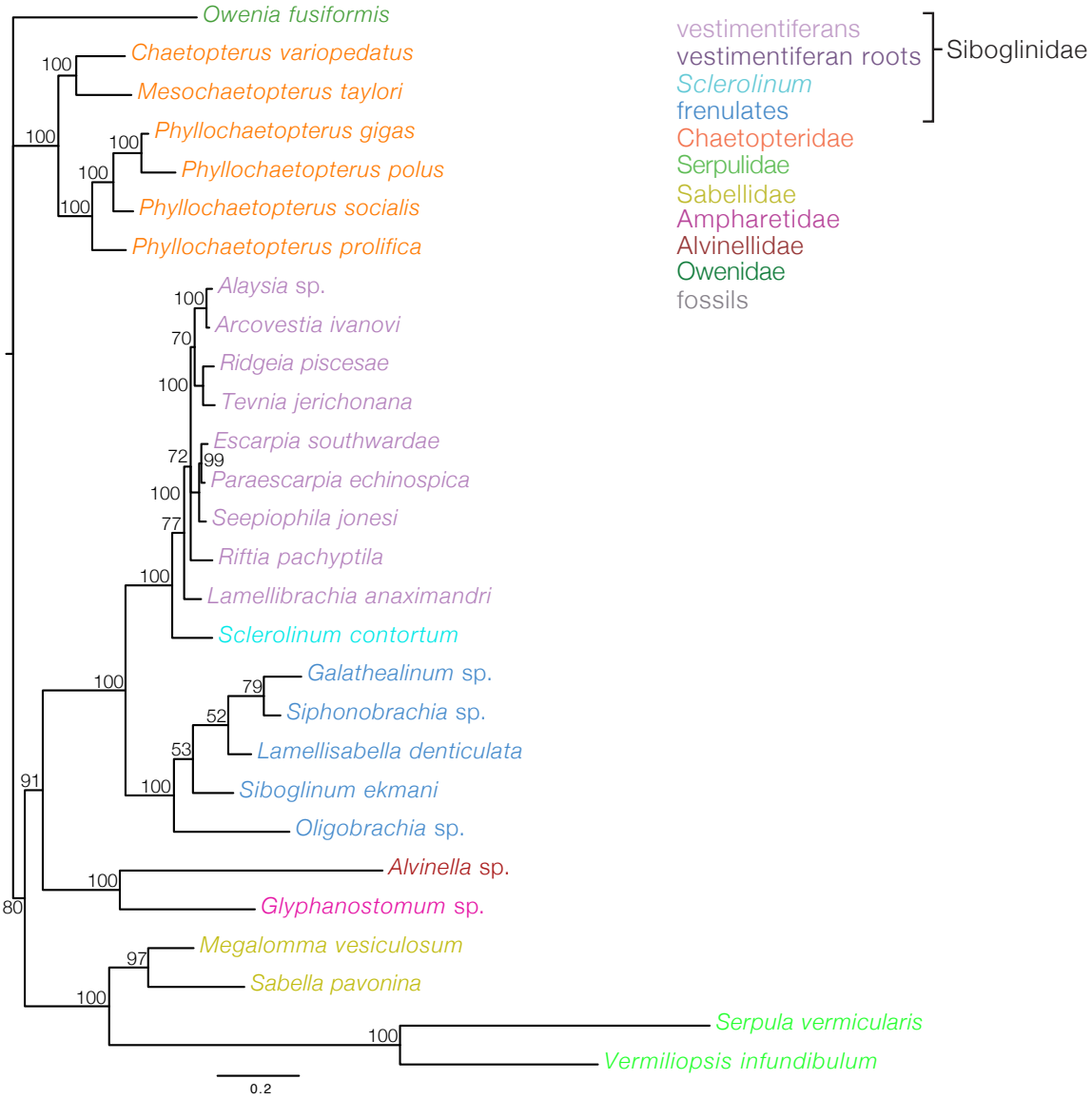

Figure D.1 Molecular data-only phylogeny of modern annelids for which tube morphology was assessed during this study. This analysis was performed using a Bayesian approach, and a combined dataset of the genes COI, 28S, 18S and 16S. The phylogeny is a 50 % consensus tree, in which numbers represent posterior probability values out of 100. The scale bar indicates substitutions per site.

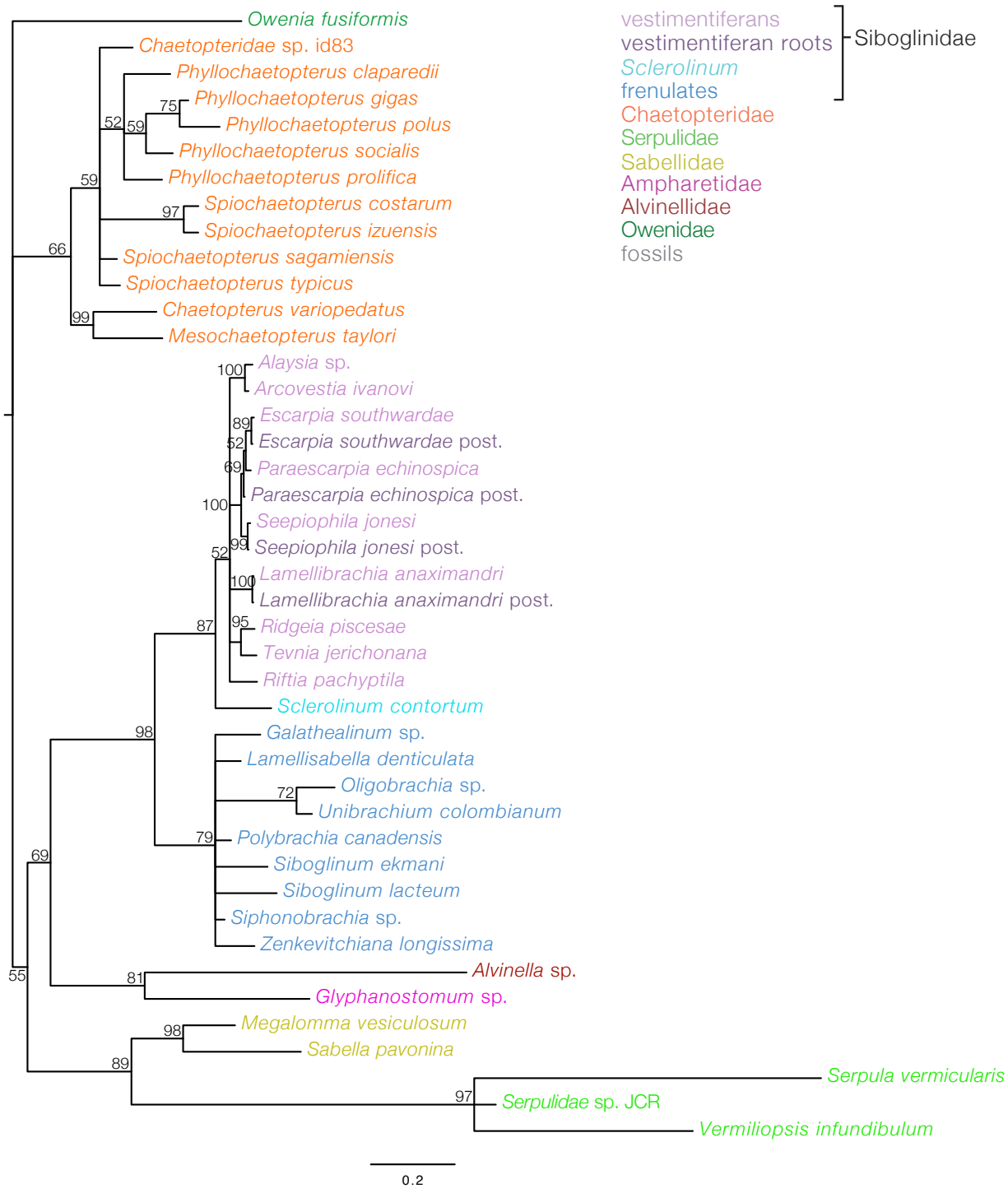

Figure D.2 Molecular and tube data phylogeny of modern annelids, for which tube morphology was assessed during this study. This analysis was performed using a Bayesian approach, and a combined dataset of the genes COI, 28S, 18S and 16S as well as data from the morphological character matrix (Table D.4). The phylogeny is a 50 % consensus tree, in which numbers represent posterior probability values out of 100. The scale bar indicates substitutions per site.

Figure D.3 Molecular and tube data phylogeny of modern and fossil annelids, for which tube morphology was assessed during this study. This analysis was performed using a Bayesian approach, and a combined dataset of the genes COI, 28S, 18S and 16S as well as data from the morphological character matrix (Table D.4). The phylogeny is a 50 % consensus tree, in which numbers represent posterior probability values out of 100. The scale bar indicates substitutions per site.

Table D.7 Results of pyrolysis gas chromatography mass spectrometry (py-GC-MS) analyses of modern tube material. Relative abundance is indicated by plus and minus symbols, and base peak ions are in bold.

Compound	Origin	MS characteristics	*Alvinella* sp.	*R. pisce-sae anterior*	*E. south-wardae* anterior	*E. south-wardae* posterior	*L. luymesi* posterior	*S. tripeira*	*S. contor-tum*	*C.* cf. *vario-pedatus*	*M. taylori*	*P. polus*	*P. gigas*	*S. izuensis*
Acetic acid	Chitin	**60**	+++	+++	+++	+++	?	+++	+++	?	-	-	+++	?
Pyridine	Chitin	**79**, 52	+++	+++	+++	+++	?	+++	+++	+++	+++	-	+++	+++
Methylpyridine	Chitin	**93**, 66	+++	+++		+++	+++	+++	+++	+++	+++	+++	+++	+++
Acetamide	Chitin	**59**	+++	+++	+++	+++	+++	+++	+++	+++	-	-	-	-
Ethylpyridine or 2-Pyridinecarboxaldehyde	Chitin	107, **79**, 51, 78	+	-	?	?	-	+	-	?	+	-	-	-
2-Pyrrolecarboxaldehyde	Chitin	**95**, 66	-	?	-	++	-	?	?	?	-	-	-	-
N-methyl-N-ethenylacetamide	Chitin	99, **56**	-	?	-	++	-	?	?	-	-	?	?	?
N-acetyl-N-ethenylacetamide	Chitin	127, **42**, 85, 56	-	?	-	?	-	?	?	-	-	-	-	-
Acetyldihydropyridine	Chitin	123, **80**, 81, 52	-	++	?	?	++	?	+	+	-	-	-	-
Acetylpyridones	Chitin	137, **109**, 95, 81, 68, 53	-	?	-	+++	-	?	-	-	-	-	-	-
3-Acetamidofuran	Chitin	125, **83**, 54, 42, 53	-	+++	-	+++	-	+++	+++	-	-	-	-	-
3-Acetamido-5-methylfuran	Chitin	139, **97**, 69, 42, 53	-	+++	+++	+++	+++	+++	+++	-	-	-	-	-
Acetamido-pyrones	Chitin	153, **111**, 82, 42, 83	-	+++	+++	+++	+++	+++	+++	-	-	-	-	-
Oxazoline derivatives	Chitin	185, **84**, 55, 83, 42	-	-	-	-	?	++	?	-	-	-	-	-
Trianhydro-2-acetamido-2-deoxyglucose	Chitin	167, **42**, 125, 54, 83	-	?	?		-	?	?	-	-	-	-	-
Dianhydro-2-acetamido-2-deoxyglucose	Chitin	185, **69**, 97, 81, 111	-	-	?	?	?	?	-	-	-	-	-	-
1,6-anhydro-2-acetamido-2-deoxyglucose	Chitin	204, **59**, 101, 114, 57	-	-	-	?	-	?	-	-	-	-	-	-
Furan		82, 81, 53	-	+	+	-	-	-	-	+	?	+++	+++	++
Pyrrole	Ch, Pro	**67**, 55	-	-	-	?	-	-	-	-	-	-	-	-
Benzene		78, 51	-	?	++	-	-	-	?	?	?	+++	+++	?
Toluene	Phe	92, **91**	+++	+++	+++	+++	+++	+++	+++	+++	+++	+++	+++	+++
Furfural		96, 95	-	-	-	-	-	-	-	+++	+++	+++	+++	-
C1-pyrrole	Pro, Hpro	81, **80**, 52, 50	++	++	+++	+++	+++	++	+++	+++		+++	++	++

Ethylpyrrole	Pro	**95**, 94, 66	-	+	-	-	?	-	-	-	?	-		-
Styrene		104, 78, 51	+++	+++	+++	+++	+++	+++	+++	+++	+++	+	+	+++
Phenol	Tyr	**94**, 66	+++	+++	-	+++	++	+++	+++	++	+++	+++	+++	+++
Indene		116	-	?	-		?	+	+	+++	?	?	?	+++
4-Methylphenol	Tyr	108, **107**, 77, 79	+++	+++	+++	+++	+++	+++	+++	+++	+++	+++	+++	+++
Ethylcyanobenzene	Phe	117, **90**, 116, 89	+++	-	?	?	?	?	-	?	-	+	?	-
Indole	Trp	**117**, 90, 89, 63	+++	+++	?	+++	+++	+++	+++	+++	++	+++	+	+++
C1-indole	Trp	131, **130**, 77	-	+++	-	+++	+++	+++	+++	+++	?	++	++	+++

Table D.8 Results of pyrolysis gas chromatography mass spectrometry (py-GC-MS) analyses of recently mineralised tube material. Relative abundance is indicated by plus and minus symbols, and base peak ions are in bold.

Compound	Origin	MS characteristics	*Alvinella* sp. mineralised	*R. piscesae* mineralised	*E. southwardae* mineralised (3)	*E. southwardae* mineralised (14)	*E. southwardae* mineralised (18)	*L. luymesi* posterior (6)	*L. luymesi* posterior (7)
Acetic acid	Chitin	**60**	-	-	-	+++	-	-	-
Pyridine	Chitin	**79**, 52	-	-	-	+++	-	+++	++
Methylpyridine	Chitin	**93**, 66	-	-	+	++	+	+++	+++
Acetamide	Chitin	**59**	-	-	-	-	-	-	-
Ethylpyridine or 2-Pyridinecarboxaldehyde	Chitin	107, **79**, 51, 78	-	-	-	-	-	?	-
2-Pyrrolecarboxaldehyde	Chitin	**95**, 66	-	-	-	-	?	?	-
N-methyl-N-ethenylacetamide	Chitin	99, **56**	-	-	-	-	-	-	-
N-acetyl-N-ethenylacetamide	Chitin	127, **42**, 85, 56	-	-	-	-	-	-	-
Acetyldihydropyridine	Chitin	123, **80**, 81, 52	-	-	-	-	-	+	-
Acetylpyridones	Chitin	137, **109**, 95, 81, 68, 53	-	-	-	-	-	-	-
3-Acetamidofuran	Chitin	125, **83**, 54, 42, 53	-	-	-	-	-	-	-
3-Acetamido-5-methylfuran	Chitin	139, **97**, 69, 42, 53	-	-	-	-	-	-	-
Acetamido-pyrones	Chitin	153, **111**, 82, 42, 83	-	-	-	-	-	-	-
Oxazoline derivatives	Chitin	185, **84**, 55, 83, 42	-	-	-	-	-	-	-
Trianhydro-2-acetamido-2-deoxyglucose	Chitin	167, **42**, 125, 54, 83	-	-	-	-	-	-	-
Dianhydro-2-acetamido-2-deoxyglucose	Chitin	185, **69**, 97, 81, 111	-	-	-	-	-	-	-
1,6-anhydro-2-acetamido-2-deoxyglucose	Chitin	204, **59**, 101, 114, 57	-	-	-	-	-	-	-
Furan		82, 81, 53	-	-	-	+++	-	-	-
Pyrrole	Ch, Pro	**67**, 55	-	-	-	-	?	-	-
Benzene		78, 51	-	-	+++	+++	++	?	+++
Toluene	Phe	92, **91**	-	-	+++	+++	+++	+++	+++
Furfural		96, 97	-	-	-	-	-	-	-
C1-pyrrole	Pro	81, **80**, 52, 50	-	-	+++	+++	+++	+++	+++
Ethylpyrrole	Pro	**95**, 94, 66	-	-	-		-	?	-
Styrene		104, 78, 51	-	-	+	+++	++	+++	+++
Phenol	Tyr	**94**, 66	-	-	?	+++	+	+++	++
Indene		116	-	-	+++	+++	+++	+++	+++
4-Methylphenol	Tyr	108, **107**, 77, 79	-	-	++	+++	+++	+++	+++
Ethylcyanobenzene	Phe	117, **90**, 116, 89	-	-	?		+++	+	++
Indole	Trp	**117**, 90, 89, 63	-	-	+++	+++	+++	+++	+++
C1-indole	Trp	131, **130**, 77	-	-	+	+++	+++	+++	+++

Table D.9 Results of pyrolysis gas chromatography mass spectrometry (py-GC-MS) analyses of ancient tube material. Relative abundance is indicated by plus and minus symbols, and base peak ions are in bold.

Compound	Origin	MS characteristics	Rocky Knob 12-RK (smal)	Rocky Knob 12-RK (big)	Rocky Knob RNT-1	Rocky Knob RNT-2	Upper Waiau River UWT 3-4	Waipiro Stream WAIP 1	Humptulips	Omagari OMG 03-1	Omagari OMG 03-2	Omagari OMG 03-4a	Okukinenbetsu OKb 4	Okukinenbetsu OKb 4-3	Okukinenbetsu OKb 4-5	Christopher Fm. (PPI1)	Christopher Fm. (PPI2)	Christopher Fm. (ERI)
Acetic acid	Chitin	**60**	-	-	-	-	-	-	-	?	-	-	-	-	-	-	-	?
Pyridine	Chitin	**79**, 52	-	-	-	-	-	-	-	-	-	-	-	-	-	?	-	-
Methylpyridine	Chitin	**93**, 66	+	-	-	-	-	-	++	-	-	-	++	-	-	+	-	-
Acetamide	Chitin	**59**	?	-	-	-	-	-	-	-	-	-	-	-	-	-	-	-
Ethylpyridine or 2-Pyridinecarboxaldehyde	Chitin	107, **79**, 51, 78	-	-	-	-	-	-	-	-	-	-	-	-	-	-	-	-
2-Pyrrolecarboxaldehyde	Chitin	**95**, 66	-	-	-	-	-	-	-	-	-	-	-	-	-	-	-	-
N-methyl-N-ethenylacetamide	Chitin	99, **56**	-	-	-	-	-	-	-	-	-	-	-	-	-	-	-	-
N-acetyl-N-ethenylacetamide	Chitin	127, **42**, 85, 56	-	-	-	-	-	-	-	-	-	-	-	-	-	-	-	-
Acetyldihydropyridine	Chitin	123, **80**, 81, 52	-	-	-	-	-	-	-	-	-	-	-	-	-	-	-	-
Acetylpyridones	Chitin	137, **109**, 95, 81, 68, 53	-	-	?	-	-	-	-	-	-	-	-	-	-	-	-	-
3-Acetamidofuran	Chitin	125, **83**, 54, 42, 53	-	-	-	-	-	-	-	-	-	-	-	-	-	-	-	-
3-Acetamido-5-methylfuran	Chitin	139, **97**, 69, 42, 53	-	-	-	-	-	-	-	-	-	-	-	-	-	-	-	-
Acetamido-pyrones	Chitin	153, **111**, 82, 42, 83	-	-	-	-	-	-	-	-	-	-	-	-	-	-	-	-
Oxazoline derivatives	Chitin	185, **84**, 55, 83, 42	-	-	-	-	-	-	-	-	-	-	-	-	-	-	-	-
Trianhydro-2-acetamido-2-deoxyglucose	Chitin	167, **42**, 125, 54, 83	-	-	-	-	-	-	-	-	-	-	-	-	-	-	-	-
Dianhydro-2-acetamido-2-deoxyglucose	Chitin	185, **69**, 97, 81, 111	-	-	-	-	-	-	-	-	-	-	-	-	-	-	-	-
1,6-anhydro-2-acetamido-2-deoxyglucose	Chitin	204, **59**, 101, 114, 57	-	-	-	-	-	-	-	-	-	-	-	-	-	-	-	-
Furan		82, 81, 53	-	-	-	-	-	-	?	-	?	-	?	-	-	-	-	-
Pyrrole	Ch, Pro	**67**, 55	-	-	-	-	-	-	-	-	-	-	-	-	-	?	-	?
Benzene		78, 51	++	+++	+++	+++	+++	+++	+++	+++	+++	+++	+++	+++	+++	++	+++	++
Toluene	Phe	92, **91**	+++	++	+++	+++	+++	+++	+++	+++	+++	+++	+++	+++	+++	+++	+++	++
Furfural		96, 97	-	-	-	-	-	-	-	-	-	-	-	-	-	-	-	-
C1-pyrrole	Pro	81, **80**,	+	-	-	-	+	-	++	-	-	-	?	-	-	+++	++	-

		52, 50													
Ethylpyrrole	Pro	**95**, 94, 66	?	-	-	-	-	-	-	-	-	?	-	?	
Styrene		104, 78, 51	++	++	-	+	++	?	+	+	+	++	++	-	
Phenol	Tyr	**94**, 66	++	++	-	-	?	++	?	-	+++	?	?	+	
Indene		116	+++	+++	+++	+++	+++	?	+++	-	+++	+++	++	+++	+++
4-Methylphenol	Tyr	108, **107**, 77, 79	++	+++	+	-	++	+++	-	-	+++	++	+++	++	++
Ethylcyanobenzene	Phe	117, **90**, 116, 89	?	-	-	-	-	-	?	?	-	-	++	-	?
Indole	Trp	**117**, 90, 89, 63	+++	-	-	-	-	++	-	-	-	-	+++	++	?
C1-indole	Trp	131, **130**, 77	++	-	-	+	-	?	-	-	-	-	++	++	?

References

Andersen, A. C., Hourdez, S., Marie, B., Jollivet, D., Lallier, F. H. and Sibuet, M. (2004) *Escarpia southwardae* sp. nov., a new species of vestimentiferan tubeworm (Annelida, Siboglinidae) from West African cold seeps. *Canadian Journal of Zoology* **82**, 980–999. doi:10.1139/z04-049.

Banks, D. A. (1985) A fossil hydrothermal worm assemblage from the Tynagh lead–zinc deposit in Ireland. *Nature* **313**, 128–131.

Barnes, R. (1964) Tube-building and feeding in the chaetopterid polychaete, *Spiochaetopterus oculatus*. *The Biological Bulletin* **127**, 397–412.

Beauchamp, B. and Savard, M. (1992) Cretaceous chemosynthetic carbonate mounds in the Canadian Arctic. *Palaios* **7**, 434–450.

Beauchamp, B., Harrison, J. C., Nassichuk, W. W., Krouse, H. R. and Eliuk, L. S. (1989) Cretaceous cold-seep communities and methane-derived carbonates in the Canadian Arctic. *Science* **244**, 53–6. doi:10.1126/science.244.4900.53.

Boirat, J. M. and Fouquet, Y. (1986) Decouverte de tubes de vers hydrothermaux fossils dans un amas sulfure de l'Eocene superieur (Barlo, ophiolite de Zambales, Philippines). *Comptes Rendue, Serie II* **302**, 941–946.

Boyce, A. J., Little, C. T. S. and Russel, M. J. (2003) A new fossil vent biota in the Ballynoe barite deposit, Silvermines, Ireland: evidence for intracratpnic sea-floor hydrothermal activity about 352 Ma. *Ecolomic Geology* **98**, 649–656.

Buschmann, B. and Maslennikov, V. V. (2006) The late Ordovican or earliest Silurian hydrothermal vent fauna from Yaman Kasy VMS deposit (South Uralides, Russia). *Freiberger Forschungshefte* **14**, 139–172.

Campbell, K. A. (1995) Dynamic development of Jurassic-Pliocene cold-seeps, convergent margin of western North America. PhD Thesis, University of Southern California.

Campbell, K. A. (2006) Hydrocarbon seep and hydrothermal vent paleoenvironments and paleontology: past developments and future research directions. *Palaeogeography, Palaeoclimatology, Palaeoecology* **232**, 362–407. doi:10.1016/j.palaeo.2005.06.018.

Campbell, K. A., Farmer, J. D. and Des Marais, D. (2002) Ancient hydrocarbon seeps from the Mesozoic convergent margin of California: carbonate geochemistry, fluids and palaeoenvironments. *Geofluids* **2**, 63–94. doi:10.1046/j.1468-8123.2002.00022.x.

Campbell, K. A., Francis, D. A., Collins, M., Gregory, M. R., Nelson, C. S., Greinert, J. and

Aharon, P. (2008a) Hydrocarbon seep-carbonates of a Miocene forearc (East Coast Basin), North Island, New Zealand. *Sedimentary Geology* **204**, 83–105. doi:10.1016/j.sedgeo.2008.01.002.

Campbell, K. A., Francis, D. A., Collins, M., Gregory, M. R., Nelson, C. S., Greinert, J. and Aharon, P. (2008b) Hydrocarbon seep-carbonates of a Miocene forearc (East Coast Basin), North Island, New Zealand. *Sedimentary Geology* **204**, 83–105. doi:10.1016/j.sedgeo.2008.01.002.

Dube, T. E. (1988) Tectonic significance of Upper Devonian igneous rocks and bedded barite, Roberts Mountain allochthon, Nevada, U.S.A. In *Devonian of the World (Sedimentation), Vol. II.* (ed. McMillan, S. M., Embry, A. F., and Glass, D. J.), pp. 235–249. Canadian Society of Petroleum Geologists, Calgary.

Eichinger, I., Hourdez, S. and Bright, M. (2013) Morphology, microanatomy and sequence data of *Sclerolinum contortum* (Siboglindae, Annelida) of the Gulf of Mexico. *Organisms Diversity and Evolution* **13**, 311–329. doi:10.1007/s13127-012-0121-3.

Enders, H. E. (1909) A study of the life history and habits of *Chaetopterus variopedatus*. *Journal of Morphology* **20**, 479–532.

Gaill, F. and Hunt, S. (1986) Tubes of deep sea hydrothermal vent worms *Riftia pachyptila* (Vestimentifera) and *Alvinella pompejana* (Annelida). *Marine Ecology Progress Series* **3**, 267–274.

Gardiner, S. L. and Hourdez, S. (2003) On the occurrence of the vestimentiferan tube worm *Lamellibrachia luymesi* van der Land and Nørrevang, 1975 (Annelida: Pogonophora) in hydrocarbon seep communities in the Gulf of Mexico. *Proceedings of the Biological Society of Washington* **116**, 380–394.

Gardiner, S. L., McMullin, E. and Fisher, C. R. (2001) *Seepiophila jonesi*, a new genus and species of vestimentiferan tube worm (Annelida: Pogonophora) from hydrocarbon seep communities in the Gulf of Mexico. *Proceedings of The Biological Society of Washington* **114**, 694–707.

Gill, F. L., Harding, I. C., Little, C. T. S. and Todd, J. A. (2005) Palaeogene and Neogene cold seep communities in Barbados, Trinidad and Venezuela: An overview. *Palaeogeography, Palaeoclimatology, Palaeoecology* **227**, 191–209. doi:10.1016/j.palaeo.2005.04.024.

Goedert, J. and Campbell, K. (1995) An early Oligocene chemosynthetic community from the Makah Formation, northwestern Olympic Peninsula, Washington. *Veliger* **38**, 22–

29.

Goedert, J. L. and Squires, R. L. (1990a) Eocene deep-sea communities in localized limestones formed by subduction-related methane seeps, southwestern Washington. *Geology* **18**, 1182–1185. doi:10.1130/0091-7613(1990)018<1182:EDSCIL>2.3.CO;2.

Goedert, J. L. and Squires, R. L. (1990b) Eocene deep-sea communities in localized limestones formed by subduction-related methane seeps, southwestern Washington. *Geology* **18**, 1182–1185. doi:10.1130/0091-7613(1990)018.

Goedert, J. L. and Squires, R. L. (1993) First Oligocene records of *Calyptogena* (Bivalvia: Vesicomyidae). *Veliger* **36**, 72–77.

Goedert, J., Peckmann, J. and Reitner, J. (2000) Worm tubes in an allochthonous cold-seep carbonate from lower Oligocene rocks of western Washington. *Journal of Paleontology* **74**, 992–999.

Goedert, J. L., Thiel, V., Schmale, O., Rau, W. W., Michaelis, W. and Peckmann, J. (2003) The Late Eocene Whiskey Creek methane-seep deposit (western Washington State). Part I: Geology, palaeontology, and molecular geobiology. *Facies* **48**, 223 – 240.

Gomez-Perez, I. (2003) An Early Jurassic deep-water stromatolitic bioherm related to possible methane seepage (Los Molles Formation, Neuquen, Argentina). *Palaeogeography, Palaeoclimatology, Palaeoecology* **201**, 21–49.

Hammer, Ø., Nakrem, H. a., Little, C. T. S., Hryniewicz, K., Sandy, M. R., Hurum, J. H., Druckenmiller, P., Knutsen, E. M. and Høyberget, M. (2011) Hydrocarbon seeps from close to the Jurassic–Cretaceous boundary, Svalbard. *Palaeogeography, Palaeoclimatology, Palaeoecology* **306**, 15–26. doi:10.1016/j.palaeo.2011.03.019.

Haymon, R. and Koski, R. (1985) Evidence of an ancient hydrothermal vent community: fossil worm tubes in Cretaceous sulfide deposits of the Samail Ophiolite, Oman. *Bulletin of the Biological Society of Washington* **6**, 57–65.

Haymon, R. M., Koski, R. A. and Sinclair, C. (1984) Fossils of hydrothermal vent worms from Cretaceous sulfide ores of the Samail Ophiolite, Oman. *Science* **223**, 1407–1409.

Hikida, Y., Suzuki, S., Togo, Y. and Ijiri, A. (2003) An exceptionally well-preserved fossil seep community from the Cretaceous Yezo Group in the Nakagawa area, Hokkaido, northern Japan. *Paleontological Research* **7**, 329–342.

Hilário, A. and Cunha, M. R. (2008) On some frenulate species (Annelida: Polychaeta: Siboglinidae) from mud volcanoes in the Gulf of Cadiz (NE Atlantic). *Scientia Marina*

72, 361–371.

Himmler, T., Freiwald, A., Stollhofen, H. and Peckmann, J. (2008) Late Carboniferous hydrocarbon-seep carbonates from the glaciomarine Dwyka Group, southern Namibia. *Palaeogeography, Palaeoclimatology, Palaeoecology* **257**, 185–197. doi:10.1016/j.palaeo.2007.09.018.

Hryniewicz, K., Hammer, Ø., Nakrem, H. a. and Little, C. T. S. (2012) Microfacies of the Volgian-Ryazanian (Jurassic-Cretaceous) hydrocarbon seep carbonates from Sassenfjorden, central Spitsbergen, Svalbard. *Norsk Geologisk Tidsskrift* **92**, 113–131.

Hryniewicz, K., Nakrem, H. A., Hammer, Ø., Little, C. T. S., Kaim, A., Sandy, M. R. and Hurum, J. H. (2015) The palaeoecology of the latest Jurassic-earliest Cretaceous hydrocarbon seep carbonates from Spitsbergen, Svalbard. *Lethaia* **48**, 353–374. doi:10.1111/let.12112.

Ivanov, A. (1963) *Pogonophora*. Academic Press, London.

Jones, M. L. (1985) On the Vestimentifera, new phylum: six new species, and other taxa, from hydrothermal vents and elsewhere. *Bulletin of the Biological Society of Washington* **6**, 117–158.

Kauffman, E. G., Arthur, M. a., Howe, B. and Scholle, P. a. (1996) Widespread venting of methane-rich fluids in Late Cretaceous (Campanian) submarine springs (Tepee Buttes), Western Interior Seaway, U.S.A. *Geology* **24**, 799–802. doi:10.1130/0091-7613(1996)024<0799:WVOMRF>2.3.CO;2.

Kiel, S. (2010) An Eldorado for paleontologists: the Cenozoic seeps of western Washington State, USA. In *The Vent and Seep Biota* (ed. Kiel, S.), pp. 433-448. Springer Netherlands, Dordrecht. doi:10.1007/978-90-481-9572-5_14.

Kiel, S. and Campbell, K. A. (2005) *Lithomphalus enderlini* gen. et sp. nov. from cold-seep carbonates in California - a Cretaceous neomphalid gastropod? *Palaeogeography, Palaeoclimatology, Palaeoecology* **227**, 232–241. doi:10.1016/j.palaeo.2005.04.022.

Kiel, S., Campbell, K. A., Elder, W. P. and Little, C. T. S. (2008a) Jurassic and Cretaceous gastropods from hydrocarbon seeps in forearc basin and accretionary prism settings, California. *Acta Palaeontologica Polonica* **53**, 679–703. doi:10.4202/app.2008.0412.

Kiel, S., Amano, K. and Jenkins, R. G. (2008b) Bivalves from cretaceous cold-seep deposits on Hokkaido, Japan. *Acta Palaeontologica Polonica* **53**, 525–537. doi:10.4202/app.2008.0310.

Little, C. T. S., Herrington, R. J., Maslennikov, V. V., Morris, N. J. and Zaykov, V. V. (1997) Silurian hydrothermal-vent community from the southern Urals, Russia. *Nature* **385**, 146–148. doi:10.1038/385146a0.

Little, C. T. S., Herrington, R. J., Maslennikov, V. V. and Zaykov, V. V. (1998) The fossil record of hydrothermal vent communities. *Geological Society, London, Special Publications* **148**, 259–270. doi:10.1144/GSL.SP.1998.148.01.14.

Little, C. T. S., Cann, J. R., Herrington, R. J. and Morisseau, M. (1999a) Late Cretaceous hydrothermal vent communities from the Troodos ophiolite, Cyprus. *Geology* **27**, 1027–1030.

Little, C. T. S., Herrington, R. J., Haymon, R. M. and Danelian, T. (1999b) Early Jurassic hydrothermal vent community from the Franciscan Complex, San Rafael Mountains, California. *Geology* **27**, 167–170.

Little, C. T. S., Maslennikov, V. V, Morris, N. J. and Gubanov, A. P. (1999c) Two Palaeozoic hydrothermal vent communities from the southern Ural mountains, Russia. *Palaeontology* **42**, 1043–1078.

Little, C. T. S., Danelian, T., Herrington, R. and Haymon, R. (2004) Early Jurassic hydrothermal vent community from the Franciscan Complex, California. *Journal of Paleontology* **78**, 542–559.

Majima, R., Nobuhara, T. and Kitazaki, T. (2005) Review of fossil chemosynthetic assemblages in Japan. *Palaeogeography, Palaeoclimatology, Palaeoecology* **227**, 86–123. doi:10.1016/j.palaeo.2005.04.028.

Minisini, D. and Schwartz, H. (2007) An early Paleocene cold seep system in the Panoche and Tumey Hills, central California (United States). In *Sand Injectites: Implications for Hydrocarbon Exploration and Production* (ed. Hurst, A. and Cartwright, J.), pp. 185–197. AAPG Memoir 87 doi:10.1306/1209862M873264.

Moore, D. W., Young, L. E., Modene, J. S. and Plahuta, J. T. (1986) Geologic setting and genesis of the Red Dog zinc–lead–silver deposit, western Brooks Range, Alaska. *Economic Geology* **81**, 1696–1727.

Morineaux, M., Nishi, E., Ormos, A. and Mouchel, O. (2010) A new species of *Phyllochaetopterus* (Annelida: Chaetopteridae) from deep-sea hydrothermal Ashadze-1 vent field, Mid-Atlantic Ridge: taxonomical description and partial COI DNA sequence. *Cahiers Biologie Marine* **51**, 239–248.

Natalicchio, M., Dela Pierre, F., Clari, P., Birgel, D., Cavagna, S., Martire, L. and Peckmann, J. (2013) Hydrocarbon seepage during the Messinian salinity crisis in the Tertiary Piedmont Basin (NW Italy). *Palaeogeography, Palaeoclimatology, Palaeoecology* **390**, 68–80. doi:10.1016/j.palaeo.2012.11.015.

Nishi, E. and Rouse, G. W. (2014) First whale fall chaetopterid; a gigantic new species of *Phyllochaetopterus* (Chaetopteridae: Annelida) from the deep sea off California. *Proceedings of the Biological Society of Washington* **126**, 287–298.

Nishi, E., Miura, T. and Bhaud, M. (1999) A new species of *Spiochaetopterus* (Chaetopteridae: Polychaeta) from a cold-seep site off Hatsushima in Sagami Bay, central Japan. *Proceedings of the Biological Society of Washington* **112**, 210–215.

Nishi, E., Bhaud, M. R. and Koh, B. S. (2004) Two new species of *Spiochaetopterus* (Annelida: Polychaeta) from Sagami Bay and Tokyo Bay, central Japan with a comparative table of species from Japanese and adjacent waters. *Zoological Science* **21**, 457–464.

Nobuhara, T., Onda, D., Kikuchi, N., Kondo, Y., Matsubara, K., Amano, K., Jenkins, R. G., Hikida, Y. and Majima, R. (2008) Lithofacies and fossil assemblages of the Upper Cretaceous Sada limestone, Shimanto City, Kochi Prefecture, Shikoku, Japan. *Fossils* **84**, 47–60.

Oudin, E. and Constantinou, G. (1984) Black smoker chimney fragments in Cyprus sulphide deposits. *Nature* **308**, 349–353. doi:10.1038/308349a0.

Oudin, E., Bouladon, J. and Paris, J. P. (1985) Vers hydrothermaux fossils dans une mineralisation sulfuree des ophiolites de Nouvelle–Caledonie. *Academie des Sciences, Compte Rendus, Serie II* **301**, 157–162.

Peckmann, J., Thiel, V., Michaelis, W., Clari, P., Gaillard, C., Martire, L. and Reitner, J. (1999) Cold seep deposits of Beauvoisin (Oxfordian, southeastern France) and Marmorito (Miocene, northern Italy): microbially induced authigenic carbonates. *International Journal of Earth Sciences* **88**, 60–75.

Peckmann, J., Goedert, J. L., Thiel, V., Michaelis, W. and Reitner, J. (2002) A comprehensive approach to the study of methane-seep deposits from the Lincoln Creek Formation, western Washington State, USA. *Sedimentology* **49**, 855–873. doi:10.1046/j.1365-3091.2002.00474.x.

Peckmann, J., Little, C. T. S., Gill, F. and Reitner, J. (2005) Worm tube fossils from the Hollard Mound hydrocarbon-seep deposit, Middle Devonian, Morocco: Palaeozoic

seep-related vestimentiferans? *Palaeogeography, Palaeoclimatology, Palaeoecology* **227**, 242–257. doi:10.1016/j.palaeo.2005.04.021.

Radwanska, U. (1994) A new group of microfossils: Middle Miocene (Badenian) opercular caps (calottae) of the tube-dwelling polychaetes *Vermiliopsis* Saint-Joseph, 1894. *Acta Geologica Polonica* **44**, 83–96.

Reuscher, M., Fiege, D. and Wehe, T. (2009) Four new species of Ampharetidae (Annelida: Polychaeta) from Pacific hot vents and cold seeps, with a key and synoptic table of characters for all genera. *Zootaxa* **2191**, 1–40.

Reuscher, M., Fiege, D. and Imajima, M. (2015) Ampharetidae (Annelida: Polychaeta) from Japanese waters. Part IV. Miscellaneous genera. *Journal of the Marine Biological Association of the United Kingdom* **95**, 1105–1125. doi:10.1017/S0025315415000545.

Revan, M. K., Unlu, T. and Genc, Y. (2010) Preliminary findings on the fossil traces in the massive sulphite deposits of eastern Black Sea region (Lahanos, Killik and Cayeli). *Mineral Resources Exploitation Bulletin* **140**, 73–79.

Saether, K. P. (2011) A taxonomic and palaeobiogeographic study of the fossil fauna of Miocene hydrocarbon seep deposits, North Island, New Zealand. PhD Thesis, University of Auckland.

Schwartz, H., Sample, J., Weberling, K. D., Minisini, D. and Moore, J. C. (2003) An ancient linked fluid migration system: cold-seep deposits and sandstone intrusions in the Panoche Hills California, USA. *Geo-Marine Letters* **23**, 340–350.

Sendall, K. A., Fontaine, A. R., O'Foighill, D. and O'Foighil, D. (1995) Tube morphology and activity patterns related to feeding and tube building in the polychaete *Mesochaetopterus taylori* Potts. *Canadian journal of zoology* **73**, 509–517.

Shapiro, R. and Fricke, H. (2002) Tepee Buttes: fossilized methane-seep ecosystems. In *GSA Field Guide 3: Science at the Highest Level*, pp. 94 – 101. Geological Society of America, Boulder, Colorado.

Smirnov, R. V. (2000) Two new species of Pogonophora from the arctic mud volcano off northwestern Norway. *Sarsia* **85**, 141–150. doi:10.1080/00364827.2000.10414563.

Southward, E. C. (1962) A new species of *Galathealinum* (Pogonophora) from the Canadian Arctic. *Canadian Journal of Zoology* **40**, 385–389.

Southward, E. C. (1963) *Siboglinum lacteum* sp. nov. In *Pogonophora* (ed. Ivanov, A. V.), pp. 322–325. Academic Press, London.

Southward, E. C. (1969) Growth of a pogonophore: a study of *Polybrachia canadensis* with a discussion of the development of taxonomic characters. *Journal of Zoology* **157**, 449–467.

Southward, E. C. (1972) On some Pogonophora from the Carribbean and the Gulf of Mexico. *Bulletin of Marine Science* **22**, 739–776.

Southward, E. C. (1978a) A new species of *Lamellisabella* (Pogonophora) from the North Atlantic. *Journal of the Marine Biological Association of the United Kingdom* **58**, 713–718.

Southward, E. C. (1978b) Description of a new species of *Oligobrachia* (Pogonophora) from the North Atlantic, with a survey of the Oligobrachiidae. *Journal of the Marine Biological Association of the United Kingdom* **58**, 357–366.

Southward, E. C. (1991) Three new species of Pogonophora, including two vestimentiferans, from hydrothermal sites in the Lau Back-arc Basin (Southwest Pacific Ocean). *Journal of Natural History* **25**, 859–881. doi:10.1080/00222939100770571.

Southward, E. C. and Galkin, S. V. (1997) A new vestimentiferan (Pogonophora: Obturata) from hydrothermal vents in the Manus back-arc basin (Bismarck Sea, Papua New Guinea, southwest Pacific Ocean). *Journal of Natural History* **31**, 43–55.

Southward, E. C., Tunnicliffe, V. and Black, M. (1995) Revision of the species of *Ridgeia* from northeast Pacific hydrothermal vents, with a redescription of *Ridgeia piscesae* Jones (Pogonophora: Obturata = Vestimentifera). *Canadian Journal of Zoology* **73**, 282–295. doi:10.1139/z95-033.

Southward, E. C., Schulze, A. and Tunnicliffe., V. (2002) Vestimentiferans (Pogonophora) in the Pacific and Indian Oceans: A new genus from Lihir Island (Papua New Guinea) and the Java Trench, with the first report of *Arcovestia ivanovi* from the North Fiji Basin. *Journal of Natural History* **36**, 1179–1197.

Southward, E. C., Andersen, A. C. and Hourdez, S. (2011) *Lamellibrachia anaximandri* n. sp., a new vestimentiferan tubeworm (Annelida) from the Mediterranean, with notes on frenulate tubeworms from the same habitat. *Zoosystema* **33**, 245–279.

Squires, R. L. and Gring, M. P. (1996) Late Eocene chemosynthetic? Bivalves from suspect cold seeps, Wagonwheel Mountain, central California. *Journal of Paleontology* **70**, 63–73.

Torres, M. E., Bohrmann, G., Dube, T. E. and Poole, F. G. (2003) Formation of modern and Paleozoic stratiform barite at cold methane seeps on continental margins. *Geology*

31, 897–900. doi:10.1130/G19652.1.

Vinn, O., Kupriyanova, E. K. and Kiel, S. (2013) Serpulids (Annelida, Polychaeta) at Cretaceous to modern hydrocarbon seeps: Ecological and evolutionary patterns. *Palaeogeography, Palaeoclimatology, Palaeoecology* **390**, 35–41. doi:10.1016/j.palaeo.2012.08.003.

Vinn, O., Hryniewicz, K., Little, C. T. S. and Nakrem, H. A. (2014) A Boreal serpulid fauna from Volgian-Ryazanian (latest Jurassic-earliest Cretaceous) shelf sediments and hydrocarbon seeps from Svalbard. **36**, 527–540.

Williscroft, K. (2013) Early Cretaceous methane seepage system and associated carbonates, biota and geochemistry, Sverdrup Basin, Ellef Ringnes Island, Nunavut. MSc Thesis, University of Calgary.

Appendix E: Supplementary material to Chapter 5

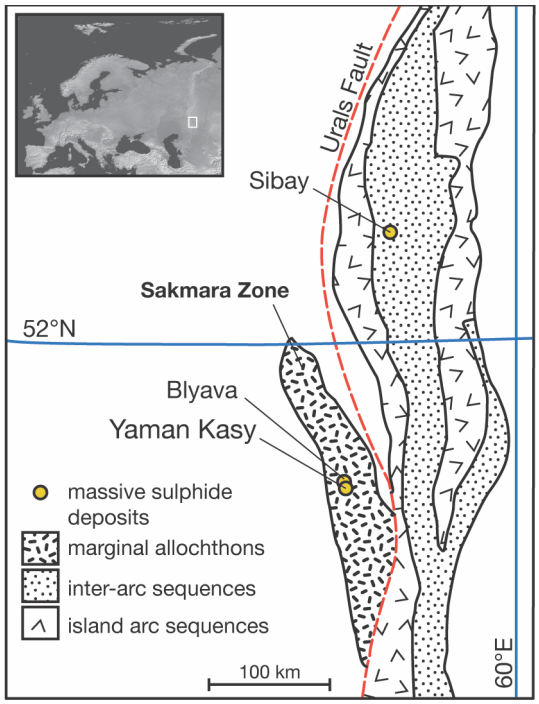

Figure E.1 Location of Yaman Kasy and other nearby massive sulphide deposits. Inset shows the location of the enlarged map area. Map adapted from Little *et al.* (1999).

Methods Supplement: Electron probe microanalysis

Previous studies of the mineralisation of polychaete tubes at hydrothermal vents indicate that elevated levels of phosphorus may be associated with mineralised organic matter (Maginn *et al.*, 2002). Pyrite content and phosphorus occurrence around Yaman Kasy microstructures was assessed using wavelength-dispersive spectrometry (WDS) point analyses, within a Cameca SX-100 electron microprobe (EPMA; Natural History Museum UK). The instrument was operated using an accelerating voltage of 20 kV and a probe current of 20 nA, and locations of data points are shown in Figures E.2 to E.5. These analyses showed that in all of the data points, phosphorus was either not present or present in amounts below the detection limits of the instrument (Tables E.1 to E.2).

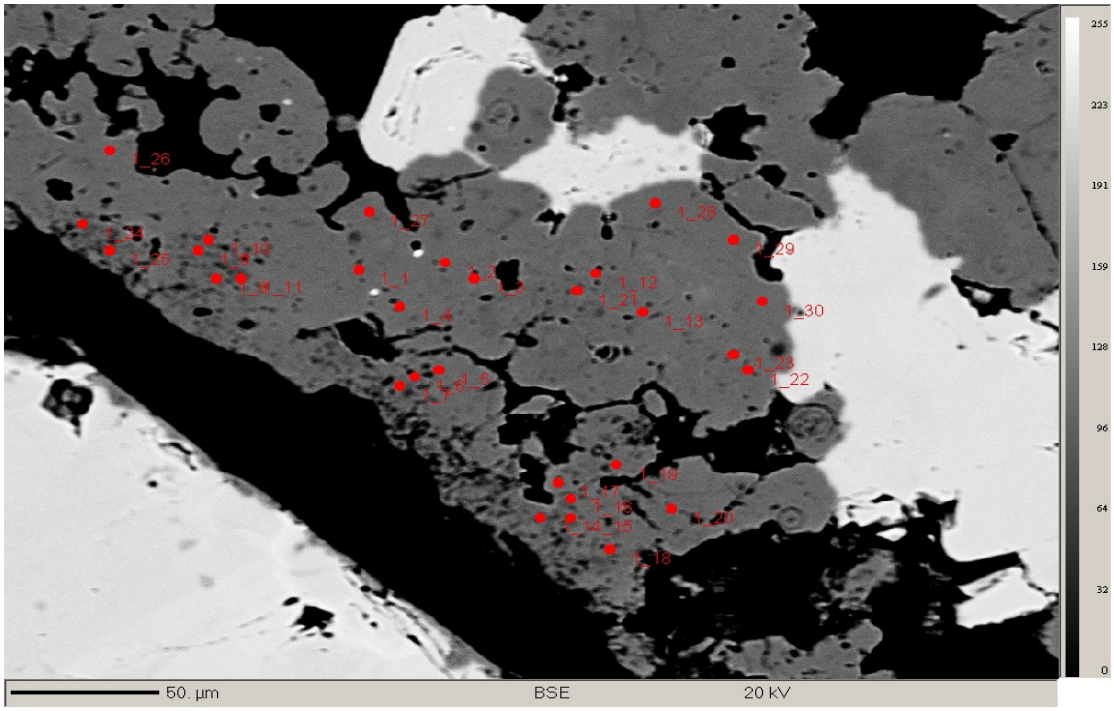

Figure E.2 Location of EPMA data points within Area 1, sample Yr_61633.

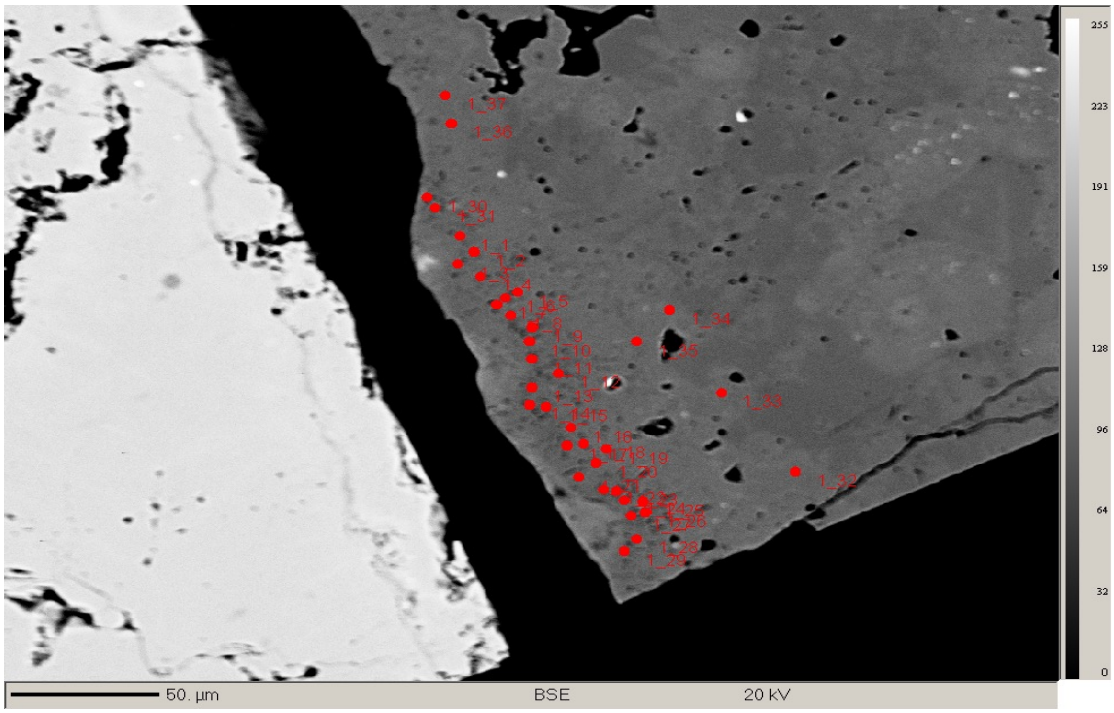

Figure E.3 Location of EPMA data points within Area 2, sample Yr_61633.

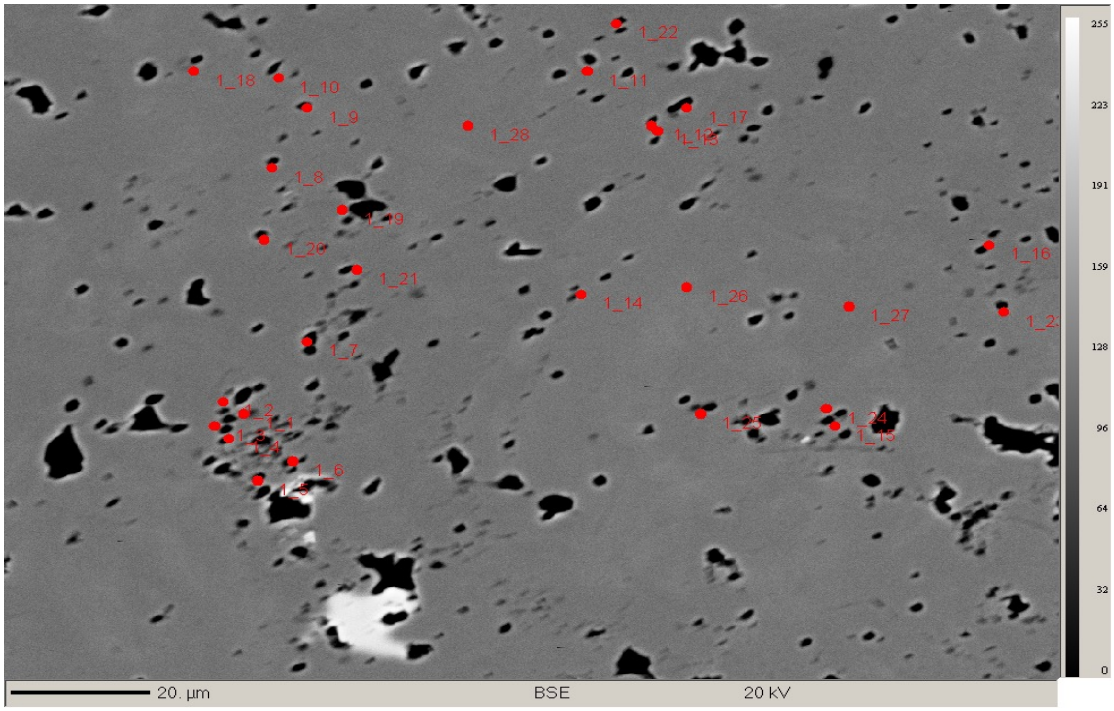

Figure E.4 Location of EPMA data points within Area 3, sample Yr_OR6468.

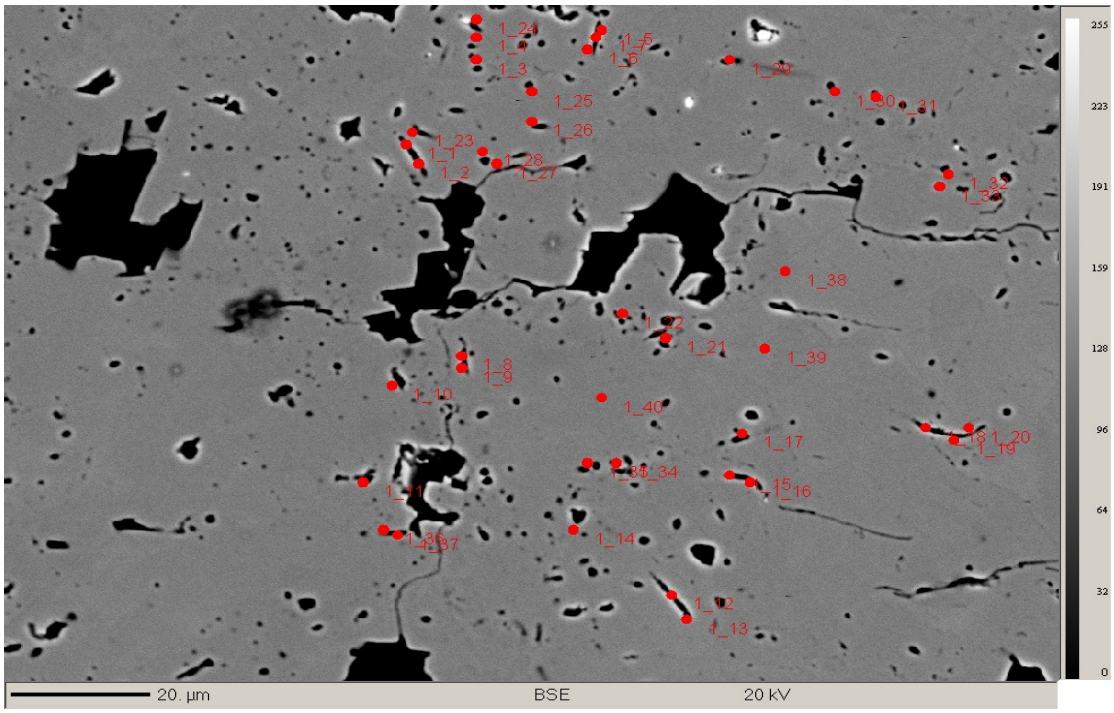

Figure E.5 Location of EPMA data points within Area 4, sample Yr_OR6468.

Table E.1 Pyrite composition (in weight %) from EPMA analyses of pyrite around Yaman Kasy microfossils and in adjacent pyrite that does not contain them (grey rows).

Figure E.2 (Area 1, Yr_61633)																		
Point	P	V	Mn	Fe	Co	Ni	Cu	Zn	Si	S	Cr	Ti	Ca	Mg	As	Sr	Ba	Pb
1 / 1.	0.00	0.00	0.03	44.45	-0.01	0.00	0.09	0.12	0.01	52.58	0.00	0.00	0.00	0.01	0.15	-0.05	0.00	0.54
1 / 2 .	0.01	0.00	0.02	44.33	-0.02	0.00	0.10	0.54	0.00	52.04	0.01	0.00	-0.01	0.01	0.08	-0.02	0.00	0.51
1 / 3 .	0.00	0.01	0.02	44.31	-0.01	0.00	0.15	0.14	0.00	51.94	0.00	0.00	0.00	0.00	0.18	-0.04	0.02	0.56
1 / 4 .	0.01	-0.01	0.03	44.30	0.03	0.00	0.09	0.22	0.00	51.59	-0.01	0.00	-0.01	0.01	0.08	-0.03	0.01	0.63
1 / 5 .	0.01	0.00	0.03	44.06	-0.02	0.00	0.09	0.12	0.00	51.27	0.00	-0.01	0.00	0.00	0.16	-0.02	0.01	0.65
1 / 6 .	0.01	0.00	0.03	43.12	-0.02	0.01	0.18	0.24	0.03	48.17	0.01	-0.01	0.02	-0.02	0.51	-0.09	-0.02	0.69
1 / 7 .	0.03	0.00	0.02	42.86	0.02	0.00	0.18	0.52	0.07	45.56	-0.02	-0.01	0.07	-0.01	0.70	-0.24	-0.01	0.77
1 / 8 .	-0.01	0.01	0.03	43.69	0.01	0.00	0.16	0.23	0.01	51.25	0.01	0.00	0.01	-0.01	0.58	-0.07	-0.01	0.44
1 / 9 .	0.01	0.00	0.03	43.60	0.01	0.00	0.19	0.20	0.02	50.50	0.01	0.00	0.01	-0.01	0.59	-0.08	0.00	0.45
1 / 10 .	0.00	0.00	0.03	44.42	0.00	-0.02	0.09	0.16	0.01	51.79	-0.01	-0.01	0.00	0.00	0.19	-0.02	0.01	0.56
1 / 11 .	0.00	0.00	0.02	43.85	-0.01	-0.01	0.17	0.27	0.01	49.71	-0.01	0.00	0.00	-0.01	0.55	-0.07	0.00	0.37
1 / 12 .	0.00	0.00	0.02	44.13	0.01	-0.01	0.14	0.17	0.01	51.15	0.01	-0.01	0.00	0.00	0.13	-0.05	0.01	0.59
1 / 13 .	0.00	0.00	0.02	44.42	-0.01	0.00	0.11	0.11	0.00	51.80	-0.02	0.00	-0.01	0.01	0.18	-0.02	-0.03	0.55
1 / 14 .	0.00	0.00	0.01	43.70	0.01	0.01	0.17	0.42	0.03	47.69	-0.01	0.00	0.05	-0.01	0.65	-0.09	-0.01	0.58
1 / 15 .	0.01	0.00	0.04	43.57	0.01	0.00	0.14	0.25	0.02	50.02	0.00	0.01	0.04	-0.01	0.41	-0.07	0.01	0.55
1 / 16 .	0.00	0.00	0.03	43.84	0.01	0.00	0.21	0.29	0.02	50.55	0.00	-0.01	0.04	-0.01	0.47	-0.09	0.00	0.57
1 / 17 .	0.00	-0.01	0.04	44.34	-0.01	0.00	0.10	0.20	0.00	51.57	-0.01	-0.02	0.00	0.00	0.18	-0.02	-0.01	0.69
1 / 18 .	0.01	0.00	0.05	44.12	0.00	0.01	0.13	0.30	0.01	51.61	0.00	0.00	0.01	0.01	0.29	-0.05	-0.01	0.57
1 / 19 .	0.00	0.00	0.02	44.55	-0.02	0.00	0.10	0.23	0.00	52.01	0.00	0.00	0.00	0.00	0.14	-0.02	0.00	0.46
1 / 20 .	0.00	0.00	0.05	44.25	0.00	0.00	0.21	0.31	0.01	51.91	0.01	0.00	0.00	0.00	0.28	-0.04	-0.01	0.55
1 / 21 .	0.01	0.00	0.03	44.19	0.00	0.01	0.18	0.28	0.02	51.23	0.00	0.00	0.01	0.01	0.23	-0.08	0.02	0.60
1 / 22 .	0.01	0.00	0.04	44.01	-0.01	0.00	0.09	0.74	0.00	52.13	0.00	-0.01	0.00	0.00	0.13	-0.04	-0.01	0.55
1 / 23 .	0.00	0.00	0.03	43.25	0.01	-0.02	0.13	2.08	0.00	51.05	0.00	0.00	0.00	0.00	0.12	-0.01	0.00	0.60
1 / 24 .	0.00	-0.01	0.08	44.02	0.01	0.00	0.12	0.46	0.01	51.68	0.02	0.00	0.00	0.00	0.27	-0.04	0.00	0.53
1 / 25 .	0.00	0.00	0.04	43.81	0.00	0.00	0.12	0.46	0.02	51.00	0.01	0.05	0.00	0.01	0.29	-0.08	-0.02	0.54
1 / 26 .	0.00	0.00	0.04	44.44	0.00	0.00	0.10	0.14	0.03	52.39	0.01	0.00	0.00	0.01	0.28	-0.11	-0.01	0.45
1 / 27 .	0.00	-0.01	0.03	44.46	0.01	0.01	0.11	0.25	0.10	52.04	0.02	0.01	0.00	0.00	0.13	-0.37	-0.01	0.50
1 / 28 .	0.00	0.00	0.05	44.72	0.00	0.01	0.07	0.50	0.00	52.40	-0.02	-0.01	0.00	0.01	0.08	-0.03	0.02	0.57
1 / 29 .	0.01	0.00	0.08	44.30	0.01	-0.01	0.08	0.43	0.02	50.62	0.00	0.00	0.00	-0.02	0.70	-0.07	-0.01	0.42
1 / 30 .	0.01	0.00	0.03	44.31	0.00	-0.01	0.09	0.81	0.00	52.18	-0.01	0.00	0.00	0.00	0.09	-0.03	0.00	0.69

Figure E.3 (Area 2, Yr_61633)

Point	P	V	Mn	Fe	Co	Ni	Cu	Zn	Si	S	Cr	Ti	Ca	Mg	As	Sr	Ba	Pb
1 / 1 .	0.00	0.00	0.01	43.09	0.01	0.00	0.10	1.01	0.01	50.69	-0.01	-0.01	0.00	-0.01	0.57	-0.04	0.02	0.42
1 / 2 .	0.00	0.00	0.01	43.58	0.01	0.00	0.09	0.31	0.00	51.03	0.00	0.00	-0.01	0.00	0.34	-0.03	-0.01	0.67
1 / 3 .	0.00	0.00	0.02	43.34	-0.01	0.00	0.11	0.53	0.01	50.55	0.00	-0.01	0.00	-0.02	0.72	-0.01	0.01	0.44
1 / 4 .	-0.01	0.00	0.03	43.93	0.02	0.00	0.06	0.39	0.00	50.79	0.00	0.00	0.00	-0.01	0.29	-0.07	0.00	0.57
1 / 5 .	0.01	0.00	0.02	44.00	0.00	0.02	0.07	0.23	0.00	51.52	-0.01	-0.01	0.00	0.00	0.18	-0.02	-0.01	0.60
1 / 6 .	0.01	0.00	0.01	43.85	-0.01	0.00	0.07	0.29	0.01	51.93	-0.01	0.00	0.00	0.01	0.22	-0.05	0.00	0.54
1 / 7 .	0.01	0.00	0.02	43.91	-0.01	0.00	0.09	0.39	0.05	51.24	0.00	0.00	0.00	0.03	0.25	-0.13	0.00	0.30
1 / 8 .	0.01	0.00	0.04	42.89	0.01	0.01	0.09	0.34	0.03	49.55	-0.01	0.00	0.00	-0.02	0.85	-0.08	0.02	0.47
1 / 9 .	0.00	0.01	0.02	43.62	0.00	0.00	0.10	0.42	0.01	50.39	0.01	-0.01	0.01	-0.01	0.41	-0.07	-0.01	0.39
1 / 10 .	0.00	-0.01	0.02	42.93	0.01	0.01	0.11	0.40	0.03	49.51	0.00	0.00	0.00	-0.02	0.83	-0.09	-0.02	0.49
1 / 11 .	0.00	0.00	0.04	42.85	0.01	0.01	0.10	0.48	0.00	50.32	0.01	0.01	0.00	-0.03	0.84	-0.02	0.00	0.51
1 / 12 .	0.00	0.00	0.03	43.77	0.01	0.00	0.07	0.35	0.01	51.52	0.00	-0.01	0.00	0.00	0.39	-0.03	-0.01	0.40
1 / 13 .	0.00	0.00	0.03	43.55	0.00	0.01	0.09	0.47	0.01	51.53	-0.01	0.00	-0.01	-0.01	0.41	-0.03	-0.01	0.31
1 / 14 .	0.00	0.00	0.03	43.55	0.01	-0.01	0.10	0.72	0.00	51.02	-0.01	0.00	0.00	0.00	0.51	-0.05	0.00	0.32
1 / 15 .	0.00	0.00	0.04	43.34	-0.01	0.00	0.06	0.38	0.01	50.69	0.02	0.00	0.00	-0.01	0.48	-0.07	0.02	0.30
1 / 16 .	0.00	-0.01	0.03	43.28	0.01	0.00	0.08	0.39	0.01	50.77	0.00	0.00	0.00	-0.01	0.59	-0.05	0.00	0.45
1 / 17 .	0.01	0.00	0.05	43.10	0.01	0.01	0.11	0.48	0.02	49.81	0.01	-0.01	0.01	-0.01	0.72	-0.06	-0.01	0.40
1 / 18 .	0.00	0.01	0.05	43.81	0.00	0.01	0.10	0.33	0.00	51.30	0.00	0.00	0.00	0.00	0.29	-0.05	0.00	0.60
1 / 19 .	-0.01	0.00	0.03	43.88	0.01	0.01	0.06	0.21	0.06	51.60	-0.01	0.00	0.00	0.01	0.18	-0.07	0.00	0.54
1 / 20 .	0.00	0.00	0.02	43.94	-0.01	-0.01	0.08	0.30	0.01	51.61	0.01	-0.01	0.00	0.00	0.21	-0.04	0.01	0.52
1 / 21 .	0.00	0.00	0.04	42.90	0.00	0.00	0.11	0.51	0.03	50.45	-0.01	0.00	0.00	-0.03	0.71	-0.10	-0.01	0.61
1 / 22 .	0.00	0.00	0.03	42.32	0.01	0.00	0.14	0.32	0.02	49.89	-0.01	-0.01	0.00	-0.03	1.20	-0.06	-0.02	0.78
1 / 23 .	0.00	0.00	0.03	42.81	0.02	-0.01	0.10	0.38	0.02	50.55	-0.01	-0.01	0.00	-0.02	0.87	-0.08	0.02	0.49
1 / 24 .	0.00	0.00	0.05	42.84	0.01	0.01	0.14	0.30	0.01	51.12	0.00	0.00	0.00	-0.02	0.83	-0.04	0.01	0.57
1 / 25 .	0.01	0.00	0.04	43.33	0.01	0.00	0.06	0.20	0.01	50.63	0.00	0.00	0.00	-0.01	0.45	-0.04	0.02	0.41
1 / 26 .	-0.01	0.00	0.04	43.37	0.01	0.01	0.06	0.23	0.01	51.69	0.00	0.00	0.00	0.00	0.31	-0.05	0.01	0.43
1 / 27 .	0.00	0.00	0.04	43.40	-0.01	0.00	0.08	0.30	0.01	50.70	0.02	0.00	0.00	0.00	0.54	-0.06	0.00	0.39
1 / 28 .	0.00	0.00	0.04	43.40	0.01	0.01	0.10	0.28	0.02	50.77	-0.02	0.00	0.00	-0.01	0.62	-0.06	0.00	0.31
1 / 29 .	-0.01	0.01	0.02	43.23	0.02	0.01	0.10	0.40	0.01	51.49	-0.01	0.00	0.00	-0.01	0.56	-0.05	0.01	0.41
1 / 30 .	0.00	0.00	0.06	43.54	0.00	0.00	0.11	0.63	0.01	50.63	0.00	-0.01	0.01	0.00	0.43	-0.04	0.02	0.29
1 / 31 .	0.00	0.00	0.03	43.56	0.02	0.02	0.12	0.54	0.01	51.03	-0.02	-0.01	0.00	-0.02	0.47	-0.05	0.00	0.37
1 / 32 .	0.00	0.00	0.04	44.37	0.01	0.01	0.07	0.02	0.00	52.79	0.01	-0.01	0.00	0.01	0.07	-0.02	-0.01	0.14
1 / 33 .	-0.01	0.00	0.04	43.46	-0.02	0.02	0.12	0.47	0.00	51.33	0.01	0.00	0.01	-0.01	0.23	-0.04	-0.02	0.60
1 / 34 .	0.00	0.00	0.02	44.62	0.00	0.00	0.13	0.08	-0.01	52.17	0.00	-0.01	-0.01	0.00	0.46	-0.02	-0.01	0.41
1 / 35 .	0.00	0.01	0.04	43.42	0.01	0.00	0.18	0.17	0.00	51.73	0.01	0.00	0.00	0.00	0.38	-0.03	0.00	0.58

1 / 36 .	0.00	0.00	0.00	44.47	-0.01	0.01	0.02	0.29	0.00	51.92	0.01	0.01	-0.01	0.01	0.06	-0.03	0.00	0.43
1 / 37 .	0.00	0.00	0.02	44.55	-0.01	-0.01	0.04	0.24	0.00	52.09	0.00	-0.01	0.00	0.00	0.10	-0.03	0.01	0.40

Figure E.4 (Area 3, Yr_OR6468)

Point	P	V	Mn	Fe	Co	Ni	Cu	Zn	Si	S	Cr	Ti	Ca	Mg	As	Sr	Ba	Pb
1 / 1 .	0.01	0.00	0.01	46.97	0.00	0.00	0.00	0.01	0.00	53.81	0.01	0.01	-0.01	0.01	0.12	-0.05	-0.01	0.14
1 / 2 .	0.00	0.00	0.02	46.76	-0.01	0.00	0.00	0.01	0.04	53.58	0.02	-0.01	-0.01	0.00	0.12	-0.17	-0.01	0.14
1 / 3 .	0.00	0.01	0.03	46.85	0.00	-0.01	0.00	-0.02	0.01	53.19	0.01	0.00	-0.01	0.00	0.15	-0.06	-0.01	0.11
1 / 4 .	0.00	0.00	0.01	47.12	0.01	-0.01	0.00	0.02	0.00	53.50	0.00	0.00	0.00	0.00	0.15	-0.04	-0.01	0.14
1 / 5 .	0.01	0.00	0.05	46.32	0.01	0.00	-0.01	0.02	0.01	52.95	0.00	0.00	-0.01	0.00	0.15	-0.05	0.01	0.30
1 / 6 .	0.01	0.00	0.02	46.98	-0.01	0.00	0.01	0.06	0.02	52.99	0.00	-0.01	0.00	-0.01	0.25	-0.07	0.01	0.30
1 / 7 .	0.00	0.00	0.02	46.34	-0.01	-0.01	0.03	0.02	0.04	53.18	0.02	0.00	0.00	-0.01	0.18	-0.18	0.00	0.20
1 / 8 .	0.00	0.01	0.02	47.22	-0.01	0.01	0.02	0.00	0.01	53.43	-0.02	0.00	0.00	0.00	0.07	-0.03	0.01	0.14
1 / 9 .	0.01	0.01	0.01	47.20	-0.01	0.01	-0.01	-0.02	0.00	53.64	0.01	0.00	-0.01	0.00	0.17	-0.03	-0.02	0.15
1 / 10 .	0.00	0.00	0.02	47.06	0.01	0.00	0.00	0.02	0.00	53.64	0.00	0.00	0.00	0.01	0.14	-0.03	0.00	0.14
1 / 11 .	0.00	0.00	0.00	47.02	0.01	-0.01	0.01	-0.02	0.00	53.66	0.00	0.00	-0.02	0.00	0.23	-0.04	0.02	0.15
1 / 12 .	0.00	0.00	0.01	47.22	0.00	0.00	-0.02	0.03	0.00	53.55	0.00	0.00	-0.01	0.00	0.15	-0.05	-0.01	0.12
1 / 13 .	0.00	0.00	0.00	47.13	-0.02	0.01	0.00	-0.02	0.02	53.33	0.01	0.00	0.00	0.00	0.14	-0.10	-0.03	0.13
1 / 14 .	0.00	-0.01	0.01	47.28	-0.01	0.00	-0.02	-0.01	0.00	53.45	-0.01	-0.01	-0.01	0.00	0.19	-0.03	-0.02	0.13
1 / 15 .	0.01	0.00	0.00	46.75	0.02	0.01	0.02	-0.02	0.01	52.20	0.02	0.00	-0.01	0.00	0.23	-0.08	0.00	0.24
1 / 16 .	0.00	0.00	0.02	47.07	-0.01	-0.01	0.03	0.00	0.00	53.39	0.02	0.00	-0.01	0.00	0.13	-0.04	-0.01	0.10
1 / 17 .	0.00	0.01	0.02	47.09	-0.01	0.00	0.01	0.00	0.01	53.47	0.00	0.00	0.00	0.00	0.13	-0.05	0.00	0.13
1 / 18 .	0.00	0.00	0.01	47.13	0.01	-0.02	0.00	-0.01	0.01	53.45	0.01	0.00	-0.01	0.00	0.16	-0.04	0.01	0.13
1 / 19 .	0.00	0.01	0.07	43.41	0.01	0.00	0.06	-0.01	1.36	49.14	0.00	-0.01	-0.01	-0.01	0.30	0.00	0.00	0.33
1 / 20 .	0.00	0.01	0.02	46.97	0.00	0.00	-0.01	0.00	0.00	53.26	0.00	0.00	0.00	0.00	0.26	-0.04	0.02	0.22
1 / 21 .	0.00	-0.01	0.01	46.05	0.02	-0.01	-0.01	0.05	0.01	52.25	0.00	0.00	0.00	0.00	0.24	-0.04	0.00	1.04
1 / 22 .	0.00	0.00	0.01	47.27	-0.01	0.02	0.01	0.01	0.00	53.71	0.00	0.00	0.00	0.01	0.20	-0.02	0.01	0.14
1 / 23 .	0.01	0.00	0.01	46.97	0.02	0.00	-0.01	0.02	0.01	53.30	0.00	0.00	0.00	-0.01	0.32	-0.03	0.01	0.13
1 / 24 .	0.00	0.01	0.01	46.86	-0.03	0.00	0.00	-0.02	0.03	53.81	0.01	0.00	0.00	0.00	0.21	-0.15	0.00	0.21
1 / 25 .	0.00	0.01	0.02	47.13	0.00	0.00	-0.01	0.02	0.01	53.26	-0.02	0.00	-0.01	0.01	0.18	-0.04	-0.01	0.13
1 / 26 .	0.01	0.00	0.02	47.16	-0.01	0.00	-0.01	-0.04	0.01	53.54	0.00	-0.01	-0.01	0.00	0.19	-0.04	-0.01	0.09
1 / 27 .	0.00	0.00	0.01	47.33	0.00	-0.01	0.01	0.01	0.00	53.39	0.01	0.00	-0.01	0.00	0.23	-0.03	-0.01	0.16
1 / 28 .	0.00	0.00	0.03	47.07	-0.01	0.00	0.00	-0.01	0.01	53.75	-0.01	0.00	0.00	0.00	0.19	-0.04	0.00	0.15

Figure E.5 (Area 4, Yr_OR6468)

Point	P	V	Mn	Fe	Co	Ni	Cu	Zn	Si	S	Cr	Ti	Ca	Mg	As	Sr	Ba	Pb
1 / 1 .	0.00	0.00	0.02	46.76	-0.01	0.00	0.00	0.01	0.03	53.92	0.00	-0.01	0.00	0.00	0.24	-0.07	0.02	0.21
1 / 2 .	0.00	-0.01	0.01	46.57	0.00	0.00	0.01	0.02	0.03	53.63	0.01	0.00	0.00	0.00	0.31	-0.13	-0.01	0.28
1 / 3 .	0.03	0.00	0.01	46.57	0.00	0.02	0.01	0.05	0.15	48.91	0.00	0.00	0.01	-0.01	0.23	-0.26	0.01	0.23

1 / 4 .	0.00	0.00	0.00	46.68	0.01	-0.01	-0.01	0.05	0.01	53.25	0.01	0.00	-0.01	-0.01	0.27	-0.04	-0.02	0.19
1 / 5 .	0.00	0.01	0.01	47.27	0.01	-0.01	-0.01	0.00	0.01	53.49	0.00	0.00	0.00	0.00	0.17	-0.04	0.02	0.24
1 / 6 .	0.01	0.00	0.01	47.03	0.00	0.00	0.00	0.02	0.01	53.58	0.00	0.00	0.00	0.00	0.16	-0.05	-0.01	0.17
1 / 7 .	0.00	0.00	0.01	46.63	-0.01	0.01	0.02	0.01	0.07	53.42	0.00	-0.01	0.00	0.00	0.20	-0.17	-0.04	0.21
1 / 8 .	0.00	0.00	0.01	46.79	0.00	0.00	0.02	0.00	0.11	53.71	0.00	0.01	-0.01	0.14	0.26	-0.39	-0.02	0.20
1 / 9 .	0.00	0.00	0.01	46.80	-0.01	0.01	0.02	0.04	0.02	53.52	0.01	0.00	-0.01	-0.01	0.21	-0.12	-0.01	0.18
1 / 10 .	0.00	-0.01	0.02	47.16	-0.01	-0.01	0.01	0.01	0.00	53.88	0.00	0.01	-0.01	0.00	0.11	-0.06	0.01	0.14
1 / 11 .	0.00	0.01	0.01	47.35	0.01	0.00	-0.02	-0.03	0.00	53.97	0.00	0.00	0.00	0.00	0.04	-0.04	-0.02	0.14
1 / 12 .	0.00	0.00	0.00	46.76	0.01	0.00	0.00	0.03	0.01	53.48	0.00	0.00	0.00	0.00	0.34	-0.06	-0.03	0.22
1 / 13 .	0.00	0.00	0.01	47.07	0.01	0.00	0.00	0.04	0.01	53.66	-0.01	-0.01	0.00	0.00	0.22	-0.03	0.00	0.18
1 / 14 .	0.00	0.00	-0.01	47.13	-0.02	0.00	-0.01	0.02	0.00	53.65	-0.01	0.00	-0.01	0.00	0.24	-0.03	0.00	0.24
1 / 15 .	0.01	0.00	0.02	46.70	0.01	0.01	-0.02	0.03	0.00	53.75	0.00	0.00	-0.01	0.00	0.28	-0.05	-0.01	0.22
1 / 16 .	0.00	0.00	0.02	46.95	-0.01	-0.02	0.00	0.04	0.01	53.42	-0.01	0.00	0.00	0.00	0.16	-0.06	0.01	0.15
1 / 17 .	0.00	0.00	0.00	47.08	0.00	0.00	-0.01	0.03	0.01	53.70	-0.01	0.00	0.00	0.00	0.23	-0.04	0.01	0.15
1 / 18 .	0.00	0.00	0.01	47.20	0.01	-0.01	0.00	0.02	0.00	53.29	0.00	0.00	0.00	0.00	0.22	-0.03	0.01	0.11
1 / 19 .	0.00	0.00	0.02	46.61	0.00	0.00	0.02	0.01	0.50	53.07	0.00	0.00	-0.01	0.00	0.27	0.00	0.02	0.25
1 / 20 .	0.00	0.00	0.00	46.74	0.01	0.00	0.00	0.06	0.04	53.34	-0.01	0.00	0.00	0.00	0.19	-0.14	0.01	0.24
1 / 21 .	-0.01	0.00	0.01	47.14	0.00	0.00	-0.01	0.02	0.00	53.72	-0.01	-0.01	0.00	0.01	0.20	-0.03	0.02	0.18
1 / 22 .	0.00	-0.01	0.00	46.99	0.01	0.01	0.01	0.00	0.01	53.34	-0.02	-0.01	0.00	0.00	0.22	-0.04	-0.01	0.18
1 / 23 .	0.00	0.00	0.01	46.57	0.00	0.00	0.01	0.03	0.07	53.56	-0.01	0.00	0.00	0.00	0.25	-0.24	0.01	0.21
1 / 24 .	0.00	0.01	-0.01	46.77	0.00	0.00	0.01	0.02	0.02	53.20	0.01	0.01	-0.01	0.00	0.22	-0.06	0.00	0.27
1 / 25 .	0.00	-0.01	0.02	46.96	-0.01	-0.02	0.00	0.04	0.01	53.59	0.01	0.00	-0.01	0.01	0.24	-0.04	0.01	0.19
1 / 26 .	0.00	0.00	0.01	47.03	0.00	0.00	0.03	0.02	0.02	53.47	0.01	0.00	0.00	-0.01	0.16	-0.06	0.00	0.18
1 / 27 .	0.01	0.00	0.00	46.79	0.01	0.02	0.01	0.02	0.15	52.47	0.00	0.00	0.00	-0.01	0.31	-0.36	-0.02	0.25
1 / 28 .	0.00	0.00	0.02	43.60	0.02	0.00	0.03	0.03	0.14	49.97	-0.01	-0.01	0.00	0.00	0.35	-0.45	0.01	0.30
1 / 29 .	0.00	0.00	0.02	46.98	-0.04	-0.01	0.01	0.00	0.00	53.58	0.00	-0.01	-0.01	0.00	0.17	-0.01	0.01	0.15
1 / 30 .	-0.01	0.00	0.01	46.94	-0.01	0.00	-0.01	0.04	0.00	53.52	0.00	0.00	-0.02	0.00	0.22	-0.05	0.00	0.18
1 / 31 .	0.01	0.00	0.04	46.94	0.01	0.01	-0.01	0.04	0.01	53.46	-0.02	0.00	0.00	0.00	0.22	-0.04	-0.01	0.20
1 / 32 .	0.00	-0.01	0.01	46.89	0.00	0.01	-0.01	0.01	0.01	53.39	0.01	0.00	0.00	0.00	0.22	-0.03	-0.01	0.20
1 / 33 .	0.00	0.01	0.02	46.79	0.00	-0.01	0.01	0.01	0.02	53.42	-0.02	-0.01	0.00	-0.01	0.23	-0.08	0.02	0.18
1 / 34 .	0.00	0.00	0.03	46.83	0.00	-0.01	-0.01	0.05	0.00	53.43	0.01	0.00	-0.01	0.00	0.22	-0.03	0.00	0.21
1 / 35 .	0.00	0.00	0.00	47.06	0.01	0.00	0.00	0.02	0.00	53.64	0.00	0.01	-0.01	-0.01	0.19	-0.03	0.00	0.15
1 / 36 .	0.01	0.00	0.02	47.03	0.00	-0.01	0.00	0.01	0.00	53.85	-0.01	-0.01	-0.01	0.01	0.07	-0.05	0.01	0.14
1 / 37 .	0.00	0.00	0.04	47.02	0.01	0.00	0.01	-0.02	0.04	53.89	-0.01	0.00	-0.01	0.00	0.08	-0.12	-0.01	0.12
1 / 38 .	0.00	0.00	0.02	47.22	-0.02	0.01	0.00	0.01	0.00	53.41	0.00	0.00	-0.01	0.00	0.19	-0.03	0.01	0.16
1 / 39 .	0.00	0.00	0.00	46.98	-0.02	0.00	-0.01	0.02	0.00	53.22	-0.01	0.00	0.00	0.00	0.22	-0.04	0.01	0.12
1 / 40 .	-0.01	0.00	0.03	46.91	0.00	-0.01	-0.01	0.04	0.00	53.40	0.01	0.00	-0.01	0.00	0.21	-0.03	-0.02	0.12

Table E.2 Detection limits (in weight %) for EPMA analyses of pyrite composition around Yaman Kasy microfossils and in adjacent pyrite that does not contain them (grey rows).

Detection limits - Figure E.2 (Area 1, Yr_61633)																		
Point	P	V	Mn	Fe	Co	Ni	Cu	Zn	Si	S	Cr	Ti	Ca	Mg	As	Sr	Ba	Pb
1 / 1 .	0.02	0.02	0.03	0.04	-0.01	0.03	0.04	0.06	0.01	0.05	0.04	0.02	0.02	0.01	0.02	0.03	0.05	0.05
1 / 2 .	0.01	0.02	0.03	0.04	-0.02	0.03	0.04	0.06	0.01	0.05	0.04	0.02	0.02	0.01	0.02	0.03	0.05	0.05
1 / 3 .	0.01	0.02	0.03	0.04	0.00	0.03	0.04	0.06	0.01	0.05	0.04	0.02	0.02	0.01	0.02	0.03	0.05	0.05
1 / 4 .	0.01	0.02	0.03	0.04	0.01	0.03	0.04	0.05	0.01	0.05	0.04	0.02	0.02	0.01	0.02	0.03	0.05	0.05
1 / 5 .	0.01	0.02	0.03	0.04	-0.03	0.03	0.04	0.06	0.01	0.06	0.04	0.02	0.02	0.01	0.02	0.03	0.05	0.05
1 / 6 .	0.01	0.02	0.03	0.04	-0.02	0.03	0.04	0.06	0.01	0.05	0.03	0.02	0.01	0.01	0.02	0.03	0.05	0.05
1 / 7 .	0.01	0.02	0.03	0.04	0.01	0.03	0.04	0.05	0.01	0.05	0.04	0.02	0.01	0.01	0.02	0.03	0.05	0.05
1 / 8 .	0.02	0.02	0.03	0.04	0.01	0.03	0.04	0.06	0.01	0.05	0.03	0.02	0.02	0.01	0.02	0.03	0.05	0.05
1 / 9 .	0.01	0.02	0.03	0.04	0.00	0.03	0.04	0.06	0.01	0.05	0.04	0.02	0.02	0.01	0.02	0.03	0.05	0.05
1 / 10 .	0.01	0.02	0.03	0.04	0.00	0.03	0.04	0.05	0.01	0.06	0.04	0.02	0.02	0.01	0.02	0.03	0.05	0.05
1 / 11 .	0.01	0.02	0.03	0.04	-0.01	0.03	0.04	0.06	0.01	0.05	0.04	0.02	0.02	0.01	0.02	0.03	0.05	0.05
1 / 12 .	0.01	0.02	0.03	0.04	0.01	0.03	0.04	0.06	0.01	0.06	0.03	0.02	0.02	0.01	0.02	0.03	0.05	0.05
1 / 13 .	0.01	0.02	0.03	0.04	-0.02	0.03	0.04	0.06	0.01	0.05	0.04	0.02	0.02	0.01	0.02	0.03	0.05	0.05
1 / 14 .	0.01	0.02	0.03	0.04	0.01	0.03	0.04	0.05	0.01	0.05	0.04	0.02	0.02	0.01	0.02	0.03	0.05	0.05
1 / 15 .	0.01	0.02	0.03	0.04	0.01	0.03	0.04	0.05	0.01	0.05	0.04	0.02	0.02	0.01	0.02	0.03	0.05	0.05
1 / 16 .	0.02	0.02	0.03	0.04	0.00	0.03	0.04	0.05	0.01	0.06	0.04	0.02	0.02	0.01	0.02	0.03	0.05	0.05
1 / 17 .	0.01	0.02	0.03	0.04	-0.01	0.03	0.04	0.05	0.01	0.06	0.04	0.02	0.02	0.01	0.02	0.03	0.05	0.05
1 / 18 .	0.01	0.02	0.03	0.04	0.00	0.03	0.04	0.05	0.01	0.05	0.04	0.02	0.02	0.01	0.02	0.03	0.05	0.05
1 / 19 .	0.02	0.02	0.03	0.04	-0.02	0.03	0.04	0.06	0.01	0.05	0.04	0.02	0.02	0.01	0.02	0.03	0.05	0.05
1 / 20 .	0.02	0.02	0.03	0.04	0.00	0.03	0.04	0.05	0.01	0.05	0.04	0.02	0.02	0.01	0.02	0.03	0.05	0.05
1 / 21 .	0.01	0.02	0.03	0.04	0.00	0.03	0.04	0.06	0.01	0.05	0.03	0.02	0.01	0.01	0.02	0.03	0.05	0.05
1 / 22 .	0.01	0.02	0.03	0.04	-0.01	0.03	0.04	0.06	0.01	0.06	0.04	0.02	0.02	0.01	0.02	0.03	0.05	0.05
1 / 23 .	0.01	0.02	0.03	0.04	0.00	0.03	0.04	0.06	0.01	0.05	0.04	0.02	0.02	0.01	0.02	0.03	0.05	0.05
1 / 24 .	0.01	0.02	0.03	0.04	0.00	0.03	0.04	0.05	0.01	0.06	0.03	0.02	0.02	0.01	0.02	0.03	0.05	0.05
1 / 25 .	0.01	0.01	0.03	0.04	0.00	0.03	0.04	0.05	0.01	0.05	0.04	0.02	0.02	0.01	0.02	0.03	0.05	0.05
1 / 26 .	0.02	0.02	0.03	0.04	0.00	0.03	0.04	0.06	0.01	0.05	0.04	0.02	0.02	0.01	0.02	0.03	0.05	0.05
1 / 27 .	0.02	0.02	0.03	0.04	0.01	0.03	0.04	0.06	0.01	0.06	0.03	0.02	0.02	0.01	0.02	0.04	0.05	0.05
1 / 28 .	0.01	0.02	0.03	0.04	0.00	0.03	0.04	0.05	0.01	0.06	0.04	0.02	0.02	0.01	0.02	0.03	0.05	0.05
1 / 29 .	0.01	0.02	0.03	0.04	0.01	0.03	0.04	0.06	0.01	0.05	0.03	0.02	0.02	0.01	0.03	0.03	0.05	0.05
1 / 30 .	0.01	0.02	0.03	0.04	0.00	0.03	0.04	0.06	0.01	0.05	0.04	0.02	0.02	0.01	0.03	0.03	0.05	0.05
Detection limits - Figure E.3 (Area 2, Yr_61633)																		
Point	P	V	Mn	Fe	Co	Ni	Cu	Zn	Si	S	Cr	Ti	Ca	Mg	As	Sr	Ba	Pb

1 / 1 .	0.02	0.02	0.03	0.04	0.01	0.03	0.04	0.05	0.01	0.06	0.04	0.02	0.02	0.01	0.02	0.03	0.05	0.05
1 / 2 .	0.02	0.02	0.03	0.04	0.00	0.03	0.04	0.05	0.01	0.05	0.04	0.02	0.02	0.01	0.02	0.03	0.05	0.05
1 / 3 .	0.01	0.02	0.03	0.04	0.00	0.03	0.04	0.05	0.01	0.05	0.04	0.02	0.01	0.01	0.02	0.03	0.05	0.05
1 / 4 .	0.02	0.02	0.03	0.04	0.01	0.03	0.04	0.05	0.01	0.05	0.04	0.02	0.02	0.01	0.02	0.03	0.05	0.05
1 / 5 .	0.01	0.02	0.03	0.04	0.00	0.03	0.04	0.05	0.01	0.05	0.04	0.02	0.02	0.01	0.02	0.03	0.05	0.05
1 / 6 .	0.01	0.02	0.03	0.04	-0.02	0.03	0.04	0.05	0.01	0.05	0.04	0.02	0.02	0.01	0.03	0.03	0.05	0.05
1 / 7 .	0.01	0.02	0.03	0.04	-0.01	0.03	0.04	0.05	0.01	0.05	0.04	0.02	0.02	0.01	0.02	0.03	0.05	0.05
1 / 8 .	0.01	0.02	0.03	0.04	0.01	0.03	0.04	0.05	0.01	0.06	0.04	0.02	0.02	0.01	0.02	0.03	0.05	0.05
1 / 9 .	0.02	0.02	0.03	0.04	0.00	0.03	0.04	0.05	0.01	0.05	0.04	0.02	0.01	0.01	0.02	0.03	0.05	0.05
1 / 10 .	0.02	0.02	0.03	0.04	0.01	0.03	0.04	0.06	0.01	0.05	0.04	0.02	0.02	0.01	0.02	0.03	0.05	0.05
1 / 11 .	0.01	0.02	0.03	0.04	0.01	0.03	0.04	0.06	0.01	0.05	0.03	0.02	0.02	0.01	0.02	0.03	0.05	0.05
1 / 12 .	0.02	0.02	0.03	0.04	0.01	0.03	0.04	0.06	0.01	0.06	0.04	0.02	0.02	0.01	0.02	0.03	0.05	0.05
1 / 13 .	0.01	0.02	0.03	0.04	0.00	0.03	0.04	0.06	0.01	0.06	0.04	0.02	0.02	0.01	0.02	0.03	0.05	0.05
1 / 14 .	0.02	0.02	0.03	0.04	0.01	0.03	0.04	0.06	0.01	0.06	0.04	0.02	0.02	0.01	0.02	0.03	0.05	0.06
1 / 15 .	0.02	0.02	0.03	0.04	-0.01	0.03	0.04	0.06	0.01	0.05	0.04	0.02	0.01	0.01	0.02	0.03	0.05	0.05
1 / 16 .	0.01	0.02	0.03	0.04	0.00	0.03	0.04	0.05	0.01	0.05	0.03	0.02	0.02	0.01	0.02	0.03	0.05	0.05
1 / 17 .	0.01	0.02	0.03	0.04	0.00	0.03	0.04	0.05	0.01	0.06	0.04	0.02	0.02	0.01	0.02	0.03	0.05	0.05
1 / 18 .	0.02	0.02	0.03	0.04	0.00	0.03	0.04	0.05	0.01	0.06	0.04	0.02	0.02	0.01	0.02	0.03	0.05	0.05
1 / 19 .	0.02	0.02	0.03	0.04	0.00	0.03	0.04	0.06	0.01	0.05	0.04	0.02	0.02	0.01	0.02	0.03	0.05	0.05
1 / 20 .	0.02	0.01	0.03	0.04	0.00	0.03	0.04	0.06	0.01	0.05	0.04	0.02	0.01	0.01	0.02	0.03	0.05	0.06
1 / 21 .	0.02	0.02	0.03	0.04	0.00	0.03	0.04	0.05	0.01	0.05	0.04	0.02	0.02	0.01	0.02	0.03	0.05	0.05
1 / 22 .	0.02	0.02	0.03	0.04	0.00	0.03	0.04	0.06	0.01	0.05	0.04	0.02	0.02	0.01	0.02	0.03	0.05	0.05
1 / 23 .	0.02	0.02	0.03	0.04	0.01	0.03	0.04	0.05	0.01	0.05	0.04	0.02	0.02	0.01	0.02	0.03	0.05	0.05
1 / 24 .	0.01	0.02	0.03	0.04	0.01	0.03	0.04	0.05	0.01	0.05	0.04	0.02	0.02	0.01	0.03	0.03	0.05	0.05
1 / 25 .	0.01	0.02	0.03	0.04	0.01	0.03	0.04	0.05	0.01	0.05	0.04	0.02	0.02	0.01	0.02	0.03	0.05	0.05
1 / 26 .	0.02	0.02	0.03	0.04	0.00	0.03	0.04	0.05	0.01	0.05	0.04	0.02	0.02	0.01	0.02	0.03	0.05	0.06
1 / 27 .	0.01	0.02	0.03	0.04	-0.01	0.03	0.04	0.05	0.01	0.05	0.03	0.02	0.02	0.01	0.02	0.03	0.05	0.05
1 / 28 .	0.02	0.02	0.03	0.04	0.00	0.03	0.04	0.06	0.01	0.06	0.04	0.02	0.02	0.01	0.02	0.03	0.05	0.05
1 / 29 .	0.02	0.02	0.03	0.04	0.01	0.03	0.04	0.06	0.01	0.05	0.04	0.02	0.02	0.01	0.02	0.03	0.05	0.05
1 / 30 .	0.01	0.02	0.03	0.04	0.00	0.03	0.04	0.06	0.01	0.05	0.04	0.02	0.02	0.01	0.02	0.03	0.05	0.05
1 / 31 .	0.02	0.02	0.03	0.04	0.01	0.03	0.04	0.05	0.01	0.05	0.04	0.02	0.02	0.01	0.02	0.03	0.05	0.05
1 / 32 .	0.01	0.02	0.03	0.04	0.00	0.03	0.04	0.05	0.01	0.06	0.04	0.02	0.02	0.01	0.02	0.03	0.05	0.05
1 / 33 .	0.02	0.02	0.03	0.04	-0.04	0.03	0.04	0.06	0.01	0.05	0.04	0.02	0.02	0.01	0.02	0.03	0.05	0.05
1 / 34 .	0.01	0.00	0.03	0.04	0.00	0.03	0.04	0.05	0.01	0.06	0.04	0.02	0.02	0.01	0.02	0.03	0.05	0.05
1 / 35 .	0.01	0.02	0.03	0.04	0.01	0.03	0.04	0.05	0.01	0.05	0.04	0.02	0.02	0.01	0.02	0.03	0.05	0.05
1 / 36 .	0.01	0.02	0.03	0.04	-0.02	0.03	0.04	0.06	0.01	0.05	0.04	0.02	0.02	0.01	0.02	0.03	0.05	0.05
1 / 37 .	0.02	0.02	0.03	0.04	-0.01	0.03	0.04	0.06	0.01	0.05	0.04	0.02	0.02	0.01	0.02	0.03	0.05	0.06

Detection limits - Figure E.4 (Area 3, Yr_OR6468)

Point	P	V	Mn	Fe	Co	Ni	Cu	Zn	Si	S	Cr	Ti	Ca	Mg	As	Sr	Ba	Pb
1 / 1 .	0.01	0.02	0.03	0.04	0.00	0.03	0.04	0.05	0.01	0.06	0.04	0.02	0.02	0.01	0.02	0.03	0.05	0.05
1 / 2 .	0.02	0.02	0.03	0.04	-0.01	0.03	0.04	0.05	0.01	0.06	0.04	0.02	0.02	0.01	0.02	0.03	0.05	0.05
1 / 3 .	0.01	0.02	0.03	0.04	0.00	0.03	0.04	0.06	0.01	0.05	0.04	0.02	0.02	0.01	0.02	0.03	0.05	0.06
1 / 4 .	0.01	0.02	0.03	0.04	0.00	0.03	0.09	0.06	0.01	0.05	0.04	0.02	0.02	0.01	0.02	0.03	0.05	0.06
1 / 5 .	0.01	0.02	0.03	0.04	0.01	0.03	0.04	0.06	0.01	0.06	0.04	0.02	0.02	0.01	0.02	0.03	0.05	0.05
1 / 6 .	0.01	0.02	0.03	0.04	-0.01	0.03	0.04	0.06	0.01	0.06	0.04	0.02	0.02	0.01	0.02	0.03	0.05	0.05
1 / 7 .	0.01	0.02	0.03	0.04	-0.01	0.03	0.04	0.05	0.01	0.06	0.03	0.02	0.02	0.01	0.03	0.03	0.05	0.05
1 / 8 .	0.01	0.02	0.03	0.04	-0.02	0.03	0.04	0.06	0.01	0.05	0.04	0.02	0.02	0.01	0.03	0.03	0.05	0.05
1 / 9 .	0.01	0.02	0.03	0.04	-0.01	0.03	0.04	0.06	0.01	0.05	0.04	0.02	0.02	0.01	0.02	0.03	0.05	0.05
1 / 10 .	0.01	0.02	0.03	0.04	0.01	0.03	0.04	0.06	0.01	0.05	0.04	0.02	0.02	0.01	0.03	0.03	0.05	0.05
1 / 11 .	0.01	0.02	0.03	0.04	0.01	0.03	0.04	0.06	0.01	0.05	0.04	0.02	0.02	0.01	0.02	0.03	0.05	0.05
1 / 12 .	0.02	0.02	0.03	0.04	0.00	0.03	0.04	0.05	0.01	0.05	0.04	0.02	0.02	0.01	0.02	0.03	0.05	0.05
1 / 13 .	0.01	0.02	0.03	0.04	-0.02	0.03	0.04	0.06	0.01	0.06	0.04	0.02	0.02	0.01	0.02	0.03	0.05	0.05
1 / 14 .	0.01	0.02	0.03	0.04	0.00	0.03	0.04	0.06	0.01	0.06	0.04	0.02	0.02	0.01	0.02	0.03	0.05	0.05
1 / 15 .	0.01	0.02	0.03	0.04	0.01	0.03	0.04	0.06	0.01	0.06	0.04	0.02	0.02	0.01	0.02	0.03	0.05	0.05
1 / 16 .	0.01	0.02	0.03	0.04	-0.01	0.03	0.04	0.05	0.01	0.05	0.04	0.02	0.02	0.01	0.02	0.03	0.05	0.05
1 / 17 .	0.01	0.02	0.03	0.04	-0.01	0.03	0.04	0.06	0.01	0.05	0.04	0.02	0.02	0.01	0.02	0.03	0.05	0.05
1 / 18 .	0.02	0.02	0.03	0.04	0.01	0.03	0.04	0.06	0.01	0.05	0.04	0.02	0.02	0.01	0.02	0.03	0.05	0.05
1 / 19 .	0.01	0.02	0.03	0.04	0.01	0.03	0.04	0.06	0.01	0.05	0.03	0.02	0.02	0.01	0.02	0.00	0.05	0.05
1 / 20 .	0.02	0.02	0.03	0.04	0.00	0.03	0.04	0.06	0.01	0.05	0.04	0.02	0.02	0.01	0.02	0.03	0.05	0.05
1 / 21 .	0.02	0.02	0.03	0.04	0.01	0.03	0.04	0.06	0.01	0.05	0.04	0.02	0.02	0.01	0.02	0.03	0.05	0.05
1 / 22 .	0.01	0.02	0.03	0.04	-0.01	0.03	0.04	0.06	0.01	0.06	0.04	0.02	0.02	0.01	0.02	0.03	0.05	0.05
1 / 23 .	0.01	0.02	0.03	0.04	0.01	0.03	0.04	0.05	0.01	0.05	0.04	0.02	0.02	0.01	0.02	0.03	0.05	0.05
1 / 24 .	0.01	0.02	0.03	0.04	-0.05	0.03	0.04	0.06	0.01	0.06	0.04	0.02	0.02	0.01	0.02	0.03	0.05	0.05
1 / 25 .	0.01	0.02	0.03	0.04	0.00	0.03	0.04	0.05	0.01	0.05	0.04	0.02	0.02	0.01	0.02	0.03	0.05	0.05
1 / 26 .	0.01	0.02	0.03	0.04	-0.01	0.03	0.04	0.06	0.01	0.06	0.04	0.02	0.02	0.01	0.02	0.03	0.05	0.06
1 / 27 .	0.02	0.02	0.03	0.04	0.00	0.03	0.04	0.05	0.01	0.05	0.04	0.02	0.02	0.01	0.02	0.03	0.05	0.05
1 / 28 .	0.02	0.01	0.03	0.04	-0.02	0.03	0.04	0.06	0.01	0.06	0.04	0.02	0.02	0.01	0.02	0.03	0.05	0.05

Detection limits - Figure E.5 (Area 4, Yr_OR6468)

Point	P	V	Mn	Fe	Co	Ni	Cu	Zn	Si	S	Cr	Ti	Ca	Mg	As	Sr	Ba	Pb
1 / 1 .	0.01	0.01	0.03	0.04	-0.01	0.03	0.04	0.06	0.01	0.06	0.04	0.02	0.02	0.01	0.02	0.03	0.05	0.05
1 / 2 .	0.01	0.02	0.03	0.04	0.00	0.03	0.04	0.06	0.01	0.06	0.04	0.02	0.02	0.01	0.02	0.03	0.05	0.05
1 / 3 .	0.02	0.02	0.03	0.04	0.00	0.03	0.04	0.05	0.01	0.05	0.04	0.02	0.02	0.01	0.02	0.04	0.05	0.05
1 / 4 .	0.02	0.02	0.04	0.04	0.01	0.03	0.04	0.05	0.01	0.06	0.04	0.02	0.02	0.01	0.02	0.03	0.05	0.06
1 / 5 .	0.01	0.02	0.03	0.04	0.01	0.03	0.04	0.06	0.01	0.06	0.04	0.02	0.02	0.01	0.02	0.03	0.05	0.05

1 / 6 .	0.01	0.02	0.03	0.04	0.00	0.03	0.04	0.06	0.01	0.06	0.04	0.02	0.02	0.01	0.02	0.03	0.05	0.05				
1 / 7 .	0.02	0.02	0.03	0.04	-0.01	0.03	0.04	0.06	0.01	0.06	0.04	0.02	0.01	0.01	0.02	0.03	0.05	0.05				
1 / 8 .	0.01	0.01	0.03	0.04	0.00	0.03	0.04	0.06	0.01	0.06	0.04	0.02	0.02	0.01	0.03	0.04	0.05	0.05				
1 / 9 .	0.01	0.02	0.03	0.04	-0.02	0.03	0.04	0.06	0.01	0.06	0.04	0.02	0.02	0.01	0.02	0.03	0.05	0.05				
1 / 10 .	0.02	0.02	0.03	0.04	-0.01	0.03	0.04	0.06	0.01	0.05	0.03	0.02	0.02	0.01	0.02	0.03	0.05	0.05				
1 / 11 .	0.01	0.02	0.03	0.04	0.01	0.03	0.04	0.06	0.01	0.06	0.04	0.02	0.02	0.01	0.02	0.03	0.05	0.05				
1 / 12 .	0.02	0.02	0.03	0.04	0.00	0.03	0.04	0.06	0.01	0.06	0.04	0.02	0.02	0.01	0.02	0.03	0.05	0.05				
1 / 13 .	0.02	0.02	0.03	0.04	0.01	0.03	0.04	0.06	0.01	0.06	0.04	0.02	0.02	0.01	0.02	0.03	0.05	0.05				
1 / 14 .	0.02	0.02	0.03	0.04	-0.02	0.03	0.04	0.06	0.01	0.06	0.04	0.02	0.02	0.01	0.03	0.03	0.05	0.05				
1 / 15 .	0.01	0.02	0.03	0.04	0.01	0.03	0.04	0.06	0.01	0.06	0.04	0.02	0.02	0.01	0.02	0.03	0.05	0.05				
1 / 16 .	0.01	0.01	0.03	0.04	-0.01	0.03	0.04	0.06	0.01	0.05	0.04	0.02	0.02	0.01	0.03	0.03	0.05	0.05				
1 / 17 .	0.02	0.02	0.03	0.04	0.00	0.03	0.04	0.06	0.01	0.06	0.04	0.02	0.02	0.01	0.02	0.03	0.05	0.05				
1 / 18 .	0.02	0.02	0.03	0.04	0.01	0.03	0.04	0.06	0.01	0.06	0.04	0.02	0.02	0.01	0.02	0.03	0.05	0.06				
1 / 19 .	0.01	0.02	0.03	0.04	0.00	0.03	0.04	0.06	0.01	0.05	0.04	0.02	0.02	0.01	0.02	0.00	0.05	0.05				
1 / 20 .	0.01	0.02	0.03	0.04	0.01	0.02	0.04	0.05	0.01	0.05	0.04	0.02	0.02	0.01	0.02	0.03	0.05	0.06				
1 / 21 .	0.02	0.02	0.03	0.04	0.00	0.03	0.04	0.06	0.01	0.05	0.04	0.02	0.02	0.01	0.02	0.03	0.05	0.05				
1 / 22 .	0.02	0.02	0.04	0.04	0.01	0.03	0.04	0.06	0.01	0.05	0.04	0.02	0.02	0.01	0.02	0.03	0.05	0.05				
1 / 23 .	0.02	0.02	0.03	0.04	0.00	0.03	0.04	0.06	0.01	0.06	0.04	0.02	0.02	0.01	0.03	0.04	0.05	0.05				
1 / 24 .	0.02	0.02	0.04	0.04	0.00	0.03	0.04	0.06	0.01	0.05	0.04	0.02	0.02	0.01	0.02	0.03	0.05	0.06				
1 / 25 .	0.01	0.02	0.03	0.04	0.00	0.03	0.04	0.06	0.01	0.05	0.04	0.02	0.02	0.01	0.02	0.03	0.05	0.05				
1 / 26 .	0.01	0.02	0.03	0.04	0.00	0.03	0.04	0.06	0.01	0.05	0.04	0.02	0.02	0.01	0.02	0.03	0.05	0.05				
1 / 27 .	0.01	0.01	0.03	0.04	0.01	0.03	0.04	0.06	0.01	0.06	0.04	0.02	0.02	0.01	0.02	0.04	0.05	0.06				
1 / 28 .	0.01	0.02	0.03	0.04	0.01	0.03	0.04	0.05	0.01	0.05	0.04	0.02	0.01	0.01	0.02	0.04	0.05	0.05				
1 / 29 .	0.02	0.02	0.03	0.04	-0.14	0.03	0.04	0.06	0.01	0.05	0.04	0.02	0.02	0.01	0.02	0.03	0.05	0.05				
1 / 30 .	0.02	0.02	0.03	0.04	-0.01	0.03	0.04	0.06	0.01	0.05	0.04	0.02	0.02	0.01	0.02	0.03	0.05	0.05				
1 / 31 .	0.01	0.02	0.03	0.04	0.00	0.03	0.04	0.06	0.01	0.05	0.04	0.02	0.02	0.01	0.02	0.03	0.05	0.05				
1 / 32 .	0.02	0.02	0.03	0.04	0.00	0.03	0.04	0.06	0.01	0.05	0.04	0.02	0.02	0.01	0.02	0.03	0.05	0.05				
1 / 33 .	0.01	0.02	0.03	0.04	0.00	0.03	0.04	0.06	0.01	0.06	0.04	0.02	0.02	0.01	0.02	0.03	0.05	0.05				
1 / 34 .	0.01	0.02	0.03	0.04	0.00	0.03	0.04	0.05	0.01	0.06	0.04	0.02	0.02	0.01	0.03	0.03	0.05	0.05				
1 / 35 .	0.02	0.02	0.03	0.04	0.00	0.03	0.04	0.06	0.01	0.06	0.04	0.02	0.02	0.01	0.02	0.03	0.05	0.05				
1 / 36 .	0.01	0.02	0.03	0.04	0.00	0.03	0.04	0.06	0.01	0.06	0.04	0.02	0.02	0.01	0.03	0.03	0.05	0.05				
1 / 37 .	0.01	0.02	0.03	0.04	0.00	0.03	0.04	0.06	0.01	0.06	0.04	0.02	0.02	0.01	0.02	0.03	0.05	0.05				
1 / 38 .	0.02	0.02	0.03	0.04	-0.02	0.03	0.04	0.06	0.01	0.06	0.04	0.02	0.02	0.01	0.02	0.03	0.05	0.05				
1 / 39 .	0.01	0.02	0.03	0.04	-0.02	0.03	0.04	0.06	0.01	0.05	0.04	0.02	0.02	0.01	0.02	0.03	0.05	0.05				
1 / 40 .	0.02	0.02	0.03	0.04	0.00	0.03	0.04	0.06	0.01	0.06	0.04	0.02	0.02	0.01	0.02	0.03	0.05	0.06				

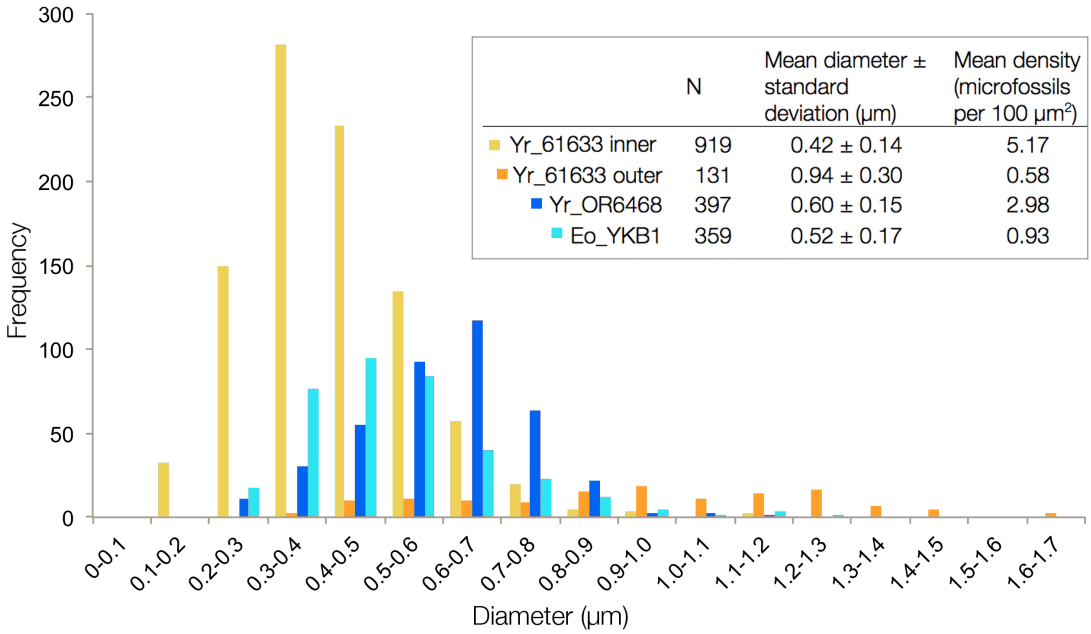

Figure E.6 Diameter distributions and density measurements for Yaman Kasy microfossils. Bars are coloured according to the four around-tube locations where microfossils were found (Yr_61633 inner rim of colloform pyrite; Yr_61633 outer rim of colloform pyrite; Yr_OR6468; Eo_YKB1).

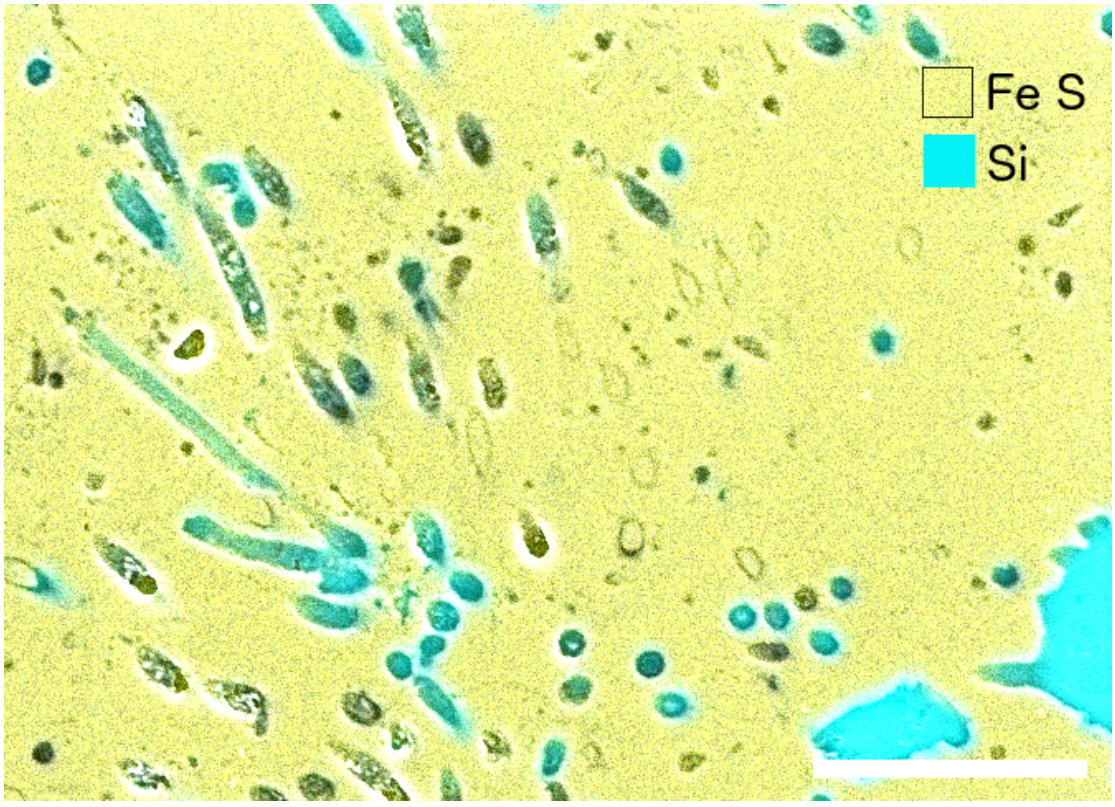

Figure E.7 Elemental composition of mineralised microbial filaments preserved alongside the tubes of *Alvinella* sp. Scale bar is 7 µm.

Table E.3 Results of Shapiro-Wilk normality tests of microstructure diameter distributions. Non-significant results are highlighted, TS - transverse section, LS - longitudinal section.

	N	W	p-value
Yr_61633 inner	919	0.9665	1.069e-13
Yr_61633 outer	131	0.9837	0.1183
Yr_OR6468	397	0.9869	0.001239
Eo_YKB1	359	0.9152	2.437e-13

Table E.4 Results of *F*-tests for the comparison of variance between dataset pairs of microstructure diameter measurements. Non-significant results are highlighted.

	Yr_61633 inner	Yr_61633 outer	Yr_OR6468
Yr_61633 outer	F = 0.2072, num df = 918, denom df = 130, p-value < 2.2e-16		
Yr_OR6468	F = 0.8954, num df = 918, denom df = 396, p-value = 0.1872	F = 4.3224, num df = 130, denom df = 396, p-value < 2.2e-16	
Eo_YKB1	F = 0.6952, num df = 918, denom df = 358, p-value = 2.248e-05	F = 3.356, num df = 130, denom df = 358, p-value < 2.2e-16	F = 0.7764, num df = 396, denom df = 358, p-value = 0.01406

Table E.5 Results of Kolmogorov-Smirnov tests for comparison of microstructure diameter distributions between dataset pairs.

	Yr_61633 inner	Yr_61633 outer	Yr_OR6468
Yr_61633 outer	D = 0.7438, p-value < 2.2e-16		
Yr_OR6468	D = 0.5445, p-value < 2.2e-16	D = 0.634, p-value < 2.2e-16	
Eo_YKB1	D = 0.2737, p-value < 2.2e-16	D = 0.6477, p-value < 2.2e-16	D = 0.347, p-value < 2.2e-16

References

Little, C. T. S., Maslennikov, V. V, Morris, N. J. and Gubanov, A. P. (1999) Two Palaeozoic hydrothermal vent communities from the southern Ural mountains, Russia. *Palaeontology* **42**, 1043–1078.

Maginn, E., Little, C. T. S., Herrington, R. and Mills, R. (2002) Sulphide mineralisation in the deep sea hydrothermal vent polychaete, *Alvinella pompejana*: implications for fossil preservation. *Marine Geology* **181**, 337–356.